Fundamental Studies of Carbon Oxygen Bond Activation in Nickel Diphosphine Ether Complexes

and

Metallomacrocycles as Ligands: Synthesis and Characterization of Aluminum-Bridged Bisglyoximato Complexes of Iron and Cobalt

Thesis by
Paul Kelley

In Partial Fulfillment of the Requirements
for the Degree of Doctor of Philosophy

CALIFORNIA INSTITUTE OF TECHNOLOGY
Division of Chemistry and Chemical Engineering
Pasadena, California
2014
(Defended on April 10, 2014)

"See! Caltech made you happy."

-Agnes Tong

ACKNOWLEDGEMENTS

Graduate school can be a series of trials, most of these trials are too much for a single being to handle alone. Fortunately no one has to undertake these tasks alone. Family, mentors, and friends are all critical to ones success in graduate school. Admittingly, without these forementioned resources I would have never been able to complete my PhD. It is to them that I owe my success. I would like to thank my mentors, friends, and family and anyone I may not list in the following statement. I want you to know that you have all touched my life in a special way and I am glad to have met you.

Thank you.

Prof. Theodor Agapie, I need to thank you first of all for taking me into your group back in 2008. It has been a long journey. In your group, I have had the opportunity to work on many projects and explore many different areas of chemistry and I thank you for that. Throughout my years at Caltech you have been a source of guidance and inspiration both in and out of the lab. Theo, I cannot thank you enough for the support you have given me. I will always remember my first years in lab and how you worked beside me teaching me how to use a schlenk line. Thank you for all that you taught me about inorganic and organometallic chemistry. Thank you for all the time you have taken pouring over my many presentations and teaching me how to be a respectable presenter. I thank you for all the times you allowed me to TA 102 with you. The lessons I learned from watching you teach and craft that class will be invaluable to me in the future, and I thank you for the time that you spent imparting that to me. I am also grateful that I got to observe (and partake) in the development

and management of a newly founded research group. I would be lying if I said I didn't enjoy helping to build the Agapie group. Most of all, thank you for teaching me how to be a scientist and an overall better person, your rigor and passion for chemistry will always inspire me.

Prof. John Bercaw, thank you so much for being the chair of my thesis committee. Your advice and guidance has got me out of a rut numerous times. To the other members of my committee, Profs. Jonas C. Peters and Greg C. Fu, thank you for all your honest feedback on my scientific endeavors. Your words inside and outside my meetings helped me feel that you are genuinely invested in my development as a scientist. Thank you both for coming back to Caltech!

Many thanks to the members of the Gray group who provided a tremendous amount of time and effort in helping me when I was working on a bioinorganic project. Similarly I need to thank the members of the Bercaw group who provided advice and help on numerous occasions. Alex Miller, Ian Tonks, Paul Oblad, and Ted Weintrob thank you for all your help. The Bercaw group shrunk significantly near the end of my PhD studies. However, what the group lacked in size was made up with character and heart. Tom Teets, Dave Leitch, and Aaron Sattler, thank you all for making so many BP meetings enjoyable, and I wish you all luck in your careers!

Most of my time at Caltech was spent with my homies, by that I mean the Agapie group. I have spent many years with this group of people, I have shared their success and failures, while I can maybe convince myself that I helped them all in some fashion during their journeys, I feel what I may have done for them pales in comparison to what they have done for me.

Thanks to all my box mates of the past and present Jessica Sampson, Justin Henthorn, Josh Wiensch, and Madalyn Radlauer for putting up with me. I have always enjoyed the chemistry you guys would produce and I know you will keep up the good work! Maddy kudos to you for being an awesome safety officer, keeping us safe, and encouraging us to get regular healthy hours of sleep, I will always miss your peppy and chipper attitude. Sibo thanks for all your support over the years, thanks for all your comments, experimental suggestions, and just being overall helpful when I was in a scientific rut. Emily Tsui thanks for being an awesome friend all these years, hopefully we can continue the party in our postdocs! To Sandy, you will always be the best of the best to me. Thanks for all your help, from those early years of the bioinorganic projects to now. Davide thanks for all your hard work in making our group parties enjoyable! Thanks for all your tireless work as our dungeon master in our grand D&D adventure! The time when we encountered the Gnolls in our campaign is one of my top 5 greatest moments in graduate school. Thank you for that. Jacob thanks for always being a great guy, from your taste in music, to the kind words you would say sometimes, to that time your unbuttoned my shirt, thanks for all that! (Some more than others though...) Guy A. Edouard thanks for being an awesome co-worker! I really enjoyed working with you and still wake up in a cold sweat sometimes due to that paper we co-authored, but at least we both now know the source of the hydrogen! Justin Henthorn thanks for being a great bay mate. You would always remind me when my bay was getting to dirty by cleaning yours first, oh the shame. Guy, Justin, and Josh Wiensch thanks for allowing me to hang out with you guys I will always remember the lunches that we would get... I felt like a Goon. Kyle Horak, thanks for being an

awesome friend, although you never answer my text messages ☹. Kyle, never forget your style, for it is uniquely your own. Buss thanks for being a fun guy to hang around you will always be my Boo. To all the first years, the most painful thing about moving on is that I won't get to hang out and see what you guys come up with. Good luck to all three of you in your amazing Agapie group journey! I'm certain we will meet again at a conference or something I look forward to all the chemistry you guys do!

Thanks also to Dr Dave Herbert for all you input during my studies of the nickel diphosphine chemistry. Po-Heng Lin thanks you so much for having a great sense of humor and always being your jolly self.

Many thanks to the exceptional staff at Caltech with whom, I had a chance to interact. Thank you Drs. Scott Virgil, Dave VanderVelde, Larry Henling, Mona Shahgholi, and the late Mike Day. You guys provided so much support to me over the years and I wouldn't have been able to make it here without you.

Thanks to all my friends and family who helped me when I was not in lab. Many thanks especially to my friends from other groups mainly Peter Agbo, Ryan Henning, and Joey Varghese thanks so much for being great to just hang out with! I am certain there are other people I am not listing and for all those, from me to you, "You are awesome!"

Many thanks to the Caltech Center for Diversity and their amazing staff! I unfortunately only became envolved in the CCD near the end of my PhD studies, mostly due to the urging of Agnes Tong.

I also would like to thank my good friend Agnes Tong. While there are many things I need to thank you for I am going to list the ones I feel are most important.

Agnes you have always been there for me when I have felt like I had no one to turn to. For issues I would encounter at Caltech or issues at home you were always there and I felt like I could talk to you about it and for that I thank you. Thank you for all the administrative help you have given me over the years of my PhD study and making things so much easier to understand. Interestingly, you were the only person who ever asked me wether I was attracted to females and I thank you for that. I thank you for making me question myself and become more truthful to myself. Thank you Agnes for always being there for me and simply being someone I could always talk to. Thanks for being someone I could confide in, someone who would actually listen. Agnes you have helped me through so much and you will always (along with Sandy and Emily) rank with the best of the best, thank you so much for being my friend.

ABSTRACT

In order to develop better catalysts for the cleavage of aryl-X bonds fundamental studies of the mechanism and individual steps of the mechanism have been investigated in detail. As the described studies are difficult at best in catalytic systems, model systems are frequently used. To study aryl-oxygen bond activation, a terphenyl diphosphine scaffold containing an ether moiety in the central arene was designed. The first three chapters of this dissertation focus on the studies of the nickel complexes supported by this diphosphine backbone and the research efforts in regards to aryl-oxygen bond activation.

Chapter 2 outlines the synthesis of a variety of diphosphine terphenyl ether ligand scaffolds. The metallation of these scaffolds with nickel is described. The reactivity of these nickel(0) systems is also outlined. The systems were found to typically undergo a reductive cleavage of the aryl oxygen bond. The mechanism was found to be a subsequent oxidative addition, β-H elimination, reductive elimination and (or) decarbonylation.

Chapter 3 presents kinetic studies of the aryl oxygen bond in the systems outlined in Chapter 2. Using a series of nickel(0) diphosphine terphenyl ether complexes the kinetics of aryl oxygen bond activation was studied. The activation parameters of oxidative addition for the model systems were determined. Little variation was observed in the rate and activation parameters of oxidative addition with varying electronics in the model system. The cause of the lack of variation is due to the ground state and oxidative addition transition state being affected similarly. Attempts were made to extend this study to catalytic systems.

Chapter 4 investigates aryl oxygen bond activation in the presence of additives. It was found that the addition of certain metal alkyls to the nickel(0) model system lead to an increase in the rate of aryl oxygen bond activation. The addition of excess Grignard reagent led to an order of magnitude increase in the rate of aryl oxygen bond activation. Similarly the addition of $AlMe_3$ led to a three order of magnitude rate increase. Addition of $AlMe_3$ at -80 °C led to the formation of an intermediate which was identified by NOESY correlations as a system in which the $AlMe_3$ is coordinated to the ether moiety of the backbone. The rates and activation parameters of aryl oxygen bond activation in the presence of $AlMe_3$ were investigated.

The last two chapters involve the study of metalla-macrocycles as ligands. Chapter 5 details the synthesis of a variety of glyoxime backbones and diphenol precursors and their metallation with aluminum. The coordination chemistry of iron on the aluminum scaffolds was investigated. Varying the electronics of the aluminum macrocycle was found to affect the observed electrochemistry of the iron center.

Chapter 6 extends the studies of chapter 5 to cobalt complexes. The synthesis of cobalt dialuminum glyoxime metal complexes is described. The electrochemistry of the cobalt complexes was investigated. The electrochemistry was compared to the observed electrochemistry of a zinc analog to identify the redox activity of the ligand. In the presence of acid the cobalt complexes were found to electrochemically reduce protons to dihydrogen. The electronics of the ancillary aluminum ligands were found to affect the potential of proton reduction in the cobalt complexes. These potentials were compared to other diglyoximate complexes.

TABLE OF CONTENTS

LIST OF FIGURES

LIST OF SCHEMES

LIST OF TABLES

CHAPTER 1

General Introduction

This dissertation is focused on two main areas, specifically the study of aryl oxygen bond activation in a nickel(0) diphosphine terphenyl ether complex and the study of aluminum glyoxime macrocycles and the effects of sterics and electronics on the coordination and chemistry of the central metal center.

The efficient elaboration of aryl oxygen bonds to a variety of functional groups is emerging as a versatile tool in organic methodology. One very important use of aryl oxygen moieties is for the facile modification of arene rings. These substituents can be introduced into the aromatic ring via a number of pathways, notably electrophilic aromatic substitution. One widely used example is for the lithiation of arene rings where the aryl-lithium salt can be quenched with an electrophilic species leads to derivertization of the ring.

Although the utility of aryl oxygen groups cannot be understated, their removal is not straightforward. The aryl oxygen bond is strong and hence resists efforts at its activation. Some catalytic systems have been developed albeit the systems typically suffer from low turnover and low rates. Another utility of this cleavage is in cross coupling. Cross coupling of aryl ethers allows for the utilization of phenolic precursors in organic synthesis. While catalytic systems have been developed few in-depth mechanistic studies have been done on the reactivity of aryl oxygen bonds with nickel.

While few experimental studies had been done some computational studies had been undertaken where it was found that a nickel arene interaction was of present prior to the activation of the aryl oxygen bond. Our group has been focusing on several novel terphenyl diphosphine scaffolds. These terphenyl diphosphines were found to encourage metal arene interactions with a variety of metals. Given that the ligands predisposed the metal to interact with the arene we envisioned observing intramolecular reactivity with an ether moiety in close proximity with the central arene

ring. Hence we come to the main ligand of this thesis. We developed a diphosphine terphenyl containing an ether moiety in the central arene of the terphenyl. Using this novel diphosphine studies were undertaken to gain mechanistic insight into the mechanism of aryl oxygen bond activation. From this system, in collaboration with my colleagues Sibo Lin and Guy A. Edouard, a mechanism for the reductive cleavage of aryl oxygen bond was able to be worked out, which we were able to extend to catalytic systems.

From there I directed myself to studies on the effect of electronics in aryl oxygen bond activation (Chapter 3). I was able study the rate of oxidative addition in great detail in variants of the nickel diphosphine discussed in chapter two. I was able to show that the rates and kinetics of oxidative addition are not affected significantly by the electronics of the ether. This is proposed to result from similar changes in the energy of the fround and transition states. Attempts were made to extend these studies to actual catalytic systems however due to the complexity of the systems the conclusions were always less than satisfying.

However, during the kinetic studies I was able to observe the acceleration of aryl oxygen bond activation in the presence of Lewis metal alkyls. Through careful low temperature studies we were able to ascertain that the Lewis acidic metal is coordinated to the ether moiety. The rate was found to show a dependence on Lewis acidic metal alkyl hinting a much more complicated mechanism.

The second part of my thesis deals with the study of iron and cobalt glyoxime complexes. What sets these compounds apart is the large aluminum linker between the glyoximes. The aluminum linkers and the ancillary ligands on the aluminum were found to affect the chemistry and geometry of the metal center. The structural and

electrochemical parameters of the iron complex were investigated. Analogous cobalt complexes were studied for proton reduction as a function of the aluminum linkers.

CHAPTER 2

MECHANISTIC STUDIES OF ARYL-OXYGEN BOND ACTIVATION IN A NICKEL(0) DIPHOSPHINE-ETHER COMPLEX

The text for this chapter was taken in part from:

Kelley, P.; Lin, S.; Edouard, G.; Day, M. W.; Agapie, T. *J. Am. Chem. Soc.* **2012**, *134*, 5480-5483.

Abstract

In order to understand the mechanism of the reductive cleavage of aryl ethers by nickel, the reactivity of terphenyl diphosphine aryl alkyl ethers with nickel precursors was studied. A series of nickel(0) complexes containing nickel-arene interactions adjacent to a methyl aryl ether bond were isolated. Heating these systems led to aryl-oxygen bond activation and generation of nickel-aryl-alkoxide complexes. Formal β-H elimination from these species produced a nickel-aryl-hydride that can undergo reductive elimination and decarbonylation in the presence of the formed aldehyde to regenerate a nickel(0) complex. Upon observing reactivity with aryl methyl ethers the investigations were extended to ethyl, isopropyl, aryl, and benzyl aryl ether linkages, which are structurally relevant to lignin biomass. The reported complexes map out a plausible mechanism for the reductive cleavage of aryl ethers catalyzed by nickel, involving β-H elimination from a nickel alkoxide rather than cleavage of the nickel-oxygen bond by H_2. The studies provide insight into the mechanistic possibilities of the cleavage of aryl oxygen bonds in both small organics and also lignin biomass.

INTRODUCTION:

The elaboration of the aryl carbon-oxygen bond to a variety of functional groups has emerged as a versatile synthetic tool in organic methodology,[1] as phenol precursors are readily available and synthetic modification of the aromatic ring is facile. Phenol derived electrophiles are very valuable. Phenol derived electrophiles are naturally abundant and or can be readily prepared from other accessible aromatic compounds. Currently there are over 50000 phenol and aryl polyol derivatives commercially available. This is in direct contrast with aryl, polyaryl, vinyl, allyl, and alkyl halides, which are typically used as electrophiles in cross coupling. Although a variety of these precursors can be provided on large scale industrially, they are still far less naturally available, and at times economically and environmentally challenging.[1a,1b]

Substitution of arenes containing oxygen moieties is quite facile, indicating another advantage of phenolic precursors. Electrophilic aromatic substituents can be introduced into the aromatic ring via a number of pathways, notably through substitution. It is possible to control the formation of *ortho*-substituted arenes through the use of directed *ortho*-metallation. Oxygen containing moieties such as phenols, ethers, carbamates, and sulfonates have been shown to direct lithiation of the *ortho* position of the arene (Scheme 2.1).[1a,1b] Quenching of the lithium species with an electrophilic species leads to the functionalization of the arene. These functionalized arenes can be used as electrophiles in cross coupling reactions leading to the facile synthesis of complex organic compounds.

Scheme 2.1 Ortho directed lithiation

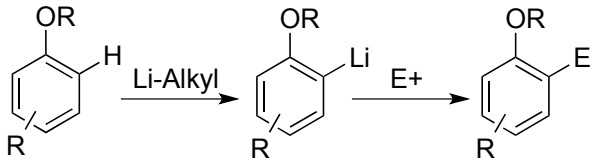

While the availability and ease of functionalization of phenolic precursors makes their advantages apparent, the implication of an aryl oxygen cleaving strategy is not simple. Aryl ether bonds are significantly stronger than their aryl halide counterparts making the direct activation of aryl-oxygen substrates challenging. Typically aryl oxygen moieties must be converted to the more reactive phosphinates, sulfunates, or triflates. Because of the strength of the aryl oxygen bonds, harsh conditions are typically required, which lead to deleterious side reactions hindering formation of the desired cross-coupled product.

Nickel-based catalysts have proven versatile in the conversion of substrates with aryl C-O[2] or C-S[3] bonds in comparison to well-known palladium catalysts. Although cross-coupling of phenolic substrates tends to require prior conversion to the more reactive sulfonates,[2a] recent advances show that aryl phosphates, aryl esters, aryl carbamates, aryl ethers and even free phenols can be used as electrophiles in cross-coupling reactions.[2b-l] In a complementary approach, the conversion of aryl C-O to aryl-H bonds has been recognized as a valuable strategy for removing an oxygen-based directing group from an aryl ring. Silanes have been utilized as a hydride source for this transformation.[2i,2j] Additionally, stoichiometric intramolecular aryl C-O activation has been reported with rhodium and palladium pincer complexes.[4] In the context of biomass conversion to alternative fuels and chemicals, the depolymerization of lignin, a significant component of biomass containing aryl ether linkages, is a considerable

challenge.[5] Recently, an appealing strategy involving the cleavage of lignin-like aryl C-O bonds via nickel-catalyzed hydrogenolysis was reported by Hartwig *et al* (Scheme 2.2).[6] Given the general interest in the conversion of aryl C-O bonds, detailed mechanistic insight including the nature of the intermediates is instrumental in developing practical catalysts.

Scheme 2.2 Several Catalytic Nickel Systems for the Cross Coupling and or Reductive Cleavage of Aryl Oxygen Bonds in Relevant Substrates

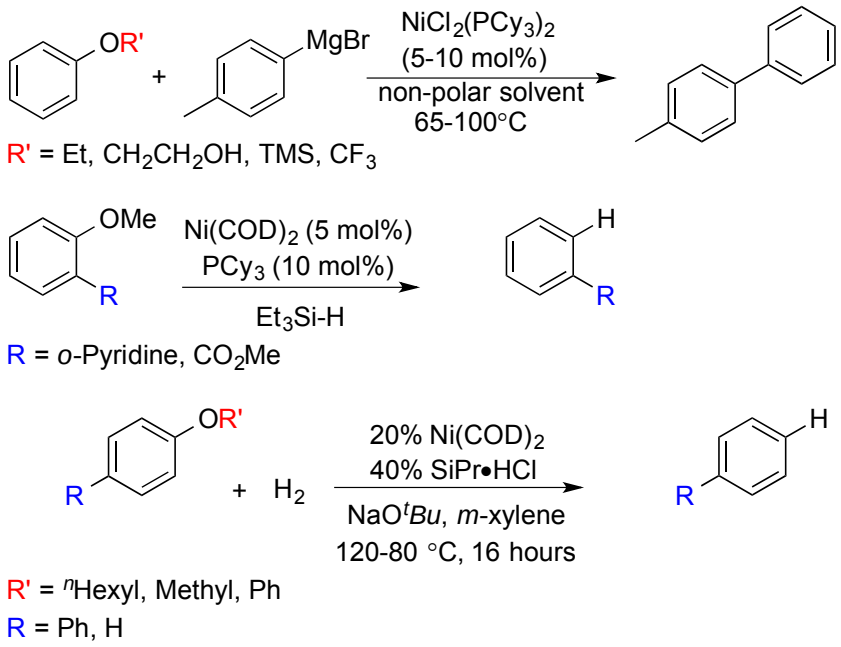

In the Agapie group several diphosphine terphenyl ligand precusors have been previously synthesized. When metallated with nickel, these scaffolds were found to support mono- and dinuclear complexes that exhibit a variety of strong nickel-arene interactions (Scheme 2.3).[7] Specifically the *meta*-terphenyl diphosphine was found to predispose the nickel center toward an interaction with the carbon at the 2'-position of the central arene ring or an interaction with the arene π–system in that area. As metal-arene interactions have been proposed to precede the cleavage of aryl-X bonds, we envisioned this m-terphenyl diphosphine as a scaffold for a model system to provide

mechanistic insight into the reductive cleavage of aryl-oxygen bonds. A m-terphenyl diphosphine could be synthesized containing a carbon-O bond in the ipso-position of the central terphenyl ring (Scheme 2.4).[8] The close proximity of the central arene and carbon-O bond should engender reactivity. Herein, we report detailed mechanistic studies of the nickel-mediated reductive cleavage of an aryl-ether with pendant phosphines.

Scheme 2.3 Several Nickel Terphenyl Diphsophine Systems

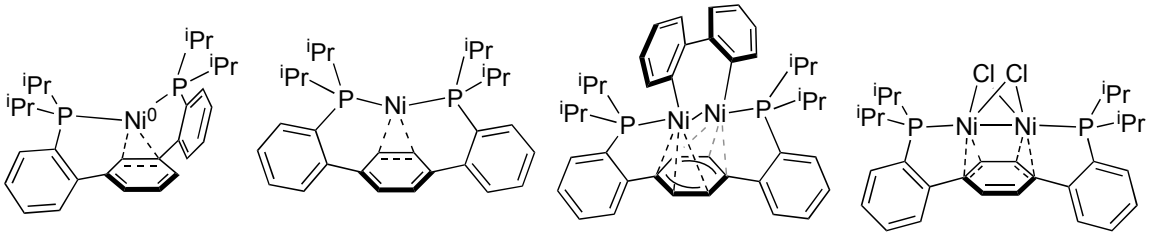

Scheme 2.4 Design of Alkyl Ether Terphenyl Scaffold

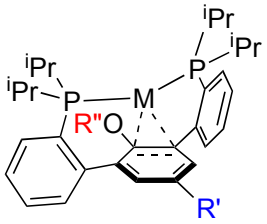

RESULTS & DISCUSSION:

Ligand Synthesis:

Synthesis of the alkyl ether terphenyl ligands was accomplished via the procedure shown in Scheme 2.1. A substituted phenol can be treated with a 2:1 mixture of sodium iodide and sodium chlorite in the presence of acid to form the desired diiodophenol. The diiodophenol can be alkylated with a variety of alkyl halides in acetone utilizing potassium carbonate as a base to form the diiodoalkoxybenzene. Treatment of the diiodo precursor with 2-bromophenyl boronic acid under Suzuki coupling conditions yields the dibromide terphenyl ether backbone. A lithium halogen exchange followed by treatment with diisopropylchlorophosphine leads to the formation of the desired diphosphine terphenyl ether ligand. This synthesis is highly modular and several ligand variants have been synthesized. The functional group in 4'-position of the phenol can easily be changed by varying the starting phenol, which allows for variation of the electronics of the central arene.

Scheme 2.5 Diphosphine Terphenyl Methyl Ether Synthesis

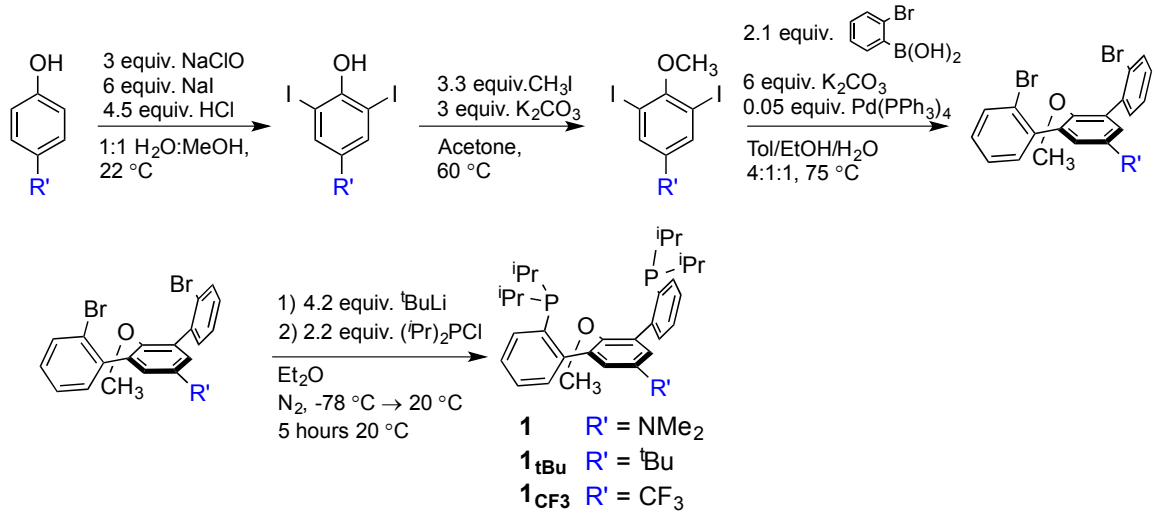

Using the general procedure outlined in Scheme 2.5 several variants of ligands were synthesized. The main diphosphine discussed in this chapter, contains a dimethylamino group in the *para*-position of the central ring and was synthesized using a modified procedure (Scheme 2.6). Starting from 4-nitrophenol, the dibromide terphenyl ether with a para-nitro group can be synthesized in a fashion similar to other substituted phenols. Variation of the ether can be achieved by reaction of the phenol with different alkyl halide precursors (Scheme 2.5). Reduction of the nitro group was achieved via treatment of the dibromo terphenyl with ammonium chloride in the presence of excess iron powder in an acetone water mixture. This transformation can also be done in a 10:1 ethanol water mixture using excess iron powder and concentrated hydrochloric acid. Reductive amination of the terphenyl amine leads to the desired dibromo terphenyl dimethylamine ligand precursor after purification via flash chromatography. This dimethylamine terphenyl can be used to synthesize the diphosphine analogous to that shown in the general procedure (Scheme 2.6).

Scheme 2.6 Diphosphine dimethylamino terphenyl alkyl ether synthesis

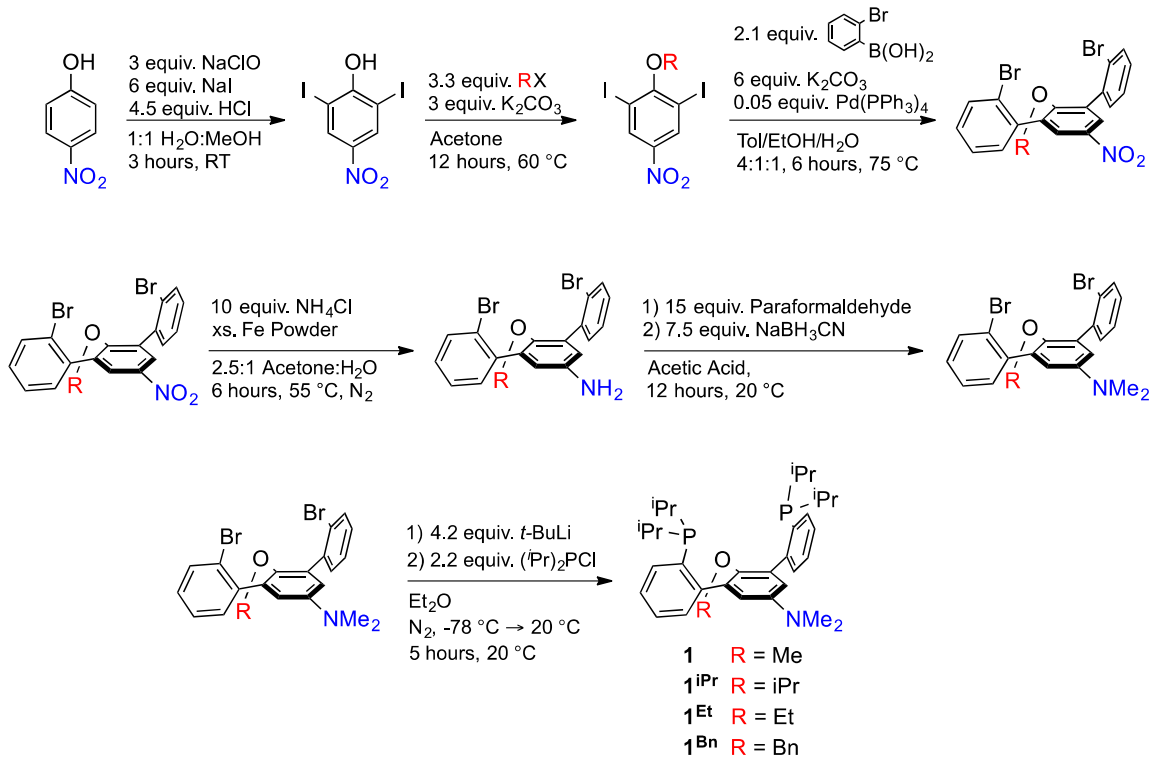

Ligands containing alkyl ethers can easily be synthesized via reaction of a diiodo phenolic precursor with the desired alkyl halide. The synthesis of a diaryl ether on this scaffold, however, requires a different approach to install the aryl group. The most promising method was found to be coupling of a phenol with a diaryl iodonium triflate salt.[9] Asymmetric diaryl iodonium triflate salts can easily be synthesized through a one-pot reaction of an aryl iodide with benzene in the presence of m-chloroperoxybenzoic acid and triflic acid. Coupling of these asymmetric diaryl iodonium reagents with a phenol leads to the formation of a diaryl ether containing the most electronegative arene of the diaryl iodonium reagent.

With this in mind the synthesis of a terphenyl diaryl ether ligand was attempted starting from the diiodo phenol (Scheme 2.7). Treatment of the 2,6-diiodo-4-

nitrophenol with sodium hydroxide in the presence of a variety of diaryl iodonium triflate salts did not result in the formation of the desired diaryl ether presumably due to the electronics of the arene. However, coupling of the more electron rich 2,6-diiodo-4-tertbutylphenol with (4-nitrophenyl)(phenyl) iodonium triflate proceeded smoothly to form the desired 4-nitrophenyoxy-2,6-diiodo-4-tertbutylbenzene cross coupling precursor (Scheme 2.7).[10] Cross coupling followed by a reduction and reductive amination of the nitro substituent lead to the desired dibromide. Analogous to the previous diphosphines the terphenyl dibromide can be phosphinated upon purification by flash chromatography to yield the desired diaryl ether terphenyl diphosphine (Scheme 2.7).

Scheme 2.7 Diphosphine terphenyl diaryl ether synthesis

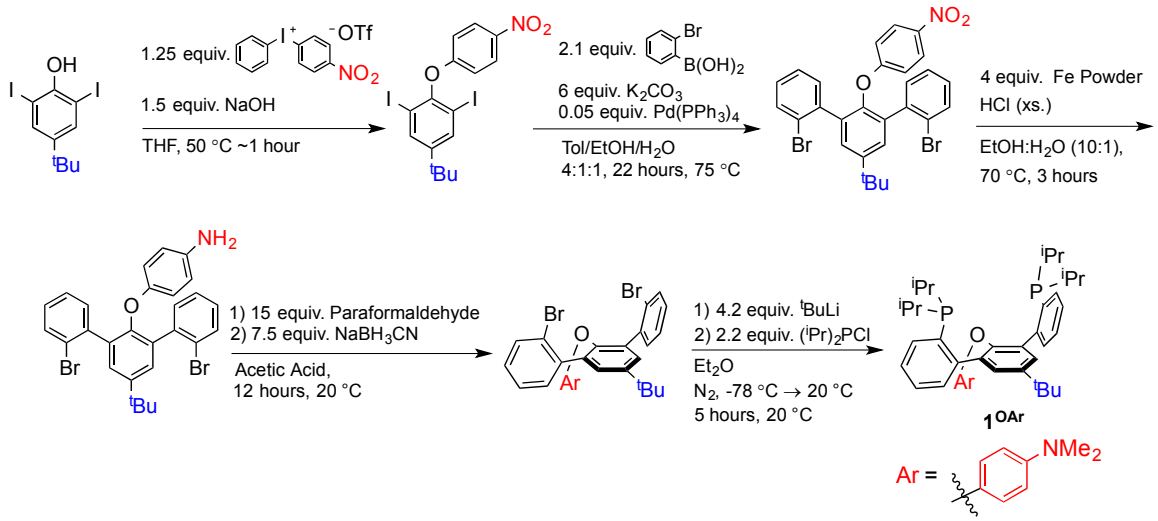

All the diphosphine ether ligands synthesized exhibit NMR behavior consistent with hindered rotation around the carbon-carbon bond between the central terphenyl ring and the outer terphenyl arenes (Figure 2.1). These properties arise due to the ether moiety at the *ipso*-carbon at the central terphenyl ring and the isopropyl substituted phosphines. Analysis of the diphosphine ether ligands via ^{31}P NMR spectroscopy typically reveals two peaks between 0 and 5 ppm. Changes in the ratio of the ^{31}P resonances are dependent on the identity of the ether in the *ipso*-position. A similar analysis by ^{1}H NMR spectroscopy reveals broadening of the resonances corresponding to the ether moiety and resonances for the outer rings. For the benzyl variant **1**$^{\mathbf{Bn}}$ (Scheme 2.6) a pair of doublets and a singlet is observed for the methylene protons. This is consistent with two species in solution, the major species, which gives the two doublets, is consistent with an *anti* like configuration where the phosphines are on different sides of the plane of the central arene ring (Figure 2.1). In such a configuration, the two methylene protons are in different environments, and hence diastereotopic. Each diastereotopic proton would split the resonance of the other

proton causing the observation of two doublets. Similarly the observed singlet is consistent with a *syn* conformation of the two outer phosphines (Figure 2.1). With both phosphine groups on the same side of the central arene plane the methylene protons would be in similar environments and a singlet is observed by ^{1}H NMR spectroscopy.

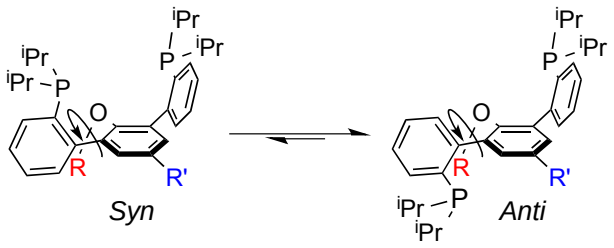

Figure 2.1. Hindered rotation around substituted terphenyl rings. *Syn* atropisomer corresponds to both phosphines on the same side of the central arene ring. The *anti* atropisomer corresponds to phosphines on either side of the central ring.

Interconversion between the *syn* and *anti* atropisomers can be achieved at higher temperatures. Variable temperature ^{1}H NMR studies show a coalescence of peaks in the aromatic region and the isopropyl methane protons and sharpening of the resonances of the isopropyl methyl groups and the methoxy group as shown in Figure 2.2. Similarly variable temperature ^{31}P NMR studies show coalescence of the phosphorous resonances assigned to the *syn* and *anti* atropisomers at higher temperatures. All diphosphine ethers synthesized exhibit similar peak coalescence at higher temperatures.

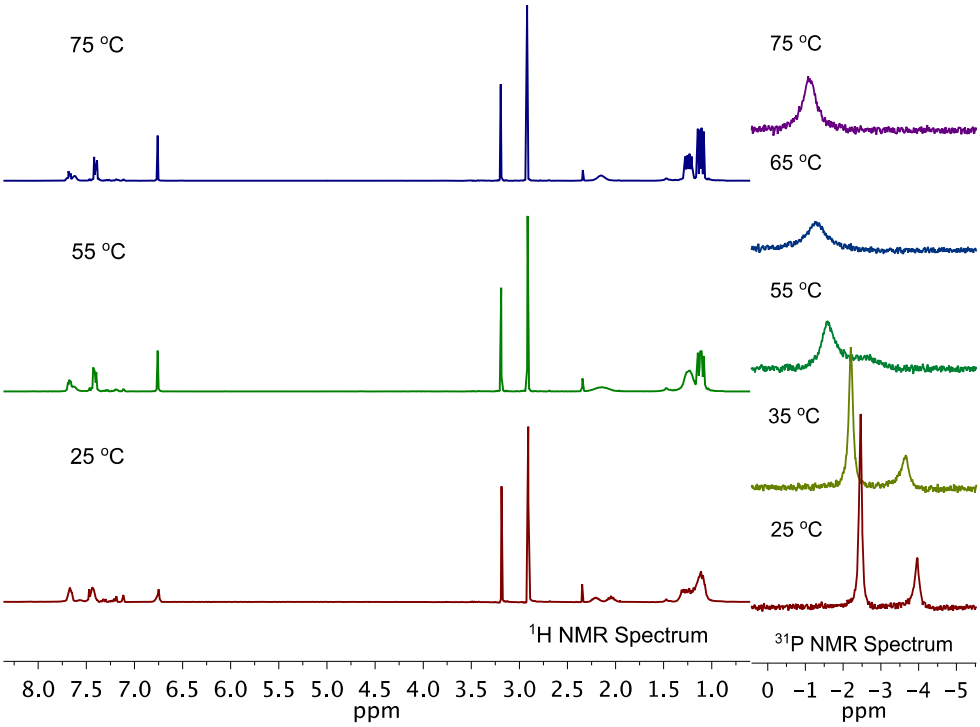

Figure 2.2. Variable temperature NMR spectra of **1**. Stacked ^{1}H NMR spectra on the left and ^{31}P NMR spectra on the right.

Metallation of the Methyl Ether Diphosphine: Nickel(0) Model Systems

Methyl ether

Addition of an equivalent of Ni(COD)$_2$ to the diphosphine scaffold **1** at 20 °C led to generation of a new species **2** over the course of 13 hours, according to NMR spectroscopy (Scheme 2.8). Metallation of **1** with Ni(COD)$_2$ is slow (13 hours) consistent with hindered rotation of the terphenyl backbone. Comparatively, para- and meta-terphenyl diphosphines, which do not contain ether backbones, are metallated at a much faster rate. The ^{31}P and ^{1}H NMR spectra give a singlet and sharp resonances respectively indicative of the absence of the rotation of the terphenyl backbone that is observed in the free ligand. The ^{31}P NMR chemical shift of **2** (40.7 ppm) is similar to

that reported for the *p*-terphenyl diphosphine supported nickel(0) (40.4 ppm).[7] Similarly, the protons assigned to the central arene resonate almost 1 ppm more upfield (5.84 ppm) compared with those of the free phosphine (6.73 ppm) in the ^{1}H NMR spectrum of **2**, whereas the ether OC*H*$_3$ peak is only slightly shifted (3.13 ppm vs. 3.17 ppm, **1** vs. **2**). These data are consistent with the formation of a nickel(0) species with interactions between the metal center and the aromatic π-system, but not the ether oxygen. Through the aforementioned NMR studies, complex **2** was assigned as a nickel(0) complex with the metal center coordinated to the two phosphine and central arene (Scheme 2.8).

Scheme 2.8 Synthesis of nickel(0) compound 2

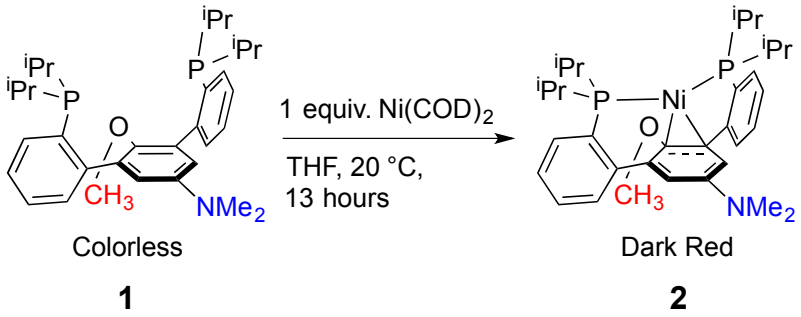

The assignment and spectroscopic findings of **2** were confirmed by a single-crystal X-ray diffraction (XRD). X-ray quality crystals of **2** were grown out of pentane at -32 °C. In the solid state the metal center is bound by two phosphines and interacts with two carbon centers of the central arene as predicted by NMR studies (Figure 2.3). The short Ni-C distances (1.96-2.09 Å) indicate strong interactions between the metal center and central arene. Consequently, some C-C distances of the central ring are consistent with partial localization of the double bonds. For **2** the C8-C9 and C10-C11 bonds (1.368(2) and 1.360(2) Å, respectively) are shorter than the rest of the central

arene C-C bonds by >0.06 Å. The aryl C-O bond is angled 16.76 ° away from the metal center, consistent with partial sp^3 hybridization of the 2′-position of the central ring (C18, (Figure 2.3)) due to the Ni-C interaction. Notably, an intermediate displaying η^2-interactions between Ni(0) and the double bond adjacent to the oxygen was found computationally to precede C-O bond activation in the cross coupling of phenolic derivatives.[2g,11] Complex **2** is the only example of such an arrested intermediate characterized by crystallography, according to a Cambridge Structural Database search.[12]

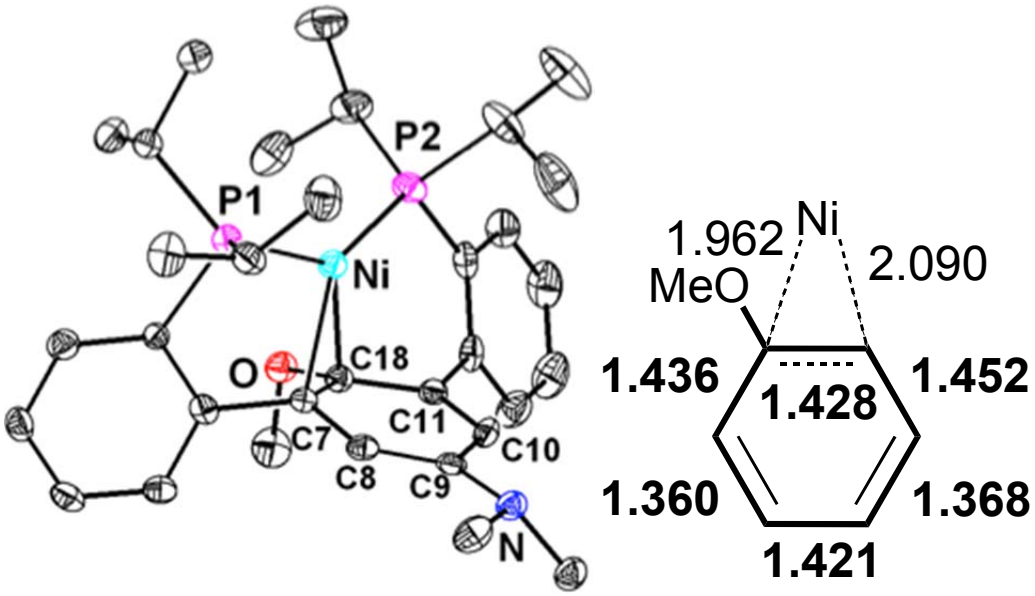

Figure 2.3 Solid-state structure of **2** (left). Solvent molecules, anions, and select hydrogen atoms not shown for clarity. Diagram of central arene bond lengths in **2** (right).

Complex **2** was found to convert to new species in solution at 45 °C or over an extended period of time at 20 °C (Scheme 2.9). After the first 12 hours at 45 °C a new product **3** was observed by NMR spectroscopy, in mixture with starting material. The same species can also be observed in a mixture after five days at 20 °C. Monitoring the reaction mixture by ^{1}H NMR spectroscopy reveals a shift in the peak corresponding to

the central arene ring downfield at 6.78 ppm, which is very close to the central arene resonances of the ligand precursor **1** (6.72 ppm). Additionally, the OC*H*$_3$ resonance is shifted nearly 0.5 ppm downfield from 3.17 ppm in **2** to 3.66 ppm in complex **3**. Hydrolysis of **3** and analysis of the liberated organic products by ESI mass spectrometry reveals a terphenyl diphosphine moiety without the methoxy group. This is consistent with activation of the aryl-oxygen bond to form a nickel(II) methoxide. Due to the shifts in the central arene and methoxy resonances and the identity of the ligand complex **3** was assigned as a nickel(II) methoxy species where the nickel has activated the sp^2 aryl-oxygen bond. Compound **3** is similar to a nickel(II) PCP complex which gives similar ^{1}H NMR resonances for the central arene and methoxy group at 6.85 ppm and 3.90 ppm respectively.[13]

Scheme 2.9 Synthesis of nickel(II) methoxide complex 3

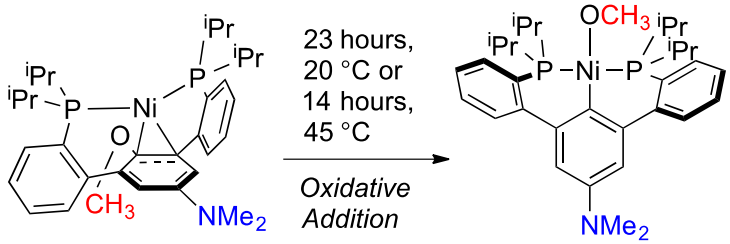

Dark Red
2

Orange
3

Upon further heating of **3**, a new species, **4**, is observed (Scheme 2.10). The central arene protons of this complex are also shifted relative to **2** in the aromatic region (6.79 ppm vs. 5.84 ppm) and are quite similar to the arene resonances in the nickel(II) methoxide complex **3** (6.78 ppm). Intriguingly, the OC*H*$_3$ signal is absent and upfield triplet is observed in the hydride region of the ^{1}H NMR spectrum (-2.87 ppm). This upfield peak is consistent with the formation of a Ni(II) hydride.

Compound **4** was found to be isolable in *55%* yield by precipitation from THF upon stirring **2** at 20 °C for seven days. The central arene resonances suggest a PCP pincer type coordination similar to that of **3**. Analysis of the ligand by ESI mass spectrometry also supports this assignment for **4**. Unfortunately, efforts to obtain X-ray quality single crystals of **4** or **3** have been unsuccessful to date.

Scheme 2.10 Synthesis of nickel(II) hydride 4 from complex 2

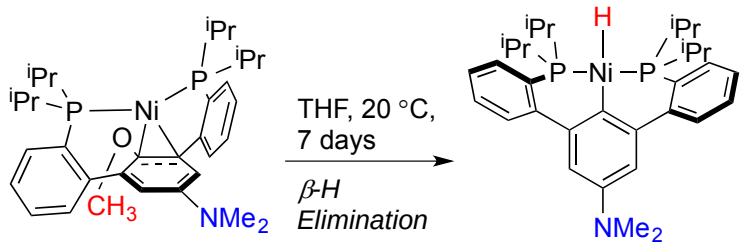

Dark Red **2** Yellow **4**

In order to obtain structural insight into compounds **3** and **4** an analog with a better crystallization profile was synthesized. Treatment of **4** with excess methyl iodide at 20 °C for 14 hours generated a new species assigned as a Ni(II) iodide, *5*; an XRD study of this species confirmed the above assignments for compounds **3** and **4** (Scheme 2.11). Gratifyingly, the nickel center was found in the same plane as the central arene as predicted by cleavage of the aryl–O bond. The Ni–C distance (1.919(1) Å) is consistent with an aryl C–Ni bond and is similar to other PCP pincer complexes.[13] The diphosphine ligand framework, bound in *pseudo-C*$_2$ fashion, acts as a classical tridentate diphosphine-aryl pincer,[14] but with six-member chelates involving aryl-aryl linkages.[15] The solid-state structure is consistent with the NMR spectroscopic data for **4** and *5* indicating the absence of the methoxy group and the lack of

interaction with the π-system of the arene. Most importantly, the structure shows cleavage of the aryl C–O bond and displacement of oxygen by nickel.

Scheme 2.11 Synthesis of nickel (II) iodide *5* from complex 4

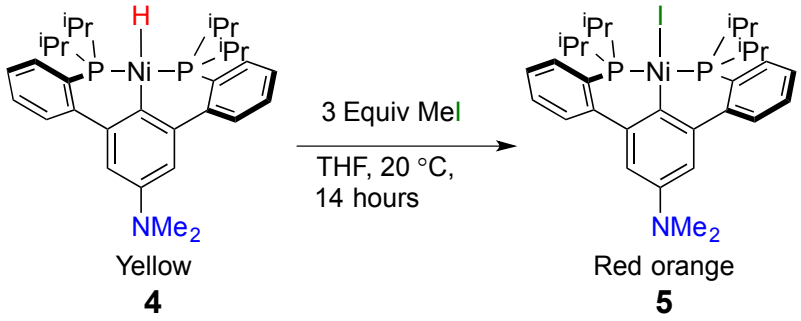

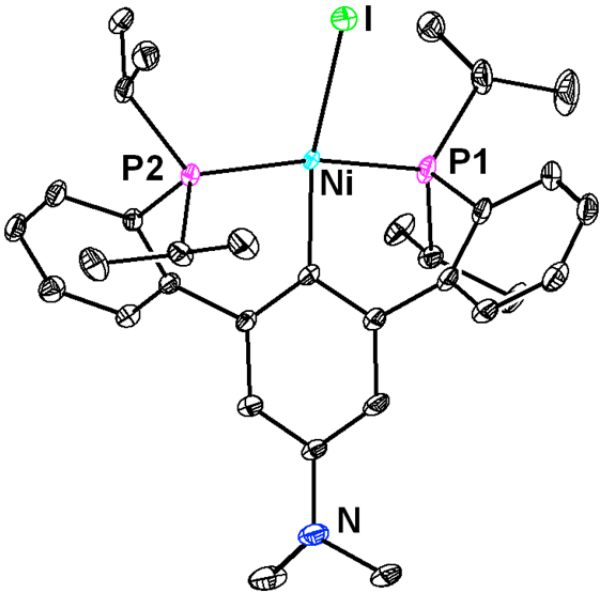

	angles (°)
P2-Ni-P1	166.680(17)
C-Ni-I	161.06(4)
P2-Ni-I	99.972(12)
P1-Ni-I	93.156(13)
C-Ni-P2	84.30(4)
C-Ni-P1	83.98(4)

Figure 2.4 Solid-state structure of *5* (left). Solvent molecules, anions, and select hydrogen atoms not shown for clarity. Table of relevant angles in *5* (right).

Attempts were made to independently synthesize a nickel(II) methoxide on this PCP backbone in order to confirm the identity of **3**. One route to **3** is the reaction of **4** with methanol. Sigma bond metathesis of the methanol and **4** could form **3** and release

hydrogen. Treatment of **4** with methanol at 20 °C, gratifyingly, led to the reformation of species **3**, albeit not quantitatively (as identified by ^{1}H and ^{31}P NMR spectroscopy). Alternatively complex **3** can be synthesized through a salt metathesis between **5** and sodium methoxide. Indeed, treatment of **5** with sodium methoxide at 20 °C does led to the formation of **3**, albeit in a mixture with **4** and other unidentified species. Although the nickel(II) methoxide could not be synthesized by these alternate routes without contamination from **4**, the independent methods of generation are consistent with identity of **3** being a nickel(II) aryl-methoxide. This is the product of oxidative addition of the aryl C–O bond to nickel(0).[16] Similar stoichiometric reactions mediated by rhodium and palladium have been reported.[4]

Scheme 2.12 Alternate Syntheses of 3 from 4 and *5*

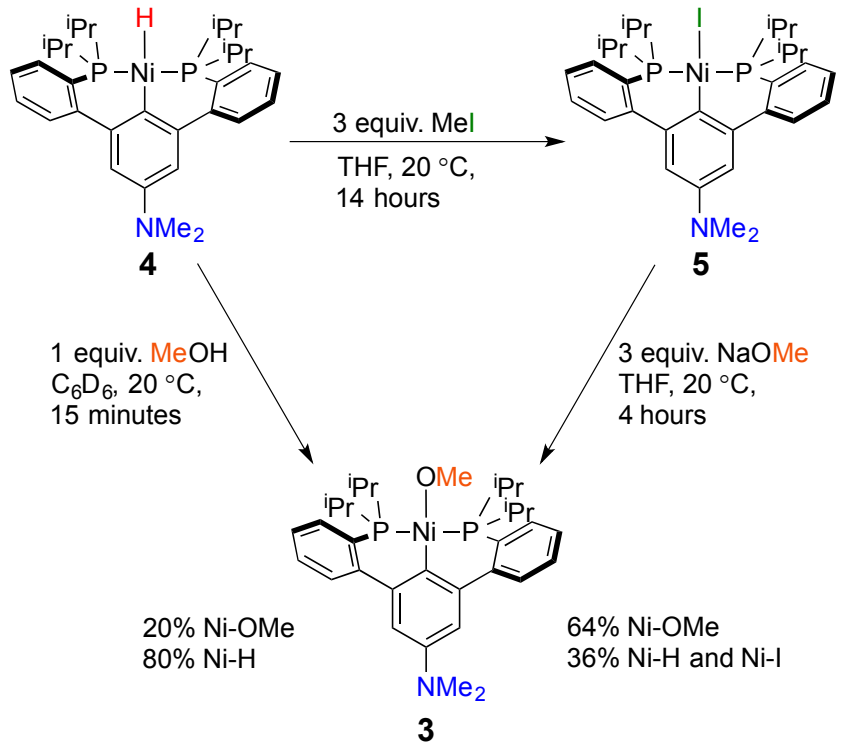

The mechanism of the hydride formation in **4** was probed through deuterium labeling studies. A ligand containing a deuterated methoxide was synthesized through the use of d_3-iodomethane in the phenol protection. **1-d_3** metallation with nickel(0) produced **2-d_3** the deuterated analog of **2**. Subjection of **2-d_3** to elevated temperatures in this complex leads to a nickel methoxide complex **3-d_3**, which is identical to **3**, albeit without resonances for the methoxy group. Further heating of **3**^{d3} leads to the formation of the nickel(II) deuteride **4-d_1**. Complex **4-d_1** gives no signal in the hydride region of the ^{1}H NMR spectrum, but otherwise displays the same peaks as **4**. This is consistent with the formation of a nickel-deuteride through a β-hydrogen elimination of the methoxide to presumably form formaldehyde, as the methoxy group is the only source of deuterium in the reaction mixture other than d_6-benzene. This study

confirms the methoxy group as the source of hydrogen (deuterium). *β*-hydrogen elimination could occur via a five-coordinate intermediate,[17] although, in coordinatively saturated systems it has been proposed to occur via alkoxide dissociation[18] or in bimolecular fashion.[19] Given the strain observed in the chelates in **5**, dissociation of a phosphine arm may also be possible,[17a,17b,20] opening up a *cis* coordination site for *β*-hydrogen elimination. Further studies will be required to elucidate the mechanism of *β*-hydrogen in the present system.

Scheme 2.13 Synthesis of 4-*d*$_1$ from 2-*d*$_3$

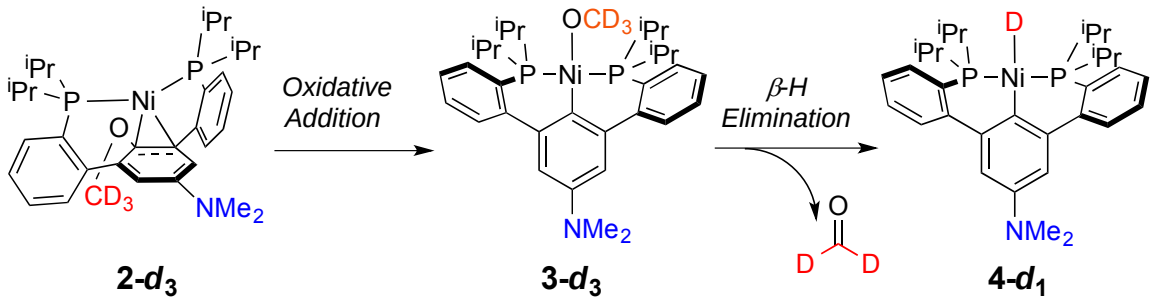

Although its generation does not require dihydrogen, hydride **4** is a potential intermediate in the hydrogenolysis of the aryl-O bond. Complex **2** was heated to 100 °C, generating new species, **6**, in over 90% yield (^{1}H NMR spectroscopy) within two hours. The Ni-*H* peak is absent from the ^{1}H NMR spectra of the product and a new triplet is present (**6**, 6.51 ppm) assigned to an aryl *ipso*-C-*H*. Infrared (IR) spectroscopy revealed an absorption indicative of a terminal Ni(0)–CO (**6**, 1917 cm^{-1}) (Scheme 2.14). The identity of this complex was confirmed through the independent synthesis of the Nickel(0) ipso-H complex **7**. Addition of a sub stoichiometric amount of carbon monoxide to this complex leads to the formation of **6** and starting material as identified by NMR and IR spectroscopy (Scheme 2.15).

Scheme 2.14 Synthesis of Ni(0) carbonyl complex 6 from 2

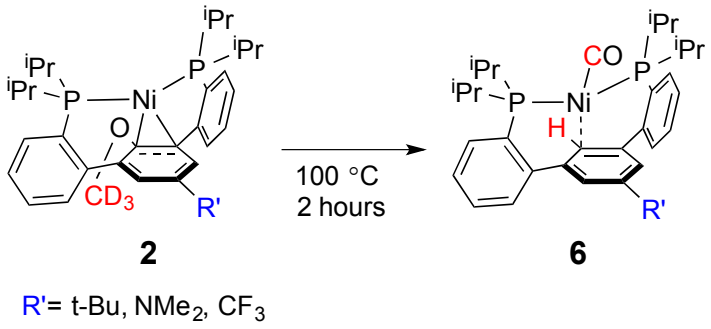

Scheme 2.15 Alternate Synthesis of 6 from 7

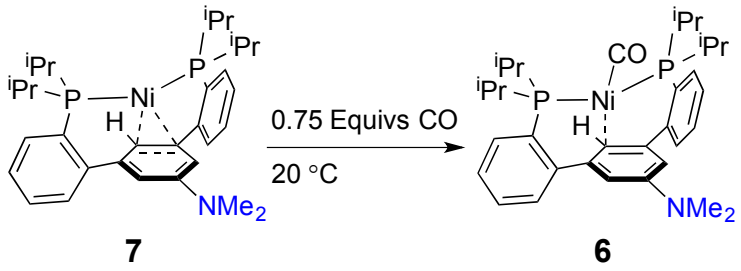

Intrigued by the presence of the *ipso*-H and the carbonyl group, we hypothesized that the *ipso*-H and carbonyl in **6** were the product of a reductive elimination and decarbonylation of formaldehyde from the previously isolated nickel(II) hydride **4**. To this end, reductive elimination in the **4** was investigated as the source of the *ipso*-H. Surprisingly, heating **4** to 100 °C for over 6 hours does not result in reductive elimination to form **7** and heating for extended periods resulted in decomposition of **4**. However, the addition of sub stoichiometric amounts of carbon monoxide to **4** does result in the generation of **6**, albeit slowly in a mixture with several other unidentifiable products. This behavior indicates that another ligand facilitates the reductive elimination step in **4**.

π-Acidic ligands have been previously reported to facilitate reductive elimination in nickel(II) square planar complexes. Intrigued by the ligand facilitated reductive elimination, other ligands were investigated. The addition of less π-acidic ligands such as pyridine or trimethyl phosphine did not result in reductive elimination in **4** even after heating at 100 °C. As formaldehyde is proposed to be generated through the β-H elimination to form **4**, paraformaldehyde was tested for facilitation of the reductive elimination. Treatment of **4** with paraformaldehyde immediately leads to the formation of several unidentified species at room temperature. Heating this mixture to 60 °C results in the formation of **6** within four hours.

The reaction of the hydride **4** with formaldehyde could proceed through several mechanisms. The nickel(II) hydride could undergo a sigma bond metathesis with formaldehyde to release dihydrogen forming a nickel(II) formyl complex. The formyl can undergo a deinsertion of the carbonyl to form a five coordinate nickel(II) carbonyl hydride, this transient species could undergo reductive elimination to form **6**. Alternatively formaldehyde can act as a fifth ligand and coordinate to the **4** and facilitate reductive elimination to form **7**, which can then decarbonylate formaldehyde releasing dihydrogen and forming **6**.

In order to gain insight into these mechanistic possibilities the nickel(0) complexes were tested for decarbonylation reactivity. Treatment of **7** with paraformaldehyde quickly resulted in a vigorous release of dihydrogen and a color change from dark red to red orange. Analysis by ^{1}H and ^{31}P NMR spectroscopy revealed the quantitative formation of **6** in under 10 minutes at 20 °C. Interestingly, all the meta nickel(0) complexes (**7**, **2**, $\mathbf{2}_{tBu}$, and $\mathbf{2}_{CF3}$)discussed undergo decarbonylation

with paraformaldehyde. As the nickel(0) complexes are competent for the decarbonylation of formaldehyde it is entirely possible that **4** coordinates formaldehyde as a fifth ligand and undergoes reductive elimination to form **7** with formaldehyde coordinated. As we have observed experimentally **7** can quickly undergo decarbonylation to quantitatively generate **6**.

A possible mechanism for the reductive cleavage of anisoles with nickel has been outlined using the nickel(0) diphosphine ether model system **2** (Scheme 2.16). Starting from a nickel(0) metal center (**2**) the complex can undergo oxidative addition to form a nickel(II) methoxide (**3**). The nickel(II) methoxide species (**3**) undergoes β-hydrogen elimination to form a nickel(II) hydride (**4**) and formaldehyde. In the presence of formaldehyde, the hydride (**4**) undergoes reductive elimination and decarbonylation to form a nickel(0) carbonyl complex (**6**). Overall, an anisole has been reductively cleaved forming an arene, carbon monoxide, and dihydrogen, with the methoxy group providing the required reducing equivalents (Scheme 2.17).

Scheme 2.16 Observed Model System Reactivity

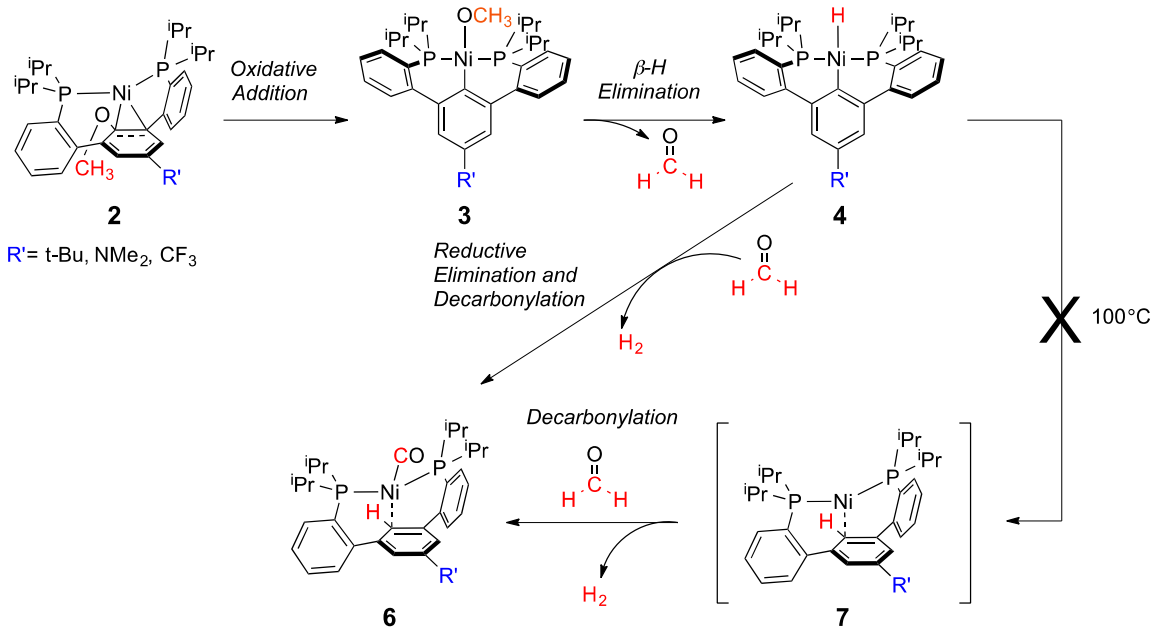

Scheme 2.17 Overall Anisole Reductive Cleavage Products

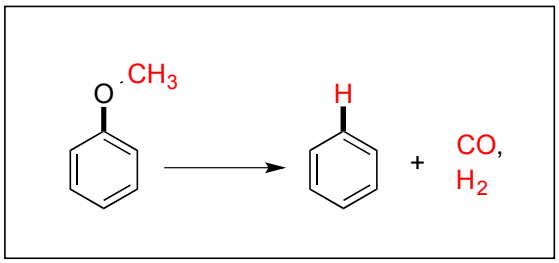

Inspired by these mechanistic results, the reactivity of the nickel model complex **2** was assessed in the presence of two prominent reductive cleavage additives, hydrogen and silanes. In a catalytic system with dihydrogen it is feasible to propose that the nickel(0) can add into the aryl oxygen bond forming a nickel(II) alkoxide, which could undergo sigma bond metathesis with dihydrogen to form a nickel(II) hydride and an alcohol. To investigate the feasibility of this mechanistic possibility the reactivity of **2** was explored in the presence of dihydrogen. Using **2-*d*$_8$** it should be possible to observe whether sigma bond metathesis is feasible through a labeling study,

as a successful sigma bond metathesis would lead to the formation of **4**. A vessel charged with **2-*d*$_3$** and 4 atm of dihydrogen was heated to 45 °C. Under these conditions only *β*-hydrogen elimination was observed as only **4-d$_1$** was identifiable by ^{1}H NMR spectroscopy. The results of the labeling study show that in this system, *β*-hydrogen elimination from the alkoxide is more favorable than sigma bond metathesis of dihydrogen, for the formation of **4** (Scheme 2.18). Overall this suggests that the sigma bond metathesis of dihydrogen through a nickel(II) intermediate might not be a viable mechanistic step for the reductive cleavage of aryl bonds.

Scheme 2.18 Reactivity of 2-*d*$_3$ in the presence of H$_2$

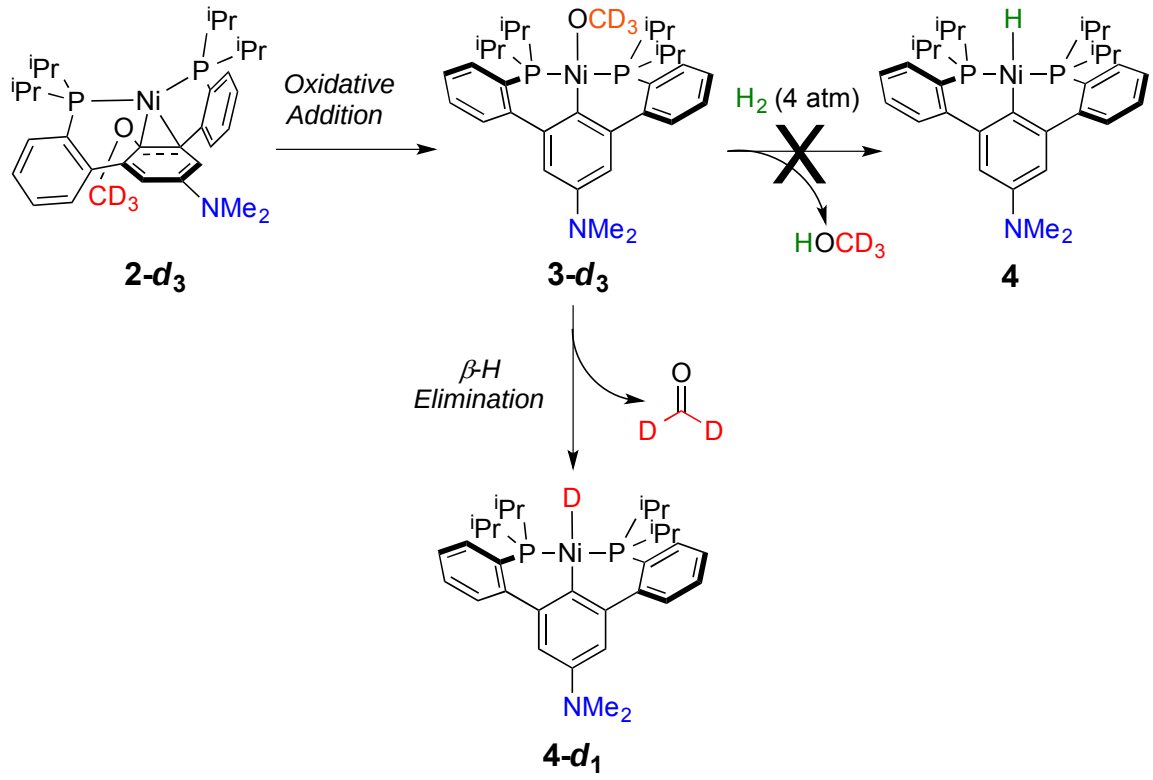

As silyl hydrides are also used as hydride sources in the reductive cleavage of aryl oxygen bonds, the reactivity of the model complex was investigated in the presence of triethylsilane (Scheme 2.19). In a catalytic system one can postulate that a

nickel(0) catalyst could undergo oxidative addition of an aryl ether to form a nickel(II) alkoxide, which can undergo transmetallation with silane, producing a nickel(II) hydride, followed by reductive elimination releasing arene and forming the nickel(0) catalytic species. This mechanistic possibility can be probed through a labeling study of **2** and labeled silane, where the identity of the ipso-H, in **6** will indicate silane transmetallation. Heating **2** to 80 °C in benzene in the presence of two equivalents of Et_3SiD for three hours generated less than 10% **6-*d*$_1$**. A larger excess of Et_3SiD (10 equivalents) led to more deuterium incorporation (ca 20% **6-*d*$_1$**).

As there is an isotope effect favoring the formation of **6**, the effect of triethylsilane with **2-*d*$_1$** was also investigated. Treatment of **2-*d*$_1$** with Et_3SiH (2 equiv) generated **6-*d*$_1$** and **6** in a 1:1 ratio. The increased isotopic incorporation from Et_3SiH vs. Et_3SiD is consistent with normal isotope effects for *β*-hydrogen elimination (conversion of **3** to **4**) and σ-bond metathesis between **3** and silane to generate **4**. An unidentified species was observed by ^{1}H and ^{31}P NMR spectroscopy, in amount proportional to the label incorporation from SiX (X=D or H) into **6**. This is consistent with decreased generation of formaldehyde and hence lower formation of the nickel carbonyl species upon reductive elimination / decarbonylation. These results indicate that the mechanism involving β-hydrogen elimination (Scheme 2.19) is favored vs. interception of the nickel methoxide by silane, at low concentration of silane.

Scheme 2.19 Labeling studies of 2 with Triethylsilane

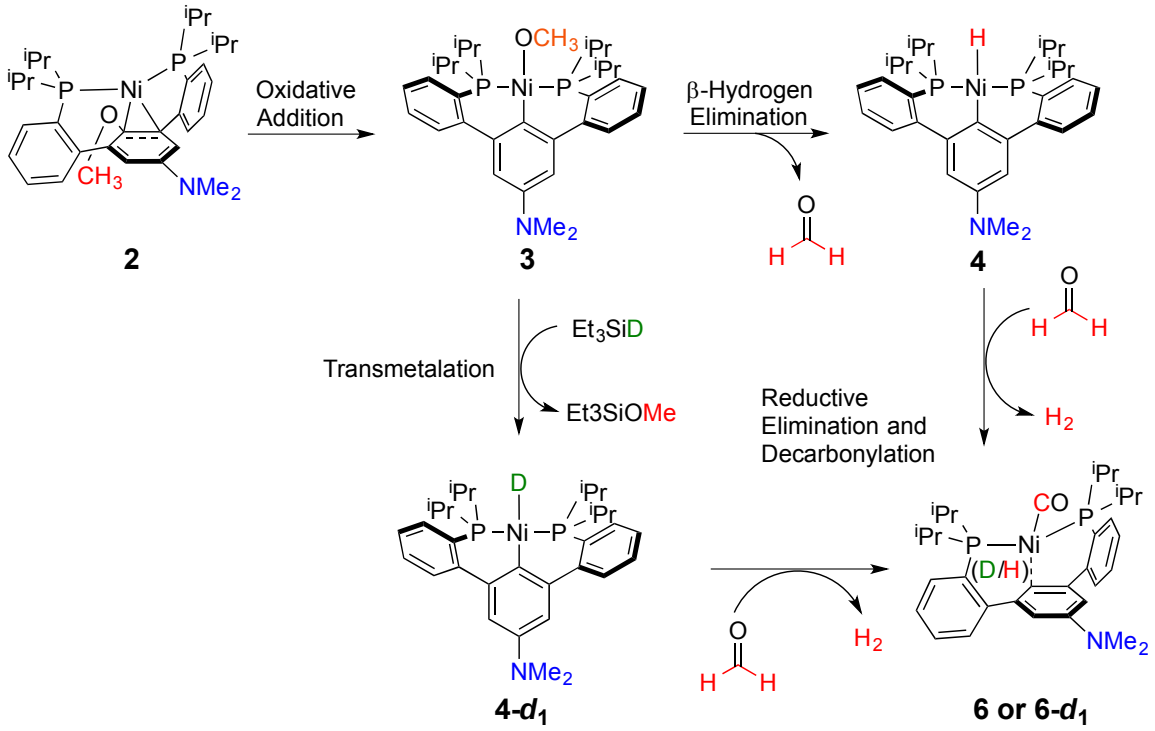

The mechanism for the reductive cleavage of the aryl-oxygen bond outlined with complex **2** was found to be the same for the other nickel(0) terphenyl diphosphine methyl ether variants. The tert-butyl variant $\mathbf{2}_{t\mathrm{Bu}}$ was found to undergo a mechanism identical to the dimethyl amino variant. Interestingly the trifluoromethyl variant $\mathbf{2}_{\mathrm{CF3}}$ showed some deviation in the formation of the final nickel(0) carbonyl product. Heating of $\mathbf{2}_{\mathrm{CF3}}$ to 100 °C for 1.5 hours produces both $\mathbf{6}_{\mathrm{CF3}}$ and $\mathbf{7}_{\mathrm{CF3}}$ in a 1:1 ratio. This could be due to the lack of reactivity between $\mathbf{3}_{\mathrm{CF3}}$ and formaldehyde and formaldehyde acts like a fifth ligand promoting reductive elimination to form $\mathbf{4}_{\mathrm{CF3}}$. $\mathbf{7}_{\mathrm{CF3}}$ undergoes decarbonylation much slower (3 hours) than the more electron donating **7** (less than 10 minutes), which can explain the observed $\mathbf{7}_{\mathrm{CF3}}$, reductive elimination followed by a slow decarbonylation leads to a mixture of species.

Metallation of the Methyl Ether Diphosphine: Nickel(II) Phenoxide Halide Systems

Treatment of a colorless solution of the diphosphine terphenyl ether **1** with an equivalent of yellow Ni(II)Cl_2(DME) (DME = dimethoxyethane) in THF results in the formation of a green compound (**8**) (Scheme 2.20) over the course of several hours. The ^{31}P NMR spectrum shows a shift in the phosphorous resonances of the free diphosphine to a new resonance at 13.46 ppm. The ^{1}H NMR reveals several broad resonances in the alkyl region between 0 and 4 ppm which can be assigned to the dimethylamine group and isopropyl groups of the ligand, however there is no assignable methoxy resonance indicating C–O bond activation. Mass analysis of the organics after hydrolysis of **8** reveals the mass for the diphosphine phenol, leading to the assignment of **8** as a nickel(II) phenoxide chloride complex (as shown scheme 2.20). This is consistent with Ni(II)X_2 reacting in a fashion similar to boron tribromide, where the Lewis acidic nickel center coordinates to the methoxy group and eliminates MeX, forming a nickel(II) phenoxide chloride. This is reminiscent of reactivity observed in the treatment of other phosphine ethers and diphosphine ethers with group 10 metals.[4] The observed reactivity appears to be limited to metal halides, treatment of the ligand with other nickel(II) salts such as Ni(II)OTf_2 (OTf = trifluoromethyl sulfate) does not lead to the formation of a similar phenoxide complex and only starting materials are observed by ^{1}H and ^{31}P NMR spectroscopy. The rate of the formation of the phenoxide complex is also dependent on the identity of the ether. Treatment of $\mathbf{1}^{Et}$ or $\mathbf{1}^{iPr}$ leads to the formation of the same nickel(II) phenoxide chloride complex albeit at a significantly reduced rate with $\mathbf{1}^{iPr}$ being the slowest, while addition of a nickel(II) halide to $\mathbf{1}^{OAr}$ does not lead to the formation of **8**.

Scheme 2.20 Reactivity of 1 with $NiCl_2$(DME)

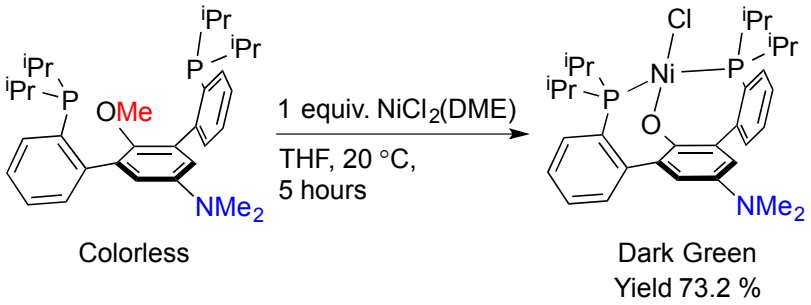

Colorless

Dark Green
Yield 73.2 %

A single crystal X-ray diffraction study of a crystal of **8** grown from a concentrated solution in benzene confirmed the tentative structure (Figure 2.5). From the solid state structure we can see that the Ni(II)Cl_2 has activated the sp^3 C–O bond to form a nickel phenoxide species. Interestingly two different structures were obtained from the crystal and differ in the structural identity of the dimethylamine group on the central arene. One structure contains what appears to be a dimethylamine in the backbone and displays C–N–C angles of 111.42°, 109.77°, and 115.64° which are consistent with a tetrahedral geometry (angles 109.5°) around the amine nitrogen. The other structure contains what appears to be a planar imine as the angles around the nitrogen are 120.53°, 118.57°, and 119.62° which is consistent with planar geometry (angles 120°) making this more consistent with an imine group rather than an amine group. The N–C_{Ar} bond length is much shorter in the imine like system (1.383 Å) than in the amine structure (1.432 Å). Observation of the imine and amine structures in the unit cell suggests that the dimethylamino phenoxide is capable of redox chemistry similar to iminoquinones.

Although the geometry of the amino group hints at redox activity of the phenoxide, the bond lengths of the arene do not. Little difference is observed in the bond lengths of the two central arene rings in the crystal structures (Figure 2.5). For a *para*-iminoquinone both the N–Ar and O–Ar bonds are shorter than typical N and O-Ar bonds. As an alternate explanation the two structures could differ due to packing of the molecules in the crystal. Further investigation of the molecules of this type is needed to identify whether the aminophenoxide is capable of acting as a redox active ligand in these Ni-POP complexes.

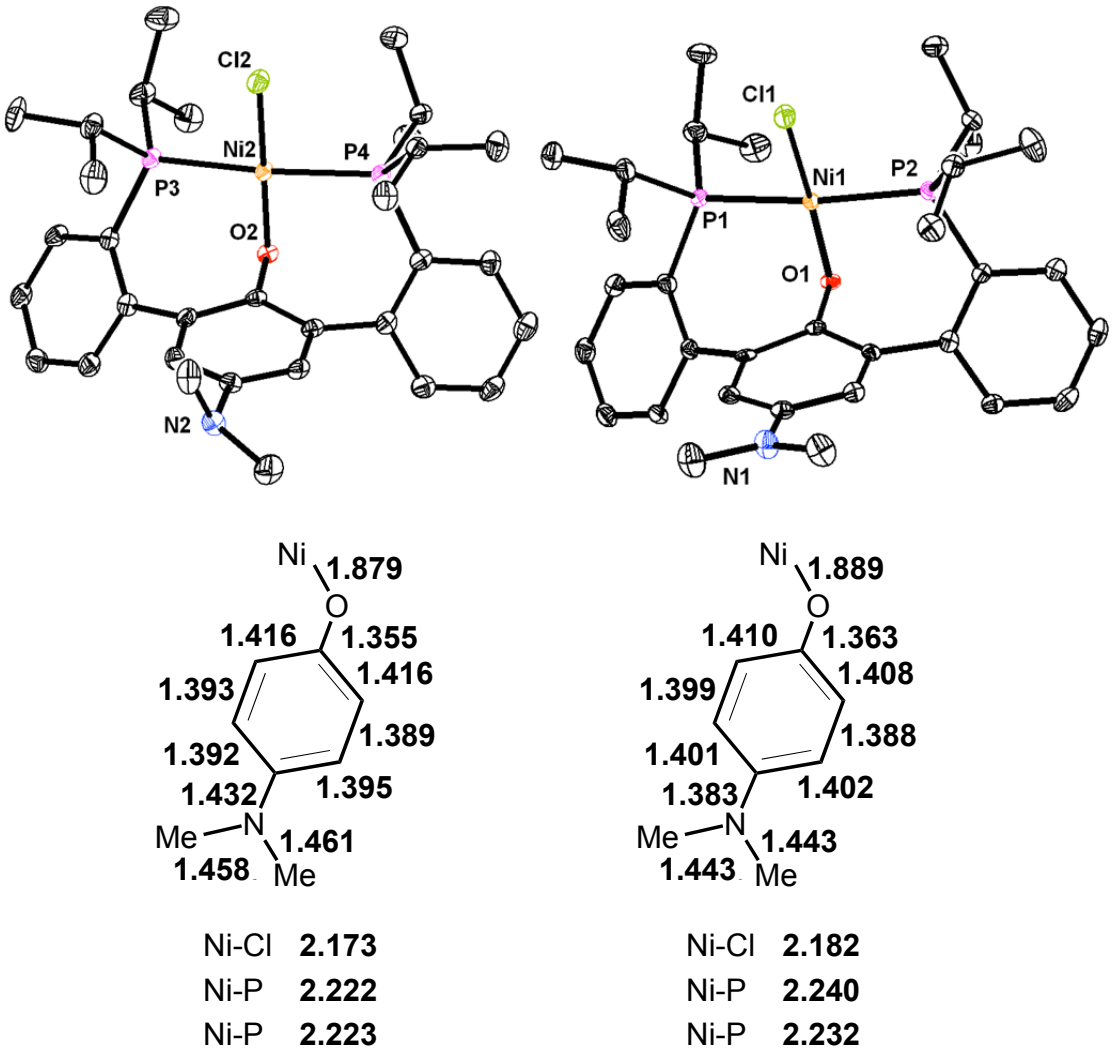

Figure 2.5 Solid-state structure of **8** (top). Solvent molecules, anions, and select hydrogen atoms not shown for clarity. Table of relevant bond lengths in **8** (bottom).

Metallation of the Methyl Ether Diphosphine: Nickel(I) Systems

The cleavage of C–X bonds are typically proposed to proceed through a nickel(0/II) mechanism, where a nickel(0) catalyst undergoes oxidative addition of a substrate to form a nickel(II) species which can transmetallate and undergo reductive elimination to reform the nickel(0) catalyst. Analogies can quickly be drawn between mechanism and observed intermediates in nickel(0/II) mechanisms as intermediates

are readily and conveniently observable by NMR spectroscopy. Although nickel(0/II) appears to be common, it has been proposed that the cleavage of some C-X bonds can proceed through a nickel(I/III) mechanism in addition or lieu of a nickel(0/II) mechanism (Scheme 2.21). This mechanism has been proposed for the cross coupling of aryl halides, alkyl halides and more recently in the activation of aryl oxygen bonds.

Scheme 2.21 A possible nickel(I/III) mechanism for cross coupling

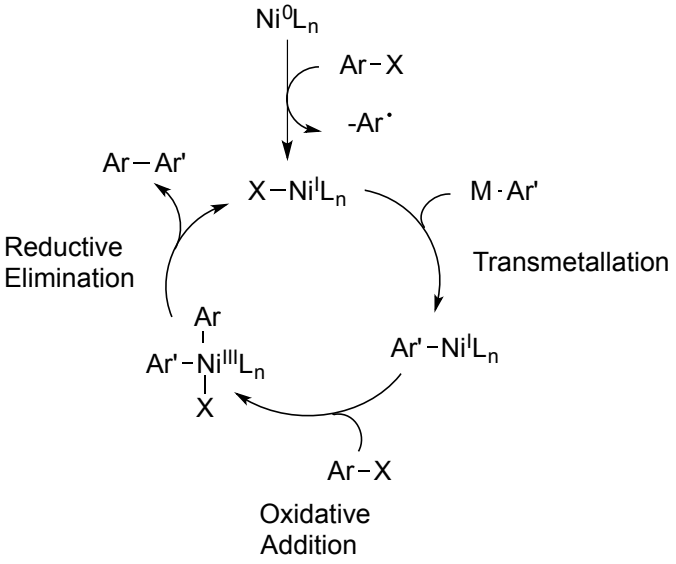

For aryl ethers, Martin et. al. developed a system for the reductive cleavage of C–O bonds based on nickel(0), tricyclohexylphosphine, and silane as the reducing agent.[2i] Using this system the reductive cleavage of aryl ethers was observed catalytically, however only when the phosphine was tricyclohexylphosphine. Through further experimental and computational investigations of the system, it was proposed that the catalytic cycle goes through a nickel(I) intermediate (Scheme 2.22). In the catalytic cycle a nickel(I) diphosphine silane is generated from $Ni(COD)_2$, PCy_3, and Et_3SiH through a comproportionation event. The nickel(I) diphosphine silane is the key catalytic species. The nickel(I) silane coordinates the substrate in an η^2-fashion and

undergoes a migratory insertion event and generate a benzyl nickel species. From this benzyl nickel species $MeOSiR_3$ is eliminated followed by a migration of the nickel center, resulting in the formation of the nickel(I) arene. This complex undergoes transmetallation with triethylsilane to generate the reduced arene and regenerating the nickel(I) silane catalyst. In order to gain insight into the possibility of a nickel(I) intermediate and investigate the cleavage of aryl-O bonds by nickel(I) a nickel(I) terphenyl diphosphine ether was synthesized.

Scheme 2.22 Proposed mechanism for aryl-O bond activation containing nickel(I) species

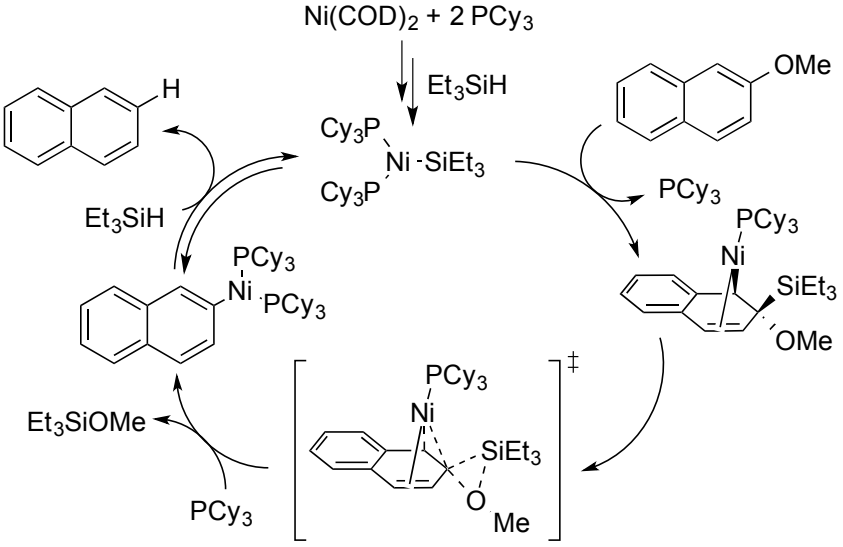

We have studied aryl–oxygen bond activation facilitated by nickel in a terphenyl diphosphine ether system. From our studies *vide supra* the activation of the aryl–oxygen bond proceeds through a nickel(0/II) mechanism in the model system. Given the evidence for nickel(I) species in activation of aryl–X bonds in catalytic systems, attempts were made to gain mechanistic insight in the role of nickel(I) in aryl–O bond activation using our model system.

Nickel(I) systems have been previously synthesized on similar terphenyl diphosphine scaffolds in our group through a comproportionation of nickel(II) and

nickel(0) precursors. Treatment of the dimethylamino terphenyl diphosphine methyl ether **1** with a 1:1 mixture of $NiCl_2DME$ and $NiCOD_2$ led to a mixture of nickel(II) phenoxide chloride **8**, and **2** (Scheme 2.23 A). This mixture of products emphasizes the reactivity of the ligand with nickel(II) halide precursors. The nickel(II) phenoxide forms at a rate faster than **2**. This is due either to the dissociation of COD from the nickel(0) precursor or the nickel(II) halide only needs to coordinate a single phosphine to undergo the cleavage of the sp^3 C-O bond. Fortunately, the nickel(0) complex **2** can be oxidized to form a nickel(I) complex, i.e. **2** can be oxidized by $NiCl_2DME$ to form a nickel(I) chloride complex **9** and nickel black (Scheme 2.23 B). Filtration from the nickel black led to the isolation of **9** as a bright yellow solid.

Scheme 2.23 Synthesis of 9 from $Ni(COD)_2$ and $NiCl_2(DME)$

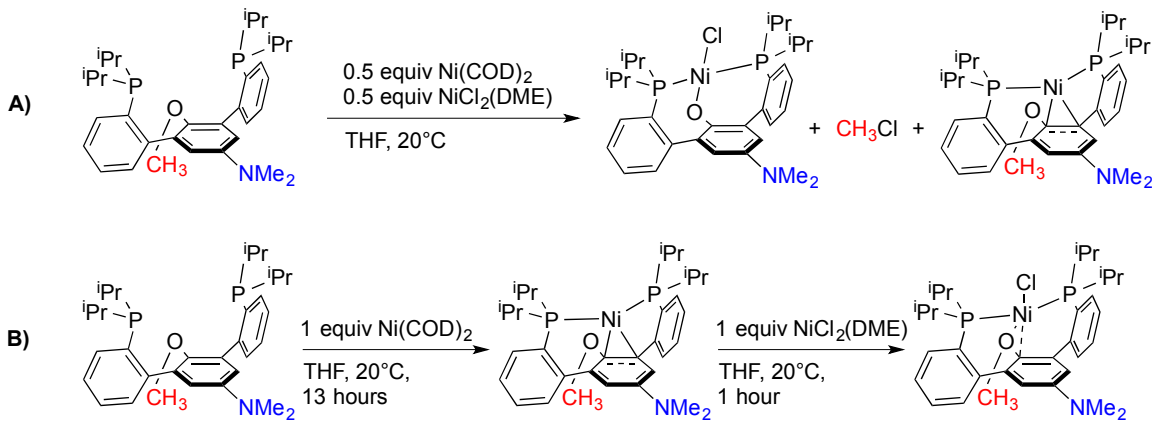

Complex **9** is paramagnetic and hence gives broad peaks ranging from -5 to 20 ppm in the ^1H NMR spectrum. No resonances are observed by ^{31}P NMR spectroscopy for compound **9**. Hydrolysis of the complex with HCl and subsequent analysis by ESI mass spectrometry gives the mass of the terphenyl diphosphine **1**. The mass of **1** provides evidence for a nickel(I) chloride coordinated to the two diphosphines with

the ether still intact (Scheme 2.23). Treatment of **9** with a halide abstraction agent such as AgOTf or TlOTf leads to the formation of a nickel(I) triflate complex $\mathbf{9}^{OTf}$. Compound $\mathbf{9}^{OTf}$ can be reduced with cobaltocene to regenerate the nickel(0) complex **2** providing further evidence for the identity of both complexes **9** and $\mathbf{9}^{OTf}$. Nickel(I) complexes can be synthesized with different anions through the use of other oxidizing agents, for example treatment of **2** with ferrocenium hexafluorophosphate leads to the formation of complex $\mathbf{9}^{PF6}$. With several nickel(I) complexes the reactivity of the nickel(I) center with the aryl-O bond was investigated.

Scheme 2.24 Synthesis of different variants of 9

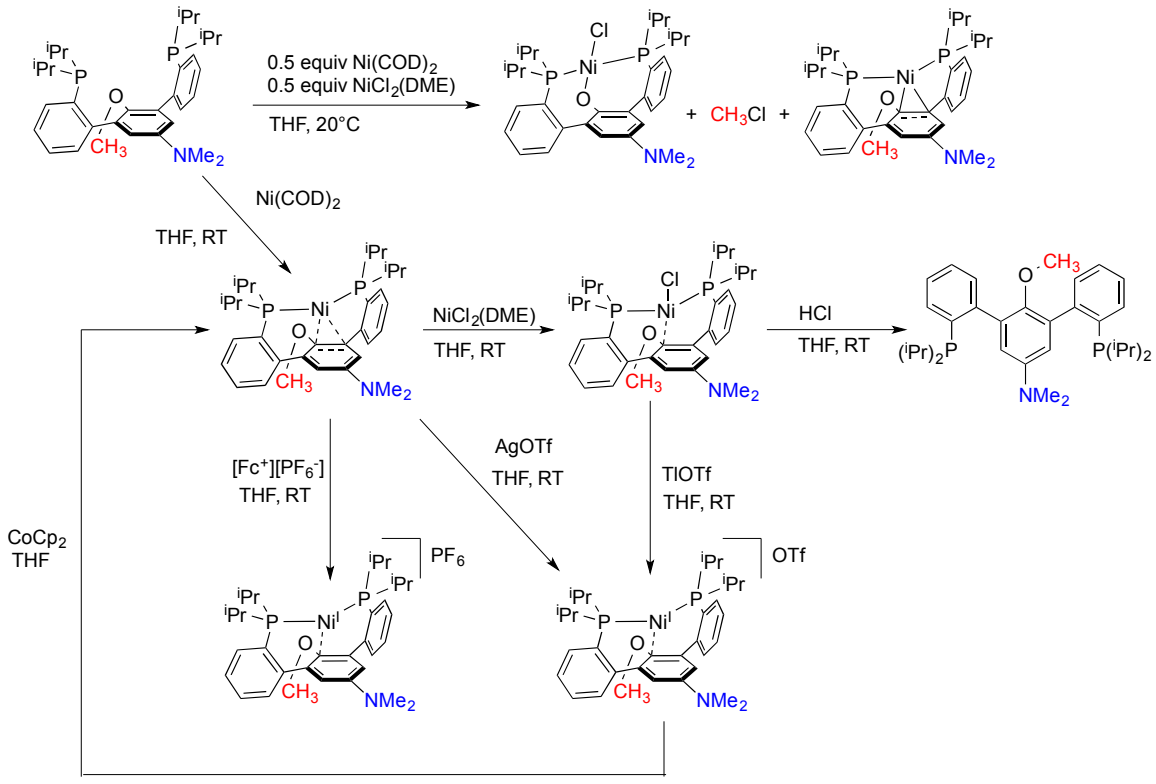

Complex **9** was found to be very robust. Heating **9** in benzene to 80 °C did not lead to any observed reactivity. Similarly heating complex **9** to 140 °C in xylenes does not result in aryl-O bond cleavage or any form of reactivity as only **9** was observed by

^{1}H NMR after heating and the diphosphine **1** was observed by ESI mass spectrometry after hydrolysis of the reaction mixture. It was hypothesized that the lack of reactivity in **9** was due to coordination of the chloride to the nickel center, to this end reactivity was investigated with nickel(I) complexes without coordinating anions $\mathbf{9}^{OTf}$ and $\mathbf{9}^{PF6}$. Heating $\mathbf{9}^{OTf}$ in xylenes (140 °C) or the $\mathbf{9}^{PF6}$ in MeCN (80 °C) did not lead to any observed reactivity.

In the mechanism proposed by Martin et. al. the silane of the nickel(I) species plays a critical part in the cleavage of the aryl oxygen bond (migratory insertion and silanol elimination). To investigate the possibility of aryl oxygen bond activation by migratory insertion and alcohol elimination the synthesis of other nickel(I) complexes was attempted. Initially the synthesis of nickel(I) aryl and alkyl complexes were targeted. Treatment of **9** with MeMgBr or MeMgCl in THF, toluene, or benzene leads to the clean generation of **2** within minutes. The addition of larger Grignards such as benzyl, phenyl, and mesityl also leads to the formation of **2** and the coupled aryls (as observed by GC-MS) within minutes. Complex **9** presumably quickly undergoes transmetallation to form a nickel(I) aryl complex. Two of these nickel(I) aryl species rapidly undergo either a radical recombination or a bimolecular reductive elimination to form the biaryl and **2**. Treatment of **9** with other reagents such as lithium or sodium triethylborohydride, triethyl silane (to form a nickel(I) hydride), and triethyl silyl potassium (to form a nickel(I) silyl species) all led to formation of **2**.

Scheme 2.25 Transmetallation reactivity of 9

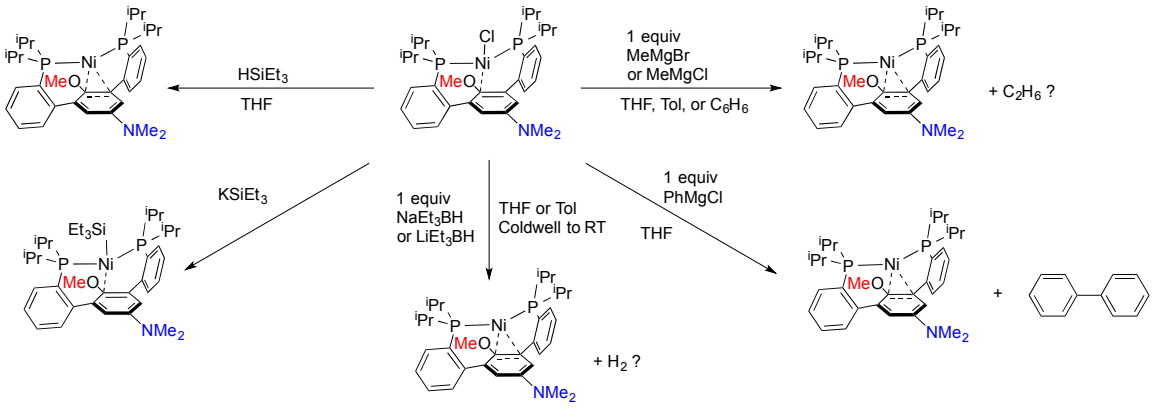

Isopropyl Ether

Intrigued by the observed mechanism for the terphenyl diphosphine methyl ether system, our investigation was expanded to observe if this mechanism is general to all aryl ethers. Nickel(0) model systems were targeted containing a variety of different ethers. To model the reductive cleavage of secondary alcohols, an isopropyl aryl ether was targeted. Synthesis of the diphosphine terphenyl isopropyl ether ligand proceeded according to scheme 2.6 and resulted in the diphosphine $\mathbf{1}^{\mathbf{iPr}}$. Treatment of $\mathbf{1}^{\mathbf{iPr}}$ with nickel(0) COD_2 at 20 °C in THF resulted in the formation of the nickel(0) diphosphine terphenyl isopropyl ether complex $\mathbf{2}^{\mathbf{iPr}}$ (Scheme 2.26). A shift is observed in the ^{31}P NMR spectrum where a single peak is observed at 39.20 ppm (vs. -2.41 and -4.54 of $\mathbf{1}^{\mathbf{iPr}}$) for $\mathbf{2}^{\mathbf{iPr}}$, this is comparable to the ^{31}P NMR shift of the methoxy variant **2** (40.7 ppm). By ^{1}H NMR spectroscopy a downfield shift in the central arene ring resonance of $\mathbf{2}^{\mathbf{iPr}}$ is observed, in comparison to the free ligand (5.78 ppm vs. 6.75 ppm) similar to what is observed in complex **2** (5.84 ppm). A doublet is observed at 0.68 ppm along with a septet at 3.90 ppm assigned to the isopropyl ether methyl groups and methine respectively. The resonances are relatively unchanged from what is observed

in the free terphenyl isopropyl ether where two doublets are observed at 0.70 and 0.73 ppm and a septet at 3.83 ppm.

Scheme 2.26 Synthesis of 2^{iPr}

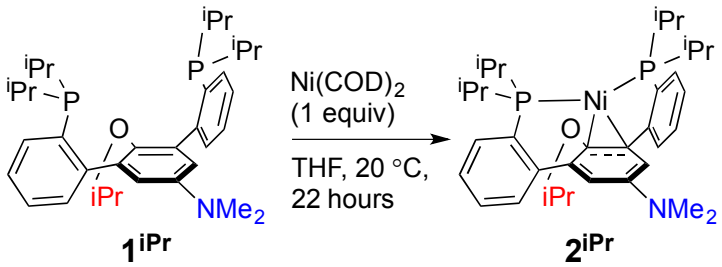

With $\mathbf{2}^{iPr}$ in hand, reactivity studies were undertaken. Unsurprisingly the nickel(0) complex $\mathbf{2}^{iPr}$ undergoes oxidative addition to form a proposed nickel(II) isopropoxide species $\mathbf{3}^{iPr}$ as identified by ^{31}P NMR spectroscopy. To date attempts to isolate complex $\mathbf{3}^{iPr}$ have resulted in failure. The proposed nickel(II) isopropoxide gives a ^{31}P NMR resonance at 23.65 ppm, which is in the range of the ^{31}P resonance of **2** (27.23 ppm). β-H elimination quickly occurs in $\mathbf{3}^{iPr}$ to form the previously characterized **4** and acetone as observed by ^{1}H and ^{31}P NMR. The reductive elimination in the presence of acetone is facile forming **7** (Scheme 2.27). All four species ($\mathbf{2}^{iPr}$, $\mathbf{3}^{iPr}$, **4**, and **7**) can be observed by ^{1}H and ^{31}P NMR after 22 hours in THF at 20 °C. In comparison, with **2** the final product **6** is not observed by ^{1}H and ^{31}P NMR under these conditions (20 °C for 22 hours) only **3** and a small amount of **4** could be observed in addition to starting material. Heating of $\mathbf{2}^{iPr}$ at 100 °C for one hour results in complete conversion to **7** and acetone. The reductive cleavage of a secondary aryl ether results in the formation of a ketone and an arene (Scheme 2.28). The observed mechanism mirrors that observed with the methyl terphenyl ether diphosphine oxidative addition, followed by β-H elimination and subsequent reductive elimination.

However, in the ether case the formed acetone shows that a ketone can act as a fifth ligand to promote reductive elimination to form the arene.

Scheme 2.27 Observed 2^{iPr} Model System Reactivity

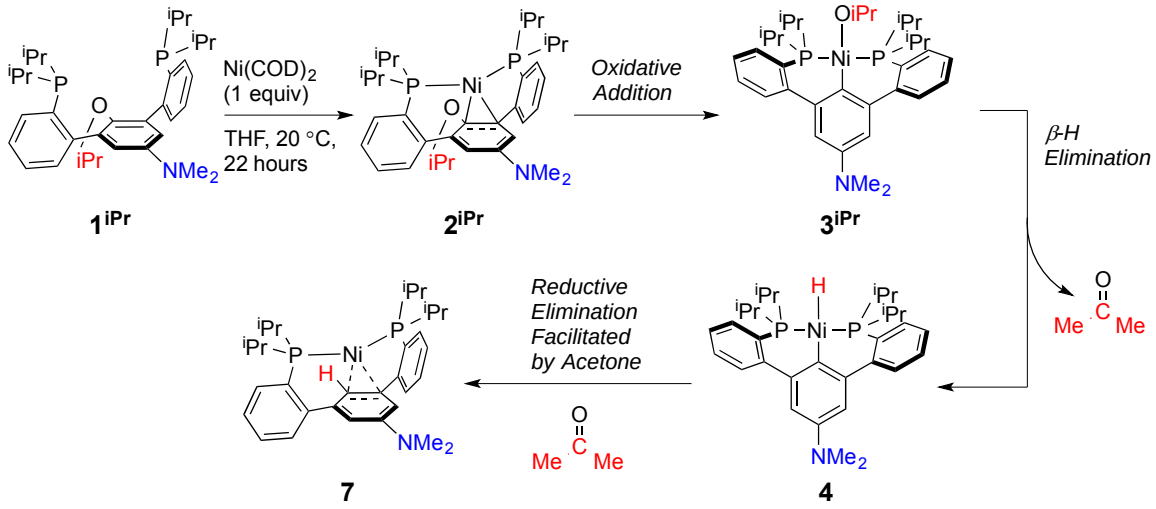

Scheme 2.28 Overall Isopropyl aryl ether Reductive Cleavage Products

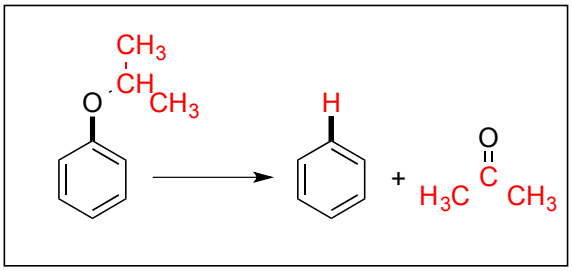

Ethyl Ether

As acetone showed no reactivity with the nickel(0) precursor in comparison to formaldehyde, which displayed decarbonylation under the same conditions, it was hypothesized that a more complex aldehyde could engender composite reactivity within the system. To explore this possibility a terphenyl diphosphine ethyl ether 1^{Et}

was targeted. Compound $\mathbf{1^{Et}}$ was synthesized via the fore mentioned synthesis route (Scheme 2.29). Mixing a solution of $\mathbf{1^{Et}}$ with Ni(0)COD_2 at 20 °C results in the formation of a new Ni(0) terphenyl diphosphine ether complex $\mathbf{2^{Et}}$. A resonance is observed by ^{31}P NMR at an unremarkable shift of 40.56 ppm, consistent with the other synthesized terphenyl diphosphine ether complexes. ^{1}H NMR shows a similar shift in the central arene resonances (5.85 ppm) indicative of a metal arene interaction as seen with other variants. The ethoxide moiety of $\mathbf{2^{Et}}$ shows resonances (a quartet and doublet) at 3.58 and 0.51 ppm corresponding to the methylene and methyl of the ethoxide respectively. These shifts are similar for the ethoxide peaks observed in $\mathbf{1^{Et}}$ (3.48 and 0.63 ppm for the methylene and methyl respectively) albeit without the isomer broadening.

Scheme 2.29 Synthesis of $\mathbf{2^{Et}}$

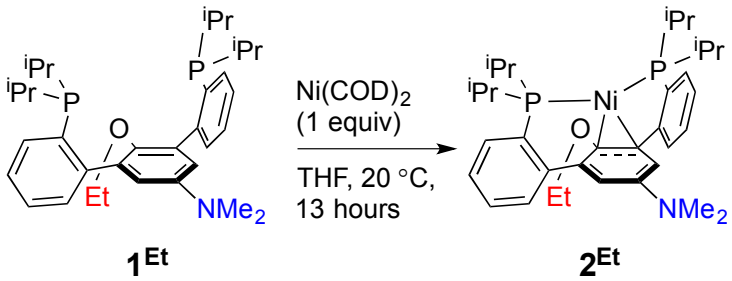

$\mathbf{1^{Et}}$ $\mathbf{2^{Et}}$

Upon heating the Ni^0 center of $\mathbf{2^{Et}}$ undergoes an oxidative addition of the aryl oxygen bond resulting in a new species $\mathbf{3^{Et}}$. ^{31}P NMR spectroscopy reveals a resonance at 27.33 ppm. This new species is believed to be the nickel(II) oxidative addition product similar to **3**. Further heating results in reductive elimination to form the nickel(II) hydride **4** as observed by NMR spectroscopy and acetaldehyde. Further heating results in the formation of a mixture of three complexes in varying ratios dependent on the heating temperature. The three species were identified as, the

previously identified Ni^0 carbonyl complex **6**, a Ni^0 species generated from reductive elimination of a proton **7**, and a Ni^0 complex resulting from the reductive elimination of a methyl group **10** (Scheme 2.30). The overall reaction is the reductive cleavage of an ethyl aryl ether and formation of benzene, toluene, carbon monoxide and hydrogen (Scheme 2.31).

Scheme 2.30 Observed 2^{Et} Model System Reactivity

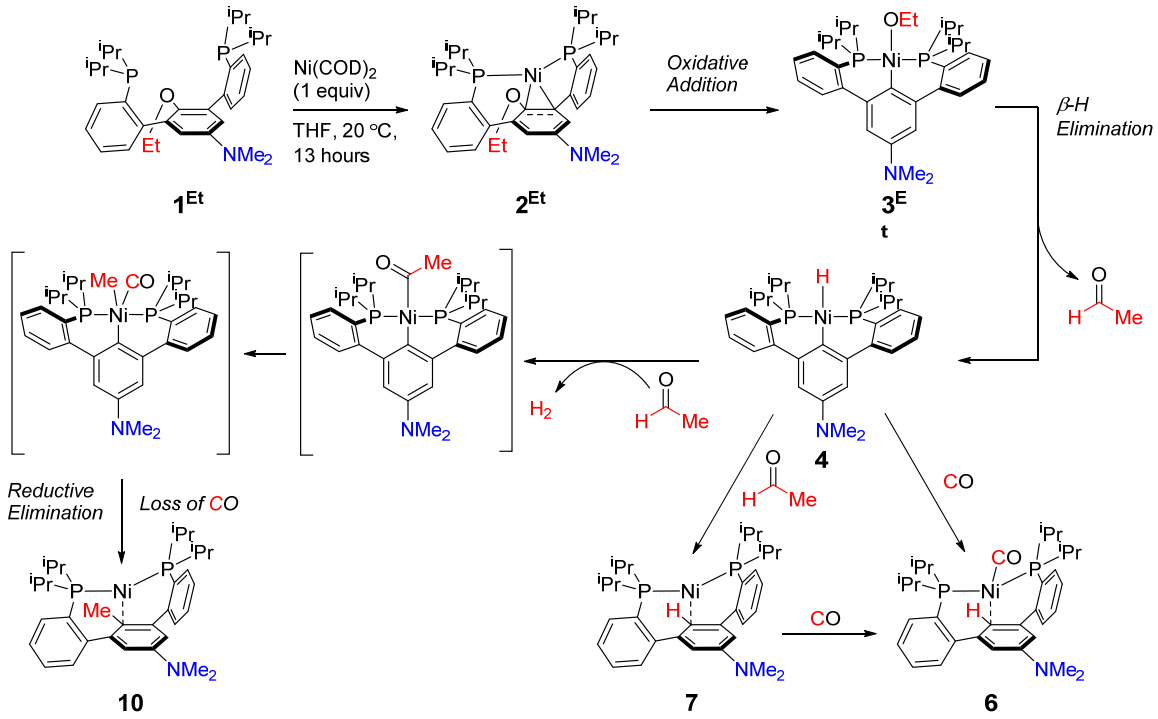

From the mixture of species formed it is probable that there are several competing processes active. For the formation of tolyl complex **10** from heating 2^{Et} it is postulated that the nickel(II) hydride **4** reacts with the formed acetaldehyde resulting in a transient nickel(II)-acyl complex and hydrogen. This species is proposed to quickly undergo decarbonylation and reductive elimination to form complex **10** (Scheme 2.24). The carbon monoxide generated could be used to form complex **6** as the nickel(II) hydride **4** is capable of reacting with carbon monoxide to form the

reductively eliminated product **7**. The formation of the proton species could also arise from **4** coordinating acetaldehyde as a fifth ligand, leading to reductive elimination.

Scheme 2.31 Overall Ethyl aryl ether Reductive Cleavage Products

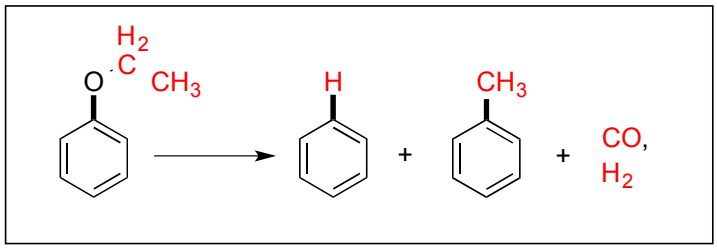

In order to probe the mechanism of $\mathbf{2}^{Et}$ further studies were carried out. If the proposed mechanism was possible, the isolable nickel hydride **4** should be able to react with acetaldehyde to form the observed ratio of products. When **4** is mixed with excess acetaldehyde little reactivity is seen at room temperature, however heating to reaction conditions identical to the aforementioned studies results in the formation of the methyl reductive elimination product coordinated to a carbonyl ligand **11** which was not observed in the heating of $\mathbf{2}^{Et}$ (Scheme 2.32). It is also possible that the acetaldehyde can undergo decarbonylation from a nickel(0) species forming carbon monoxide and methane similar to what is observed in reactions of **2** or **7** in the presence of formaldehyde at room temperature. However, acetaldehyde does not react with **2**, **7**, and $\mathbf{7}_H$ at room temperature and reacts over the course of days with heating at 90°C resulting in a small amount of nickel(0) carbonyl species, starting material, and small amounts of decomposition products as denoted by the observation of free ligand by ^{31}P NMR spectroscopy (Scheme 2.33). Due to the lessened reactivity of the acetaldehyde it is probable that the two described mechanisms result in the observed products, as the acetaldehyde can act as a fifth ligand for **4** resulting in the formation

of the reductive elimination species **7** and alternatively acetaldehyde can react with the hydride to undergo deacylation to form dihydrogen and a nickel(II) acyl complex, which can follow the ascribed pathway and form **10**.

Scheme 2.32 Reactivity of 4 with acetaldehyde

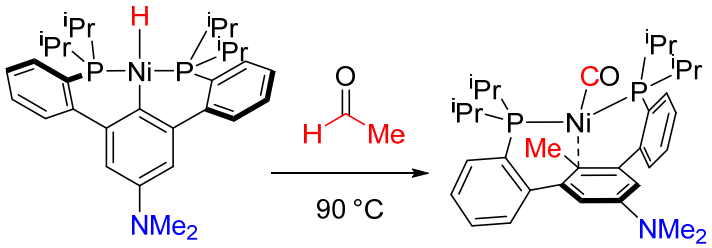

4 **11**

Scheme 2.33 Reactivity of nickel(0) model systems with acetaldehyde

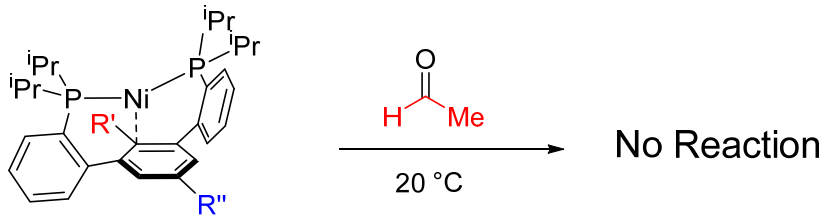

2 R'= OMe R''= NMe_2
7 R'= H R''= NMe_2
7_H R'= H R''= H

Benzyl Ether

In an attempt to further study the effect of variation of the ether a ligand containing a benzyl ether in the ipso position was synthesized. Treatment of the ligand with $Ni(COD)_2$ in THF for 25 hours results in the formation of a new species **12**. Analysis by ^{31}P NMR spectroscopy reveals a single resonance at 18.42 ppm which is inconsistent with the aforementioned nickel(0) systems, but similar to a previously reported nickel(II) chloride phenoxide complex (**8**) which gives a ^{31}P NMR resonance at 13.45 ppm. By ^{1}H NMR spectroscopy the protons on the central aryl ring of the

terphenyl core resonate at 7.15 ppm, which is closer to that of the free ligand indicating the absence of interactions between the central arene and the Ni center. Similarly the benzyl methylene protons are shifted from the doublets centered at 4.43 ppm observed in the free ligand to a triplet at 1.35 ppm, which is similar to resonances for nickel alkyl species. The observation of a triplet for the benzyl methylene protons indicates coupling from the phosphines, suggesting the methylene is interacting with the nickel metal center. This data lead to the assignment of **12** as a Ni(II) benzyl phenoxide complex (Scheme 2.34).

Scheme 2.34 Synthesis of 12 from 1^{Bn}

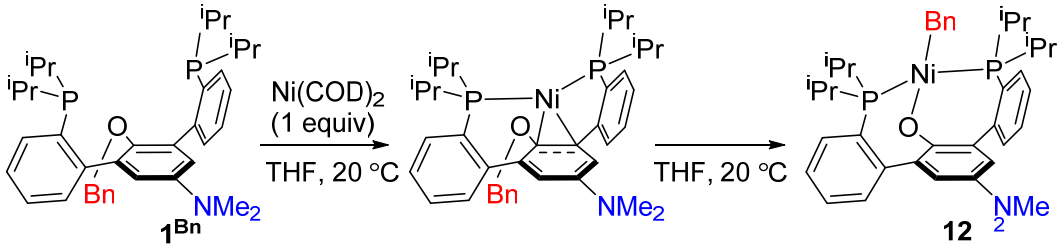

Gratifyingly, single crystals were grown from diethyl ether at room temperature, which upon preliminary analysis by single crystal x-ray diffraction resulted in the expected **12** structure. In order to further probe this system the reaction of the Benzyl ether ligand over time revealed the presence of another species by ^{31}P NMR spectroscopy with a phosphorous resonance at 40.60 ppm, which is consistent with the other nickel(0) systems. Due to the weak benzyl oxygen bond this nickel(0) species quickly undergoes oxidative addition to form the isolated nickel(II) species **12**. This result is unsurprising, as the benzyl oxygen bond is known to be weaker than the aryl oxygen bond.

Diaryl Ether

The need for a β-hydrogen is essential for the reductive cleavage of alkyl ethers in our nickel(0) model system. The absence of a β-hydrogen would lead to an inhibition of formation of a nickel(II) hydride and hence no reductive elimination. Investigation of this possibility lead to the synthesis of a terphenyl diphosphine containing an diaryl ether. A diaryl ether variant was synthesized via a coupling of a sufficiently nucleophilic 2,6-diiodophenol with a diaryliodonium triflate salt in the presence of base and following the route outlined in scheme 2.7. The developed synthesis can be used on the diaryl precursor to result in a ligand containing a diaryl ether $\mathbf{1^{OAr}}$. Treatment of the terphenyl ligand with $Ni(COD)_2$ at room temperature results in the formation of a new species **13** (Scheme 2.35).

Scheme 2.35 Synthesis of 13

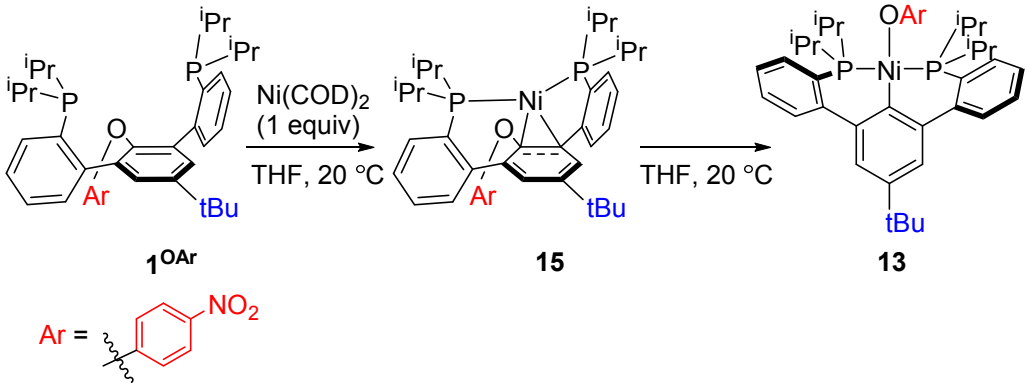

Analysis of **13** by ^{31}P NMR spectroscopy reveals a new peak at 29.73 ppm. Analysis by 1H NMR spectroscopy reveals a subtle shift in the proton resonance for the central terphenyl ring, from 7.51 ppm in the free ligand to 7.22 ppm for the nickel complex. The subtle shift in the central arene ring and shift of the phosphine resonances leads to the assignment of the nickel complex **13** as a nickel(II) complex where the nickel has undergone oxidative addition to the aryl oxygen bond of the

terphenyl ring resulting in a complex similar to the nickel(II) alkoxide complexes previously synthesized. Treatment of **13** with an equivalent of MeMgBr results in the formation of a nickel(II)-methyl species **14**, which is the same nickel(II) complex observed when **3** is treated with MeMgBr, providing further corroboration of the assignment. It was proposed that upon metallation with nickel(0) COD_2 a nickel(0) complex **15** is formed however this species quickly undergoes oxidative addition to form **13**. Indeed analysis of the reaction of $\mathbf{1}^{OAr}$ over time reveals a peak at 41.56 ppm by ^{31}P NMR consistent with a nickel(0) complex. **15** quickly undergoes oxidative addition to form **13** at 20 °C. The rate of oxidative addition is much faster due to the electronics on the phenoxide making it a better leaving group than alkoxides resulting in a weaker aryl ether bond (Scheme 2.36).

Scheme 2.36 Treatment of 13 with Methyl Grignard

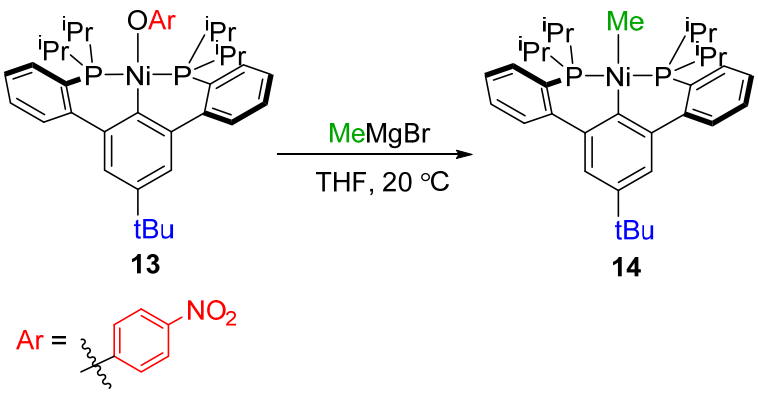

The nickel(II) complex **13** was investigated for further reactivity. Heating **13** to 100 °C does not result in any further reactivity. As predicted the lack of a β-hydrogen inhibits further reactivity in the aryl-aryl ether system. However its lack of reactivity makes it perfect for the study of sigma bond metathesis. The treatment of **13** with 4 atm of dihydrogen does not result in any reactivity, neither at 20 °C or when heated to 100 °C. Treating **13** with excess paraformaldehyde also does not result in any observed

reactivity at 20 °C, however upon heating at 100 °C for extended periods of time (72 hours) results in the formation of a small amount of **6**. **6** could be formed from **13** from a sigma bond metathesis with formaldehyde to form a phenol and a nickel(II) formyl that can deinsert carbon monoxide and undergo reductive elimination to make **6**. This study shows that in our model system although sigma bond metathesis or a sigma bond metathesis like mechanism may be possible it is not kinetically favorable in comparison to β-H elimination for the formation of the nickel(II) hydride.

CONCLUSIONS:

In summary, the mechanism of nickel-mediated reductive cleavage of aryl-ethers was investigated. Substrates with pendant phosphines allowed the isolation and characterization of intermediates along the reaction pathway. These intermediates were found to support a mechanism involving nickel(0) coordination to an arene, oxidative addition of the aryl carbon oxygen bond, followed by β-hydride elimination, and aldehyde or ketone-assisted reductive elimination of the aryl-H bond. Dihydrogen (4 atm) does not compete with the above processes. Overall the present studies provide mechanistic snapshots of a transformation of interest in organic methodology and with potential for biomass conversion.

EXPERIMENTAL SECTION:

General considerations:

Unless otherwise specified, all compounds were manipulated using a glove box under a nitrogen atmosphere. Solvents for all reactions were dried by Grubbs' method.[21] Benzene-d_6 was purchased from Cambridge Isotope Laboratories and vacuum distilled from sodium benzophenone ketyl. Chloroform-*d* was also purchased from Cambridge Isotope Laboratories and vacuum distilled from calcium hydride. Alumina and Celite were activated by heating under vacuum at 200 °C for 12 h. 2,6-diiodo-4-nitrophenol, 1,3-diiodo-2-methoxy-5-nitrobenzene, and its isotopolog with a deuterated methoxy ether were synthesized following literature procedures.[22] 2,6-diiodo-4-nitroaniline was purchased from Sigma-Aldrich. All other materials were used as received. ^{1}H, ^{13}C, and ^{31}P NMR spectra were recorded on a Varian Mercury 300 spectrometer at ambient temperature, unless denoted otherwise. Chemical shifts are reported with respect to internal solvent: 7.16 ppm and 128.06 (t) ppm (C_6D_6) and 7.26 ppm and 77.16 ppm ($CDCl_3$) for ^{1}H and ^{13}C NMR data, respectively. ^{31}P NMR chemical shifts are reported with respect to the instrument solvent lock when a deuterated solvent was used. IR spectra were recorded on a Thermo-Fisher Scientific Nicolet 6700 FT-IR spectrometer. Gas chromatography-mass spectrometry (GC-MS) analysis was performed upon filtering the sample through a plug of silica gel. Fast atom bombardment-mass spectrometry (FAB-MS) analysis was performed with a JEOL JMS-600H high-resolution mass spectrometer. Elemental analysis was conducted by Midwest Microlab, LLC (Indianapolis, IN). In the following complexes, the carbons of the terphenyl backbone are assigned using the following scheme:

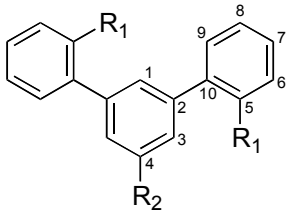

2,6-diiodo-4-nitrophenol

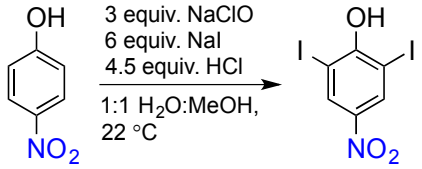

2,6-diiodo-4-nitrophenol was synthesized according to a modified literature procedure.[22b] A solution of 2,6-diiodo-4-nitrophenol (50.01 g, 359.5 mmol) in MeOH (1 L) was mixed with an aqueous solution (1 L in H_2O) of $NaClO_2$ (123.64 g, 1.09 mol) and NaI (321.04 g, 2.15 mol) in a 3 L round bottom flask. To this dark purple solution 4.5 equivalents of 12M HCl (120 ml) was added slowly using an addition funnel to prevent the temperature from rising over 35C. Upon HCl addition the solution quickly became a slurry. The solution was stirred overnight at 20 °C. After the allocated time the slurry was filtered over Celite using a glass frit. The brown solid was eluted with ethyl acetate and washed three times with a saturated solution of sodium metabisulfite. The solvent was removed from the bright yellow organic fraction under vacuum yielding a yellow crystalline powder. Yield: 121.32 g, 86.3% ^{1}H NMR (*d*$_6$-Acetone, 300 MHz) δ 8.61 (s, 2H, central Ar-*H*)

1,3-diiodo-2-alkoxy-5-nitrobenzene

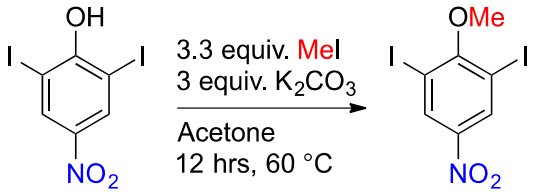

The 1,3-diiodo-2-alkoxy-5-nitrobenzene compounds were synthesized using a modified literature procedure for the synthesis of 1,3-diiodo-2-methoxy-5-nitrobenzene.[22a] In a 500 ml round bottom flask potassium carbonate (21.69 g, 156.9 mmol) was mixed with 20.13 g (51.5 mmol) 2,6-diiodo-4-nitrophenol in acetone (150 ml). To this slurry 10.5 ml (168.7 mmol) methyl iodide was added to the slurry via syringe. The round bottom was equipped with a reflux condenser and sealed with a septum and heated to 55°C for 12 hours. After 12 hours the solvent was removed from the orange slurry via rotovap. The solid residue was taken up in water and the organics were extracted three times with ethyl acetate (50 ml). The yellow organic fractions were combined and dried with magnesium sulfate. The ethyl acetate was removed by rotovap yielding an orange yellow solid, which smells vaguely of garlic.

1,3-diiodo-2-methoxy-5-nitrobenzene Yield: 19.08 g, 91.5% ^{1}H NMR ($CDCl_3$, 300 MHz) δ 8.64 (s, 2H), 3.94 (s, 3H)

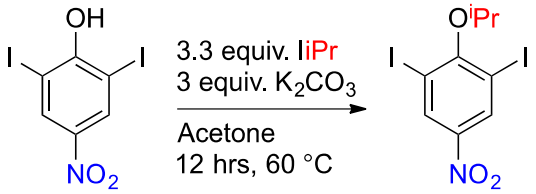

1,3-diiodo-2-isopropoxy-5-nitrobenzene Yield: 4.13 g, 52.3% ^{1}H NMR ($CDCl_3$, 300 MHz) δ 8.66 (s, 2H), 4.96 (septet, 1H), 1.46 (d, 6H)

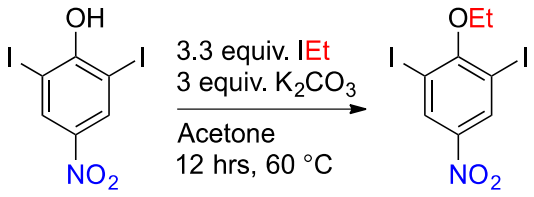

1,3-diiodo-2-ethoxy-5-nitrobenzene Yield: 6.23 g, 62.7% ^{1}H NMR ($CDCl_3$, 300 MHz) δ 8.66 (s, 2H), 4.04 (quartet, 2H), 1.20 (t, 3H)

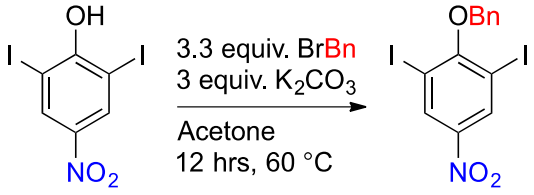

1,3-diiodo-2-benzyl-5-nitrobenzene Yield: 19.08 g, 91.5% ^{1}H NMR ($CDCl_3$, 300 MHz) δ 8.16 (s, 2H), 7.53 (d, 2H), 7.24 (t, 2H), 7.19 (t, 1H), 4.67 (s, 2H)

1,3-diiodo-2-phenoxy-5-nitrobenzene

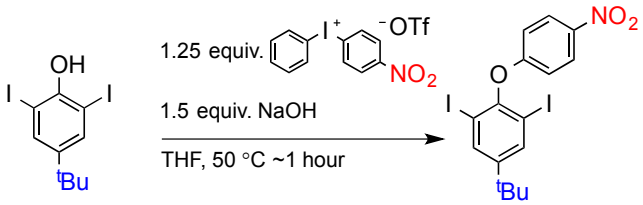

1,3-diiodo-2-(4-nitrophenoxy)-5-tertbutylbenzene was synthesized using a modified literature procedure for the arylation of malonates of diaryl iodonium salts.[9d] In a round bottom flask 0.75 g NaOH (18.6 mmol) and 5.00 g 2,6-diiodo-4-tertbutylphenol (12.4 mmol) were stirred in 20 ml THF. To this slurry was added 7.38 g (15.5 mmol) of the diaryl iodonium triflate salt. This dark brown mixture was heated to 50 °C for one hour. After the allotted time the solvent was removed *in vacuo* and the residue was dissolved in a 90:10 Hexanes:Et_2O mixture. A yellow solid precipitated from solution. The solid was collected via filtration yielding 1,3-diiodo-2-(4-nitrophenoxy)-5-

tertbutylbenzene. Yield: 4.30 g, 66.3% ^{1}H NMR ($CDCl_3$, 300 MHz) δ 8.22 (d, 2H), 7.84 (s, 2H), 6.89 (d, 2H), 1.33 (s, 9H)

1,3-bis(2´-bromophenyl)-2-methoxy-4-nitrobenzene

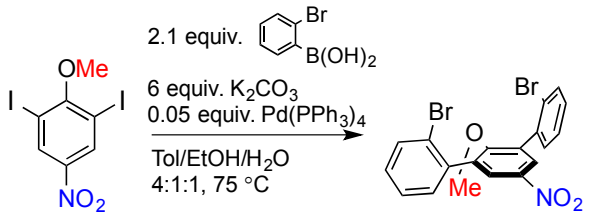

The 1,3-bis(2´-bromophenyl)-2-alkoxy-4-nitrobenzene compounds were synthesized according to the procedure for 1,3-bis(2'-bromophenyl)-2-methoxy-4-nitrobenzene. Suzuki coupling conditions were adapted from a previously published procedure.[6] 1,3-diiodo-2-methoxy-5-nitrobenzene (2.48 g, 6.58 mmol, 1 equiv), 2-bromo-phenylboronic acid (2.77 g, 13.80 mmol, 2.1 equiv), K_2CO_3 (5.46 g, 39.47 mmol, 6 equiv), 140 mL toluene, 40 mL ethanol, and 40 mL water were added to a 500 mL Schlenk tube fitted with a screw-in Teflon stopper. The mixture was degassed by three freeze-pump-thaw cycles, after which $Pd(PPh_3)_4$ (380 mg, 0.38 mmol, 0.05 equiv) was added as a solid with a counterflow of nitrogen. The reaction vessel was then placed in an oil bath pre-heated to 75°C. After stirring for 6 h, the reaction mixture was allowed to cool to room temperature, concentrated via rotary evaporation and diluted with 200 mL H_2O. The solution was extracted with three portions of CH_2Cl_2. The combined organic fractions were dried over $MgSO_4$, filtered and concentrated via rotary evaporation. The crude 1,3-bis(2'-bromophenyl)-2-methoxy-4-nitrobenzene

was reduced without purification. 1,3-bis(2'-bromophenyl)-2-methoxy-4-nitrobenzene ^{1}H NMR ($CDCl_3$, 300 MHz) δ 8.17 (s, 2H, central Ar-*H*), 7.71 (d, 2H, Ar-*H*), 7.40 (m, 4H, Ar-*H*), 7.30 (d, 2H, Ar-*H*), 3.27 (s, 3H, OC*H*$_3$)

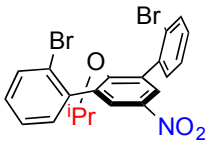

1,3-bis(2'-bromophenyl)-2-isopropoxy-4-nitrobenzene ^{1}H NMR ($CDCl_3$, 300 MHz) δ 8.21 (s, 2H, central Ar-*H*), 7.72 (d, 2H, Ar-*H*), 7.42 (m, 4H, Ar-*H*), 7.29 (d, 2H, Ar-*H*), 3.64 (septet, 1H, OC*H*(CH_3)$_2$), 0.68 (d, 6H, OCH(C*H*$_3$)$_2$)

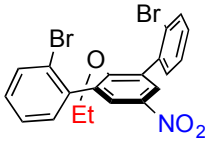

1,3-bis(2'-bromophenyl)-2-ethoxy-4-nitrobenzene ^{1}H NMR ($CDCl_3$, 300 MHz) δ 8.18 (s, 2H, central Ar-*H*), 7.71 (d, 2H, Ar-*H*), 7.39 (m, 4H, Ar-*H*), 7.30 (d, 2H, Ar-*H*), 3.43 (m, 2H, OC*H*$_2$$CH_3$), 0.75 (t, 2H, OCH_2C*H*$_3$)

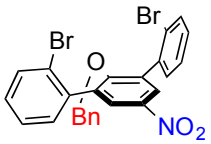

1,3-bis(2'-bromophenyl)-2-benzyl-4-nitrobenzene ^{1}H NMR ($CDCl_3$, 300 MHz) δ 8.11 (s, 2H, central Ar-*H*), 7.38 (m, 2H, Ar-*H*), 6.80 (m, 9H, Ar-*H*), 6.57 (d, 2H, Ar-*H*), 4.30 (dd, 2H, OC*H*$_2$Ph)

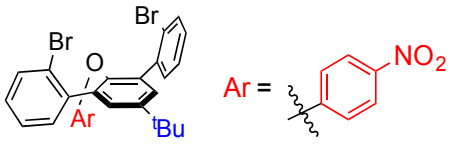

1,3-bis(2'-bromophenyl)-2-phenoxy-4-nitrobenzene ^{1}H NMR ($CDCl_3$, 300 MHz) δ 7.86 (d, 2H, Ar-*H*), 7.54 (d, 2H, Ar-*H*), 7.44 (d, 2H, Ar-*H*), 7.31 (s, 2H, Ar-*H*), 7.19 (m, 2H, Ar-*H*), 7.09 (m, 2H, Ar-*H*), 6.61 (d, 2H, Ar-*H*), 1.41 (s, 9H, $C(CH_3)_3$)

4-amino-1,3-bis(2'-bromophenyl)-2-methoxybenzene

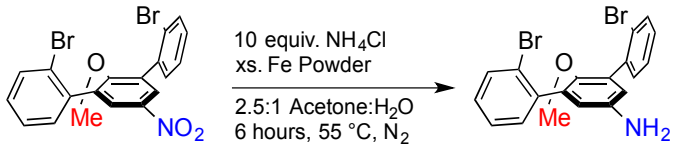

4-amino-1,3-bis(2'-bromophenyl)-2-methoxybenzene was synthesized using a literature procedure[7]. The crude 4-amino-1,3-bis(2'-bromophenyl)-2-methoxybenzene was methylated without purification. ^{1}H NMR ($CDCl_3$, 300 MHz) δ 7.65 (d, 2H, Ar-*H*), 7.36 (m, 4H, Ar-*H*), 7.20 (t, 2H, Ar-*H*), 6.59 (s, 2H, central Ar-*H*), 3.63 (s, 2H, NH_2), 3.27 (s, 3H, OCH_3)

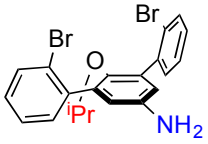

4-amino-1,3-bis(2'-bromophenyl)-2-isopropoxybenzene ^{1}H NMR ($CDCl_3$, 300 MHz) δ 7.66 (d, 2H, Ar-*H*), 7.41 (d, 2H, Ar-*H*), 7.32 (t, 2H, Ar-*H*), 7.18 (t, 2H, Ar-*H*), 6.67 (s, 2H, central Ar-*H*), 3.94 (s, 2H, NH_2), 3.38 (septet, 1H, $OCH(CH_3)_2$), 0.55 (d, 6H, $OCH(CH_3)_2$)

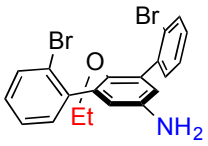

4-amino-1,3-bis(2'-bromophenyl)-2-ethoxybenzene ^{1}H NMR ($CDCl_3$, 300 MHz) δ 7.66 (d, 2H, Ar-*H*), 7.38 (m, 4H, Ar-*H*), 7.18 (t, 2H, Ar-*H*), 6.60 (s, 2H, central Ar-*H*), 3.63 (s, 2H, N*H*$_2$), 3.27 (s, 2H, OC*H*$_2$CH$_3$), 0.60 (s, 3H, OC*H*$_2$CH$_3$)

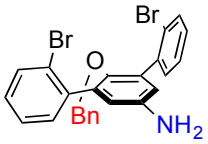

4-amino-1,3-bis(2'-bromophenyl)-2-benzylbenzene ^{1}H NMR ($CDCl_3$, 300 MHz) δ 7.78 (d, 2H, Ar-*H*), 7.52 (m, 4H, Ar-*H*), 7.31 (t, 2H, Ar-*H*), 6.90 (m, 3H, Ar-*H*), 6.73 (t, 1H, Ar-*H*), 6.31 (s, 2H, central Ar-*H*), 4.46 (dd, 2H, OC*H*$_2$Ph), 3.64 (br s, 2H, N*H*$_2$)

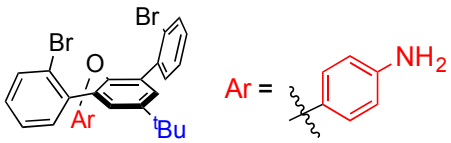

4-amino-1,3-bis(2'-bromophenyl)-2-phenoxybenzene ^{1}H NMR ($CDCl_3$, 300 MHz) δ 7.54 (d, 2H, Ar-*H*), 7.36 (s, 2H, central Ar-*H*), 7.31 (d, 2H, Ar-*H*), 7.18 (t, 2H, Ar-*H*), 7.07 (t, 2H, Ar-*H*), 6.28 (m, 4H, Ar-*H*), 3.26 (br s, 2H, N*H*$_2$), 1.38 (s, 9H, C(C*H*$_3$)$_3$)

1,3-bis(2'-bromophenyl)-4-dimethylamino-2-methoxybenzene

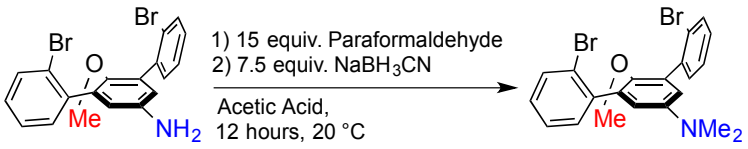

1,3-bis(2'-bromophenyl)-4-dimethylamino-2-methoxybenzene was synthesized using a literature procedure[8]. The product was purified by Flash chromatography (dichloromethane) and isolated as a colorless solid. 1,3-bis(2'-bromophenyl)-4-

dimethylamino-2-methoxybenzene Yield: 41.9% ^{1}H NMR (C_6D_6, 399.80 MHz) δ 7.57 (d, 2H, Ar-*H*$_6$), 7.41 (d, 2H, Ar-*H*$_9$), 7.01 (t, 2H, Ar-*H*$_7$), 6.81 (t, 2H, Ar-*H*$_8$), 6.68 (s, 2H, Ar-*H*$_3$), 3.12 (s, 3H, OC*H*$_3$), 2.48 (s, 6H, N(C*H*$_3$)$_2$), ^{13}C NMR (C_6D_6, 100.54 MHz) δ 146.72 (s, Ar-*C*$_1$), 146.66 (s, Ar-*C*$_4$), 141.21 (s, Ar-*C*$_{10}$), 135.74 (s, Ar-*C*$_2$), 132.98 (s, Ar-*C*$_9$), 132.31 (s, Ar-*C*$_6$), 128.97 (s, Ar-*C*$_7$), 127.09 (s, Ar-*C*$_8$), 124.54 (s, Ar-*C*$_5$), 115.73 (s, Ar-*C*$_3$), 60.77 (s, O-*C*H$_3$), 40.69 (N(*C*H$_3$)$_2$), MS (m/z): calcd, 460.9813 (M+); found, 460.9822 (FAB+, M+).

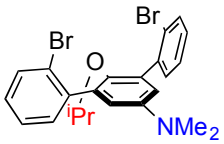

1,3-bis(2'-bromophenyl)-4-dimethylamino-2-isopropoxybenzene Yield: 37.4% ^{1}H NMR ($CDCl_3$, 300 MHz) δ 7.66 (d, 2H, Ar-*H*$_6$), 7.45 (d, 2H, Ar-*H*$_9$), 7.34 (t, 2H, Ar-*H*$_7$), 7.19 (t, 2H, Ar-*H*$_8$), 6.69 (s, 2H, Ar-*H*$_3$), 3.39 (septet, 1H, OC*H*(CH$_3$)$_2$), 2.96 (s, 6H, N(C*H*$_3$)$_2$), 0.59 (d, 6H, OCH(C*H*$_3$)$_2$)

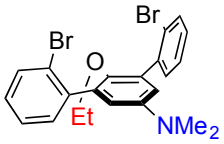

1,3-bis(2'-bromophenyl)-4-dimethylamino-2-ethoxybenzene Yield: 41.9% ^{1}H NMR ($CDCl_3$, 300 MHz) δ 7.67 (d, 2H, Ar-*H*$_6$), 7.45 (d, 2H, Ar-*H*$_9$), 7.34 (t, 2H, Ar-*H*$_7$), 7.20 (t, 2H, Ar-*H*$_8$), 6.64 (s, 2H, Ar-*H*$_3$), 3.27 (br q, 3H, OC*H*$_2$CH$_3$), 2.95 (s, 6H, N(C*H*$_3$)$_2$), 0.62 (t, 3H, OC*H*$_2$CH$_3$)

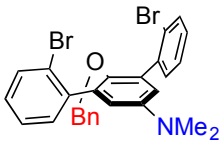

1,3-bis(2'-bromophenyl)-4-dimethylamino-2-benzylbenzene Yield: 41.9% ^{1}H NMR (C_6D_6, 300 MHz) δ 7.55 (d, 2H, Ar-*H*$_6$), 7.44 (d, 2H, Ar-*H*$_9$), 6.92 (t, 2H, Ar-*H*$_7$), 6.77 (t, 2H, Ar-*H*$_8$), 6.72 (s, 2H, Ar-*H*$_3$), 4.50 (br m, 2H, OC*H*$_2$Ph), 2.48 (s, 6H, N(C*H*$_3$)$_2$)

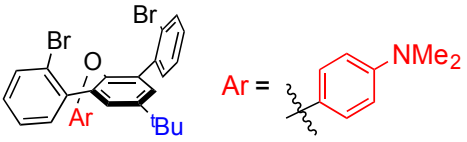

1,3-bis(2'-bromophenyl)-4-dimethylamino-2-phenoxybenzene Yield: 41.9% ^{1}H NMR (C_6D_6, 300 MHz) δ 7.55 (s, 2H, Ar-*H*), 7.38 (d, 4H, Ar-*H*), 6.79 (d, 2H, Ar-*H*), 6.57 (dd, 2H, Ar-*H*), 6.20 (d, 2H, Ar-*H*), 2.25 (s, 6H, N(C*H*$_3$)$_2$), 1.24 (s, 9H, C(C*H*$_3$)$_3$)

1,3-bis(2'-diisopropylphosphino)-4-dimethylamino-2-methoxybenzene (1)

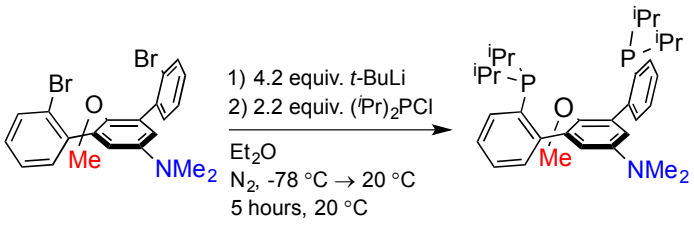

In a glovebox a 100 mL Schlenk tube was charged with a colorless solution of 1,3-bis(2'-diisopropylphosphino)-4-dimethylamino-2-methoxybenzene (50.1 mg, 0.11 mmol) in Et_2O (30 mL) and a stir bar. The Schlenk tube was removed from the glove box and cooled to -78°C in a dry ice/acetone bath. Under N2, ^{t}BuLi in pentane (1.5 M, 303.5 µL, 0.46 mmol) was added via syringe slowly to the cold solution. The resulting dark yellow mixture was stirred for one hour at -78°C. After an hour chlorodiisopropylphosphine (36.5 µl, 0.23 mmol) was added to the cold solution

slowly via syringe. After addition the reaction mixture was allowed to warm to and stir at room temperature for 8 hours. The volatile materials were then removed under vacuum and the pale yellow/white residue was mixed in hexanes and filtered through Celite. The volatiles were removed from the filtrate *in vacuo*, and the resulting pale yellow/colorless oil was mixed in pentane and stirred with alumina. The mixture was filtered through a bed of alumina and the alumina was rinsed with toluene. Removal of volatile materials under vacuum yielded 1,3-bis(2'-diisopropylphosphino)-4-dimethylamino-2-methoxybenzene (**1**) as a white solid (0.68 g, 1.20 mmol) in 92.9% yield. ^{1}H NMR (C_6D_6, 300 MHz, 75°C) δ 7.65 (m, 2H, Ar-*H*$_6$), 7.48 (m, 2H, Ar-*H*$_9$), 7.19 (m, 4H, Ar-*H*$_{7\text{-}8}$), 6.73 (s, 2H, Ar-*H*$_3$), 3.14 (s, 3H, OC*H*$_3$), 2.65 (s, 6H, N(C*H*$_3$)$_2$), 2.06 (m, 2H, C*H*(CH$_3$)$_2$) , 1.92 (m, 2H, C*H*(CH$_3$)$_2$) , 1.08 (m, 24H, CH(C*H*$_3$)$_2$) ^{13}C{^{1}H} NMR (C_6D_6, 100.54 MHz) δ 148.52 (m, Ar-*C*$_{10}$), 147.49 (s, Ar-*C*$_1$), 145.61 (s, Ar-*C*$_4$), 136.85 (d, Ar-*C*$_5$), 136.44 (d, Ar-*C*$_2$), 132.43 (s, Ar-*C*$_9$), 131.68 (d, Ar-*C*$_6$), 128.19 (s, Ar-*C*$_8$), 126.68 (s, Ar-*C*$_7$), 117.41 (s, Ar-*C*$_3$), 60.18 (s, O-*C*H$_3$), 41.21 (N(*C*H$_3$)$_2$), 26.79 (*C*H-(CH$_3$)$_2$), 24.96 (*C*H-(CH$_3$)$_2$), 20.83 (CH-(*C*H$_3$)$_2$), ^{31}P{^{1}H} NMR (C_6D_6, 121.48 MHz) δ -2.72 (s), -4.09 (s) MS (m/z): calcd, 535.3133 (M+); found, 535.3134 (FAB+, M+). 1,3-

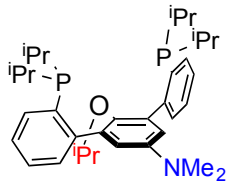

bis(2'-diisopropylphosphino)-4-dimethylamino-2-isopropoxybenzene (1^{iPr})

(0.91 g, 1.61 mmol) in 83.1% yield. ^{1}H NMR (C_6D_6, 499.85 MHz, 70°C) δ 7.66 (br s, 2H, Ar-*H*$_6$), 7.49 (d, 2H, Ar-*H*$_9$), 7.20 (t, 2H, Ar-*H*$_{7\text{-}8}$), 7.15 (t, 2H, Ar-*H*$_3$), 6.70 (s, 2H, Ar-*H*$_3$), 3.76 (septet, 1H, OC*H*(CH$_3$)$_2$), 2.67 (s, 6H, N(C*H*$_3$)$_2$), 2.13 (m, 2H, C*H*(CH$_3$)$_2$)

, 1.91 (m, 2H, C*H*(CH$_3$)$_2$) , 1.08 (m, 24H, CH(C*H*$_3$)$_2$), 0.59 (d, 6H, OCH(C*H*$_3$)$_2$), ^{13}C{^{1}H} NMR (C$_6$D$_6$, 125.70 MHz) δ 149.04 (d, Ar-*C*$_{10}$), 145.41 (s, Ar-*C*$_1$), 145.20 (s, Ar-*C*$_4$), 137.24 (d, Ar-*C*$_5$), 137.03 (d, Ar-*C*$_2$), 132.18 (s, Ar-*C*$_{6\text{-}9}$), 132.06 (d, Ar-*C*$_{6\text{-}9}$), 128.12 (s, Ar-*C*$_{7\text{-}8}$), 126.55 (s, Ar-*C*$_{7\text{-}8}$), 117.48 (d, Ar-*C*$_3$), 74.61 (s, O*C*H-(CH$_3$)$_2$), 41.32 (N(*C*H$_3$)$_2$), 27.08 (*C*H-(CH$_3$)$_2$), 24.53 (*C*H-(CH$_3$)$_2$), 22.86 (OCH-(*C*H$_3$)$_2$), 22.27 (OCH-(*C*H$_3$)$_2$), 21.32 (CH-(*C*H$_3$)$_2$), 20.86 (CH-(*C*H$_3$)$_2$), 20.64 (CH-(*C*H$_3$)$_2$), 20.53 (CH-(*C*H$_3$)$_2$), ^{31}P{^{1}H} NMR (C$_6$D$_6$, 121.48 MHz) δ -2.41 (s), -4.53 (s)

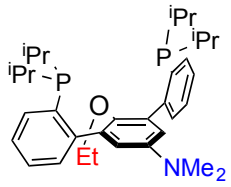

1,3-bis(2'-diisopropylphosphino)-4-dimethylamino-2-ethoxybenzene (1^{Et})

(0.97 g, 1.76 mmol) in 93.9% yield. ^{1}H NMR (C$_6$D$_6$, 499.85 MHz, 75°C) δ 7.54 (m, 2H, Ar-*H*$_6$), 7.48 (m, 2H, Ar-*H*$_9$), 7.15 (m, 4H, Ar-*H*$_{7\text{-}8}$), 6.68 (s, 2H, Ar-*H*$_3$), 3.39 (s, 3H, OC*H*$_2$CH$_3$), 2.67 (s, 6H, N(C*H*$_3$)$_2$), 1.99 (m, 4H, C*H*(CH$_3$)$_2$), 1.12 (m, 12H, CH(C*H*$_3$)$_2$), 1.01 (m, 12H, CH(C*H*$_3$)$_2$), 0.57 (m, 3H, OCH$_0$C*H*$_3$), ^{13}C{^{1}H} NMR (C$_6$D$_6$, 125.70 MHz) δ 148.29 (d, Ar-*C*$_{10}$), 146.39 (s, Ar-*C*$_1$), 145.11 (s, Ar-*C*$_4$), 136.90 (m, Ar-*C*$_5$), 136.48 (m, Ar-*C*$_2$), 132.04 (s, Ar-*C*$_{6\text{-}9}$), 131.89 (s, Ar-*C*$_{6\text{-}9}$), 131.39 (s, Ar-*C*$_{6\text{-}9}$), 130.76 (s, Ar-*C*$_{6\text{-}9}$), 128.17 (s, Ar-*C*$_{7\text{-}8}$), 126.24 (s, Ar-*C*$_{7\text{-}8}$), 116.96 (s, Ar-*C*$_3$), 116.74 (s, Ar-*C*$_3$), 68.79 (s, O*C*H$_2$CH$_3$), 68.27 (s, O*C*H$_2$CH$_3$), 40.85 (N(*C*H$_3$)$_2$), 26.44 (*C*H-(CH$_3$)$_2$), 25.91 (*C*H-(CH$_3$)$_2$), 24.47 (*C*H-(CH$_3$)$_2$), 20.58 (CH-(*C*H$_3$)$_2$), 20.28 (CH-(*C*H$_3$)$_2$), 19.48 (CH-(*C*H$_3$)$_2$), 15.20 (OCH$_2$*C*H$_3$), ^{31}P{^{1}H} NMR (C$_6$D$_6$, 121.48 MHz) δ -2.84 (s), -4.30 (s)

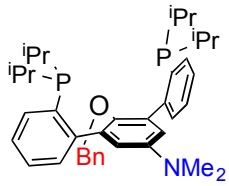

1,3-bis(2'-diisopropylphosphino)-4-dimethylamino-2-benzylbenzene (1^{Bn})

(0.19 g, 0.30 mmol) in 92.9% yield. ^{1}H NMR (C_6D_6, 300 MHz, 20 °C) δ 7.68 (m, 1H, Ar-*H*$_6$), 7.48 (m, 3H, Ar-*H*$_9$), 7.21 (m, 4H, Ar-*H*$_{7\text{-}8}$), 6.93 (m, 3H, Ar-*H*$_3$), 6.77 (s, 2H, Ar-*H*$_3$), 6.62 (m, 2H, Ar-*H*$_3$), 4.50 (dd, 2H, OC*H*$_2$Ph), 2.67 (s, 6H, N(C*H*$_3$)$_2$), 2.02 (m, 2H, C*H*(CH$_3$)$_2$) , 1.91 (m, 2H, C*H*(CH$_3$)$_2$) , 1.01 (m, 18H, CH(C*H*$_3$)$_2$), 0.86 (m, 6H, CH(C*H*$_3$)$_2$), ^{13}C{^{1}H} NMR (C_6D_6, 125.70 MHz) δ 148.27 (d, Ar-*C*$_{10}$), 146.00 (s, Ar-*C*$_5$), 138.41 (s, Ar-*C*$_1$), 137.35 (s, Ar-*C*$_4$), 137.14 (s, Ar-*C*$_3$), 132.44 (s, Ar-*C*$_{6\text{-}9}$), 131.89 (s, Ar-*C*$_{6\text{-}9}$), 131.33 (s, Ar-*C*$_{6\text{-}9}$), 128.33 (s, OCH$_2$*Ph*), 128.16 (s, Ar-*C*$_{7\text{-}8}$), 127.32 (s, OCH$_2$*Ph*), 126.74 (s, Ar-*C*$_{7\text{-}8}$), 117.16 (s, Ar-*C*$_3$), 75.29 (s, O*C*H$_2$Ph), 75.00 (s, O*C*H$_2$Ph), 41.15 (N(*C*H$_3$)$_2$), 26.82 (*C*H-(CH$_3$)$_2$), 26.34 (*C*H-(CH$_3$)$_2$), 24.47 (*C*H-(CH$_3$)$_2$), 21.14 (CH-(*C*H$_3$)$_2$), 20.50 (CH-(*C*H$_3$)$_2$), ^{31}P{^{1}H} NMR (C_6D_6, 121.48 MHz) δ -2.67 (s), -4.20 (s)

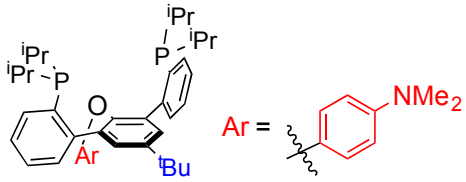

1,3-bis(2'-diisopropylphosphino)-4-dimethylamino-2-phenoxybenzene (1^{OAr})

(0.53 g, 0.83 mmol) in 92.9% yield. ^{1}H NMR (C_6D_6, 300 MHz, 70 °C) δ 7.58 (br s, 2H, Ar-*H*), 7.44 (s, 2H, Ar-*H*), 7.40 (d, 2H, Ar-*H*), 7.01 (m, 4H, Ar-*H*), 6.54 (m, 2H, Ar-*H*), 6.23 (d, 2H, Ar-*H*), 2.38 (s, 6H, N(C*H*$_3$)$_2$), 1.94 (br s, 2H, C*H*(CH$_3$)$_2$), 1.39 (s, 3H, C(C*H*$_3$)$_3$), 1.12 (br m, 18H, CH(C*H*$_3$)$_2$), 1.01 (br m, 6H, CH(C*H*$_3$)$_2$) ^{13}C{^{1}H} NMR (C_6D_6, 125.70 MHz) δ 151.82 (s, Ar-*C*$_1$), 150.91 (s, Ar-*C*$_1$), 148.23 (s, Ar-*C*$_{10}$), 147.39 (s,

Ar-C_{10}), 147.07 (s, Ar-C_2), 146.83 (s, Ar-C_2), 145.51 (s, OAr), 145.22 (s, OAr), 145.02 (s, OAr), 144.69 (s, Ar-C_4), 136.60 (s, Ar-C_5), 136.35 (s, Ar-C_5), 131.83 (s, Ar-$C_{6\text{-}9}$), 131.45 (s, Ar-$C_{6\text{-}9}$), 130.59 (s, Ar-$C_{6\text{-}9}$), 129.81 (s, Ar-C_3), 129.61 (s, Ar-C_3), 127.95 (s, Ar-$C_{7\text{-}8}$), 126.40 (s, Ar-$C_{7\text{-}8}$), 116.96 (s, OAr), 116.22 (s, OAr), 113.89 (s, OAr), 113.64 (s, OAr), 40.84 (Ar-N(CH$_3$)$_2$), 34.24 (C(CH$_3$)$_3$), 31.39 (C(CH$_3$)$_3$), 26.50 (CH-(CH$_3$)$_2$), 25.61 (CH-(CH$_3$)$_2$), 24.43 (CH-(CH$_3$)$_2$), 20.55 (CH-(CH$_3$)$_2$), 19.50 (CH-(CH$_3$)$_2$), ^{31}P{^{1}H} NMR (C_6D_6, 121.48 MHz) δ -2.61 (s), -3.98 (s)

2,6-diiodo-4-trifluoromethylphenol

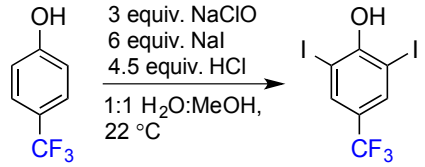

2,6-diiodo-4-trifluoromethylphenol was synthesized using the same procedure listed for 2,6-diiodo-4-nitrophenol. Yield: 5.32 g, 73.3% ^{1}H NMR (CDCl$_3$, 300 MHz) δ 7.92 (s, 2H, central Ar-H) ^{19}F{^{1}H} NMR δ 61.75

1,3-diiodo-2-methoxy-5-trifluoromethylbenzene

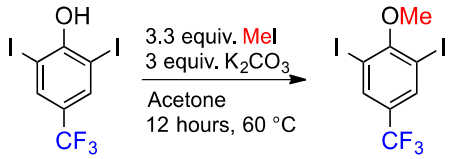

1,3-diiodo-2-methoxy-5-trifluoromethylbenzene was synthesized using the same procedure listed for 1,3-diiodo-2-methoxy-5-nitrobenzene. Yield: 4.52 g, 87.0% ^{1}H NMR (CDCl$_3$, 300 MHz) δ 8.01 (s, 2H, central Ar-H) 3.90 (s, 3H, OCH_3)

1,3-bis(2´-bromophenyl)-2-methoxy-5-trifluoromethylbenzene

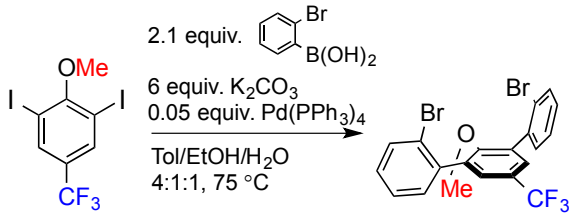

1,3-bis(2'-bromophenyl)-2-methoxy-5-trifluoromethylbenzene was synthesized using the same procedure listed for 1,3-bis(2'-bromophenyl)-2-methoxy-5-nitrobenzene. Yield: 2.31 g, 53.9% ^{1}H NMR ($CDCl_3$, 300 MHz) δ 7.49 (s, 2H, central Ar-*H*), 7.41 (d, 2H, Ar-*H*), 7.00 (d, 2H, Ar-*H*), 6.89 (t, 2H, Ar-*H*), 6.73 (t, 2H, Ar-*H*), 2.94 (s, 3H, OC*H*$_3$) ^{19}F{^{1}H} NMR δ 61.31

1,3-bis(2'-diisopropylphosphino)-2-methoxy-5-trifluoromethylbenzene (1_{CF3})

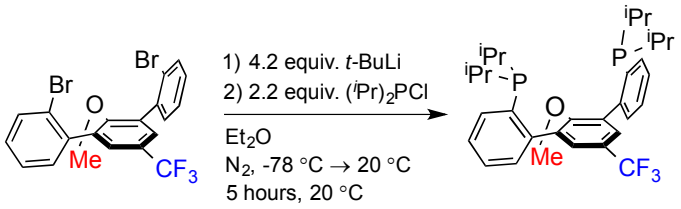

1,3-bis(2'-2'-diisopropyphosphinophenyl)-2-methoxy-5-trifluoromethylbenzene was synthesized using the same procedure listed for 1,3-bis(2'-2'-diisopropyphosphinophenyl)-2-methoxy-5-nitrobenzene. ^{1}H NMR ($CDCl_3$, 300 MHz) δ 7.60 (br m, 2H, Ar-*H*), 7.33 (br m, 4H, Ar-*H*), 7.12 (br m, 4H, Ar-*H*), 3.00 (m, 3H, OC*H*$_3$), 1.93 (septet, 2H, C*H*(CH_3)), 1.71 (septet, 2H, C*H*(CH_3)), 1.01 (m, 6H, CH(C*H*$_3$)), 0.87 (m, 18H, CH(C*H*$_3$)),^{19}F{^{1}H} NMR δ 61.31, ^{31}P{^{1}H} NMR δ -2.55, -4.24

1,3-diiodo-5-nitrobenzene.

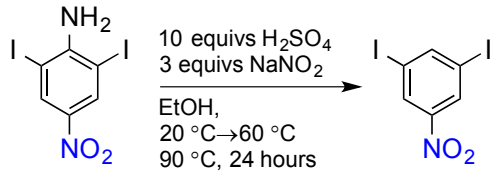

A modified literature procedure was used for the synthesis of 1,3-diiodo-5-nitrobenzene.[23] A solution of 2,6-diiodo-4-nitroaniline in ethanol (5.851 g; 15.0 mmol in 100 ml) was cooled to 0 °C using an ice bath. Upon cooling 8 ml (150 mmol) of concentrated H_2SO_4 was added drop wise over 1 hour using an addition funnel. This slurry was heated to 60 °C and 3.152 g (45.7 mmol) of sodium nitrite was added slowly to the reaction mixture. Upon addition the reaction mixture was heated to 90 °C for 24 hours. After the allocated time the reaction mixture was poured into ice water. The formed yellow solid was filtered off and extracted using water and ethyl acetate. The ethyl acetate fraction was concentrated to dryness to give the desired compound as a yellow solid. Yield 4.045g (71%) ^{1}H NMR (300 MHz, $CDCl_3$) δ 8.52 (d, 2H, *meta*Ar-*H*), 8.37 (t, 1H, *ipso*Ar-*H*) ppm.

1,3-bis(2´-bromophenyl)-5-nitrobenzene.

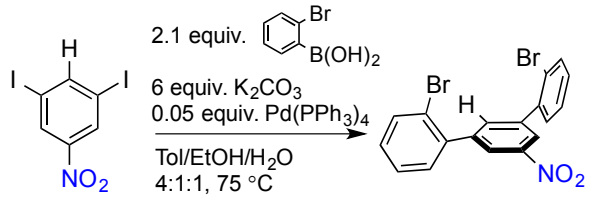

1,3-bis(2'-bromophenyl)-5-nitrobenzene was synthesized using the same procedure listed for 1,3-bis(2'-bromophenyl)-2-methoxy-5-nitrobenzene. Yield: 2.48 g (79% yield, 5.22 mmol) of the desired terphenyl dibromide as a white solid. ^{1}H NMR ($CDCl_3$, 300

MHz) δ 8.32 (d, 2H, *ipso*Ar-*H*), 7.82 (t, 1H, *meta*Ar-*H*), 7.72 (d, 2H, Ar-*H*), 7.43 (m, 2H, Ar-*H*), 7.30 (m, 4H, Ar-*H*).

1,3-bis(2´-bromophenyl)-5-dimethylaminobenzene.

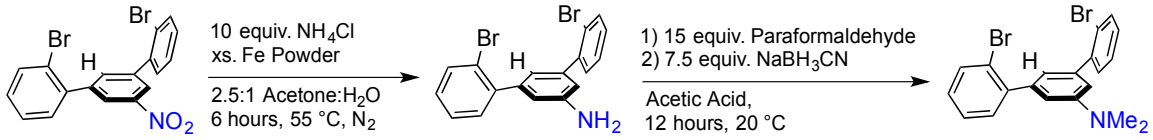

1,3-bis(2'-bromophenyl)-5-dimethylaminobenzene was synthesized from 1,3-bis(2'-bromophenyl)-5-nitrobenzene using the same procedure that was used for the reduction and amination of 1,3-bis(2'-bromophenyl)-4-dimethylamino-2-methoxybenzene. 1,3-bis(2'-bromophenyl)-5-dimethylaminobenzene was purified by Flash chromatography (dichloromethane) and isolated as a colorless solid. ^{1}H NMR ($CDCl_3$, 300 MHz) δ 7.62 (d, 2H, Ar-*H*), 7.42 (d, 2H, Ar-*H*), 7.35 (t, 2H, Ar-*H*), 7.20 (t, 2H, Ar-*H*), 6.78 (m, 3H, Ar-*H*), 3.03 (s, 6H, N(CH_3)$_2$.

1,3-bis(2'-diisopropylphosphino)-5-dimethylaminobenzene.

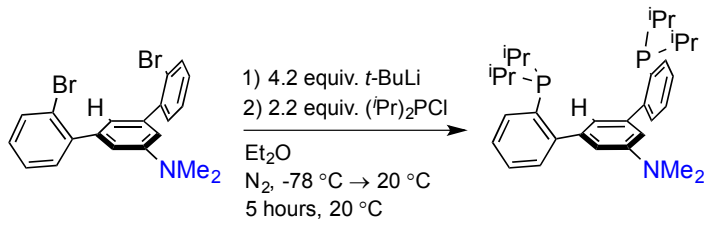

1,3-bis(2'-diisopropyphosphinophenyl)-5-dimethylaminobenzene was synthesized using the same procedure listed for 1,3-bis(2'-2'-diisopropyphosphinophenyl)-2-methoxy-5-nitrobenzene. ^{1}H NMR ($CDCl_3$, 300 MHz) δ 7.59 (br m, 2H, Ar-*H*), 7.47 (br m, 2H, Ar-*H*), 7.18 (br m, 4H, Ar-*H*), 7.03 (s, 1H, Ar-*H*), 6.91 (s, 2H, Ar-*H*), 2.68 (s, 6H,

N(C*H*$_3$)$_2$), 1.94 (septet, 4H, C*H*(CH$_3$)), 1.02 (m, 24H, CH(C*H*$_3$)), ^{13}C{^{1}H} NMR (C_6D_6, 125.70 MHz) δ 151.58 (d, Ar-*C*$_{10}$), 148.79 (s, Ar-*C*$_4$), 142.65 (s, Ar-*C*$_1$), 135.42 (d, Ar-*C*$_3$), 132.28 (s, Ar-*C*$_{7\text{-}8}$), 130.49 (s, Ar-*C*$_{7\text{-}8}$), 128.15 (s, Ar-*C*$_{6\text{-}9}$), 126.22 (d, Ar-*C*$_2$), 122.04 (d, Ar-*C*$_{6\text{-}9}$), 114.66 (d, Ar-*C*$_5$), 40.12 (N(*C*H$_3$)$_2$), 25.02 (CH-(*C*H$_3$)$_2$), 20.26 (*C*H-(CH$_3$)$_2$), 19.85 (CH-(*C*H$_3$)$_2$), ^{31}P{^{1}H} NMR δ -4.62

2,6-diiodo-4-trifluoromethylaniline

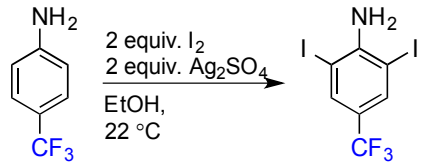

A literature procedure was used for the synthesis of 2,6-diiodo-4-trifluoromethylaniline.[24] Yield 4.734 g, 91.7% ^{1}H NMR (300 MHz, $CDCl_3$) δ 8.52 (d, 2H, *meta*Ar-*H*), 4.96(br s, 2H, N*H*$_2$) ppm

1,3-diiodo-3-trifluoromethylbenzene

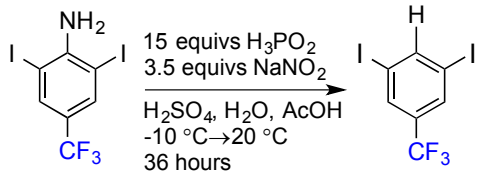

A literature procedure was used for the synthesis of 1,3-diiodo-5-trifluoromethylbenzene.[25] 0.883 g, 19.3% ^{1}H NMR (300 MHz, $CDCl_3$) δ 8.03 (br m, 1H, *ipso*Ar-*H*), 7.91(br m, 2H, Ar-*H*) ppm

1,3-bis(2´-bromophenyl)-5-trifluoromethylbenzene

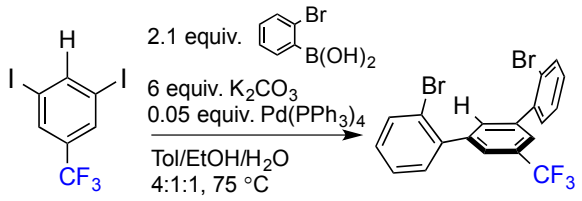

1,3-bis(2'-bromophenyl)-5-trifluoromethylbenzene was synthesized using the same procedure listed for 1,3-bis(2'-bromophenyl)-2-methoxy-5-nitrobenzene. Yield: 0.663 g (66.1% yield, 1.45 mmol) of the desired terphenyl dibromide as a white solid. ^{1}H NMR ($CDCl_3$, 300 MHz) δ 7.59 (s, 2H, Ar-*H*), 7.32 (m, 3H, Ar-*H*), 6.87 (d, 4H, Ar-*H*), 6.72 (m, 2H, Ar-*H*) ^{19}F{^{1}H} NMR δ 61.99

1,3-bis(2'-diisopropylphosphino)-5-trifluoromethylbenzene.

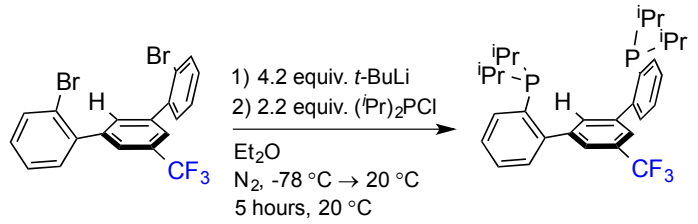

1,3-bis(2'-diisopropylphosphinophenyl)-5-trifluoromethylbenzene was synthesized using the same procedure listed for 1,3-bis(2'-diisopropyphosphinophenyl)-2-methoxy-5-nitrobenzene. Yield: 0.710 g (92.4% yield, 1.34 mmol) of the desired terphenyl dibromide as a white solid. ^{1}H NMR ($CDCl_3$, 300 MHz) δ 7.86 (s, 2H, Ar-*H*), 7.77 (s, 1H, Ar-*H*), 7.42 (m, 2H, Ar-*H*), 7.31 (m, 2H, Ar-*H*), 7.14 (m, 4H, Ar-*H*), 1.82 (m, 4H, C*H*(CH_3)), 1.13 (m, 12H, CH(C*H*$_3$)), 0.88 (m, 12H, CH(C*H*$_3$)), ^{13}C{^{1}H} NMR (C_6D_6, 125.70 MHz) δ 150.04 (d, Ar-C_{10}), 143.70 (s, Ar-C_4), 137.66 (s, Ar-C_1), 136.14 (d, Ar-C_5), 133.60 (s, Ar-$C_{7\text{-}8}$), 131.26 (s, Ar-$C_{7\text{-}8}$), 129.48 (s, Ar-$C_{6\text{-}9}$), 128.83 (d, Ar-C_2), 127.98 (d, Ar-$C_{6\text{-}9}$), 127.43 (Ar-CF$_3$) 127.08 (d, Ar-C_3), 25.74 (CH-(*C*H$_3$)$_2$), 25.62 (CH-

(CH_3)$_2$), 21.09 (CH-(CH_3)$_2$), 20.94 (CH-(CH_3)$_2$), 20.51 (CH-(CH_3)$_2$), 20.42 (CH-(CH_3)$_2$), ^{19}F{^{1}H} NMR δ 62.03, ^{31}P{^{1}H} NMR δ -5.31

[1,3-bis(2'-diisopropylphosphino)-4-dimethylamino-2-methoxybenzene]nickel(0) (2)

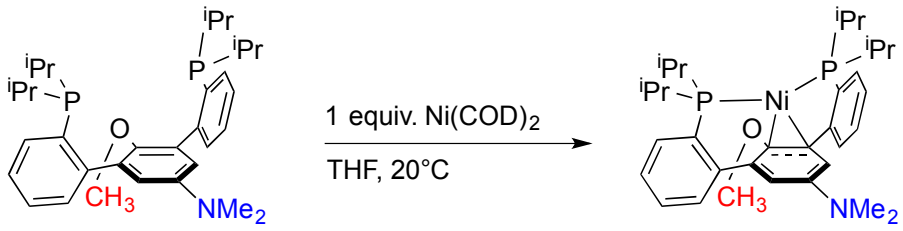

A colorless solution of 1,3-bis(2'-diisopropylphosphino)-4-dimethylamino-2-methoxybenzene (937.2mg, 1.74 mmol) in THF (35 ml) was mixed with a yellow slurry of Ni(COD)$_2$ (477.7 mg, 1.74 mmol) in THF (5 ml) at RT. The mixture changed color to dark red and was stirred for 11 hours. Volatiles were removed *in vacuo* yielding a dark red solid. The crude solid was taken up in MeCN and filtered through Celite to remove solids. MeCN was removed from the filtrate under vacuum. The dark red solid was dissolved in hexanes and cooled to neigh freezing temperatures in a liquid nitrogen cooled cold well and filtered through a Celite packed frit. The hexanes were removed under vacuum yielding a dark red solid. **(2)** Yield: 872.9 mg, 84.4% ^{1}H NMR (C_6D_6, 399.80 MHz) δ 7.70 (d, 2H, Ar-H_6), 7.32 (m, 2H, Ar-H_5), 7.24 (mm, 4H, Ar-$H_{7\text{-}8}$), 5.84 (t, 2H, Ar-H_3), 3.17 (s, 3H, OCH_3), 2.58 (s, 6H, N(CH_3)$_2$), 2.33 (m, 2H, CH(CH_3)$_2$), 2.04 (m, 2H, CH(CH_3)$_2$), 1.25 (mm, 6H, CH(CH_3)$_2$), 1.16 (mm, 12H, CH(CH_3)$_2$), 1.06 (m, 6H, CH(CH_3)$_2$) ^{13}C{^{1}H} NMR (C_6D_6, 100.54 MHz) δ 151.42 (t, Ar-C_{10}), 143.50 (s, Ar-C_4), 140.43 (t, Ar-C_2), 130.82 (s, Ar-C_6), 129.74 (t, Ar-C_9), 128.95 (s, Ar-C_8), 127.11 (s, Ar-C_7), 115.72 (t, Ar-C_2), 109.32 (t, Ar-C_3), 100.69 (t, Ar-C_1), 59.55 (s, O-CH_3), 42.03 (N(CH_3)$_2$), 27.25 (CH-(CH_3)$_2$), 21.82 (CH-(CH_3)$_2$),

20.15 (CH-(CH$_3$)$_2$), 20.09 (CH-(CH$_3$)$_2$), 19.80 (CH-(CH$_3$)$_2$), 19.33 (CH-(CH$_3$)$_2$), ^{31}P{^{1}H} NMR (C_6D_6, 121.48 MHz) δ 40.65 (s) Anal. Calcd. for $C_{33}H_{47}NNiOP_2$ (%): C, 66.68; H, 7.97; N, 2.36 Found C, 66.45; H, 7.94; N, 2.11.

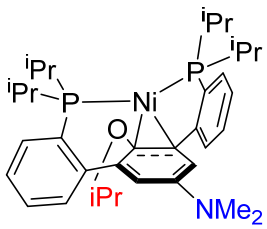

(2^{iPr}) Yield: 124.3 mg, 56.3% ^{1}H NMR (C_6D_6, 300 MHz) δ 7.72 (d, 2H, Ar-H), 7.31 (m, 2H, Ar-H), 7.23 (mm, 4H, Ar-H), 5.78 (t, 2H, Ar-H), 3.89 (septet, 1H, OCH(CH$_3$)$_2$), 2.60 (s, 6H, N(CH_3)$_2$), 2.331(m, 2H, CH(CH$_3$)$_2$), 1.99 (m, 2H, CH(CH$_3$)$_2$), 1.25 (mm, 6H, CH(CH_3)$_2$), 1.16 (mm, 12H, CH(CH_3)$_2$), 1.06 (m, 6H, CH(CH_3)$_2$), 0.67 (d, 6H, OCH(CH$_3$)$_2$), ^{13}C{^{1}H} NMR (C_6D_6, 100.54 MHz) δ 151.50 (t, Ar-C_{10}), 143.43 (s, Ar-C_4), 140.05 (t, Ar-C_5), 130.35 (s, Ar-C_6), 128.26 (t, Ar-C_9), 127.96 (s, Ar-C_8), 126.68 (s, Ar-C_7), 117.94 (t, Ar-C_2), 107.73 (t, Ar-C_3), 99.56 (t, Ar-C_1), 73.36 (s, O-CH(CH$_3$)$_2$), 41.59 (N(CH$_3$)$_2$), 27.04 (CH-(CH$_3$)$_2$), 23.02 (s, O-CH(CH$_3$)$_2$), 21.72 (CH-(CH$_3$)$_2$), 20.00 (CH-(CH$_3$)$_2$), 19.52 (CH-(CH$_3$)$_2$), 19.23 (CH-(CH$_3$)$_2$), 18.97 (CH-(CH$_3$)$_2$), ^{31}P{^{1}H} NMR (C_6D_6, 121.48 MHz) δ 39.20 (s) Anal. Calcd. for $C_{33}H_{51}NNiOP_2$ (%): C, 67.54; H, 8.26; N, 2.25 Found C, 66.68; H, 8.09; N, 2.26.

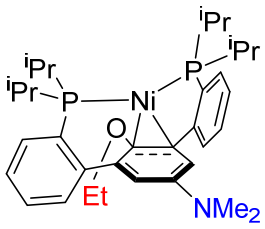

(2^{Et}) Yield: 279.0 mg, 63.0% ^{1}H NMR (C_6D_6, 500 MHz) δ 7.70 (d, 2H, Ar-*H*), 7.31 (m, 2H, Ar-*H*), 7.23 (mm, 4H, Ar-*H*), 5.84 (t, 2H, Ar-*H*), 3.57 (q, 2H, OC*H*$_2$CH$_3$), 2.59 (s, 6H, N(C*H*$_3$)$_2$), 2.35 (m, 2H, C*H*(CH$_3$)$_2$), 2.03 (m, 2H, C*H*(CH$_3$)$_2$), 1.25 (mm, 6H, CH(C*H*$_3$)$_2$), 1.16 (mm, 12H, CH(C*H*$_3$)$_2$), 1.06 (m, 6H, CH(C*H*$_3$)$_2$), 0.50 (t, 3H, OCH$_2$C*H*$_3$), ^{13}C{^{1}H} NMR (C_6D_6, 100.54 MHz) δ 151.05 (t, Ar-*C*), 143.14 (s, Ar-*C*), 140.01 (t, Ar-*C*), 130.38 (s, Ar-*C*), 129.31 (t, Ar-*C*), 128.43 (s, Ar-*C*), 126.65 (s, Ar-*C*), 116.03 (t, Ar-*C*), 108.57 (t, Ar-*C*), 99.99 (t, Ar-*C*), 67.65 (s, O*C*H$_2$CH$_3$), 41.65 (N(*C*H$_3$)$_2$), 26.85 (*C*H-(CH$_3$)$_2$), 21.57 (*C*H-(CH$_3$)$_2$), 19.76 (CH-(*C*H$_3$)$_2$), 18.96 (CH-(*C*H$_3$)$_2$), 15.42 (OCH$_2$*C*H$_3$), ^{31}P{^{1}H} NMR (C_6D_6, 121.48 MHz) δ 40.57 (s) Anal. Calcd. for $C_{34}H_{49}NNiOP_2$ (%): C, 67.12; H, 8.12; N, 2.30 Found C, 65.34; H, 8.46; N, 2.21.

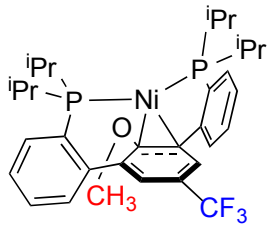

(2$_{CF3}$) Yield: 613.1 mg, 73.7% ^{1}H NMR (C_6D_6, 499.85 MHz) δ 7.44 (m, 2H, Ar-*H*), 7.23 (m, 2H, Ar-*H*), 7.18 (m, 4H, Ar-*H*), 6.62 (s, 2H, Ar-*H*), 3.01 (s, 3H, OC*H*$_3$), 2.23 (m, 2H, C*H*(CH$_3$)$_2$), 1.94 (m, 2H, C*H*(CH$_3$)$_2$), 1.08 (mm, 18H, CH(C*H*$_3$)$_2$), 0.91 (mm, 6H, CH(C*H*$_3$)$_2$), ^{19}F{^{1}H} NMR (C_6D_6, 282.33 MHz) δ -61.34 (s), ^{31}P{^{1}H} NMR (C_6D_6, 121.48 MHz) δ 41.12 (s) ^{13}C{^{1}H} NMR (C_6D_6, 125.70 MHz) δ 150.14 (t, Ar-*C*), 138.90 (t, Ar-

*C*3), 130.96 (s, Ar-*C*9), 129.75 (t, Ar-*C*6), 129.68 (s, Ar- *C*7-8), 128.35 (s, Ar-*C*2), 127.48 (s, Ar-*C*7-8), 118.89 (s, Ar-*C*3), 117.81 (q, Ar-*C*F3), 111.29 (s, Ar-*C*1), 99.40 (s, Ar-*C*4), 58.98 (O(*C*H3)), 27.38 (*C*H-(CH3)2), 21.71 (*C*H-(CH3)2), 19.77 (CH-(*C*H3)2), 19.60 (CH-(*C*H3)2), 19.06 (CH-(*C*H3)2), Anal. Calcd. for $C_{32}H_{41}F_3NiOP_2$ (%): C, 62.06; H, 6.67 Found C, 61.77; H, 6.60.

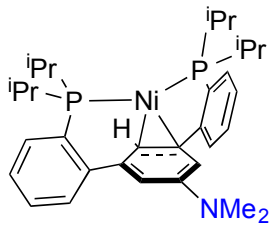

(7) Yield: 473.8 mg, 84.9% ^{1}H NMR (C_6D_6, 499.85 MHz) δ 7.65 (d, 2H, Ar-*H*), 7.25 (m, 2H, Ar-*H*), 7.15 (mm, 4H, Ar-*H*), 5.82 (s, 2H, Ar-*H*), 5.37 (s, 1H, Ar-*H*), 2.59 (s, 6H, N(C*H*3)2), 2.30 (m, 2H, C*H*(CH3)2), 2.04 (m, 2H, C*H*(CH3)2), 1.23 (mm, 6H, CH(C*H*3)2), 1.16 (mm, 6H, CH(C*H*3)2), 1.05 (m, 12H, CH(C*H*3)2), ^{31}P{^{1}H} NMR (C_6D_6, 121.48 MHz) δ 38.55 (s) ^{13}C{^{1}H} NMR (C_6D_6, 125.70 MHz) δ 153.93 (t, Ar-*C*10), 147.74 (s, Ar-*C*4), 139.81 (t, Ar-*C*9), 131.44 (s, Ar-*C*8), 129.77 (t, Ar-*C*5), 129.30 (s, Ar-*C*6), 127.81 (t, Ar-*C*7), 122.37 (s, Ar-*C*10), 107.71 (s, Ar-*C*3), 90.26 (s, Ar-*C*4), 70.33 (s, Ar-*C*1), 41.80 (N(*C*H3)2), 27.76 (*C*H-(CH3)2), 22.32 (*C*H-(CH3)2), 20.66 (CH-(*C*H3)2), 20.55 (CH-(*C*H3)2), 20.37 (CH-(*C*H3)2), 19.94 (CH-(*C*H3)2), Anal. Calcd. for $C_{32}H_{45}NNiP_2$ (%): C, 68.10; H, 8.04; N, 2.48 Found C, 59.35; H, 7.41; N, 2.16

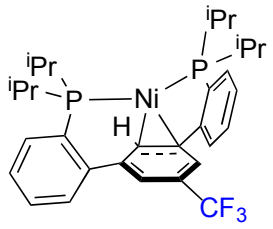

(7$_{CF3}$) Yield: 872.9 mg, 84.4% ^{1}H NMR (C_6D_6, 499.85 MHz) δ 7.35 (d, 2H, Ar-*H*), 7.18 (m, 2H, Ar-*H*), 7.12 (mm, 2H, Ar-*H*), 7.07 (mm, 2H, Ar-*H*), 6.60 (s, 2H, Ar-*H*), 4.64 (s, 1H, Ar-*H*), 2.20 (m, 2H, C*H*(CH_3)$_2$), 1.95 (m, 2H, C*H*(CH_3)$_2$), 1.07 (mm, 12H, CH(C*H*$_3$)$_2$), 0.94 (mm, 12H, CH(C*H*$_3$)$_2$), ^{31}P{^{1}H} NMR (C_6D_6, 121.48 MHz) δ 41.93 (s) ^{19}F{^{1}H} NMR (C_6D_6, 282.33 MHz) δ -62.59 (s) ^{13}C{^{1}H} NMR (C_6D_6, 125.70 MHz) δ 152.33 (t, Ar-*C*$_{10}$), 137.92 (t, Ar-*C*$_9$), 131.17 (s, Ar-*C*$_5$), 129.63 (s, Ar-*C*$_7$), 128.84 (t, Ar-*C*$_8$), 127.69 (s, Ar-*C*$_6$), 125.85 (s, Ar-*C*$_2$), 121.32 (q, Ar-Ar-*C*F$_3$), 117.49 (s, Ar-*C*$_3$), 112.85 (s, Ar-*C*$_4$), 63.96 (s, Ar-*C*$_1$), 27.22 (t, *C*H-(CH_3)$_2$), 21.55 (t, *C*H-(CH_3)$_2$), 19.72 (CH-(*C*H$_3$)$_2$), 19.66 (CH-(*C*H$_3$)$_2$), 19.50 (CH-(*C*H$_3$)$_2$), 19.12 (CH-(*C*H$_3$)$_2$) Anal. Calcd. for $C_{31}H_{39}F_3NiP_2$ (%): C, 63.18; H, 6.67 Found C, 63.12; H, 6.74.

[1,3-bis(2'-diisopropylphosphino)-4-dimethylaminophenyl]nickel(II)methoxide (3)

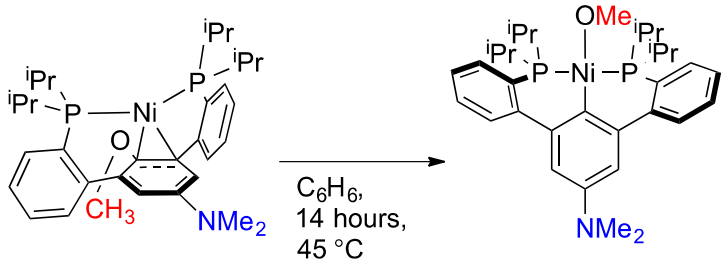

A dark red solution of purified [1,3-bis(2'-diisopropylphosphino)-4-dimethylamino-2-methoxybenzene]nickel(0) (105.2 mg, 0.18 mmol) in C_6H_6 was warmed to 45°C in a Schlenk tube. After 14 hours the solvent was removed under vacuum. The resulting red orange solid was washed with pentane and extracted with ether. The ether was

pumped off resulting in an orange solid (**3b**). Yield: 82.7 mg, 78.6% ^{1}H NMR (C_6D_6, 399.80 MHz) δ 7.76 (d, 2H, Ar-*H*$_6$), 7.44 (d, 2H, Ar-*H*$_9$), 7.37 (t, 2H, Ar-*H*$_7$), 7.17 (t, 2H, Ar-*H*$_8$), 6.78 (s, 2H, Ar-*H*$_3$), 3.67 (s, 3H, OC*H*$_3$), 2.56 (s, 6H, N(C*H*$_3$)$_2$), 2.52 (br, 2H, C*H*(CH$_3$)$_2$), 1.76 (br, 2H, C*H*(CH$_3$)$_2$), 1.66 (br, 6H, CH(C*H*$_3$)$_2$), 1.28 (br, 6H, CH(C*H*$_3$)$_2$), 0.96 (br, 6H, CH(C*H*$_3$)$_2$), 0.80 (br, 6H, CH(C*H*$_3$)$_2$) ^{13}C{^{1}H} NMR (C_6D_6, 100.54 MHz) δ 153.23 (t, Ar-*C*$_{10}$), 150.95 (s, Ar-*C*$_4$), 147.19 (t, Ar-*C*$_5$), 130.26 (s, Ar-*C*$_7$), 129.41 (s, Ar-*C*$_9$), 128.40 (s, Ar-*C*$_2$), 128.35 (s, Ar-*C*$_6$), 126.99 (s, Ar-*C*$_1$), 126.60 (s, Ar-*C*$_8$), 113.59 (s, Ar-*C*$_3$), 54.84 (s, O*C*H$_3$), 40.56 (s, N(*C*H$_3$)$_2$), 23.83 (s, *C*H(CH$_3$)$_2$), 21.09 (s, *C*H(CH$_3$)$_2$), 20.45 (s, CH(*C*H$_3$)$_2$), 19.77 (s, CH(*C*H$_3$)$_2$), 18.90 (s, CH(*C*H$_3$)$_2$), 18.12 (s, CH(*C*H$_3$)$_2$), ^{31}P{^{1}H} NMR (C_6D_6, 161.85 MHz) δ 27.26 (s) Anal. Calcd. for $C_{33}H_{47}NNiOP_2$ (%): C, 66.68; H, 7.97; N, 2.36 Found C, 66.60; H, 8.10; N, 2.23.

[1,3-bis(2'-diisopropylphosphino)-4-dimethylaminophenyl]nickel(II)hydride (4)

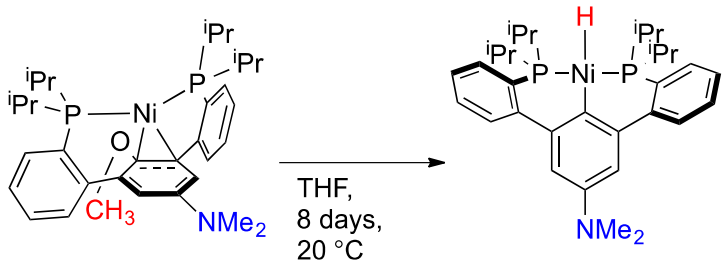

A dark red solution of crude [1,3-bis(2'-diisopropylphosphino)-4-dimethylamino-2-methoxybenzene]nickel(0) (100.1 mg, 0.17 mmol) in THF (10 ml) was stirred at RT for 8 days. Over the course of 8 days a yellow solid precipitated. The solid was collected on a pad of Celite. The solid was extracted from the Celite with toluene. Removal of solvent under vacuum yielded a yellow solid. Yield: 52.3 mg, 55% ^{1}H NMR (C_6D_6, 300 MHz) δ 7.87 (d, 2H, Ar-*H*$_6$), 7.44 (t, 2H, Ar-*H*$_7$), 7.29 (d, 2H, Ar-*H*$_9$),

7.14 (t, 2H, Ar-*H*$_8$), 6.79 (s, 2H, Ar-*H*$_5$), 2.54 (t, 6H, N(C*H*$_3$)$_2$), 2.27 (br m, 2H, C*H*(CH$_3$)$_2$), 1.70 (br m, 6H, CH(C*H*$_3$)$_2$), 1.61 (br m, 2H, C*H*(CH$_3$)$_2$), 1.28 (mm, 6H, CH(C*H*$_3$)$_2$), 1.12 (mm, 6H, CH(C*H*$_3$)$_2$), 0.70 (m, 6H, CH(C*H*$_3$)$_2$), -2.80 (t, 1H, Ni-*H*), ^{13}C{^{1}H} NMR (CD_2Cl_2, 100.54 MHz) δ 152.69 (t, Ar-*C*$_{10}$), 150.79 (s, Ar-*C*$_4$), 147.09 (t, Ar-*C*$_3$), 130.40 (s, Ar-*C*$_7$), 129.13 (s, Ar-*C*$_9$), 128.70 (s, Ar-*C*$_2$), 128.15 (s, Ar-*C*$_6$), 126.61 (s, Ar-*C*$_8$), 126.41 (s, Ar-*C*$_1$), 114.03 (s, Ar-*C*$_3$), 41.07 (s, N(*C*H$_3$)$_2$), 24.08 (s, *C*H(CH$_3$)$_2$), 20.48 (s, CH(*C*H$_3$)$_2$), 20.34 (s, CH(*C*H$_3$)$_2$), 20.08 (s, *C*H(CH$_3$)$_2$), 18.75 (s, CH(*C*H$_3$)$_2$), 18.08 (s, CH(*C*H$_3$)$_2$), ^{31}P{^{1}H} NMR (C_6D_6, 121.48 MHz) δ 30.41 (s) Anal. Calcd. for $C_{32}H_{45}NNiP_2$ (%): C, 68.10; H, 8.04; N, 2.48 Found. C, 67.63; H, 7.85; N, 2.05

[1,3-bis(2'-diisopropylphosphino)-4-dimethylaminophenyl]nickel(II)iodide (*5*)

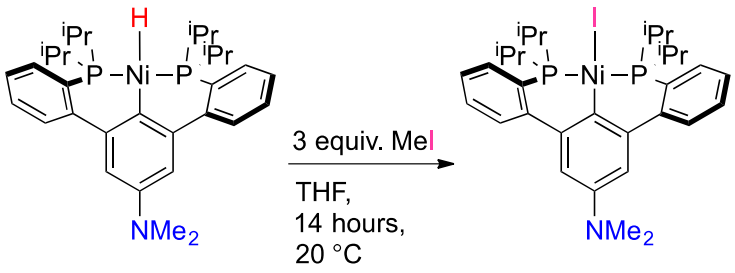

A yellow solution of [1,3-bis(2'-diisopropylphosphino)-4-dimethylaminophenyl]nickel(II)hydride (35.3 mg, 0.063 mmol) was made in THF (7 ml). To this solution was added dry methyl iodide (28.5 mg, 0.20 mmol) at room temperature. The solution was stirred for 14 hours at room temperature in the dark. After 14 hours the volatiles were removed under vacuum leaving a red orange residue. The residue was washed with hexanes and extracted with ether. The ether was removed under vacuum yielding a red orange solid. X-ray quality crystals were grown from a concentrated solution in ether. Yield: 27.4 mg, 63.5%^{1}H NMR (C_6D_6, 399.80

MHz) δ 7.72 (d, 2H, Ar-*H*$_6$), 7.40 (d, 2H, Ar-*H*$_9$), 7.37 (t, 2H, Ar-*H*$_8$), 7.13 (t, 2H, Ar-*H*$_7$), 6.78 (s, 2H, Ar-*H*$_3$), 3.03 (m, 2H, C*H*(CH$_3$)$_2$), 2.52 (m, 6H, N(C*H*$_3$)$_2$), 1.77 (m, 2H, C*H*(CH$_3$)$_2$), 1.51 (q, 6H, CH(C*H*$_3$)$_2$), 1.31 (m, 6H, CH(C*H*$_3$)$_2$), 0.91 (m, 6H, CH(C*H*$_3$)$_2$), 0.77 (m, 6H, CH(C*H*$_3$)$_2$), ^{13}C{^{1}H} NMR (C$_6$D$_6$, 100.54 MHz), δ 151.38 (t, Ar-*C*$_{10}$), 151.20 (s, Ar-*C*$_4$), 146.92 (t, Ar-*C*$_5$), 130.39 (s, Ar-*C*$_8$), 129.78 (t, Ar-*C*$_9$), 127.98 (s, Ar-*C*$_2$), 127.95 (s, Ar-*C*$_6$), 127.16 (s, Ar-*C*$_7$), 126.19 (t, Ar-*C*$_1$), 113.86 (t, Ar-*C*$_3$), 40.28 (N(*C*H$_3$)$_2$), 24.29 (*C*H-(CH$_3$)$_2$), 23.59 (*C*H-(CH$_3$)$_2$), 20.55 (CH-(*C*H$_3$)$_2$), 20.21 (CH-(*C*H$_3$)$_2$), 19.39 (CH-(*C*H$_3$)$_2$), 18.91 (CH-(*C*H$_3$)$_2$), ^{31}P{^{1}H} NMR (C$_6$D$_6$, 121.48 MHz) δ 34.35 (s) Anal. Calcd. for C$_{32}$H$_{44}$NNiP$_2$ (%): C, 58.01; H, 6.51; N, 1.90 Found. C, 58.23; H, 6.62; N, 2.00

[1,3-bis(2'-diisopropylphosphino)-4-dimethylaminobenzenel]nickel(0)carbonyl (6)

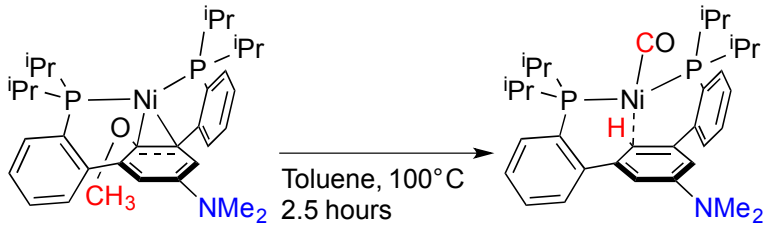

A dark red solution of crude [1,3-bis(2'-diisopropylphosphino)-4-dimethylamino-2-methoxybenzene]nickel(0) (96.9 mg, 0.16 mmol) in toluene was heated to 100 °C in a sealed Schlenk tube. The tube was heated for 2.5 hours. After 2.5 hours the solvent was removed under vacuum giving an orange solid. The solid was washed with hexanes and dried under vacuum yielding a red orange solid. Yield: 83.8 mg, 86.7% ^{1}H NMR (C$_6$D$_6$, 399.80 MHz) δ 7.49 (br m, 2H, Ar-*H*$_6$), 7.44 (br m, 2H, Ar-*H*$_9$), 7.18 (m, 4H, Ar-*H*$_{7-8}$), 6.56 (s, 2H, Ar-*H*$_3$), 6.51 (t, 1H, Ar-*H*$_1$), 2.65 (s, 6H, N(C*H*$_3$)$_2$), 2.40 (m, 2H, C*H*(CH$_3$)$_2$), 2.18 (m, 2H, C*H*(CH$_3$)$_2$), 1.24 (q, 6H, CH(C*H*$_3$)$_2$), 1.16 (q, 6H,

CH(C*H*$_3$)$_2$), 1.10 (q, 6H, CH(C*H*$_3$)$_2$), 1.02 (q, 6H, CH(C*H*$_3$)$_2$) ^{13}C{^{1}H} NMR (C$_6$D$_6$, 100.54 MHz) δ 195.98 (t, Ni-*C*O), 152.54 (s, Ar-*C*$_1$), 151.06 (t, Ar-*C*$_{10}$), 145.58 (s, Ar-*C*$_2$), 136.50 (t, Ar-*C*$_5$), 131.26 (s, Ar-*C*$_9$), 130.81 (s, Ar-*C*$_6$), 128.90 (s, Ar-*C*$_8$), 127.29 (s, Ar-*C*$_7$), 110.03 (s, Ar-*C*$_3$), 84.65 (s, Ar-*C*$_1$), 40.68 (N(*C*H$_3$)$_2$), 29.44 (*C*H-(CH$_3$)$_2$), 26.79 (*C*H-(CH$_3$)$_2$), 20.40 (CH-(*C*H$_3$)$_2$), 19.62 (CH-(*C*H$_3$)$_2$), 18.90 (CH-(*C*H$_3$)$_2$), 18.60 (CH-(*C*H$_3$)$_2$) ^{31}P{^{1}H} NMR (C$_6$D$_6$, 121.48 MHz) δ 34.17 (s) EA Calcd. C, 66.91; H, 7.66; N, 2.36 Found. C, 67.13; H, 7.67; N, 2.38 IR (C$_6$D$_6$): ν_{CO} = 1917 cm^{-1}.

General Synthesis of Nickel(II) Phenoxide Halide Systems (8)

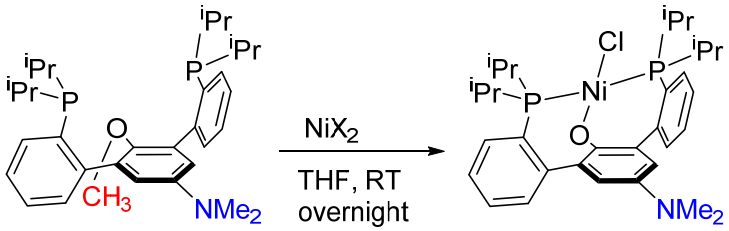

To a colorless solution of **1** in THF is added a slurry of NiX$_2$ in THF. Upon mixing the solution develops a deep green color overtime. The solution was allowed to stir overnight. After the allotted time the solvent was removed under vacuum resulting in a dark green solid. The dark green solid was rinsed with Et$_2$O and Hexanes resulting in pure **8** as a dark green solid. Yield: 72% ^{1}H NMR (C$_6$D$_6$, 500 MHz) δ 7.22 (br m, 4H, Ar-*H*), 7.05 (s, 2H, Ar-*H*), 6.99 (m, 4H, Ar-*H*), 2.75 (s, 6H, N(C*H*$_3$)$_2$), 2.57 (m, 2H, C*H*(CH$_3$)$_2$), 2.12 (m, 2H, C*H*(CH$_3$)$_2$), 1.83 (m, 12H, Ar-C*H*$_3$), 1.19 (m, 6H, CH(C*H*$_3$)$_2$), 0.66 (m, 6H, CH(C*H*$_3$)$_2$), ^{13}C{^{1}H} NMR (C$_6$D$_6$, 100.54 MHz) δ 147.15 (t, Ar-*C*), 134.71 (s, Ar-*C*), 132.85 (s, Ar-*C*), 130.79 (s, Ar-*C*), 128.19 (s, Ar-*C*), 124.90 (s, Ar-*C*), 122.73 (t, Ar-*C*), 119.04 (s, Ar-*C*), 42.22 (N(*C*H$_3$)$_2$), 22.85 (*C*H-(CH$_3$)$_2$), 20.83 (*C*H-(CH$_3$)$_2$), 19.23 (CH-(*C*H$_3$)$_2$), 19.04 (CH-(*C*H$_3$)$_2$), 18.55 (CH-(*C*H$_3$)$_2$), 14.88 (CH-

(CH_3)$_2$), $^{31}P\{^1H\}$ NMR (C_6D_6, 121.48 MHz) δ 13.60 (s) Anal. Calcd. for $C_{32}H_{44}ClNNiOP_2$ (%): C, 62.52; H, 7.21; N, 2.28 Found C, 60.76; H, 7.10; N, 2.08.

General Synthesis of Nickel(I) Systems (9)

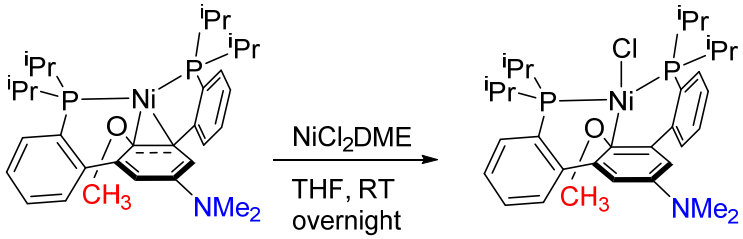

To a dark red solution of **2** in THF is added a slurry of oxidant in THF. Upon mixing the solution lightens to a yellow color overtime. The solution was stirred overnight. After the allotted time the solvent was removed under vacuum resulting in a dark yellow residue. The yellow solid was rinsed with Et_2O and Hexanes resulting in **9** as a pale yellow solid. Paramagnetically broadened peaks are observed in the ^1H and ^{31}P NMR spectra of these compounds. Anal. Calcd. for $C_{34}H_{47}ClNNiOP_2$ (**9**) (%): C, 62.93; H, 7.52; N, 2.22 Found C, 62.23; H, 7.35; N, 2.12. Anal. Calcd. for $C_{34}H_{47}F_3NNiO_4P_2S$ ($\mathbf{9}^{OTf}$) (%): C, 54.93; H, 6.37; N, 1.88 Found C, 52.54; H, 6.46; N, 1.81.

[1,3-bis(2'-diisopropylphosphino)-4-dimethylamino-2-methylbenzene]nickel(0) (10)

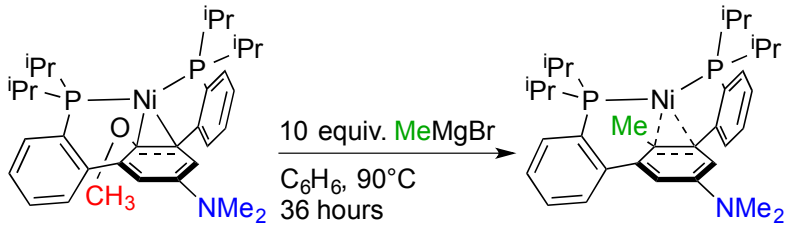

A dark red solution of crude [1,3-bis(2'-diisopropylphosphino)-4-dimethylamino-2-methoxybenzene]nickel(0) (100.1 mg, 0.17 mmol) in toluene was treated with 10 equivalents of MeMgBr and heated to 90 °C in a sealed Schlenk. The tube was heated for 36 hours. After 36 hours the solvent was removed under vacuum giving a dark red solid. The solid was triterated with pentanes and hexanes to precipitate excess Grignard reagent. The resulting slurry was filtered through Celite. **10** was obtained from the elute as a dark red solid. Yield: 52.4 mg, 53.3% ^{1}H NMR (C_6D_6, 300 MHz) δ 7.62 (br m, 2H, Ar-*H*), 7.24 (br m, 2H, Ar-*H*), 7.20 (m, 4H, Ar-*H*), 5.80 (s, 2H, Ar-*H*), 2.60 (s, 6H, N(C*H*$_3$)$_2$), 2.26 (m, 2H, C*H*(CH$_3$)$_2$), 1.98 (m, 2H, C*H*(CH$_3$)$_2$), 1.52 (s, 3H, Ar-C*H*$_3$), 1.12 (m, 24H, CH(C*H*$_3$)$_2$), ^{31}P{^{1}H} NMR (C_6D_6, 121.48 MHz) δ 36.83 (s)

[1,3-bis(2'-diisopropylphosphino)-4-dimethylamino-2-methylbenzene]nickel(0)carbonyl (11)

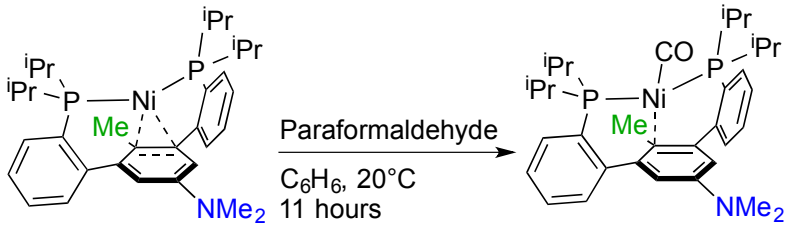

Method A: To a yellow solution of **4** (12.3 mg, 0.022 mmol) in benzene was added 10 equivalents of acetaldehyde. The solution was heated to 90 °C for 24 hours. After 24 hours the excess acetaldehyde was removed resulting in **11** as a red orange solid.

Method B: A dark red solution of **8** (32.9 mg, 0.057 mmol) in toluene was treated with 5 equivalents of paraformaldehyde (8.7 mg, 0.29 mmol). The solution was mixed at room temperature for 11 hours. After 11 hours the solvent was removed *in vacuo* and the residue was filtered through Celite with hexanes. The solvent was removed from the organic fraction yielding **11** as a red orange solid. Yield: 30.9 mg, 89.8% ^{1}H NMR (C_6D_6, 300 MHz) δ 7.44 (br m, 2H, Ar-*H*), 7.37 (br m, 2H, Ar-*H*), 7.20 (m, 4H, Ar-*H*), 6.62 (s, 2H, Ar-*H*), 2.72 (s, 6H, N(C*H*$_3$)$_2$), 2.42 (m, 2H, C*H*(CH$_3$)$_2$), 2.02 (m, 2H, C*H*(CH$_3$)$_2$), 1.66 (s, 3H, Ar-C*H*$_3$), 1.08 (m, 24H, CH(C*H*$_3$)$_2$), ^{31}P{^{1}H} NMR (C_6D_6, 121.48 MHz) δ 35.90 (s)

[1,3-bis(2'-diisopropylphosphino)-4-dimethylaminophenoxide]nickel(II)benzyl (12)

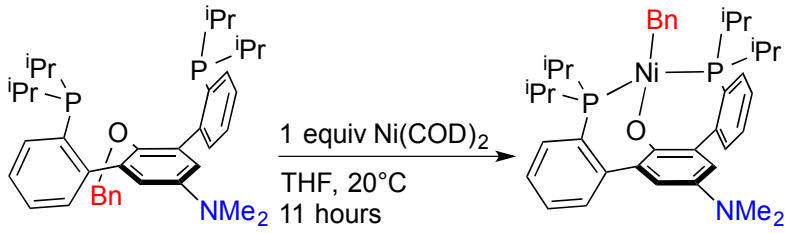

A colorless solution of 1,3-bis(2'-diisopropylphosphino)-4-dimethylamino-2-benzyloxybenzene (114.6 mg, 0.187 mmol) in THF (10 ml) was mixed with a yellow slurry of $Ni(COD)_2$ (48.9 mg, .178 mmol) in THF (2.5 ml) at RT. The mixture changed color to dark red and was stirred for 11 hours. Volatiles were removed *in vacuo* yielding a dark red purple solid. The crude solid was washed with hexanes and Et_2O yielding a purple red solid. Crystals were grown from a concentrated solution in Et_2O at 20 °C. (**12**) Yield: 103.9 mg, 82.9% ^1H NMR (C_6D_6, 300 MHz) δ 7.74 (d, 2H, Ar-*H*), 7.24 (m, 2H, Ar-*H*), 7.20 (mm, 2H, Ar-*H*), 7.15 (s, 2H, Ar-*H*), 7.04 (mm, 2H, Ar-*H*), 2.93 (s, 6H, $N(CH_3)_2$), 2.30 (m, 2H, $CH(CH_3)_2$), 1.88 (m, 2H, $CH(CH_3)_2$), 1.72 (mm, 6H, $CH(CH_3)_2$), 1.63 (mm, 6H, $CH(CH_3)_2$), 1.35 (mm, 2H, CH_2Ph) 0.71 (mm, 6H, $CH(CH_3)_2$), 0.36 (m, 6H, $CH(CH_3)_2$) $^{13}C\{^1H\}$ NMR (C_6D_6, 100.54 MHz) δ 148.02 (t, Ar-C_{10}), 144.27 (s, Ar-C_4), 139.69 (t, Ar-C_5), 134.04 (s, Ar), 132.37 (s, Ar), 131.96 (s, Ar), 129.98 (s, Ar-C_6), 129.64 (t, Ar-C_9), 126.82 (s, Ar-C_8), 125.73 (t, Ar-C_2), 124.51 (s, Ar-C_7), 123.60 (s, Ar-C_3), 118.25 (s, Ar-C_1), 42.05 ($N(CH_3)_2$), 23.68 (CH-$(CH_3)_2$), 20.60 (CH-$(CH_3)_2$), 19.40 (CH-(CH_3)$_2$), 19.06 (CH-(CH_3)$_2$), 18.18 (CH-(CH_3)$_2$), 16.02 (CH-(CH_3)$_2$), -0.04 (t, CH_2-Ar), $^{31}P\{^1H\}$ NMR (C_6D_6, 121.48 MHz) δ 18.42 (s) Anal. Calcd. for $C_{39}H_{51}NNiOP_2$ (%): C, 69.86; H, 7.67; N, 2.09 Found C, 69.62; H, 7.49; N, 1.96.

[1,3-bis(2'-diisopropylphosphino)-4-dimethylaminophenyl]nickel(II)phenoxide (13)

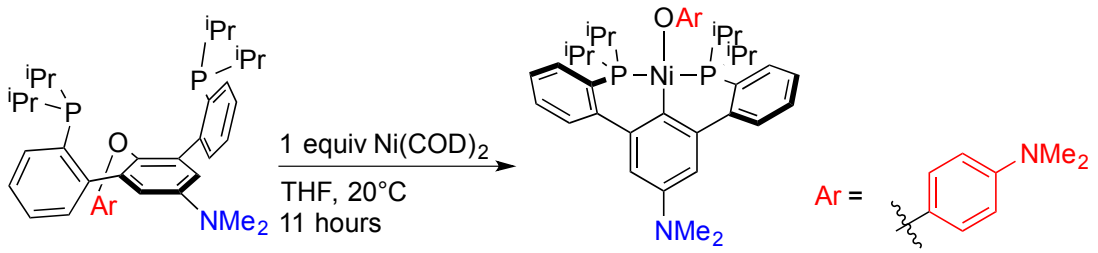

A colorless solution of 1,3-bis(2'-diisopropylphosphino)-4-dimethylamino-2-phenoxybenzene (110.5 mg, 0.17 mmol) in THF (5 ml) was mixed with a yellow slurry of $Ni(COD)_2$ (46.8 mg, .17 mmol) in THF (2.5 ml) at RT. The mixture changed color to orange and was stirred for 13 hours. Volatiles were removed *in vacuo* yielding a orange solid. The crude solid was washed with hexanes and Et_2O yielding a orange solid. (**13**) Yield: 116.3 mg, 97.8% ^{1}H NMR (C_6D_6, 300 MHz) δ 7.73 (d, 2H, Ar-*H*), 7.40 (m, 2H, Ar-*H*), 7.26 (mm, 2H, Ar-*H*), 7.23 (s, 2H, Ar-*H*), 7.14 (mm, 2H, Ar-*H*), 6.98 (mm, 2H, Ar-*H*), 6.78 (mm, 2H, Ar-*H*), 2.66 (s, 6H, N(CH_3)$_2$), 2.16 (m, 2H, CH(CH_3)$_2$), 1.56 (m, 2H, CH(CH_3)$_2$), 1.46 (mm, 6H, CH(CH_3)$_2$), 1.23 (mm, 9H, C(CH_3)$_3$), 0.85 (mm, 12H, CH(CH_3)$_2$) 0.68 (mm, 6H, CH(CH_3)$_2$), ^{13}C{^{1}H} NMR (C_6D_6, 100.54 MHz), δ 163.17 (Ar-*C*), 152.11 (t, Ar-C_{10}), 149.13 (s, Ar-C_4), 147.01 (t, Ar-C_5), 140.07 (Ar-*C*), 130.29 (s, Ar-C_8), 129.52 (s, Ar-C_9), 127.47 (s, Ar-C_2), 126.54 (s, Ar-C_6), 126.12 (t, Ar-C_7), 124.07 (t, Ar-C_1), 119.87 (s, Ar-*C*), 117.16 (s, Ar-C_3), 43.32 (N(CH_3)$_2$), 33.77 (C(CH_3)$_3$), 31.14 (C(CH_3)$_3$), 22.94 (CH-(CH_3)$_2$), 20.50 (CH-(CH_3)$_2$), 20.02 (CH-(CH_3)$_2$), 18.77 (CH-(CH_3)$_2$), 18.58 (CH-(CH_3)$_2$), 17.54 (CH-(CH_3)$_2$), ^{31}P{^{1}H} NMR (C_6D_6, 121.48 MHz) δ 29.74 (s) Anal. Calcd. for $C_{42}H_{57}NNiOP_2$ (%): C, 70.80; H, 8.06; N, 1.97 Found C, 70.95; H, 7.98; N, 1.96.

[1,3-bis(2'-diisopropylphosphino)-4-dimethylaminophenyl]nickel(II)methyl (14)

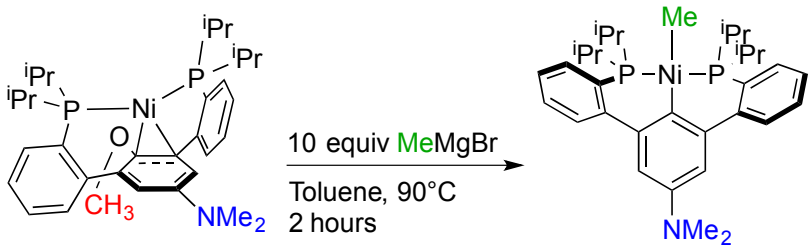

A dark red solution of crude [1,3-bis(2'-diisopropylphosphino)-4-dimethylamino-2-methoxybenzene]nickel(0) (50.1 mg, 0.08 mmol) in toluene was treated with 10 equivalents of MeMgBr and heated to 90 °C in a sealed Schlenk. The tube was heated for 2 hours. After 2 hours the solvent was removed under vacuum giving a orange red solid. The solid was triterated with pentanes and hexanes to precipitate excess Grignard reagent. The resulting slurry was filtered through Celite. (**12**) was obtained from the elute as a yellow solid. Yield: 39.8 mg, 86.2% ^{1}H NMR (C_6D_6, 300 MHz) δ 7.74 (br d, 2H, Ar-*H*), 7.34 (br d, 2H, Ar-*H*), 7.24 (m, 2H, Ar-*H*), 7.10 (m, 2H, Ar-*H*), 6.92 (m, 2H, Ar-*H*), 2.61 (s, 6H, N(CH_3)$_2$), 2.46 (m, 2H, CH(CH_3)$_2$), 1.92 (m, 2H, CH(CH_3)$_2$), 1.05 (s, 24H, CH(CH_3)$_2$), 0.36 (t, 3H, CH_3), ^{13}C{^{1}H} NMR (CD_2Cl_2, 100.54 MHz) δ 152.12 (t, Ar-C_{10}), 150.57 (s, Ar-C_4), 147.49 (t, Ar-C_5), 129.42 (s, Ar-C_7), 128.42 (s, Ar-C_9), 127.78 (s, Ar-C_2), 126.79 (s, Ar-C_6), 125.83 (s, Ar-C_8), 126.41 (s, Ar-C_1), 112.99 (s, Ar-C_3), 40.88 (s, N(CH_3)$_2$), 23.13 (s, CH(CH_3)$_2$), 19.97 (s, CH(CH_3)$_2$), 18.57 (s, CH(CH_3)$_2$), -18.20 (s, Ni-CH_3), ^{31}P{^{1}H} NMR (C_6D_6, 121.48 MHz) δ 44.51 (s) Anal. Calcd. for $C_{33}H_{47}NNiP_2$ (%): C, 68.53; H, 8.19; N, 2.42 Found C, 68.33; H, 8.35; N, 2.15.

Table 2.X. Crystal and refinement data for complexes **2**, *5* and **8**.

	2	*5*	**8**
CCDC Number	859840	859841	
Empirical formula	$C_{33}H_{47}NOP_2Ni$	$C_{32}H_{44}NP_2INi \cdot C_4H_{10}O$	$C_{32}H_{44}ClNNiOP_2$
Formula weight	594.37	764.35	614.78
T (K)	100(2)	100(2)	100(2)
a, Å	10.6162(4)	9.0551(6)	17.0566(7)
b, Å	19.6007(8)	17.5696(12)	10.9300(4)
c, Å	15.6192(6)	11.5133(8)	33.5079(14)
, deg	90	90	90
, deg	103.887(2)	102.374(3)	97.838(2)
, deg	90	90	90
Volume, Å^3	3155.1(2)	1789.2(2)	6188.5(4)
Z	4	2	8
Crystal system	Monoclinic	Monoclinic	Monoclinic
Space group	P2$_1$/*n*	P 2$_1$	P2(1)/n
d_{calc}, g/cm^3	1.251	1.419	1.320
range, deg	2.08 to 33.20	1.81 to 36.41	0.92 to 25.00
μ, mm^{-1}	0.742	1.522	0.842
Abs. Correction	None	Semi-empirical from equivalents	None
GOF	1.604	1.924	1.050
R_1,[a] wR_2[b] [I>2(I)]	R1 = 0.0489, *w*R2 = 0.0501	R1 = 0.0266, *w*R2 = 0.0483	R1 = 0.0570, wR2 = 0.1043

[a] $R_1 = \sum||F_o| - |F_c||/\sum|F_o|$. [b] $wR_2 = [\sum[w(F_o^2-F_c^2)^2]/\sum[w(F_o^2)^2]]^{1/2}$.

REFERENCES

(1) (a) Rosen, B. M.; Quasdorf, K. W.; Wilson, D. A.; Zhang, N.; Resmerita, A.-M.; Garg, N. K.; Percec, V. *Chem. Rev.* **2010**, *111*, 1346. (b) Han, F.-S. *Chemical Society Reviews* **2013**, *42*, 5270. (c) Yu, D.-G.; Li, B.-J.; Shi, Z.-J. *Accounts of Chemical Research* **2010**, *43*, 1486. (d) Mesganaw, T.; Garg, N. K. *Organic Process Research & Development* **2012**, *17*, 29.

(2) (a) Zim, D.; Lando, V. R.; Dupont, J.; Monteiro, A. L. *Org. Lett.* **2001**, *3*, 3049. (b) Dankwardt, J. W. *Angew. Chem. Int. Ed.* **2004**, *43*, 2428. (c) Johnstone, R. A. W.; Neil McLean, W. *Tetrahedron Lett.* **1988**, *29*, 5553. (d) Guan, B.-T.; Xiang, S.-K.; Wu, T.; Sun, Z.-P.; Wang, B.-Q.; Zhao, K.-Q.; Shi, Z.-J. *Chem. Commun.* **2008**, 1437. (e) Tobisu, M.; Shimasaki, T.; Chatani, N. *Angew. Chem. Int. Ed.* **2008**, *47*, 4866. (f) Quasdorf, K. W.; Tian, X.; Garg, N. K. *J. Am. Chem. Soc.* **2008**, *130*, 14422. (g) Quasdorf, K. W.; Antoft-Finch, A.; Liu, P.; Silberstein, A. L.; Komaromi, A.; Blackburn, T.; Ramgren, S. D.; Houk, K. N.; Snieckus, V.; Garg, N. K. *J. Am. Chem. Soc.* **2011**, *133*, 6352. (h) Guan, B.-T.; Wang, Y.; Li, B.-J.; Yu, D.-G.; Shi, Z.-J. *J. Am. Chem. Soc.* **2008**, *130*, 14468. (i) Álvarez-Bercedo, P.; Martin, R. *J. Am. Chem. Soc.* **2010**, *132*, 17352. (j) Tobisu, M.; Yamakawa, K.; Shimasaki, T.; Chatani, N. *Chem. Commun.* **2011**, *47*, 2946. (k) Wenkert, E.; Michelotti, E. L.; Swindell, C. S. *J. Am. Chem. Soc.* **1979**, *101*, 2246. (l) Antoft-Finch, A.; Blackburn, T.; Snieckus, V. *J. Am. Chem. Soc.* **2009**, *131*, 17750.

(3) (a) Vicic, D. A.; Jones, W. D. *J. Am. Chem. Soc.* **1997**, *119*, 10855. (b) Vicic, D. A.; Jones, W. D. *J. Am. Chem. Soc.* **1999**, *121*, 7606. (c) Torres-Nieto, J.; Brennessel, W. W.; Jones, W. D.; García, J. J. *J. Am. Chem. Soc.* **2009**, *131*, 4120.

(4) (a) van der Boom, M. E.; Liou, S.-Y.; Ben-David, Y.; Shimon, L. J. W.; Milstein, D. *J. Am. Chem. Soc.* **1998**, *120*, 6531. (b) van der Boom, M. E.; Liou, S.-Y.; Ben-David, Y.; Vigalok, A.; Milstein, D. *Angew. Chem. Int. Ed.* **1997**, *36*, 625.

(5) (a) Rinaldi, R.; Schuth, F. *Energy Environ. Sci.* **2009**, *2*, 610. (b) Zakzeski, J.; Bruijnincx, P. C. A.; Jongerius, A. L.; Weckhuysen, B. M. *Chem. Rev.* **2010**, *110*, 3552. (c) Hicks, J. C. *J. Phys. Chem. Lett.* **2011**, *2*, 2280.

(6) Sergeev, A. G.; Hartwig, J. F. *Science* **2011**, *332*, 439.

(7) Velian, A.; Lin, S.; Miller, A. J. M.; Day, M. W.; Agapie, T. *J. Am. Chem. Soc.* **2010**, *132*, 6296.

(8) Kelley, P.; Lin, S.; Edouard, G.; Day, M. W.; Agapie, T. *J. Am. Chem. Soc.* **2012**, *134*, 5480.

(9) (a) Zhu, M.; Jalalian, N.; Olofsson, B. *Synlett* **2008**, *2008*, 592. (b) Bielawski, M.; Aili, D.; Olofsson, B. *The Journal of Organic Chemistry* **2008**, *73*, 4602. (c) Bielawski, M.; Zhu, M.; Olofsson, B. *Advanced Synthesis & Catalysis* **2007**, *349*, 2610. (d) Oh, C. H.; Kim, J. S.; Jung, H. H. *The Journal of Organic Chemistry* **1999**, *64*, 1338

(10) (a) Oh, C. H.; Kim, J. S.; Jung, H. H. *The Journal of Organic Chemistry* **1999**, *64*, 1338. (b) Petersen, T. B.; Khan, R.; Olofsson, B. *Organic Letters* **2011**, *13*, 3462.

(11) Li, Z.; Zhang, S.-L.; Fu, Y.; Guo, Q.-X.; Liu, L. *J. Am. Chem. Soc.* **2009**, *131*, 8815.

(12) An η^6-aryl ether nickel complex has been characterized: Campora, J.; del Mar Conejo, M.; Reyes, M. L.; Mereiter, K.; Passaglia, E. *Chem. Commun.* **2003**, 78.

(13) Cámpora, J.; Palma, P.; del Río, D.; Conejo, M. M.; Álvarez, E. *Organometallics* **2004**, *23*, 5653.

(14) van der Boom, M. E.; Milstein, D. *Chem. Rev.* **2003**, *103*, 1759.

(15) (a) Steinke, T.; Shaw, B. K.; Jong, H.; Patrick, B. O.; Fryzuk, M. D. *Organometallics* **2009**, *28*, 2830. (b) Kaufhold, O.; Stasch, A.; Pape, T.; Hepp, A.; Edwards, P. G.; Newman, P. D.; Hahn, F. E. *J. Am. Chem. Soc.* **2008**, *131*, 306.

(16) Reaction of **1** with Ni(II) reagents results in stoichiometric cleavage of the ArO-CH_3 bond. Investigations of this transformation will be reported in a future manuscript.

(17) (a) Ozawa, F.; Ito, T.; Yamamoto, A. *J. Am. Chem. Soc.* **1980**, *102*, 6457. (b) Komiya, S.; Morimoto, Y.; Yamamoto, A.; Yamamoto, T. *Organometallics* **1982**, *1*, 1528. (c) Bryndza, H. E.; Calabrese, J. C.; Marsi, M.; Roe, D. C.; Tam, W.; Bercaw, J. E. *J. Am. Chem. Soc.* **1986**, *108*, 4805.

(18) (a) Blum, O.; Milstein, D. *J. Organomet. Chem.* **2000**, *593-594*, 479. (b) Smythe, N. A.; Grice, K. A.; Williams, B. S.; Goldberg, K. I. *Organometallics* **2008**, *28*, 277. (c) Fafard, C. M.; Ozerov, O. V. *Inorg. Chim. Acta* **2007**, *360*, 286.

(19) (a) Ritter, J. C. M.; Bergman, R. G. *J. Am. Chem. Soc.* **1998**, *120*, 6826. (b) Matas, I.; Cámpora, J.; Palma, P.; Álvarez, E. *Organometallics* **2009**, *28*, 6515.

(20) (a) McCarthy, T. J.; Nuzzo, R. G.; Whitesides, G. M. *J. Am. Chem. Soc.* **1981**, *103*, 3396. (b) Alexanian, E. J.; Hartwig, J. F. *J. Am. Chem. Soc.* **2008**, *130*, 15627.

(21) Pangborn, A. B.; Giardello, M. A.; Grubbs, R. H.; Rosen, R. K.; Timmers, F. J. *Organometallics* **1996**, *15*, 1518.

(22) (a) Pandiarajan, K.; Kabilan, S.; Sankar, P.; Kolehmainen, E.; Nevalainen, T.; Kauppinen, R. *Bulletin of the Chemical Society of Japan* **1994**, *67*, 2639. (b) Lista, L.; Pezzella, A.; Napolitano, A.; d'Ischia, M. *Tetrahedron* **2008**, *64*, 234. c) Schmittel, M.; Ammon, H. *Synlett* **1999**, *6*, 750.

(23) Görl, C.; Beck, N.; Kleiber, K.; Alt, H. G. *Journal of Molecular Catalysis A: Chemical* **2012**, *352*, 110.

(24) Lindsay, D. M.; Dohle, W.; Jensen, A. E.; Kopp, F.; Knochel, P. *Organic Letters* **2002**, *4*, 1819.

(25) Tobe, Y.; Sasaki, S.-i.; Mizuno, M.; Hirose, K.; Naemura, K. *The Journal of Organic Chemistry* **1998**, *63*, 7481.

CHAPTER 3

Examination of the Effect of Arene Electronics on Aryl-Oxygen Bond Activation in Catalytic and Model Nickel(0) Diphosphine Systems

Abstract

Studies of the kinetics of oxidative addition using a series of nickel(0) (diphosphine)aryl methyl ether complexes with electron donating and withdrawing groups were undertaken. The observed rates and activation parameters for aryl-oxygen bond activation were found to be independent of the electronics of the ring the metal is coordinated to. The rate was found to depend on the electronics of the leaving alkoxide. The lack of variation with electronics in the model system is believed to be due to the simultaneous stabilization of the ground state and oxidative addition transition state. Relative rates for the cross coupling of anisoles with the $Ni(II)(PCy_3)_2Cl_2$ catalytic system were obtained for para-substituted anisoles for comparison to the stoichiometric system. Anisoles containing electron-withdrawing groups were found to be cleaved faster than those containing electron-donating groups in the catalytic system. The difference in rates was attributed to the differences in the strength of the nickel arene interactions. This was corroborated with equilibrium studies with substituted arenes.

INTRODUCTION:

Functionalization of the aryl carbon oxygen bonds has emerged as a versatile synthetic tool in organic methodology as phenol precursors are readily available and synthetic modification of the aromatic ring is facile.[1] Aryl carbon oxygen bonds, however, are strong and difficult to activate. Nickel based catalysts have been shown to be versatile in the cleavage of aryl carbon oxygen bonds in a variety of different moieties.[1-8] The cleavage of the aryl carbon oxygen bond can be followed by the coupling of the substrate with a variety of cross-coupling partners.[1,3-7,9] While the mechanism of palladium cross-coupling have been studied extensively, fewer mechanistic studies have been carried out on nickel catalyzed cross coupling systems.[10-13] It is imperative to carry out such studies as nickel and palladium, while both group 10 metals have different reactivity profiles. For example, the smaller more nucleophilic nickel center more readily harnesses phenol-derived and less reactive electrophiles in cross coupling. Furthermore, nickel centers undergo such reactions using less exotic ligands than the palladium counterparts, in some cases ligand free conditions can be used.[1] These factors, combined with its low cost, make nickel an ideal metal for cross coupling and activation of aryl reagents.[1] Detailed mechanistic studies of nickel catalyzed aryl carbon oxygen bond activation will result in the design of better catalysts for said activation, which, as fore mentioned, is important for organic methodology and for other applications such as biomass conversion as Hartwig demonstrated.[14]

Previously we reported a nickel(0) meta-terphenyl diphosphine complex containing an aryl ether functionality on the ipso carbon of the central aryl ring. Using this system it was shown that with heating the Ni center was able to undergo a subsequent oxidative addition, followed by a beta-hydrogen elimination, and an assisted reductive elimination

and decarbonylation.[15] As this system undergoes several steps important to nickel aryl carbon oxygen bond activation relevant to cross-coupling and biomass conversion, studies of the oxidative addition were undertaken using this nickel model system.[1] Herein is described the stoichiometric oxidative addition studies as well as the efforts to compare the model studies with data obtained from nickel catalysts.

RESULTS & DISCUSSION:

Our previously described series of nickel(0) model system, which undergoes a stoichiometric intramolecular reductive cleavage of an aryl oxygen bond, provides an ideal scaffold to study nickel facilitated oxidative addition. Variation of the electronics of the terphenyl backbone can make the observed oxidative addition similar to the activation of substrates with varying aryl electronics. To this end several nickel(0) complexes were synthesized containing different functional groups on the central arene, para to the ipso methyl ether. The functional groups were selected to cover the range of the Hammett parameters with the dimethyl amino group being the most electron donating group (EDG) and trifluoromethyl being the most electron withdrawing group (EWG) (Table 1).

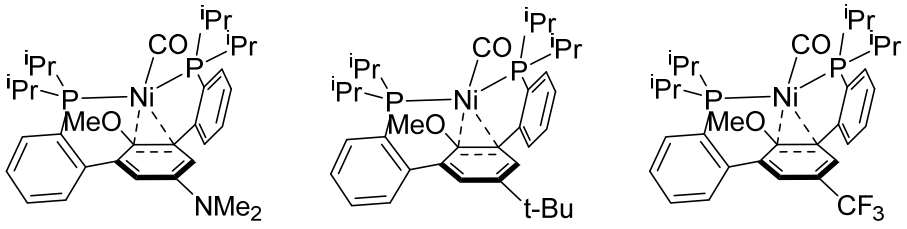

R =	NMe_2	t-Bu	CF_3
σ_p	-0.83	-0.20	0.54
ν_{CO} (cm^{-1})	1912	1919	1943

Table 3.1 Hammett parameters and carbonyl stretching frequencies of **16**, **16**$_{tBu}$, and **16**$_{CF3}$

The EDG and EWG on the central arene should modulate the strength of the metal arene interaction as a more electron deficient ring should have a stronger metal arene interaction. In order to probe the effect of the electronics on the central arene ring the carbonyl complexes **16**, **16**$_{tBu}$, and **16**$_{CF3}$ were synthesized. The carbonyl

stretching frequency will give a measure of the strength of the nickel arene interaction. The carbonyl complexes were synthesized through the decarbonylation of paraformaldehyde by the nickel(0) terphenyl diphosphines **2**, $\mathbf{2}_{t\mathrm{Bu}}$, and $\mathbf{2}_{\mathrm{CF3}}$ in THF. The rates of decarbonylation in **2**, $\mathbf{2}_{t\mathrm{Bu}}$, and $\mathbf{2}_{\mathrm{CF3}}$ varied with the electronics, with NMe_2 being much faster than CF_3. Measuring the carbonyl stretching frequencies of the three nickel variants by IR spectroscopy gave the stretching frequencies listed in table 3.1.

A low carbonyl stretching frequency is indicative of backbonding between the metal and carbonyl. Backbonding occurs between the metal and the π^*-orbital of the C-O bond. Donation into this orbital leads to a weakening of the C-O bond and a strengthening of the M-C bond. Similarly the metal binds to the central arene through donation of electron density into the π^*-orbital of the central arene ring which leads to an elongation of the central arene bond the metal interacts with. As σ_p of the arene increases ν_{CO} increases, which is consistent with less backbonding between the metal and the carbonyl and more backbonding to the arene. The backbonding gives an estimate of the metal arene interation as a stronger interaction leads to a higher ν_{CO} closer to the stretch of free CO (ν_{CO} = 2143 cm^{-1}). The stretching frequencies for the NMe_2 and t-Bu variants are quite low, indicative of a weaker nickel arene interaction. The ν_{CO} stretching frequencies are also very similar (1912 vs. 1919 cm^{-1}) although the Hammett parameters of the two are vastly different ($\sigma_{p\Delta}$ = -0.63). Substitution of a trifluoromethyl group in the central ring as in $\mathbf{16}_{\mathrm{CF3}}$ leads to a stronger nickel arene interaction and conversely a stronger ν_{CO} (1943 cm^{-1}).

The kinetics of oxidative addition in these model systems was investigated. The kinetics are believed to be first order as the observed reaction is **2** going to **3** (Scheme

3.1). **2** was dissolved in d_6-benzene and heated to 45 °C in a J-Young tube. The decay of **2** to **3** was monitored by ^{1}H NMR spectroscopy. Under the described conditions the oxidative addition of the nickel undergoes three half-lives in ca. 14 hours. At 45°C the observed rate of oxidative addition in **2** was found to be 2.09 ± 0.05 min^{-1}, while the k_{obs} for $\mathbf{2_{tBu}}$ was 2.38 ± 0.05 min^{-1}. While the oxidative addition in **2** and $\mathbf{2_{tBu}}$ was facile at 45 °C, oxidative addition was too slow in $\mathbf{2_{CF3}}$. The kinetic studies for the oxidative addition in the **2** and $\mathbf{2_{tBu}}$ suggest that there is little difference between the measured rates.

Scheme 3.1 Oxidative addition in the nickel(0) model system 2

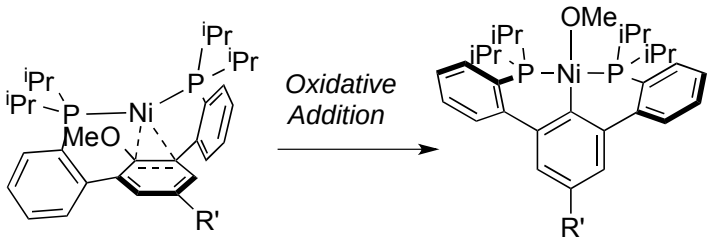

2 R'= NMe_2 **3** R'= NMe_2
$\mathbf{2_{tBu}}$ R'= tBu $\mathbf{3_{tBu}}$ R'= tBu
$\mathbf{2_{CF3}}$ R'= CF_3 $\mathbf{3_{CF3}}$ R'= CF_3

Attempts were also made to study the rate of oxidative addition at higher temperatures. At 80°C the k_{obs} of oxidative addition in **2** was found to be 83 ± 2 min^{-1} while the rates for $\mathbf{2_{tBu}}$ and $\mathbf{2_{CF3}}$ were found to be 72.3 ± 0.4 min^{-1} and 18.3 ± 0.2 min^{-1} respectively. The oxidative addition at 80°C is about 30 times faster than the determined rates at 45°C and the oxidative addition is complete after ca. 40 minutes. After collecting data on the oxidative addition at 45°C and 80°C, an attempt was made to perform a similar ^{1}H NMR kinetic analysis at 60°C. At 60°C, however, during the course of the oxidative addition significant impurities were detected. Analysis of the ^{31}P NMR spectrum collected after the depletion of **2** shows several phosphorus peaks of

unknown identity. In the ^{31}P NMR spectrum peaks, are observed at 38.59, 36.26, 34.15, 30.92, and finally 27.24 ppm (Figure 1). The peaks at 34.15 and 27.24 ppm correspond to **6** and the **3** respectively. The peak at 38.59 ppm corresponds to complex **7** while the peak at 30.92 ppm is assigned to a nickel(II) chloride, which is a decomposition product of the hydride in dichloromethane. The identity of the species that produces the peak at 36.26 ppm in the ^{31}P NMR spectrum was found to be the nickel(0)-carbonyl complex **16** by independent synthesis (Scheme 3.2).

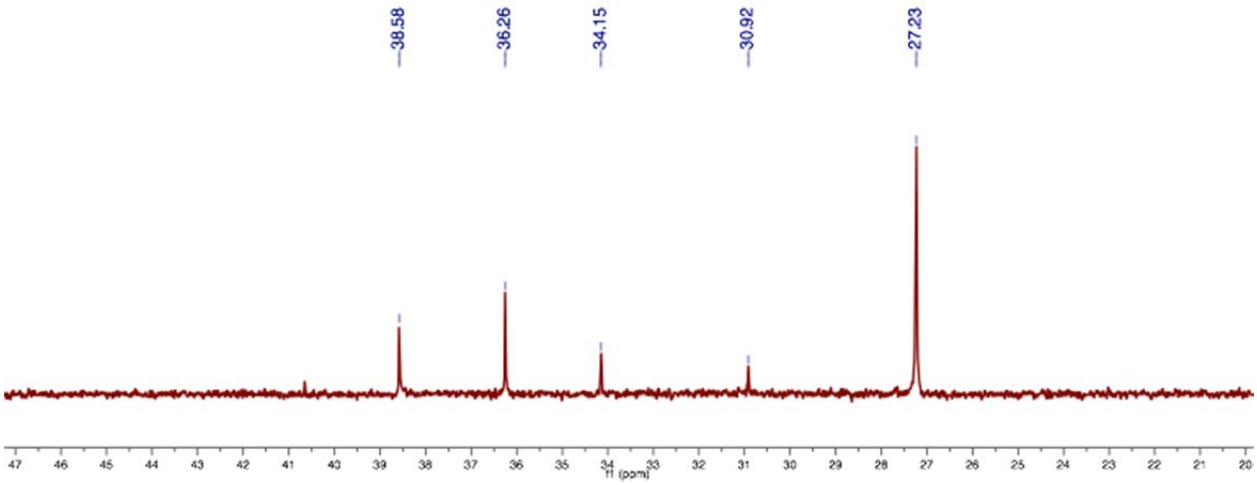

Figure 3.1: ^{31}P{^{1}H} NMR spectrum of the products of **2** at 60°C. 27.23 ppm is **3**. 30.92 ppm possible nickel(II) chloride impurity, 34.15 ppm **6**, 36.26 ppm **16**, and 38.58 ppm is the reductive elimination product of the Ni(II) hydride **7**.

Scheme 3.2 Synthesis of 16 from 2 and formaldehyde

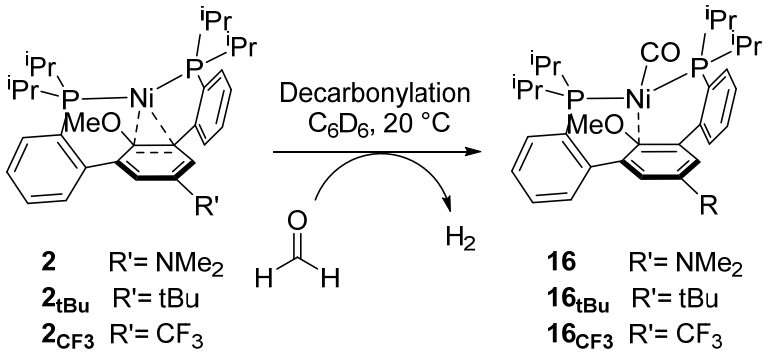

Previously the only reactivity of the nickel(0) diphosphine terphenyl species observed was the described intramolecular oxidative addition. However, **2,** at room temperature, can react with formaldehyde to undergo decarbonylation to form complex **16** (Scheme 3.2). Examination of the ^{1}H NMR for **16** gives a spectrum similar to **6** albeit with an indicative peak at 2.57 ppm, which is identified as the methoxy peak by integration. Both nickel(0)-carbonyl complexes show central aryl ring resonances at similar chemical shifts (6.58 ppm for **16** vs. 6.52 ppm for **6**). IR spectroscopy analysis of the **16** reveals a stretching frequency of 1912 cm^{-1}, which was confirmed by independent synthesis (Table 3.1). This stretching frequency is in the range of **6** and **6$_{tBu}$** (1917 cm^{-1} and 1929 cm^{-1} respectively) albeit lower as an increase in backbonding from the Ni center to the CO is consistent with a more electron rich central arene *vide supra*. **16** is quite stable at the temperatures of the kinetic experiments (no change by ^{31}P and ^{1}H NMR spectroscopy after 9 days at 80°C). Decarbonylation of formaldehyde by **2** is concerning, as the reaction of **2** will increase the observed rate for the oxidative addition, as **2** is participating in two different reactions.

Interestingly, the reaction of the Ni^{0} at 45°C or 80°C produces little of the **16** impurity. Close analysis of the ^{31}P NMR spectra of the reaction at 45°C reveals the

formation of a small amount of the nickel(II) hydride **4** and **16** and minuscule amounts of **7**. Only **16** affects the rate of oxidative addition as it is the only impurity derived from the **2**. The concentration of **16** in solution is miniscule in comparison to the remaining **1** starting material and the oxidative addition product **3**. Similarly at 80°C few impurities are generated and the end product is **6**. It is interesting how the interplay of the relative rates of oxidative addition and the beta-hydrogen elimination allow for the relatively clean reactions at 45°C and 80°C and a messy reaction at 60°C. At 45°C the rate of beta-hydrogen elimination is apparently slow compared to oxidative addition thus hindering the formation of **16**. Increasing the temperature to 80°C drastically increases the rate of oxidative addition which becomes much faster than beta-hydrogen elimination and when formaldehyde is formed from the beta-hydrogen elimination there is no **2** remaining to react with. At 60°C however, beta-hydrogen elimination proceeds at an observable pace and oxidative addition is not fast enough resulting in the generation of significant amounts of formaldehyde which proceeds to undergo decarbonylation with **2** to form the observed complex **16** (Scheme 3.3).

Scheme 3.3 Reactivity of 2 at 60 °C

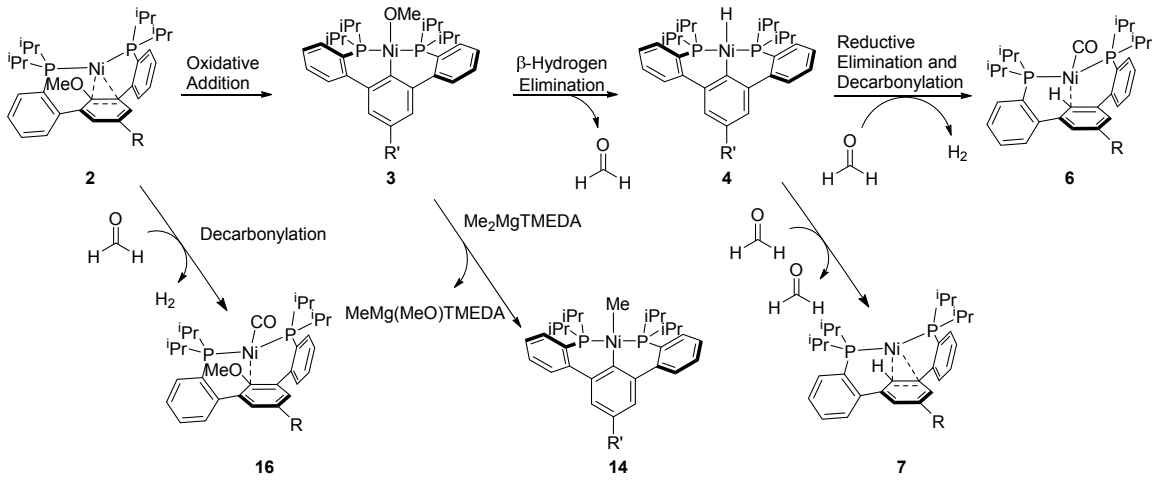

The formation of **16** from formaldehyde significantly hinders the kinetic analysis of the intramolecular oxidative addition of **2**. In order to inhibit the formation of **16**, complex **3** was reacted with a transmetallation reagent to prevent formaldehyde formation (Scheme 3.3). The addition of Me_2MgTMEDA to a solution of **2** produced no reaction at room temperature as determined by ^{31}P and ^{1}H NMR spectroscopy. Heating this mixture to 45°C led to the exclusive formation of a new species at 44.46 ppm by ^{31}P NMR spectroscopy. This species was identified as a nickel(II) methyl complex (**14**) by the upfield triplet at -0.38 ppm in the ^{1}H NMR spectrum. The observed triplet is consistent with a nickel methyl with splitting from the coordinated phosphine groups. It was hypothesized that transmetallation would be fast with respect to oxidative addition and beta-hydride elimination, indeed the reaction of **2** with Me_2MgTMEDA at 80°C for one hour leads to the formation of **14** as the sole product.

Further heating of **14** at 80°C leads to the formation of a new species as identified by ^{31}P and ^{1}H NMR spectroscopy (Scheme 3.4). Heating the Ni-Me complex several hours at 80°C leads to the observation of a new resonance at 36.85 ppm in the ^{31}P NMR spectrum. If the heating is continued for ca. 48 hours complex **14** can be

completely converted to this new species **10**, which was characterized as the product of a reductive elimination of **14** by ^{1}H NMR spectroscopy and ESI-MS. Analysis of the ^{1}H NMR spectrum of **10** shows two indicative peaks, a peak at 1.47 ppm, consistent with the aryl methyl, and a peak for the central arene at 5.76 ppm, which is consistent with the nickel center interacting with the central arene (the central arene of **2** gives a peak at 5.85 ppm by ^{1}H NMR spectroscopy).

Scheme 3.4 Reductive elimination of 14 to form nickel(0) complex 8

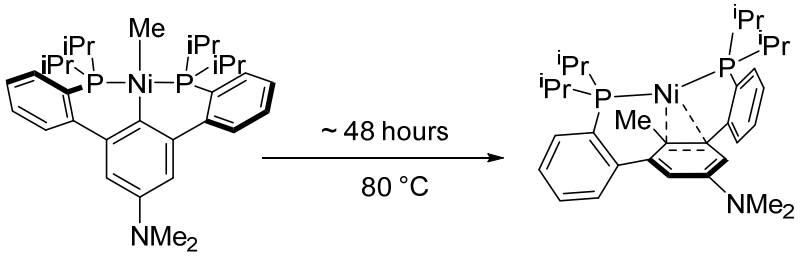

14 **10**

Using Me_2MgTMEDA as a transmetallation agent another attempt was made to measure the kinetics of intramolecular oxidative addition of **2** at 60°C. When 1.2 eq. of Me_2MgTMEDA was used a rate of $k = 10.5\text{x}10^{-3}$ min^{-1} was obtained from observing the decay of **2** by ^{1}H NMR spectroscopy (Table 3.2). To examine the possibility that the Me_2MgTMEDA is somehow affecting the rate of the oxidative addition, the rate was measured using different concentrations of the transmetallation agent. Using 10 and 23 eq. of Me_2MgTMEDA rate constants of $k = 10.2\text{x}10^{-3}$ min^{-1} and $k = 10.7\text{x}10^{-3}$ min^{-1} were obtained respectively. If the Me_2MgTMEDA was affecting the rate constant one would expect to observe a significant change in the rate with increasing concentration of transmetallating agent. From the rate constant data it appears that the addition of Me_2MgTMEDA does not affect the rate constant of oxidative addition in **2** at a given temperature.

Complex	Equivalents of $Me_2MgTMEDA$	Temp °C	k_{obs} (min^{-1})
2	1	60	$10.5x10^{-3}$
2	10	60	$10.2x10^{-3}$
2	23	60	$10.7x10^{-3}$

Table 3.2: Observed rate constants for the oxidative addition of **2** in the presence of varying amounts of $Me_2MgTMEDA$ in C_6D_6 at 60°C.

Rates of Oxidative addition from the Ni^0 model system

As MeMgTMEDA was shown to have no effect on oxidative addition rates of oxidative addition were measured at 45, 70, and 80°C (Figure 3.2) of which the results are shown in table 3.3. The rates at 45 and 80 °C without MeMgTMEDA were found to compare well with rates observed with MeMgTMEDA (2.09 ± 0.05 and 83 ± 2 vs. 2.19 ± 0.05 and 86 ± 3 (x 10^{-3})(min^{-1}) respectively). From these rates the activation parameters $\Delta H^{\ddagger}$ and $\Delta S^{\ddagger}$ were calculated using the linear form of the Eyring correlation (Equation 3.1 B, Figure 3.3, and Table 3.4).

Equation 3.1

A) $$k = \frac{k_B T}{h} \exp\left(\frac{\Delta S^{\ddagger}}{R}\right) \exp\left(-\frac{\Delta H^{\ddagger}}{RT}\right)$$

B) $$\ln\frac{k}{T} = \frac{-\Delta H^{\ddagger}}{R} \cdot \frac{1}{T} + \ln\frac{k_B}{h} + \frac{\Delta S^{\ddagger}}{R}$$

Analogous studies were undertaken using the previously synthesized tert-butyl variant $\mathbf{2}_{t\mathrm{Bu}}$. The rates of oxidative addition were measured in the presence of dimethyl magnesium TMEDA at 45, 60, and 80°C the observed rates and calculated activation parameters $\mathbf{2}_{t\mathrm{Bu}}$ are listed in tables 3.3 and 3.4 respectively. In the case of the para-

trifluoromethyl substituted $\mathbf{2}_{CF3}$ it was observed that the addition of Grignard resulted in the loss of ^{1}H and ^{31}P NMR resonances possibly due to the formation of a paramagnetic species. Due to this reactivity the rates of oxidative addition were obtained without the addition of a transmetallating agent. Fortunately, $\mathbf{2}_{CF3}$ reacts much slower with formaldehyde than either **2** or $\mathbf{2}_{tBu}$. The rates of oxidative addition obtained from $\mathbf{2}_{CF3}$ were found to be only three times slower than that for **2** or $\mathbf{2}_{tBu}$ (Table 3.3).

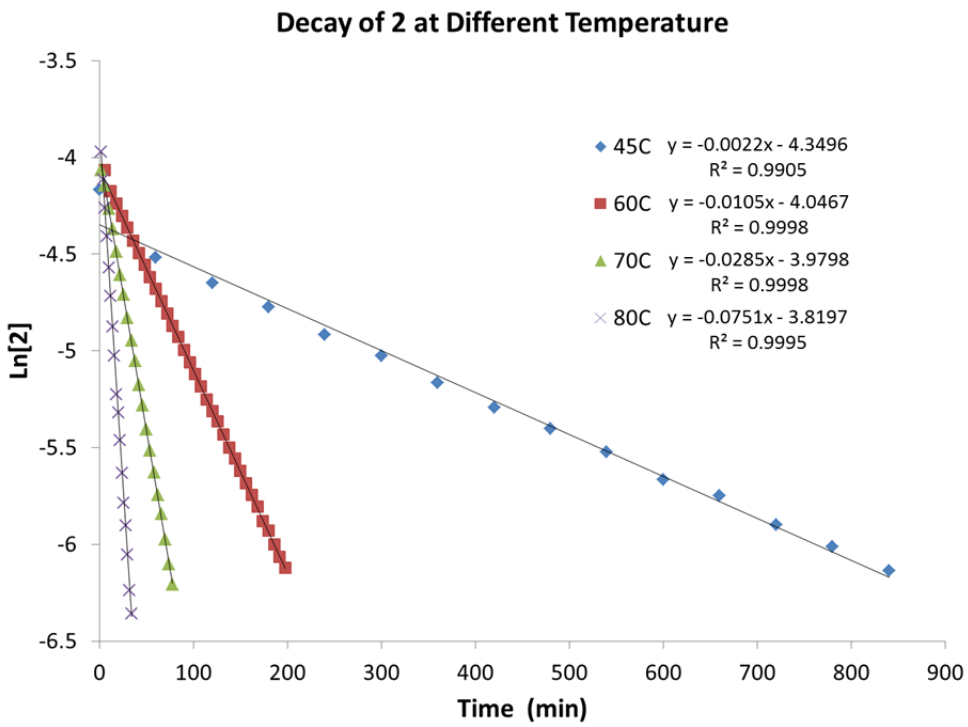

Figure 3.2: Kinetic plots of the first order Decay of **2** at 318, 333, 343, and 353 K.

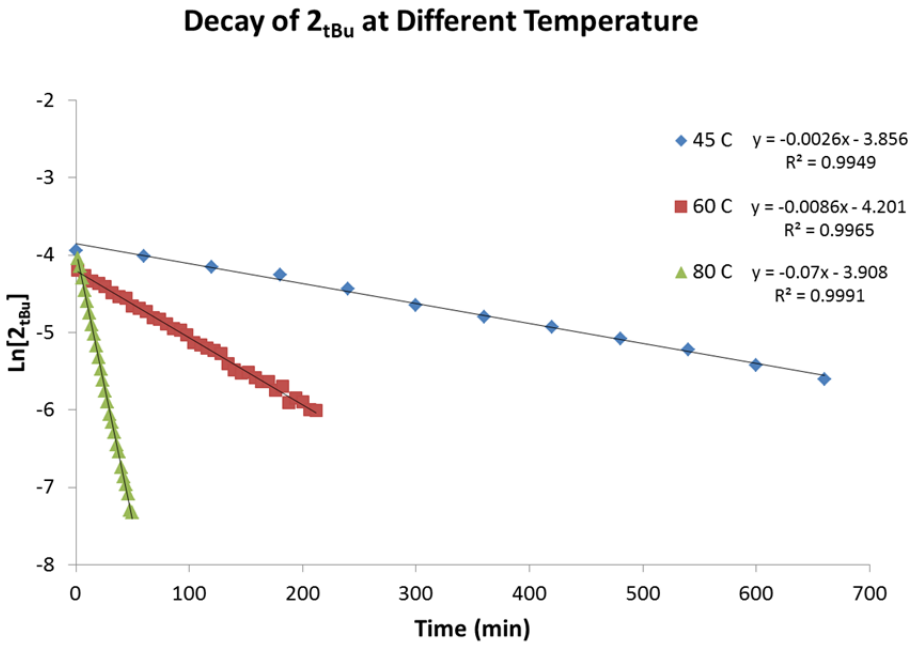

Figure 3.3: Kinetic plots of the first order Decay of $\mathbf{2}_{tBu}$ at 318, 333, and 353 K.

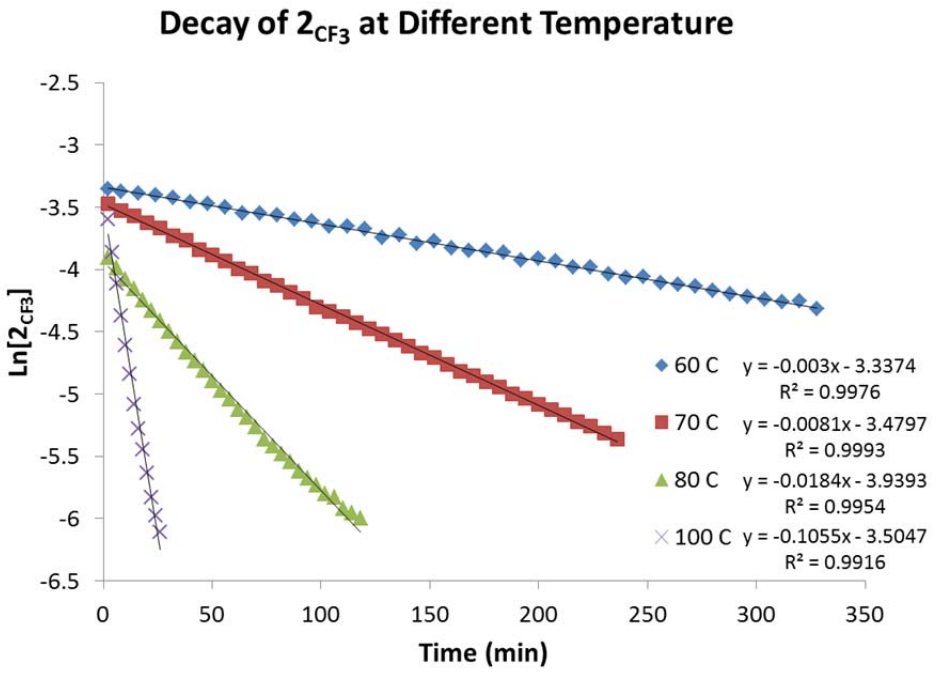

Figure 3.4: Kinetic plots of the first order Decay of 2_{CF3} at 333, 343, 353, and 373 K.

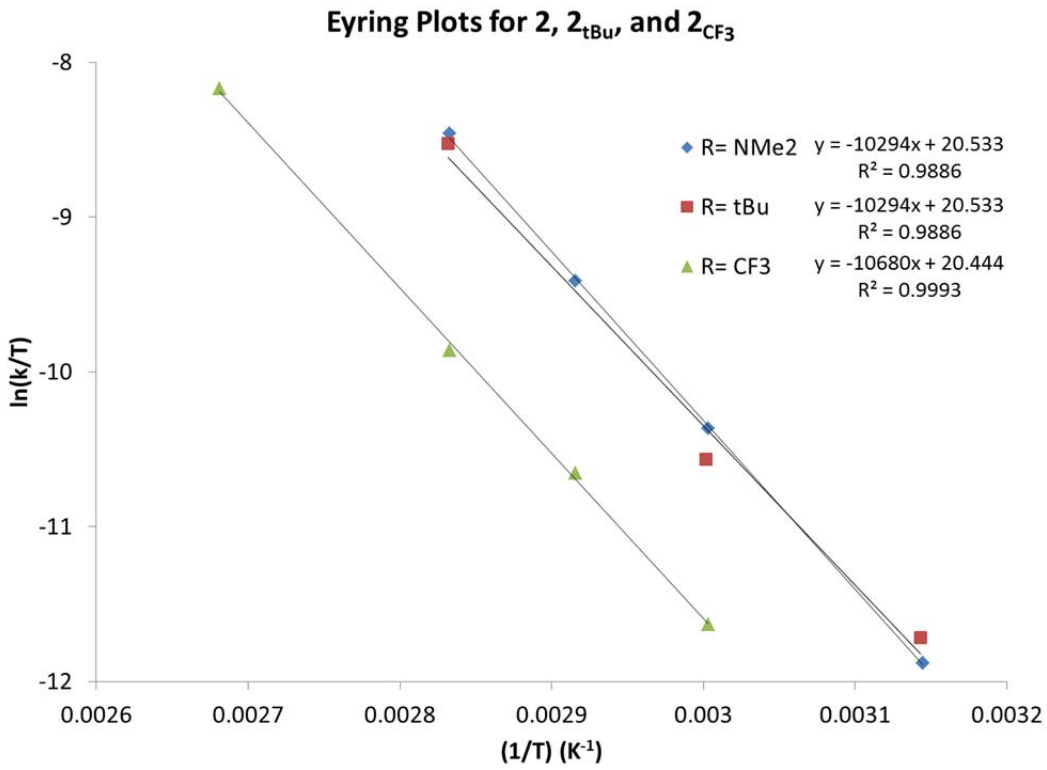

Figure 3.5: Eyring plots of **2**, 2_{tBu}, and 2_{CF3}

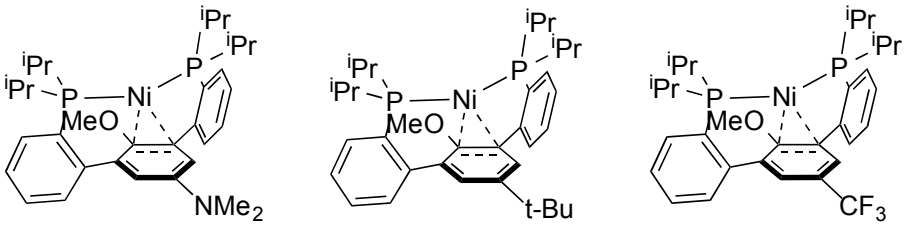

R=	NMe_2	t-Bu	CF_3
T= (K)	k_{obs} (min^{-1}) ($x10^{-3}$)	k_{obs} (min^{-1}) ($x10^{-3}$)	k_{obs} (min^{-1}) ($x10^{-3}$)
318	2.19 ± 0.05	2.58 ± 0.05	-
333	10.2 ± 0.1	8.65 ± 0.09	2.94 ± 0.04
343	28.4 ± 0.1	-	8.05 ± 0.05
353	86 ± 3	70.0 ± 0. 4	18.3 ± 0.2
363	-	-	-
373	-	-	105 ± 3

Table 3.3 Observed rate constants for **2**, $\mathbf{2}_{tBu}$, and $\mathbf{2}_{CF3}$ at different temperatures

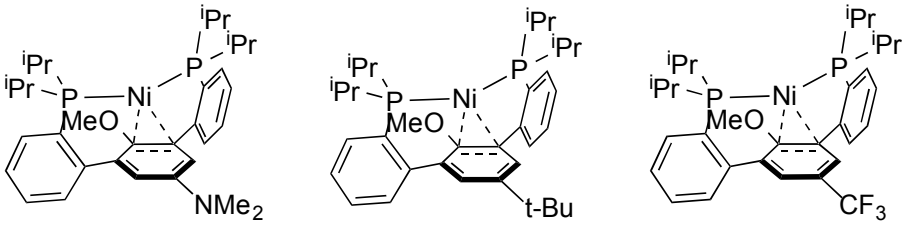

	NMe_2	t-Bu	CF_3
$\Delta H^{\ddagger}$(kcal mol^{-1})	21.7 ± 0.2	20 ± 2	21.2 ± 0.4
$\Delta S^{\ddagger}$(cal K^{-1} mol^{-1})	-2.66 ± 0.03	-6 ± 1	-6.6 ± 0.2

Table 3.4 Calculated activation parameters for **2**, $\mathbf{2}_{tBu}$, and $\mathbf{2}_{CF3}$

As can be seen from table 3.3 the rates of oxidative addition in the model systems are quite similar between the dimethylamino, tert-butyl, and trifluoromethyl groups with the trifluoromethyl group being only three times slower, despite the electronics being significantly different. Consequently the obtained activation parameters are all within error of each other. The similarities of the activation parameters could arise due to a stabilization of the nickel(0) ground state as shown in figure 3.4. This ground state stabilization arises due to the nickel arene interactions.

The nickel arene interactions could also lead to stabilization of the transition state of the aryl oxygen bond activation. But if both the ground state and transition state were stabilized similarly, overall it would appear as if there was little to no effect of electronics, which is the case in the model system. For example, **1** would form a nickel(0) complex (**2**) that is less stable than the trifluoromethyl complex (**2**$_{CF3}$) due to weaker interactions with the central arene ring. From this complex the oxidative addition transition state may be destabilized by a similar energy. This trend of thought could also be applied to **2**$_{CF3}$, stabilization of the Ni^0 and stabilization of the intermediate by similar energies and the activation parameters observed in these complexes would end up being similar (Figure 3.2).

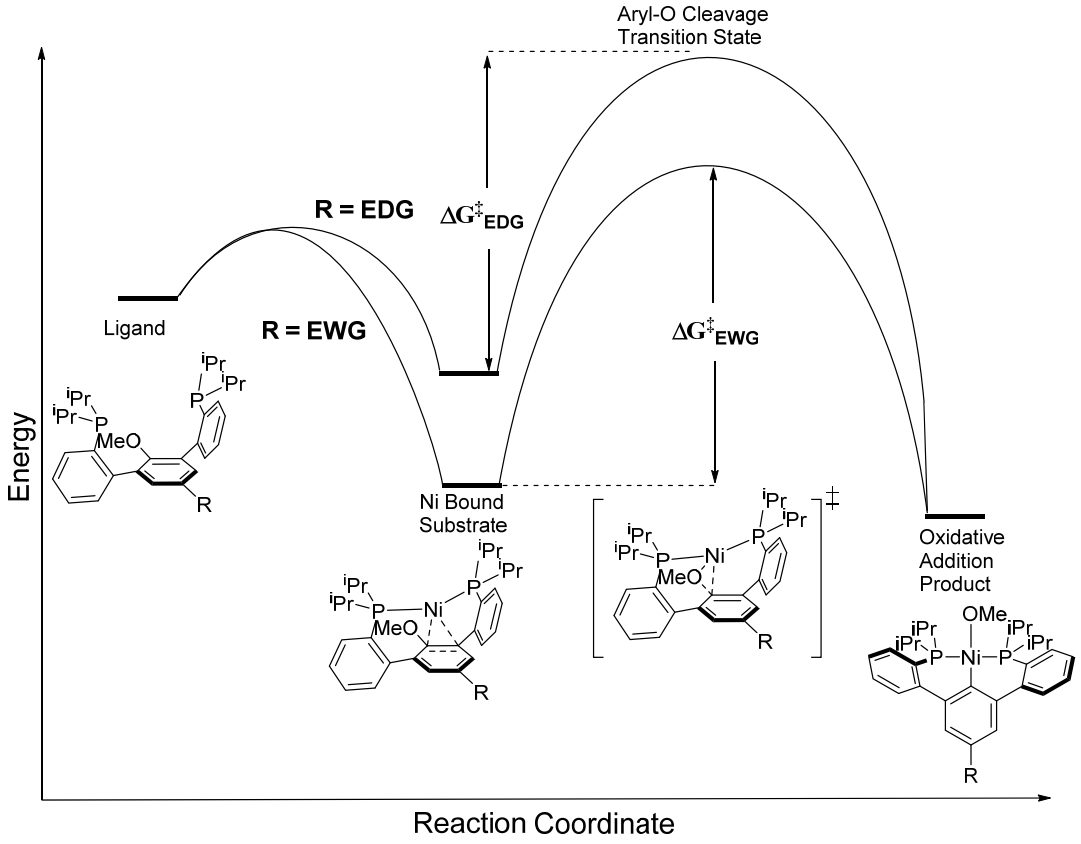

Figure 3.6 Hypothetical reaction coordinate diagram for oxidative addition in the studied nickel(0) model systems.

Given that the observed rate of oxidative addition was found to not be effected by the electronics of the arene that the nickel is coordinated to, an effort was made to change the electronics of the ether on the other side of the oxygen bond. To this end the kinetics of oxidative addition in the nickel(0) terphenyl diphosphine aryl ether complex **15** were investigated. **15** undergoes oxidative addition at 20 °C over the course of several hours to form **13**, and hence cannot be isolated *vide supra*. In order to obtain rates for oxidative addition in **15** a nickel(I) system based on the terphenyl diphosphine aryl ether backbone was used $\mathbf{9^{OAr}}$ (see Chapter 2). The nickel (I) system $\mathbf{9^{OAr}}$ can be synthesiszed via a comproportionation of $Ni(COD)_2$ and $NiCl_2(DME)$ with the diphosphine $\mathbf{1^{OAr}}$. Transmetallation of $\mathbf{9^{OAr}}$ with a Grignard leads to the formation of the reduced nickel complex **15** (presumably analoguous to the reduction observed in the forementioned nickel (I) complexes (see Chapter 2)). This method of generation of **15** was used to study the kinetics of oxidative addition.

Scheme 3.5 Synthesis of $\mathbf{9^{Oar}}$ from diphosphine $\mathbf{1^{OAr}}$

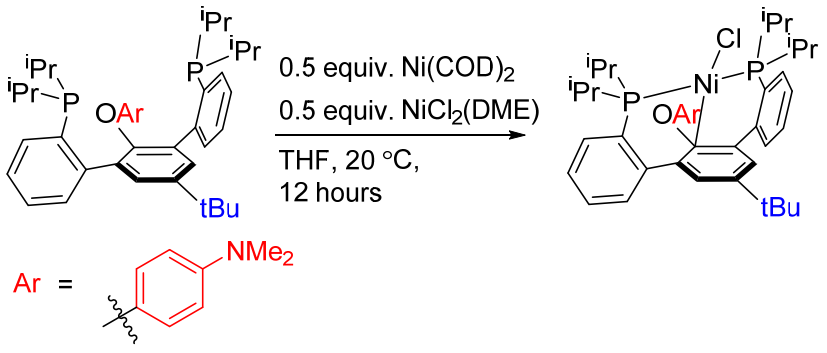

Oxidative addition was measured at 35, 40, 45, and 50°C of which the results are shown in table 3.5. The observed rates of oxidative addition in the aryl aryl ether were found to be about two orders of magnitude faster than the alkyl ethers (Table 3.5). Using the Eyring correlation (Equation 3.1) the activation parameters of the

oxidative addition were calculated as shown in table 3.6. The $\Delta H^{\ddagger}$ was found to be 19.8 ± 0.4 (k_{cal}/mol^{-1}) while $\Delta S^{\ddagger}$ was found to be 0.42 ± 1 (e.u.). The rate increase is believed to be in part due to the electronics of the phenoxide being a better leaving group than an alkoxide leading to faster oxidative addition. While the electronics of the nickel-coordinated arene have little effect on the observed rates the electronics of the ether greatly affect the favorability of oxidative addition.

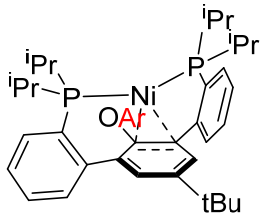

15

Temperature	k_{obs} (min^{-1})
35	0.066
40	0.108
45	0.186
50	0.310

$\Delta H^{\ddagger}$ (k_{cal}/mol^{-1})	19.8 ± 0.4
$\Delta S^{\ddagger}$ (e.u.)	0.4 ± 0.2

Table 3.5 (Left) Observed kinetics of oxidative addition in **15** at different temperatures (Right) Derived activation parameters for **15**

It is known from relative rates of palladium(0) and nickel(0) catalysts that the presence of an electron withdrawing group leads to an increase in the rate of catalysis.[16-19] One way of explaining this phenomenon in light of the data we observe, is that the starting points differ in each case. For our Ni^0 system we start with the metal center already coordinated to the substrate ligand, while in the case of the catalyst the Ni^0 is unbound. In the catalytic systems there is a fast pre-equilibrium which forms the nickel(0) arene adduct. This equilibrium is dependent on the electronics of the aryl substrate. The more electron deficient arenes form a stronger interaction with the

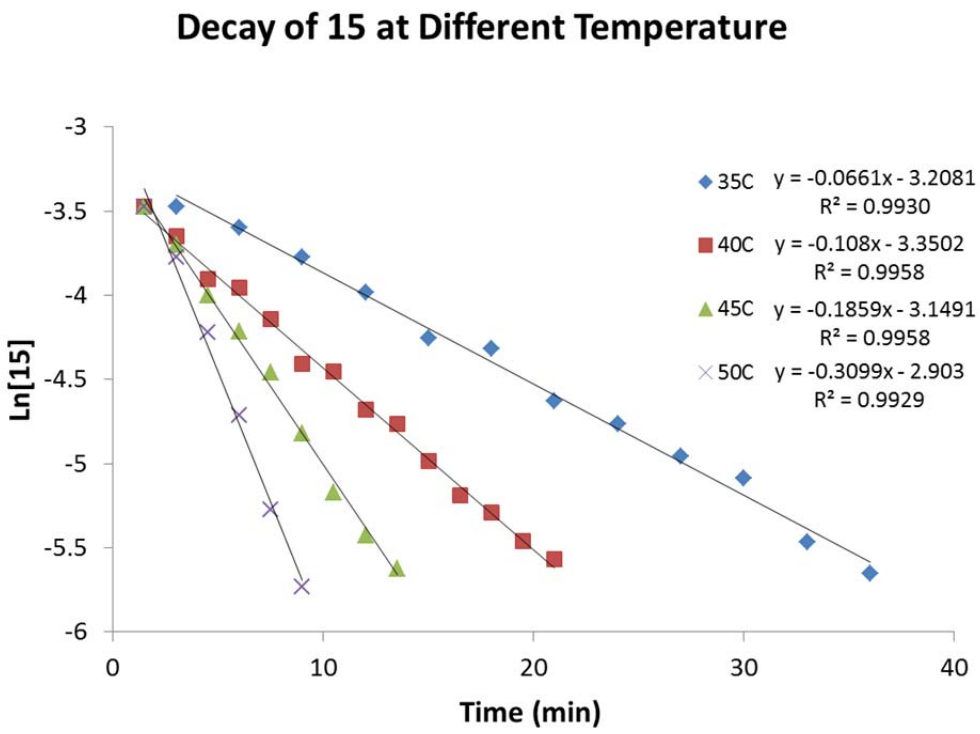

Figure 3.7: Kinetic plots of the first order Decay of **15** at 308, 313, 318, and 323 K.

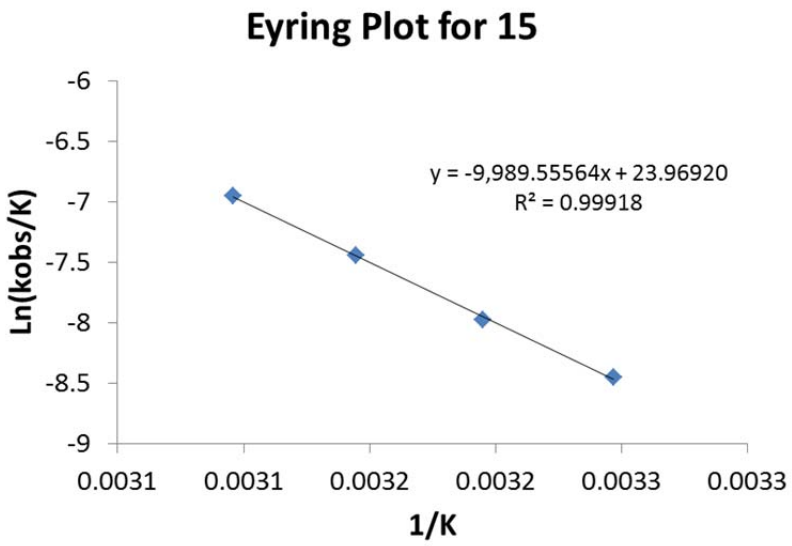

Figure 3.8: Eyring plot of **15**

nickel(0) center as shown with the nickel model systems *vide supra* (Table 3.1). This pre-equilibrium shifts the concentration of the nickel(0) arene species leading to an observed rate increase. In order to better understand the effect of the arene interactions in oxidative addition, studies were shifted from model systems to catalytic systems.

Nickel Catalyst Studies

Studies of oxidative addition in nickel catalyst systems were undertaken using two different nickel systems, the known and versatile cross coupling catalyst $Ni(II)(PCy_3)_2Cl_2$ **(17)**[1-7,9], and the structurally characterized $[Ni(PCy_3)_2]_2N_2$ complex **(18)**.[20] **17** is a known precatalyst for the Kumada coupling of aryl ethers and Grignard reagents (Scheme 3.6). It is proposed that **17** undergoes a sequential transmetallation to form a nickel(0) dialkyl species which undergoes reductive elimination leading to the formation of a nickel(0) species, which is believed to be the active catalyst. As **17** is a known catalyst for oxidative addition of anisoles, conditions similar to those found in literature were used. Initial catalysis screens yielded little to no conversion of the starting anisole. It was initially believed this limited activity could be due to the use of chloride containing Grignard reagents, however it was found that the presence of THF greatly hinders the activity of the catalyst. Removal of the THF from the Grignard reagent or the use of a Grignard containing diethyl ether resulted in catalytic activity. It was found from these initial studies that the trifluoromethyl anisole reacts faster than the dimethyl and tert-butyl variants. Similarly in 1:1 competition reactions conversion was only observed in the trifluoromethyl anisole, which indicates that the nickel

preferentially undergoes oxidative addition with the more electronegative substrate. Through competition reactions relative rates were obtained for a variety of substrates as shown in table 3.6.

Scheme 3.6 Proposed catalytic cycle for the Nickel catalyzed cross coupling of Aryl ethers with Alkyl Grignards

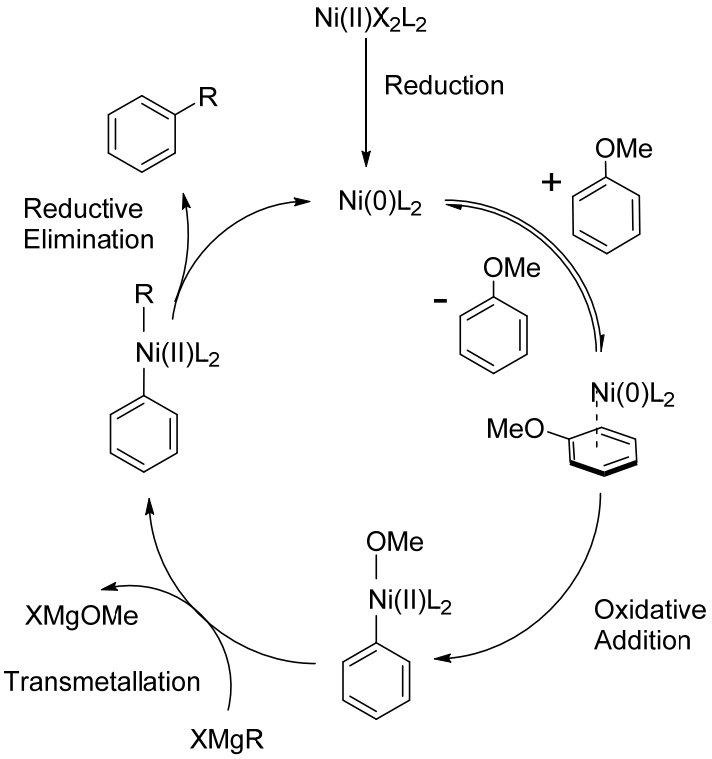

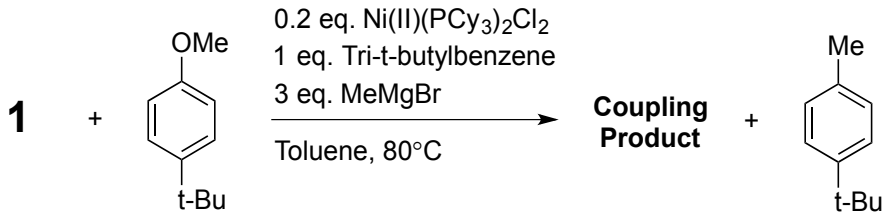

	Relative Rate$_{obs}$
Arene Electronics 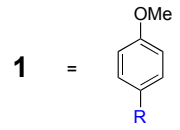	
NMe_2	1.07
CF_3	10.26
Arene Substitution 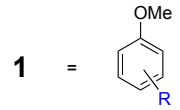	
4-Methyl	1.17
3-Methyl	1.23
2-Methyl	0.91
2,6-Methyl	0.34
Aryl Ether variation 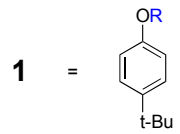	
Ethyl ether	0.90
Isopropyl ether	0.96
Trimethylsilyl ether	5.78
Carbamate	39.28
Arene Variation 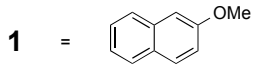	
2-Methoxynapthalene	65.00

Table 3.6 Relative rates obtained from competition reactions. All rates are relative to 4-tertbutyl anisole.

While oxidative addition is well documented for **17** it is not as well documented in the literature for oxidative addition to anisoles. For the catalysis from the $[Ni(PCy_3)_2]_2N_2$ complex **18**, conditions identical to those used for the $Ni(II)(PCy_3)_2Cl_2$ system were used. Gratifyingly, **18** was found to facilitate the coupling between an anisole and an alkyl Grignard in a fashion similar to **17**. In order to further probe oxidative addition in this system, attempts were made to directly observe oxidative addition via ^1H NMR spectroscopy in a similar fashion to the Ni model complexes i.e. a shifting of the arene or methoxy resonances. Unfortunately, no change was observed by ^1H NMR spectroscopy in a 1:1 mixture of tert-butyl anisole with **18** even when heating to 80 °C. Similarly no oxidative addition was observed to take place with trifluoromethyl anisole under similar conditions. While no oxidative addition was observed, the addition of methyl Grignard to a solution containing a catalytic amount of **18** resulted in a conversion of the tert-butyl anisole to the tert-butyl toluene. Surprisingly, one equivalent of the methyl Grignard did not result in a clean conversion of the anisole into toluene. Something similar was observed with aryl Grignards, as homo-coupled arenes were observed after the coupling reaction, when aryl Grignards were used. Although no ethane, the expected by product from methyl Grignard, was observed it is still possible homo-coupling or some other process is taking place.

The relative rates observed with the nickel systems **17** and **18** give a trend of increasing rate of reactivity with electron withdrawing substrates. This is in contrast with what was observed in our nickel model system. The observed rate of increase could be due to the nickel catalytic species having a better metal arene interaction with

the more electron withdrawing substrates as was inferred from the model complex. In order to understand the effects of the substrate pre-equilibrium (Scheme 3.6) the equilibrium constants of different arenes were investigated. One of the problems with the nickel precatalysts **17** and **18**, is the identity of the actual catalyst is unknown. The actual catalyst could be a nickel diphosphine or a nickel monophosphine, which would complicate the observed kinetics and equilibra, as phosphine dissociation/association with the catalytic species would become relevant. As phosphine dissociation/association could be a complicating factor a nickel(0) system containing a chelating diphosphine was used. Nickel(II)$(Cl)_2$(dcpe) (dcpe= 1,2-bis(dicyclohexylphosphino)ethane) can be treated with sodium naphthalene to form nickel(0)(dcpe) naphthalene (**19**) where the nickel has a metal arene interaction with the ring of the naphthalene.

Scheme 3.7 Equilibrium reaction between 19 and Arenes

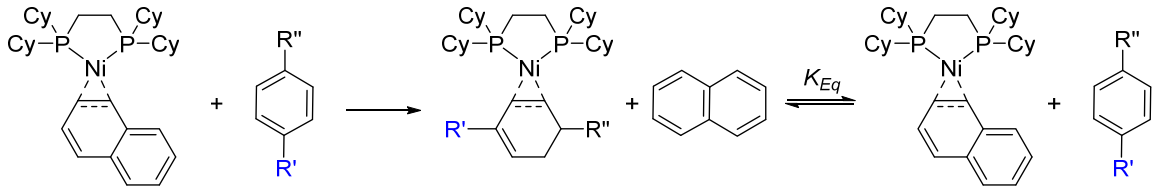

The goal was to measure the equilibrium constants of arene exchange in the nickel complex **19**. Treatment of **19** with large amounts of substituted arenes did indeed lead to arene exchange as observed by ^{31}P NMR spectroscopy (Table 3.7). The more electron withdrawing arenes were found to substitute more easily than less electron withdrawing arenes. Comparing 4-trifluoromethyltoluene and trifluoromethylbenzene one can see that the electron withdrawing groups shift the equilibrium in favor of the arene binding. 4-trifluoromethylanisole was found to bind to nickel more preferentially

than 4-trifluoromethyltoluene. This could be due to interaction with the anisole or due to the anisole moiety while being σ_p donating is actually σ_m withdrawing in comparison to the methyl group (σ_m 0.12 and -0.07 for OMe and Me groups respectively).[21] This would cause the meta position of the ring to be a site of low electron density allowing the nickel to interact with the ring. 1,4-ditrifluoromethylbenzene was found to be one of the few substrates tried that easily displaced naphthalene.

K_{eq}	$Arene_{CF}$
12.1	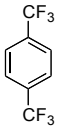
0.003	
0.0015	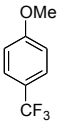
0.0008	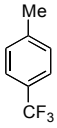

Table 3.7 Equilibrium constants for **19** with listed arenes

The equilibrium constants clearly show that the equilibrium is influenced greatly by the electron withdrawing groups. This provides support for our proposal that the substrate equilibrium plays a part in the rate acceleration observed in the catalytic systems.

CONCLUSIONS:

The kinetics of oxidative addition was studied using the previously studied nickel(0) terphenyl diphosphine model complexes. Formaldehyde was found to negatively affect the kinetics at certain temperatures. Kinetics were carried out in the presence of a Grignard reagent in order to prevent formaldehyde formation. The rates of oxidative addition were found to be similar amongst the three model systems. The trifluoromethyl was only three times slower than the tert-butyl and dimethylamino. Activation parameters were similar across the three complexes. The similarity of the kinetics and activation parameters was postulated to be due to stabilization of the ground state and oxidative addition transition state in the model complex. Unfortunately we were unable to determine the actual rates of oxidative addition in the catalytic systems, but using our model system in conjunction with the catalytic systems we were able to show that oxidative addition in the model system is unaffected by the electronics of the arene. While oxidative addition in the catalytic system shows a significant variance in rate depending on the electronics of the substrate arene, we were able to show that this is in part due to a shifting of the pre-equilibrium of the substrate.

EXPERIMENTAL SECTION:

General considerations: Unless otherwise specified, all compounds were manipulated using a glove box under a nitrogen atmosphere. Solvents for all reactions were dried by Grubbs' method. Benzene-d6 was purchased from Cambridge Isotope Laboratories and vacuum distilled from sodium benzophenone ketyl. All other materials were used as received. $Ni(II)Cl_2(PCy_3)_2$ was purchased from Strem Chemicals as a crystalline solid and was used as received. ^{1}H, ^{13}C, and ^{31}P NMR spectra were recorded on a Varian Mercury 300 spectrometer at ambient temperature, unless denoted otherwise. Chemical shifts are reported with respect to internal solvent: 7.16 ppm and 128.06 (t) ppm (C6D6) and for ^{1}H and ^{13}C NMR data, respectively. ^{31}P NMR chemical shifts are reported with respect to the instrument solvent lock when a deuterated solvent was used. IR spectra were recorded on a Thermo-Fisher Scientific Nicolet 6700 FT-IR spectrometer. Gas chromatography-mass spectrometry (GC-MS) analysis was performed upon filtering the sample through a plug of silica gel. Fast atom bombardment-mass spectrometry (FAB-MS) analysis was performed with a JEOL JMS-600H high-resolution mass spectrometer.

Synthesis of [1,3-bis(2'-diisopropylphosphino)-4-dimethylamino-2-methoxybenzene]nickel(0)carbonyl (16)

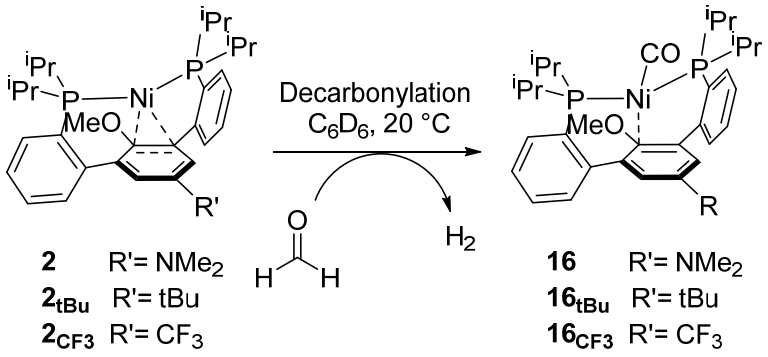

To a solution of **2** (12.3 mg, 0.021 mmol) in C_6D_6 was added 5 equivalents of formaldehyde (3.7 mg, 0.123 mmol). Upon addition hydrogen gas was vigorously evolved as the solution turned from dark red, to red orange in a matter of minutes. The solvent was removed *in vacuo* and the residue was washed with hexanes and eluted with ether. The solvent was removed from the orange ether fraction resulting in an orange residue of **16**.

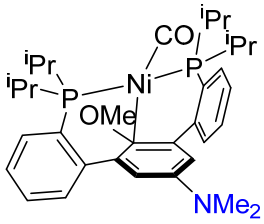

16 Yield: (11.3 mg, 0.018 mmol 87.1 %) ^{1}H NMR (C_6D_6, 300 MHz) δ 7.47 (br m, 4H, Ar-*H*), 7.22 (br m, 4H, Ar-*H*), 6.58 (br s, 2H, Ar-*H*) 2.67 (s, 6H, N(C*H*$_3$)$_2$), 2.57 (s, 3H, OC*H*$_3$), 2.48 (septet, 1H, C*H*(CH$_3$)$_2$), 2.15 (septet, 1H, C*H*(CH$_3$)$_2$), 1.25 (septet, 18H, C*H*(CH$_3$)$_2$), 0.99 (septet, 6H, C*H*(CH$_3$)$_2$), ^{13}C{^{1}H} NMR (C_6D_6, 100.54 MHz) δ 194.01 (t, Ni-*C*O), 149.57 (s, Ar-*C*$_4$), 147.94 (t, Ar-*C*$_{10}$), 138.45 (s, Ar-*C*$_2$), 136.27 (t, Ar-*C*$_5$), 130.33 (s, Ar-*C*$_9$), 129.90 (s, Ar-*C*$_6$), 127.95 (s, Ar-*C*$_8$), 126.97 (s, Ar-*C*$_7$), 122.79 (s,

Ar-*C*$_3$), 113.60 (s, Ar-*C*$_1$), 60.59 (s, Ar-*OMe*), 40.91 (N(*C*H$_3$)$_2$), 29.48 (*C*H-(CH$_3$)$_2$), 26.08 (*C*H-(CH$_3$)$_2$), 19.42 (CH-(*C*H$_3$)$_2$), 19.14 (CH-(*C*H$_3$)$_2$), 18.86 (CH-(*C*H$_3$)$_2$), 18.03 (CH-(*C*H$_3$)$_2$), ^{31}P{^{1}H} NMR δ 36.25 Anal. Calcd. for $C_{34}H_{47}NNiO_2P_2$ (%): C, 65.61; H, 7.61; N, 2.25 Found C, 68.73; H, 7.41; N, 2.09.

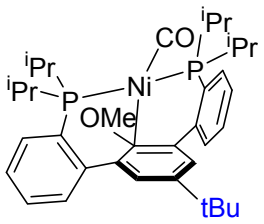

16$_{tBu}$. Yield: (10.2 mg, 0.016 mmol 85.0 %) ^{1}H NMR (C_6D_6, 300 MHz) δ 7.44 (br m, 4H, Ar-*H*), 7.21 (br m, 6H, Ar-*H*), 2.49 (s, 3H, OC*H*$_3$) 2.46 (s, 1H, C*H*(CH$_3$)$_2$), 2.15 (s, 1H, C*H*(CH$_3$)$_2$), 1.43 (s, 6H, N(CH$_3$)$_2$), 1.20 (m, 18H, CH(C*H*$_3$)$_2$), 0.95 (m, 6H, CH(C*H*$_3$)$_2$), ^{13}C{^{1}H} NMR (C_6D_6, 100.54 MHz) δ 194.80 (t, Ni-*C*O), 148.30 (s, Ar-*C*$_4$), 146.26 (t, Ar-*C*$_{10}$), 137.23 (s, Ar-*C*$_2$), 130.65 (t, Ar-*C*$_5$), 130.27 (s, Ar-*C*$_9$), 129.84 (s, Ar-*C*$_6$), 128.67 (s, Ar-*C*$_8$), 126.91 (s, Ar-*C*$_7$), 125.88 (s, Ar-*C*$_3$), 60.21 (s, Ar-*OMe*), 34.15 (*C*(CH$_3$)$_2$), 31.36 (C(*C*H$_3$)$_2$), 29.35 (*C*H-(CH$_3$)$_2$), 25.55 (*C*H-(CH$_3$)$_2$), 19.19 (CH-(*C*H$_3$)$_2$), 18.89 (CH-(*C*H$_3$)$_2$), 18.72 (CH-(*C*H$_3$)$_2$), 17.77 (CH-(*C*H$_3$)$_2$) ^{31}P{^{1}H} NMR δ 35.92

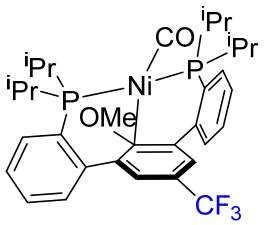

16$_{CF3}$. Yield: (13.4 mg, 0.021 mmol 92.7 %) ^{1}H NMR (C_6D_6, 300 MHz) δ 7.34 (br s, 2H, Ar-*H*), 7.32 (m, 2H, Ar-*H*), 7.23 (m, 2H, Ar-*H*), 7.15 (m, 2H, Ar-*H*), 2.42 (s, 3H, OC*H*$_3$) 2.39 (s, 2H, C*H*(CH$_3$)$_2$), 2.05 (s, 2H, C*H*(CH$_3$)$_2$), 1.11 (s, 12H, CH(C*H*$_3$)$_2$), 1.03 (m, 6H, CH(C*H*$_3$)$_2$), 0.82 (m, 6H, CH(C*H*$_3$)$_2$), ^{13}C{^{1}H} NMR (C_6D_6, 100.54 MHz) δ

195.52 (t, Ni-*C*O), 147.79 (s, Ar-*C*$_4$), 147.58 (t, Ar-*C*$_{10}$), 135.69 (s, Ar-*C*$_2$), 130.14 (t, Ar-*C*$_5$), 139.64 (s, Ar-*C*$_9$), 129.64 (s, Ar-*C*$_6$), 129.17 (s, Ar-*C*$_8$), 127.41 (s, Ar-*C*$_7$), 124.10 (s, Ar-*C*$_3$), 123.91 (Ar-*C*F$_3$), 120.26 (s, Ar-*C*$_1$), 59.96 (s, Ar-*OMe*), 28.78 (*C*H-(CH$_3$)$_2$), 24.78 (*C*H-(CH$_3$)$_2$), 18.82 (CH-(*C*H$_3$)$_2$), 18.52 (CH-(*C*H$_3$)$_2$), 18.42 (CH-(*C*H$_3$)$_2$), 17.44 (CH-(*C*H$_3$)$_2$), ^{19}F{^{1}H} NMR δ -61.30, ^{31}P{^{1}H} NMR δ 37.25 Anal. Calcd. for $C_{33}H_{11}F_3NiO_2P_2$ (%): C, 61.23; H, 6.38; Found C, 55.83; H, 6.12.

Synthesis of bis[bis(tricyclohexylphosphine)nickel] dinitrogen (18)

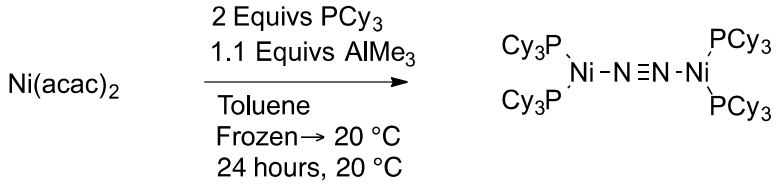

A modified literature procedure was used for the synthesis of **18**.[20] To a freshly thawed mixture of Ni(acac)$_2$ (1.00 g, 3.89 mmol) and tricyclohexylphosphine (2.19 g, 7.81 mmol) in 12 ml of toluene was added a thawed solution of AlMe$_3$ (315 mg, 4.38 mmol) in 3 ml of toluene. Upon addition of AlMe$_3$ the blue green solution turned dark red. The reaction vessel was stoppered and the reaction mixture was stirred for 24 hours. The after 24 hours the stirring was stopped and the reaction mixture was allowed to sit for 3 hours. The slurry was filtered through Celite and the solid was eluted with toluene. The flow through of the filtration was placed in the freezer to promote crystallization/precipitation. The toluene fraction was pumped down to give a dark red solid and was used as isolated. Yield: (814 mg, 1.28 mmol 33.2 %) ^{1}H NMR (C_6D_6, 300 MHz) δ 1.89 (br s, 12H, Cy-*H*), 1.72 (br m, 48H, Cy-*H*), 1.27 (br m, 72H, Cy-*H*) ^{31}P{^{1}H} NMR δ 45.98

Synthesis of 19

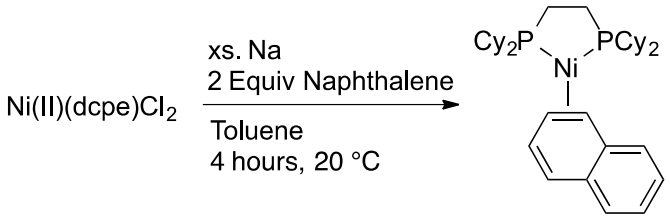

Naphthalene (47.5 mg, 0.37 mmol) was added to a vial containing a sodium mirror (65.3 mg 2.84 mmol) as a solution in THF. The sodium naphthalene solution immediately turned dark forest green. The sodium naphthalene was stirred for 30 minutes. In a separate vial Ni(II)(dcpe)Cl_2 (100.2 mg, 0.18 mmol) was stirred as a slurry in THF. The dark green sodium naphthalene solution was added to the Ni(II)(dcpe)Cl_2 mixture. The solution slurry turned from dark green to yellow and finally to red orange. The mixture was stirred for 45 minutes before filtering through Celite. The solvent was removed resulting in a red orange solid. The residue was washed with pentane and eluted with benzene resulting in 18. Yield: (203.8 mg, 88.2%) ^{1}H NMR (C_6D_6, 300 MHz) δ 7.37 (br s, 2H, Ar-*H*), 7.08 (br s, 2H, Ar-*H*), 5.85 (br d, 4H, Ar-*H*), 1.62 (br d, 32H, (dcpe)-*H*), 1.12 (br s, 20H, (dcpe-*H*), ^{31}P{^{1}H} NMR δ 53.38 (dd, J = 717.9, 81.9 Hz)

Kinetic Studies:

Special considerations: All kinetic data over 45 °C was collected on a Varian INOVA-500 MHz NMR spectrometer and all 45°C kinetic data was collected using a Varian Mercury 300 MHz NMR spectrometer. In all experiments trimethoxybenzene was used as a standard.

Example of a Kinetic Reaction:

In a glove box a J-Young tube was charged with 11.3 mg (0.019 mmol) of **2** and 1.1 mg (0.006 mmol) of trimethoxybenzene in C_6D_6 or d_8-toluene. The J-Young tube was heated to the desired temperature in either an oil bath or in an NMR spectrometer. NMR spectra were collected at regular intervals.

Catalytic Studies:

Special Considerations: All catalytic reactions were performed using 1,3,5-tritert-butylbenzene as an internal standard. All conversions listed were calculated via amounts of analytes based on gas chromatography.

Example of a Catalytic Reaction:

In a glove box a Schlenk tube containing 40.2 mg (0.244 mmol) of tert-butyl anisole , 16.4 mg (0.024 mmol) $Ni(PCy_3)_2Cl_2$, 12.7 mg (0.045 mmol) of PCy_3, and 61.2 mg (0.025 mmol) of 1,3,5-tritert-butylbenzene was charged with 2.7 ml of dry toluene. This solution was allowed to stir for five minutes before 300 µl of MeMgBr (3M in Et_2O) was added via syringe. The slurry immediately turned yellow. The Schlenk was sealed and heated to 80°C for 17 hours after which the reaction was quenched with water and the organics were extracted by DCM. The organic fraction was analyzed via gas chromatography.

Example of an Equilibrium Reaction:

In a glove box a J-Young tube containing 10.3 mg of **19** (0.017 mmol) was treated with 10 equivalents of naphthalene and one equivalent of 1,4-ditrifluorobenzene in C_6D_6. The solution was mixed by shaking. The mixture was analyzed by ^{31}P NMR spectroscopy and the concentration of the resulting species was calculated. Using the observed concentrations of the nickel species and the added concentrations of the naphthalene and substituted benzene the equilibrium constants were calculated.

REFERENCES

1. Rosen, B. M.; Quasdorf, K. W.; Wilson, D. A.; Zhang, N.; Resmerita, A.-M.; Garg, N. K.; Percec, V. *Chemical Reviews* **2010**, *111*, 1346-1416.
2. Álvarez-Bercedo, P.; Martin, R. *Journal of the American Chemical Society* **2010**, *132*, 17352-17353.
3. Guan, B.-T.; Wang, Y.; Li, B.-J.; Yu, D.-G.; Shi, Z.-J. *Journal of the American Chemical Society* **2008**, *130*, 14468-14470.
4. Guan, B.-T.; Xiang, S.-K.; Wu, T.; Sun, Z.-P.; Wang, B.-Q.; Zhao, K.-Q.; Shi, Z.-J. *Chemical Communications* **2008**, 1437-1439.
5. Hie, L.; Ramgren, S. D.; Mesganaw, T.; Garg, N. K. *Organic Letters* **2012**, *14*, 4182-4185.
6. Quasdorf, K. W.; Antoft-Finch, A.; Liu, P.; Silberstein, A. L.; Komaromi, A.; Blackburn, T.; Ramgren, S. D.; Houk, K. N.; Snieckus, V.; Garg, N. K. *Journal of the American Chemical Society* **2011**, *133*, 6352-6363.
7. Quasdorf, K. W.; Tian, X.; Garg, N. K. *Journal of the American Chemical Society* **2008**, *130*, 14422-14423.
8. Tobisu, M.; Yamakawa, K.; Shimasaki, T.; Chatani, N. *Chemical Communications* **2011**, *47*, 2946-2948.
9. Dankwardt, J. W. *Angewandte Chemie International Edition* **2004**, *43*, 2428-2432.
10. Tamao, K.; Sumitani, K.; Kiso, Y.; Zembayashi, M.; Fujioka, A.; Kodama, S.-i.; Nakajima, I.; Minato, A.; Kumada, M. *Bulletin of the Chemical Society of Japan* **1976**, *49*, 1958-1969.
11. Tamao, K.; Sumitani, K.; Kumada, M. *Journal of the American Chemical Society* **1972**, *94*, 4374-4376.
12. Hartwig, J. F. *Inorganic Chemistry* **2007**, *46*, 1936-1947.
13. Culkin, D. A.; Hartwig, J. F. *Organometallics* **2004**, *23*, 3398-3416.
14. Sergeev, A. G.; Hartwig, J. F. *Science* **2011**, *332*, 439-443.
15. Kelley, P.; Lin, S.; Edouard, G.; Day, M. W.; Agapie, T. *Journal of the American Chemical Society* **2012**, *134*, 5480-5483.
16. Littke, A. F.; Fu, G. C. *Angewandte Chemie International Edition* **2002**, *41*, 4176-4211.
17. Stambuli, J. P.; Kuwano, R.; Hartwig, J. F. *Angewandte Chemie International Edition* **2002**, *41*, 4746-4748.
18. Saito, S.; Oh-tani, S.; Miyaura, N. *The Journal of Organic Chemistry* **1997**, *62*, 8024-8030.
19. Amatore, C.; Pfluger, F. *Organometallics* **1990**, *9*, 2276-2282.
20. Jolly, P. W.; Jonas, K.; Krüger, C.; Tsay, Y. H. *Journal of Organometallic Chemistry* **1971**, *33*, 109-122.
21. Corwin, H.; Leo, A.; Taft, R. W.; *Chemical Review* **1991**, *91*, 165-195.

CHAPTER 4

Effect of Lewis Acidic Metals on Aryl-Oxygen Bond Activation in Nickel(0) Diphosphine Model Systems

Abstract

The addition of Lewis acidic metal alkyls to a nickel terphenyl diphosphine aryl ether complex led to an acceleration of the observed aryl oxygen bond activation. It was found that Grignard reagents led to an order of magnitude increase while trialkyl aluminium species led to an up to three orders of magnitude rate increase over the unaccelerated rate. Treatment with trimethyl aluminum at -80 °C led to the observation of a nickel aluminum intermediate. Through low temperature ^{1}H NOESY NMR studies the intermediate was indentified as a complex where the aluminum center is coordinated to the ether moiety of the terphenyl ring on the face *trans* to the nickel center. The kinetics and activation parameters of aryl activation with trimethylaluminum are described and the proposed mechanism is discussed.

INTRODUCTION:

Aryl oxygen bonds are significantly stronger than their aryl halide counterparts making the direct activation of aryl-oxygen substrates challenging.[1] Typically aryl oxygen moieties must be converted to the more reactive phosphinates, sulfunates, or triflates. While catalytic systems are known for the cleavage and cross coupling of aryl-oxygen bonds these systems are typically limited by low turnover numbers or poor reactivity for anisoles.[1] Another strategy for the cleavage of aryl-X bonds is the assisted cleavage of aryl-X bonds in the presence of lewis acidic metals.

Currently there are several different nickel systems for the cross coupling of aryl oxygen bonds.[1] Most of these systems use high temperatures and long reaction times for homogeneous systems. The most common of these systems contain basic phosphines such as tricyclohexylphosphine or carbenes. The common catalytic systems for these activations are $Ni(COD)_2$ with 2 equivalents of PCy_3,[2] $NiCl_2(PCy_3)_2$,[2a 3] or $Ni(COD)_2$ with 2 equivalents of SIPr-HCl or a N-hetrocyclic carbene.[4] Others systems also use less basic phosphines.[5] While the phosphines vary, the presence of the Lewis acid does not. The transmetallation species in these reactions is typically either a Grignard reagent or an alkyl borane both of which are Lewis acidic species which can aid in aryl oxygen bond activation.

Lewis acids have been used in conjuction with nickel catalysts for the activation of nitrile groups. In 1984, Tolman et. al. observed that the catalytic hydrocyanation of olefins by Ni(0) phosphite complexes was changed in the presence of Lewis acids.[3g] This concept was later carried out in the carbocyanation of alkynes by nickel system by Nakao et al. in 2007. What the researchers observed was a large effect of the Lewis

acid on the activation of the arene nitrile bond where the increase in the rate of activation varied with the strength of the Lewis acidity of the additive.[3h] Using aluminum based Lewis acids they were able to determine the crystal structure of one of the intermediate species which among other things, revealed an aluminum center coordinated directly to the nitrogen of the nitrile group while the nickel center coordinated to the pi bond of the nitrile group, showing that the metal centers do indeed react in concert for the activation of the nitrile groups.[3i]

There is also precedence for the use of a secondary Lewis acidic metal center to assist the activation of aryl oxygen bonds in the literature. While the studies are not numerous, there are some reports, such as the catalytic system reported by Hartwig being able to cleave aryl oxygen bonds at lower temperatures with an equivalent of added trimethylaluminum.[4] More extensive studies in this area have been done by Shi et al. who found the presence of a Lewis acidic Grignard reagent allowed for cleavage of the aryl oxygen bond in napthanol and benzylic alcohols.[6] They proposed that the naptholate interacts with multiple Lewis acidic Grignards to form a regular framework. In these frameworks they hypothesized that the coordination would induce reorganization of the electronic structure of the phenolic aryl-oxygen bond (Figure 1).

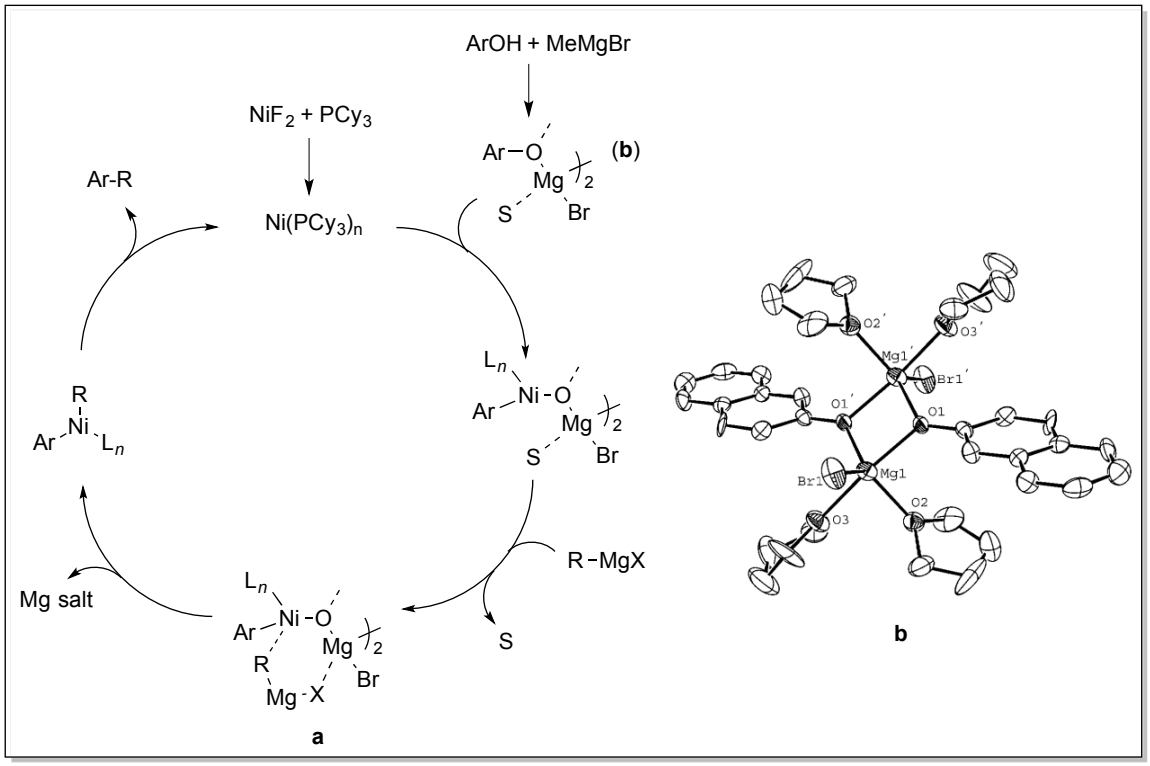

Figure 4.1: a: Catalytic cycle of Ni(0) catalyst with magnesium napthalate substrate. b: X-ray crystal structure of magnesium napthalate dimer.

This reorganization of electron density would activate the aryl oxygen bond for cleavage. Essentially, the metals would act both as electron withdrawing groups, simultaneously weakening the oxygen carbon bond and making the oxygen moiety a better leaving group. However, they noted that phenol derivatives did not successfully undergo this transformation.[6a]

More recently the Shi group extended this research to non-metallic Lewis acids.[6b] Using aryl boronic reagents the Shi group could observe a similar effect on the activation of phenolates. The addition of excess boronic reagents and triethyl borane leads to a similar effect as the Grignards on the phenolates. It is postulated that there is a double Lewis acid effect on the phenolate as they propose that both the boronic

acid and the triethyl borane contribute Lewis acidic effects on the phenolic aryl oxygen bond.

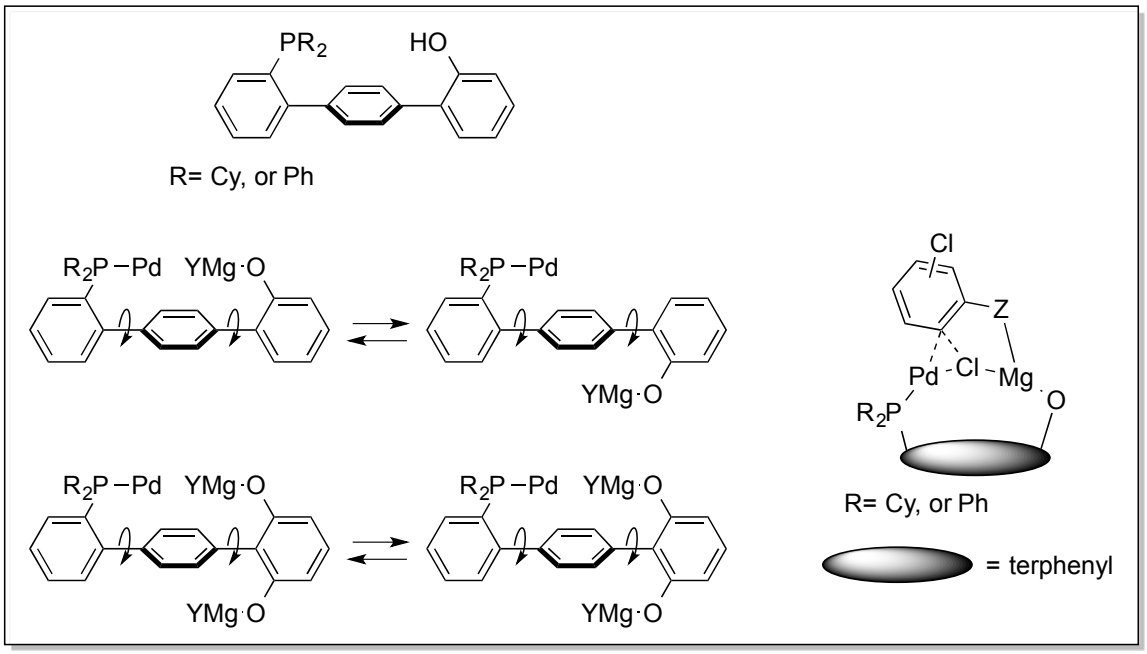

Figure 4.2: Palladium magnesium bimetallic system for the directed activation of aryl halide bonds

Some bimetallic systems have been developed where the Lewis acidic metal center has been used to impart selectivity on the activation of aryl heteroatom bonds. For example Manabe et. al. explored the use of a Lewis acid to guide the reactivity of a palladium center in oligoarene and terphenyl systems.[7] Their terphenyl system contains a phosphine arm and a phenolic arm. The phosphine arm is envisioned to bind a palladium(0) metal center for arene heteroatom bond activation while the phenolic arm is envisioned to bind a Lewis acidic Grignard reagent (Figure 5).

Using this system, Manabe et al. they were able to activate ortho arene heteroatom bonds on phenolate substrates preferentially to any other ortho arene

bonds. They proposed that substrate binds to the magnesium coordinated to the phenolic arm of the ligand allowing for the ortho positions of the substrate to be accessible to the palladium(0) center.[44] Substitution of both sides of the phenol arm led to an increase in the bond selectivity providing more support for their proposed mechanism and reactivity.[7d]

As these examples have shown the cleavage of aryl oxygen bonds can be activated through the use of a bimetallic system containing an electron-rich nickel center to coordinate the arene and a Lewis acidic metal to help activate the substrate. However systematic studies on the effect of the Lewis acid and the acceleration of the rate have not been undertaken. Such studies as described would allow for the development of better heterometallic catalysts for the cleavage of aryl oxygen bonds. As our group has recently developed a nickel(0) model system. In this model system the nickel readily undergoes oxidative addition giving us a unique platform from which to probe oxidative addition facilitated by nickel mechanistically and kinetically. With this in mind we extended our studies to aryl oxygen bond activation in the presence of Lewis acids. Herein is described the studies of Lewis acidic accelerated aryl oxygen bond activation in a nickel(0) model system.

RESULTS & DISCUSSION:

In our investigations of the rate of aryl-oxygen bond activation in nickel(0) diphosphine aryl ether complexes we have observed a rate acceleration in the presence of Grignard reagents. The treatment of **2** with ten equivalents of MeMgBr in toluene leads to an order of magnitude rate increase in the aryl-oxygen bond activation (Scheme 4.1, Table 4.1, and Figure 4.3). Interestingly, the addition of one to twenty three equivalents of Me_2MgTMEDA does not lead to a rate increase in aryl-oxygen bond activation *vide supra*. This is postulated to be due to the Lewis acidity of the metal as has been observed in other systems. The less Lewis acidic Me_2MgTMEDA does not lead to acceleration due to the bidentate ligand TMEDA, which effectively quenches the Lewis acidity of the metal center. Indeed the treatment of **2** with ten equivalents of MeMgBr in the presence of THF does not lead to an increase in the rate of oxidative addition. This is consistent with the coordinating solvent THF binding to the Grignard reagent, resulting in a less Lewis acidic metal center. It is possible that the MeMgBr is coordinating to the methoxy moiety of the terphenyl backbone weakening the oxygen arene oxygen bond and simultaneously making the methoxy a better leaving group leading to an accelerated oxidative addition forming a nickel(II) species. This nickel(II) can either be transmetallated by the coordinated Grignard reagent (a concerted process between the methoxy Grignard adduct) or transmetallated via another equivalent of the Grignard.

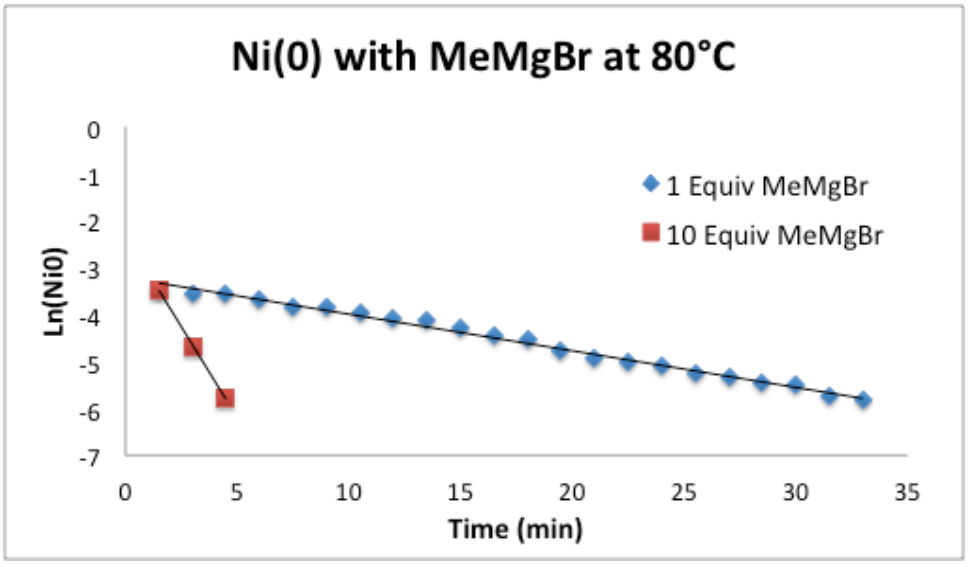

Figure 4.3: Rate acceleration of aryl-oxygen bond activation in 2 with 1 and 10 equivalents of MeMgBr.

	T(°C)	k_{obs} (min^{-1}) (x10^{-3})
Ni^0 w/1 Equiv MeMgBr	80	78
Ni^0 w/1.25 Equiv $Me_2MgTMEDA$	80	70
Ni^0 w/10 Equiv MeMgBr	80	774

Table 4.1: Rate acceleration of aryl-oxygen bond activation in 2

Scheme 4.1: Reactivity of 2 with excess Grignard reagent

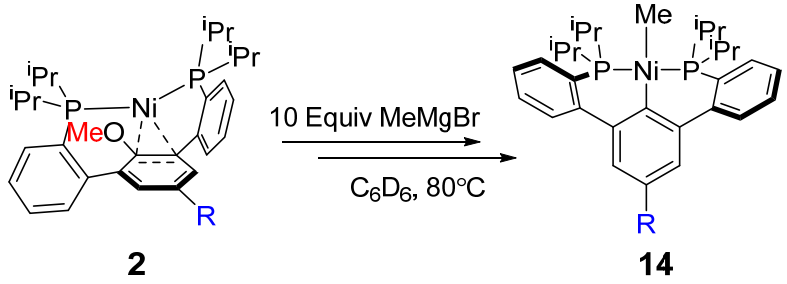

Intrigued by the results with MeMgBr the effect of other Grignard reagents were investigated. It was found that other alkyl and aryl Grignard reagents also accelerate the rate of oxidative addition in **2**. Ethyl, phenyl, benzyl, and mesityl

Grignards all resulted in rate increases. It was quite surprising that the bulkier Grignards (mesityl and phenyl) still resulted in an observed increase in rate.

Emboldened by the effect of Grignard reagents on aryl oxygen bond activation, other Lewis acids were tested for similar effects. The addition of MeLi lead to an increase in rate similar to what was observed with Grignard reagents. Surprisingly diethyl, dimethyl, and dipentafluorobenzyl zinc species did not result in an increase in aryl oxygen bond activation. Similarly metal tert-butoxides (Li, Na, and K) did not result in an increase in rate. It was proposed that the solubility of the metal tert-butoxides might inhibit their effect on the reactivity of the nickel complex, however, while changing the solvent to difluorobenzene did increase the amount of solubilized tert-butoxide the rate of aryl-oxygen bond activation was not found to increase. Even when a more soluble metal alkoxide was used (potassium 2-methylbutan-2-olate) no effect was observed. Several Lewis acidic metal salts were tried (MgX_2, FeX_3, FeX_2, $AlCl_3$, and CrX_3) however the salts were found to be insoluble under the reaction conditions and while difluorobenzene did seem to increase the amount of the metal salt solubilized the rate of aryl-oxygen bond cleavage was found to be the same as the rate without additive. Although no rate acceleration was observed, the addition of $AlCl_3$ did result in the formation and precipitation of a dark solid, which did not change upon heating. Hydrolysis of this solid with HCl and investigation of the oragnics by ESI mass spectrometry revealed the mass of the free diphosphine terphenyl anisole showing that the aryl-oxygen bond had not been cleaved.

Unexpectedly, the addition of alkyl boranes did not lead to increased reactivity in **2**. Alkyl boranes have been shown to increase oxidative addition in nickel catalytic systems for the activation of cyano groups and other catalytic systems.[8] Fortunately, the

addition of alkyl aluminum reagents led to increased rate of oxidative addition in **2**.[8c,8d,9] Addition of one equivalent of $AlMe_3$ lead to complete conversion of **2** into the previously characterized **14** (oxidative addition followed by a subsequent transmetallation) within minutes (Scheme 4.2). Without any additive the **2** undergoes complete conversion to the **3** within approximately seven days at 20 °C. This leads to an estimate of a three order of magnitude rate increase for the addition of $AlMe_3$.

Scheme 4.2: Addition of $AlMe_3$ to 2 leads to a room temperature aryl oxygen bond activation

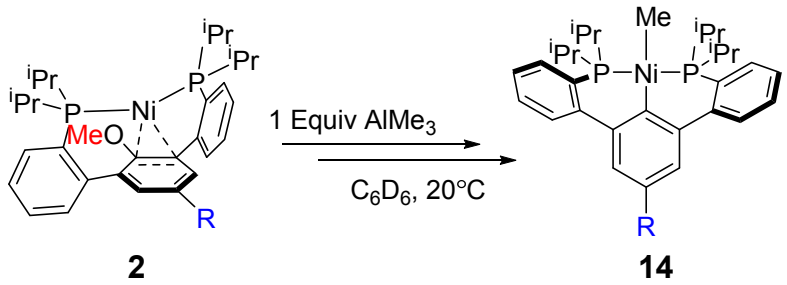

2 **14**

The addition of other alkyl aluminum reagents also leads to an observed rate increase. $AliBu_3$, $AlEt_3$, and $AlPh_3$ all lead to a rate acceleration for the formation of a nickel(II) species. The $AlPh_3$ lead to significantly slower rates than that observed for the aluminum alkyls ($AlMe_3$, $AliBu_3$, and $AlEt_3$), possibly due to the steric bulk of the triphenyl species.

In order to better understand the observed effect of Lewis acidic additives, studies were undertaken to better understand the binding of AlR_3 to the nickel(0) system and the method of aryl-oxygen bond activation. To test if nickel was required for the aryl-oxygen bond activation the diphosphine terphenyl anisole (**1**) was treated with ten equivalents of $AlMe_3$. Upon mixing a new species formed as observed by NMR spectroscopy. ^{1}H NMR shows shifts in the isopropyl methyls and methine

protons, where one methine shows a large shift upfield from 1.87 ppm to 1.18 ppm. Upfield shifts are also observed for the -NMe_2 and –OMe functional groups from 2.60 to 2.25 ppm and 3.10 to 2.63 ppm respectively. ^{31}P NMR shows two broad peaks at 18.25 and -4.82 ppm. The spectroscopic data is consistent with the aluminum coordinating to the diphosphine terphenyl anisole. There are multiple points where the $AlMe_3$ could coordinate, either through the methoxy group, the dimethyl amine, or through the phosphines. Coordination through the methoxy or dimethyl amine would not account for the large phosphorous shift in the ^{31}P NMR. It is likely that the $AlMe_3$ is coordinating through the phosphine, although coordination of multiple equivalents of $AlMe_3$ could be possible. Regardless, hydrolysis of this adduct results in the recovery of **1**. Trimethylaluminum does not cleave the aryl oxygen bond in the absence of nickel (Scheme 4.3).

Scheme 4.3: Reactivity of $AlMe_3$ with 1

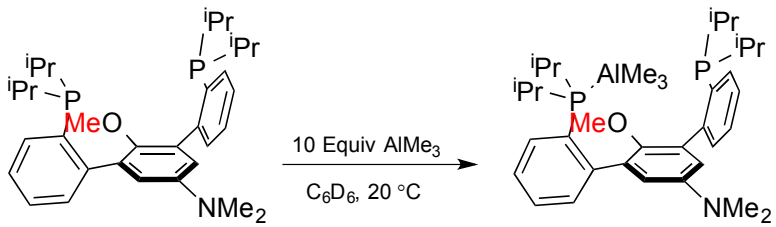

1

As nickel is required to cleave the aryl-oxygen bond it is possible that AlR_3 coordinates through nickel and the adduct cleaves the aryl-oxygen bond. To this end a nickel(0) diphosphine meta-terphenyl containing no *ipso*- or *para*- functionalities (**7$_H$**) was treated with $AlMe_3$. The addition of $AlMe_3$ leads to no change in the nickel complex as observed by NMR spectroscopy (Scheme 4.4). This suggests that the nickel does not interact with an added AlR_3 in the absence of the ligand functionalities.

Scheme 4.4: Reactivity of $AlMe_3$ with 7_H

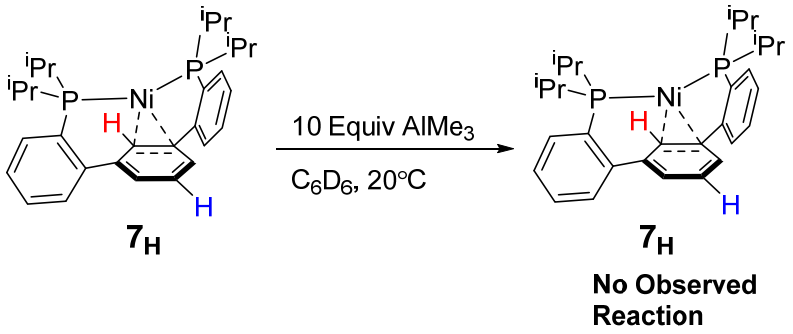

Introduction of a $-NMe_2$ group in the *para*- position of the ligand backbone (**7**) leads to the observed coordination of $AlMe_3$ by spectroscopy. An upfield shift is observed for the $-NMe_2$ group resonance from 2.58 ppm to 2.36 ppm upon coordination. A similar shift is observed in the resonance of the *ipso*- proton from 5.37 to 4.85 ppm, while the while the central arene resonance shifts downfield from 5.83 to 6.04. There is a small shift of 2.8 ppm by ^{31}P NMR spectroscopy (38.55 to 41.33 ppm upon $AlMe_3$) indicating there is not much interaction of $AlMe_3$ with the phosphines in the nickel(0) model complexes. The shifts observed upon $AlMe_3$ coordination are mainly localized to the central arene ring of the terphenyl backbone in **7**, which leads to the proposal that the added aluminum is interacting with the free lone pair on the $-NMe_2$ group (Scheme 4.5).

Scheme 4.5: Coordination of $AlMe_3$ to 7 through the NMe_2 moiety

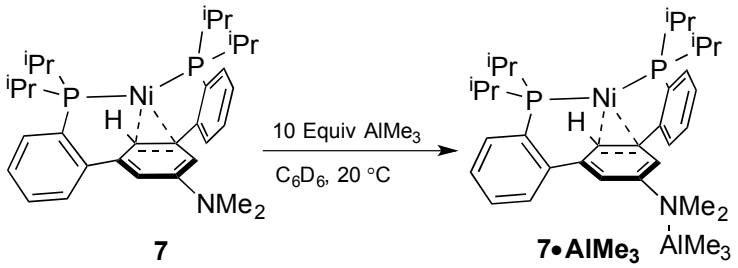

7 **7•AlMe$_3$**

When the backbone contains a –NMe_2 group the AlR_3 coordinates to the –NMe_2 group, however it is not clear how that will accelerate the aryl-oxygen bond activation. Changing the *para*= group to a tBu should prevent *para*- coordination. As a tBu group should eliminate *para* coordination and binding is not observed in the absence of any groups, complex **2$_{tBu}$** should allow us to test for coordination of AlR_3 to the methoxy moiety of the terphenyl backbone. Treatment of **2$_{tBu}$** with ten equivalents of $AlMe_3$ leads to the formation of **13$_{tBu}$**. As the methoxy group is the only group capable of binding $AlMe_3$ (*vide supra*) this provides evidence that the $AlMe_3$ (and other AlR_3 or Lewis acidic reagents) is coordinating to the methoxy group when accelerating the rate of oxidative addition (Scheme 4.6).

Scheme 4.6: Addition of $AlMe_3$ to 2$_{tBu}$

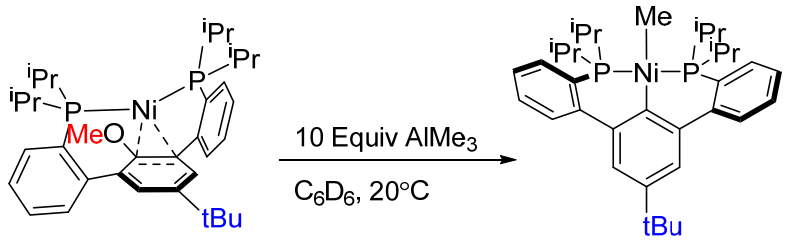

2$_{tBu}$ **14$_{tBu}$**

Low temperature NMR spectroscopy studies were carried out in an attempt to observe intermediates in the Lewis acid accelerated aryl oxygen bond activation. At -80 °C, **2$_{tBu}$** gives a broad ^{1}H NMR spectrum with –OMe and central arene resonances at

3.19 and 6.44 ppm respectively. The addition of one equivalent of $AlMe_3$ leads to a downfield shift in the methoxy resonance to 3.39 ppm and an upfield shift in the central arene resonances to 6.15 ppm. A curious downfield shift is observed for the ortho protons of the outer terphenyl rings from 7.73 to 8.00 ppm upon $AlMe_3$ coordination (Figure 4.4). This intermediate is stable surprisingly stable at low temperatures, at -80 °C no decomposition was observed after eight hours. Warming leads to aryl-oxygen bond activation and formation of $\mathbf{14_{tBu}}$. No other intermediates are observed by 1H NMR for the conversion of the nickel aluminum intermediate to $\mathbf{14_{tBu}}$.

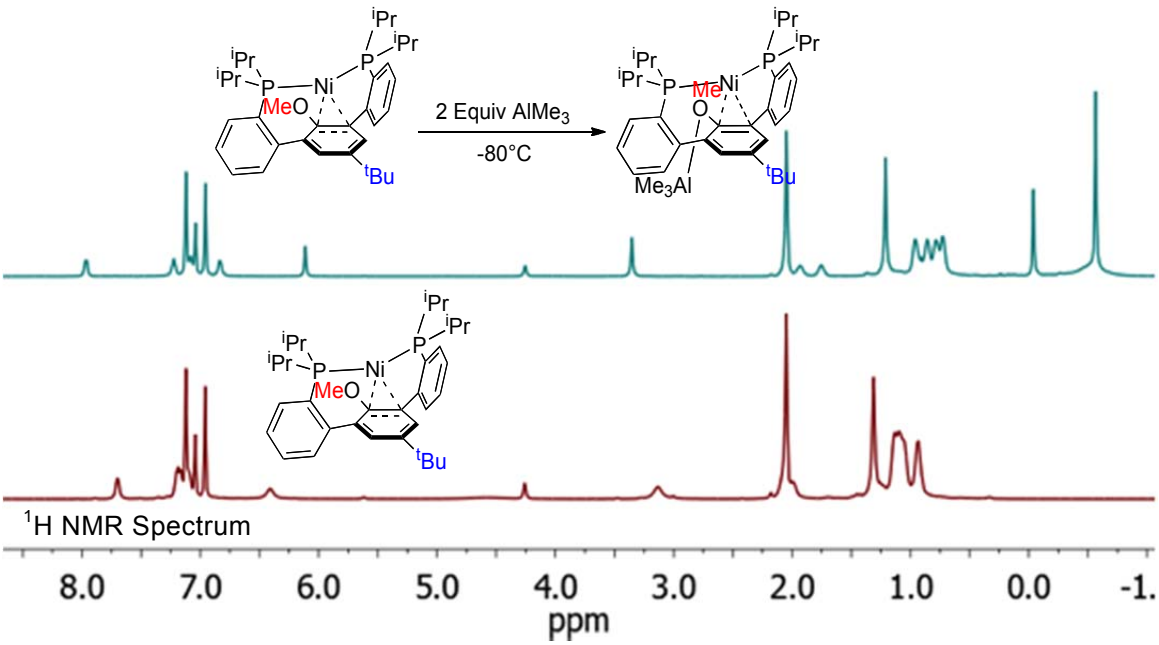

Figure 4.4: Addition of $AlMe_3$ to $\mathbf{2_{tBu}}$ at -80 °C

NOE experiments were used to provide further insight into structure of the intermediate. Homonuclear 2D NOESY spectra collected at -80 °C gratifyingly reveal interaction between the $AlMe_3$ methyl groups and the ipso methoxy group as observed as a cross peak at -0.5 and 3.5 ppm (Figure 4.5). Interestingly there is also an interaction between the aluminum alkyl and the ortho protons of the outer terphenyl

rings as shown by the cross peak at -0.5 and 8.0 ppm (Figure 4.5). The low temperature NOE data suggests that the $AlMe_3$ is coordinated to the methoxy on the face of the central arene ring opposite that of the nickel center. The methoxy group shows correlations to the isopropyl groups relating their close proximity in space (cross peak between 1 and 3.5 ppm, Figure 4.5). No methyl correlations were observed between the isopropyl groups of the phosphine and $AlMe_3$, which would be present if the aluminum center resided on the same side as the nickel center.

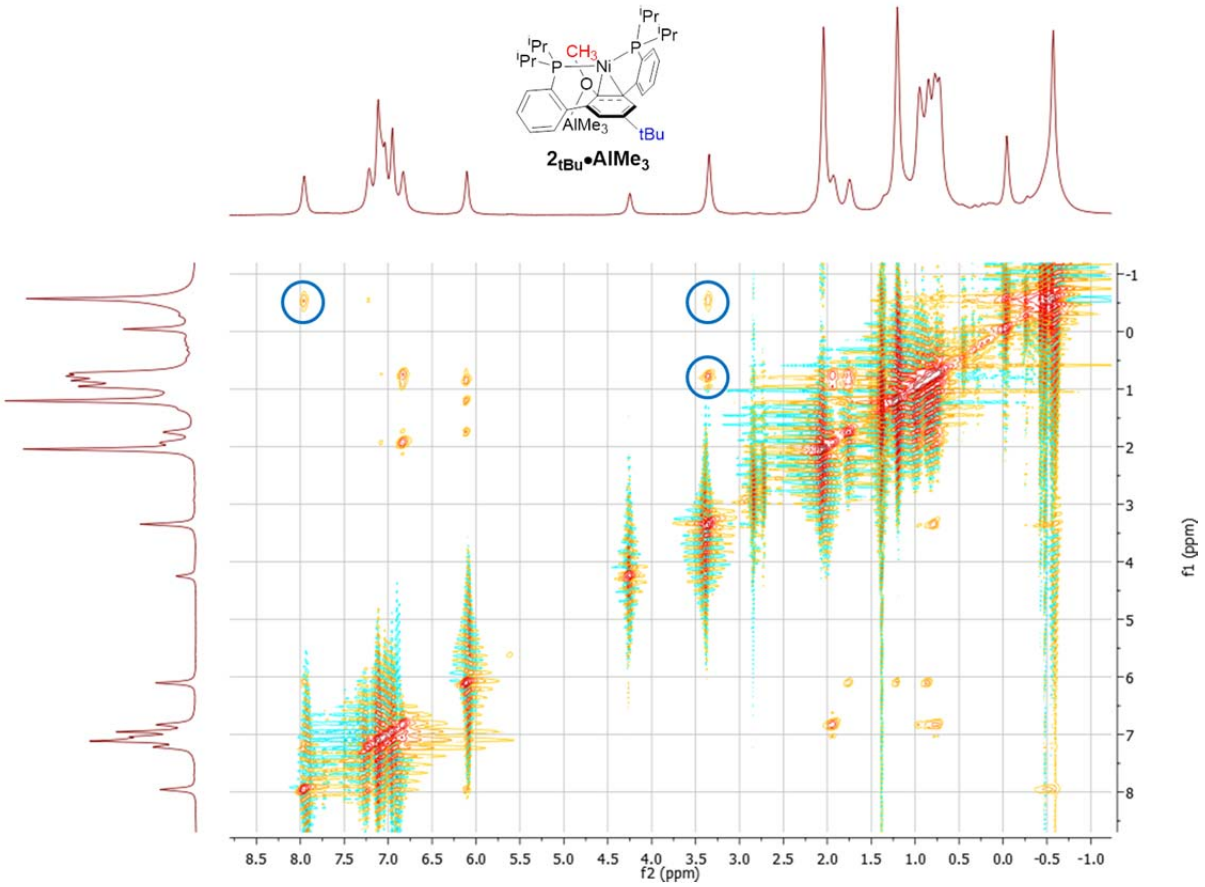

Figure 4.5: NOESY spectra of $\mathbf{2_{tBu}•AlMe_3}$ collected at -80 °C

With a better understanding of where and how the aluminum alkyl is accelerating the rate of aryl oxygen bond activation in depth studies of the rate were under taken. The decay of the nickel(0) trimethyl aluminum intermediate ($\mathbf{2_{tBu}•AlMe_3}$)

was observed over time for three reaction half lives using 10 to 100 equivalents of $AlMe_3$ (Figure 4.6). As one can see from the rate data there is an increase in the rate of the aryl oxygen bond activation with increasing concentrations of $AlMe_3$. It should be noted that a similar rate increase is observed with increasing concentration with Grignard reagents. This rate increase is consistent with a bimolecular mechanism. However there is also a significant increase with just one equivalent of $AlMe_3$.

Determination of the activation parameters for the aryl oxygen bond assisted cleavage were undertaken with two and ten equivalents of $AlMe_3$. Suprisingly both two and ten equivalents gave similar values for $\Delta S^{\ddagger}$ (-4.83 and -2.23 cal K^{-1} respectively) and $\Delta H^{\ddagger}$ (14.78 and 14.92 kcal mol^{-1} respectively) of activation (Table 4.2). The small negative $\Delta S^{\ddagger}$ suggests that the mechanism is intramolecular, which is not consistent with the effect of $AlMe_3$ concentration on the rate that is observed. It is possible that there are two alternate mechanisms for the activation of the aryl oxygen bond. The first mechanism would only require a single equivalent of $AlMe_3$ coordinated to the oxygen bond. This single equivalent leads to a large rate increase (about three orders of magnitude) over what is observed in the absence of any additive. The second mechanism would involve several equivalents of $AlMe_3$, possibly to further activate the aryl-oxygen bond or form a lower energy transition state. Calculations performed by Sibo Lin suggest that the aryl oxygen bond activation in the presence of $AlMe_3$ proceeds through an intermediate where the $AlMe_3$ and Ni metal center are on the same side. While this is not observed by NOE studies, it does provide a possible explanation of how the presence of excess $AlMe_3$ could accelerate the rate of the assisted oxidative addition. Upon addition of one equivalent of $AlMe_3$, the aluminum

center coordinates to the face opposite of the metal center, possibly due to sterics (Scheme 4.7).

Scheme 4.7: Possible Mechanism for rate acceleration with excess $AlMe_3$

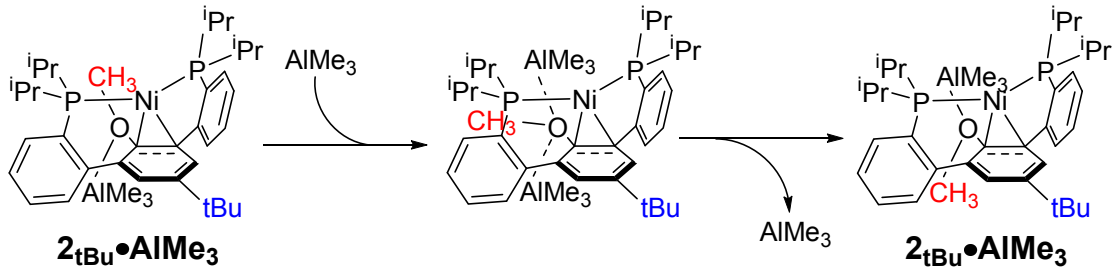

From here since the activation energy for oxidative addition in this intermediate is large the $AlMe_3$ must rearrange somehow from the local minimum to the active transition state. Another equivalent of $AlMe_3$ could coordinate to the methoxy from the top face of the ring causing dissociation of the first $AlMe_3$ equivalent leading to the calculated more favorable transition state for oxidative addition (Scheme 4.7). Increases in the concentration of $AlMe_3$ would lead to greater concentrations of this unstable intermediate leading to a faster rate, which coincides with what is observed. However, the rate increase by the additional equivalents of $AlMe_3$ is not as substantial as the first. Increasing the $AlMe_3$ from 2 to 10 equivalents only results in a 2.5x increase in rate. Similarly increasing the rate from 10 to 100 equivalents affords only a 5 fold increase.

	$\Delta H^{\ddagger}$ (kcal mol^{-1})	$\Delta S^{\ddagger}$ (cal K^{-1})
Ni(0) with No Additive	20 ± 2	-6 ± 1
Ni(0) with 2 Equivs of $AlMe_3$	15 ± 1	-5 ± 2
Ni(0) with 10 Equivs of $AlMe_3$	14.9 ± 0.7	-2 ± 1

Table 4.2: Observed activation parameters of aryl oxygen bond activation in $\mathbf{2_{tBu}}$ with 2 and 10 equivalents of $AlMe_3$

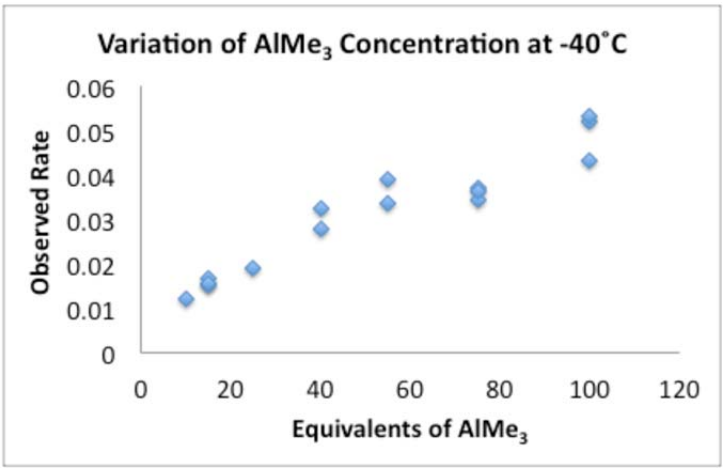

Figure 4.6: Rate of aryl oxygen bond activation in $\mathbf{2_{tBu}}$•$\mathbf{AlMe_3}$ with varying concentration of $AlMe_3$ at -40 °C

CONCLUSIONS:

The rate of oxidative addition observed in the nickel(0) diphosphine terphenyl ether model system was found to increase in the presence of Lewis acidic metals. Grignard reagents were found to increase the rate an order of magnitude while trimethylaluminum increases the rate about three orders of magnitude. At -80 °C an intermediate was identified by NOE coorelations where the $AlMe_3$ is coordinated to the ether moiety of the terphenyl ether trans to the nickel metal center. Warming this intermediate lead to the activation of the aryl ether bond. Increases in the concentration of $AlMe_3$ or MeMgBr leads to an increase in the observed rate. Although the rate increase is not as substantial as the increase from 0 to 1 equivalents of $AlMe_3$. This leads to the possibility two different mechanisms, one which requires only one equivalent and another, which requires multiple $AlMe_3$ centers.

EXPERIMENTAL SECTION:

General considerations: Unless otherwise specified, all compounds were manipulated using a glove box under a nitrogen atmosphere. Solvents for all reactions were dried by Grubbs' method. Benzene-d6 was purchased from Cambridge Isotope Laboratories and vacuum distilled from sodium benzophenone ketyl. All other materials were used as received. ^{1}H, ^{13}C, and ^{31}P NMR spectra were recorded on a Varian Mercury 300 spectrometer at ambient temperature, unless denoted otherwise. Chemical shifts are reported with respect to internal solvent: 7.16 ppm and 128.06 (t) ppm (C_6D_6) and for ^{1}H and ^{13}C NMR data, respectively. ^{31}P NMR chemical shifts are reported with respect to the instrument solvent lock when a deuterated solvent was used. IR spectra were recorded on a Thermo-Fisher Scientific Nicolet 6700 FT-IR spectrometer. Gas chromatography-mass spectrometry (GC-MS) analysis was performed upon filtering the sample through a plug of silica gel. Fast atom bombardment-mass spectrometry (FAB-MS) analysis was performed with a JEOL JMS-600H high-resolution mass spectrometer.

Kinetic Studies:

Special considerations: All kinetic data was collected on a Varian INOVA-500 MHz NMR spectrometer. In all experiments tri-*tert*-butylbenzene was used as a standard.

Example of a Kinetic Reaction:

In a glove box a J-Young tube was charged with 7.3 mg (0.012 mmol) of **2**$_{tBu}$ and 1.1 mg (0.004 mmol) of trimethoxybenzene in 200 µL d_8-toluene. This mixture in the J-Young tube was frozen in a liquid N_2 cooled cold well. After the solution was frozen a 100 µL d_8-toluene buffer layer was added to the tube and the frozen. On top of this layer was

added a solution of $AlMe_3$ in d_8-toluene. The J-Young tube was frozen and transferred to a dry ice acetone bath. The tube was transferred to the NMR at the desired temperature. NMR spectra were collected at regular intervals.

REFERENCES

(1) (a) Rosen, B. M.; Quasdorf, K. W.; Wilson, D. A.; Zhang, N.; Resmerita, A.-M.; Garg, N. K.; Percec, V. *Chemical Reviews* **2010**, *111*, 1346. (b) Yu, D.-G.; Li, B.-J.; Shi, Z.-J. *Accounts of Chemical Research* **2010**, *43*, 1486. (c) Li, B.-J.; Yu, D.-G.; Sun, C.-L.; Shi, Z.-J. *Chemistry – A European Journal* **2011**, *17*, 1728. (d) Mesganaw, T.; Garg, N. K. *Organic Process Research & Development* **2012**, *17*, 29. (e) Han, F.-S. *Chemical Society Reviews* **2013**, *42*, 5270.

(2) (a) Guan, B.-T.; Xiang, S.-K.; Wu, T.; Sun, Z.-P.; Wang, B.-Q.; Zhao, K.-Q.; Shi, Z.-J. *Chemical Communications* **2008**, 1437. (b) Tobisu, M.; Shimasaki, T.; Chatani, N. *Angewandte Chemie International Edition* **2008**, *47*, 4866. (c) Tang, Z.-Y.; Hu, Q.-S. *Journal of the American Chemical Society* **2004**, *126*, 3058.

(3) (a) Quasdorf, K. W.; Tian, X.; Garg, N. K. *Journal of the American Chemical Society* **2008**, *130*, 14422. (b) Quasdorf, K. W.; Antoft-Finch, A.; Liu, P.; Silberstein, A. L.; Komaromi, A.; Blackburn, T.; Ramgren, S. D.; Houk, K. N.; Snieckus, V.; Garg, N. K. *Journal of the American Chemical Society* **2011**, *133*, 6352. (c) Antoft-Finch, A.; Blackburn, T.; Snieckus, V. *Journal of the American Chemical Society* **2009**, *131*, 17750. (d) Guan, B.-T.; Wang, Y.; Li, B.-J.; Yu, D.-G.; Shi, Z.-J. *Journal of the American Chemical Society* **2008**, *130*, 14468. (e) Dankwardt, J. W. *Angewandte Chemie International Edition* **2004**, *43*, 2428. (f) Zim, D.; Lando, V. R.; Dupont, J.; Monteiro, A. L. *Organic Letters* **2001**, *3*, 3049. (g) Tolman, C. A.; Seidel, W. C.; Druliner, J. D.; Domaile, P. J. *Organometallics* **1984**, *3*, 33. (h) Nakao, Y.; Yada, A.; Ebata, S.; Hiyama, T. *Journal of the American Chemical Society* **2007**, *129*, 2428 (i) Nakao, Y.; Ebata, S.; Yada, A.; Hiyama, T.; Ikawa, M.; Ogoshi, S. *Journal of the American Chemical Society* **2008**, *130*, 12874

(4) Sergeev, A. G.; Hartwig, J. F. *Science* **2011**, *332*, 439.

(5) (a) Wenkert, E.; Michelotti, E. L.; Swindell, C. S. *Journal of the American Chemical Society* **1979**, *101*, 2246. (b) Wenkert, E.; Michelotti, E. L.; Swindell, C. S.; Tingoli, M. *The Journal of Organic Chemistry* **1984**, *49*, 4894.

(6) (a) Yu, D.-G.; Li, B.-J.; Zheng, S.-F.; Guan, B.-T.; Wang, B.-Q.; Shi, Z.-J. *Angewandte Chemie International Edition* **2010**, *49*, 4566. (b) Yu, D.-G.; Shi, Z.-J. *Angewandte Chemie International Edition* **2011**, *50*, 7097. (c) Yu, D.-G.; Wang, X.; Zhu, R.-Y.; Luo, S.; Zhang, X.-B.; Wang, B.-Q.; Wang, L.; Shi, Z.-J. *Journal of the American Chemical Society* **2012**, *134*, 14638.

(7) (a) Ishikawa, S.; Manabe, K. *Chemistry Letters* **2007**, *36*, 1302. (b) Ishikawa, S.; Manabe, K. *Organic Letters* **2007**, *9*, 5593. (c) Ishikawa, S.; Manabe, K. *Synthesis* **2008**, *2008*, 3180. (d) Ishikawa, S.; Manabe, K. *Angewandte Chemie International Edition* **2010**, *49*, 772. (e) Manabe, K.; Ishikawa, S. *Chemical Communications* **2008**, 3829.

(8) (a) Koester, D. C.; Kobayashi, M.; Werz, D. B.; Nakao, Y. *J. Am. Chem. Soc.* **2012**, *134*, 6544. (b) Minami, Y.; Yoshiyasu, H.; Nakao, Y.; Hiyama, T. *Angewandte Chemie International Edition* **2013**, *52*, 883. (c) Nakao, Y. *Bulletin of the Chemical Society of Japan* **2012**, *85*, 731. (d) Yada, A.; Ebata,

S.; Idei, H.; Zhang, D.; Nakao, Y.; Hiyama, T. *Bulletin of the Chemical Society of Japan* **2010**, *83*, 1170.

(9) Nakao, Y.; Ebata, S.; Yada, A.; Hiyama, T.; Ikawa, M.; Ogoshi, S. *J. Am. Chem. Soc.* **2008**, *130*, 12874.

CHAPTER *5*

Metallomacrocycles as Ligands: Synthesis and Characterization of Aluminuim-Bridged Bisglyoximato Complexes of Iron

The text for this chapter was taken in part from:

Kelley, P.; Radlauer, M. R.; Yanez, A. J.; Day, M. W.; Agapie, T. *Dalton Trans.* **2012**, *41*, 8086-8092.

Abstract

Dialuminiummacrocycles based on bisglyoximato moieties were prepared and their coodination chemistry with FeII was investigated. The nature of the ancillary ligands bound to aluminum affect the overall geometry of the metallomacrocycles. Additionally, remote substituents on aluminium-bound ligands affect the binding mode, electrochemistry, and electronic properties of the central iron.

INTRODUCTION:

Metallomacrocycles have been studied for a variety of applications including the synthesis of extended solids, catalysis, selective binding of ions and sensing.[1-18] Rational selection of metal precursors and ligands has afforded metallomacrocycles with diverse shape and size. Incorporation of binding sites for additional metals into the metallomacrocycles typically relies on the ability of coordinating atoms to bridge between the macrocycle metals and the incoming metals. Such systems, known as metallacrowns, have been extensively studied.[2, 3, 19] An alternative approach to coordinating additional metals involves orthogonal metal-binding atoms on the organic units of the macrocycles. Systems with monodentate phosphines, phenanthroline, phenols or diimines donors capable of binding diverse transition metals are known.[20-24]

Transition metal complexes supported by bisglyoximato moieties exhibit the interesting ability to bind metal centres in a coordination environment similar to biologically relevant macrocycles. Iron bisglyoximato complexes have chemistry reminiscent of heme species.[25, 26] The reactivity of cobalt bisglyoximato complexes was investigated in the context of vitamin B12 chemistry[27, 28] and, recently, in the context of catalytic proton reduction to dihydrogen.[29-34] The large majority of these species display proton or boron bridges between the oxygen atoms. Boron-bridged variants are generally constructed from the preformed, proton-bridged, metal-bisglyoximate species.[35-38] Metallomacrocycles consisting of two glyoximato ligands and bridges other than hydrogen or boron are rare, but examples are known with aluminium, gallium, indium or copper moities.[39, 40] Additionally there are several examples of cryptands consisting of tris-glyoximato moieties with the oxygen donors bound to antimony, tin,

iron, manganese, and chromium.[41-47] We report herein on the synthesis of metallomacrocycles based on aluminium bridged bisglyoximato frameworks and their coordination chemistry with iron.

RESULTS & DISCUSSION:

In order to assemble metallomacrocycles capable of chelating a variety of metals, a strategy to link two dioximato ligands was employed. Aluminium precursors supported by tetradentate ligands capable of affording two open *cis*-coordination sites were selected. Diphenoxide diamines have been used as ancillary ligands for olefin polymerization precisely due to the availability of two *cis* coordination sites.[48-50] Furthermore, the synthesis of these ligands is modular and allows for steric and electronic variation as well as changes in the linkages between the donor atoms. Methylaluminium species were prepared *in situ* by a modification of literature procedures and used as precursors for protonolysis reactions with glyoximes (Scheme 5.1).[51, 52]

Scheme 5.1: Synthesis of metal complexes supported by aluminum macrocycles.

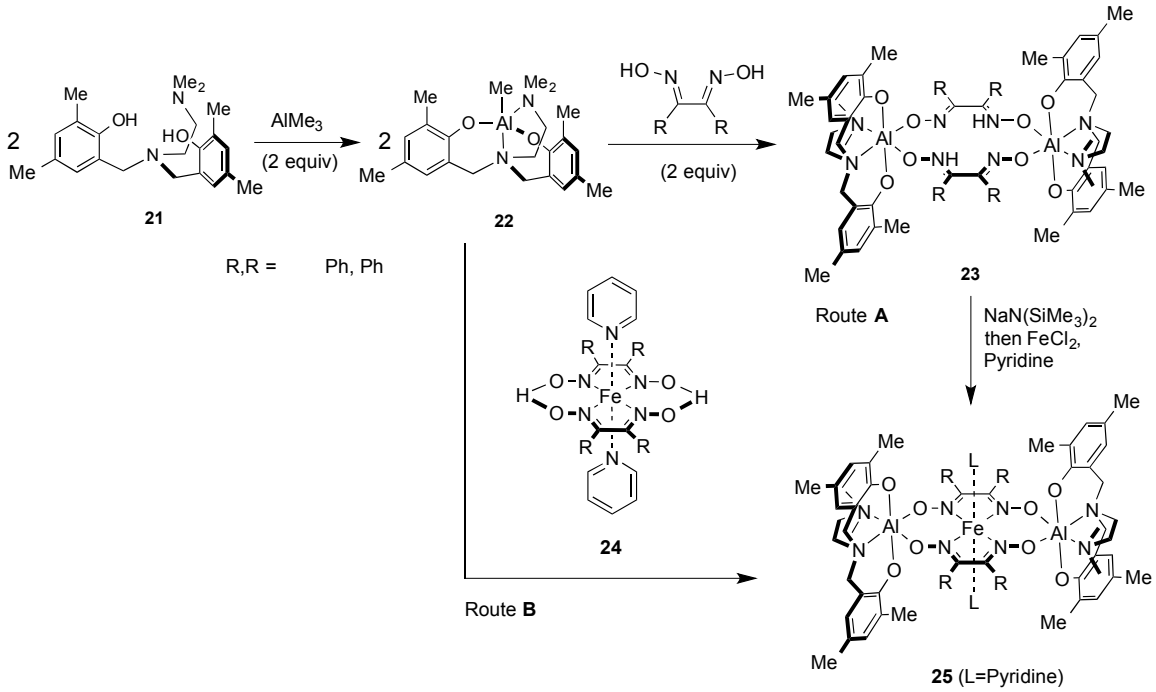

Treatment of diphenylglyoxime (Scheme 5.1), which is sparingly soluble in THF, with **21** led to a homogeneous mixture indicating that a reaction occurred. The

^{1}H NMR spectrum in C_6D_6 contains signals corresponding to both the phenoxide ligand and the dioximato backbone. Additionally, a peak slightly downfield of 14 ppm indicated protonation of two of the nitrogen atoms of the glyoximato moiety. To investigate the binding mode of the aluminiummacrocycle to metal centres that can access six-coordinate geometry, Fe(II) complexes were synthesized. Via synthetic route B, previously reported iron diglyoximato complex (**24**),[26,53] was treated with methylaluminium species 3a in THF. Precursor **24** is sparingly soluble in THF, but slowly dissolved as the reaction proceeded to generate a bright purple solution. Purification by fractional precipitation afforded the isolation of a red-purple solid. Using route A, treatment of **23** with base followed by $FeCl_2$ and pyridine allows the isolation of a red-purple solid with spectroscopic properties identical to the product obtained from route B. The ^{1}H NMR spectrum of the red-purple residue in C_6D_6 shows a single major peak for each of the three types of methyl groups, NMe_2, para-CH_3 and ortho-CH_3. Additionally, two coordinated pyridines are present (by integration of 1H NMR peaks). Similar to previously synthesized palladium complexes in the group, these spectroscopic data suggest a C_{2h} structure (or fast exchange) with two pyridines bound along the C_2 axis. ESI-MS data shows a peak at m/z = 1452.7 that is consistent with assignment of the product as **25**.

Attempts of growing X-ray quality single crystals of **25** resulted in yellow crystals from a red-purple solution in THF layered with hexanes. An XRD study of this material revealed an unexpected binding for the macrocycle (**26**, Figure 5.1 and Scheme 5.2). The iron centre is six-coordinate, with a trigonal prismatic geometry. The iron ligands are two phenoxide oxygens bridging between iron and aluminium and the four oxime moieties. The conformation of the metallomacrocycle bound to iron

has the two dioximato planes departing from coplanarity with a dihedral angle of 63°. Compound **26** was prepared free of pyridine by trituration of **25** with toluene several times. **26** shows a paramagnetic 1H NMR spectrum with broad peaks between 1 and 14 ppm. Further studies were performed to elucidate the behaviour of **25** and **26** in solution. An NMR sample of **25** in CD_2Cl_2 displayed the diamagnetic peaks as described above, but also some paramagnetic peaks consistent with the presence of **26**. Addition of excess pyridine led to an increase of the diamagnetic peaks assigned to **25**.

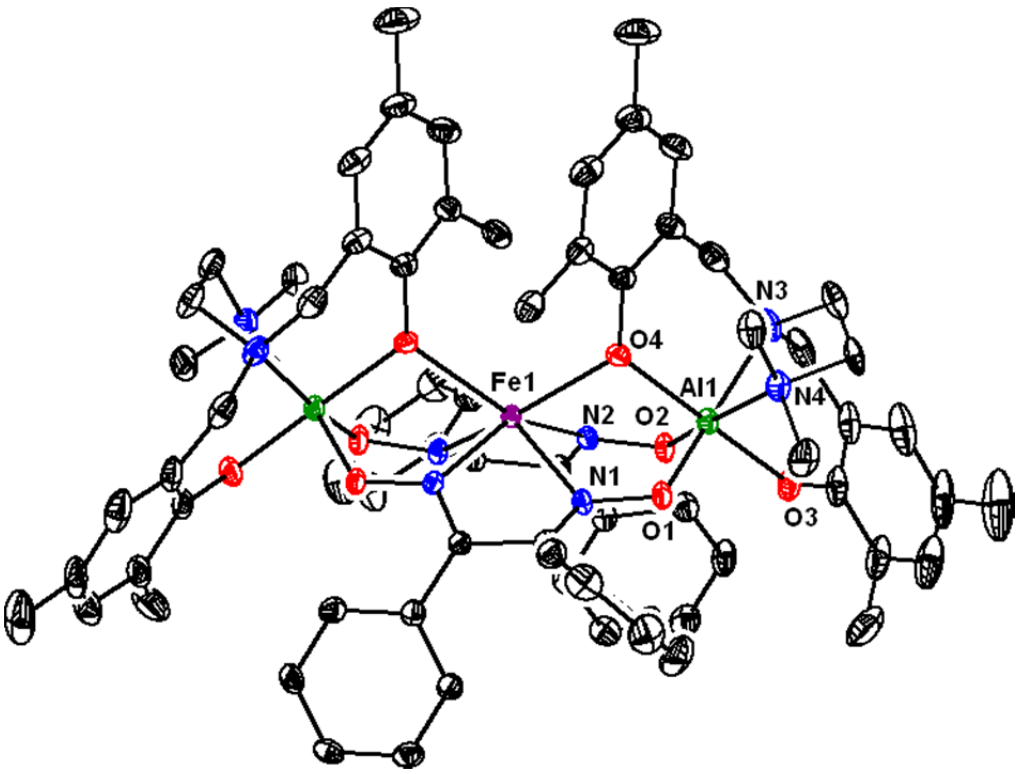

Figure 5.1. Solid-state structure of **26**. Hydrogen atoms and solvent molecules have been omitted for clarity; thermal ellipsoids are displayed at the 50% probability.

Scheme 5.2: Ancillary and Axial Ligand effects on Fe Coordination

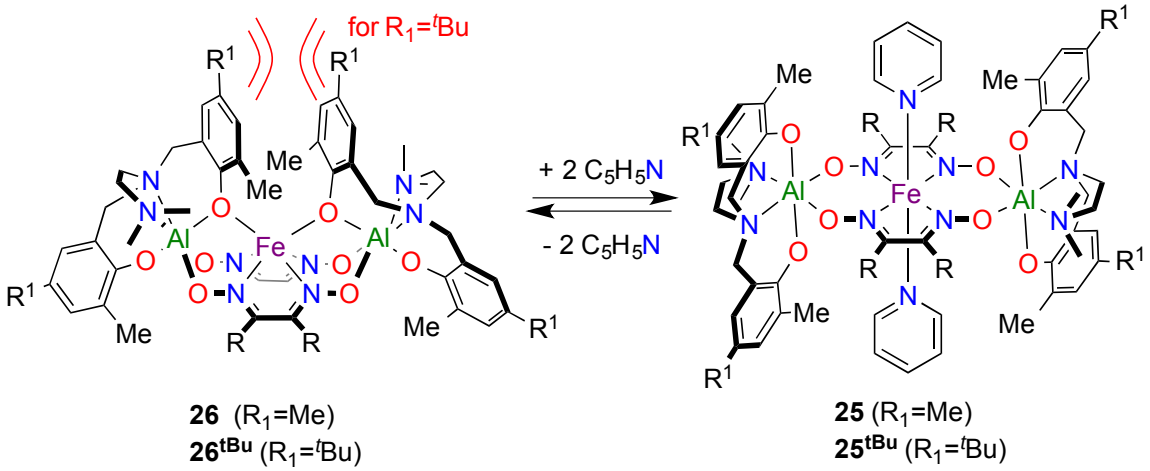

Compound **25** was dissolved in benzene and analyzed by UV-Vis spectroscopy (Figure 5.2). Two absorptions, at 461 and 548 nm were observed. Addition of pyridine led to an increase in the intensity of the band at 548 nm and decrease of the band at 461 nm. The 548 nm band is in the range previously reported for iron bisglyoximato complexes, with coplanar oximes.[26,54,55] The observed spectral shift in the presence of pyridine is consistent with an equilibrium between **25** and **26** plus free pyridine.

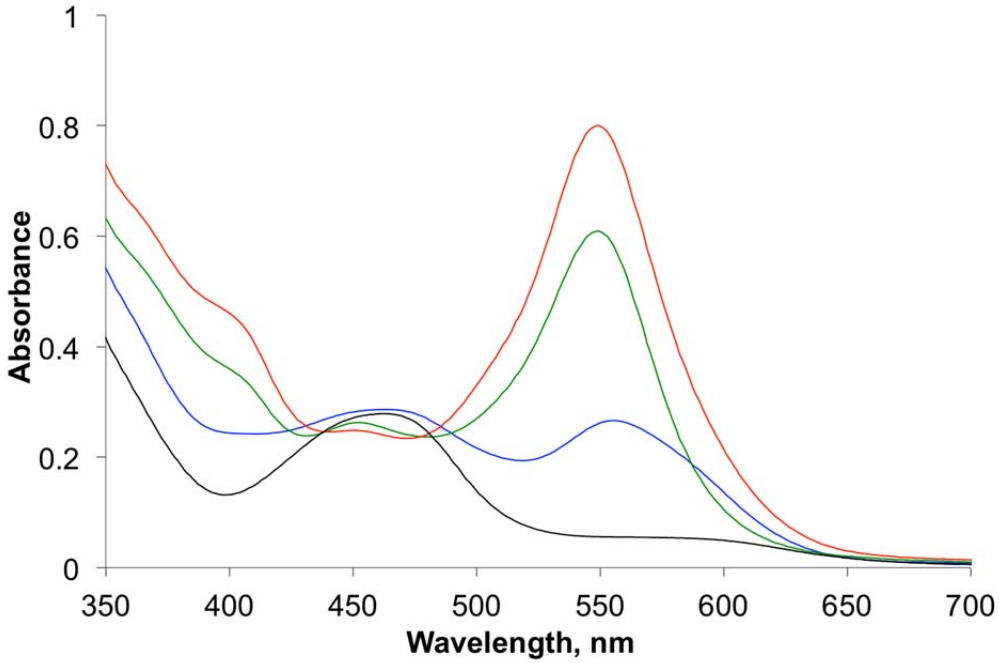

Figure 5.2. UV-Vis spectra at 70 μM of complexes **26** (black), **25** (blue), **25^{tBu}** (green) and **25** plus excess pyridine (2 mM, red).

The structural change from **25** and **26** is accompanied by a spin change from diamagnetic to paramagnetic and a change in the electronic absorption spectrum (Figure 5.2). The change in the iron coordination geometry from square bipyramid to trigonal prism is expected to lead to a smaller d-d splitting because none of the d orbitals have all lobes pointing to ligands.[56,57] Consequently a high-spin species was generated. The band at 548 nm (**25**) is consistent with a d-π^* charge transfer, as previously assigned.[54,55,58] The observed shift to higher energy is likely due to an increase in the energy of the glyoxime π^* orbital due to more direct interactions with d orbitals.

Analysis of the solid-state structure of **26** shows that the two bridging phenoxides are spatially close to each other. In order to disfavour phenoxide bridges and facilitate intermolecular binding of ligands, a bulkier phenoxide was utilized. A

variant with tert-butyl instead of methyl groups in the para position vs. the phenoxide oxygens was employed. Species **25**^{tBu} was prepared analogously to **25** and investigated by UV-Vis spectroscopy (Figure 5.2). Without added pyridine the peak at 548 nm, corresponding to the d-π^* transition in **25**^{tBu}, is almost as intense as the 548 nm peak of **25** upon addition of excess pyridine. This indicates that the increased steric bulk on the ligand periphery affects the coordination environment at the iron center, disfavouring the formation of phenoxide bridges (Scheme 5.2).

The geometry of the ancillary ligand bound to the aluminum center affects the overall symmetry of the metallomacrocycle. A tripodal N(O_2N) ligand generates an aluminium precursor of *pseudo-C*$_s$ symmetry (**21**, Scheme 5.1). Since two aluminium centres are part of the metallomacrocycle, the symmetry can be *pseudo-C*$_{2v}$ or *pseudo-C*$_{2h}$ (approximating the macrocycle as planar) dependent on the relative orientation of the Al[N(O_2N)] moiety (Scheme 5.3). If the four donors of the diphenoxide diamines ligands are linked in a linear fashion $(NO)_2$, the resulting aluminium complexes display *pseudo-C*$_2$-symmetry rendering the metal centres chiral. Again, depending on the stereochemistry at aluminium, two types of macrocycles are possible, with *pseudo-D*$_2$ or *pseudo-C*$_{2h}$ symmetry. It was envisioned that the stereochemistry at aluminium could be set by a chiral centre in the ligand backbone, such as defined by a *trans*-1,2-diaminocyclohexane moiety. Control of the stereochemistry by the ancillary ligand was expected to favour the chiral, *pseudo-D*$_2$ structure.

To examine the stereochemistry of complexes with C_2 symmetric ancillary ligands on aluminium, precursors[7,10] supported by linear diphenoxide diamine ligands were prepared using 1,2-ethylenediamine or (*R,R*)-*trans*-1,2-diaminocyclohexane backbones (Scheme 5.3). Attempts to prepare iron complexes ligated by

aluminiummacrocycles with ethylenediamine backbones resulted in a mixture of diamagnetic products likely due to the formation of both *pseudo-D*$_2$ and *pseudo-C*$_{2h}$ structures. Nevertheless, one isomer can be enriched by precipitation. Since NMR spectroscopy does not allow for determination of the symmetry of the isolated product, an XRD study was performed and showed a *pseudo-D*$_2$ structure in the solid-state (**29**^{tBu}). The iron coordination environment is *pseudo*-octahedral, with the phenoxide oxygens coordinated only to aluminium. This geometry at iron is consistent with the sharp, diamagnetic NMR spectra, and the vibrant purple colour. Since a variant with methyl groups in the position para to the phenoxide oxygen was not prepared, it is not clear if the macrocycle binding mode is a consequence of the bulky substituent or the steric demands of the linear ligand set bound to aluminium. The metallomacrocycle appears to be larger than boron or hydrogen linked versions.[59,60] The O1-O3 and O2-O4 distances in **29**^{tBu} are ca. 0.4 Å larger than the corresponding ones in difluoroborate and proton linked iron diglyoximato species (average 2.90 vs. 2.57 and 2.52 Å respectively).[59,60] This ring expansion is due to the larger aluminium centre. Ruffling of the metallocycle is observed and contrasts with the flat geometry observed for bisglyoximato complexes bridged by protons or boron moieties. This distortion could be due to *C*$_2$-twists caused by the aluminium centres or the larger size of the macrocycle.

Scheme 5.3. Effect of the ancillary ligand of aluminum on the symmetry of the metallomacrocycle.

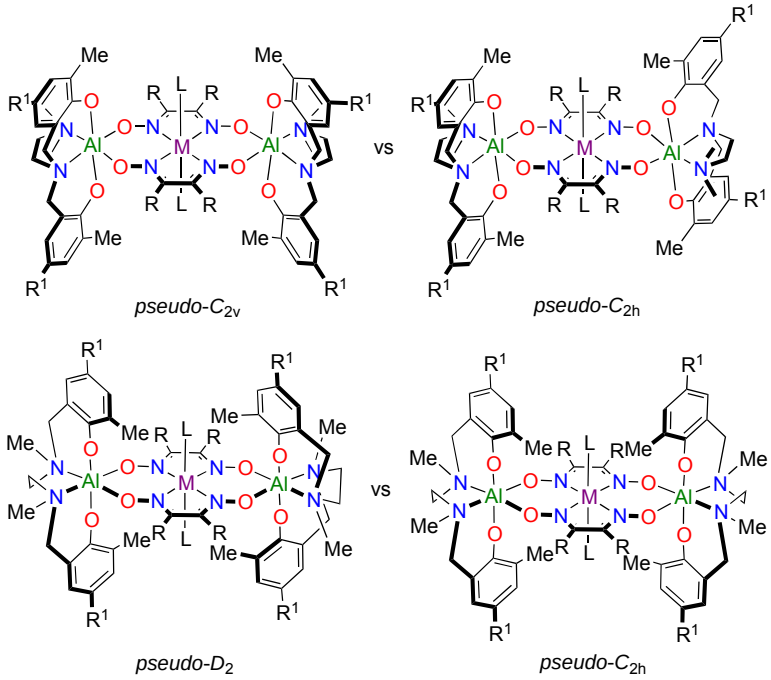

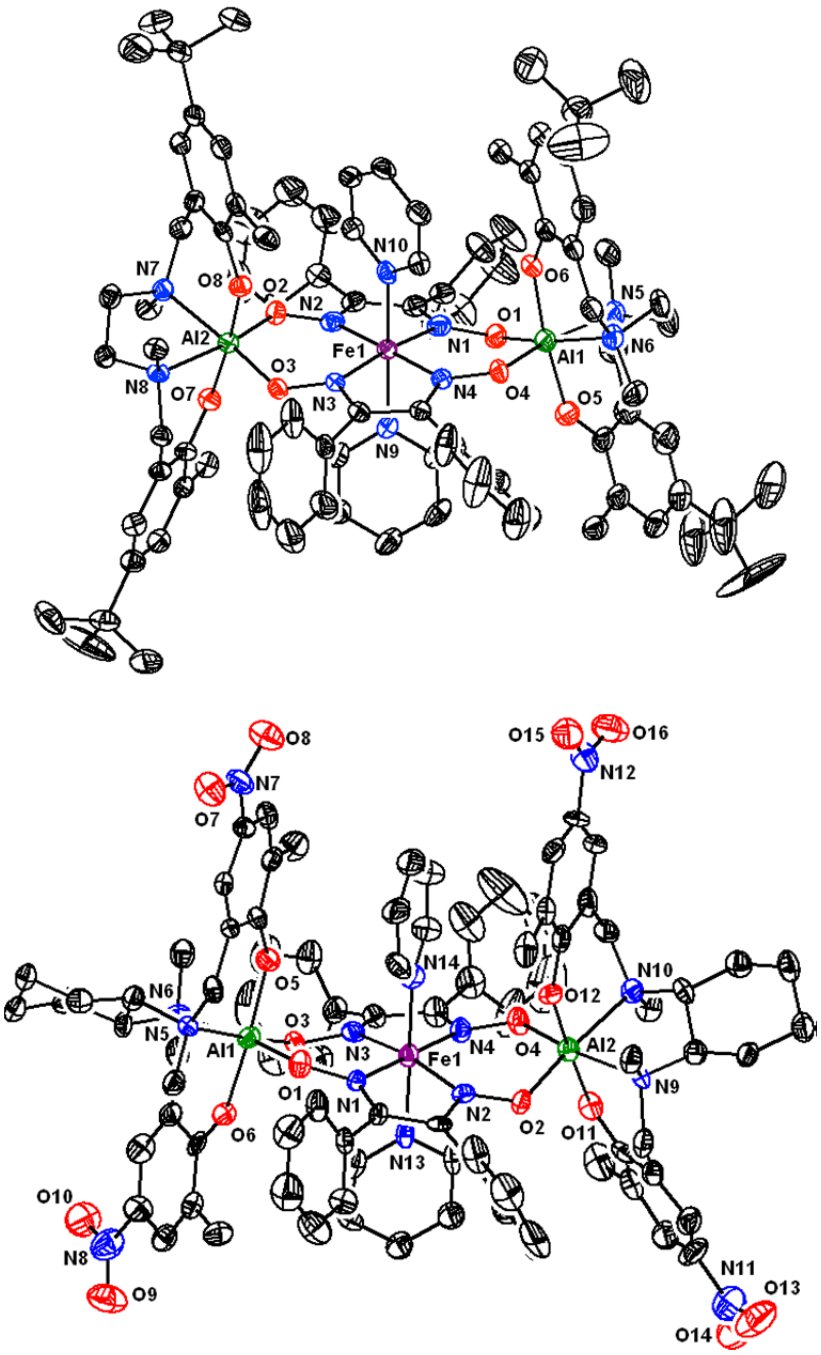

Figure 5.3. Solid state structures of 29^{tBu} and 32^{NO_2}. Hydrogen atoms and solvent molecules have been omitted for clarity; thermal ellipsoids are displayed at the 50% probability.

Utilization of enantiopure (*R,R*)-*trans*-1,2-diaminocyclohexane backbones results in significantly cleaner reactions for the synthesis of iron complexes ligated by aluminiummacrocycles, **32**^{tBu} and **32**^{NO2} (1H NMR spectroscopy). Analysis of **31**^{tBu} by ^{27}Al NMR gives a broad peak ca. 74 ppm consistent with a five coordinate aluminium center as described in literature.[52,61-63] Mixing **31**^{tBu} with diphenyl glyoxime forms the **31**^{tBu} macrocycle, which gives a broad ^{27}Al NMR peak ca. 14 ppm consistent with aluminium coordination to the glyoxime oxygens. Subsequent metallation and carbonyl coordination to form **32**^{tBu} and **33**^{tBu} does not substantionally change the shift in the ^{27}Al NMR (14 and 12 ppm respectively).[61-63] Ligand variants with *para*-NO_2 and *para*-tert-butyl substitution were employed for the phenoxides. An XRD study of complex **32**^{NO2} revealed a *pseudo*-D_2 structure. Similar to complex **29**^{tBu} supported by the ethylenediamine backbone, **32**^{NO2} shows ruffling of the macrocycle departing from an idealized D_2 structure. The control of the overall symmetry of the metallomacrocycle by the ancillary ligand on aluminium is notable as it affords enantiopure macrocycles.[18,64]

Remote substituents on the phenoxide rings were found to affect the coordination environment around the central iron, likely due to steric interactions (vide supra). To complement those findings, complexes **32**^{tBu} and **32**^{NO2} allow for studies of the electronic effect of remote groups on aluminium-bound phenoxide on chemistry at the iron centre. Cyclic voltammetry of **32**^{tBu} shows waves between 0.5 and 1 V vs. $[FeCp_2]^+$ / $FeCp_2$, which are assigned to phenoxide based redox events (Figure 5.4). Metal-bound trialkyl phenoxides were reported previously to have reduction potentials in the above range.[65,66] Complex **32**^{NO2} displays a positive shift of these potentials consistent with the presence of electron withdrawing nitro groups that

disfavouring ligand oxidation. A large peak is seen close to 1 V in $\mathbf{32}^{NO_2}$, which is assigned to the oxidation of the nitro substituted phenoxides on the ancillary aluminium centers as the $\mathbf{31}^{NO_2}$ diphenylgyoxime macrocycle also contains a large oxidation wave in that region (Figure 5.5). The redox event at -0.34 V for $\mathbf{32}^{tBu}$ was assigned to the Fe^{III}/Fe^{II} couple. This is 0.32 V more negative compared to proton-bridged iron diglyoximato species (-0.02 V vs. $[FeCp_2]^+$ / $FeCp_2$). It is not clear if this a consequence of increasing electron density at iron when six-coordinate aluminium bridges are present or of the larger macrocycle size with aluminium.[67] The presence of four *para*-NO_2 groups in $\mathbf{32}^{NO_2}$ led to a Fe^{III}/Fe^{II} couple at -0.07 V. The significant 0.27 V shift of the Fe^{III}/Fe^{II} reduction potential compared to $\mathbf{32}^{tBu}$ supports the notion that the redox properties of the central atom can be affected by remote substituents at the periphery of the macrocycle.

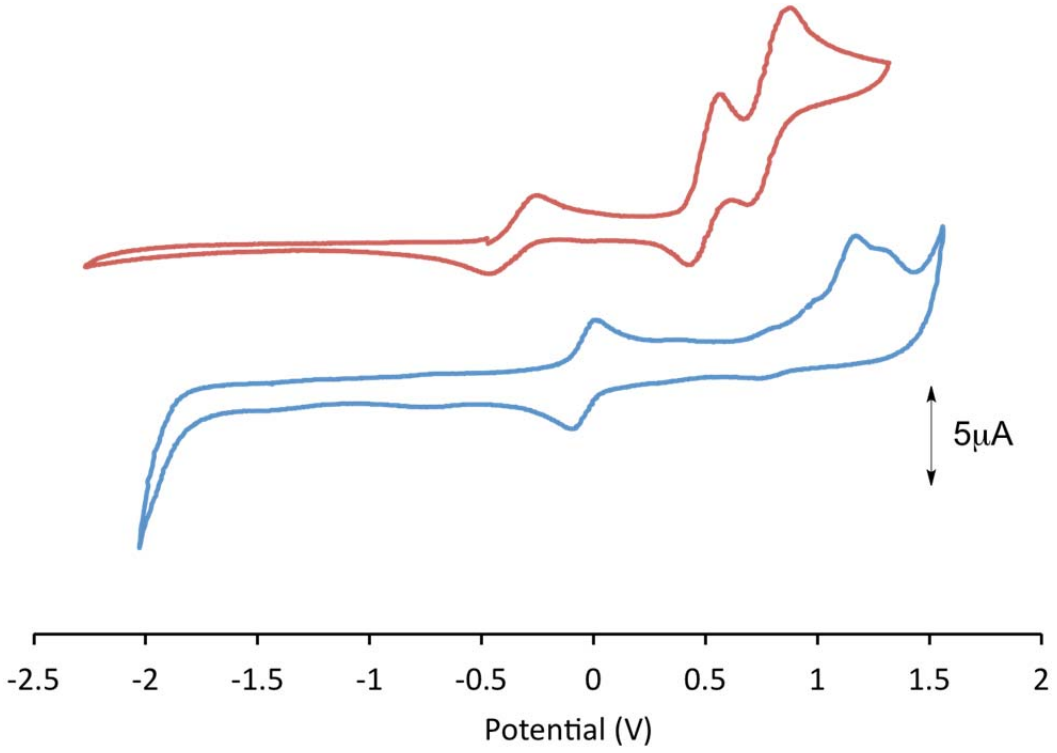

Figure 5.4. Cyclic voltammagrams of complexes $\mathbf{32}^{tBu}$ (red) and $\mathbf{32}^{NO2}$ (blue) (1 mM in 1:1 DCM:MeCN solution, 0.1 M nBu_4ClO_4, 0.01 M $AgNO_3$ reference electrode, platinum working electrode, Pt wire counter electrode, referenced to $FeCp^2/[FeCp^2]^+$).

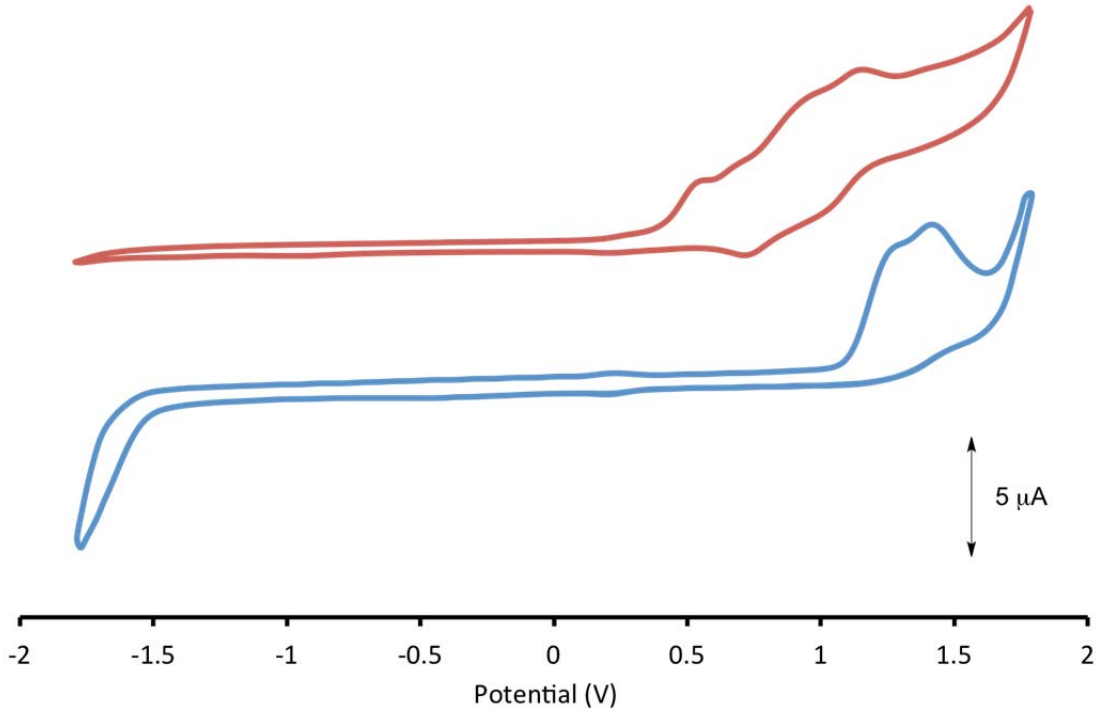

Figure 5.5. Cyclic voltammograms of complexes $\mathbf{31}^{NO2}$ (blue) and $\mathbf{31}^{tBu}$ (red), 1 mM solutions of each using a 100 mV/s scan rate, both referenced to Fc/Fc^+.

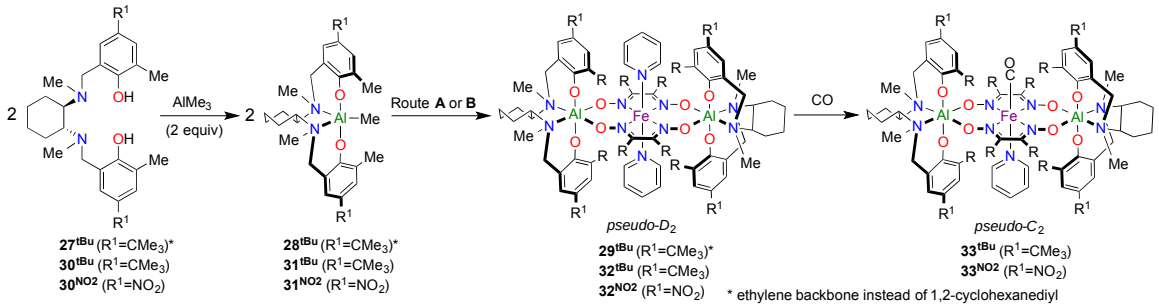

Scheme 5.4. Synthesis of iron complexes supported by aluminium macrocycles with C2-symmetric ancillary ligands.

Treatment of complexes **32^{tBu}** and **32^{NO2}** with CO generated new species cleanly by 1H NMR spectroscopy (Scheme 5.4). The number of peaks corresponding to the diphenoxide diamine ligands is doubled, consistent with a decrease in molecular symmetry. For example, the methyl groups ortho to the phenoxide oxygen display two singlets rather than one in **32^{tBu}** or **32^{NO2}**. Displacement of one pyridine with CO leads to a *pseudo-C*$_2$ structure. The two different ligands located on the C_2 axis, CO and pyridine, render chemically different the two halves of the molecule delimited by the Fe-diglyoximato moiety.[26] The carbonyl C–O stretch for complexes **33^{tBu}** and **33^{NO2}** (Scheme 5.4) appears at 2019 and 2020 cm^{-1}, respectively. The carbon monoxide adduct of the proton-bridged iron diglyoximato species (**24**) shows a C–O stretch at 2004 cm^{-1} in THF.[26] The cyclic voltammograms of the CO adducts **33^{NO2}** and **33^{tBu}** show a large shift in the Fe^{II}/Fe^{III} couple in comparison with the dipyridine complexes **32^{NO2}** and **32^{tBu}**. The Fe^{II}/Fe^{III} couple in **33^{NO2}** shows up as an irreversible oxidation at 0.71 V, which is ca. 700 mV more positive than that observed in **32^{NO2}**. Similarly, the Fe^{II}/Fe^{III} couple in the **33^{tBu}** complex is shifted, albeit obscured by the phenoxide oxidation peaks. The shift in the Fe^{II}/Fe^{III} couple is similar to what is seen in a boron-bridged

iron bisdimethylglyoxime system[38] and metal porphyrin systems upon the binding of carbon monoxide.[68,69] The similar values for $\mathbf{33}^{tBu}$ and $\mathbf{33}^{NO2}$ suggest that although the iron reduction potential is affected by the substituents, the electron density of the metal is affected to a greater extent by interactions with the carbonyl ligand. Compared to proton bridged system, $\mathbf{33}^{tBu}$ and $\mathbf{33}^{NO2}$ both appear less electron rich on the central metal based on the C–O stretch.

CONCLUSIONS:

In summary, metallomacrocycles consisting of dialuminium diglyoximato frameworks were synthesized and utilized as ligands for iron. These iron complexes were also prepared independently by first binding two glyoximato units to a central metal followed by reaction with alkyl aluminium precursors. The overall symmetry of the products is affected by the ancillary ligands bound to aluminium. Utilization of enatiopure, C_2-symmetric backbones facilitates the formation of a single, chiral isomer. The steric bulk of remote substitutents was found to affect the conformaiton of the free metallomacrocycles as well as the coordination geometry around the central metal. For iron, complexes with trigonal prismatic and square bipyramidal coordination modes were characterized. Additionally, the electronic properties of the substitutents on ligands bound to aluminium significantly influence the reduction potentials of the central metal. The present synthetic strategies and properties suggest that metallomacrocycles with a variety of ancillary ligands can be prepared and designed to affect chemistry at the central atom both sterically and electronically.

EXPERIMENTAL SECTION:

General Considerations. Unless otherwise specified, all compounds were manipulated using a glove box under a nitrogen atmosphere. Solvents for all reactions were dried by Grubbs' method. Benzene-d_6 was purchased from Cambridge Isotope Laboratories and vacuum distilled from sodium benzophenone ketyl. Chloroform-d and dichloromethane-d_2 were also purchased from Cambridge Isotope Laboratories and vacuum distilled from calcium hydride. Alumina and Celite were activated by heating under vacuum at 200 °C for 12 h. Tetradentate salan ligands (**21**^{tBu}), methyl aluminum complexes (**22**, **22**^{tBu}, and **27**^{tBu}), and metal glyoxime precursors (**24**) were all synthesized according to literature procedures.[2-4] All other materials were used as received. All ^{1}H, ^{13}C, and 2D NMR spectra were recorded on Varian Mercury 300 MHz, Varian 400 MHz, or Varian INOVA-500 or 600 MHz spectrometers at room temperature, unless denoted otherwise. Chemical shifts are reported with respect to internal solvent: 7.16 ppm and 128.06 (t) ppm (C_6D_6), 7.26 ppm and 77.16 ppm ($CDCl_3$), and 5.32 ppm and 53.84 ppm (CD_2Cl_2) for ^{1}H and ^{13}C NMR data, respectively. The chemical shifts in the ^{27}Al NMR data were referenced to a 1.1 M solution of $Al(NO_3)_3$ in D2O. Electrochemical measurements were recorded in a glovebox under a N2 atmosphere using a Pine Instrument Company Bipotentiostat, at 1mM of the complex of interest, in DCM containing 0.1 M $nBu_4N(ClO_4)$ as the supporting electrolyte. For the electrochemistry a platinum working electrode, a platinum wire auxiliary electrode, and a 0.01M $Ag/AgNO_3$ nonaqueous reference electrode were used for all measurements. Elemental analysis was performed by Midwest Microlab, LLC (Indianapolis, IN).

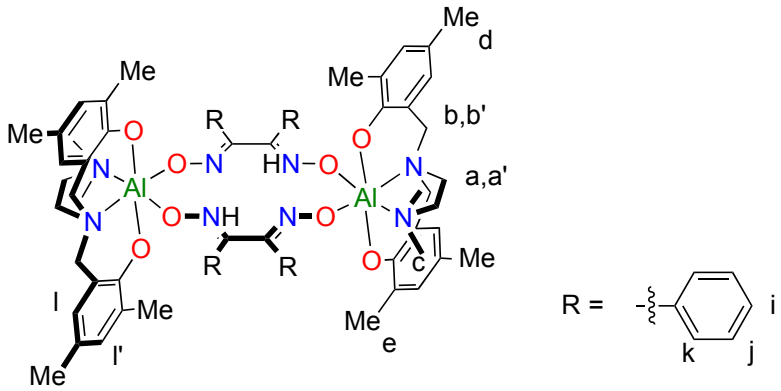

Synthesis of 23

A stirring solution of **2** (0.158 g, 0.387 mmol) in THF was treated with a slurry of diphenylglyoxime (0.096 g, 0.398 mmol) in THF. The solution was stirred for 3 hours over which the solution became yellow. The solvent was removed *in vacuo* to yield a pale yellow solid. The macrocycle **22** was used as isolated without any further purification. Yield 0.211 g, 88 %. ^{1}H NMR (300 MHz, C_6D_6) δ 14.41 (2H, s, N*H*), 7.86 (8H, m, k) 6.98 (4H, t, *J* = 7.6 Hz, i), 6.83 (8H, m, j), 6.76 (4H, s, l,l'), 6.69 (4H, s, l,l'), 4.89 (4H, d, *J* = 12.9 Hz, b,b'), 2.79 (4H, d, *J* = 13.1 Hz, b,b'), 2.38 (12H, s, e), 2.32 (4H, m, a,a'), 2.18 (12H, s, c), 2.15 (12H, s, d), 1.75 (4H, m, a,a') ppm. Anal. Calcd for $C_{72}H_{82}Al_2N_8O_8$: C, 69.66; H, 6.66; N, 9.03; Found: C, 69.07; H, 6.69; N, 8.69 %.

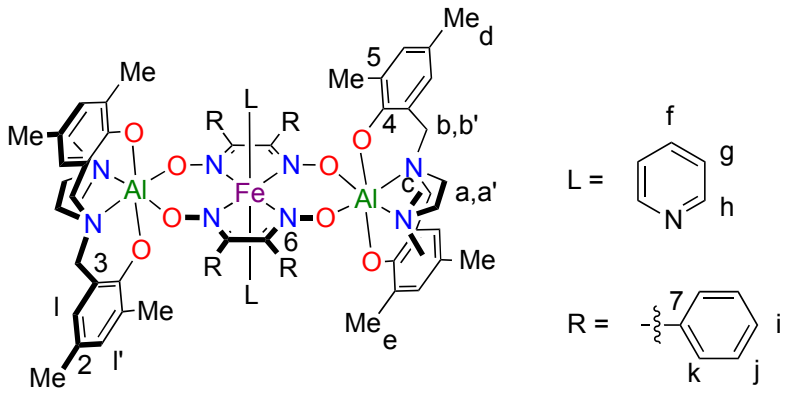

Synthesis of 25

Route B: In a 20 ml vial (0.043 g, 0.062 mmol) of **24** was stirred in about 2 ml of THF. To this was added (0.050 g, 0.126 mmol) of **22** as a solution in a small amount of THF. The reaction was stirred at ambient temperature for 3 days. Over the reaction time the solid **24** became soluble. The volatiles were removed under vacuum and the resulting purple solid was washed with Et_2O and benzene. The benzene was removed from the benzene fraction via vacuum and the resulting solid was dissolved in minimal amounts of THF. Small amounts of hexanes were added to the saturated solution resulting in precipitation of a purple solid. The solid was collected via filtration over a fine frit. Yield 0.033 g, 36 %.

Route A: Sodium hexamethyldisilazide (0.030 g, 0.163 mmol) was added to a solution of **23** (0.100 g, 0.081 mmol) in THF. The solution was stirred for 2 hours and the solvent was removed via vacuum. The resulting white residue was washed with pentane to remove the bis(trimethylsilyl)amine. The bis(trimethylsilyl)amine free solid was taken up in THF and mixed with a solution of $FeCl_2$ (0.010 g, 0.079 mmol) in THF. The solution immediately turned a dark purple and was stirred for an hour. After an hour excess pyridine was added to the solution upon which the color changed from dark purple to a reddish purple. The solvent was removed *in vacuo* yielding the a

purple red solid which was washed with ether. Yield 0.060 g, 52 %, about 90 % pure. To date, an analytically pure sample has yet to be obtained due to contamination of what is believed to be another isomer of the desired complex. ^{1}H NMR (500 MHz, C_6D_6) δ 9.30 (4H, d, *J*=5.6 Hz, h), 7.33 (4H, m, *J*=5.8 Hz, i), 6.98 (16H, m, j,l), 6.95 (4H, s, l'), 6.79 (2H, t, *J*=8.2 Hz, f), 6.63 (4H, m, g), 6.61 (4H, s, l), 4.61 (4H, d, *J*=13.0 Hz, b'), 2.61 (4H, d, *J*=12.9 Hz, b), 2.36 (6H, s, d), 2.15 (4H, m, a'), 1.97 (6H, s, e), 1.80 (6H, s, c), 1.64 (4H, m, a) ppm. ^{13}C{^{1}H} (126 MHz, C_6D_6) δ 159.08 (4), 158.35 (6), 156.67 (h), 135.70 (7), 134.57 (f), 131.41 (l'), 130.49 (i), 130.43 (k), 127.63 (j), 127.25 (l), 126.01 (5), 122.59 (g), 122.15 (3), 121.80 (2), 64.97 (b,b'), 58.18 (a,a'), 50.11 (a,a'), 47.68 (c), 20.89 (d), 16.74 (e) ppm. MS ESI (m/z): calcd, 1453.46 (M+); found 1452.7 (M+) (dipyridine) and 1390.2 (M+) (monopyridine with an oxygen)

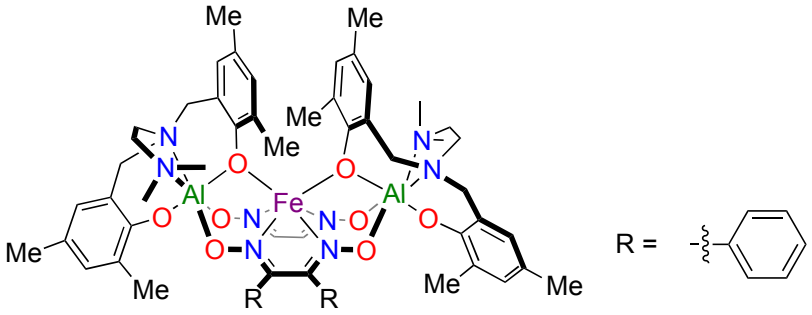

Synthesis of 26

A solution of **23** (0.248 g, 0.200 mmol) in THF was treated with a solution of Sodium hexamethyldisilazide (0.073 g, 0.400 mmol) also in THF. The solution was stirred for 3 hours over which the solution lost some of its color. After 3 hours the solvent was removed *in vacuo* resulting in a pale yellow white solid. The solid was washed with pentane resulting in a white THF soluble solid (0.116 g, 0.090 mmol, **23-Na$_2$**). To a THF solution of this disodium salt was added a slurry of $FeCl_2$ in THF (0.0115 g,

0.091 mmol). Upon addition the solution immediately became a dark black with an orange hue. The solution was stirred for 4 hours and the THF was removed *in vacuo*. The resulting dark brown solid was washed with diethyl ether resulting in an orange solid which was extracted using DCM. The DCM was removed *in vacuo* resulting in a dark orange solid paramagnetic material. Alternatively, **26** can be synthesized by removing the pyridines from **25**, by dissolving **25** in a high boiling solvent and removing the solvent *in vacuo*. Crystals were grown from a concentrated solution of **25** in THF layered with hexanes. Yield 0.066 g, 57 %. ^{1}H NMR (300 MHz, CD_2Cl_2) δ 18.46, 15.23, 12.84, 11.02, 10.67, 9.82, 8.97, 7.13, 6.68, 5.26, 4.96, 4.27 ppm.

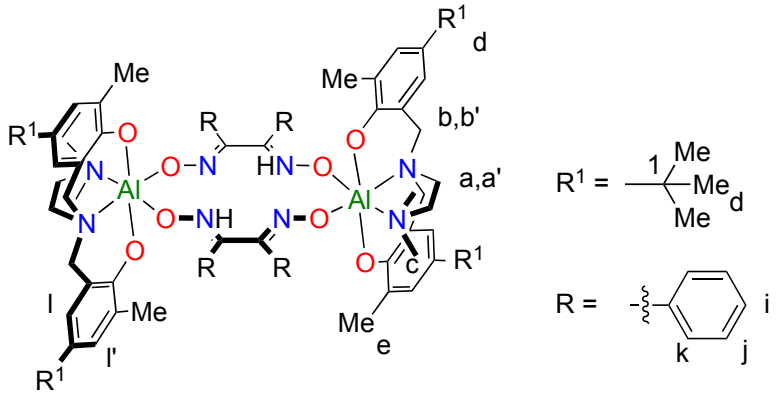

Synthesis of 23^{tBu}

The macrocycle was synthesized following the synthesis procedure for **23**. A stirring solution of **22^{tBu}** (0.100 g, 0.021 mmol) in THF was treated with a slurry of diphenylglyoxime (0.050 g, 0.021 mmol) in THF. The solution was stirred for 3 hours over which the solution became yellow. The solvent was removed *in vacuo* to yield a pale yellow solid. The Al(salan)$_2$(diphenylglyoxime)$_2$ macrocycle was used as isolated without any further purification. ^{1}H NMR (300 MHz, C_6D_6) δ 14.10 (2H, s, N*H*), 7.85 (4H, d, *J* = 6.7 Hz, l,l') 7.61 (4H, t, *J* = 7.6 Hz, l,l'), 6.92 (8H, m, k), 6.82 (8H, m, j),

6.65 (4H, m, i), 4.82 (4H, d, J = 12.7 Hz, b,b'), 2.81 (4H, d, J = 12.9 Hz, b,b'), 2.32 (12H, s, e), 2.23 (4H, m, a,a'), 2.02 (12H, s, c), 1.78 (4H, m, a,a'), 1.48 (36H, s, d) ppm.

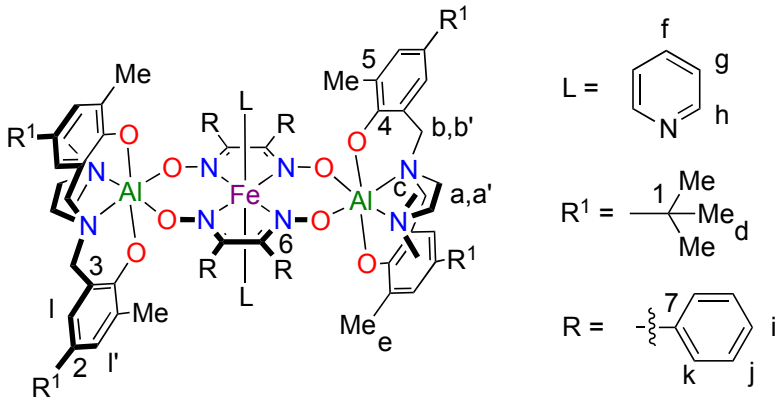

Synthesis of 25^{tBu}

25^{tBu} was synthesized and purified according to the synthesis procedures of **25**.

Route A: In a 20 ml vial 0.072 g (0.010 mmol) of **24** was stirred in about 2 ml of THF. To this was added 0.110 g (0.023 mmol) of the **22**^{tBu} complex as a solution in a small amount of THF. The reaction was stirred at ambient temperature for 16 days. Over the reaction time the solid **24** glyoxime became soluble. The volatiles were removed under vacuum and the resulting purple red solid was washed with hexanes, pentane, diethyl ether, and toluene. The toluene fraction was concentrated via vacuum and a small amount of hexanes was added to the saturated solution resulting in precipitation of a purple solid. The solid was collected via filtration over a fine frit. Yield 0.071 g, 44 %.

Route B: Sodium hexamethyldisilazide 0.036 g (0.200 mmol) was added to a solution of **23**^{tBu} (0.141 g, 0.100 mmol) in THF. The solution was stirred for 2 hours and the solvent was removed via vacuum. The resulting white residue was washed with pentane

to remove the bis(trimethylsilyl)amine. The bis(trimethylsilyl)amine free solid (0.126 g, 0.090 mmol) was taken up in THF and mixed with a solution of Fe(II)Cl_2 (0.011 g, 0.090 mmol) in THF. The solution immediately turned a dark purple and was stirred for an hour. After an hour excess pyridine was added to the solution upon which the color changed from dark purple to a reddish purple. The solvent was removed in vacuo yielding a purple red solid, which was washed with pentane and hexanes and extracted with diethyl ether. Yield 0.098 g, 67 %

^{1}H NMR (300 MHz, C_6D_6): δ 9.26 (4H, d, *J*=5.5 Hz, h), 7.41 (4H, d, *J*=8.4 Hz, g), 7.21 (8H, s, k), 6.97 (8H, s, j), 6.89 (8H, s, l), 6.83 (4H, t, *J*=6.7 Hz, i), 6.58 (2H, t, *J*=6.7 Hz, f), 4.65 (4H, d, *J*=12.9 Hz, b,b'), 2.71 (4H, d, *J*=13.3 Hz, b,b'), 2.15 (4H, m, a,a'), 2.08 (6H, s, e), 1.81 (6H, s, c), 1.63 (4H, m, a,a'), 1.44 (36H, s, d) ppm. ^{13}C{^{1}H} NMR (126 MHz, C_6D_6) δ 159.02 (4), 158.88 (6), 156.46 (h), 135.80 (7), 134.24 (2), 130.62 (f), 130.37 (k), 127.66 (j), 127.53 (i), 127.44 (l,l'), 125.67 (5), 123.18 (l,l'), 122.52 (g), 121.53 (3), 65.65 (b,b'), 58.10 (a,a'), 50.33 (a,a'), 47.64 (c), 33.90 (1), 32.33 (d), 17.12 (e) ppm. Anal. Calcd for $C_{94}H_{114}Al_2FeN_{10}O_8$: C, 69.62; H, 7.09; N, 8.64; Found C, 69.36; H, 7.33; N, 8.63

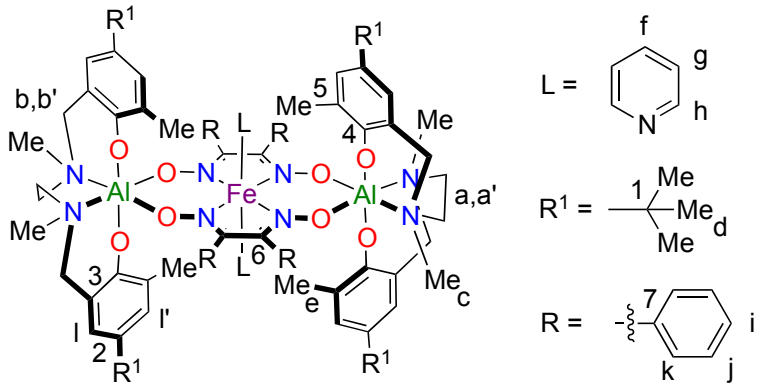

Synthesis of 29^{tBu}

In a round bottom flask **24** (0.692 g, 0.98 mmol) was stirred in 10 ml of toluene at ambient temperature. To this purple slurry was added a solution of the **28^{tBu}** (0.999 g, 2.08 mmol) in toluene. The solution was stirred for 14 hours. After 14 hours toluene was removed in vacuo yielding a purple solid. The solid was washed with hexanes, Et_2O, and toluene. The toluene washed was pumped down to a solid yielding clean 6. Yield: 0.688 g, 43 % ^{1}H NMR (500 MHz, C_6D_6) δ 9.21 (4H, d, *J* = 4.9 Hz, h), 7.31 (8H, d, *J* = 7.3 Hz, k), 7.21 (4H, d, *J* = 2.4 Hz, l'), 7.01 (8H, t, *J* = 7.5 Hz, j), 6.94 (4H, m, i), 6.75 (2H, t, *J* = 7.6 Hz, f), 6.74 (4H, d, *J* = 2.5 Hz, l), 6.30 (4H, t, *J* = 7.0 Hz, g), 4.49 (4H, d, *J* = 12.8 Hz, b,b'), 2.69 (4H, d, *J* = 9.0 Hz, a,a'), 2.57 (4H, d, *J* = 13.1 Hz, b,b'), 2.14 (12H, s, e), 1.90 (12H, s, c), 1.38 (36H ,s, d), 0.89 (4H , d, *J* = 9.1 Hz, a,a') ppm. ^{13}C{^{1}H} NMR (126 MHz, C_6D_6) δ 158.90 (4), 157.44 (6), 156.83 (h), 135.99 (2), 135.87 (7), 134.16 (f), 130.58 (k), 127.75 (j), 127.43 (i), 126.90 (l'), 126.68 (5), 123.14 (l), 122.65 (g), 120.89 (3), 63.73 (b,b'), 49.97 (a,a'), 46.85 (c), 33.88 (1), 32.30 (d), 17.62 (e) ppm. Anal. Calcd for $C_{94}H_{114}Al_2FeN_{10}O_8$: C, 69.62; H, 7.09; N, 8.64; Found, C, 69.49; H, 6.96; N, 8.44;

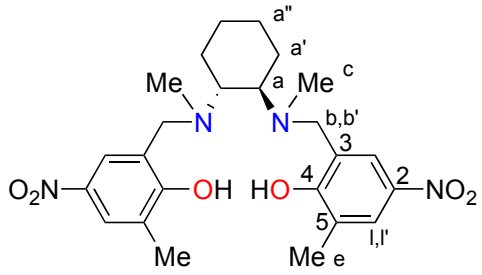

Synthesis of 30^{NO_2}

This ligand variant was synthesized using a modified literature procedure.[5] A solution of N,N'-dimethylcyclohexane-1,2-diamine (0.233 g, 1.63 mmol) and diisopropylethylamine (0.424 g, 3.28 mmol) in THF (7.5 ml) at 0°C (ice bath) was treated with a cold solution (ice bath) of 2-(chloromethyl)-6-methyl-4-nitrophenol (0.661 g, 3.28 mmol) in THF (5 ml). The solution was stirred for 16 hours during which a yellow precipitate formed. The resulting slurry was filtered using a medium glass frit and washed with 3x 20 ml of cold MeOH. The resulting off white solid was dried under vacuum. Yield 0.298 g, 38 % ^{1}H NMR (300 MHz, $CDCl_3$), δ 11.99 (2H, br s, O*H*) 8.01 (2H, d, J = 2.8 Hz, l,l'), 7.84 (2H, d, J = 2.4 Hz, l,l'), 3.91 (4H, d, J = 13.2 Hz, b,b'), 3.59 (2H, br s, b,b'), 2.83 (2H, m, a), 2.29 (6H, s, e), 2.14 (6H, s, c), 2.11 (2H, m, a"), 1.91 (2H, s, a'), 1.27 (4H, br m, a',a") ppm. ^{13}C{^{1}H} NMR (from 2D spectra, 126 MHz, $(CD_3)_2SO$) δ 166.98 (4), 135.74 (2), 126.12 (5), 125.81 (l'), 127.34 (l), 122.58 (3), 62.56 (b,b'), 25.54 (c), 22.78 (a), 16.68 (a), 16.53 (e) ppm from . ESI-MS Calc. (M) 472.2322 Found. 473.2 (MH^+)

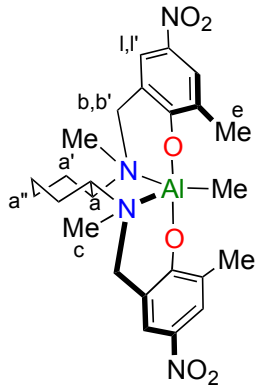

Synthesis of 31^{NO2}

The synthesis of 31^{NO2} was synthesized using trimethylaluminum following a published procedure for similar aluminium alkyl complexes.[6,7] A freshly thawed slurry of 30^{NO2} (0.024 g, 0.052 mmol) in toluene (5 ml) was treated with a thawed solution of trimethylaluminum (0.004g, 5.2 µl, 0.053 mmol). Upon mixing the solid particulates dissolved and the solution became a dark orange color which faded after a few minutes resulting in a light yellow solution. The solution was allowed to stir for 18 hours. During this time the solution became a slurry. The solvent was removed *in vacuo* resulting in a light yellow powder which was used without further purification. Yield 0.026 g, 99 % ^{1}H NMR (300 MHz, CD_2Cl_2), δ 8.04 (2H, m, l,l'), 7.85 (2H, m, l,l'), 4.00 (2H, J = 13.4 Hz, b,b'), 3.50 (2H, J = 13.0 Hz, b,b'), 2.95 (2H, m, a), 2.32 (3H, s, e), 2.28 (6H, m, e',c'), 2.18 (2H, m, a"), 2.10 (3H, s, c), 1.97 (2H, m, a'), 1.51(2H, m, a"), 1.25(2H, m, a'), -0.69 (3H, s, AlCH_3) ppm.

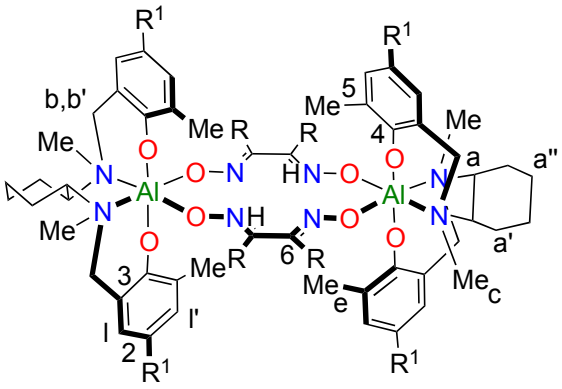

Synthesis of 31^{NO_2} Macrocycle

The macrocycle was synthesized following the synthesis procedure for **23**. A stirring solution of $\mathbf{31^{NO_2}}$ (0.100 g, 0.019 mmol) in THF was treated with a slurry of diphenylglyoxime (0.046 g, 0.019 mmol) in THF. The solution was stirred for 3 hours over which the solution became yellow. The solvent was removed *in vacuo* to yield a pale yellow solid. $\mathbf{31^{NO_2}}$ macrocycle was used as isolated without any further purification. Yield 0.139 g, 97 %. ^{1}H NMR (300 MHz, C_6D_6) δ 13.98 (2H, s, N*H*), 7.77 (4H, d, *J* = 2.9 Hz, l,l'), 7.59 (12H, m, i and j), 7.29 (12H, m, k and l,l'), 4.41 (4H, d, *J* = 13.5 Hz, b,b'), 3.25 (4H, d, *J* = 13.6 Hz, b,b'), 2.44 (4H, m, a), 2.06 (12H, s, e), 1.92 (12H, s, c), 1.72 (4H, m, a'), 1.59 (4H, m, a"), 1.03 (4H, m, a'), 0.80 (4H, m, a") ppm. ^{13}C{^{1}H} NMR (126 MHz, CD_2Cl_2) δ 165.86 (4), 149.36 (6), 136.44 (2), 130.11 (k), 128.28 (j), 127.97 (5), 127.40 (7), 126.39 (l'), 123.49 (l), 120.79 (3), 58.45 (b,b'), 56.39 (a), 39.97 (c), 24.01 (a"), 21.89 (a'), 16.18 (e) ppm. Anal. Calcd for $C_{76}H_{82}Al_2FeN_{12}O_{16}$: C, 61.95; H, 5.61; N, 11.41; Found: C, 61.91; H, 5.74; N, 11.29 %.

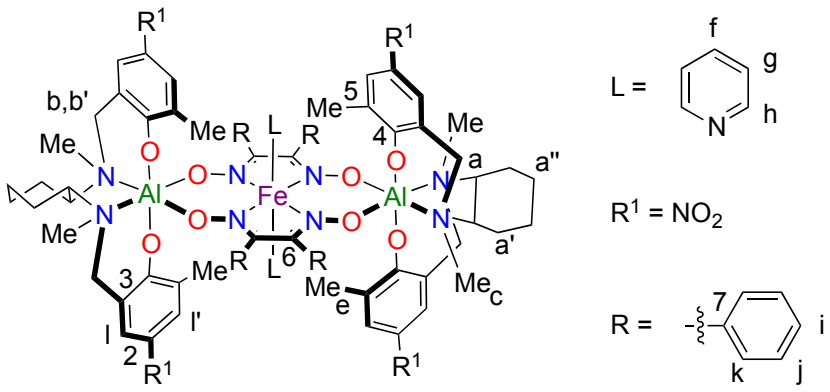

Synthesis of 32^{NO_2}

Route A: To a slurry of **31**^{NO_2} (0.150 g, 0.302 mmol) in toluene (5 ml) was added **24** (0.101 g, 0.146 mmol) with THF (3 ml). The slurry was stirred for a total of 3 days, during which the solution took on a purple orange hue. From this colored solution a solid precipitated on the walls of the vial. After the allotted time the solvent was removed *in vacuo*. The solid was washed three times with hexanes to remove the excess toluene. The solid was fractioned with hexanes, diethylether, toluene, and THF. The desired product was found in the THF fraction. Yield 0.129 g, 52 %

Route B: Sodium hexamethyldisilazide (0.030 g, 0.163 mmol) was added to a solution of **31**^{NO_2} macrocycle (0.236 g, 0.160 mmol) in THF. The solution was stirred for 12 hours and the solvent was removed via vacuum. The resulting residue was washed with pentane to remove the bis(trimethylsilyl)amine. The bis(trimethylsilyl)amine free solid (0.217 g, 0.143 mmol) was taken up in THF and mixed with a solution of Fe(II)Cl_2 (0.019 g, 0.146 mmol) in THF. The solution immediately turned a dark purple. The dark purple solution was stirred for 3 hours after which excess pyridine was added. Upon addition of pyridine the solution color changed from dark purple to a reddish purple. The solvent was removed *in vacuo* yielding a purple solid which was washed with benzene and extracted with THF. Yield 0.174 g, 72 %

^{1}H NMR (500 MHz, CD_2Cl_2), δ 8.61 (4H, s, h), δ 7.83 (4H, l',), δ 7.63 (d, 4H), δ 7.28 (m, 20H), δ 7.02 (dd, 4H), δ 6.37 (m, 2H), δ 4.15 (d, 4H), δ 2.89 (d, 4H), δ 1.80 (s, 12H), δ 1.75 (s, 12H) ^{13}C{^{1}H} NMR (126 MHz, CD_2Cl_2) δ 166.85 (4), 159.75 (6), 155.16 (h), 135.81 (2), 134.82 (k), 129.75 (j), 128.35 (5) 128.25 (7) 127.76 (f), 126.35 (l'), 123.88 (l), 123.05 (g), 121.54 (3), 58.48 (b,b') , 56.27 (a), 40.97 (c), 24.40 (a"), 22.06 (a'), 16.69 (e) ppm. Anal. Calcd for $C_{86}H_{90}Al_2FeN_{14}O_{16}$: C, 61.28; H, 5.38; N, 11.63; Found: C, 61.13; H, 5.46; N, 11.43 %

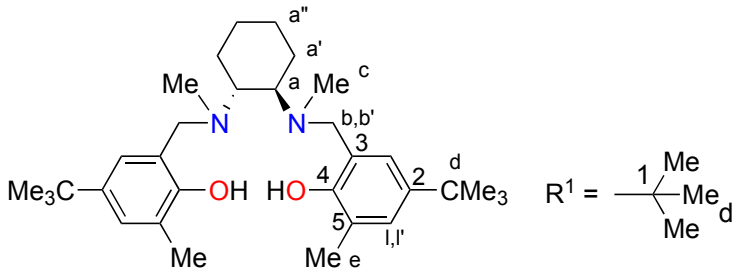

Synthesis of 30^{tBu}

This compound was synthesized via a mannich condensation of the (*R,R*)-1,2-diammoniumcyclohexane mono-(+)-tartrate salt and 2-methyl-4-tert-butylphenol using a previously published procedure.[7,8] The amines were methylated following the same procedure resulting in the compound **30^{tBu}**. ^{1}H NMR (300 MHz, $CDCl_3$), δ 10.01 (2H, br s, O*H*), 7.05 (2H, d, J = 2.1 Hz, l,l'), 6.82 (2H, d, J = 2.4 Hz, l,l'), 3.77 (2H, d, J = 13.2 Hz, b,b'), 3.66 (2H, d, J = 13.3 Hz, b,b'), 2.70 (2H, m, a), 2.20 (6H, s, e), 2.17 (6H, s, c), 2.01 (2H, m, a"), 1.81 (2H, d, a'), 1.27 (18H, s, d), 1.17 (4H, m, a',a") ppm. ^{13}C{^{1}H} NMR (126 MHz, C_6D_6) δ 154.06 (4), 140.74 (2), 127.17 (l'), 124.73 (5), 123.32 (l), 121.26 (3), 61.65 (b,b'), 33.66 (1), 31.60 (d), 25.05 (c), 21.99 (a,a',a"), 16.23 (e) ppm. ESI-MS Calc. (M) 494.3872 Found. 495.3 (MH+)

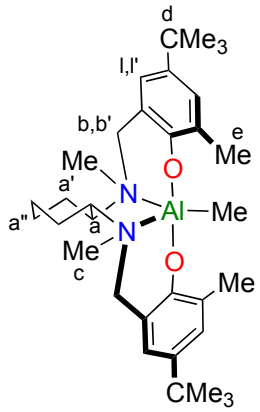

Synthesis of 31^{tBu}

Compound **31^{tBu}** was synthesized using trimethylaluminum following a published procedure for similar aluminium alkyl complexes.[6,7] A slurry of **30^{tBu}** (0.956 g, 1.93 mmol) in toluene was frozen in a coldwell. Upon freezing the solution was allowed to thaw upon which a freshly thawed solution of trimethylaluminum (0.139 g, 1.93 mmol) in toluene (3 ml) was added slowly. This mixture was allowed to warm to room temperature and left stirring for 12 hours. After 12 hours the solvent was removed in vacuo, yielding an off white solid which was used without further purification. Yield: 0.900 g, 87 % 1H NMR (300 MHz, C6D6) δ 7.32, 7.29, 6.90, 6.82, and 6.78 (l,l'), 3.61, 3.54, 3.32, 3.27, 2.79, 2.75, and 2.70 (b,b'), 2.63 and 2.43 (e), 2.29 and 1.99 (a), 1.88, 1.68, and 1.66 (c), 1.41, 1.39, and 1.39 (d), 1.21, 0.60, and 0.48 (a',a"), -0.40 (AlCH3) ppm. $^{13}C\{^{1}H\}$ NMR (126 MHz, CD_2Cl_2) δ 156.06 (4), 155.89 (4), 138.33 (2), 137.68 (2), 127.43 (l'), 127.29 (l'), 126.93 (l'), 126.68 (5), 126.55 (5), 126.01 (5), 123.04 (l), 122.84 (l), 120.03 (3), 118.54 (3), 63.81 (b,b'), 60.73 (b,b'), 60.26 (b,b'), 59.48 (b,b'), 42.67, 36.77, 33.57 (1), 31.51 (d), 24.79 (a"), 24.54 (a"), 23.13(a'), 22.89

(a'), 22.72 (a'), 16.21 (e), 16.08 (e), 15.72 (Al*C*H$_3$) ppm multiple diastereomers in solution.[27]Al NMR (104.7 MHz, 25 °C, CD_2Cl_2) δ 74.21 ppm, $\omega_{1/2}$ 6500 Hz.

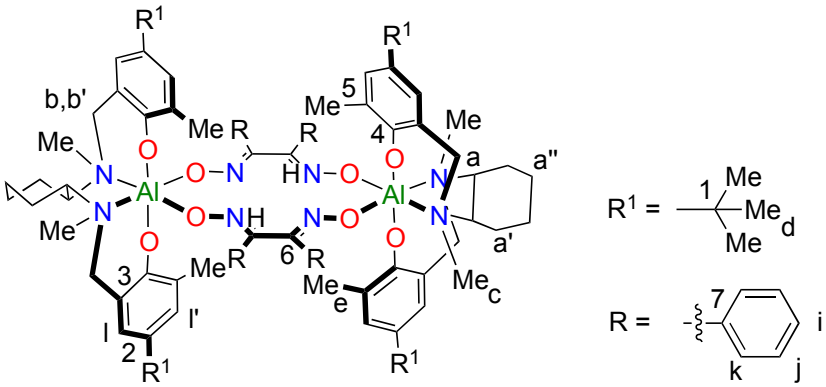

Synthesis of 31^{tBu} macrocycle

The macrocycle was synthesized following the synthesis procedure for 3a. A stirring solution of **31^{tBu}** (0.105 g, 0.197 mmol) in THF was treated with a slurry of diphenylglyoxime (0.047 g, 0.196 mmol) in THF. The solution was stirred for 3 hours over which the solution became yellow. The solvent was removed in vacuo to yield a pale yellow solid. **31^{tBu}** macrocycle was used as isolated without any further purification. It can also be purified through precipitation from pentane. Yield 0.145 g, 98 %. 1H NMR (300 MHz, C6D6) δ 14.20 (2H, s, NH), 7.67 (8H, d, J = 7.1 Hz, k), 7.29 (4H, s, l,l'), 6.91 (12H, m, j,i), 6.78 (4H, m, l,l'), 4.54 (4H, d, J = 13.0 Hz, b,b'), 2.88 (4H, d, J = 13.1 Hz, b,b'), 2.57 (4H, m, a), 2.34 (12H, s, e), 2.06 (12H, s, c), 1.45 (36H, s, d), 1.25 (8H, m, a', a"), 0.38 (8H, m, a',a") ppm. 13C{1H} NMR (126 MHz, CD2Cl2) δ 156.69 (4), 148.27 (6), 136.31 (7), 131.56 (2), 130.12 (k), 128.76 (j), 127.53 (i), 126.99 (l'), 125.54 (5), 123.17 (l), 120.29 (3), 59.40 (b,b'), 55.56 (a), 39.89 (c), 33.49 (1), 31.67 (d), 24.31 (a"), 21.83 (a'), 16.05 (e). 27Al NMR (104.7 MHz, 25 °C, CD2Cl2) δ

14.40 ppm, ω1/2 4150 Hz. Anal. Calcd for C92H118Al2FeN8O8: C, 72.80; H, 7.84; N, 7.38; Found: C, 72.68; H, 7.60; N, 7.12 %

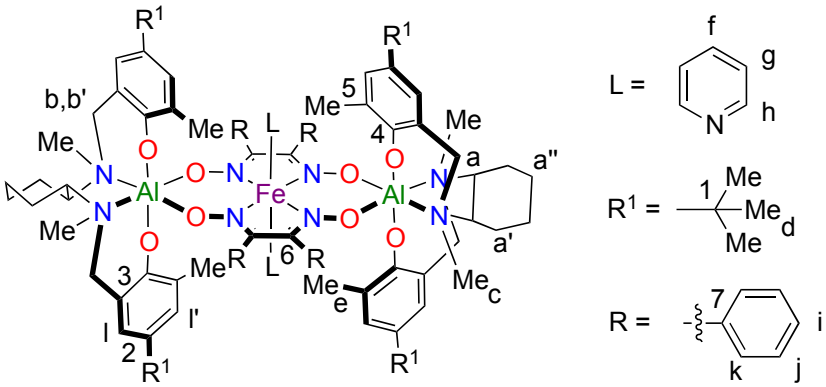

Synthesis of 32^{tBu}

Route B: In a 100 mL round bottom, a solution of **30^{tBu}** (2.167 g, 4.05 mmol) was treated with a slurry of $Fe(DPG)_2(Py)_2$ (1.334 g, 1.93 mmol) in benzene at room temperature. The solution was stirred allowing for the produced methane to escape. After 24 hours the solvent was removed in vacuo. The crude solid was taken up in hexanes and filtered. The recovered solid was washed with diethyl ether and extracted with toluene. Purified **12^{tBu}** was precipitated from toluene by adding hexanes to the toluene mixture and cooling the mixture to -35˚C overnight. Another crop of purified solid can be obtained from the hexane fraction via cooling to -35˚C overnight. Yield 2.197 g, 66 %

Route A: Sodium hexamethyldisilazide (0.013 g, 0.069 mol) was added to a solution of **31^{tBu} macrocycle** (0.503 g, 0.033 mol) in THF. The solution was stirred for 2 hours and the solvent was removed via vacuum. The resulting residue was triterated with THF to remove the bis(trimethylsilyl)amine. The bis(trimethylsilyl)amine free solid was taken up in THF and mixed with a slurry of $Fe(II)Cl_2$ (0.005 g, 0.039 mmol) in THF. The

solution immediately turned a dark purple. The dark purple solution was stirred for one hour after which excess pyridine was added. Upon addition of pyridine the solution color changed from dark purple to a reddish purple. The solvent was removed in vacuo yielding a purple solid. The solid was washed with hexanes and a small amount of diethylether before it was extracted with toluene. The solvent was removed *in vacuo* yielding the same product as Route A. Yield 0.414 g, 72 %

^{1}H NMR (500 MHz, C_6D_6) δ 9.35 (4H, d, J = 5.5 Hz, h), 7.33 (8H, d, J = 7.4 Hz, k), 7.20 (4H, s, l'), 7.06 (8H, t, J = 7.4 Hz, j), 7.00 (4H, m, J = 7.1 Hz, i), 6.77 (2H, t, J = 7.6 Hz, f), 6.74 (4H, s, l), 6.34 (4H, t, J = 6.7 Hz, g), 4.54 (4H, d, J = 13.2 Hz, b'), 2.80 (4H, d, J = 13.4 Hz, b), 2.52 (4H, s, a), 2.17 (12H, s, e), 1.93 (12H, s, c), 1.35 (36H, s, d), 1.22 (4H, m, a'), 1.02 (4H, s, a''), 0.46 (4H, m, a'), 0.28 (4H, m, a'') ppm; ^{13}C{^{1}H} NMR (125.70 MHz, C_6D_6) δ 158.77 (6), 157.80 (4), 157.01 (h), 136.14 (7), 135.90 (2), 134.17 (f), 130.62 (k), 127.78 (j), 127.41 (i), 127.08 (l'), 126.17 (5), 122.82 (l), 122.56 (g), 121.27 (3), 59.90 (b,b'), 55.45 (a), 40.90 (c), 33.86 (1), 32.29 (d), 24.26 (a"), 21.78 (a'), 17.51 (e) ppm; ^{27}Al NMR (104.7 MHz, 25 °C, C_6D_6) δ 14.19 ppm, $\omega_{1/2}$ 9000 Hz. Anal. Calcd for $C_{102}H_{126}Al_2FeN_{10}O_8$: C, 70.82; H, 7.34; 8.10; Found C, 69.90; H, 7.24; N, 7.44 %

Table 4.1. Crystal and refinement data for complexes **26**, **29^{tBu}**, and **32^{NO2}**

	26	**29^{tBu}**	**32^{NO2}**
CCDC Number	861067		861069
Empirical formula	$C_{72}H_{80}N_8O_8Al_2Fe$	$C_{94}H_{114}Al_2FeN_{10}O_8$	$C_{86}H_{90}N_{14}O_{16}Al_2Fe \cdot C_4H_{10}O \cdot 3.5(C_4H_8O)$
Formula weight	1295.25	1621.76	2012.01
T (K)	100(2)	100(2)	100(2)
a, Å	22.511(4)	14.7358(11)	23.9420(6)
b, Å	10.8586(19)	20.2952(15)	27.0271(6)
c, Å	28.663(5)	33.354(3)	15.5154(3)
, deg	90	77.202(2)	90
, deg	109.657(2)	88.031(2)	90
, deg	90	74.307(2)	90
Volume, Å^3	6598(2)	9361.2(12)	10039.7(4)
Z	4	4	4
Crystal system	Monoclinic	Triclinic	Orthorhombic
Space group	C 2/*c*	P	P 2_12_12 (#18)
d_{calc}, g/cm^3	1.304 Mg/m^3	1.151 Mg/m^3	1.331 Mg/m^3
range, deg	2.40 to 27.52	1.55 to 25.00	1.86 to 23.28
μ, mm^{-1}	0.318	none	0.246
Abs. Correction	Semi-empirical from equivalents (TWINABS)	Semi-empirical from equivalents	None
GOF	1.423	1.009	1.681
R_1,[a] wR_2[b] [I>2(I)]	R1 = 0.0537 *w*R2 = 0.0804	R1 = 0.0650 *w*R2 = 0.1428	R1 = 0.0570 *w*R2 = 0.0558

[a] $R_1 = \sum ||F_o| - |F_c|| / \sum |F_o|$. [b] $wR_2 = [\sum[w(F_o^2-F_c^2)^2] / \sum[w(F_o^2)^2]]^{1/2}$.

References

1. R. Chakrabarty, P. S. Mukherjee and P. J. Stang, *Chem. Rev.*, 2011, **111**, 6810-6918.
2. V. L. Pecoraro, A. J. Stemmler, B. R. Gibney, J. J. Bodwin, H. Wang, J. W. Kampf and A. Barwinski, in *Prog. Inorg. Chem.*, John Wiley & Sons, Inc., 2007, pp. 83-177.
3. G. Mezei, C. M. Zaleski and V. L. Pecoraro, *Chem. Rev.*, 2007, **107**, 4933-5003.
4. F. A. Cotton, C. Lin and C. A. Murillo, *Proc. Natl. Acad. Sci.*, 2002, **99**, 4810-4813.
5. F. A. Cotton, C. Lin and C. A. Murillo, *Acc. Chem. Res.*, 2001, **34**, 759-771.
6. R. S. Forgan, J.-P. Sauvage and J. F. Stoddart, *Chem. Rev.*, 2011, **111**, 5434-5464.
7. N. C. Gianneschi, M. S. Masar and C. A. Mirkin, *Acc. Chem. Res.*, 2005, **38**, 825-837.
8. C. G. Oliveri, P. A. Ulmann, M. J. Wiester and C. A. Mirkin, *Acc. Chem. Res.*, 2008, **41**, 1618-1629.
9. M. J. Wiester, P. A. Ulmann and C. A. Mirkin, *Angew. Chem. Int. Ed.*, 2011, **50**, 114-137.
10. M. Fujita, *Chem. Soc. Rev.*, 1998, **27**, 417-425.
11. M. Fujita, M. Tominaga, A. Hori and B. Therrien, *Acc. Chem. Res.*, 2005, **38**, 369-378.
12. J. Meeuwissen and J. N. H. Reek, *Nat Chem*, 2010, **2**, 615-621.
13. R. Q. Snurr, J. T. Hupp and S. T. Nguyen, *AlChE J.*, 2004, **50**, 1090-1095.
14. C. Piguet, G. Bernardinelli and G. Hopfgartner, *Chem. Rev.*, 1997, **97**, 2005-2062.
15. S. De, K. Mahata and M. Schmittel, *Chem. Soc. Rev.*, 2010, **39**, 1555-1575.
16. P. H. Dinolfo and J. T. Hupp, *Chem. Mater.*, 2001, **13**, 3113-3125.
17. J. R. Nitschke, *Acc. Chem. Res.*, 2006, **40**, 103-112.
18. S. J. Lee and W. Lin, *Acc. Chem. Res.*, 2008, **41**, 521-537.
19. M. S. Lah and V. L. Pecoraro, *J. Am. Chem. Soc.*, 1989, **111**, 7258-7259.
20. D. Li, R. Li, Z. Qi, X. Feng, J. Cai and X. Shi, *Inorg. Chem. Commun.*, 2001, **4**, 483-485.
21. T. Mizuta, T. Aotani, Y. Imamura, K. Kubo and K. Miyoshi, *Organometallics*, 2008, **27**, 2457-2463.
22. S. Ghosh, R. Chakrabarty and P. S. Mukherjee, *Inorg. Chem.*, 2008, **48**, 549-556.
23. H. Rauter, E. C. Hillgeris, A. Erxleben and B. Lippert, *J. Am. Chem. Soc.*, 1994, **116**, 616-624.
24. M. J. E. Resendiz, J. C. Noveron, H. Disteldorf, S. Fischer and P. J. Stang, *Org. Lett.*, 2004, **6**, 651-653.
25. J. F. Drake and R. J. P. Williams, *Nature*, 1958, **182**, 1084.
26. L. Vaska and T. Yamaji, *J. Am. Chem. Soc.*, 1971, **93**, 6673-6674.
27. G. N. Schrauzer, *Acc. Chem. Res.*, 1968, **1**, 97-103.
28. G. N. Schrauzer and J. Kohnle, *Chem. Ber.*, 1964, **97**.
29. P. Connolly and J. H. Espenson, *Inorg. Chem.*, 1986, **25**, 2684-2688.
30. X. Hu, B. M. Cossairt, B. S. Brunschwig, N. S. Lewis and J. C. Peters, *Chem. Commun.*, 2005, 4723-4725.
31. M. Razavet, V. Artero and M. Fontecave, *Inorg. Chem.*, 2005, **44**, 4786-4795.
32. C. Baffert, V. Artero and M. Fontecave, *Inorg. Chem.*, 2007, **46**, 1817-1824.
33. J. L. Dempsey, B. S. Brunschwig, J. R. Winkler and H. B. Gray, *Acc. Chem. Res.*, 2009, **42**, 1995-2004.
34. J. L. Dempsey, J. R. Winkler and H. B. Gray, *J. Am. Chem. Soc.*, 2010, **132**, 16774-16776.
35. X. Hu, B. S. Brunschwig and J. C. Peters, *J. Am. Chem. Soc.*, 2007, **129**, 8988-8998.

36. D. V. Stynes, I. Vernik and F. Zobi, *Coord. Chem. Rev.*, 2002, **233**, 273-287.
37. D. V. Stynes, D. B. Leznoff and D. G. A. Harshani de Silva, *Inorg. Chem.*, 1993, **32**, 3989-3990.
38. D. W. Thompson and D. V. Stynes, *Inorg. Chem.*, 1990, **29**, 3815-3822.
39. U. Kohler, H. D. Hausen and J. Weidlein, *J. Organomet. Chem.*, 1984, **272**, 337-350.
40. C. H. Li, R.-J. Wang, H.-Z. Kou and Y. Li, *Acta Crystallogr. Sect. Sect. E: Struct. Rep. Online*, 2003, **59**, m608-m610.
41. P. Chaudhuri, M. Winter, P. Fleischhauer, W. Haase, U. Florke and H.-J. Haupt, *J. Chem. Soc., Chem. Commun.*, 1990, 1728-1730.
42. F. Birkelbach, U. Flörke, H.-J. Haupt, C. Butzlaff, A. X. Trautwein, K. Wieghardt and P. Chaudhuri, *Inorg. Chem.*, 1998, **37**, 2000-2008.
43. F. Birkelbach, T. Weyhermuller, M. Lengen, M. Gerdan, A. X. Trautwein, K. Wieghardt and P. Chaudhuri, *J. Chem. Soc., Dalton Trans.*, 1997, 4529-4538.
44. D. Burdinski, E. Bill, F. Birkelbach, K. Wieghardt and P. Chaudhuri, *Inorg. Chem.*, 2001, **40**, 1160-1166.
45. D. Burdinski, F. Birkelbach, T. Weyhermüller, U. Flörke, H.-J. Haupt, M. Lengen, A. X. Trautwein, E. Bill, K. Wieghardt and P. Chaudhuri, *Inorg. Chem.*, 1998, **37**, 1009-1020.
46. Y. Z. Voloshin, O. A. Varzatskii, A. S. Belov, Z. A. Starikova, A. V. Dolganov and T. V. Magdesieva, *Polyhedron*, 2008, **27**, 325-334.
47. Y. Z. Voloshin, O. A. Varzatskii, A. V. Palchik, N. G. Strizhakova, I. I. Vorontsov, M. Y. Antipin, D. I. Kochubey and B. N. Novgorodov, *New J. Chem.*, 2003, **27**, 1148-1155.
48. E. Y. Tshuva, I. Goldberg and M. Kol, *J. Am. Chem. Soc.*, 2000, **122**, 10706-10707.
49. A. Yeori, I. Goldberg, M. Shuster and M. Kol, *J. Am. Chem. Soc.*, 2006, **128**, 13062-13063.
50. E. Y. Tshuva, S. Groysman, I. Goldberg, M. Kol and Z. Goldschmidt, *Organometallics*, 2002, **21**, 662-670.
51. C.-T. Chen, C.-A. Huang and B.-H. Huang, *Dalton Trans.*, 2003, 3799-3803.
52. H. Du, A. H. Velders, P. J. Dijkstra, J. Sun, Z. Zhong, X. Chen and J. Feijen, *Chem. Eur. J.*, 2009, **15**, 9836-9845.
53. I. W. Pang and D. V. Stynes, *Inorg. Chem.*, 1977, **16**, 590-594.
54. B. A. Jillot and R. J. P. Williams, *J. Chem. Soc. Res.*, 1958, 462-467.
55. N. Sanders and P. Day, *J. Chem. Soc. A*, 1969, 2303-2308.
56. R. Hoffmann, J. M. Howell and A. R. Rossi, *J. Am. Chem. Soc.*, 1976, **98**, 2484-2492.
57. E. Cremades, J. Echeverría and S. Alvarez, *Chem. Eur. J.*, 2010, **16**, 10380-10396.
58. Y. Yamano, I. Masuda and K. Shinra, *Bull. Chem. Soc. Jpn.*, 1971, **44**, 1581-1585.
59. I. Vernik and D. V. Stynes, *Inorg. Chem.*, 1996, **35**, 6210-6220.
60. A. A. Dvorkin, Y. A. Simonov, T. I. Malinovskii, I. I. Bulgak and D. G. Batir, *Proc. Nat. Acad. Sci. USSR*, 1997, **234**, 1372.
61. R. Benn, A. Rufińska, H. Lehmkuhl, E. Janssen and C. Krüger, *Angew. Chem. Int. Ed.*, 1983, **22**, 779-780.
62. J. W. Akitt, in *Prog. Nucl. Magn. Reson. Spectrosc.*, 1989, vol. 21, pp. 1-149.
63. J. H. Wengrovius, M. F. Garbauskas, E. A. Williams, R. C. Goint, P. E. Donahue and J. F. Smith, *J. Am. Chem. Soc.*, 1986, **108**, 982-989.
64. B. Olenyuk, J. A. Whiteford and P. J. Stang, *J. Am. Chem. Soc.*, 1996, **118**, 8221-8230.
65. D. Lionetti, A. J. Medvecz, V. Ugrinova, M. Quiroz-Guzman, B. C. Noll and S. N. Brown, *Inorg. Chem.*, 2010, **49**, 4687-4697.

66. B. Adam, E. Bill, E. Bothe, B. Goerdt, G. Haselhorst, K. Hildenbrand, A. Sokolowski, S. Steenken, T. Weyhermüller and K. Wieghardt, *Chem. Eur. J.*, 1997, **3**, 308-319.
67. R. R. Gagne and D. M. Ingle, *Inorg. Chem.*, 1981, **20**, 420-425.
68. G. M. Brown, F. R. Hopf, J. A. Ferguson, T. J. Meyer and D. G. Whitten, *J. Am. Chem. Soc.*, 1973, **95**, 5939-5942.
69. G. M. Brown, F. R. Hopf, T. J. Meyer and D. G. Whitten, *J. Am. Chem. Soc.*, 1975, **97**, 5385-5390.

CHAPTER 6

Aluminum-Bridged Bisglyoximato Cobalt Complexes: Synthesis and Electrochemical Proton Reduction Properties

The text for this chapter was taken in part from:

Kelley, P.; Day, M. W.; Agapie, T. *Eur. J. Inorg. Chem.* 2013, *22-23*, 3840-3845.

EurJIC
European Journal of Inorganic Chemistry

22-23/2013
1st + 2nd August Issue

Cluster Issue:
Small-Molecule Activation by Reactive Metal Complexes

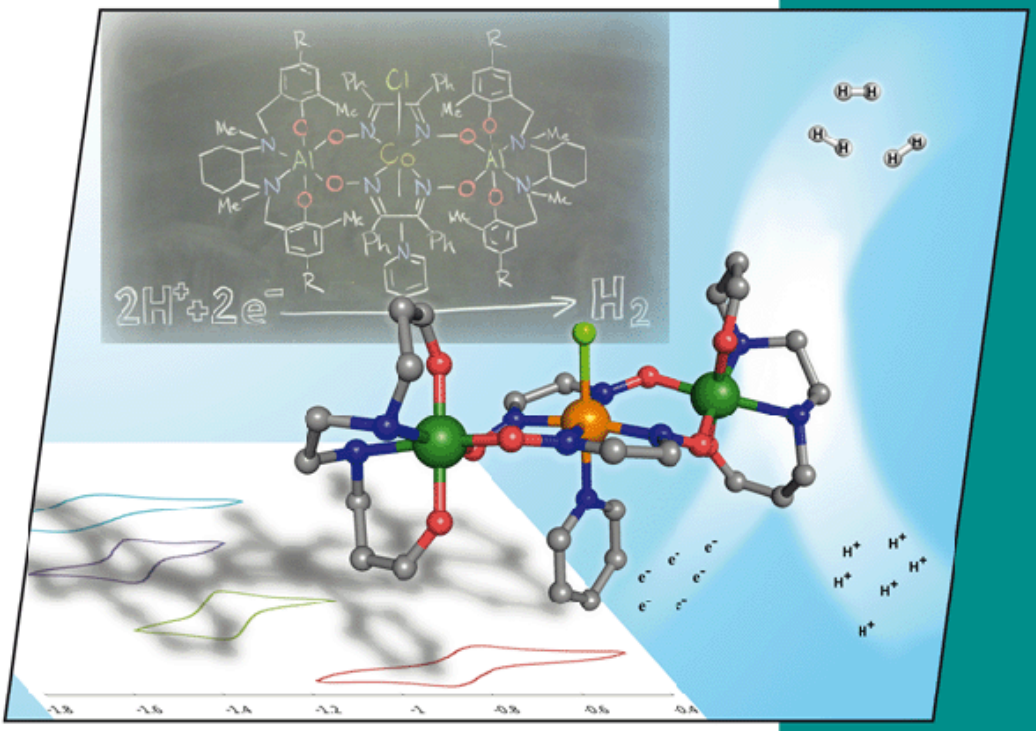

Front Cover Picture
Theodor Agapie et al.
H_2 Evolution Catalyzed by Al-Bridged Cobalt Complexes

Microreviews by
Benedict M. Gardner and Stephen T. Liddle; John Arnold et al.; Kallol Ray et al.

A Journal of
ChemPubSoc Europe

WILEY-VCH
www.eurjic.org

EJICFE (22-23) 3727–4104 (2013) · ISSN 1099-0682 · No. 22-23/2013

Abstract

The syntheses of several cobalt diglyoximato complexes connected by one or two aluminum bridges are described. The aluminum centers are supported by tunable tetradentate diamine bisphenoxide ligands. Electrochemical investigations revealed that the number of aluminum bridges and the nature of the substituents on the phenoxide ligands significantly affect the cobalt reduction potentials. The present aluminium-cobalt compounds are electrocatalysts for proton reduction to dihydrogen at potentials negative of boron-and proton-bridged analogs. The reported synthetic strategies allow for modulation of reduction potentials and secondary coordination sphere interactions by tuning the ancillary ligands bound to aluminum.

INTRODUCTION:

The reduction of protons to dihydrogen is of interest in the context of solar energy conversion and storage in chemical bonds.[1] In biological systems, this reaction is catalyzed at near thermodynamic potentials by [FeNi] and [FeFe] hydrogenases.[2] Although useful models for mechanistic studies, synthetic complexes based on hydrogenase active sites display large overpotentials and low turnover numbers.[3] Systems based on nickel tetraphosphine catalysts show high activity.[4] Several promising cobalt-based catalysts have been reported, supported by multidentate nitrogen ligands.[1c, 1d, 5] Bisglyoximato cobalt complexes, $Co(dpgX)_2(L)_2$ (dpg = diphenylglyoximato, X = H, BF_2), were reported to catalyze the reduction of protons both chemically and electrochemically.[5a-h, 6] Substitution of the protons bridging the two glyoximato groups (see complex **3**, Scheme 1) with BF_2 groups was found to affect the reduction potential of the cobalt complexes resulting in electrocatalysts active at low overpotentials.[5d-e 6a] The BF_2 moiety also imparts a greater stability towards acid in contrast to the proton-bridged species.[5d, 6j] Optimization of these catalysts has been focused either on varying the axial ligand of cobalt or the glyoxime backbone.[5d, 6a-b, 7] Herein, we report on the synthesis of bisglyoximato cobalt complexes supported by one or two aluminum-based linkers and their electrochemical properties.

RESULTS & DISCUSSION:

In analogy to the tetracoordinate boron bridges, saturated, six-coordinate aluminum linkers were targeted. Aluminum precursors having varied electronic properties were prepared, with ancillary ligands (30^{tBu} and 30^{NO2}) based on enantiopure tetradentate diamine bisphenoxide salan frameworks, starting from (*R,R*)-*trans*-1,2-diaminocyclohexane.[8] Reaction of diphenols 30^{NO2} and 30^{tBu} with $AlMe_3$ generated monoalkylaluminum diphenoxide species (31^{NO2} and 31^{tBu}, Scheme 1) as indicated by the peaks upfield of 0 ppm in the ^1H NMR spectrum assigned to the Al-CH_3 group. Monoalkylaluminum species supported by closely related ancillary ligands are formed as mixtures of inseparable isomers some of which interconvert at room temperature.[8c] Similarly, two Al-CH_3 singlets were observed for 31^{NO2}, but since the subsequent step could involve isomerizations, the mixture was used without separation.

Scheme 6.1. Synthesis of mono and dialuminum-bridged bisglyoximato cobalt complexes.

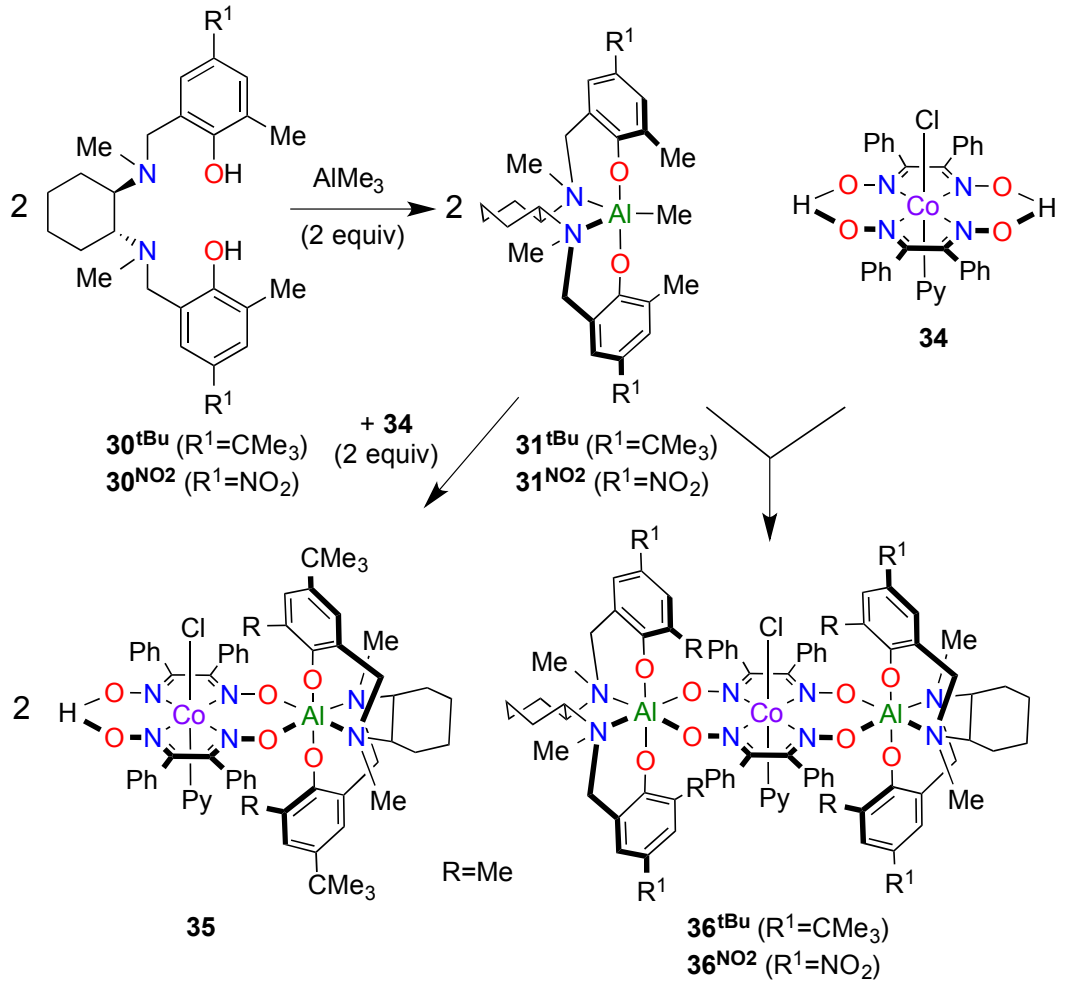

Reaction of two equivalents of $\mathbf{31}^{tBu}$ or $\mathbf{31}^{NO2}$, with cobalt diglyoximato complex **34** led to the generation of new species according to ^{1}H NMR spectroscopy. The absence of the upfield shifted singlets diagnostic of the Al-C*H*$_3$ moiety supports alkane elimination. Integrals for the *ortho* pyridine protons and the NC*H*$_3$ protons are consistent with the incorporation of two salan-supported aluminum moieties for each cobalt. The presence of four diastereotopic proton signals for the NC*H*$_2$ moieties indicates a *C*$_2$-symmetric structure, with the *C*$_2$ axis containing the cobalt center and its axial ligands. The distinct axial ligands (chloride vs pyridine) differentiate the top and bottom of the molecule, as depicted in Scheme 1. Employing the analog of **34**

displaying the dimethyl glyoxime backbone resulted in similar species (^{1}H NMR), however isolation of analytically pure samples was unsuccesfull to date due to their solubility properties.

Single crystal X-ray diffraction (XRD) studies confirmed the above structural assignment (Figure 1). The aluminum-bound glyoxime oxygen atoms are found at average O-O distances of 2.84 Å for **36^{tBu}**, 2.83 Å for **36^{NO2}**, which are significantly larger than those in H- (**3**, 2.47 Å)[9] or BF_2-linked (2.50 Å) analogs.[5e, 9b] The average Co-N distances were found to be 1.91 Å for both **36^{tBu}** and **36^{NO2}**, which are similar to those found in the H- (1.91 Å) and BF_2-linked species (1.89 Å). These structural characteristics suggest that although the macrocycles containing aluminum are larger, the effect on the Co-N distances is small. In contrast to proton- or boron-linked diglyoximato complexes that are typically planar, the cobalt-bound $N_4O_2Al_2$ macrocycle displays significant ruffling and doming distortions. The ruffling may be due to the C_2-steric strain imposed by the salan ligands found on opposite sides of the macrocycle or, as observed for porphyrins,[10] to the larger macrocycle which requires distortion to allow for binding to a central metal. The doming is likely caused by repulsive steric interaction between the pyridine and the proximal phenoxide ortho-methyl groups. Indeed, the methyl C-C distances are 7.60 and 6.86 Å on the chloride side vs 10.15 and 10.08 Å on the pyridine side, for **36^{tBu}** and **36^{NO2}**, respectively.

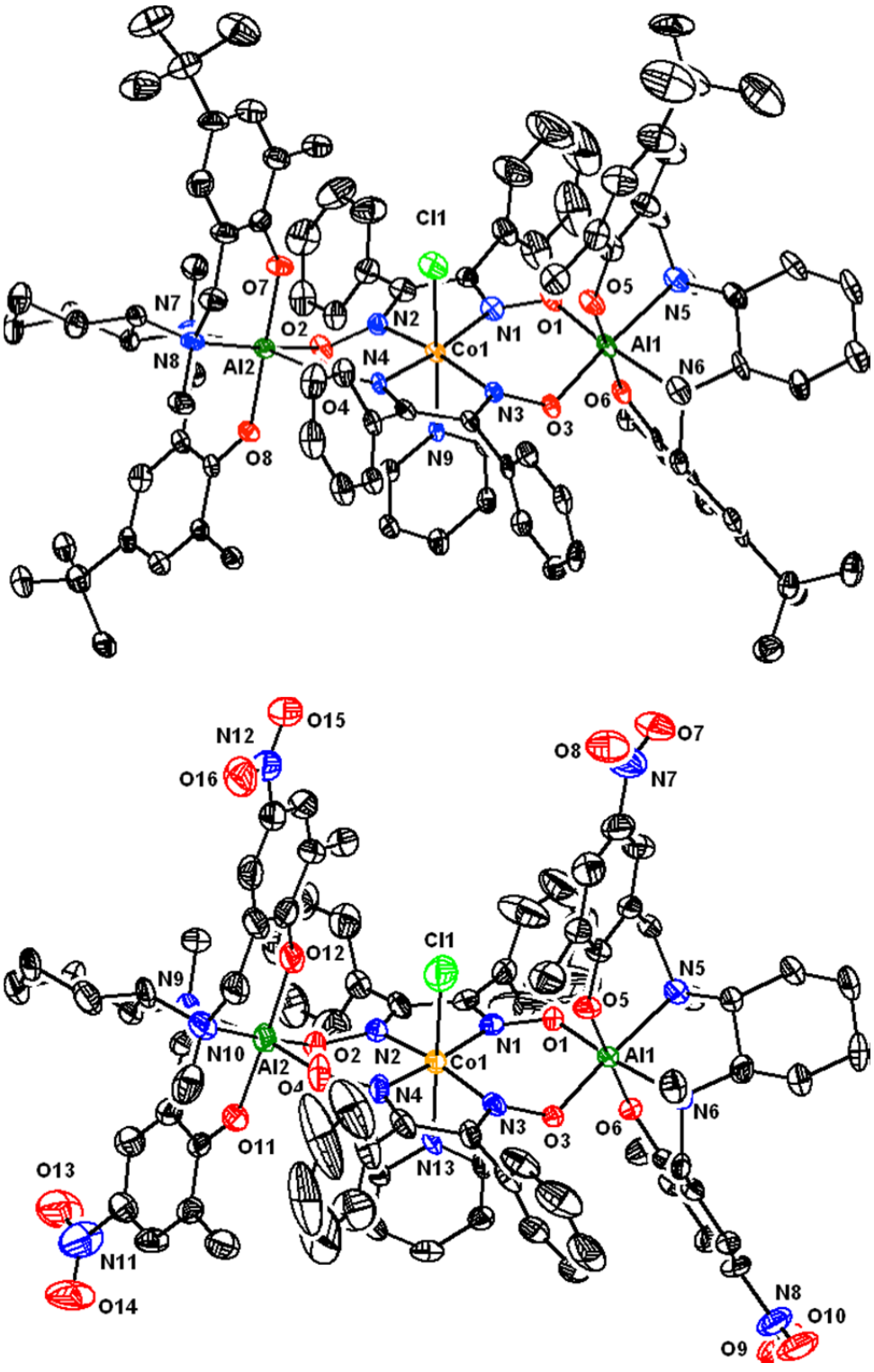

Figure 6.1. Solid state structures of 36^{tBu} and 36^{NO_2}. Hydrogen atoms and cocrystallization solvent molecules have been omitted for clarity; thermal ellipsoids are displayed at the 50% probability.

Reaction of **34** with one equivalent of **31**^{tBu} led to the generation of a new species with NMR spectroscopic features consistent with a bimetallic cobalt-aluminum complex of *C* symmetry (**35**, Scheme 1). A downfield singlet, at 20 ppm, is indicative of the proton bridging two glyoximato units. An XRD study confirms this structural assignment and highlights the effect of bridging proton and aluminum in the same cobalt diglyoximato unit. The O-O distance is 2.38 Å on the protonated side and 2.85 Å on the aluminum side. The average Co-N distances are similar on the H- and Al-sides of the macrocycle. These are in agreement with the structural parameters observed in compounds **34** and **36**.

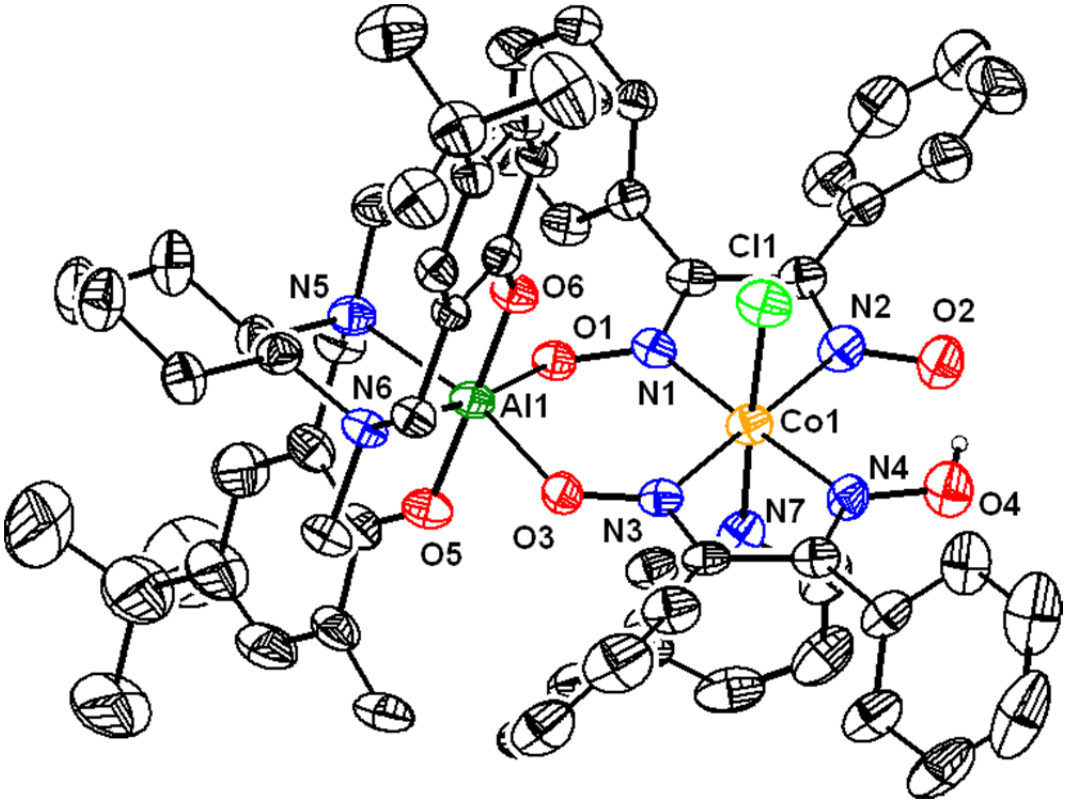

Figure 6.2. Solid state structure of **35**. Hydrogen atoms and cocrystallization solvent molecules have been omitted for clarity; thermal ellipsoids are displayed at the 50% probability.

A dialuminum zinc analog of 36^{tBu} was targeted via a complementary synthetic protocol for comparison (Scheme 2).[11] Reaction of 31^{tBu} with diphenylglyoxime led to a species (31^{tBu} macrocycle) that displays a singlet at 14 ppm (^{1}H NMR spectrum) assigned to protonated oxime nitrogens. Treatment with diethylzinc generates a new species without any signals downfield of 8 ppm, again consistent with alkane elimination. Only two doublets are observed for the NC*H*$_2$ protons consistent with the *pseudo-D*$_2$ structure assigned to the 31^{tBu} macrocycle.

Scheme 6.2. Synthesis of dialuminum-bridged bisglyoximato zinc complex via dialuminum templation of bisglyoximato macrocycle.

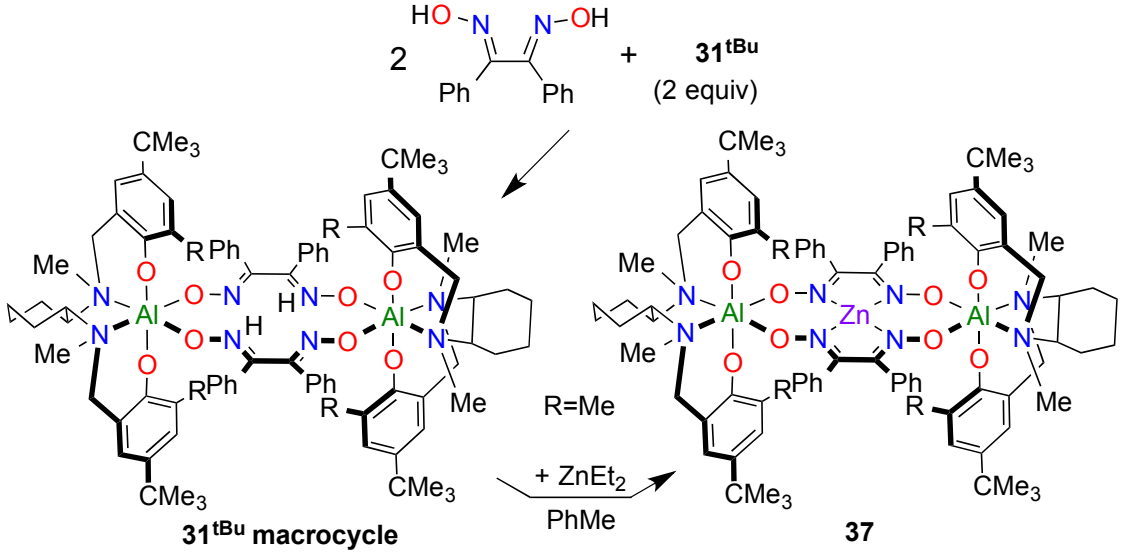

The electrochemistry of the present complexes was investigated by cyclic voltametry (CV). In dimethylformamide (DMF), the Co^{II}/Co^{I} couple was observed for **35** at -1.34 V vs Fc^{+}/Fc, 36^{tBu} at -1.59 V, and 36^{NO2} at -1.35 V (Figure 6.3 and 6.4). These are the potentials at which increase in current was observed upon addition of acid (vide infra). These couples are more negative than for boron- and proton-bridged analogs.[6a] Several redox events were also observed between 0.2 and 1 V and were assigned to ligand-based processes (Figure 6.3). These waves are in the range of previously

reported electrochemical oxidations of phenoxides coordinated to redox inactive metals.[112] As expected, compound **37**, containing Zn^{II} instead of Co^{III}, shows redox events at similar potentials and no events between -2 and 0 V, consistent with lack of redox chemistry at the central atom.

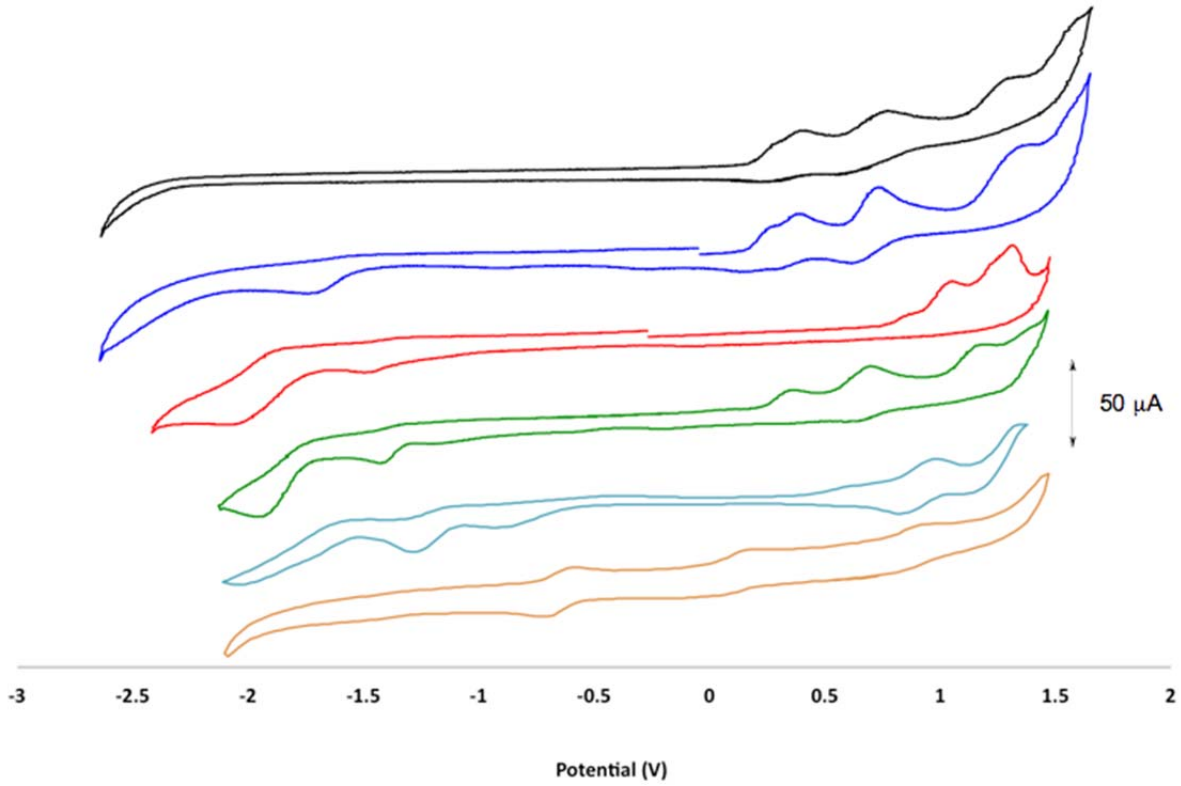

Figure 6.3. Cyclic voltammograms in 1:1 MeCN:DCM of **35** (black), $\mathbf{36}^{\mathbf{tBu}}$ (blue), $\mathbf{36}^{\mathbf{NO2}}$ (red), **37** (green), **34** (turquoise), and $\mathbf{34}^{\mathbf{BF2}}$ (orange) referenced to Fc^{+}/Fc. Cyclic voltammograms taken using a glassy carbon electrode with a scan rate was 100 mV/s initially in the positive direction. The analyte concentration was 1 mM. The electrolyte was 0.1 M NBu_4ClO_4 in MeCN:DCM.

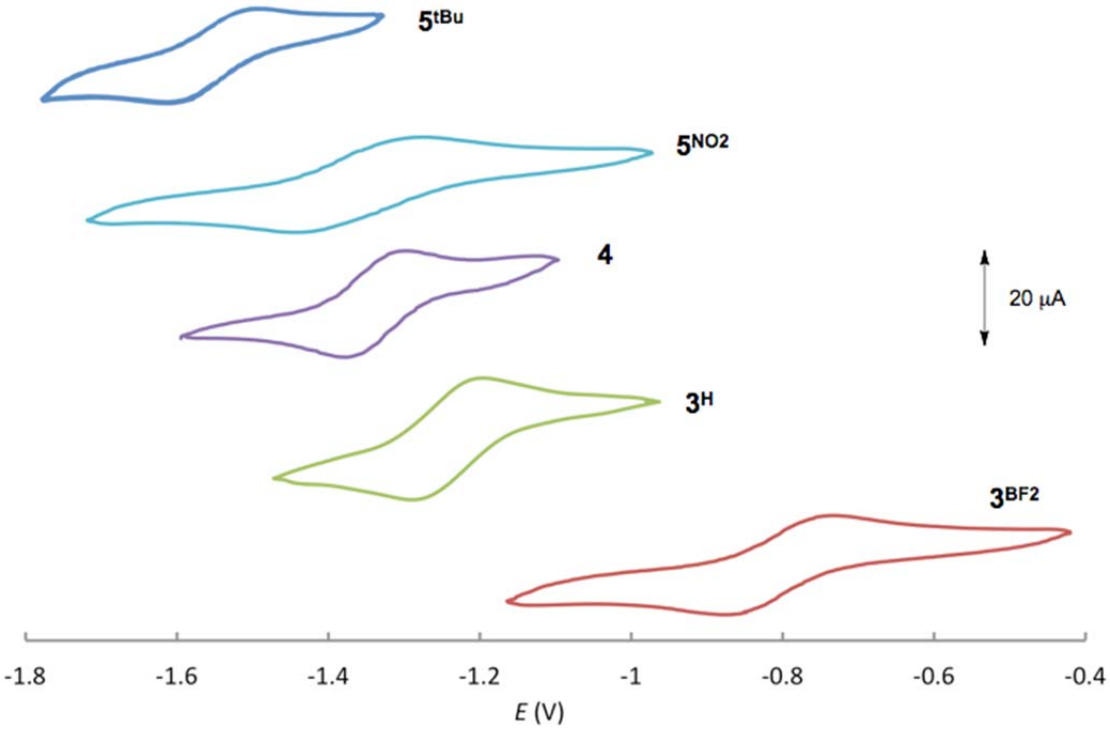

Figure 6.4. Cyclic voltammograms of the $Co^{II/I}$ couples of **36**^{tBu} (blue), **36**^{NO2} (turquoise), **35** (purple), **34**^{H} (green), and **34**^{BF2} (red) (1 mM) recorded in a 1:1 MeCN:DCM solution of $[nBu_4N][ClO_4]$ (0.1 M) at a glassy carbon working electrode using a $Ag/AgNO_3$ (0.01 M) reference electrode using a scan rate of 100 mV/s. Potentials referenced to the Fc^+/Fc couple.

Addition of trichloroacetic acid (pKa 3.5 in DMF)[13] under electrochemical conditions resulted in catalytic waves for complexes **35**, **36**^{tBu}, and **36**^{NO2} at the potentials assigned as the Co^{II}/Co^{I} couples (Figures 6.4-6.7).[5a-b, 6a] Subsequent additions of trichloroacetic acid caused cathodic shift and increase in the catalytic wave. Overpotentials were determined by comparison of the measured potential value for cobalt catalyzed proton reduction to the experimentally determined thermodynamic potential for proton reduction of trichloroacetate in DMF. Overpotentials are 680, 650, and 860 mV for the aluminum linked glyoxime complexes **35**, **36**^{tBu}, and **36**^{NO2},, respectively, and 520 and 110 mV for **34**^{H} and **34**^{BF2}, respectively with trichloroacetic acid. Bulk electrolysis experiments were performed with complexes **35** and **36**^{tBu} in a

MeCN/DCM solvent mixture, in the presence of *para*-cyanoanilinium triflate at a potential of -1.62 and -1.83 V, respectively, for two hours. Formation of H_2 was confirmed and quatified by GC analysis of the headspace. Faradaic yields of 90% and 70% were calculated for **35** and **36**^{tBu}, respectively.

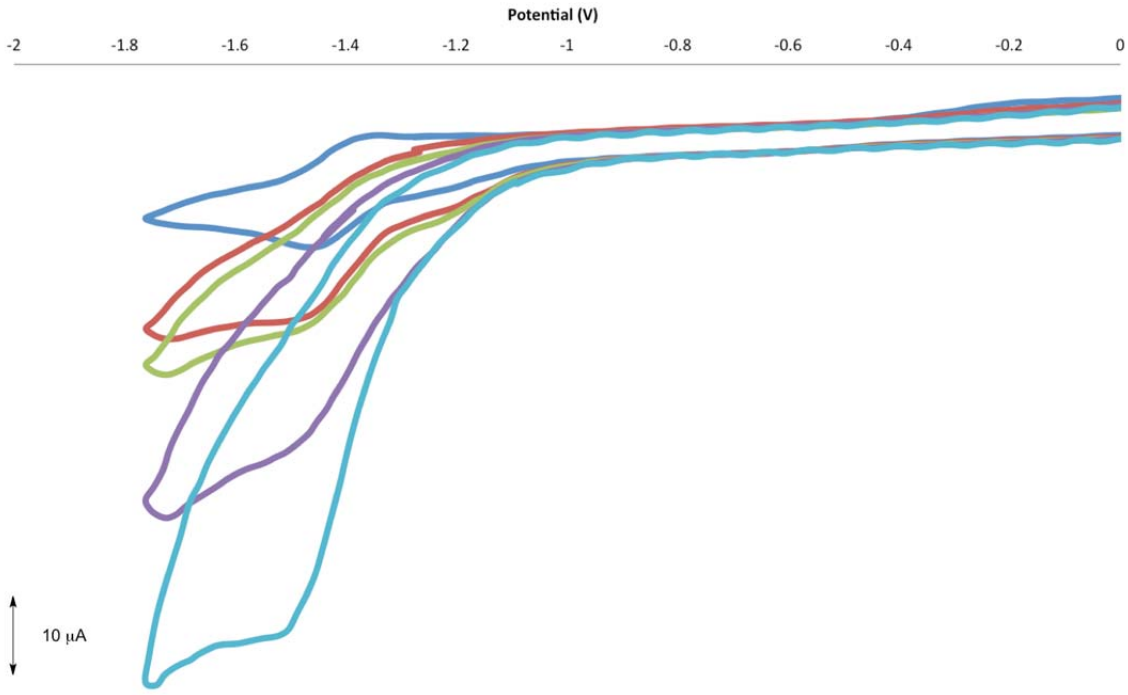

Figure 6.5. Addition of trichloroacetic acid to **35** at (1 mM) in DMF, No acid (blue), 3 mM acid (red), 6 mM acid (green), 11 mM acid (purple), 15 mM acid (turquoise). All waves referenced to Fc^+/Fc. Cyclic voltammograms taken using a glassy carbon electrode with a scan rate was 100 mV/s initially in the negative direction. The analyte concentration was 1 mM. The electrolyte was 0.1 M NBu_4ClO_4 in DMF.

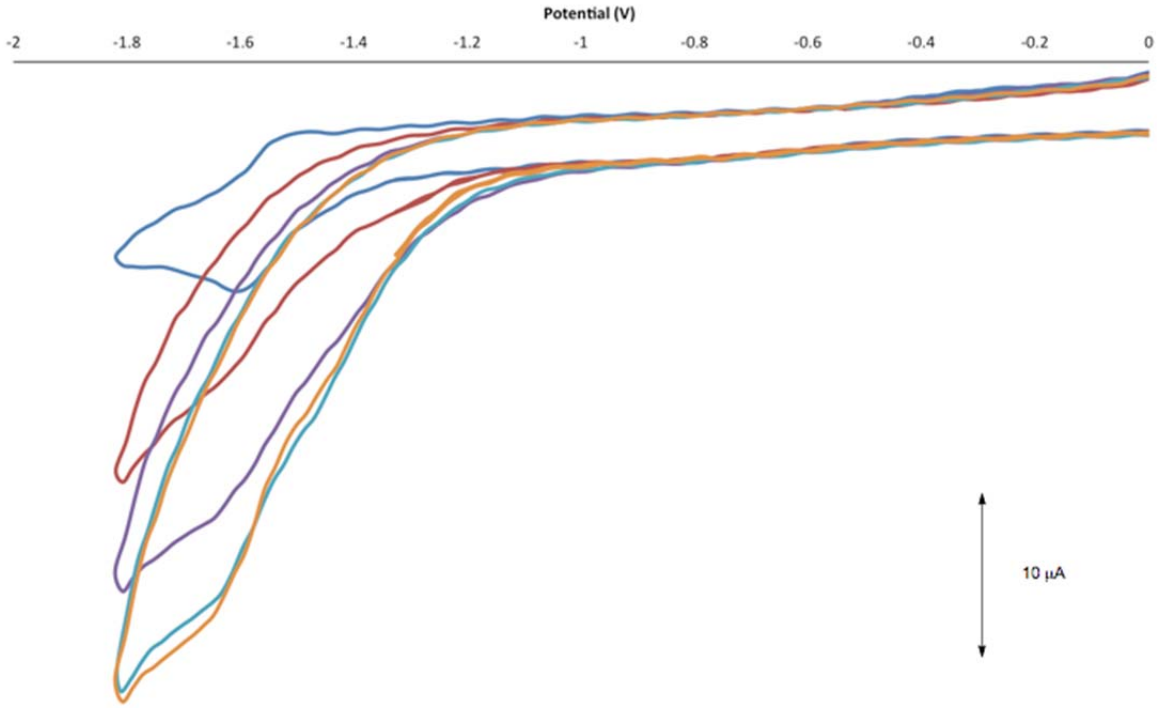

Figure 6.6. Addition of trichloroacetic acid to 36^{tBu} at (1 mM) in DMF, No acid (blue), 3 mM acid (red), 6 mM acid (purple), 10 mM acid (turquoise), 15 mM acid (orange). All waves referenced to Fc^{+}/Fc. Cyclic voltammograms taken using a glassy carbon electrode with a scan rate was 100 mV/s initially in the positive direction. The analyte concentration was 1 mM. The electrolyte was 0.1 M NBu_4ClO_4 in DMF.

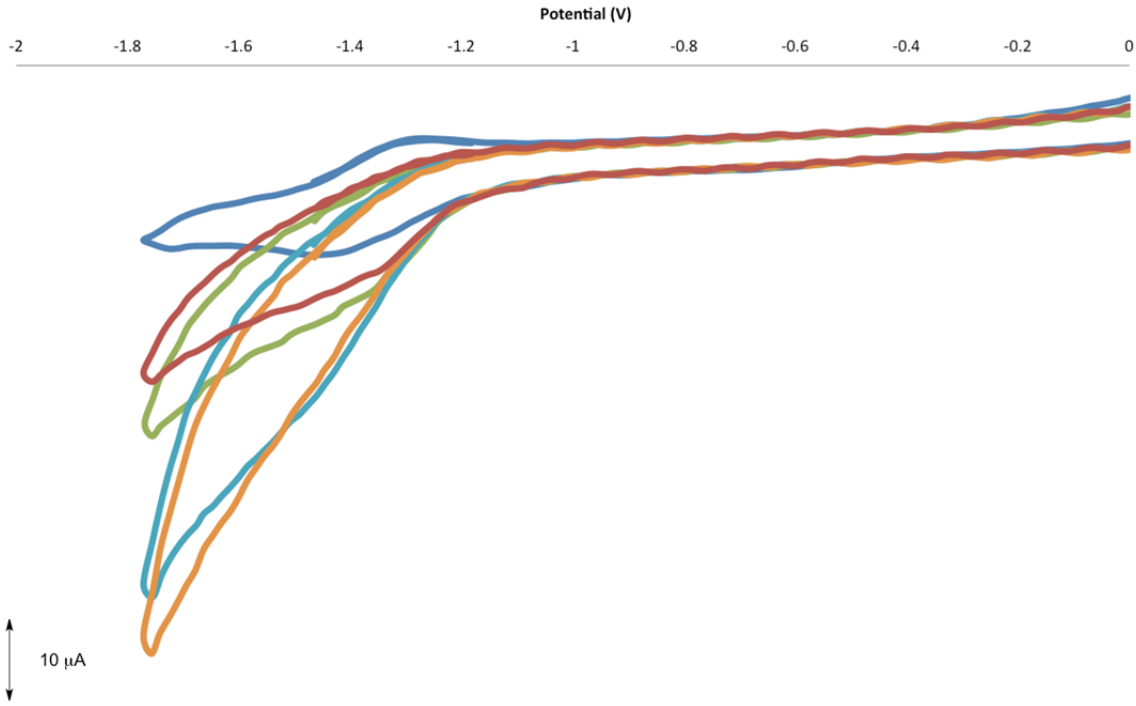

Figure 6.7. Addition of trichloroacetic acid to $\mathbf{36^{NO2}}$ at (1 mM) in DMF, No acid (blue), 3 mM acid (red), 6 mM acid (green), 10 mM acid (turquoise), 15 mM acid (orange). All waves referenced to Fc^{+}/Fc. Cyclic voltammograms taken using a glassy carbon electrode with a scan rate was 100 mV/s initially in the negative direction. The analyte concentration was 1 mM. The electrolyte was 0.1 M NBu_4ClO_4 in DMF.

Table 6.1. Potentials (V) of Synthesized Complexes in DMF (0.1 M NBu_4ClO_4). Reported potentials are referenced to Fc^{+}/Fc

	$E\,Co^{II}/\,Co^{I}$	$E\,H^{+}_{red}$
$\mathbf{34^{BF2}}$	-0.80	-0.87
34	-1.24	-1.29
$\mathbf{36^{tBu}}$	-1.55	-1.64
35	-1.34	-1.50
$\mathbf{36^{NO2}}$	-1.35	-1.49

Table 6.2. Summary of Bulk Electrolysis Studies[a]

Catalyst	Potential (V vs Fc)	Duration (hr)	Charge Passed (Coulomb)[b]	Faradiac Yield for H_2 (%)	TON
4	-1.62 V	2	38	90%	16
5^{tBu}	-1.83 V	2	30	70%	12

[a] All bulk electrolysis experiments carried out with 0.1 mM catalyst and 9 mM acid in a MeCN:DCM 1:1 solution of [nBu_4N][ClO_4] (0.1 M) using glassy carbon plate working and counter electrodes with a $Ag/AgNO_3$ (0.01 M) reference electrode. [b] All values corrected for background proton reduction on the glassy carbon plate at the listed potentials. [c] TON calculated from the amount of hydrogen produced during the duration of the bulk electrolysis experiment vs catalyst in solution.

Comparison of **35** and **34** (Co^{II}/Co^{I} at -1.25 V) indicates that substitution of a proton linker with aluminum leads to a 0.14 V negative shift of the Co^{II}/Co^{I} reduction potential and onset of catalysis. Substitution of the second proton with aluminum in **36**^{tBu} led to further cathodic shift by 0.32 V. In contrast, complex **36**^{NO2} shows an anodic shift by 0.27 V compared to **36**^{tBu}. The negative shift of the Co^{II}/Co^{I} reduction potential upon incorporation of aluminum centers vs protons may be a consequence of the electron rich, multidentate diamine bisphenoxide framework coordinated to aluminum. In agreement, the analog with electron withdrawing nitro substituents shows a significant positive potential shift.

CONCLUSIONS:

In summary, the synthesis and characterization of several aluminum-bridged bisglyoximato cobalt and zinc complexes are reported. The ligands supporting the aluminum centers were found to affect the reduction potentials of cobalt and consequently the potential for proton reduction catalysis. Electrocatalytic proton reduction occurs at potentials more negative that the boron- and proton-bridged analogs. Nevertheless, the synthetic protocols presented here may be extended to other metal bridges or ancillary ligands toward tuning the reduction potential of the central metal, improving the stability, attaching photosynthesizers or affecting the second coordination sphere.

EXPERIMENTAL SECTION:

General: All air sensitive reactions were carried out in a glovebox under a nitrogen atmosphere using oven-dried glassware cooled in vacuo. Anhydrous solvents were dried by the method of Grubbs.[14] All non-dried solvents used were of reagent grade or better and were used as is. NMR solvents were purchased from Cambridge Isotope Laboratories, Inc. C6D6 was dried over sodium/benzophnenone ketyl while CD_2Cl_2 was dried over calcium hydride, both were degassed by three freeze-pump-thaw cycles and vacuum-transferred prior to use. $CDCl_3$ was used as purchased. All proton NMR spectra were recorded on either a Varian Mercury 300MHz or a Varian INOVA-500 spectrometer with chemical shifts reported in ppm relative to the pertinent solvent peaks (7.16 ppm for C_6D_6, 7.26 ppm for $CDCl_3$, and 5.32 ppm for CD_2Cl_2). (R,R)-1,2-diaminocyclohexane was purified from a racemic mixture of 1,2-diaminocyclohexane using a literature procedure.[15] 2-(chloromethyl)-6-methyl-4-nitrophenol,[16a] N,N'-dimethylcyclohexane-1,2-diamine,[16b] **30**^{tBu},[11] **30**^{NO2},[11] **32**^{tBu},[11] **32**^{NO2},[11] **34**,[17] and **31 macrocycle**[11] were synthesized according to literature procedures. All other starting materials were used as purchased.

Electrochemical measurements were recorded in a glovebox under a N_2 atmosphere using a Pine Instrument Company Bipotentiostat, at 1mM of the complex of interest unless otherwise stated, in a mixture of 1:1 DCM:MeCN or DMF containing 0.1 M $nBu_4N(ClO_4)$ as the supporting electrolyte, a glassy carbon working electrode, a platinum wire auxiliary electrode, and a 0.01M $Ag/AgNO_3$ nonaqueous reference electrode. For proton reduction trichloroacetic acid and p-cyanoanilinium triflate were used as the proton sources. Bulk electrolysis experiments were conducted in a sealed two-chambered cell where the first chamber held the working and reference electrodes and the second chamber contained the auxiliary electrode. The two chambers were separated by a fine frit.

Glassy carbon plates (12 cm x 3 cm x 1 cm) were used as the working and auxiliary electrodes and submerged such that ca. 64 cm^2 of the plate was in the 0.1 M $nBu_4N(ClO_4)$ MeCN:DCM solution. For the bulk electrolysis studies para-cyanoanilinium triflate was used as the proton source. The amount of H_2 evolved was quantified from an analysis of the headspace of the cell with an Agilent 7890A gas chromotograph using a thermal conductivity detector. The overpotentials were determined by comparing the derivative of the catalytic wave observed with the stated catalyst in 3 mM trichloroacetic acid with the determined thermodynamic half wave potential of trichloroacetic acid in DMF. The thermodynamic half wave potential of trichloroacetic was determined to be -710 ± 20 mV by analysis of the catalytic wave for proton reduction in a 1M solution of trichloroacetic acid in a hydrogen (1 atm) saturated DMF solution.

Position labels for listed nuclear magnetic resonace spectroscopy characterization.

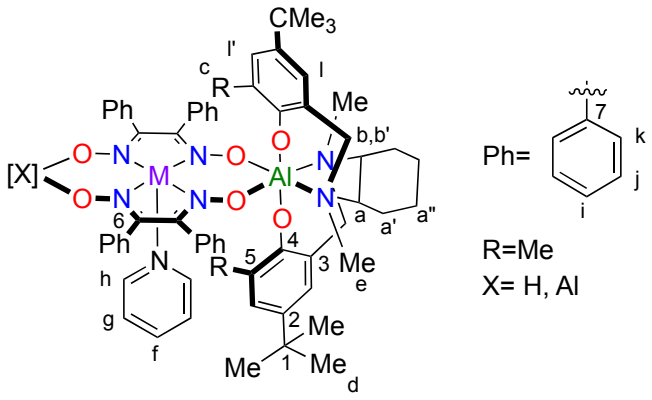

Synthesis of 35: Cobalt(III) diphenylglyoximato precursor **34** (0.127 g, 0.195 mmol) was treated with one equivalent of **31**^{tBu} (0.102 g, 0.192 mmol) in toluene (10 mL) at room temperature for 16 hours. Over time the solution became a homogeneous dark brown. The solvent was removed in vacuo resulting in a brown solid. The solid was washed with diethyl ether and extracted with benzene. The benzene solution was concentrated until solid precipitated was and filtered through celite. The filtrate was concentrated under

vacuum. To the resulting brown powder was added a small amount of benzene to barely dissolve the solid and the solution was filtered. The solvent was removed and the resulting solid was washed three times with pentane resulting in a light brown powder. Yield: 0.177 g, 79%. ^{1}H NMR (300 MHz, CD_2Cl_2) δ 19.20 (1H, s, OH), 9.13 (2H, d, J = 5.0 Hz, h), 7.75 (1H, t, J = 7.6 Hz, f), 7.29 (8H, m, j), 7.24 (2H, m, l) 7.26 (8H, m, k), 7.21 (2H, m, g), 7.16 (2H, m, i), 7.05 (2H, m, i), 6.97 (2H, d, J = 2.6 Hz, l,l'), 6.77 (2H, d, J = 2.5 Hz, l,l'), 6.50 (2H, d, J = 2.5 Hz, l,l'), 4.32 (1H, d, J = 13.4 Hz, b,b'), 3.89 (1H, d, J = 13.3 Hz, b,b'), 2.94 (1H, d, J = 13.6 Hz, b,b'), 2.75 (1H, d, J = 13.5 Hz, b,b'), 2.49 (2H, m, a), 2.12 (3H, s, e,e'), 2.07 (3H, s, e,e'), 1.85 (3H, s, c,c'), 1.66 (3H, s, c,c'), 1.63 (2H, m, a'), 1.52 (2H, m, a''), 1.35 (9H, s, d,d'), 1.25 (9H, s, d,d'), 0.96 (2H, m, a'), 0.75 (2H, m, a'') ppm. ^{13}C{^{1}H} NMR (126 MHz, CD_2Cl_2) δ 157.16 (4,4'), 157.07 (4,4'), 155.40 (6,6'), 154.31 (6,6'), 153.27 (h), 139.22 (g), 136.96 (2,2'), 135.62 (2,2'), 132.56 (i,i'), 132.36 (i,i'), 130.93 (i,i'), 130.80 (i,i'), 130.03 (k,k'), 129.97 (k,k'), 129.52 (7,7'), 129.43 (7,7'), 129.11 (7,7'), 129.02 (7,7'), 128.32 (l'), 128.17 (j), 127.54 (5,5'), 126.91 (l'), 125.87 (f), 124.98 (5,5'), 123.69 (l), 123.04 (l), 121.24 (3,3'), 119.64 (3,3'), 59.86 (b,b'), 59.57 (b,b'), 55.93 (a), 55.75 (a), 40.56 (c,c'), 40.44 (c,c'), 33.97 (1), 33.76 (1), 31.96 (d), 24.62 (a"), 22.02 (a'), 17.94 (e,e'), 17.32 (e,e') ppm. Anal. Calcd. for $C_{60}H_{69}AlClCoN_6O_6$ (%): C, 66.69; H, 6.37; N, 8.38; Found: C, 67.04; H, 6.77; N, 7.99.

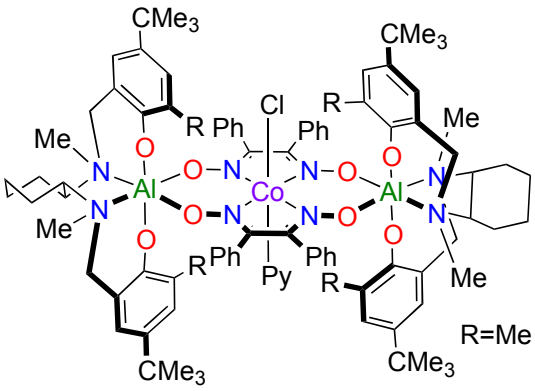

Synthesis of 36^{tBu}: A slurry of **34** (0.453 g, 0.695 mmol) in toluene (10 mL) was treated with a solution of **31^{tBu}** (0.750 g, 1.40 mmol) in toluene (10 mL) at room temperature. After 36 hours of stirring volatile materials were removed in vacuo. The crude solid was washed with hexanes. The desired product was extracted with diethyl ether and toluene. The desired product was isolated as a brown orange powder upon removing volatile material from the diethyl ether fraction. Yield: 0.437 g, 37% ^{1}H NMR (500 MHz, CD_2Cl_2) δ 9.64 (2H, d, J = 5.7 Hz, h), 7.56 (1H, t, J = 7.6 Hz, f), 7.30 (8H, m, k), 7.19 (8H, q, J = 7.8, 6.3 Hz, j), 7.13 (2H, d, J = 2.6 Hz, l'), 6.97 (2H, d, J = 2.7 Hz, l'), 6.88 (4H, d, i), 6.82 (2H, m, g), 6.64 (4H, dd, J = 12.3, 2.7 Hz, l), 4.23 (2H, d, J = 13.3 Hz, b,b'), 4.06 (2H, d, J = 13.3 Hz, b,b'), 2.90 (2H, d, J = 13.5 Hz, b,b'), 2.80 (2H, d, J = 13.5 Hz, b,b'), 2.61 (2H, m, a), 2.52 (2H, m, a), 2.26 (6H, s, e,e'), 2.21 (6H, s, e,e'), 1.84 (6H, s, c,c'), 1.66 (6H, s, c,c'), 1.60 (2H, m, a'), 1.52 (2H, m, a''), 1.29 (18H, s, d,d'), 1.28 (18H, s, d,d'), 0.96 (2H, m, a'), 0.76 (2H, m, a'') ppm. ^{13}C{^{1}H} NMR (126 MHz, CD_2Cl_2) δ 157.62 (4,4'), 157.10 (4,4'), 156.05 (6,6'), 154.89 (h), 154.38 (6,6'), 138.80 (g), 136.55 (2,2'), 135.00 (2,2'), 133.66 (7,7'), 133.12 (7,7'), 130.31 (k), 130.00 (i), 128.57 (l',l'), 128.49 (l',l'), 128.04 (j,j'), 127.90 (j,j'), 127.24 (5,5'), 126.91 (l,l), 125.16 (5,5'), 124.65 (f), 123.42 (l,l), 121.05 (3,3'), 119.30 (3,3'), 60.29 (b,b'), 59.39 (b,b'), 55.88 (a), 40.57 (c,c'), 33.90 (1), 32.01 (d), 24.69 (a''), 22.08 (a'), 18.14 (e,e'),

17.42 (e,e') ppm. Elemental Analysis $C_{97}H_{121}Al_2ClCoN_9O_8$ (%): Calc. C, 68.96; H, 7.22; N, 7.46; Found. C, 69.41; H, 7.09; N, 7.15

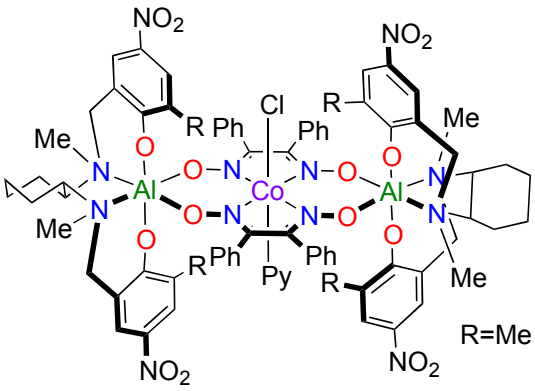

Synthesis of 36^{NO2}: A solution of 31^{NO2} (0.111 g, 0.217 mmol) in THF (5 mL) was mixed with a solution of **3** (0.063 g, 0.090 mmol) in THF (5 mL). The mixture was sealed in a Schlenk tube and heated to 66 °C for 12 hours. After the allocated time the solvent was removed in vacuo. The recovered solid was washed with diethyl ether, benzene, and extracted with THF. The product of the THF fraction was recrystallized from a vapor diffusion of diethyl ether into THF at room temperature as brown orange crystals. The ^{1}H NMR spectrum indicates the presence of an impurity that was assigned as a isomer based on its spectroscopic features. Yield: 0.063 g, 43% ^{1}H NMR (500 MHz, CD_2Cl_2) δ 9.23 (2H, d, J = 5.1 Hz, h), 8.12 (2H, d, J = 2.9 Hz, l,l'), 7.94 (2H, d, J = 2.9 Hz, l,l'), 7.76 (4H, dd, J = 4.7, 3.0 Hz, j), 7.69 (1H, m, f), 7.41 (4H, m, j), 7.29 (2H, m, i), 7.22 (4H, dd, J = 8.3, 7.2 Hz, k), 7.17 (4H, m, k), 6.86 (2H, m, i), 6.76 (4H, d, J = 7.6 Hz, l,l'), 4.31 (2H, d, J = 13.7 Hz, b,b'), 4.17 (2H, d, J = 13.8 Hz, b,b'), 3.11 (2H, d, J = 13.9 Hz, b,b'), 3.00 (2H, d, J = 14.1 Hz, b,b'), 2.45 (2H, m, a), 2.25 (6H, s, e), 2.17 (6H, s, e), 1.80 (6H, s, c,c'), 1.70 (4H, m, a'), 1.61 (4H, m, a"), 1.54 (6H, s, c,c'), 0.95 (4H, m, a"), 0.80 (4H, m, a') ppm. ^{13}C{^{1}H} NMR (126 MHz, CD_2Cl_2) δ 166.95 (4,4'), 166.24 (4,4'), 157.45 (6,6'), 156.34 (6,6'), 153.55 (h), 139.68 (f), 136.68 (2,2'), 135.82 (2,2'), 133.03 (7,7'), 131.54 (7,7'), 129.62 (k), 129.42

(i,i'), 129.33 (5,5'), 129.06 (i,i'), 128.69 (l,l'), 128.22 (l,l'), 127.29 (l,l'), 126.85 (l,l'), 126.26 (5,5'), 125.21 (g), 124.15 (j), 121.59 (3,3'), 120.09 (3,3'), 58.99 (b,b'), 58.30 (b,b'), 56.69 (a), 40.58 (c,c'), 24.41 (a"), 22.12 (a'), 17.74 (e,e'), 16.70 (e,e') ppm. Anal. Calc. $C_{81}H_{85}Al_2ClCoN_{13}O_{16}$ (%): C, 59.14; H, 5.21; N, 11.07; Found. C, 60.03; H, 5.56; N, 10.82.

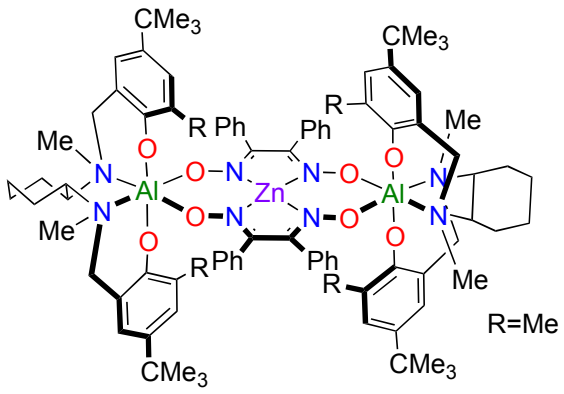

Synthesis of 37: To a just thawed solution of 31^{tBu} macrocycle (0.424 g, 0.28 mmol) in THF (10 mL) was added a freshly thawed solution of diethylzinc (0.034 g, 28.6 µl, 0.28 mmol) in THF (5 mL). The solution was allowed to warm to room temperature. After 3 hours of stirring volatile materials were removed in vacuo. The crude solid was triterated with Et_2O. The resulting solid was fractionated into hexanes and THF. Removal of volatile materials from the hexanes fraction under vacuum resulted in the desired product as an off white solid. Yield 0.305 g, 69%, ^{1}H NMR (300 MHz, C6D6) δ 7.51 (8H, d, J = 7.0 Hz, k), 6.96 (16H, m, i, j, l,l'), 6.66 (4H, d, J = 2.3 Hz, l,l'), 4.59 (4H, d, J = 12.7 Hz, b,b'), 2.72 (4H, d, J = 12.7 Hz, b,b'), 2.37 (4H, m, a), 2.31 (12H, s, e), 1.91 (12H, s, c), 1.35 (36H, s, d), 1.18 (4H, m, a"), 1.04 (4H, m, a'), 0.35 (4H, m, a"), 0.26 (4H, m, a') ppm. ^{13}C{^{1}H} NMR (126 MHz, C6D6) δ 157.80 (4), 150.92 (6), 137.65 (7), 132.79 (2), 130.97 (k), 127.61 (i), 127.52 (j), 126.95 (5), 123.75 (l), 121.90 (3), 59.94 (b,b'), 55.92 (a), 39.63 (c), 33.91 (1), 32.30 (d), 24.41 (a'), 22.33 (a"), 17.78 (e) ppm. Elemental Analysis $C_{92}H_{116}Al_2ZnN_8O_8$ (%): Calc. C, 69.88; H, 7.39; N, 7.09; Found. C, 69.90; H, 7.24; N, 7.44

Acid stability test of *35*: A solution of ***35*** (0.012 g, 0.010 mmol) in C_6D_6 was mixed with (0.040 g, 0.149 mmol) trichloroacetic acid in a J-Young tube. The tube was sealed under N_2. The degradation of ***35*** was observed over time by ^{1}H NMR spectroscopy. The amount of degradation of complex was estimated from the comparison of the benzylic protons with peaks from the degradation product in the benzylic region.

Table 6.X. Crystal and refinement data for complexes **35**, **36^{tBu}**, and **36^{NO2}**.

	35	**36^{tBu}**	**36^{NO2}**
CCDC Number	861068	863680	862110
Empirical formula	$C_{65}H_{74}ClN_7O_6AlCo \cdot C_5H_{12}$	$C_{97}H_{121}N_9O_8Al_2ClCo \cdot 1.55(C_5H_{12}) \cdot 0.45(C_6H_6)$	$C_{81}H_{84}N_{13}O_{16}Al_2ClCo$
Formula weight	1242.82	1836.69	1643.95
T (K)			
a, Å	18.2062(9)	33.3885(19)	11.8585(5)
b, Å	18.3182(9)	12.4645(7)	19.9092(8)
c, Å	20.2299(10)	26.8733(15)	22.2150(9)
, deg	90	90	90
, deg	90	111.652(3)	92.687(2)
, deg	90	90	90
Volume, Å^3	6746.8(6)	10394.8(10)	5239.0(4)
Z	4	4	2
Crystal system	Orthorhombic	Monoclinic	Monoclinic
Space group	P $2_12_12_1$	C 2	P 2_1
d_{calc}, Mg/m^3	1.224	1.174	1.042
range, deg	2.31 to 27.65°	2.31 to 27.65°	2.17 to 28.85°
μ, mm^{-1}	0.362	0.266	0.264
Abs. Correction	None	None	None
GOF	3.590	3.008	2.457
R_1,[a] wR_2[b] [I>2(I)]	R1 = 0.0610 *w*R2 = 0.0704	R1 = 0.0671 *w*R2 = 0.1146	R1 = 0.0637 *w*R2 = 0.1021

[a] $R_1 = \sum||F_o| - |F_c||/\sum|F_o|$. [b] $wR_2 = [\sum[w(F_o^2-F_c^2)^2]/\sum[w(F_o^2)^2]]^{1/2}$.

References

[1] a) H. B. Gray, *Nat. Chem.* **2009**, *1*, 7; b) N. S. Lewis, D. G. Nocera, *Proc. Natl. Acad. Sci. USA* **2006**, *103*, 15729-15735; c) P. Du, R. Eisenberg, *Energy Environ. Sci.* **2012**; d) V. Artero, M. Chavarot-Kerlidou, M. Fontecave, *Angew. Chem. Int. Ed.* **2011**, *50*, 7238-7266.

[2] a) M. Frey, *ChemBioChem* **2002**, *3*, 153-160; b) J. C. Fontecilla-Camps, A. Volbeda, C. Cavazza, Y. Nicolet, *Chem. Rev.* **2007**, *107*, 4273-4303; c) M. Y. Darensbourg, E. J. Lyon, J. J. Smee, *Coord. Chem. Rev.* **2000**, *206*, 533-561.

[3] a) G. A. N. Felton, C. A. Mebi, B. J. Petro, A. K. Vannucci, D. H. Evans, R. S. Glass, D. L. Lichtenberger, *J. Organomet. Chem.* **2009**, *694*, 2681-2699; b) C. Tard, C. J. Pickett, *Chem. Rev.* **2009**, *109*, 2245-2274.

[4] a) M. L. Helm, M. P. Stewart, R. M. Bullock, M. R. DuBois, D. L. DuBois, *Science* **2011**, *333*, 863-866; b) M. Rakowski DuBois, D. L. DuBois, *Chem. Soc. Rev.* **2009**, *38*, 62-72; c) M. Rakowski Dubois, D. L. Dubois, *Acc. Chem. Res.* **2009**, *42*, 1974-1982.

[5] a) P. Connolly, J. H. Espenson, *Inorg. Chem.* **1986**, *25*, 2684-2688; b) C. Baffert, V. Artero, M. Fontecave, *Inorg. Chem.* **2007**, *46*, 1817-1824; c) P.-A. Jacques, V. Artero, J. Pécaut, M. Fontecave, *Proc. Natl. Acad. Sci. USA* **2009**, *106*, 20627-20632; d) J. L. Dempsey, B. S. Brunschwig, J. R. Winkler, H. B. Gray, *Acc. Chem. Res.* **2009**, *42*, 1995-2004; e) X. Hu, B. S. Brunschwig, J. C. Peters, *J. Am. Chem. Soc.* **2007**, *129*, 8988-8998; f) T. Lazarides, T. McCormick, P. W. Du, G. G. Luo, B. Lindley, R. Eisenberg, *J. Am. Chem. Soc.* **2009**, *131*, 9192-9124; g) C. N. Valdez, J. L. Dempsey, B. S. Brunschwig, J. R. Winkler, H. B. Gray, *Proc. Natl. Acad. Sci. USA* **2012**, *109*, 15589-15593; h) F. Lakadamyali, M. Kato, N. M. Muresan, E. Reisner, *Angew. Chem. Int. Ed.* **2012**, *51*, 9381-9384; i) A. Fihri, V. Artero, M. Razavet, C. Baffert, W. Leibl, M. Fontecave, *Angew. Chem.-Int. Edit.* **2008**, *47*, 564-567; j) B. D. Stubbert, J. C. Peters, H. B. Gray, *J. Am. Chem. Soc.* **2011**, *133*, 18070-18073; k) N. K. Szymczak, L. A. Berben, J. C. Peters, *Chem. Commun.* **2009**, 6729-6731; l) L. A. Berben, J. C. Peters, *Chem. Commun.* **2010**, *46*, 398-400; m) J. P. Bigi, T. E. Hanna, W. H. Harman, A. Chang, C. J. Chang, *Chem. Commun.* **2010**, *46*, 958-960; n) Y. Sun, J. P. Bigi, N. A. Piro, M. L. Tang, J. R. Long, C. J. Chang, *J. Am. Chem. Soc.* **2011**, *133*, 9212-9215; o) D. K. Dogutan, R. McGuire, D. G. Nocera, *J. Am. Chem. Soc.* **2011**, *133*, 9178-9180; p) C. C. L. McCrory, C. Uyeda, J. C. Peters, *J. Am. Chem. Soc.* **2012**, *134*, 3164-3170; q) S. C. Marinescu, J. R. Winkler, H. B. Gray, *Proc. Natl. Acad. Sci. USA* **2012**, *109*, 15127-15131 r) M. Guttentag, A. Rodenberg, C. Bachmann, A. Senn, P. Hamm, R. Alberto, *Dalton Trans.* **2013**, *42*, 334-337; s) E. S. Andreiadis, P.-A. Jacques, P. D. Tran, A. Leyris, M. Chavarot-Kerlidou, B. Jousselme, M. Matheron, J. Pécaut, S. Palacin, M. Fontecave, V. Artero, *Nat Chem* **2013**, *5*, 48-53.

[6] a) X. Hu, B. M. Cossairt, B. S. Brunschwig, N. S. Lewis, J. C. Peters, *Chem. Commun.* **2005**, 4723-4725; b) M. Razavet, V. Artero, M. Fontecave, *Inorg. Chem.* **2005**, *44*, 4786-4795; c) J. L. Dempsey, J. R. Winkler, H. B. Gray, *J. Am. Chem. Soc.* **2009**, *132*, 1060-1065; d) J. L. Dempsey, J. R. Winkler, H. B. Gray, *J. Am. Chem. Soc.* **2010**, *132*, 16774-16776; e) A. Fihri, V. Artero, A. Pereira, M. Fontecave, *Dalton Trans.* **2008**, 5567-5569; f) A. Fihri, V. Artero, M. Razavet, C. Baffert, W. Leibl, M. Fontecave, *Angew. Chem. Int. Ed.* **2008**, *47*, 564-567; g) P. W. Du, K. Knowles, R. Eisenberg, *J. Am. Chem. Soc.* **2008**, *130*, 12576-12577; h) P. W. Du, J. Schneider, G. G. Luo, W. W. Brennessel, R. Eisenberg, *Inorg. Chem.* **2009**, *48*, 4952-4962; i) E.

Szajna-Fuller, A. Bakac, *Eur. J. Inorg. Chem.* **2010**, 2488-2494; j) V. Artero, M. Fontecave, *Coord. Chem. Rev.* **2005**, *249*, 1518-1535; k) D. M. Cropek, A. Metz, A. M. Muller, H. B. Gray, T. Horne, D. C. Horton, O. Poluektov, D. M. Tiede, R. T. Weber, W. L. Jarrett, J. D. Phillips, A. A. Holder, *Dalton Trans.* **2012**, *41*, 13060-13073; l) P. Zhang, P.-A. Jacques, M. Chavarot-Kerlidou, M. Wang, L. Sun, M. Fontecave, V. Artero, *Inorg. Chem.* **2012**, *51*, 2115-2120.

[7] a) B. H. Solis, S. Hammes-Schiffer, *J. Am. Chem. Soc.* **2011**, *133*, 19036-19039; b) T. M. McCormick, Z. J. Han, D. J. Weinberg, W. W. Brennessel, P. L. Holland, R. Eisenberg, *Inorg. Chem.* **2011**, *50*, 10660-10666.

[8] a) A. Yeori, I. Goldberg, M. Shuster, M. Kol, *J. Am. Chem. Soc.* **2006**, *128*, 13062-13063; b) Y.-L. Wong, Y. Yan, E. S. H. Chan, Q. Yang, T. C. W. Mak, D. K. P. Ng, *J. Chem. Soc., Dalton Trans.* **1998**, 3057-3064; c) H. Du, A. H. Velders, P. J. Dijkstra, J. Sun, Z. Zhong, X. Chen, J. Feijen, *Chem. Eur. J.* **2009**, *15*, 9836-9845.

[9] a) C. López, S. Alvarez, M. Aguiló, X. Solans, M. Font-Altaba, *Inorg. Chim. Acta* **1987**, *127*, 153-159; b) K. A. Lance, W.-K. Lin, D. H. Busch, *Acta Crystallogr. Sect. C: Commun. Online* **1991**, *C47*, 1401-1403.

[10] a) J. L. Hoard, *Science* **1971**, *174*, 1295-1302; b) K. M. Kadish, K. M. Smith, R. Guilard, *Porphyrin Handbook* **2000**, *1*.

[11] P. Kelley, M. R. Radlauer, A. J. Yanez, M. W. Day, T. Agapie, *Dalton Trans.* **2012**, *41*, 8086-8092.

[12] a) D. Lionetti, A. J. Medvecz, V. Ugrinova, M. Quiroz-Guzman, B. C. Noll, S. N. Brown, *Inorg. Chem.* **2010**, *49*, 4687-4697; b) B. Adam, E. Bill, E. Bothe, B. Goerdt, G. Haselhorst, K. Hildenbrand, A. Sokolowski, S. Steenken, T. Weyhermüller, K. Wieghardt, *Chem. Eur. J.* **1997**, *3*, 308-319.

[13] a) G. A. N. Felton, R. S. Glass, D. L. Lichtenberger, D. H. Evans, *Inorg. Chem.* **2006**, *45*, 9181-9184; b) V. Fourmond, P.-A. Jacques, M. Fontecave, V. Artero, *Inorg. Chem.* **2010**, *49*, 10338-10347.

[14] a) A. B. Pangborn, M. A. Giardello, R. H. Grubbs, R. K. Rosen, F. J. Timmers, *Organometallics.* **1996**, *15*, 1518-1520

[15] J. F. Larrow, E. N. Jacobson, Y. Gao, Y. Hong, X. Nie, C. M. Zepp, *J. Org. Chem.* **1994**, *59*, 1939-1942.

[16] a) C. A. Buehler, F. K. Kirchner, G. F. Deebel, *Organic Synthesis* **1955**, *3*, 468; b)V. Stepanenko, M. De Jesús, W. Correa, I. Guzmán, C. Vázquez, L. Ortiz, M. Ortiz-Marciales, *Tetrahedron: Asymmetry* **2007**, *18*, 2738-2745.

[17] G. N. Schrauzer, *Inorganic Synthesis* **1968**, *11*, 62-64.

Appendix A

Relevant Spectroscopic Data

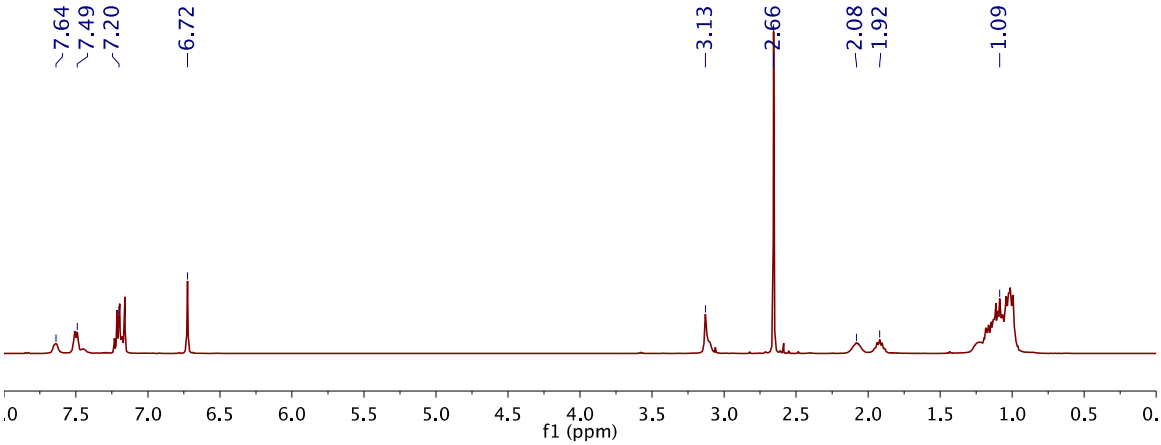

Figure A.1: ^{1}H NMR Spectrum (C_6D_6, 25°C, 399.80 MHz) of 1

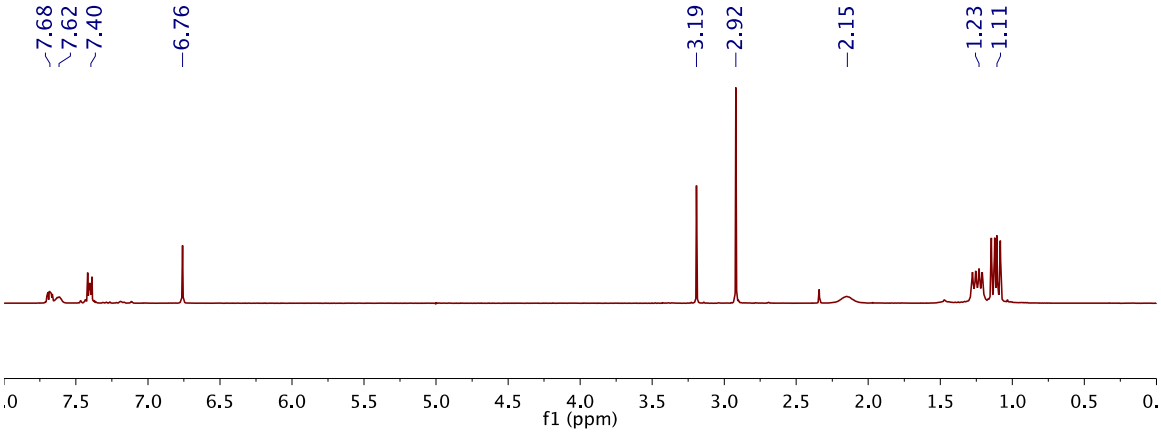

Figure A.2: ^{1}H NMR Spectrum (C_6D_6, 75°C, 300.08 MHz) of 1

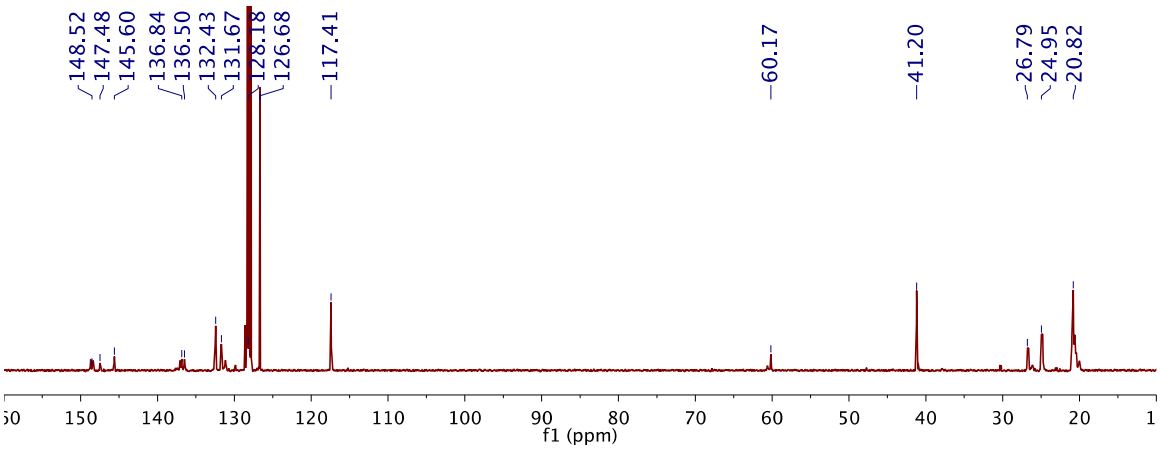

Figure A.3: ^{13}C{^{1}H} NMR Spectrum (C_6D_6, 25°C, 100.54 MHz) of 1

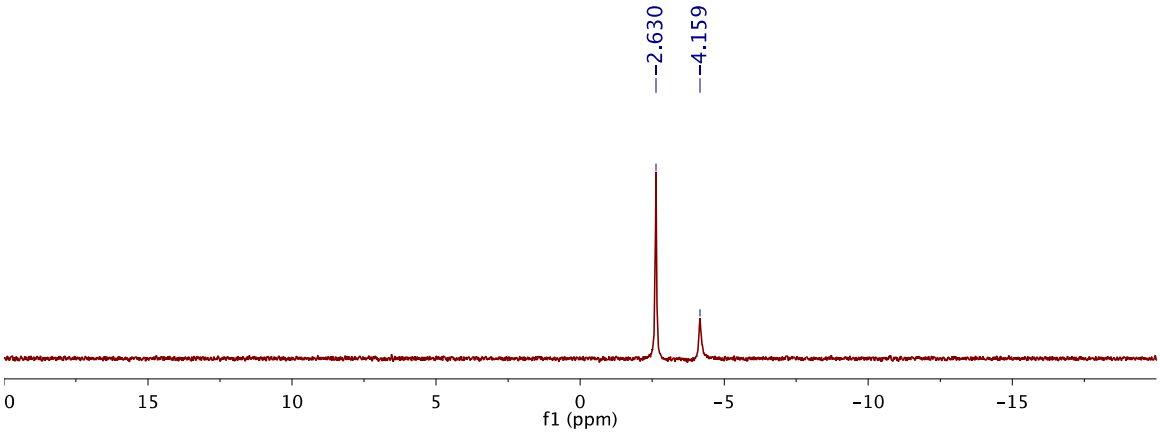

Figure A.4: $^{31}P\{^{1}H\}$ NMR Spectrum (C_6D_6, 25°C, 121.48 MHz) of 1

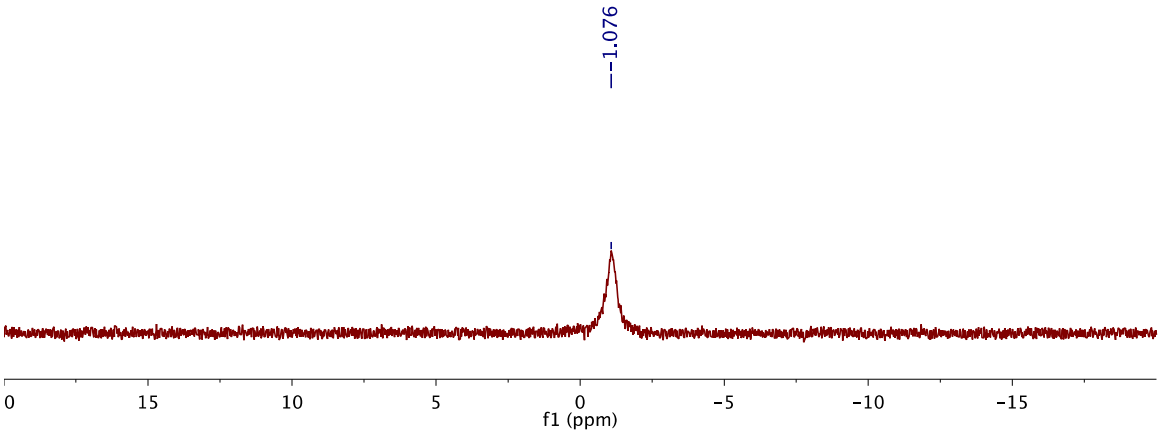

Figure A.5: $^{31}P\{^{1}H\}$ NMR Spectrum (C_6D_6, 75°C, 121.48 MHz) of 1

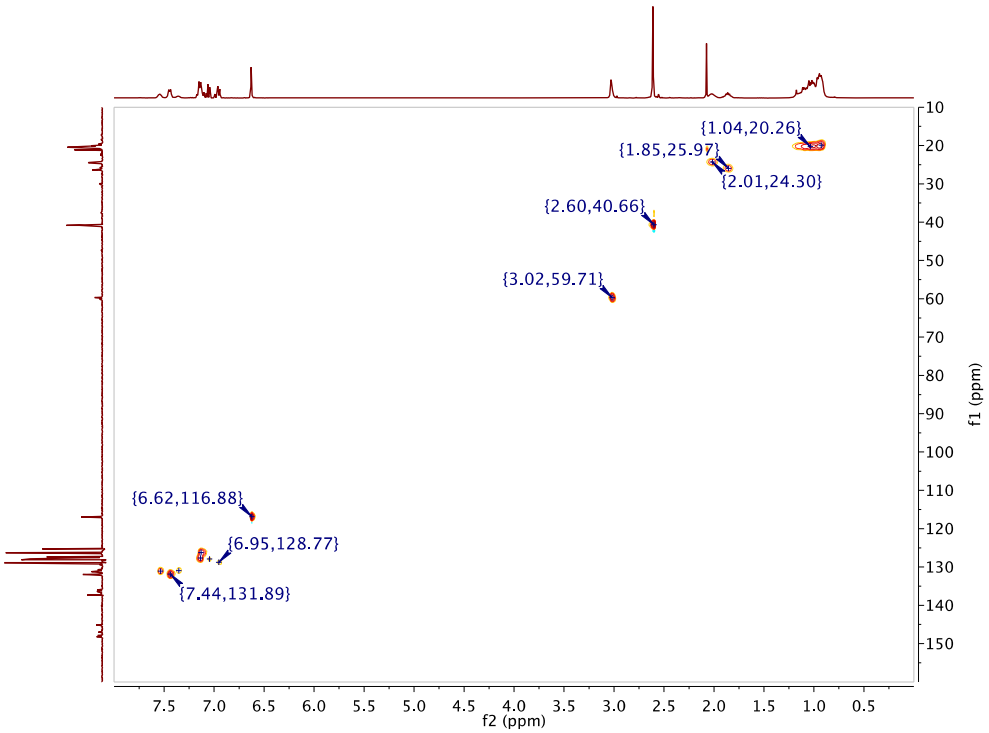

Figure A.6: ^{1}H-^{13}C HSQC NMR Spectrum (C_6D_6, 25°C, 399.80, 100.54 MHz) of 1

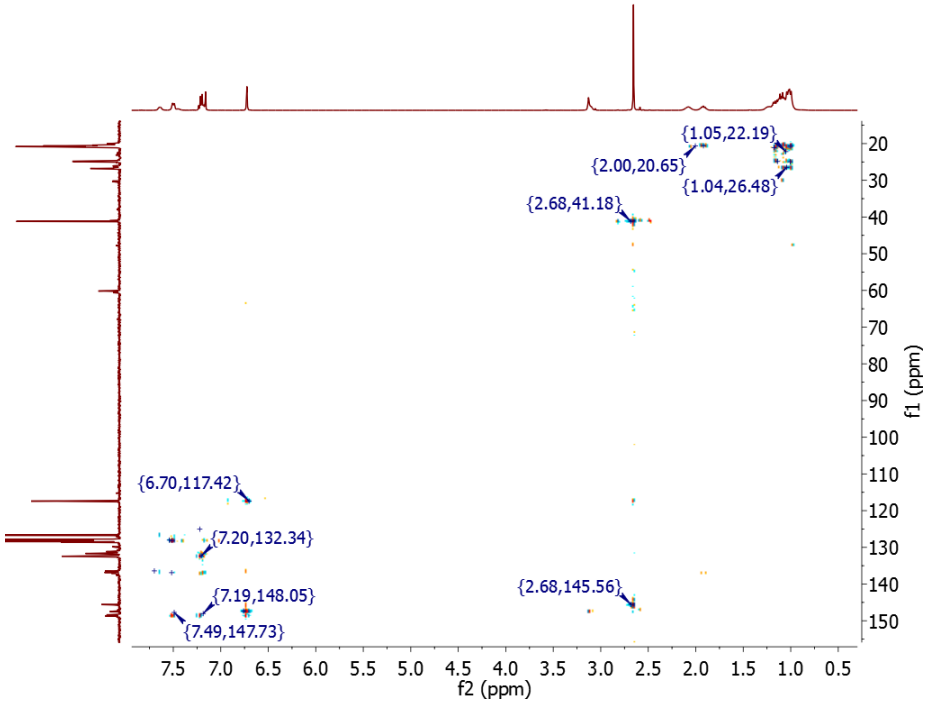

Figure A.7: ^{1}H-^{13}C HMBC NMR Spectrum (C_6D_6, 25°C, 399.80, 100.54 MHz) of 1

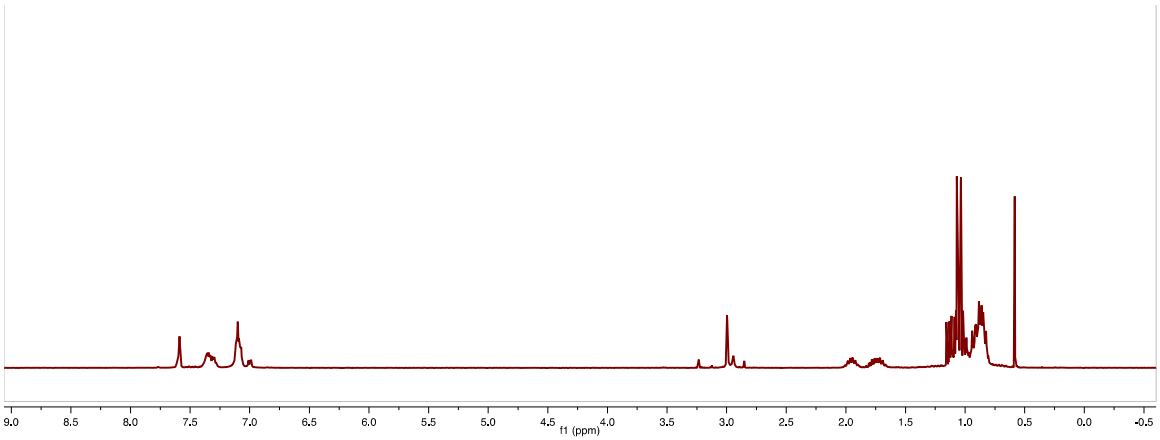

Figure A.8: ^{1}H NMR Spectrum of 1_{CF3}

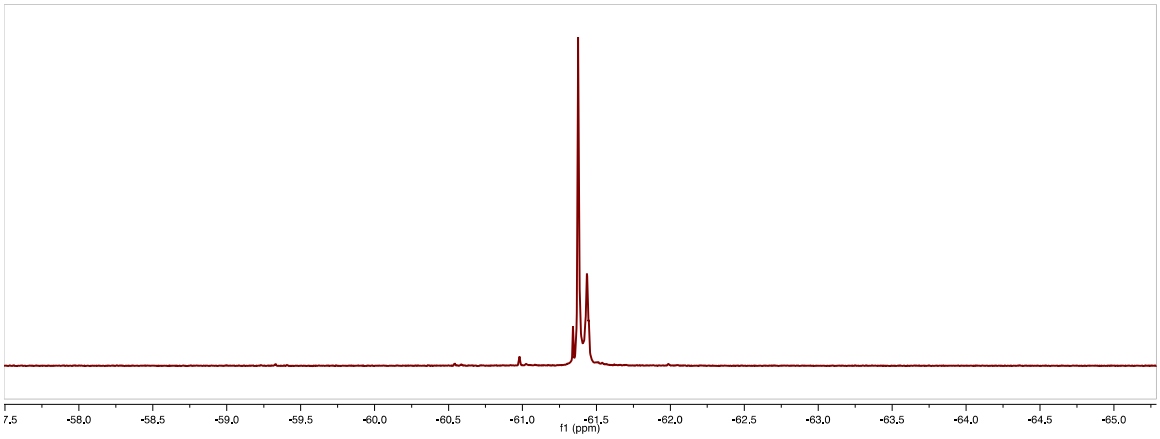

Figure A.9: $^{19}F\{^{1}H\}$ NMR Spectrum of 1_{CF3}

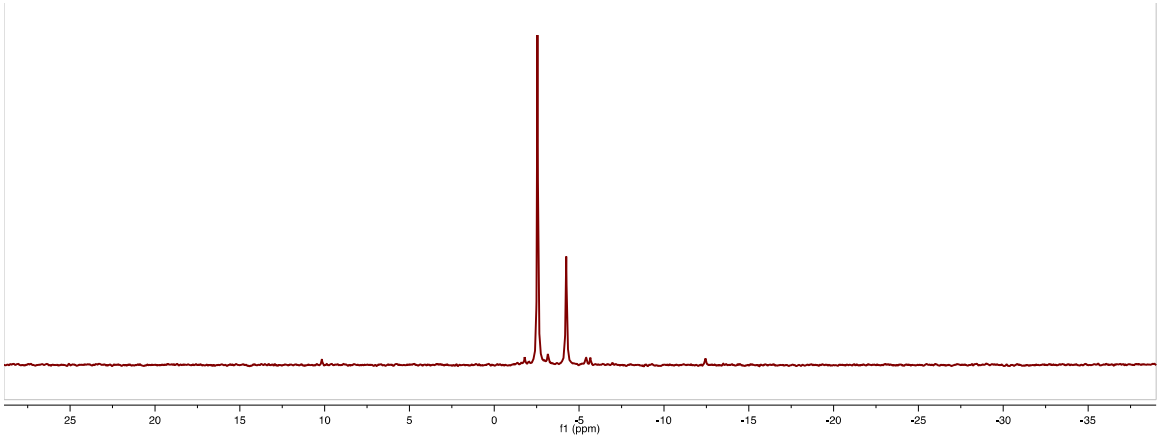

Figure A.10: $^{31}P\{^{1}H\}$ NMR Spectrum of 1_{CF3}

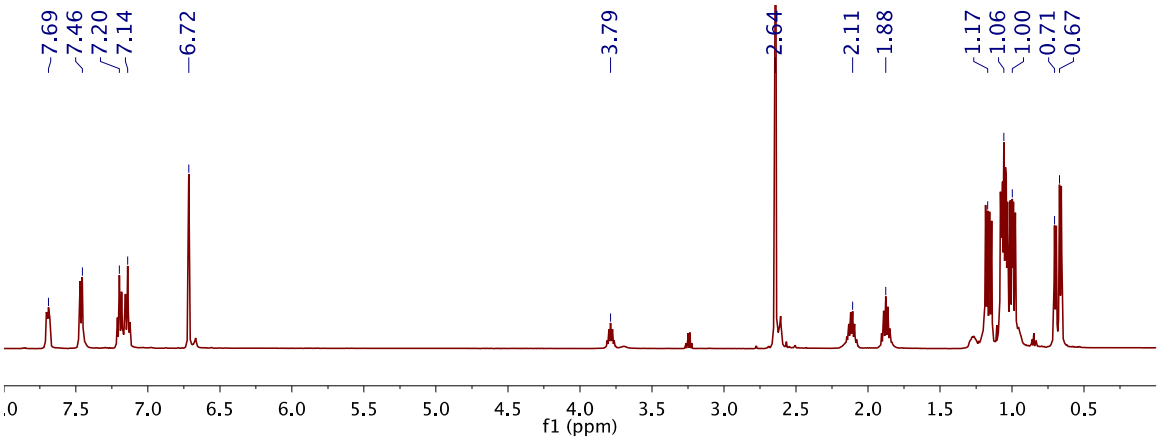

Figure A.11: ^{1}H NMR Spectrum (C_6D_6, 25°C, 499.85 MHz) of 1^{iPr}

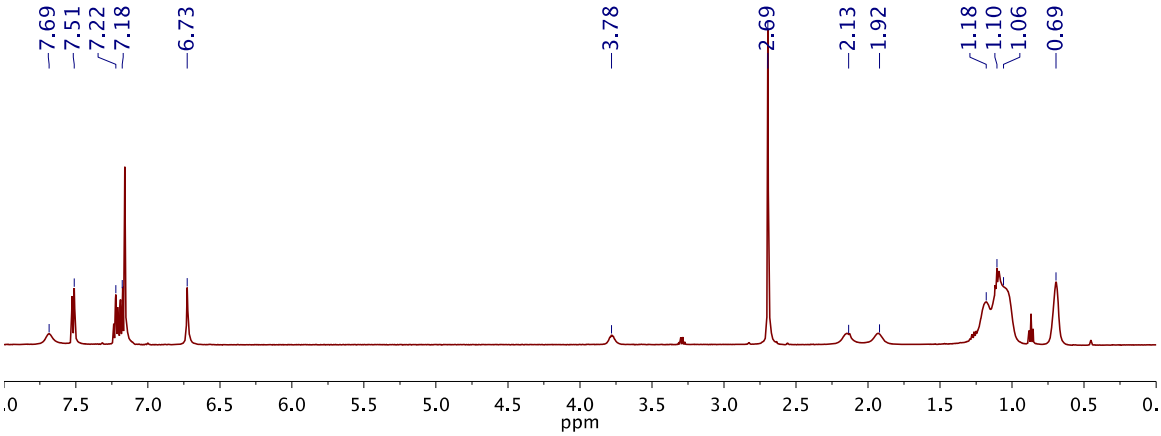

Figure A.12: ^{1}H NMR Spectrum (C_6D_6, 70°C, 499.85 MHz) of 1^{iPr}

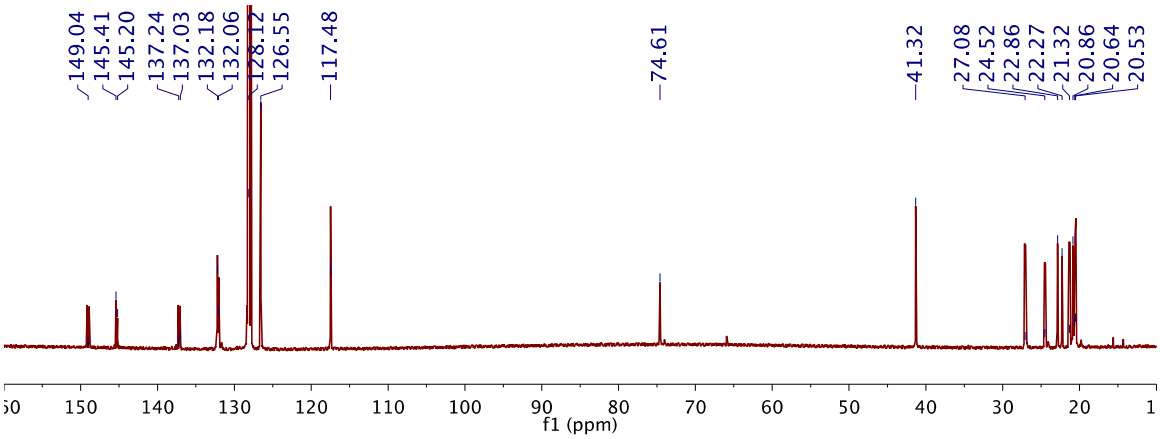

Figure A.13: ^{13}C{^{1}H} NMR Spectrum (C_6D_6, 25°C, 125.70 MHz) of 1^{iPr}

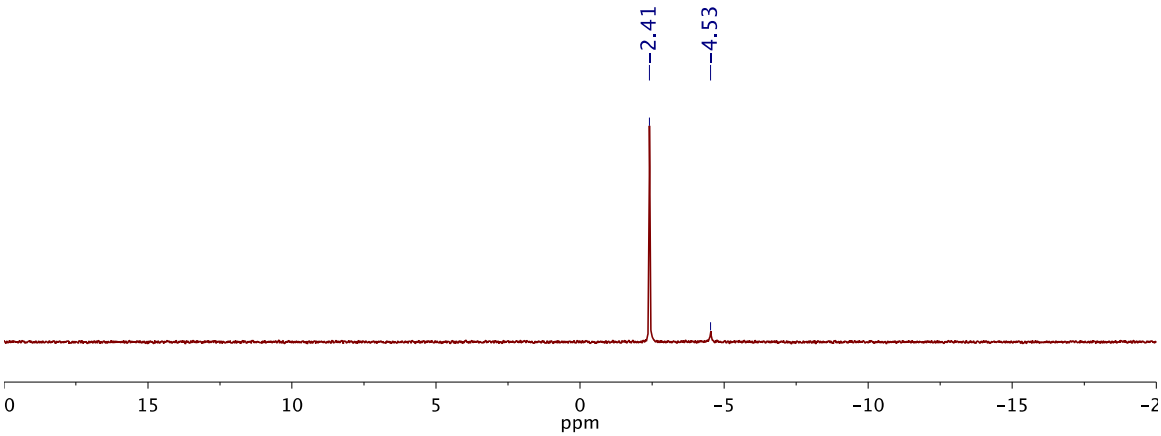

Figure A.14: $^{31}P\{^{1}H\}$ NMR Spectrum (C_6D_6, 25°C, 121.48 MHz) of 1^{iPr}

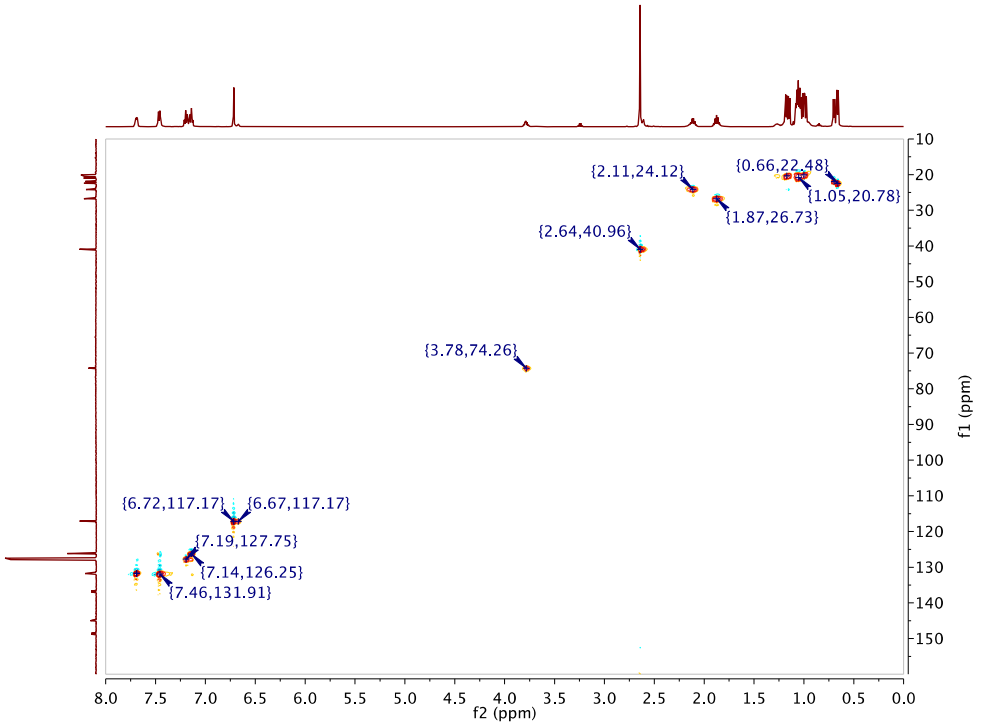

Figure A.15: ^{1}H-^{13}C HSQC NMR Spectrum (C_6D_6, 25°C, 499.85, 125.70 MHz) of 1^{iPr}

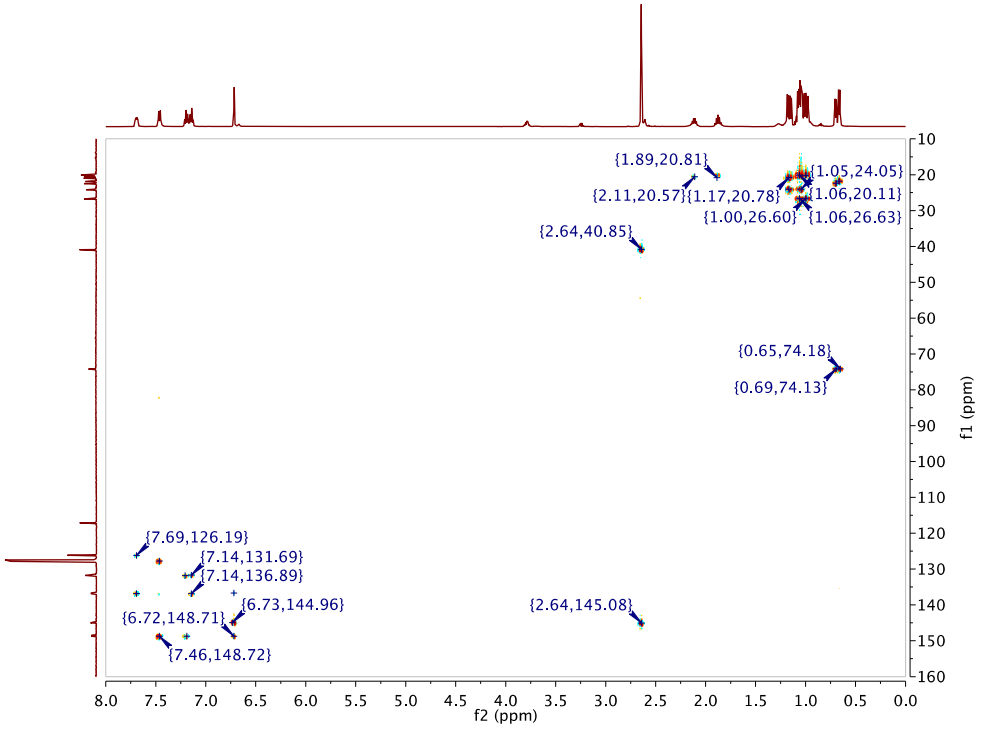

Figure A.16: ^{1}H-^{13}C HMBC NMR Spectrum (C_6D_6, 25°C, 499.85, 125.70 MHz) of 1^{iPr}

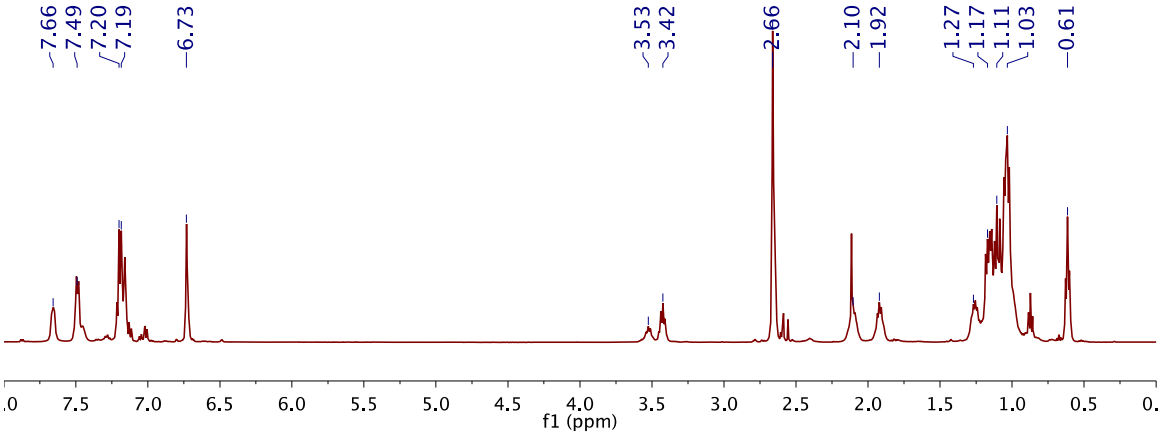

Figure A.17: ^{1}H NMR Spectrum (C_6D_6, 25°C, 499.85 MHz) of 1^{Et}

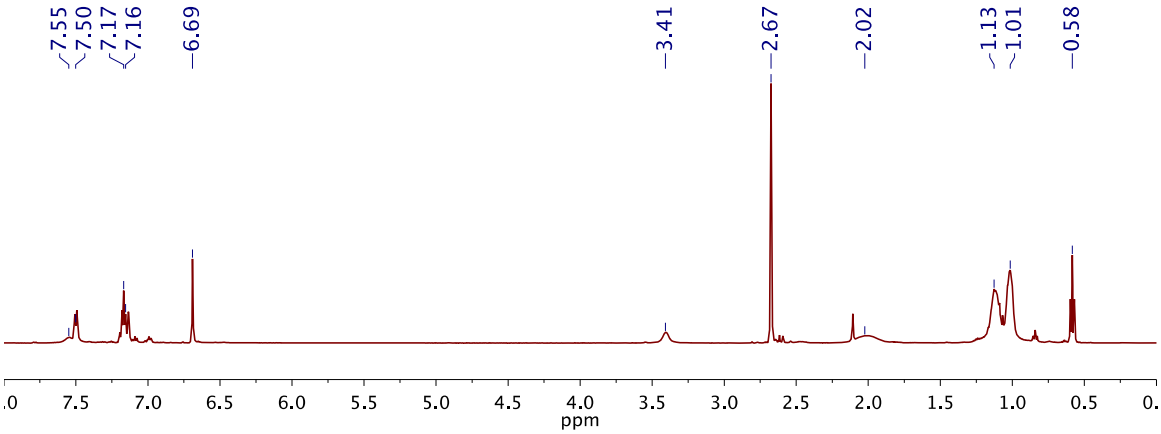

Figure A.18: ^{1}H NMR Spectrum (C_6D_6, 75°C, 499.85 MHz) of 1^{Et}

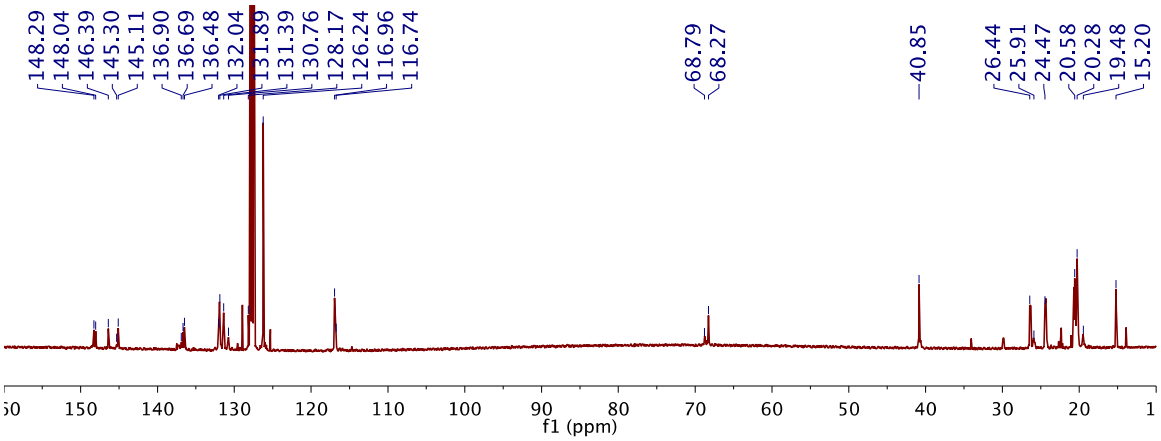

Figure A.19: ^{13}C NMR Spectrum (C_6D_6, 25°C, 125.70 MHz) of 1^{Et}

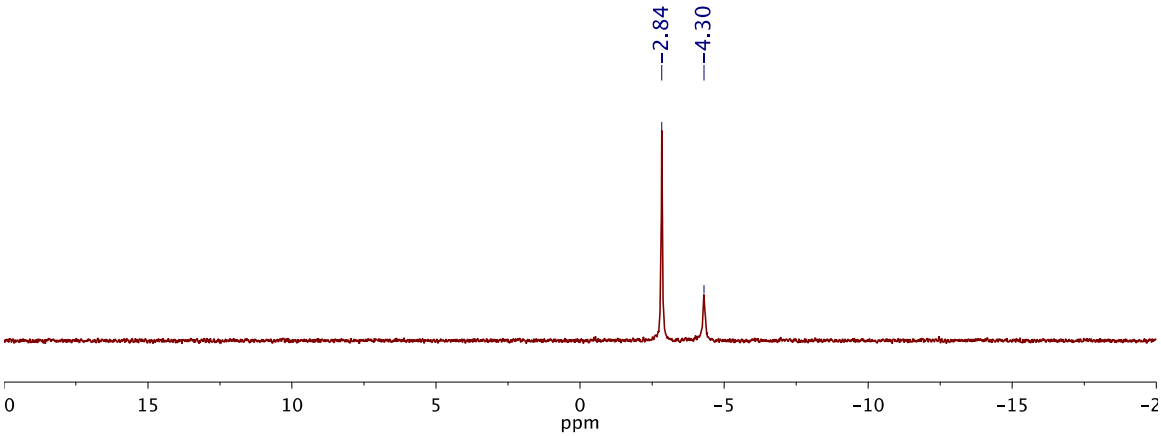

Figure A.20: $^{31}P\{^{1}H\}$ NMR Spectrum (C_6D_6, 25°C, 121.48 MHz) of 1^{Et}

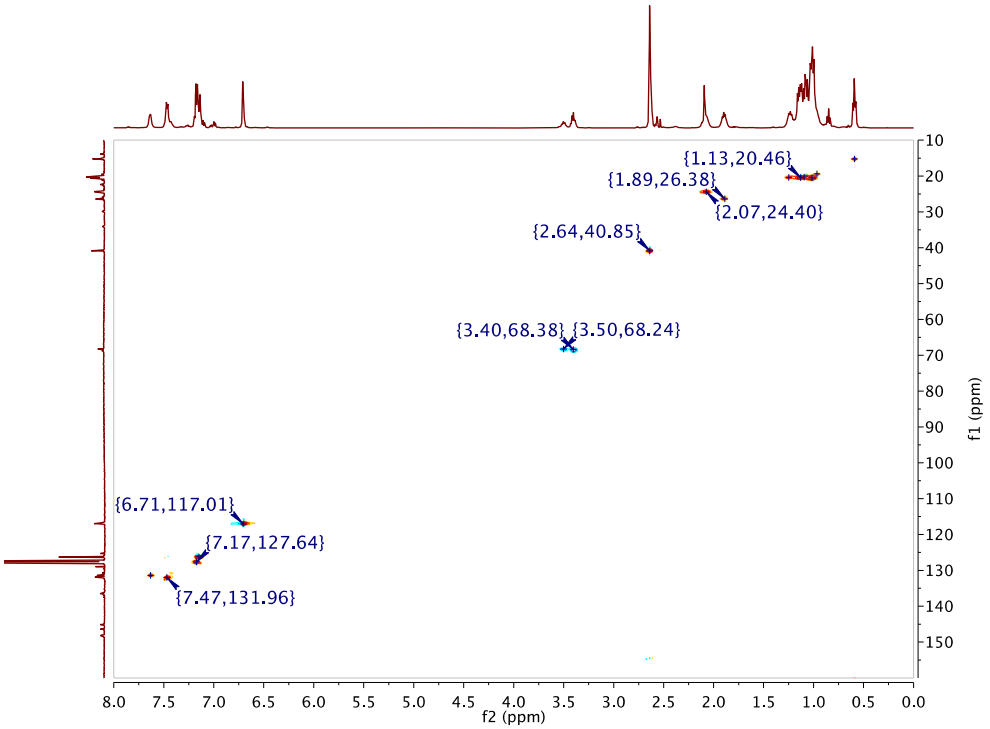

Figure A.21: ^{1}H-^{13}C HSQC NMR Spectrum (C_6D_6, 25°C, 499.85, 125.70 MHz) of 1^{Et}

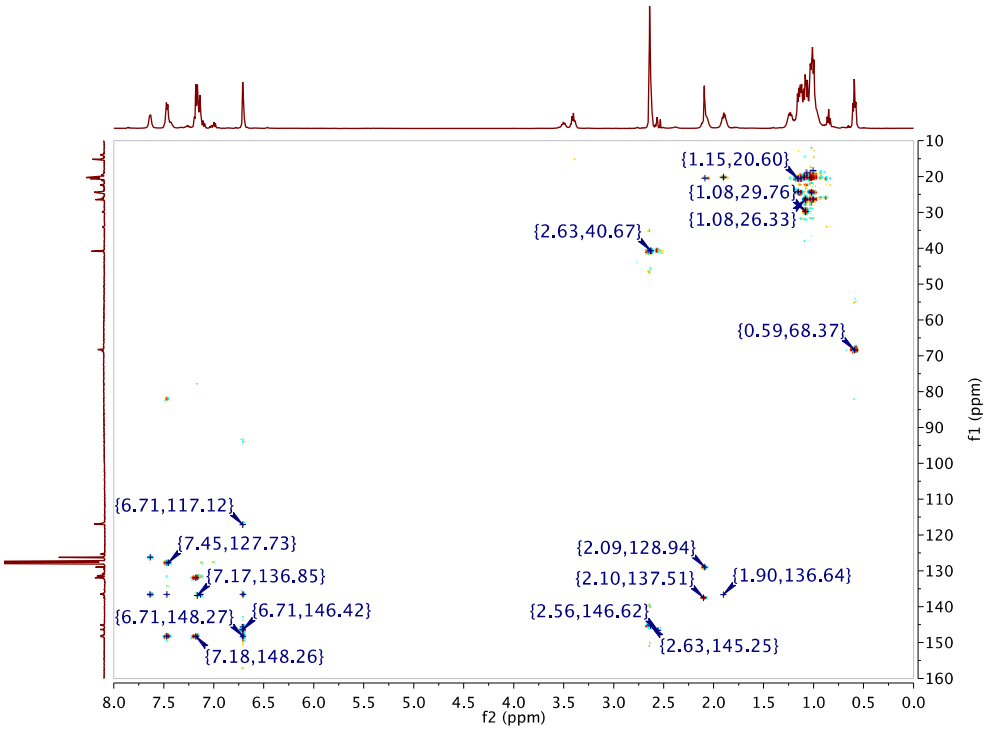

Figure A.22: ^{1}H-^{13}C HMBC NMR Spectrum (C_6D_6, 25°C, 499.85, 125.70 MHz) of 1^{Et}

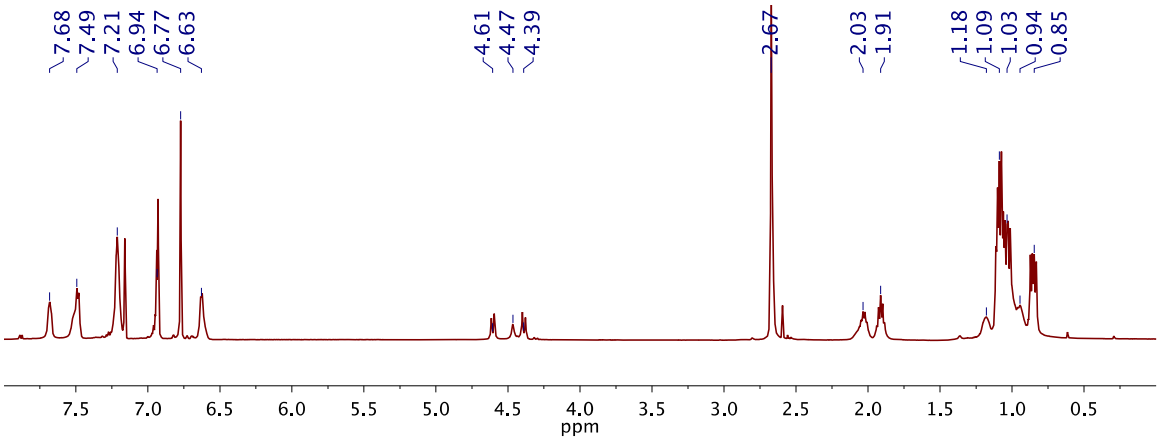

Figure A.23: ^{1}H NMR Spectrum (C_6D_6, 25°C, 499.85 MHz) of 1^{Bn}

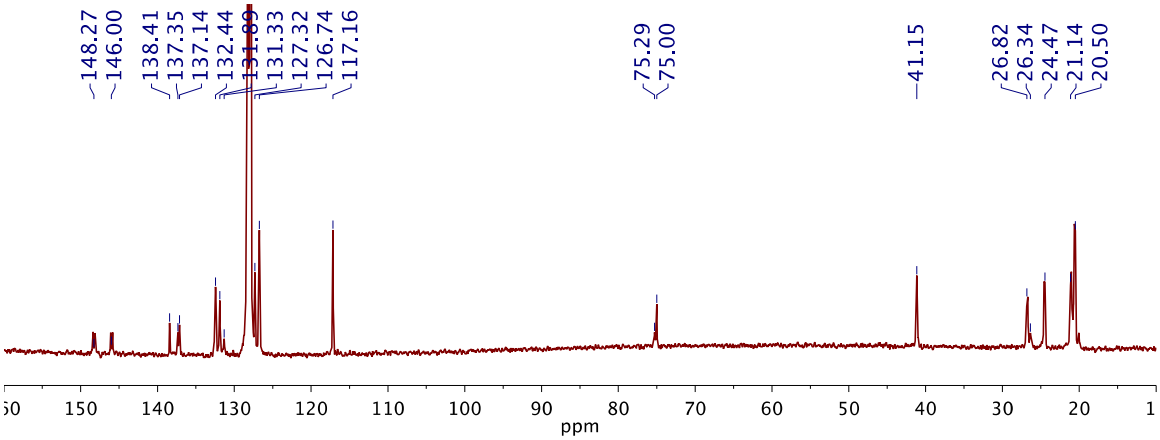

Figure A.24: $^{13}C\{^{1}H\}$ NMR Spectrum (C_6D_6, 25°C, 125.70 MHz) of 1^{Bn}

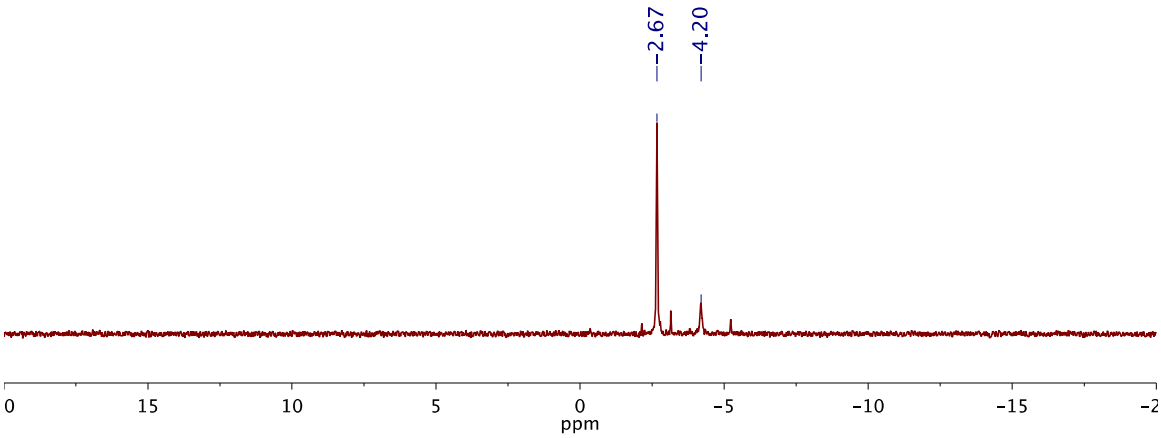

Figure A.25: $^{31}P\{^{1}H\}$ NMR Spectrum (C_6D_6, 25°C, 121.48 MHz) of 1^{Bn}

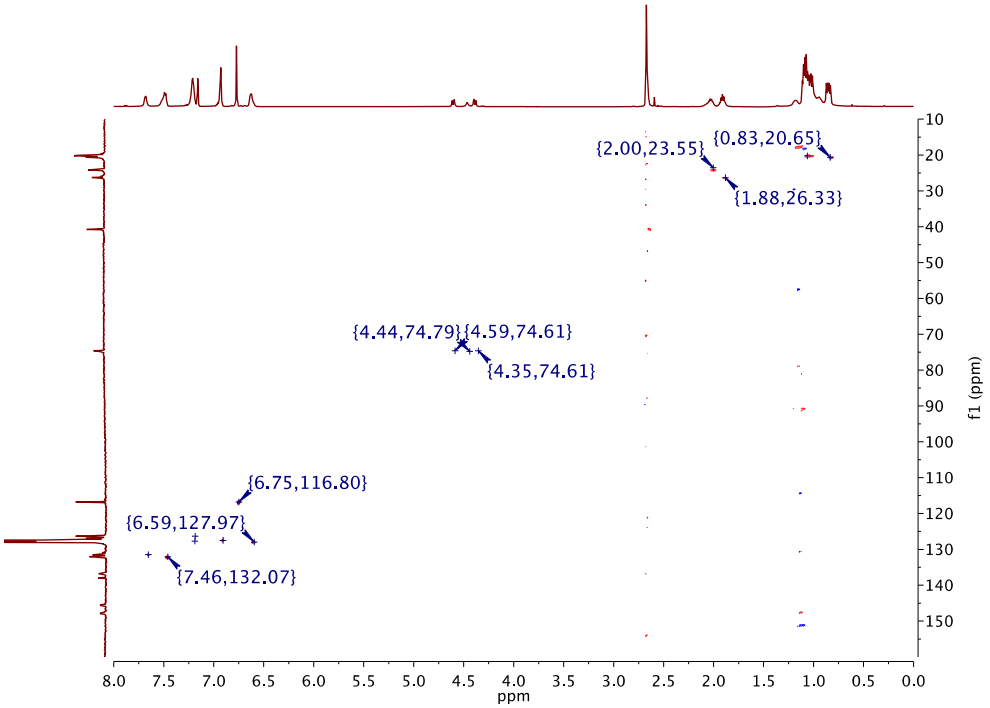

Figure A.26: ^{1}H-^{13}C HSQC NMR Spectrum (C_6D_6, 25°C, 499.85, 125.70 MHz) of 1^{Bn}

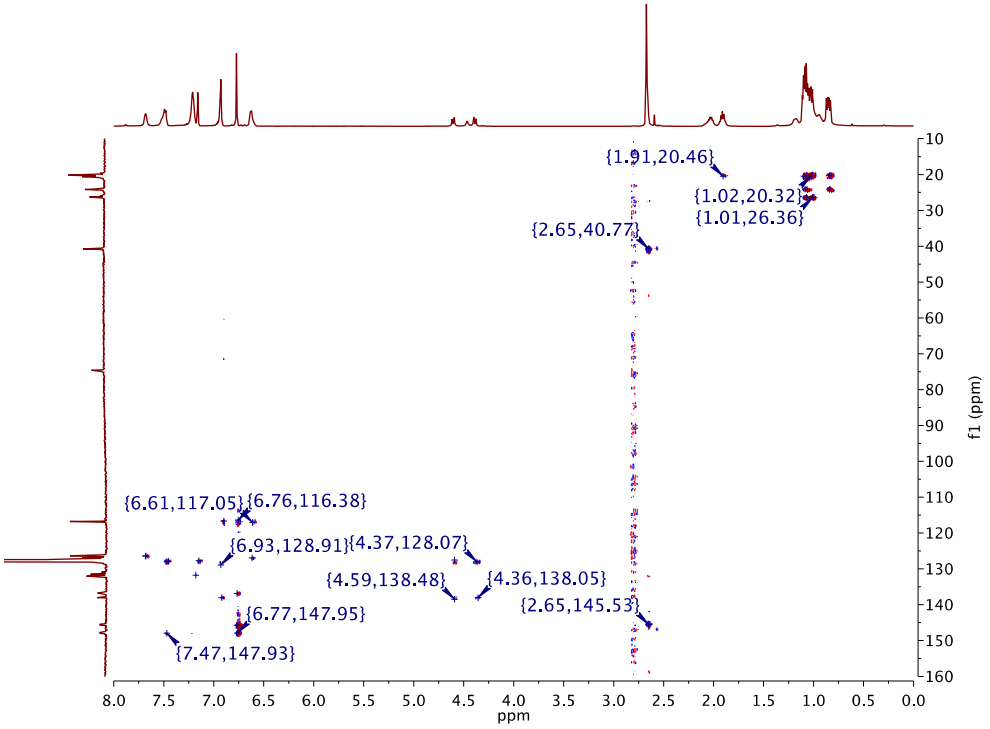

Figure A.27: ^{1}H-^{13}C HMBC NMR Spectrum (C_6D_6, 25°C, 499.85, 125.70 MHz) of 1^{Bn}

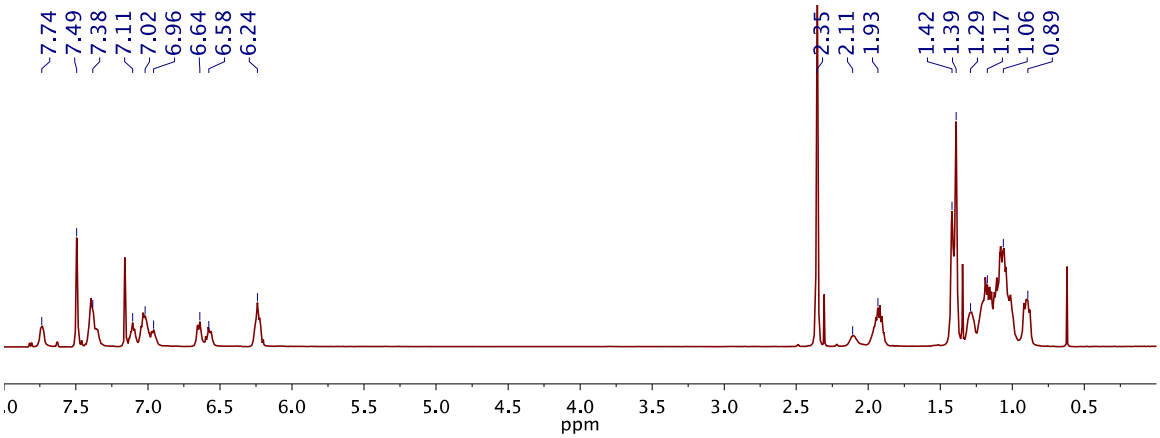

Figure A.28: ^{1}H NMR Spectrum (C_6D_6, 25°C, 499.85 MHz) of 1^{OAr}

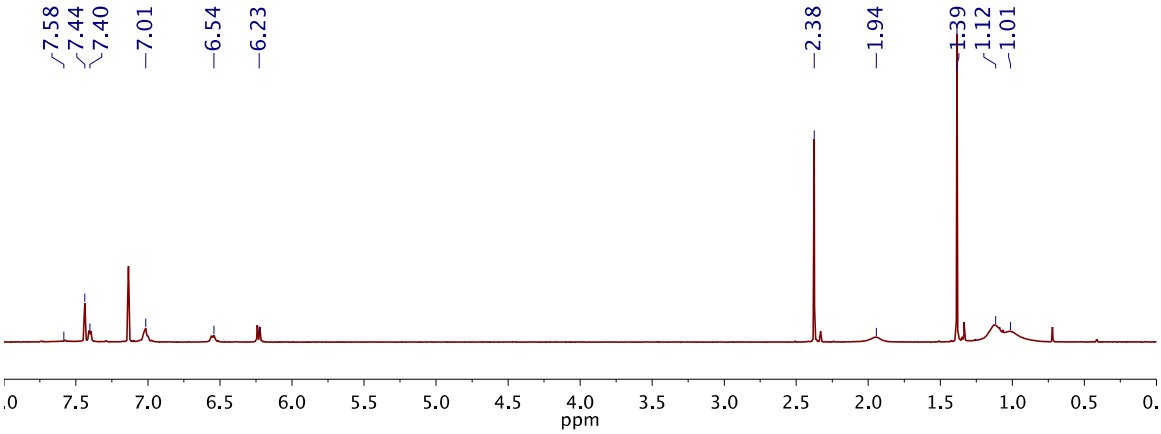

Figure A.29: ^{1}H NMR Spectrum (C_6D_6, 70°C, 499.85 MHz) of 1^{OAr}

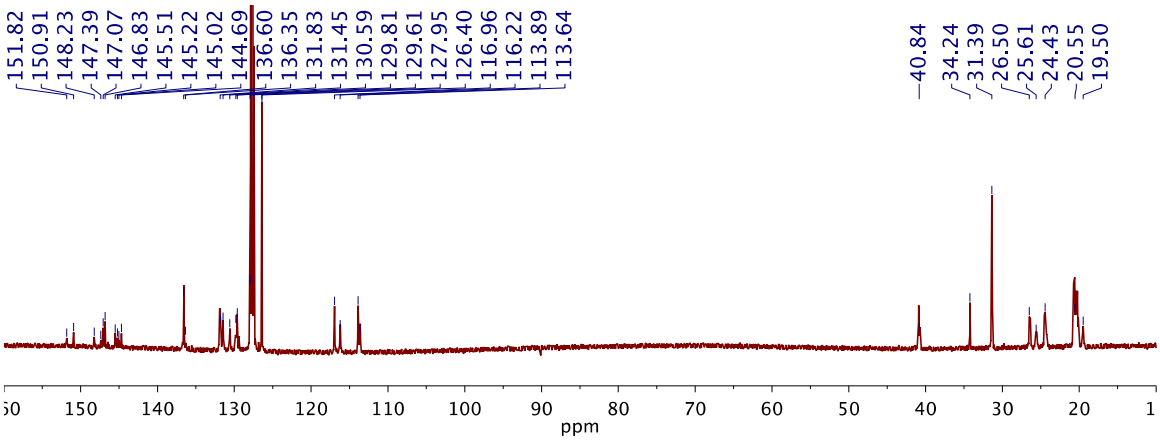

Figure A.30: ^{13}C{^{1}H} NMR Spectrum (C_6D_6, 25°C, 125.70 MHz) of 1^{OAr}

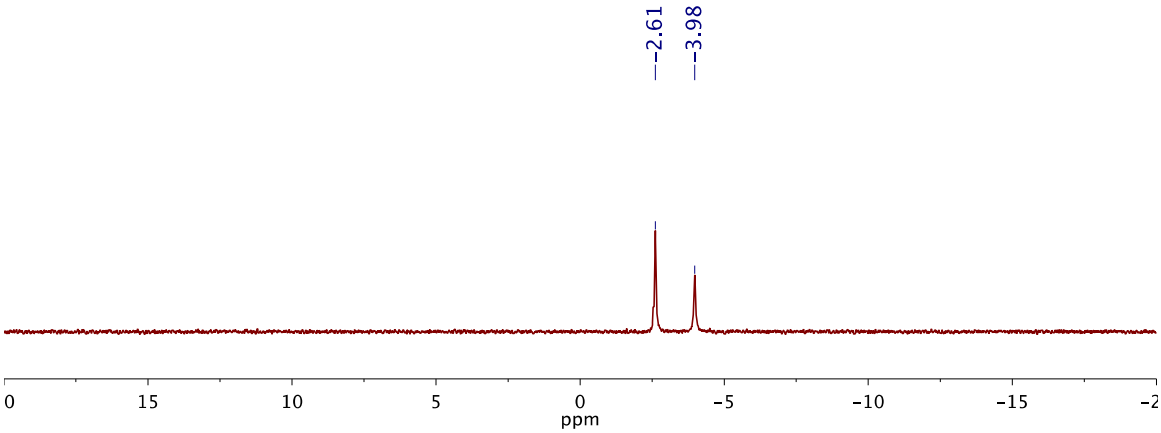

Figure A.31: $^{31}P\{^{1}H\}$ NMR Spectrum (C_6D_6, 25°C, 121.48 MHz) of 1^{OAr}

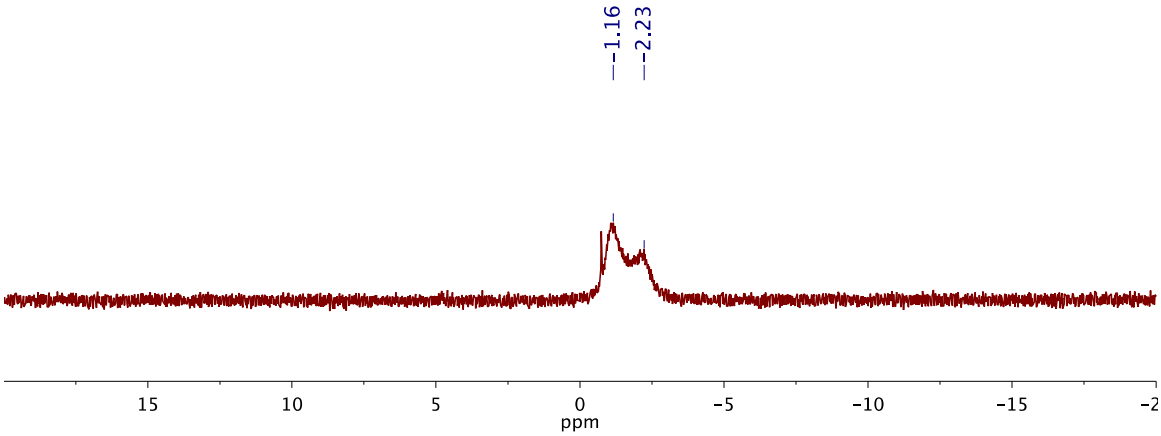

Figure A.32: $^{31}P\{^{1}H\}$ NMR Spectrum (C_6D_6, 70°C, 202.36 MHz) of 1^{OAr}

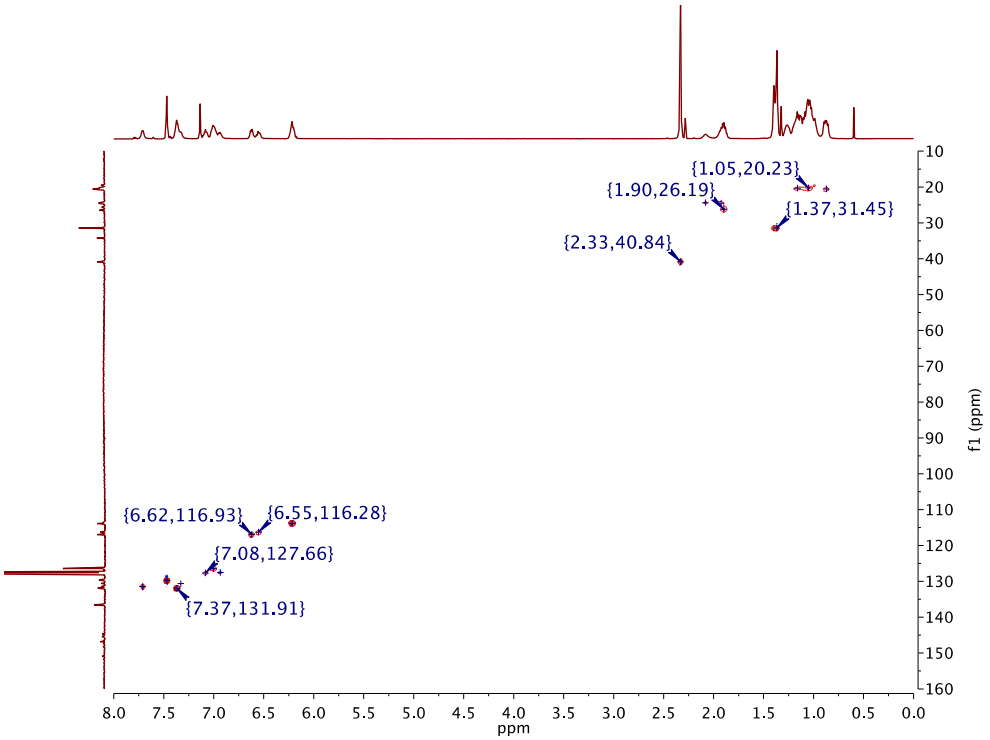

Figure A.33: ^{1}H-^{13}C HSQC NMR Spectrum (C_6D_6, 25°C, 499.85, 125.70 MHz) of 1^{OAr}

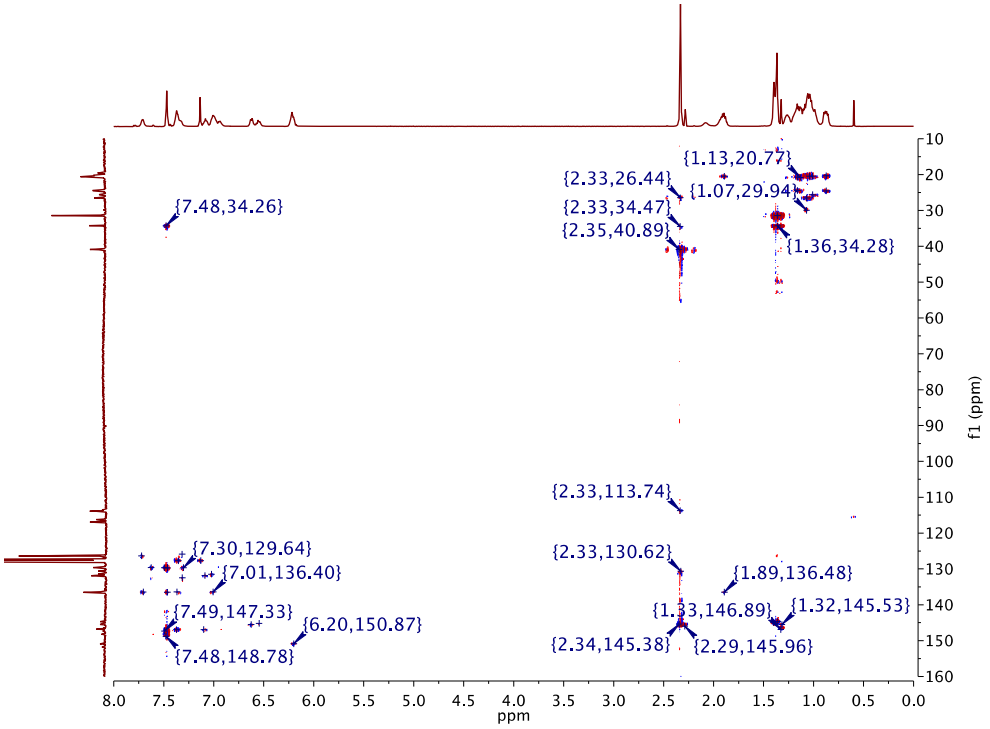

Figure A.34: ^{1}H-^{13}C HMBC NMR Spectrum (C_6D_6, 25°C, 499.85, 125.70 MHz) of 1^{Oar}

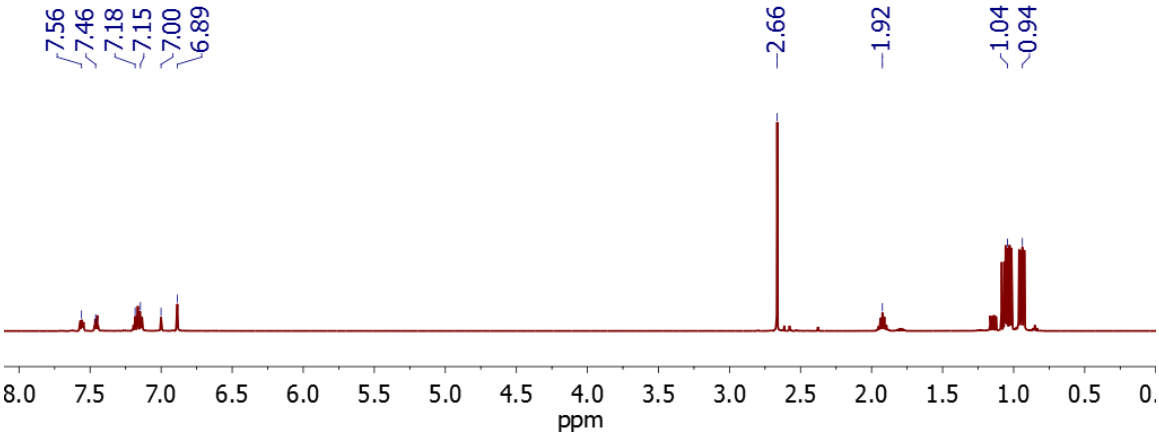

Figure A.35: ^{1}H NMR Spectrum (C_6D_6, 25°C, 499.85 MHz) of 1,3-bis(2'-diisopropylphosphino)-5-dimethylaminobenzene.

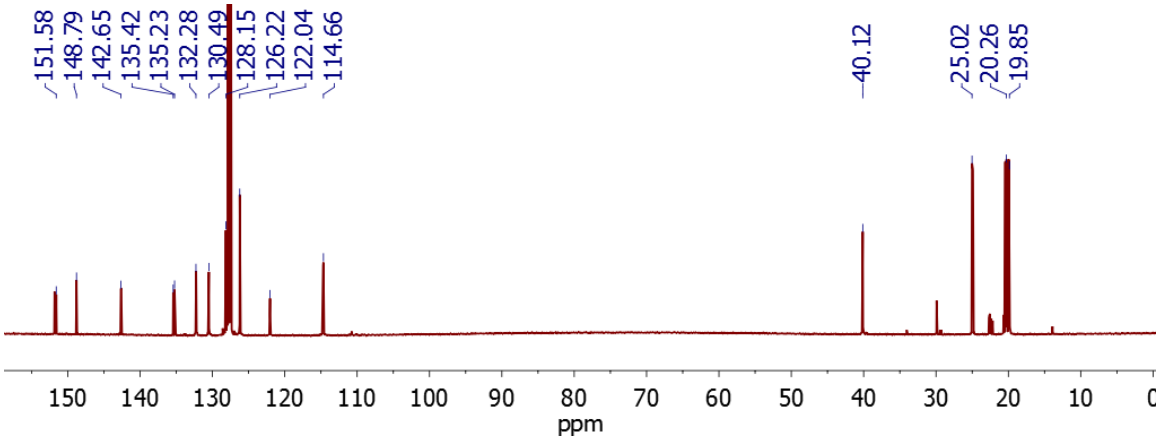

Figure A.36: $^{13}C\{^{1}H\}$ NMR Spectrum (C_6D_6, 25°C, 125.70 MHz) of 1,3-bis(2'-diisopropylphosphino)-5-dimethylaminobenzene.

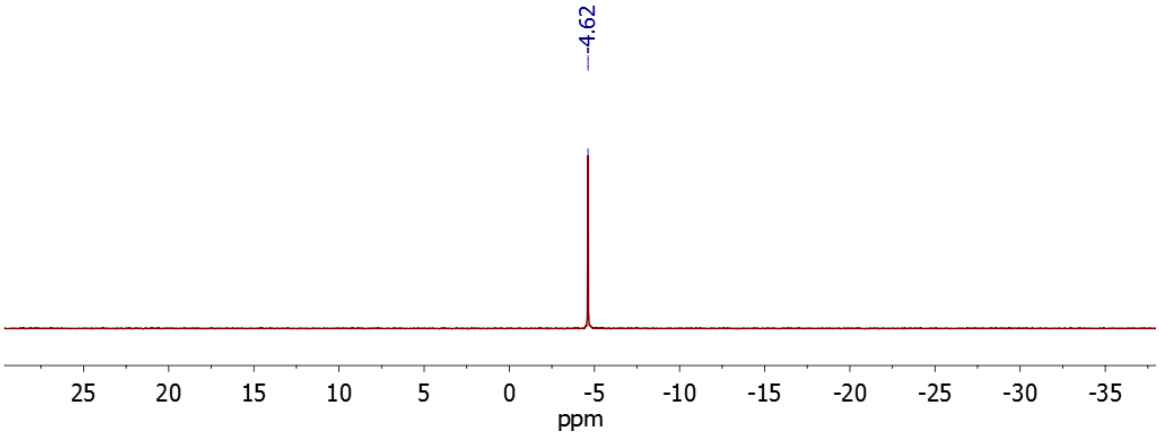

Figure A.37: $^{31}P\{^{1}H\}$ NMR Spectrum (C_6D_6, 121.48 MHz) of 1,3-bis(2'-diisopropylphosphino)-5-dimethylaminobenzene.

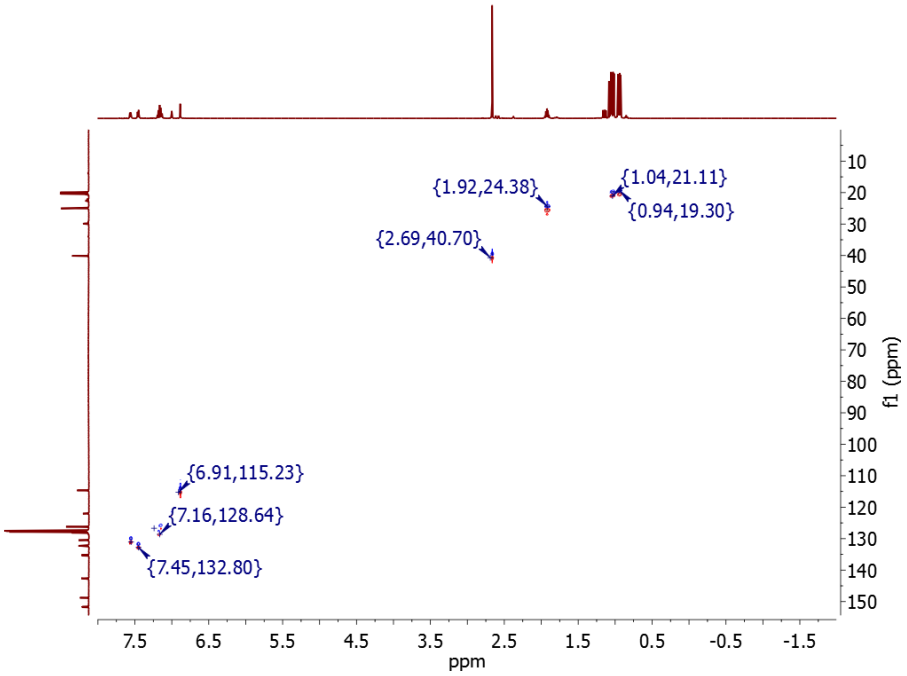

Figure A.38: ^{1}H-^{13}C HSQC NMR Spectrum (C_6D_6, 25°C, 499.85, 125.70 MHz) of 1,3-bis(2'-diisopropylphosphino)-5-dimethylaminobenzene.

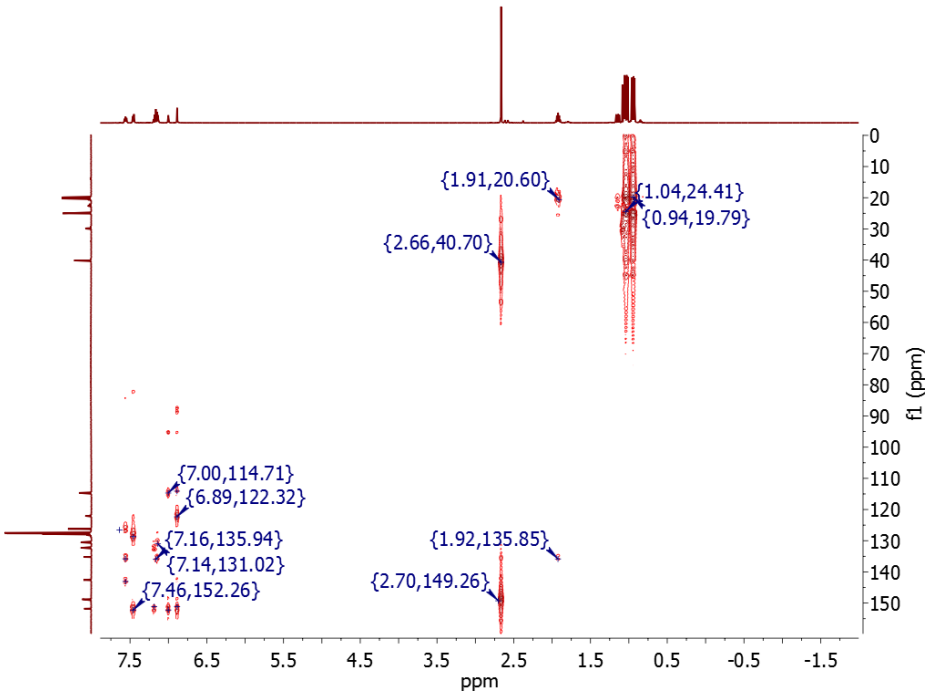

Figure A.39: ^{1}H-^{13}C HMBC NMR Spectrum (C_6D_6, 25°C, 499.85, 125.70 MHz) of 1,3-bis(2'-diisopropylphosphino)-5-dimethylaminobenzene.

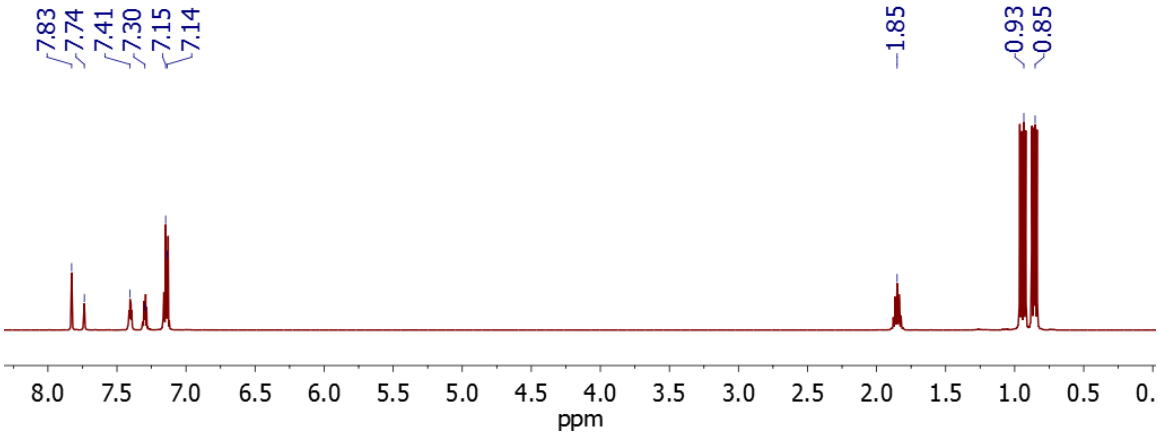

Figure A.40: ^{1}H NMR Spectrum (C_6D_6, 25°C, 499.85 MHz) of 1,3-bis(2'-diisopropylphosphino)-5-trifluoromethylbenzene.

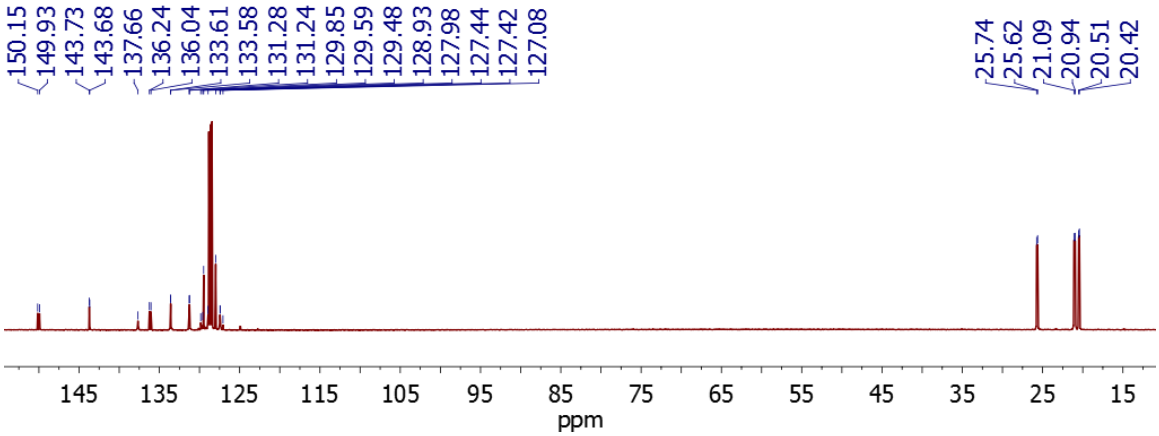

Figure A.41: ^{13}C{^{1}H} NMR Spectrum (C_6D_6, 25°C, 125.70 MHz) of 1,3-bis(2'-diisopropylphosphino)-5-trifluoromethylbenzene.

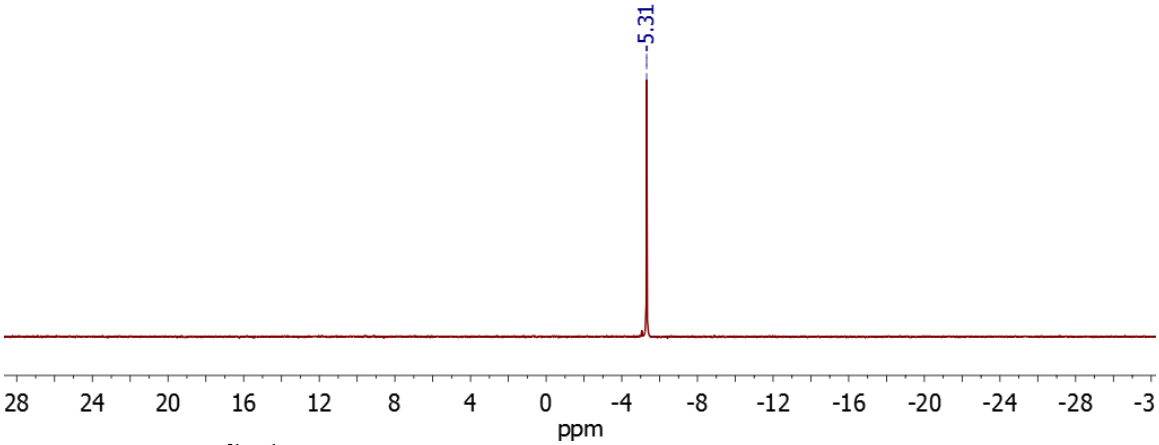

Figure A.42: ^{31}P{^{1}H} NMR Spectrum (C_6D_6, 121.48 MHz) of 1,3-bis(2'-diisopropylphosphino)-5-trifluoromethylbenzene.

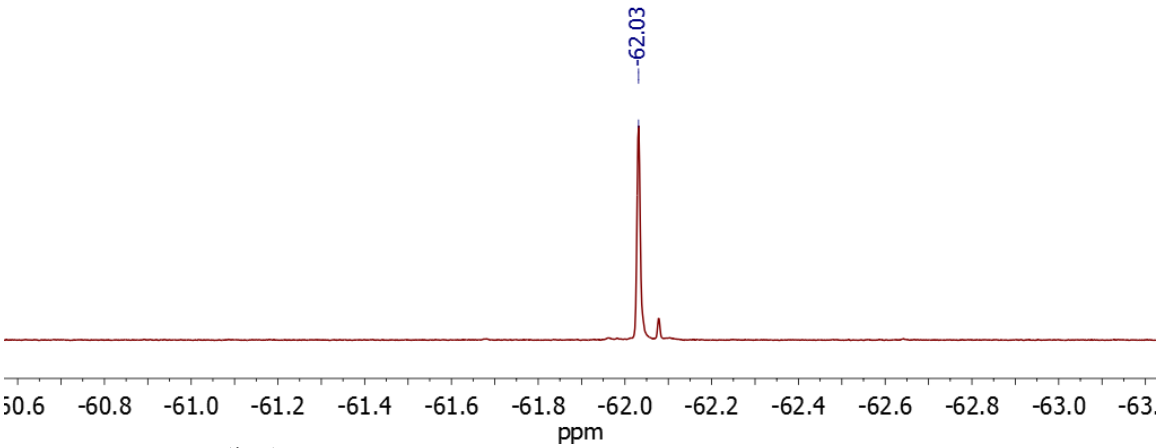

Figure A.43: $^{19}F\{^{1}H\}$ NMR Spectrum (C_6D_6, 121.48 MHz) of 1,3-bis(2'-diisopropylphosphino)-5-trifluoromethylbenzene.

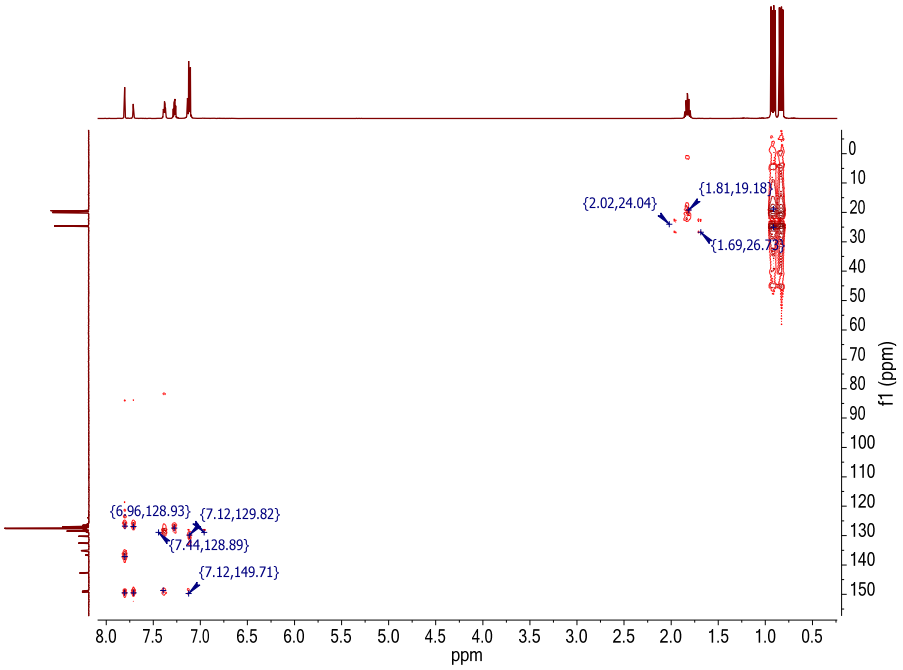

Figure A.44: ^{1}H-^{13}C HSQC NMR Spectrum (C_6D_6, 25°C, 499.85, 125.70 MHz) of 1,3-bis(2'-diisopropylphosphino)-5-trifluoromethylbenzene.

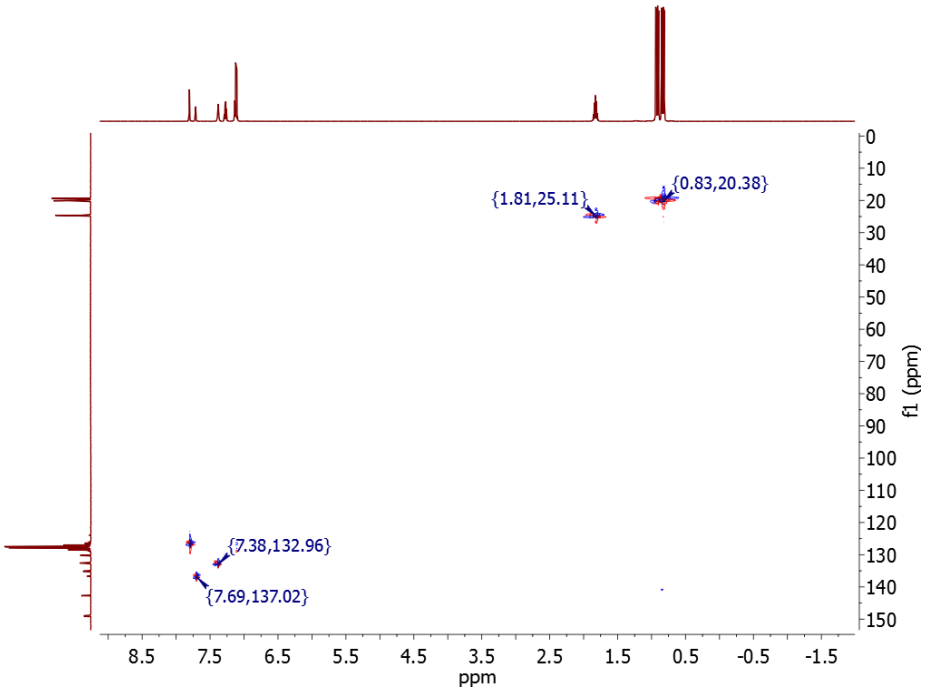

Figure A.45: ^{1}H-^{13}C HMBC NMR Spectrum (C_6D_6, 25°C, 499.85, 125.70 MHz) of 1,3-bis(2'-diisopropylphosphino)-5-trifluoromethylbenzene.

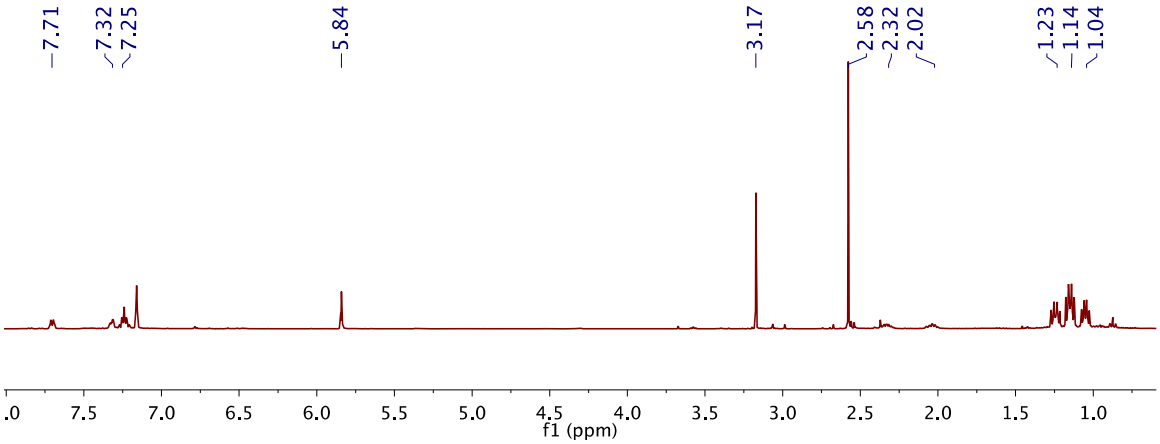

Figure A.46: ^{1}H NMR Spectrum (C_6D_6, 399.80 MHz) of 2

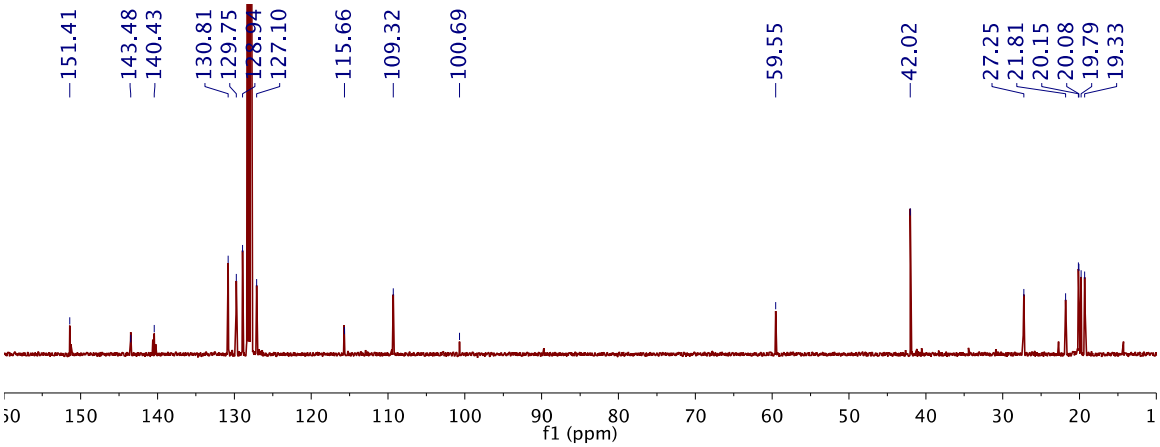

Figure A.47: ^{13}C{^{1}H} NMR Spectrum (C_6D_6, 100.54 MHz) of 2

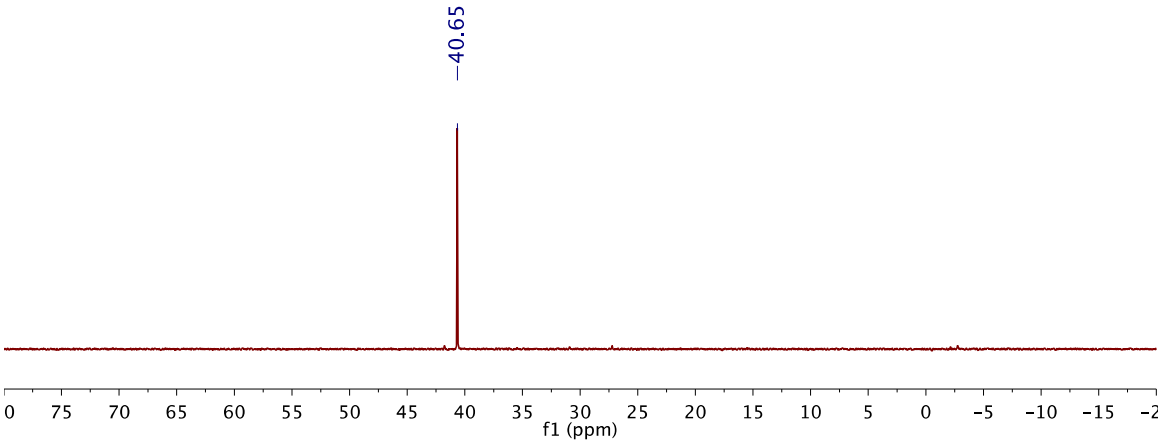

Figure A.48: ^{31}P{^{1}H} NMR Spectrum (C_6D_6, 121.48 MHz) of 2

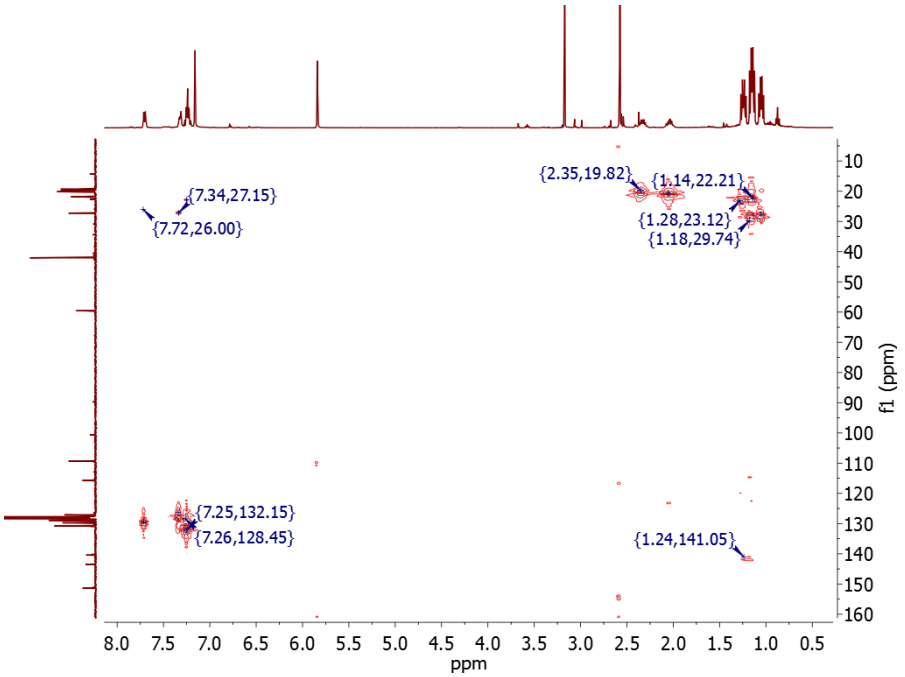

Figure A.49: ^{1}H-^{13}C H2BC NMR Spectrum (C_6D_6, 25°C, 499.85, 125.70 MHz) of 2.

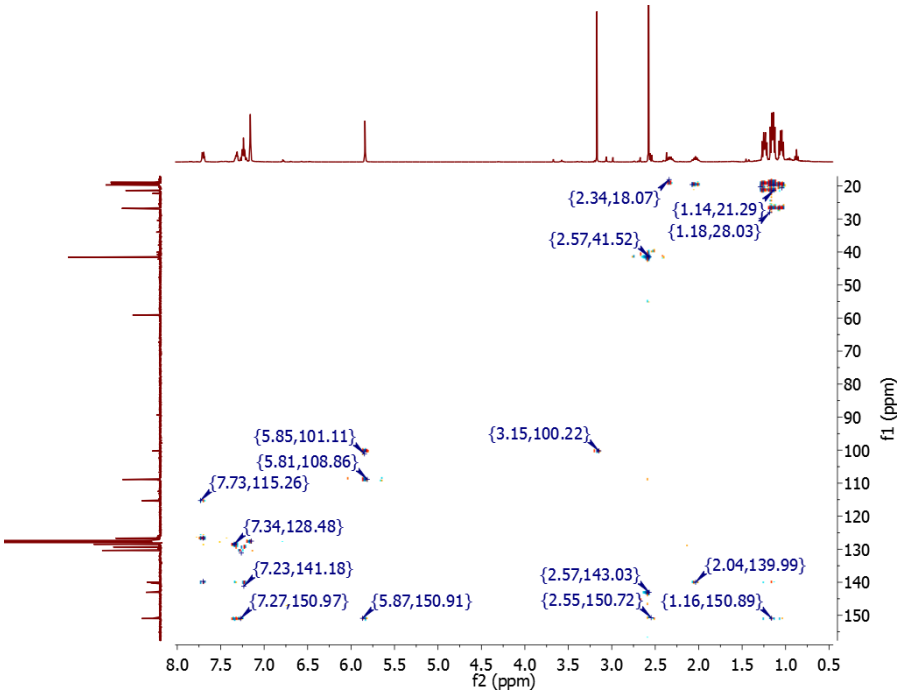

Figure A.50: ^{1}H-^{13}C HMBC NMR Spectrum (C_6D_6, 25°C, 499.85, 125.70 MHz) of 2.

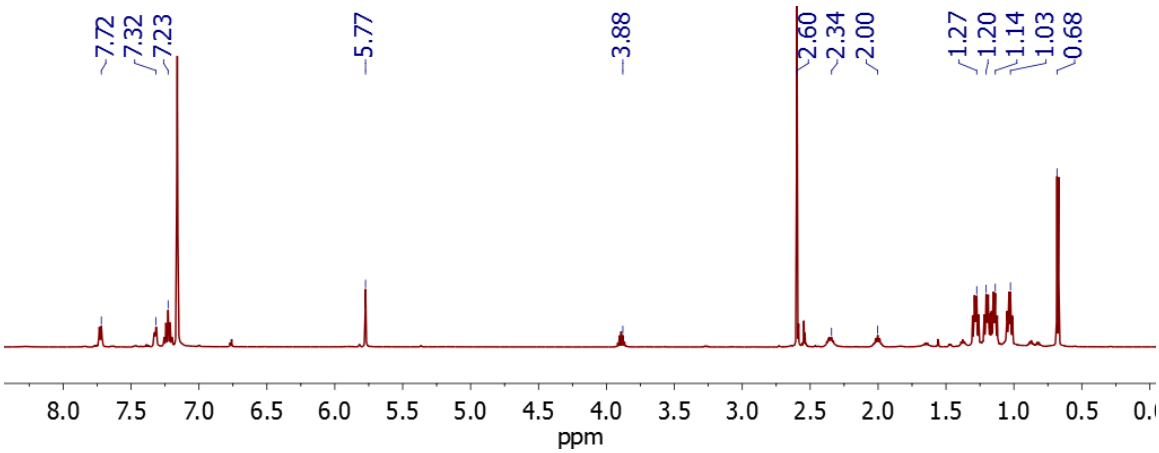

Figure A.51: ^{1}H NMR Spectrum (C_6D_6, 399.80 MHz) of 2^{iPr}

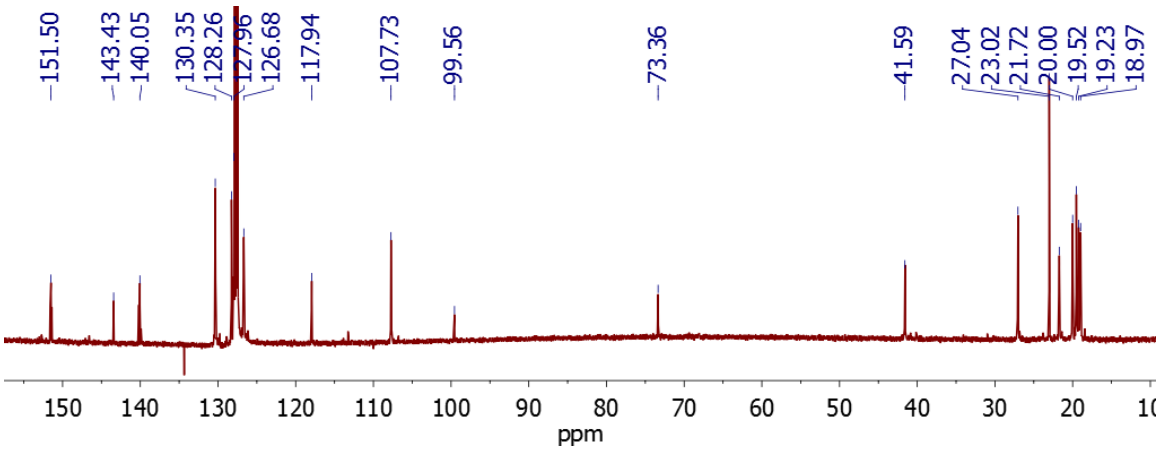

Figure A.52: ^{13}C NMR Spectrum (C_6D_6, 100.54 MHz) of 2^{iPr}

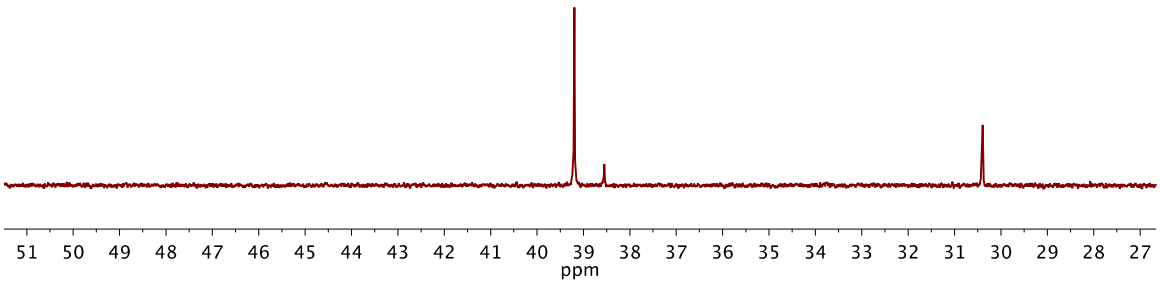

Figure A.53: ^{31}P{^{1}H} NMR Spectrum (C_6D_6, 121.48 MHz) of 2^{iPr}

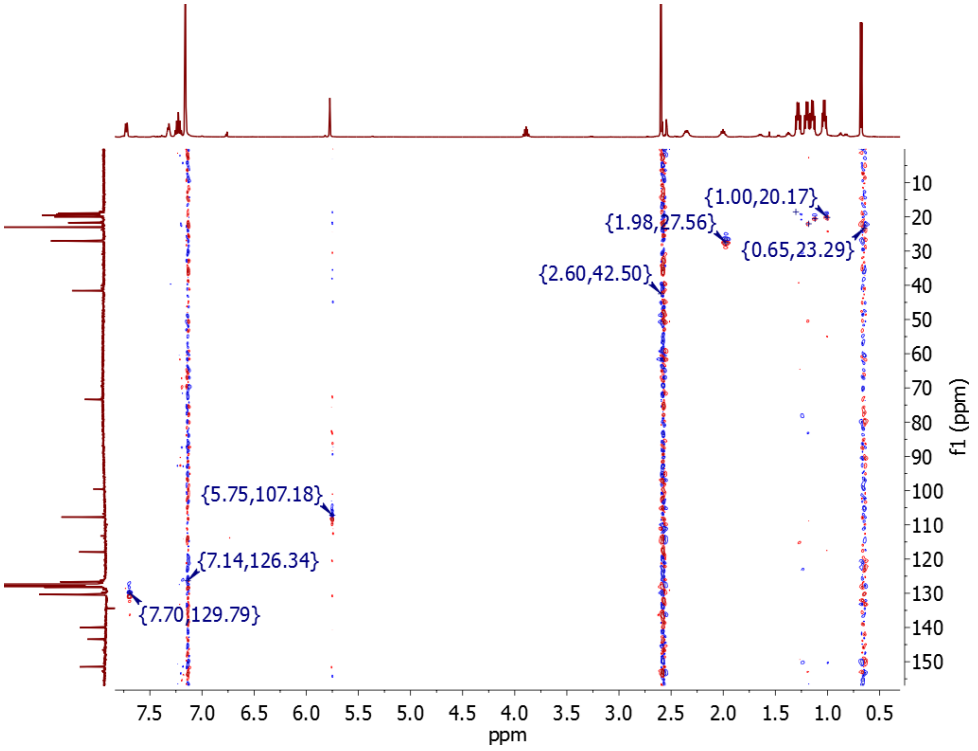

Figure A.54: ^{1}H-^{13}C HSQC NMR Spectrum (C_6D_6, 25°C, 499.85, 125.70 MHz) of 2^{iPr}.

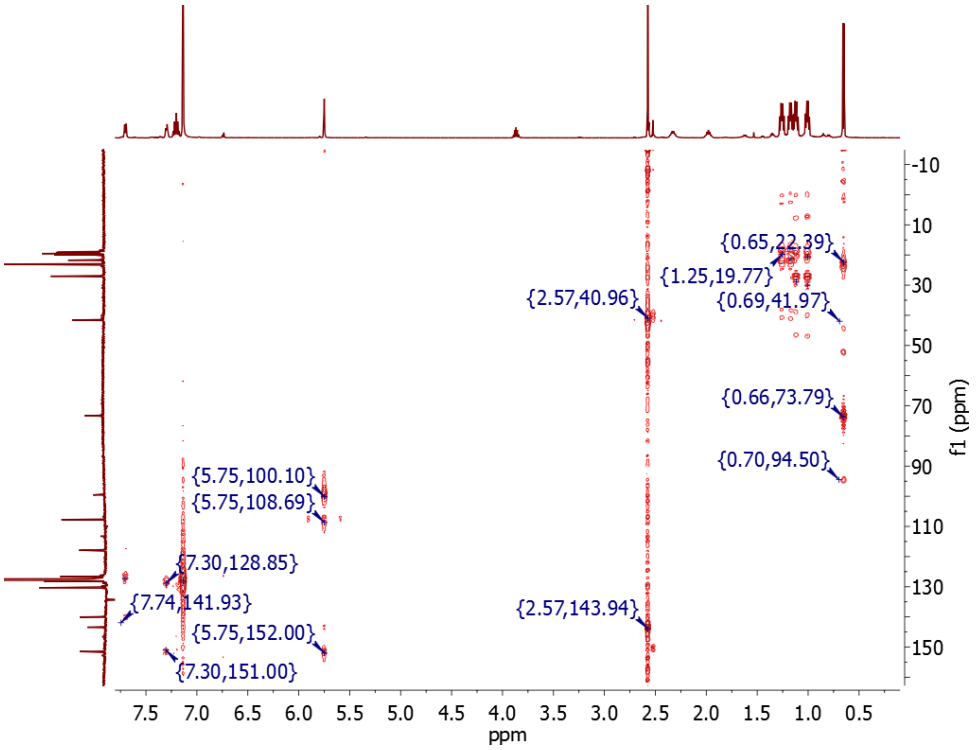

Figure A.55: ^{1}H-^{13}C HMBC NMR Spectrum (C_6D_6, 25°C, 499.85, 125.70 MHz) of 2^{iPr}.

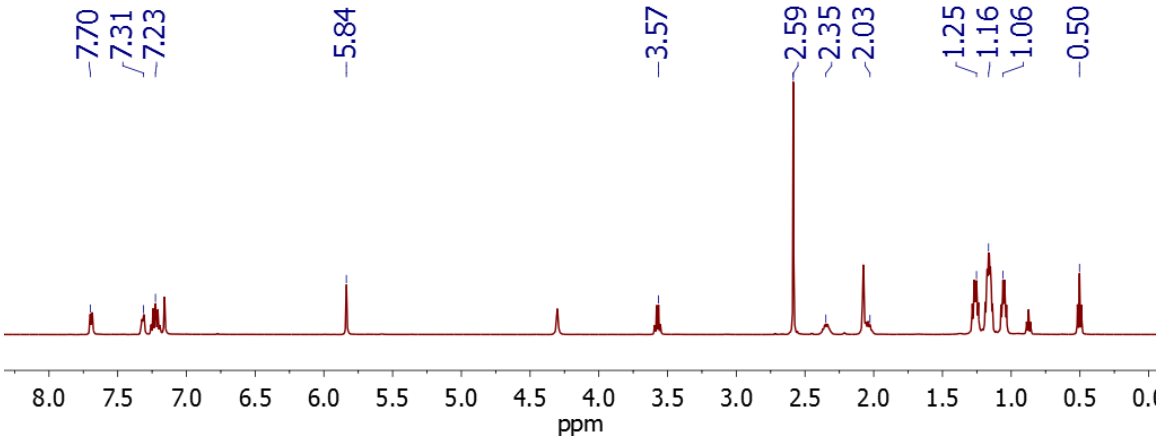

Figure A.56: ^{1}H NMR Spectrum (C_6D_6, 399.80 MHz) of 2^{Et}

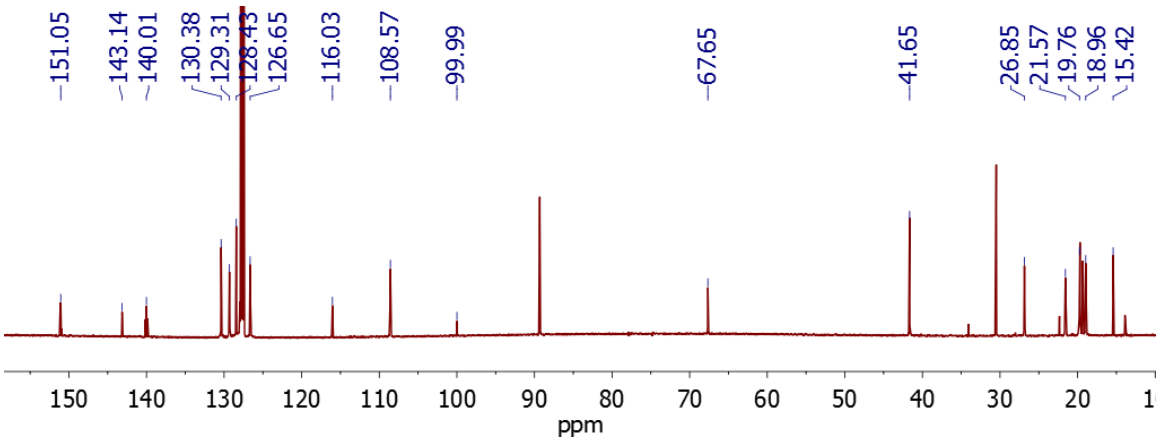

Figure A.57: ^{13}C NMR Spectrum (C_6D_6, 100.54 MHz) of 2^{Et}

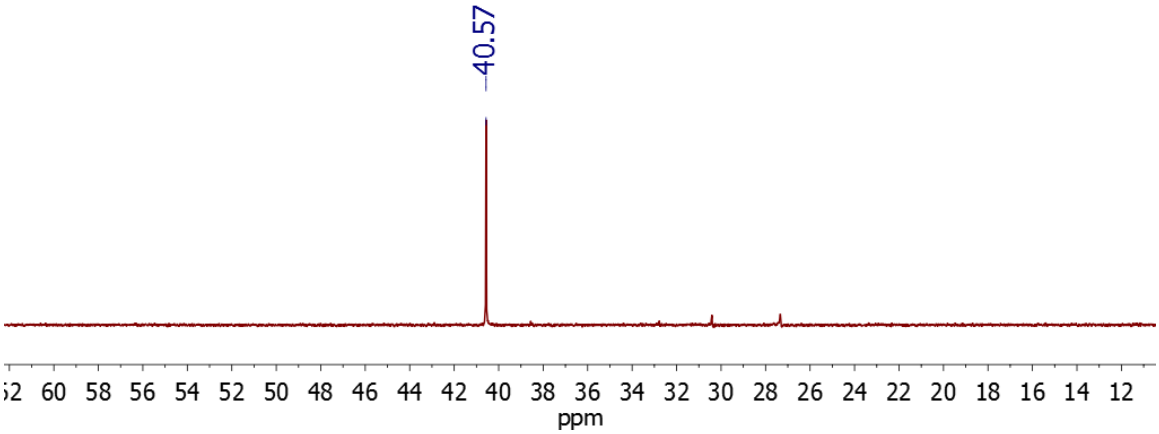

Figure A.58: ^{31}P{^{1}H} NMR Spectrum (C_6D_6, 121.48 MHz) of 2^{Et}

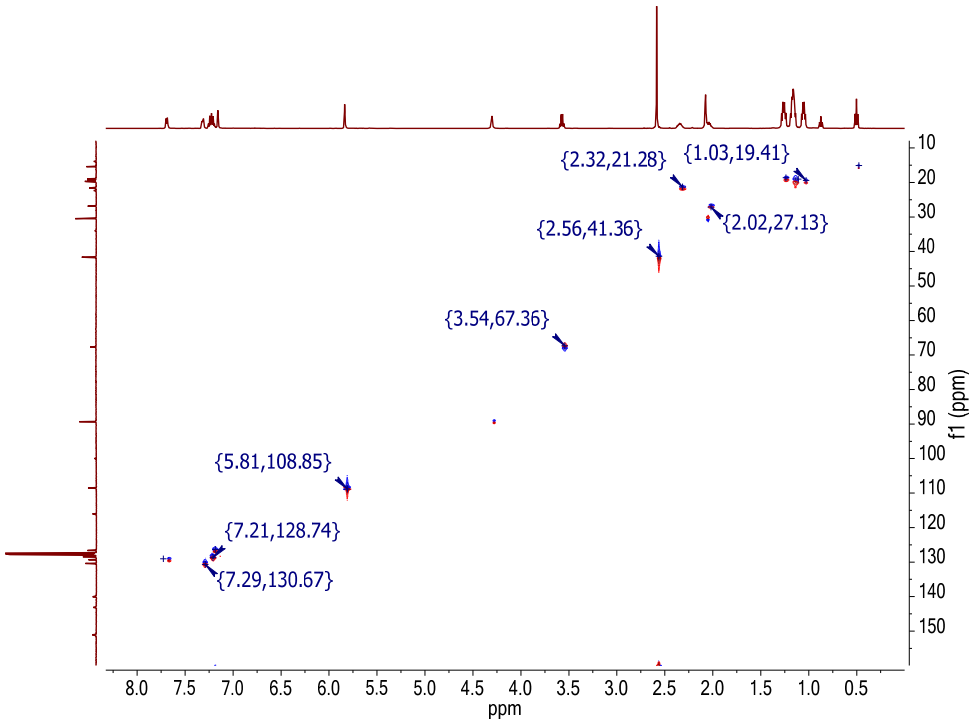

Figure A.59: ^{1}H-^{13}C HSQC NMR Spectrum (C_6D_6, 25°C, 499.85, 125.70 MHz) of 2^{Et}.

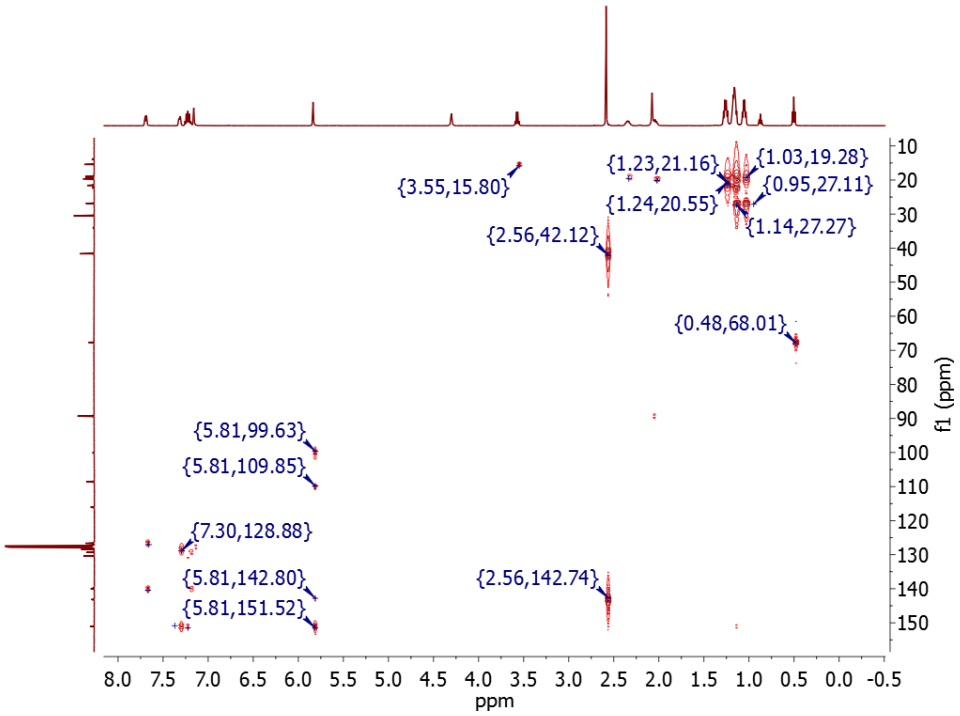

Figure A.60: ^{1}H-^{13}C HMBC NMR Spectrum (C_6D_6, 25°C, 499.85, 125.70 MHz) of 2^{Et}.

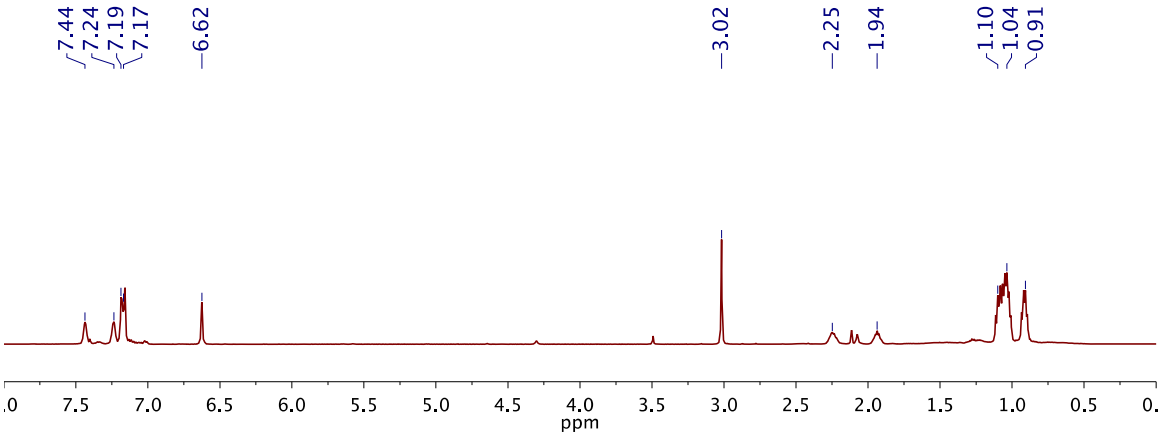

Figure A.61: ^{1}H NMR Spectrum (C_6D_6, 499.85 MHz) of 2_{CF_3}

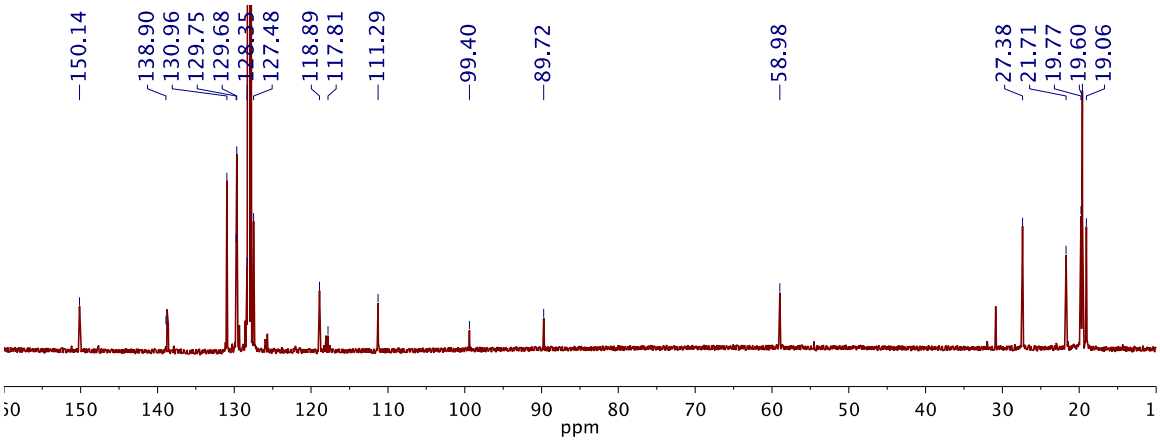

Figure A.62: ^{13}C{^{1}H} NMR Spectrum (C_6D_6, 125.70 MHz) of 2_{CF_3}

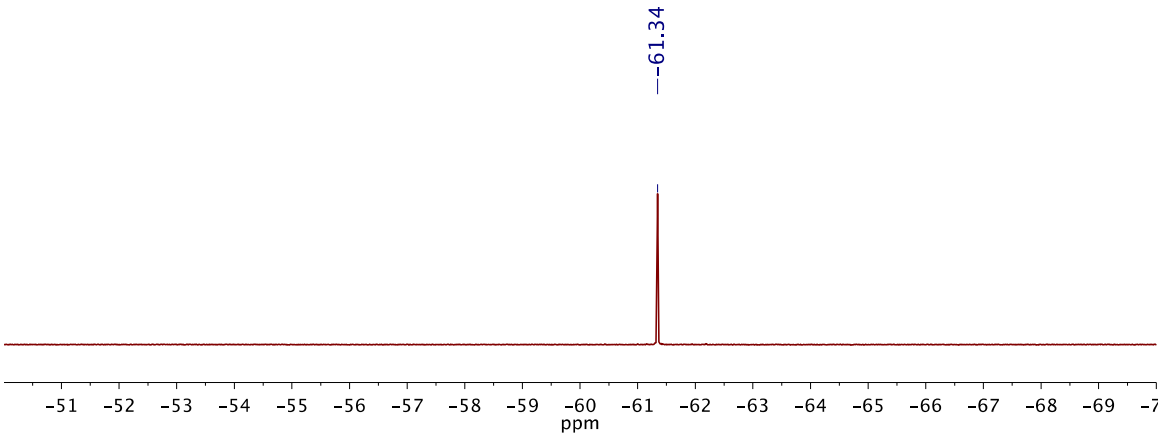

Figure A.63: ^{19}F{^{1}H} NMR Spectrum (C_6D_6, 282.33 MHz) of 2_{CF_3}

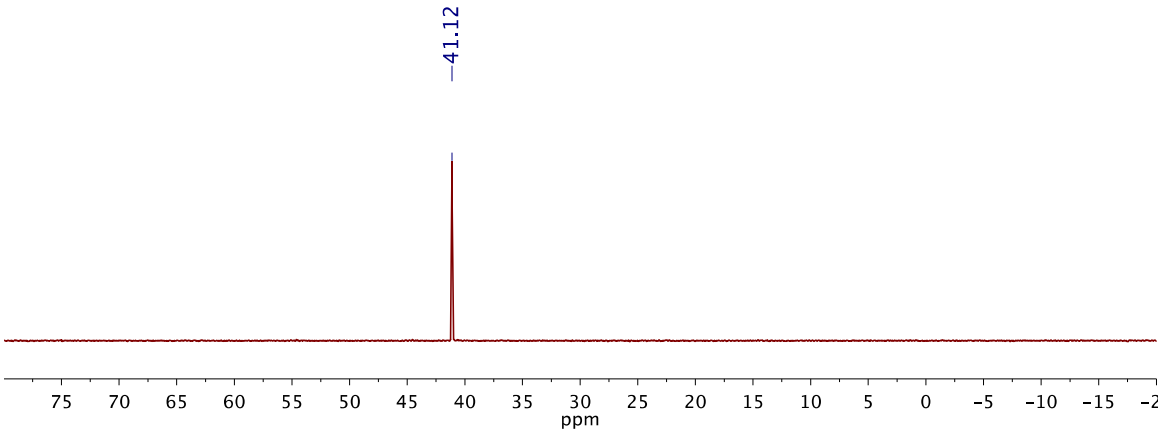

Figure A.64: $^{31}P\{^{1}H\}$ NMR Spectrum (C_6D_6, 121.48 MHz) of 2_{CF_3}

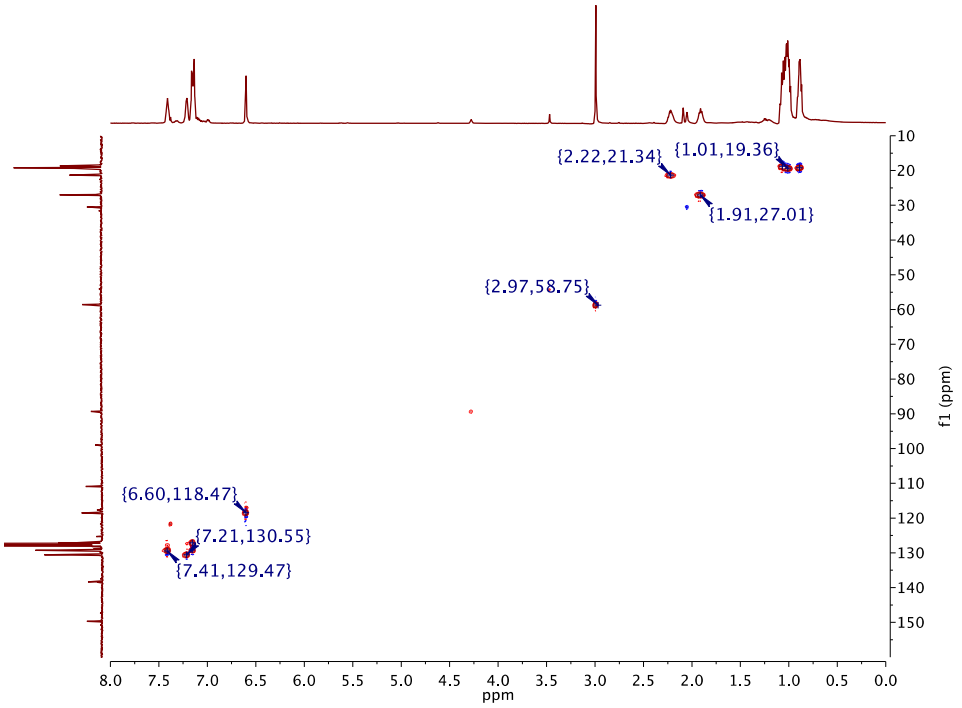

Figure A.65: ^{1}H-^{13}C HSQC NMR Spectrum (C_6D_6, 499.85, 125.70 MHz) of 2_{CF3}

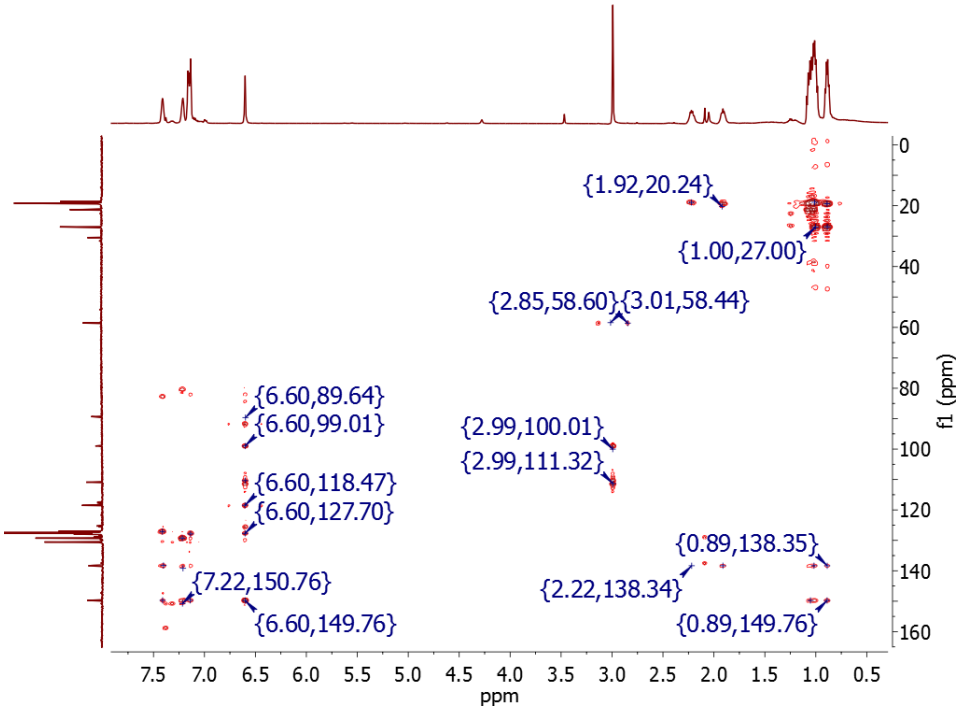

Figure A.66: ^{1}H-^{13}C HMBC NMR Spectrum (C_6D_6, 499.85, 125.70 MHz) of 2_{CF3}

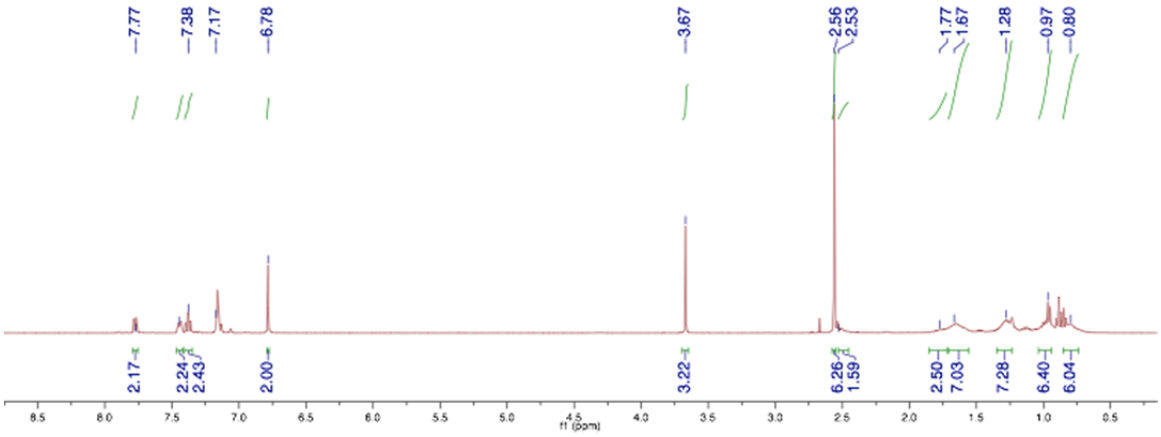

Figure A.67: ^{1}H NMR Spectrum (C_6D_6, 399.80 MHz) of 3

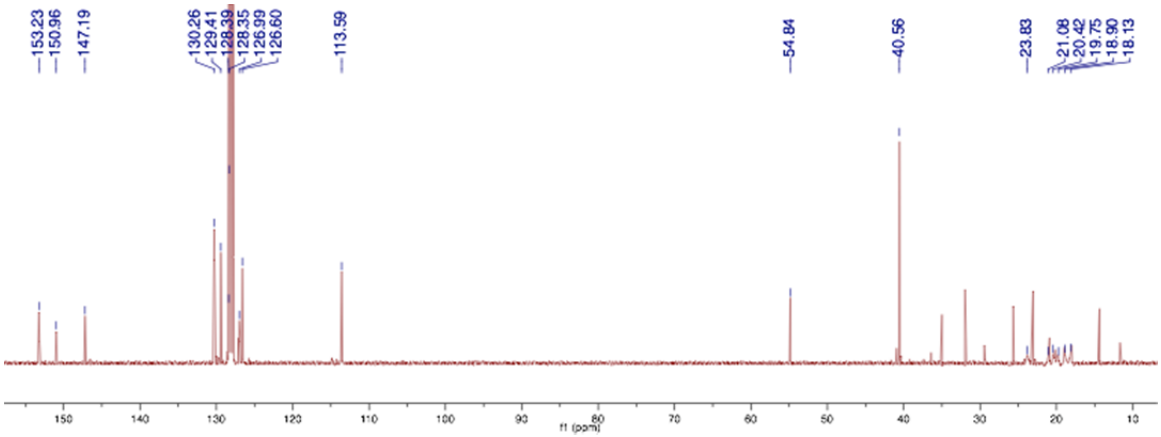

Figure A.68: ^{13}C NMR Spectrum (C_6D_6, 100.54 MHz) of 3

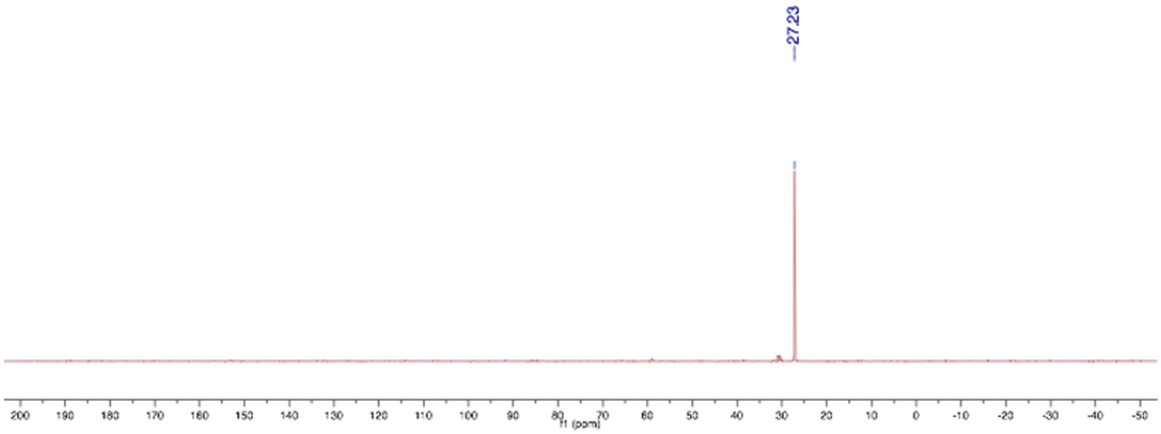

Figure A.69: ^{31}P{^{1}H} NMR Spectrum (C_6D_6, 121.48 MHz) of 3

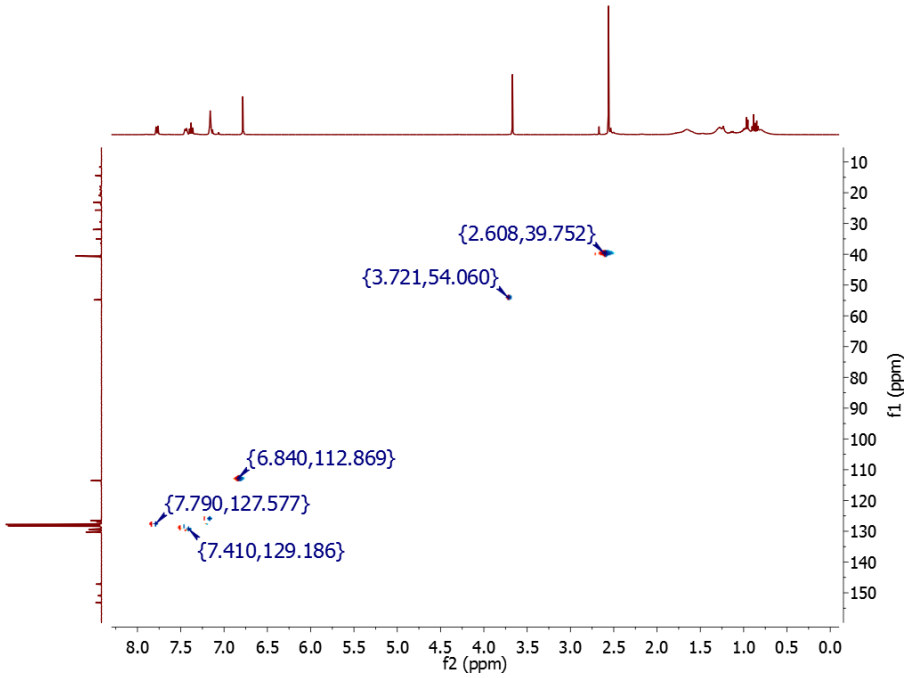

Figure A.70: ^{1}H-^{13}C HSQC NMR Spectrum (C_6D_6, 499.85, 125.70 MHz) of 3

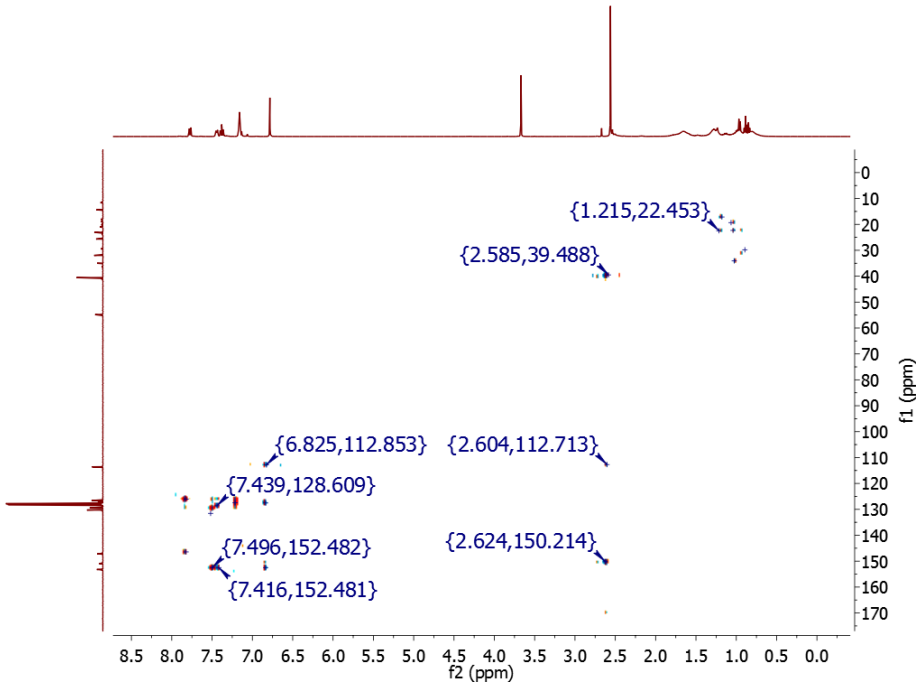

Figure A.71: ^{1}H-^{13}C HMBC NMR Spectrum (C_6D_6, 499.85, 125.70 MHz) of 3

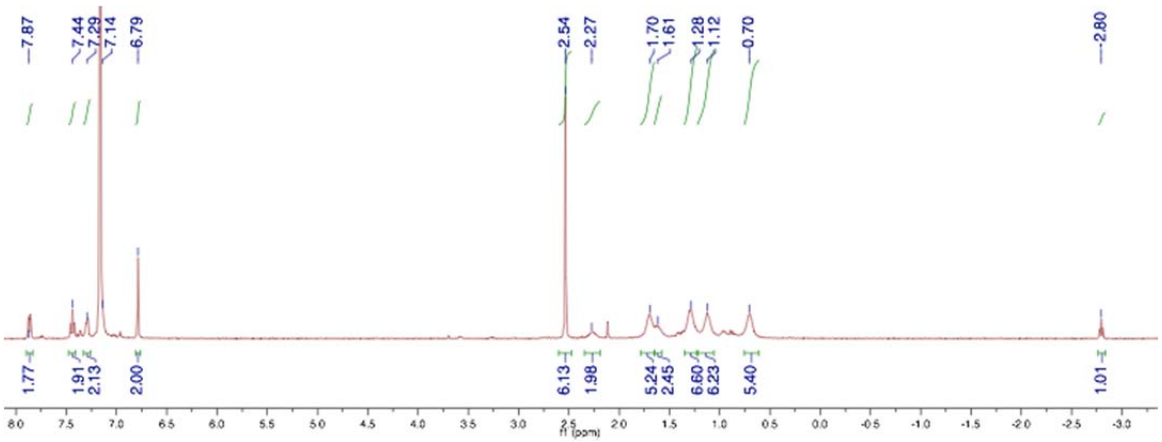

Figure A.72: ^{1}H NMR Spectrum (C_6D_6, 399.80 MHz) of 4

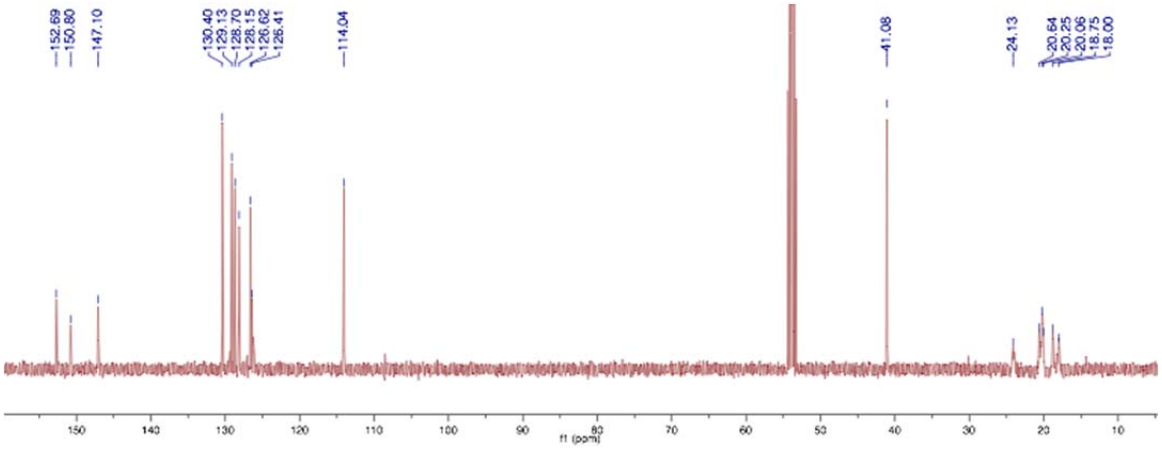

Figure A.73: ^{13}C NMR Spectrum (C_6D_6, 100.54 MHz) of 4

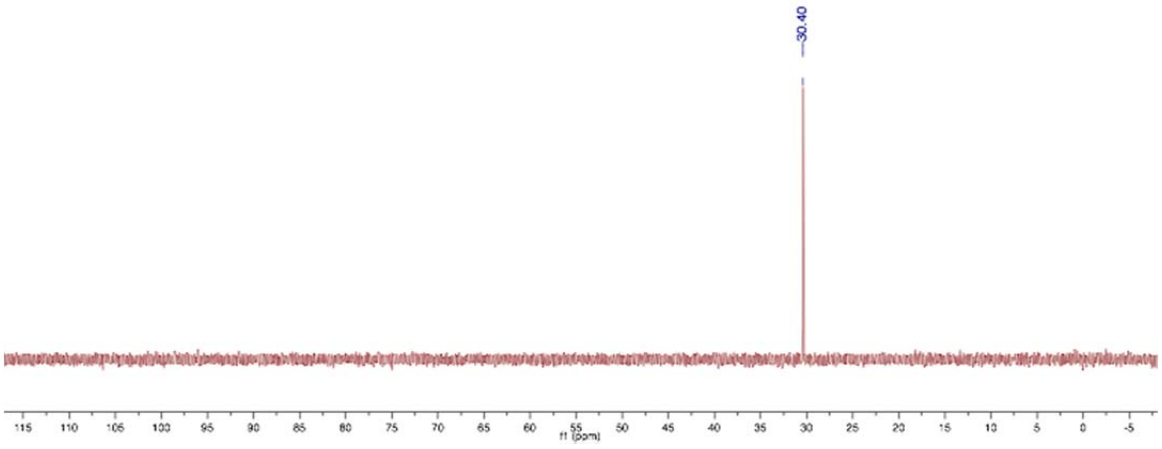

Figure A.74: ^{31}P{^{1}H} NMR Spectrum (C_6D_6, 121.48 MHz) of 4

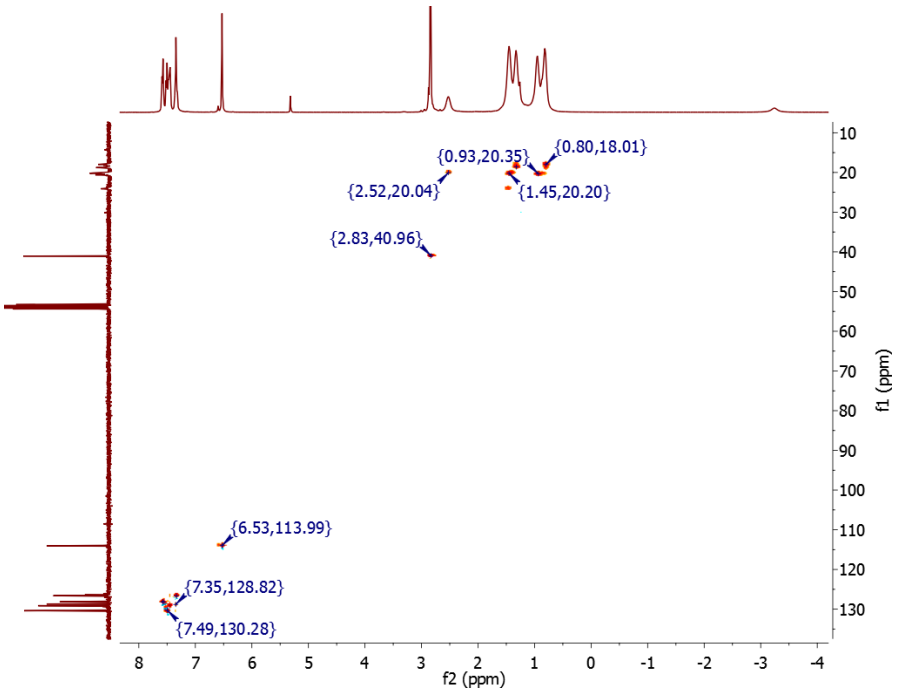

Figure A.75: ^{1}H-^{13}C HSQC NMR Spectrum (C_6D_6, 499.85, 125.70 MHz) of 4

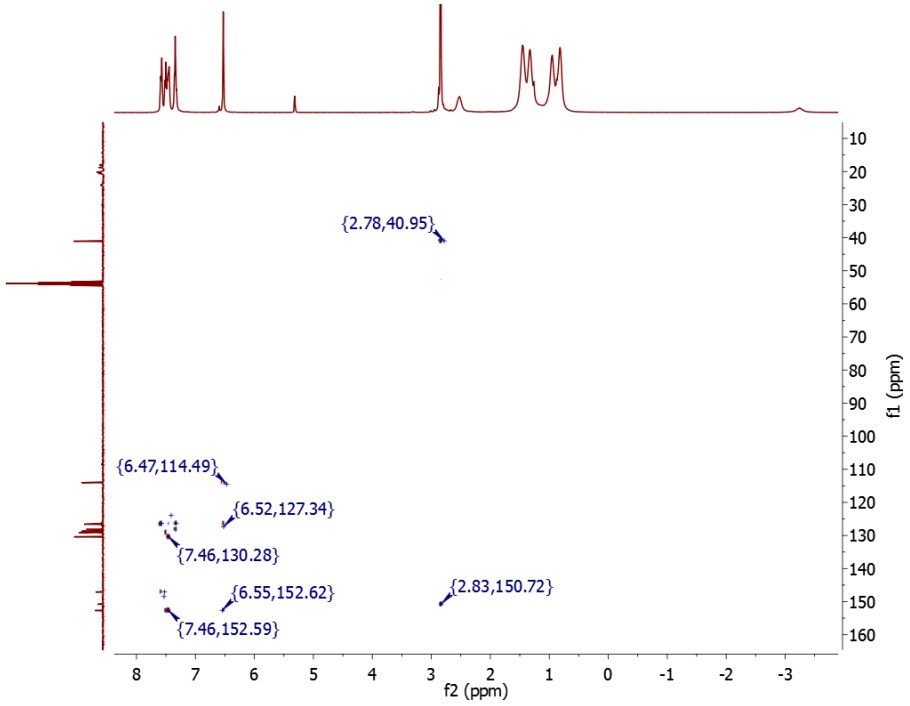

Figure A.76: ^{1}H-^{13}C HMBC NMR Spectrum (C_6D_6, 499.85, 125.70 MHz) of 4

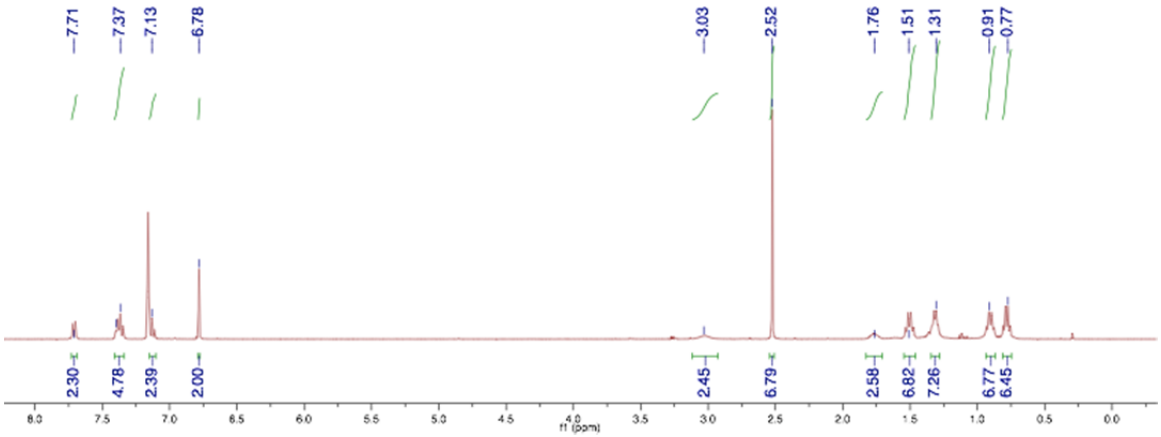

Figure A.77: ^{1}H NMR Spectrum (C_6D_6, 399.80 MHz) of *5*

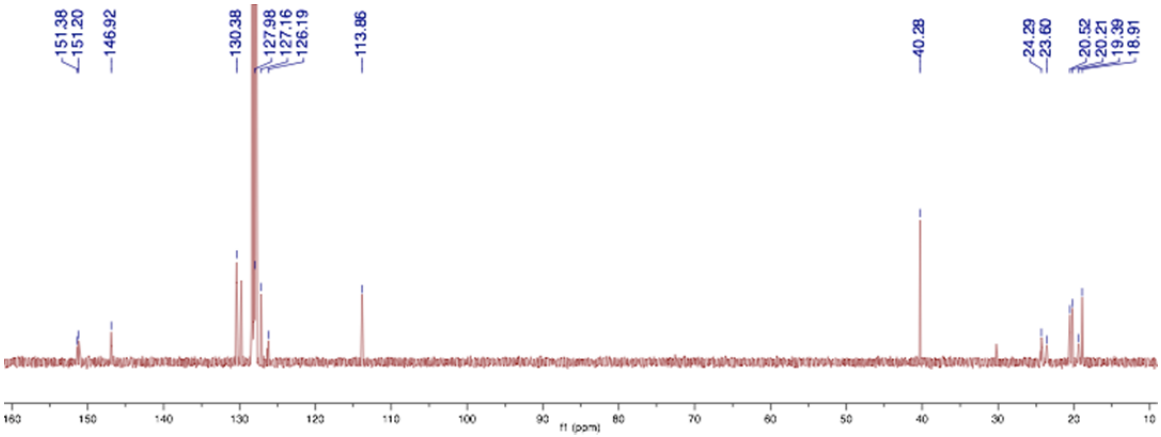

Figure A.78: ^{13}C NMR Spectrum (C_6D_6, 100.54 MHz) of *5*

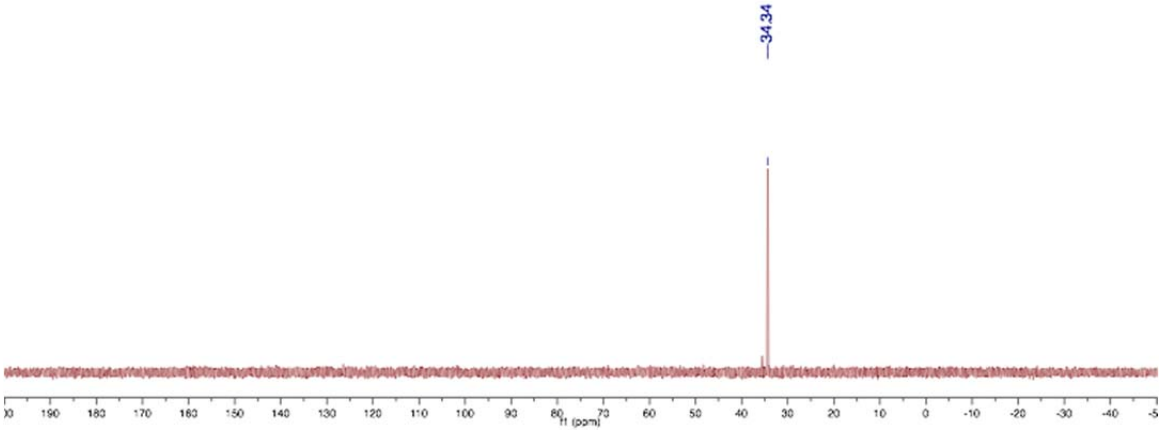

Figure A.79: ^{31}P{^{1}H} NMR Spectrum (C_6D_6, 121.48 MHz) of *5*

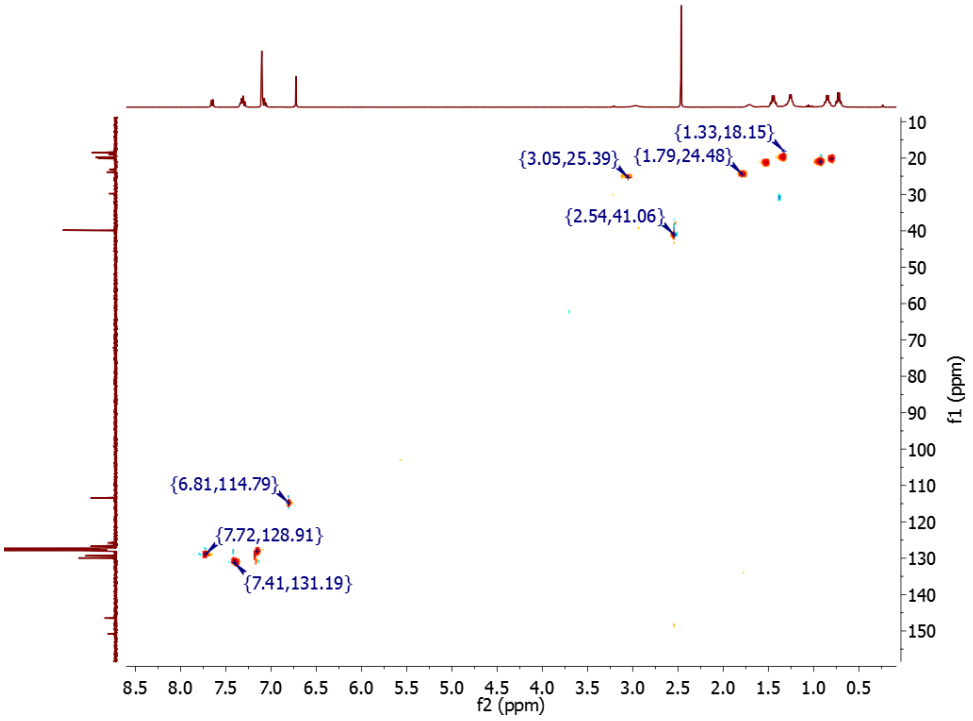

Figure A.80: ^{1}H-^{13}C HSQC NMR Spectrum (C_6D_6, 499.85, 125.70 MHz) of *5*

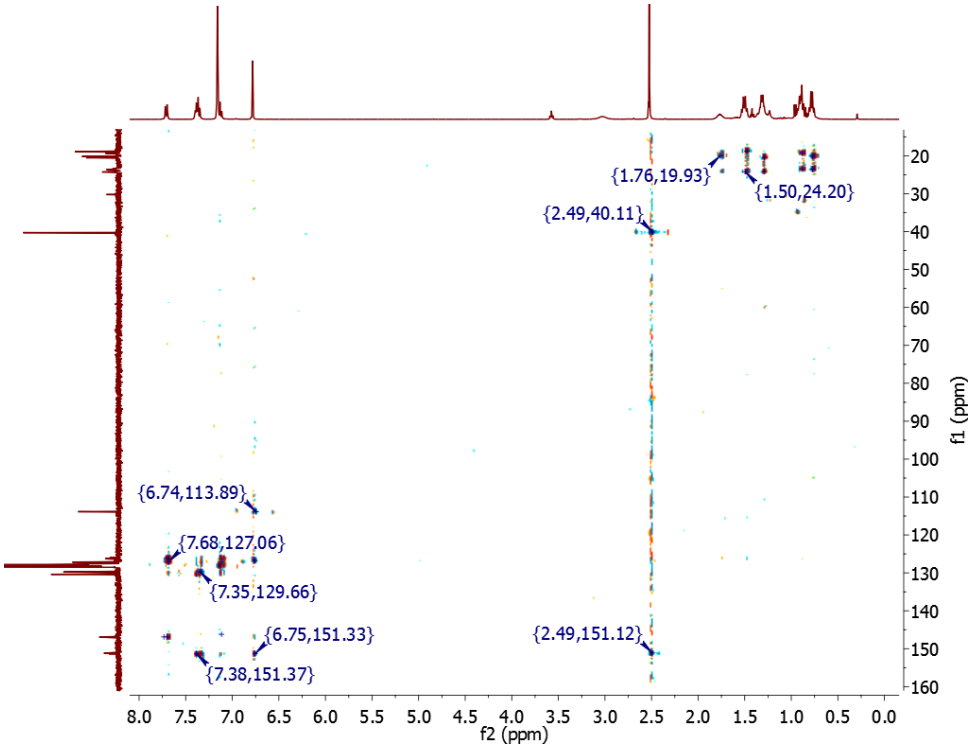

Figure A.81: ^{1}H-^{13}C HMBC NMR Spectrum (C_6D_6, 499.85, 125.70 MHz) of *5*

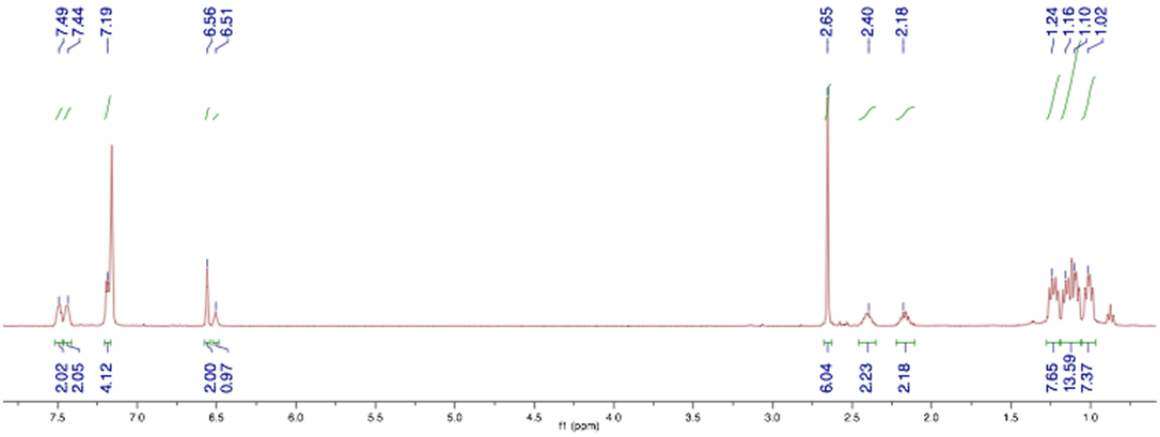

Figure A.82: ^{1}H NMR Spectrum (C_6D_6, 399.80 MHz) of 6

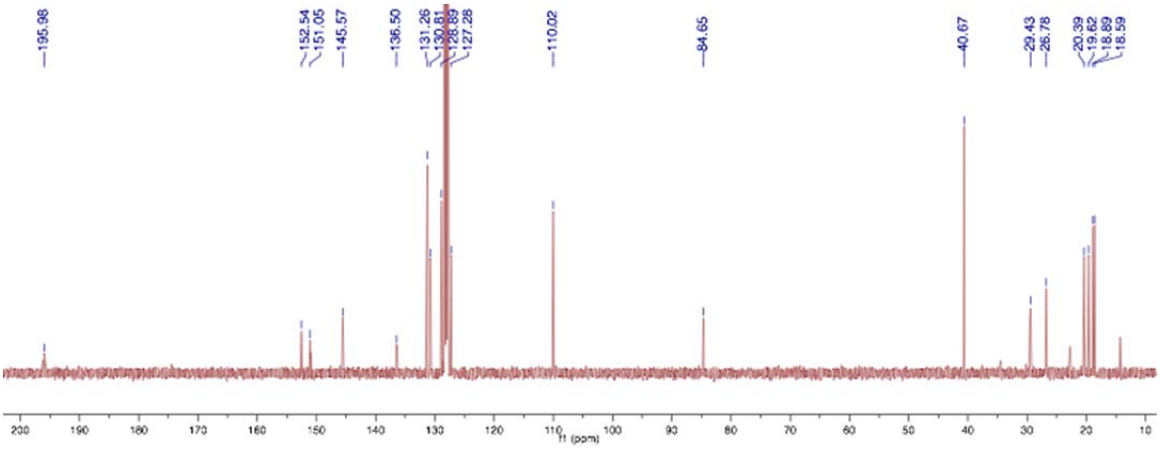

Figure A.83: ^{13}C NMR Spectrum (C_6D_6, 100.54 MHz) of 6

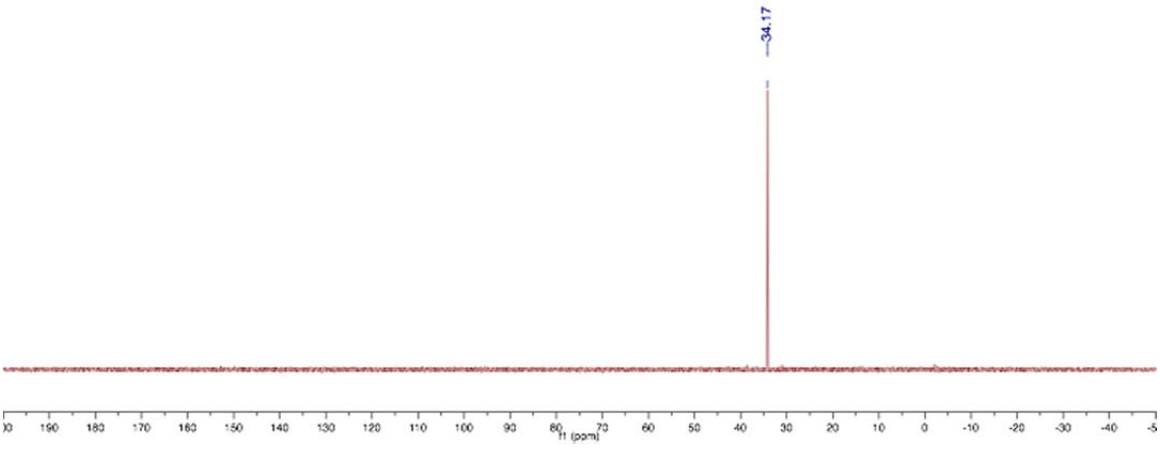

Figure A.84: ^{31}P{^{1}H} NMR Spectrum (C_6D_6, 121.48 MHz) of 6

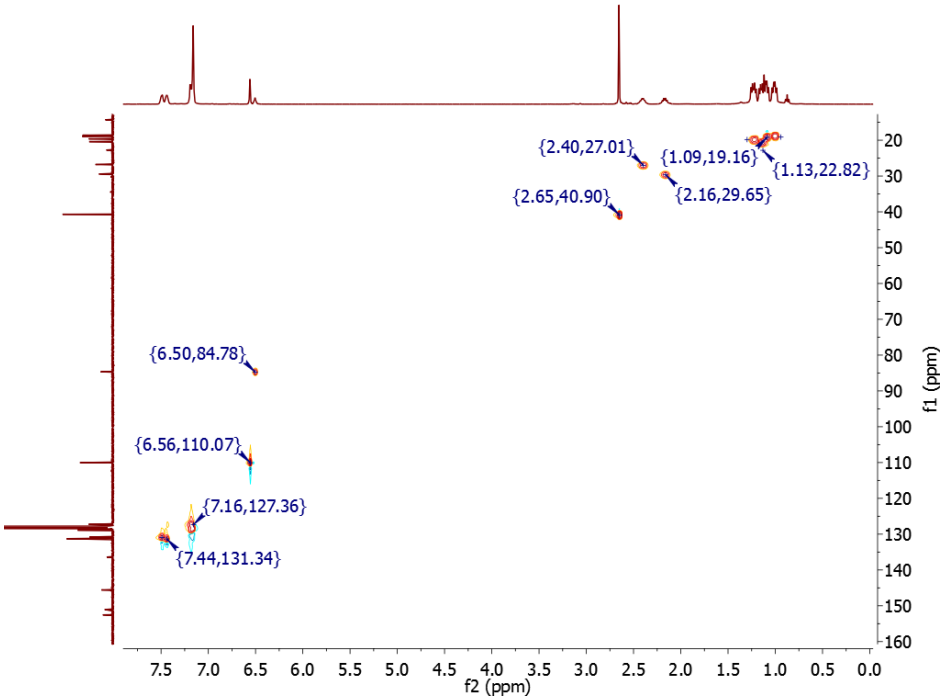

Figure A.85: ^{1}H-^{13}C HSQC NMR Spectrum (C_6D_6, 499.85, 125.70 MHz) of 6

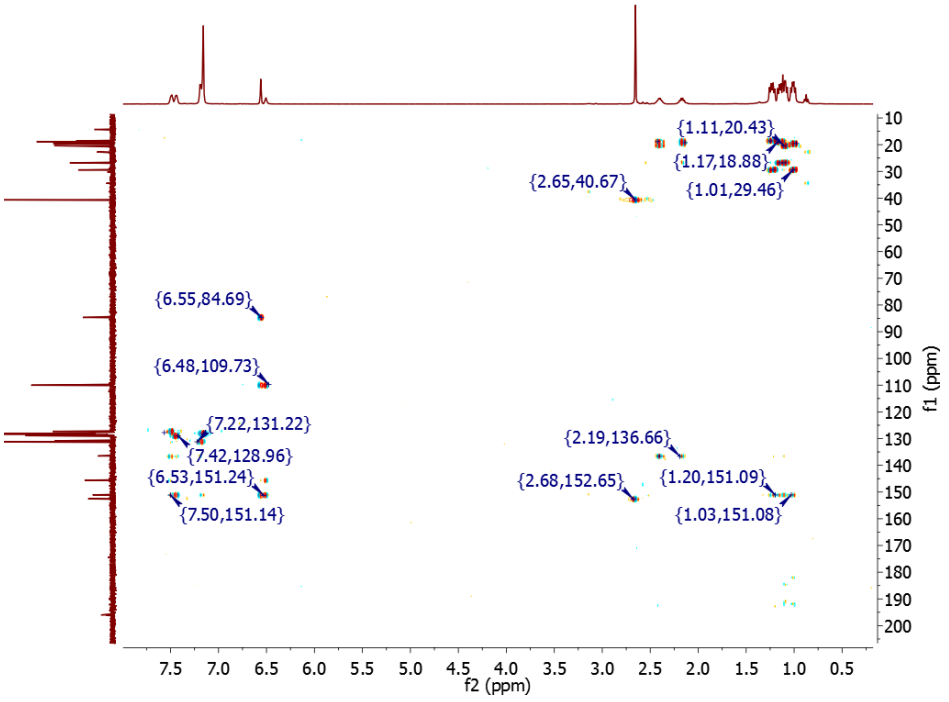

Figure A.86: ^{1}H-^{13}C HMBC NMR Spectrum (C_6D_6, 499.85, 125.70 MHz) of 6

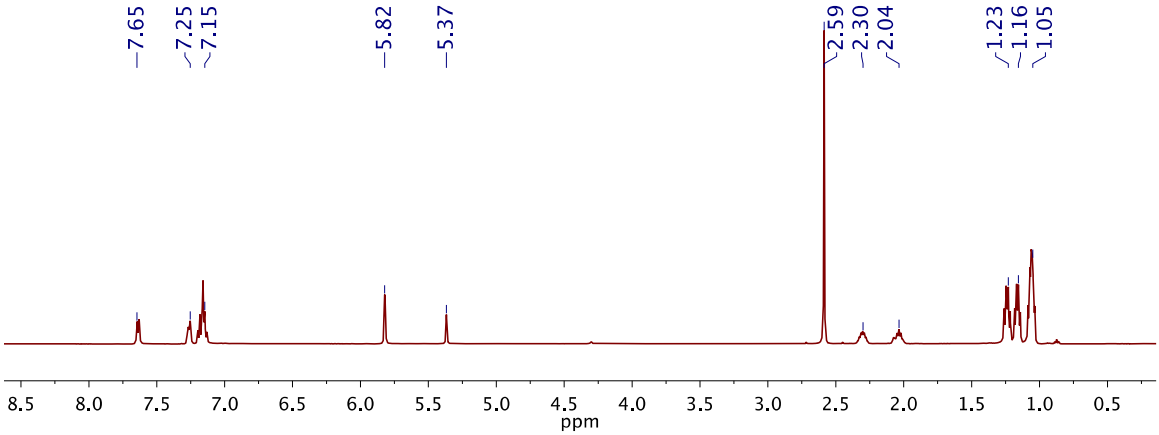

Figure A.87: ^{1}H NMR Spectrum (C_6D_6, 399.80 MHz) of 7

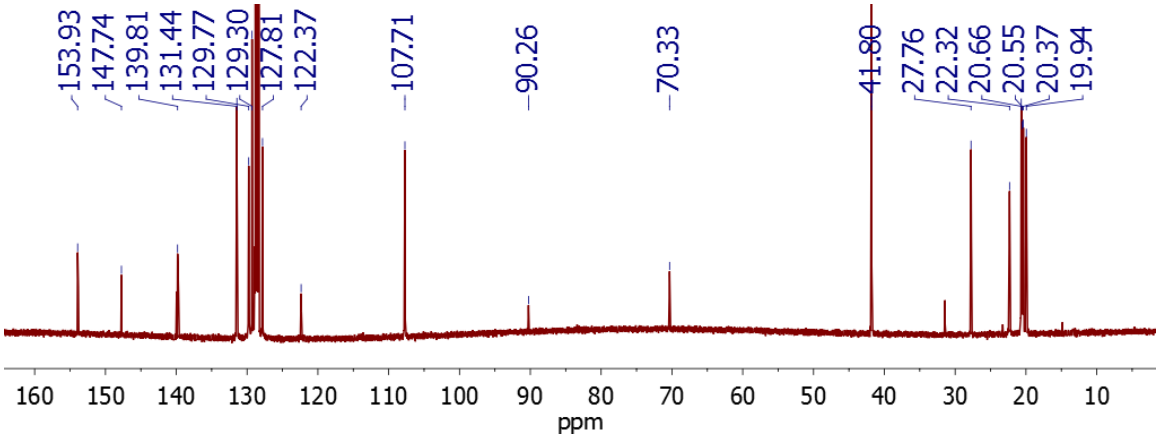

Figure A.88: ^{13}C NMR Spectrum (C_6D_6, 100.54 MHz) of 7

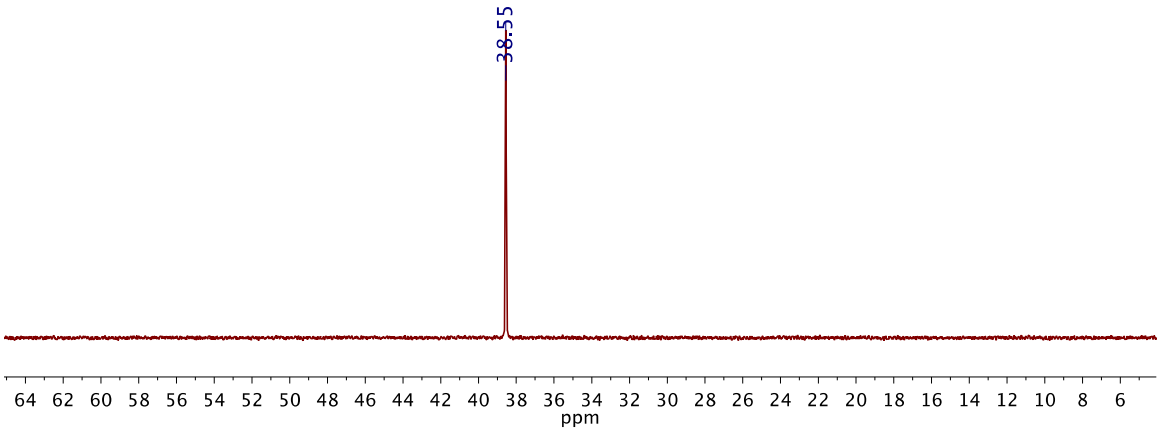

Figure A.89: $^{31}P\{^{1}H\}$ NMR Spectrum (C_6D_6, 121.48 MHz) of 7

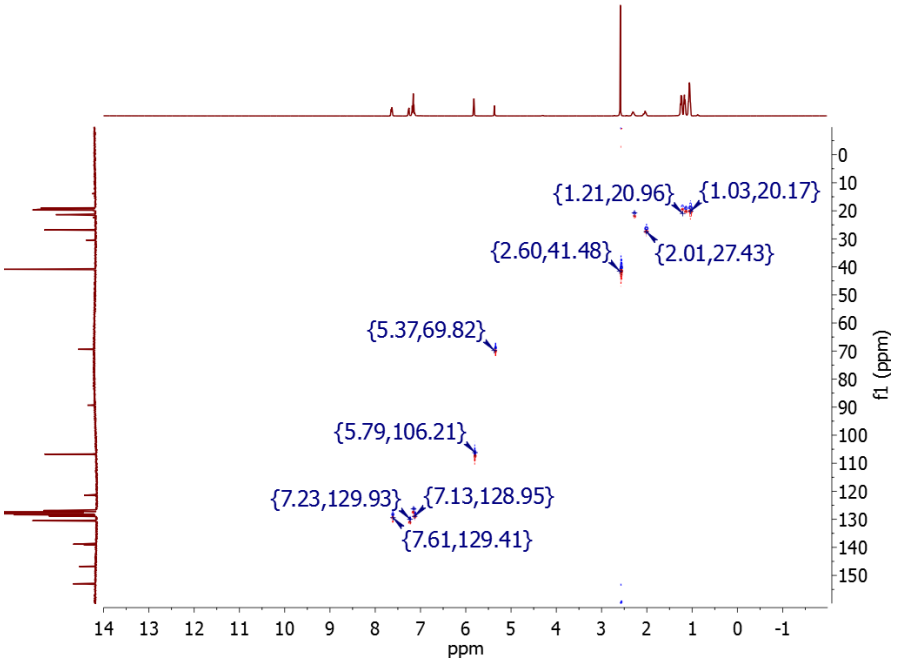

Figure A.90: ^{1}H-^{13}C HSQC NMR Spectrum (C_6D_6, 499.85, 125.70 MHz) of 7

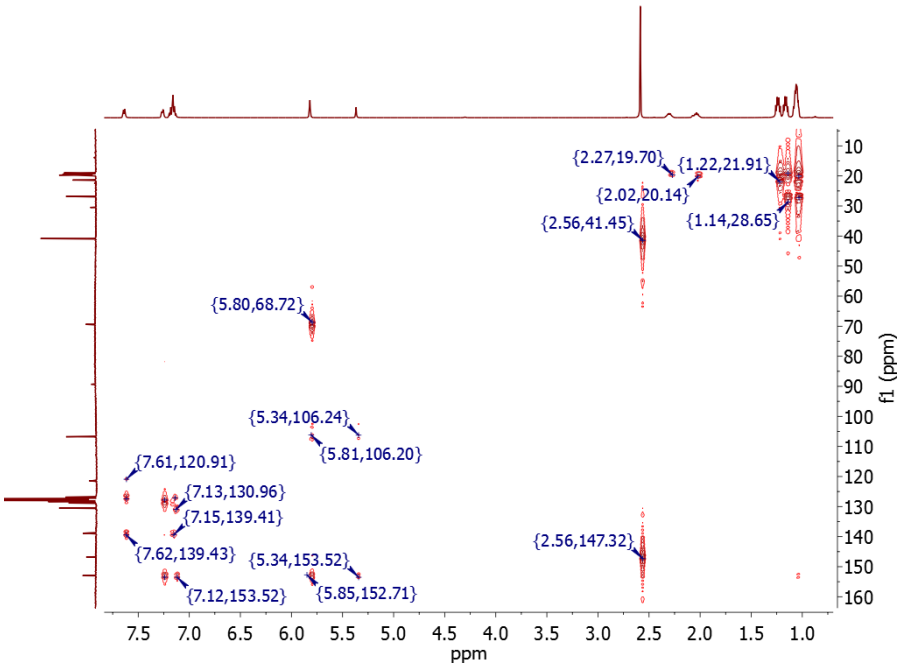

Figure A.91: ^{1}H-^{13}C HMBC NMR Spectrum (C_6D_6, 499.85, 125.70 MHz) of 7

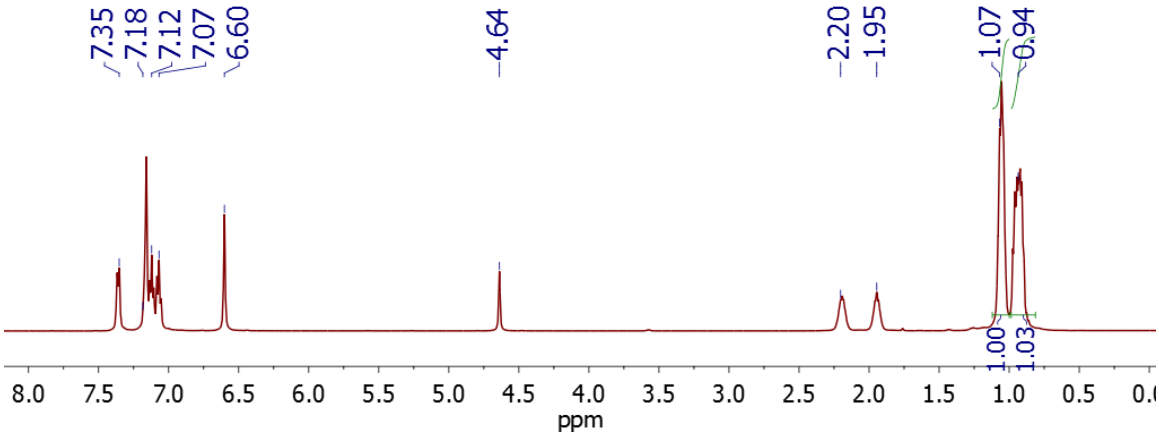

Figure A.92: ^{1}H NMR Spectrum (C_6D_6, 399.80 MHz) of 7_{CF_3}

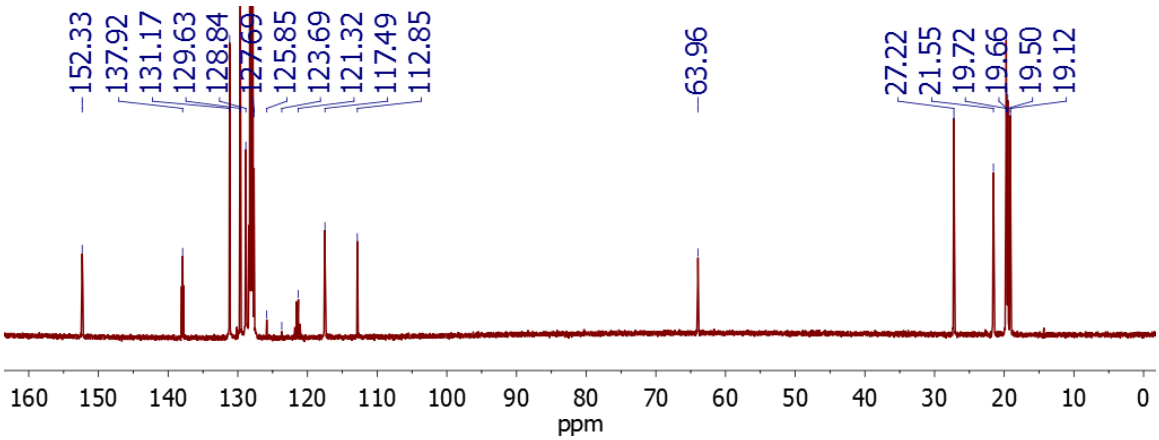

Figure A.93: ^{13}C NMR Spectrum (C_6D_6, 100.54 MHz) of 7_{CF_3}

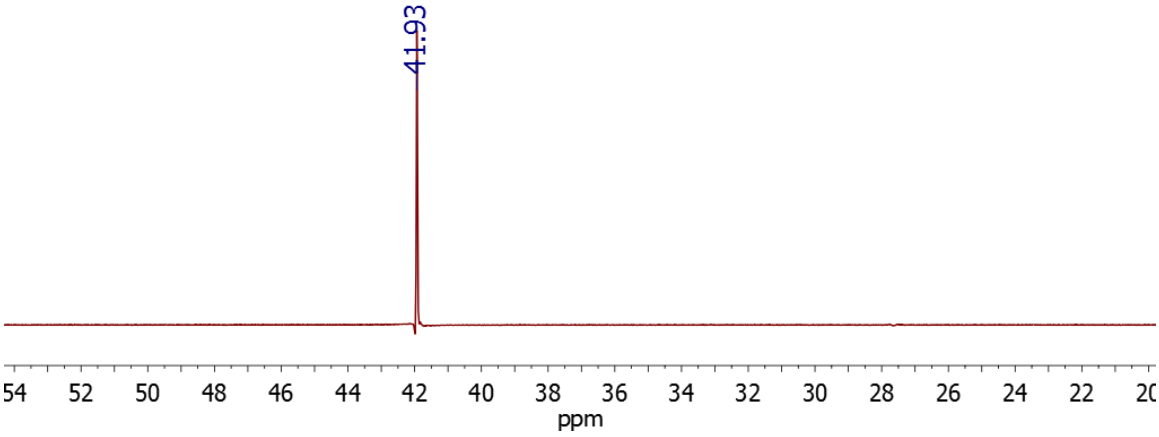

Figure A.94: $^{31}P\{^{1}H\}$ NMR Spectrum (C_6D_6, 25°C, 121.48 MHz) of 7_{CF_3}

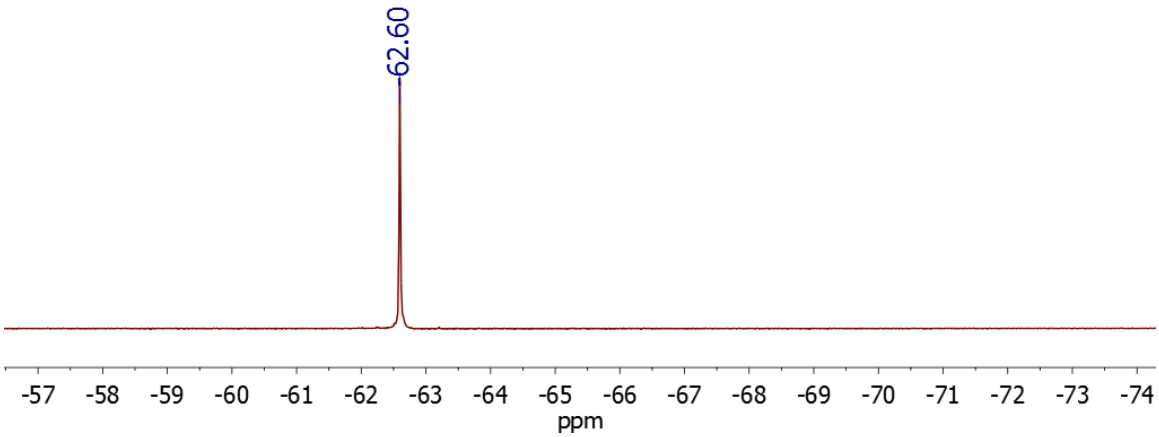

Figure A.95: $^{19}F\{^{1}H\}$ NMR Spectrum (C_6D_6, 282.33 MHz) of 7_{CF3}

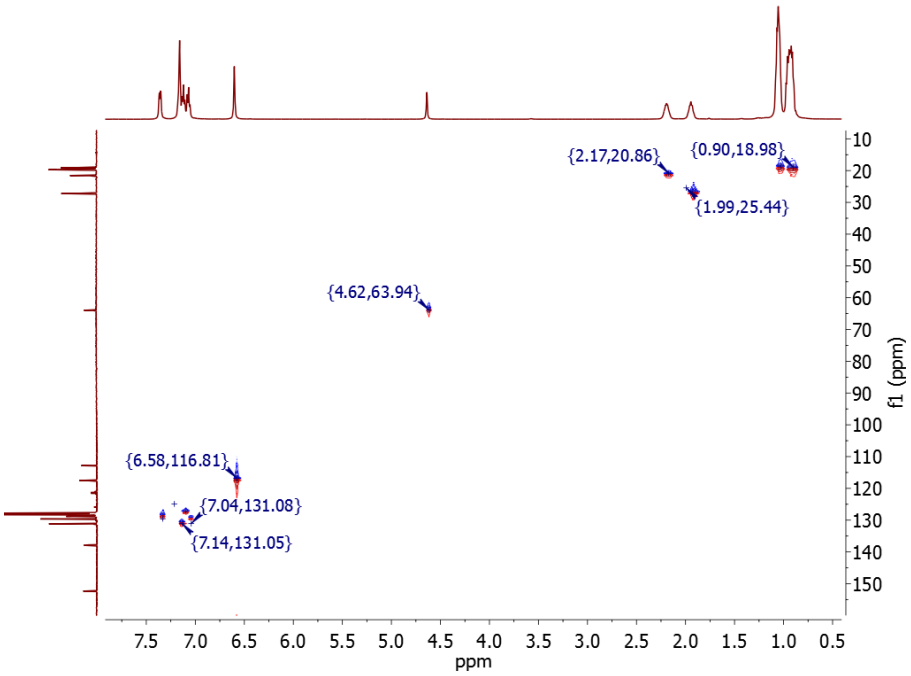

Figure A.96: ^{1}H-^{13}C HSQC NMR Spectrum (C_6D_6, 499.85, 125.70 MHz) of 7_{CF3}

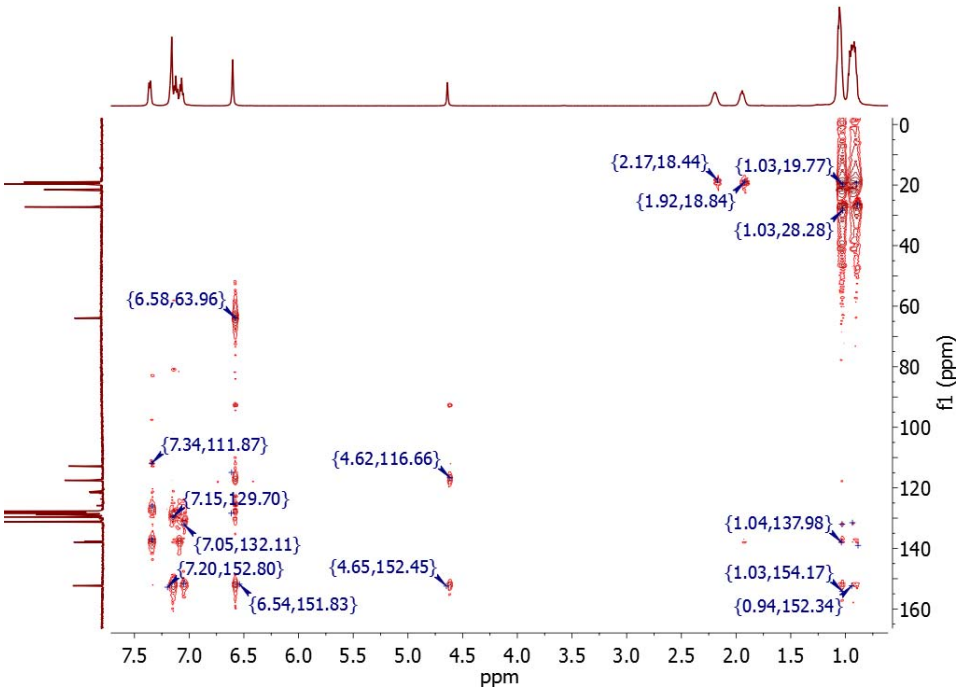

Figure A.97: ^{1}H-^{13}C HMBC NMR Spectrum (C_6D_6, 499.85, 125.70 MHz) of 7_{CF3}

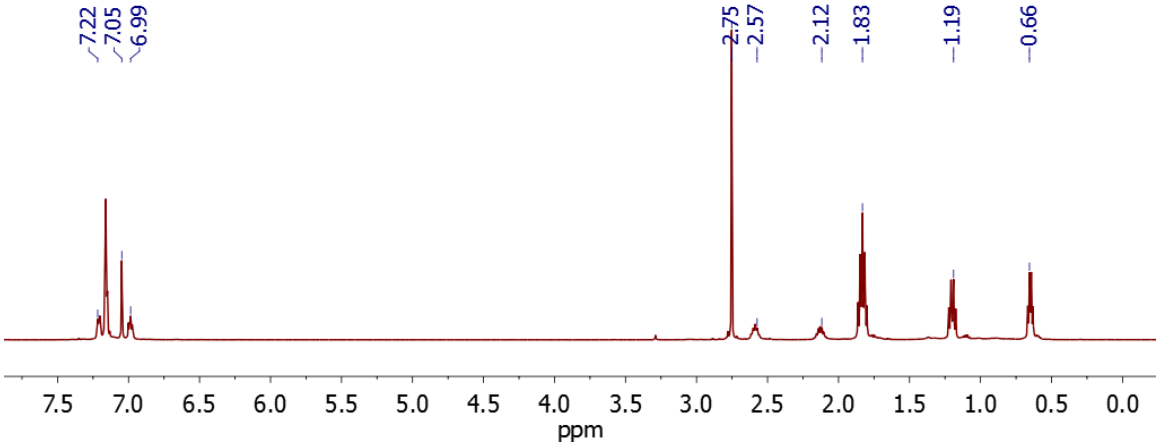

Figure A.98: ^{1}H NMR Spectrum (C_6D_6, 399.80 MHz) of 8

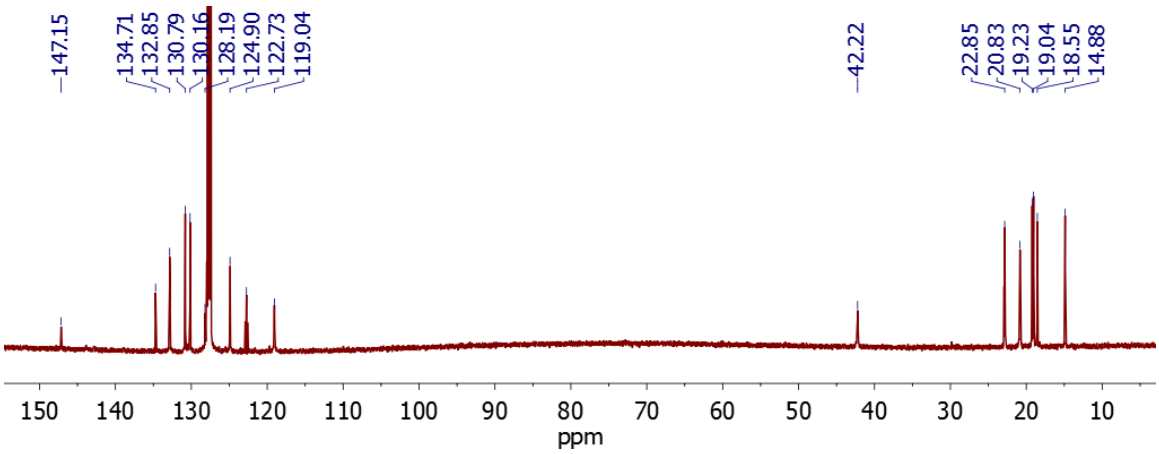

Figure A.99: ^{13}C{^{1}H} NMR Spectrum (C_6D_6, 100.54 MHz) of 8

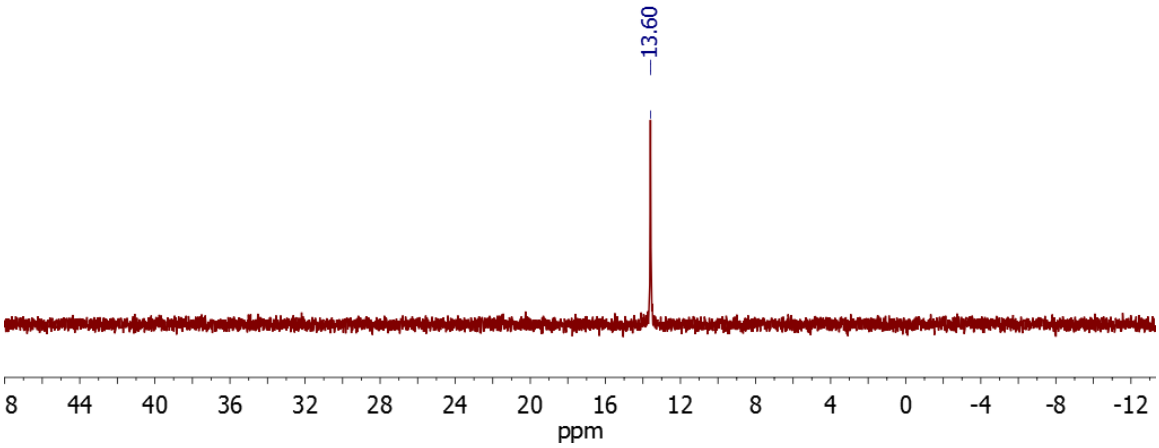

Figure A.100: ^{31}P{^{1}H} NMR Spectrum (C_6D_6, 25°C, 121.48 MHz) of 8

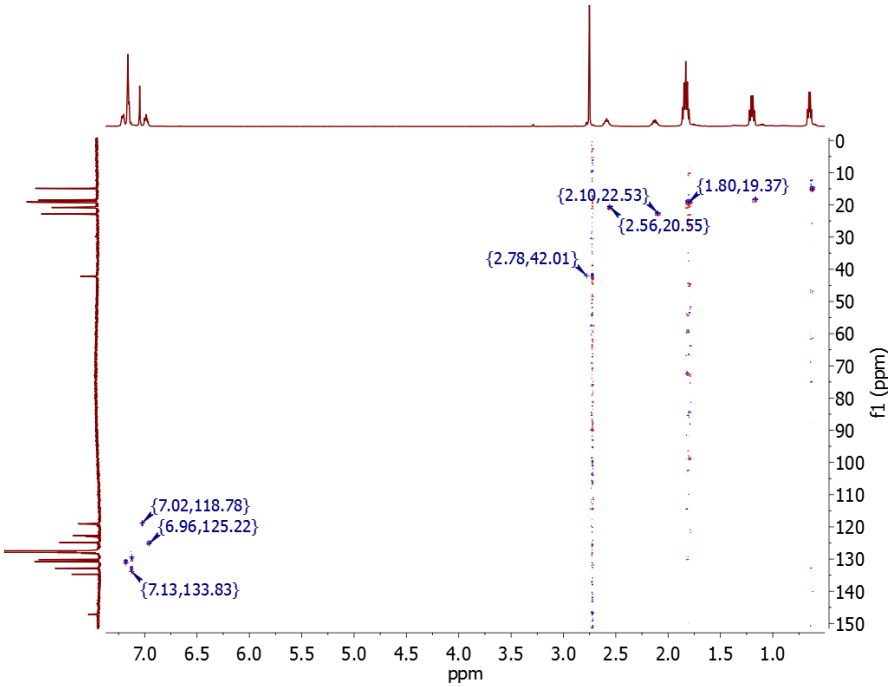

Figure A.101: ^{1}H-^{13}C HSQC NMR Spectrum (C_6D_6, 499.85, 125.70 MHz) of 8

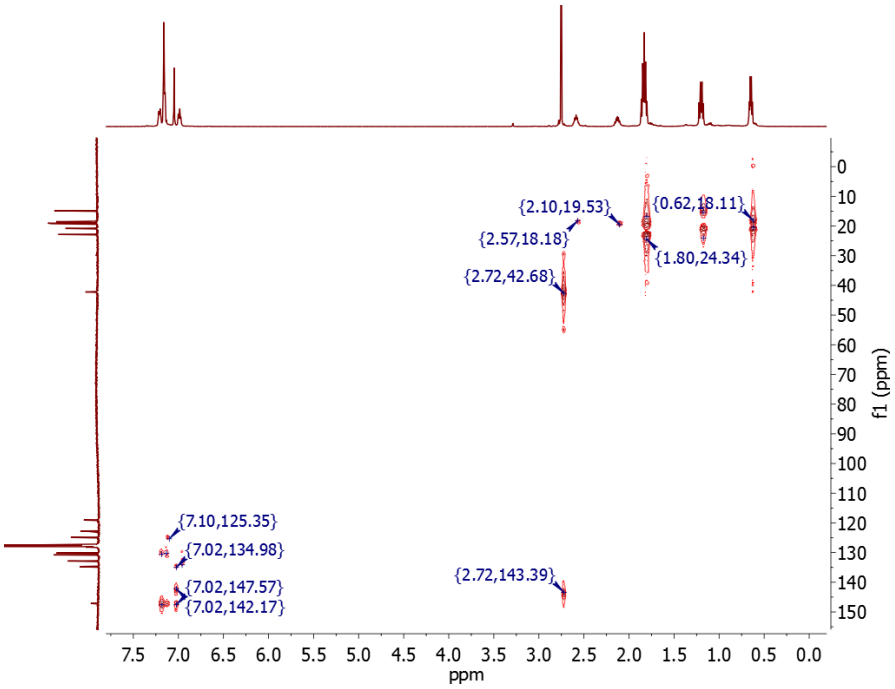

Figure A.102: ^{1}H-^{13}C HMBC NMR Spectrum (C_6D_6, 499.85, 125.70 MHz) of 8

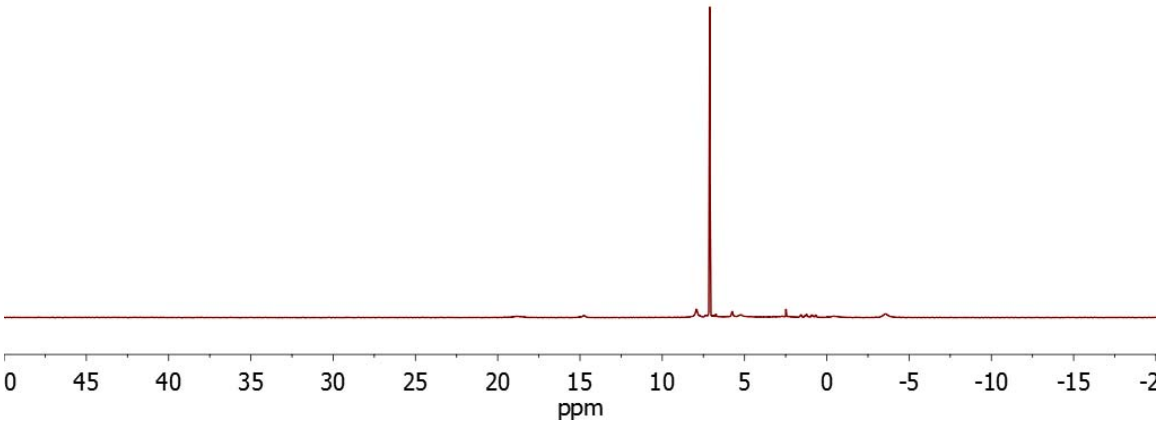

Figure A.103: ^{1}H NMR Spectrum (C_6D_6, 300 MHz)of 9

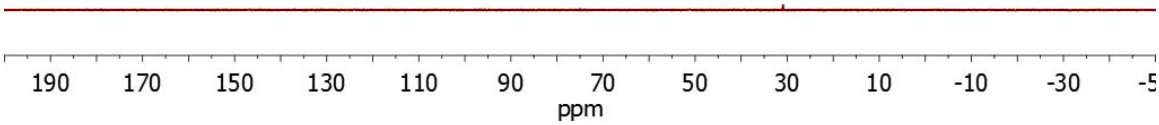

Figure A.104: $^{31}P\{^{1}H\}$ NMR Spectrum (C_6D_6, 25°C, 121.48 MHz) of 9

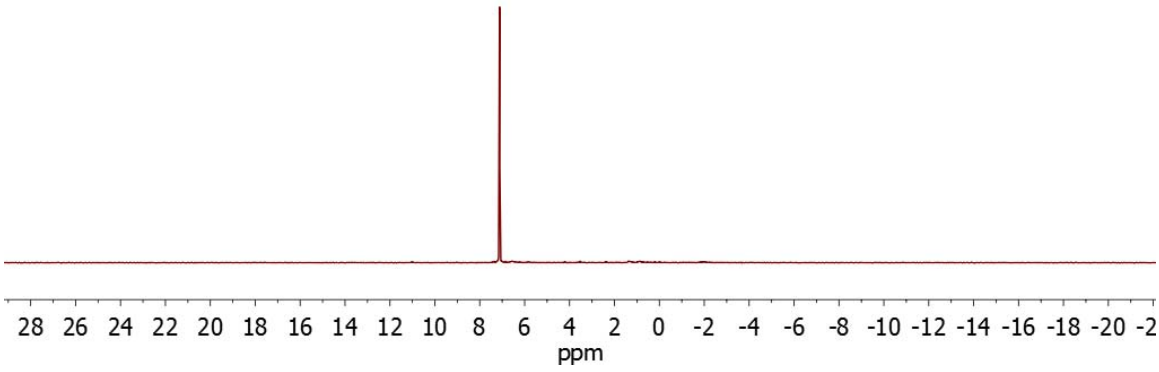

Figure A.105: ^{1}H NMR Spectrum (C_6D_6, 300 MHz) of 9^{OTF}

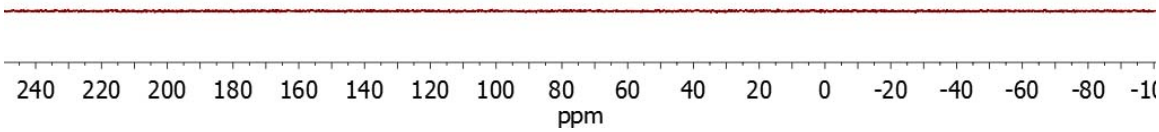

Figure A.106: $^{31}P\{^{1}H\}$ NMR Spectrum (C_6D_6, 25°C, 121.48 MHz) of 9^{OTF}

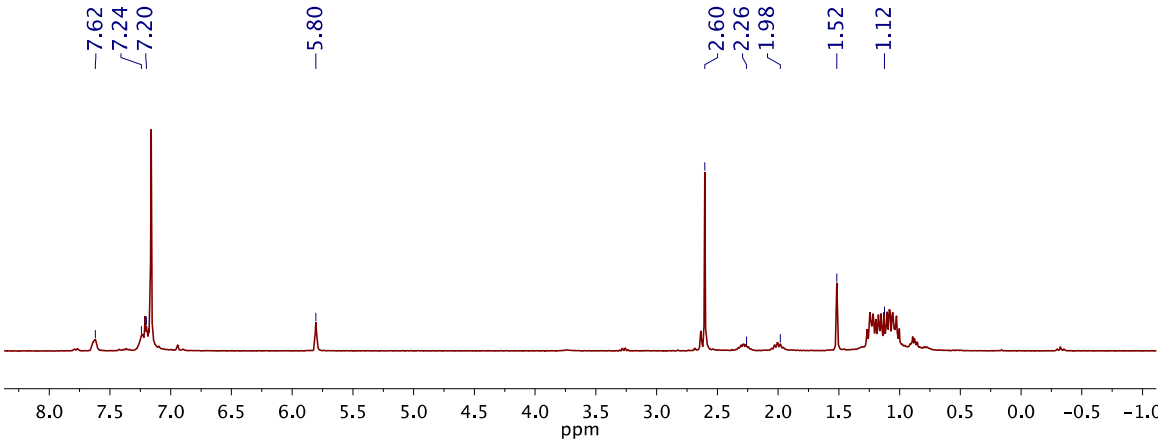

Figure A.107: ^{1}H NMR Spectrum (C_6D_6, 25°C, 499.85 MHz) of 10

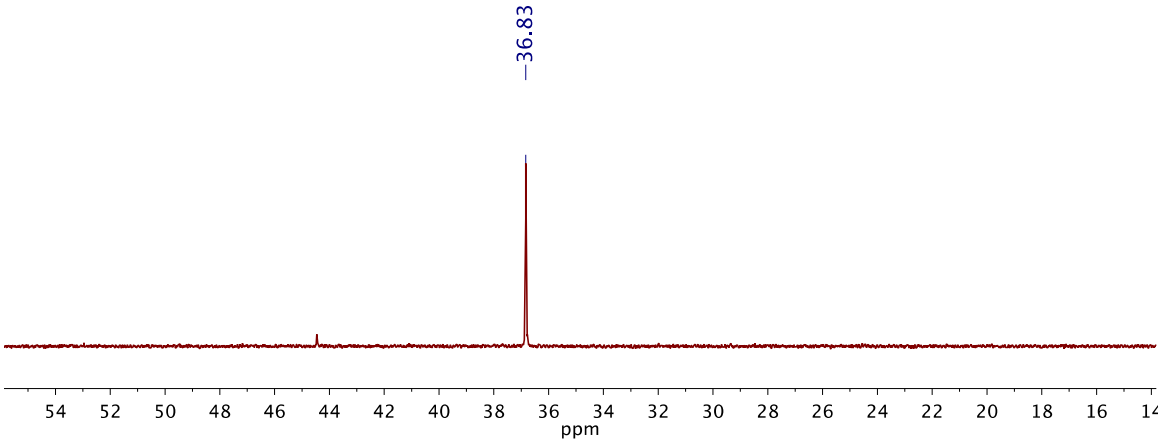

Figure A.108: $^{31}P\{^{1}H\}$ NMR Spectrum (C_6D_6, 25°C, 121.48 MHz) of 10

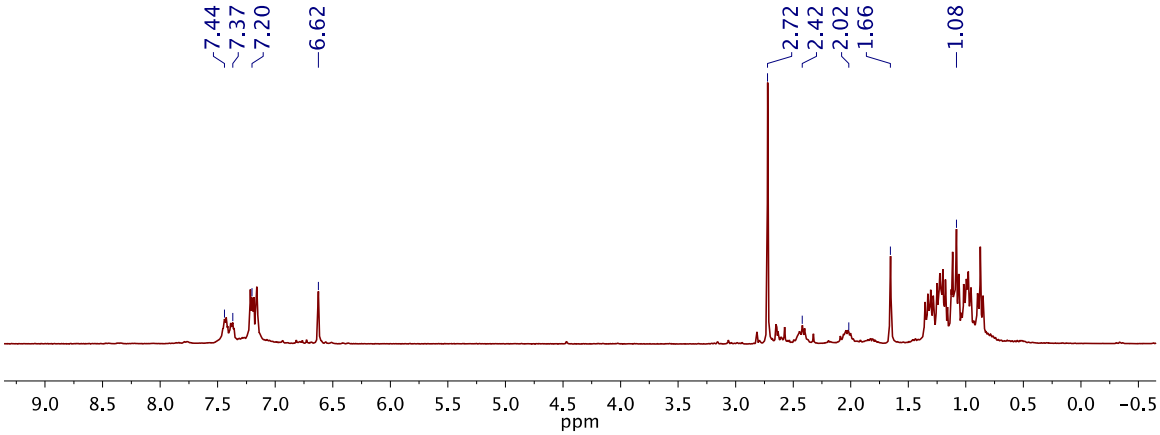

Figure A.109: ^{1}H NMR Spectrum (C_6D_6, 25°C, 499.85 MHz) of 11

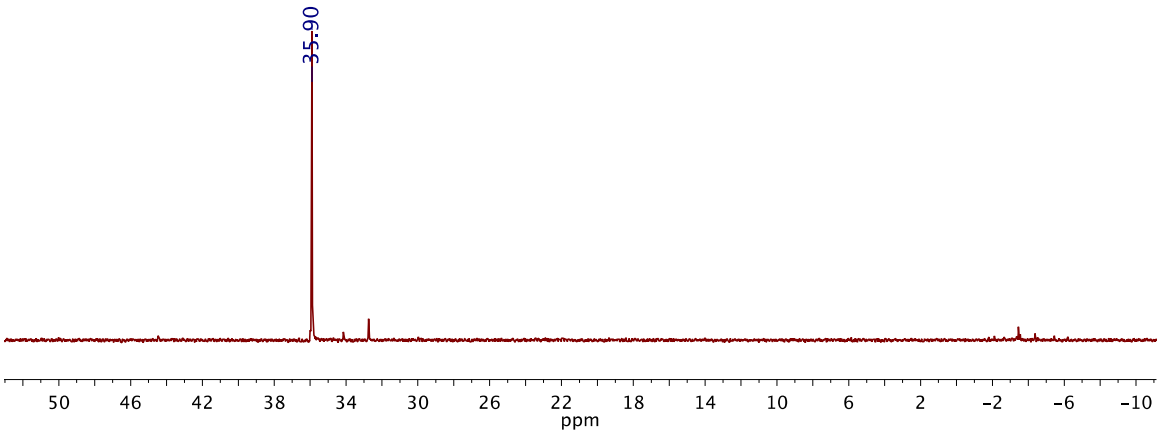

Figure A.110: $^{31}P\{^{1}H\}$ NMR Spectrum (C_6D_6, 25°C, 121.48 MHz) of 11

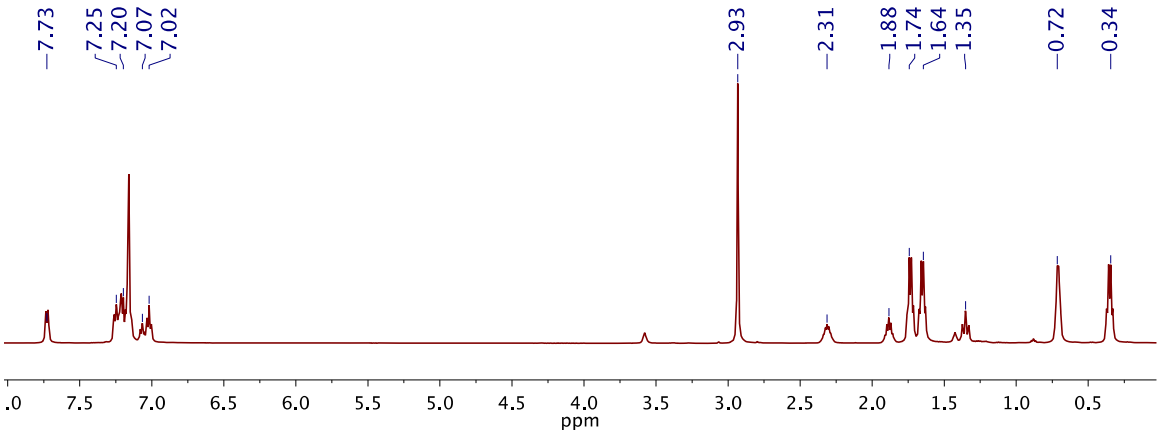

Figure A.111: ^{1}H NMR Spectrum (C_6D_6, 25°C, 499.85 MHz) of 12

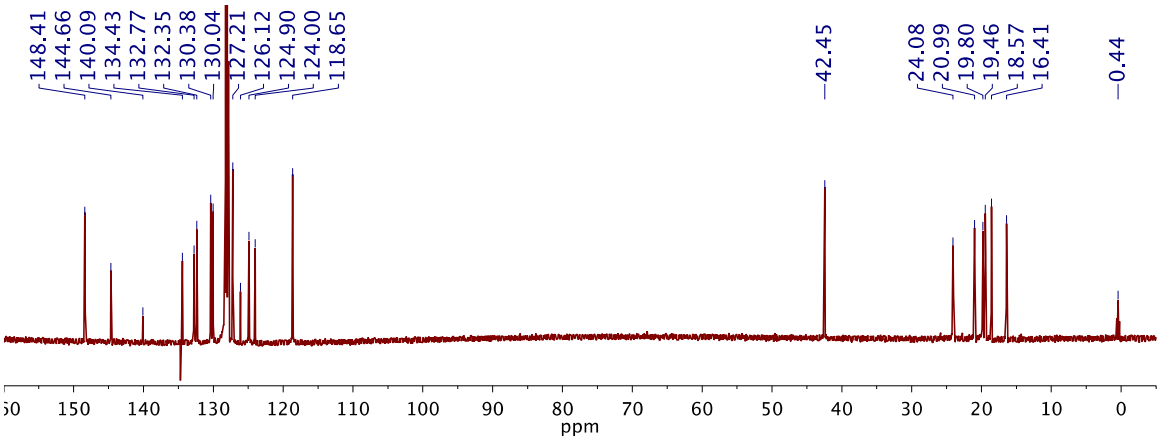

Figure D.112: $^{13}C\{^{1}H\}$ NMR Spectrum (C_6D_6, 25°C, 125.70 MHz) of 12

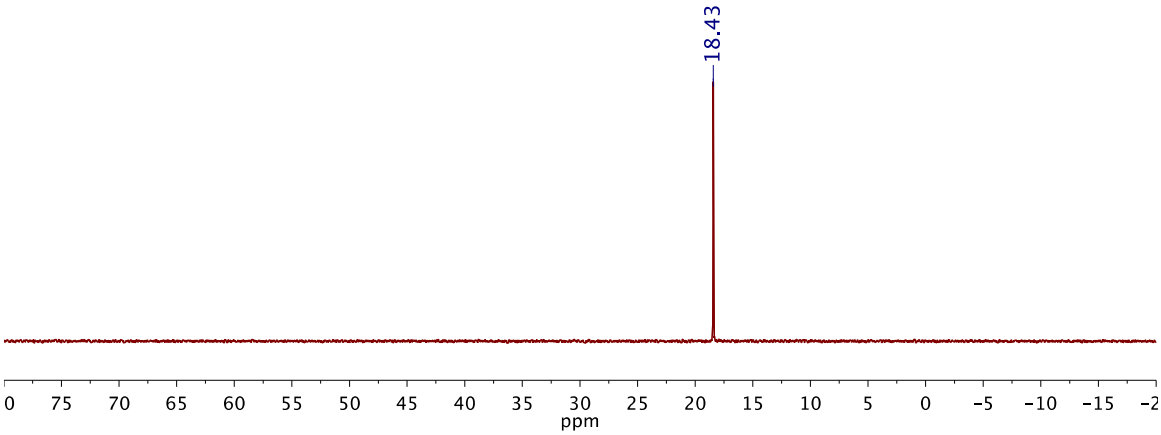

Figure A.113: $^{81}P\{^{1}H\}$ NMR Spectrum (C_6D_6, 25°C, 121.48 MHz) of 12

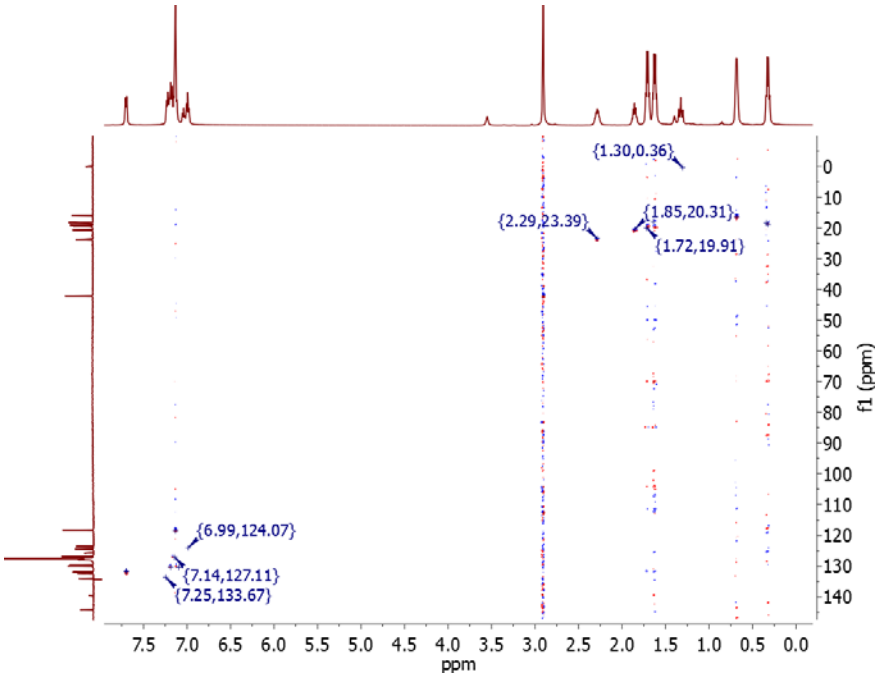

Figure A.114: ^{1}H-^{13}C HSQC NMR Spectrum (C_6D_6, 499.85, 125.70 MHz) of 12

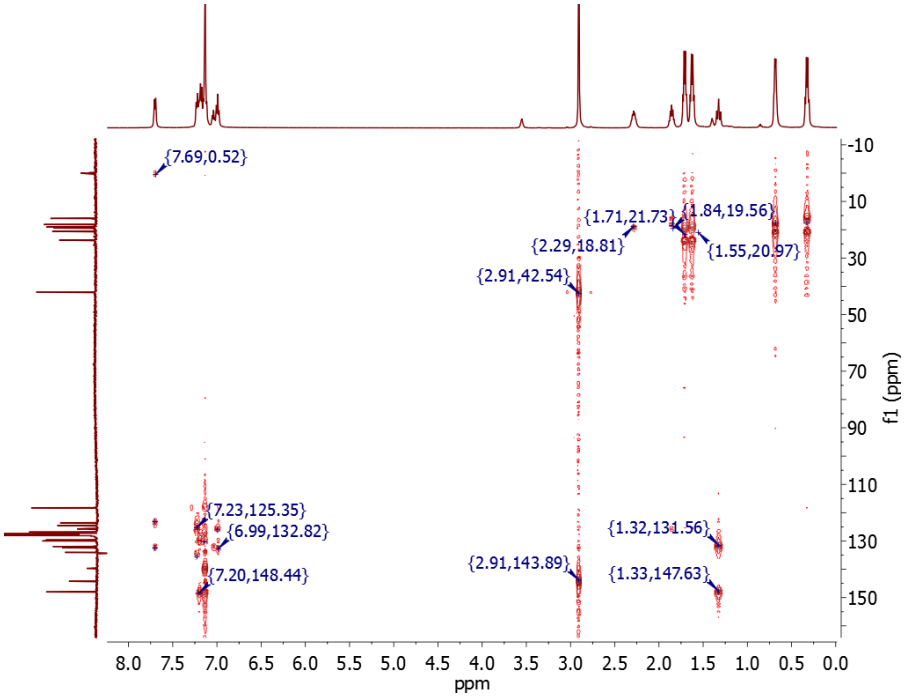

Figure A.115: ^{1}H-^{13}C HMBC NMR Spectrum (C_6D_6, 499.85, 125.70 MHz) of 12

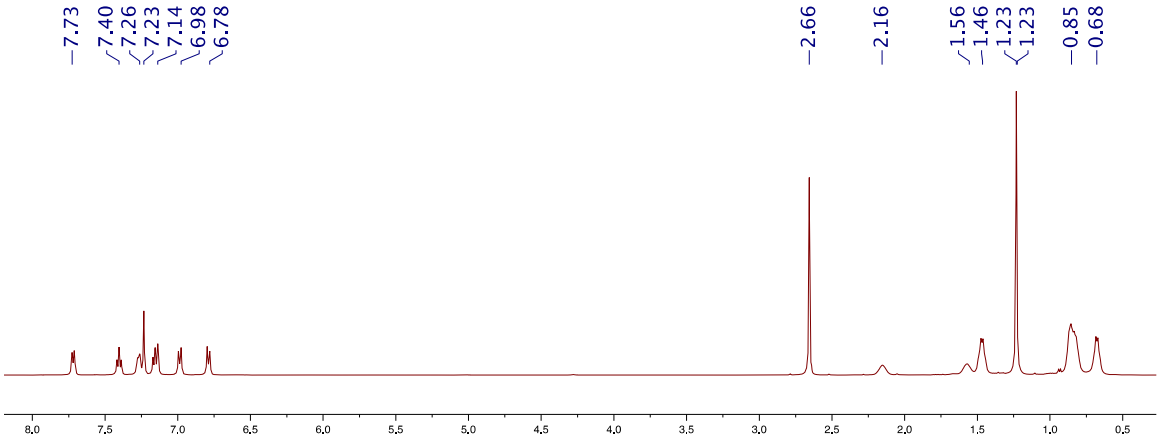

Figure A.116: ^{1}H NMR Spectrum (C_6D_6, 25°C, 499.85 MHz) of 13

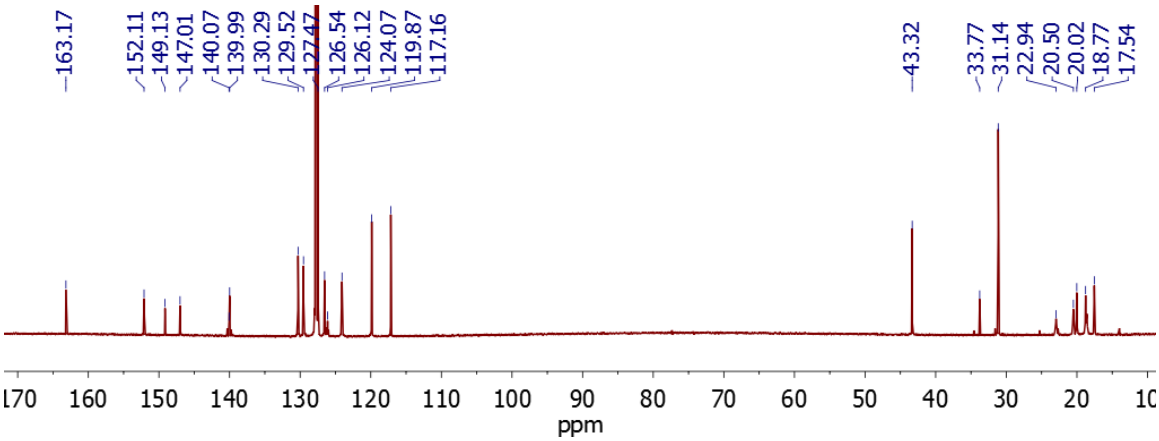

Figure A.117: ^{13}C{^{1}H} NMR Spectrum (C_6D_6, 25°C, 125.70 MHz) of 13

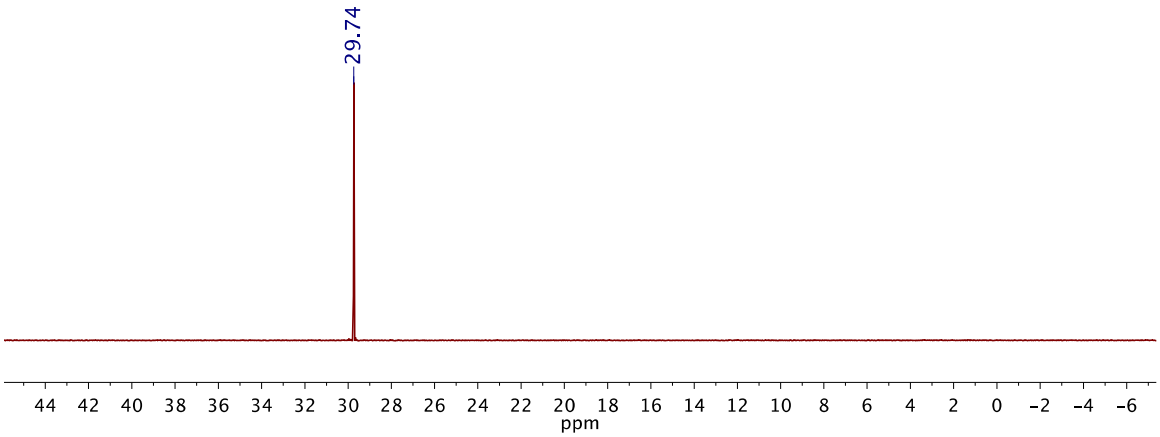

Figure A.118: ^{31}P{^{1}H} NMR Spectrum (C_6D_6, 25°C, 121.48 MHz) of 13

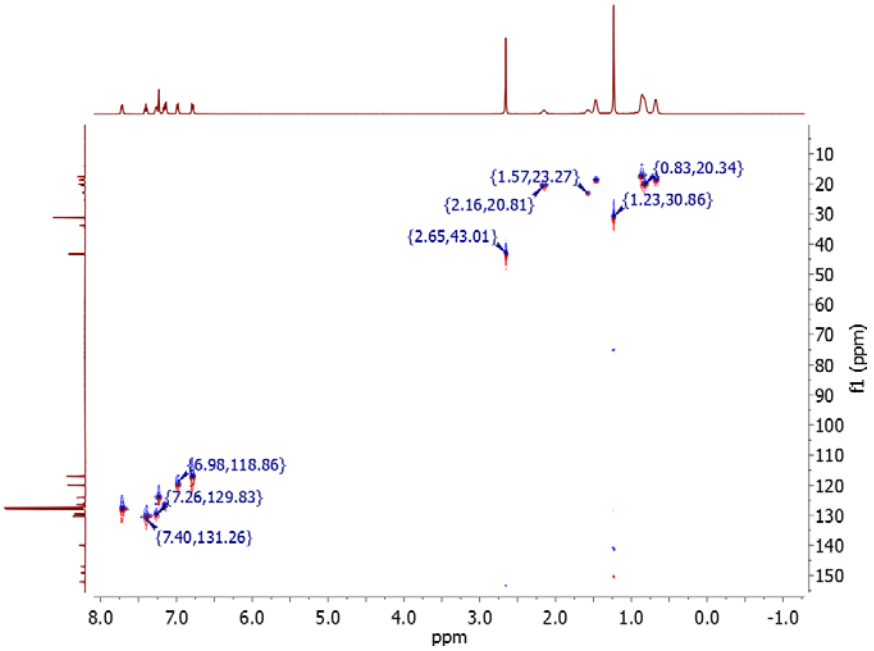

Figure A.119: ^{1}H-^{13}C HSQC NMR Spectrum (C_6D_6, 499.85, 125.70 MHz) of 13

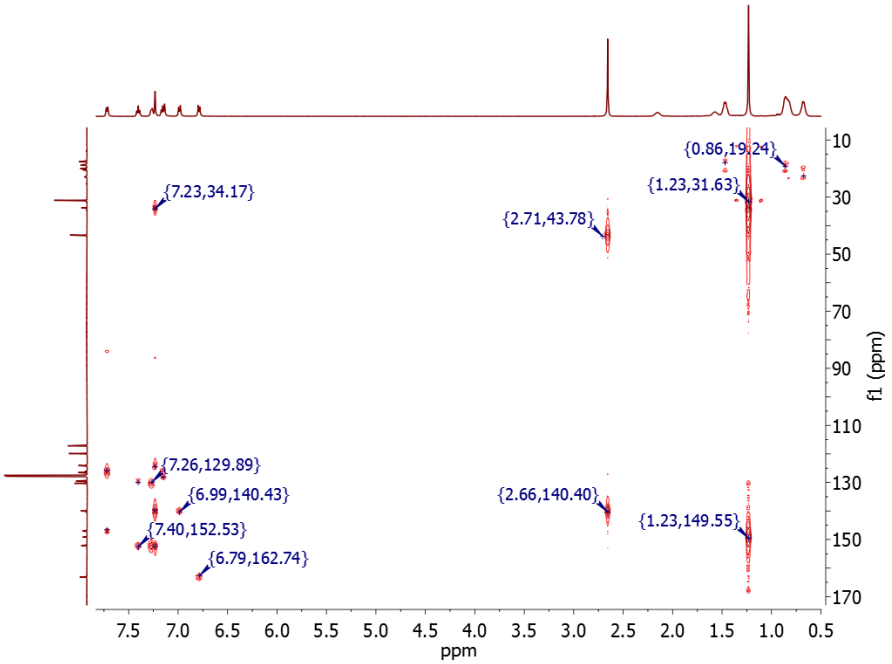

Figure A.120: ^{1}H-^{13}C HMBC NMR Spectrum (C_6D_6, 499.85, 125.70 MHz) of 13

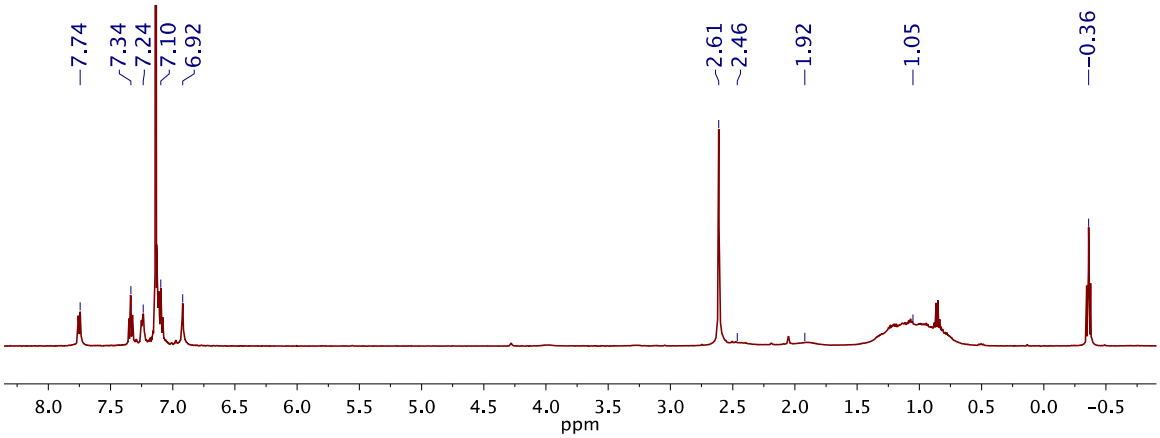

Figure A.121: ^{1}H NMR Spectrum (C_6D_6, 25°C, 499.85 MHz) of 14

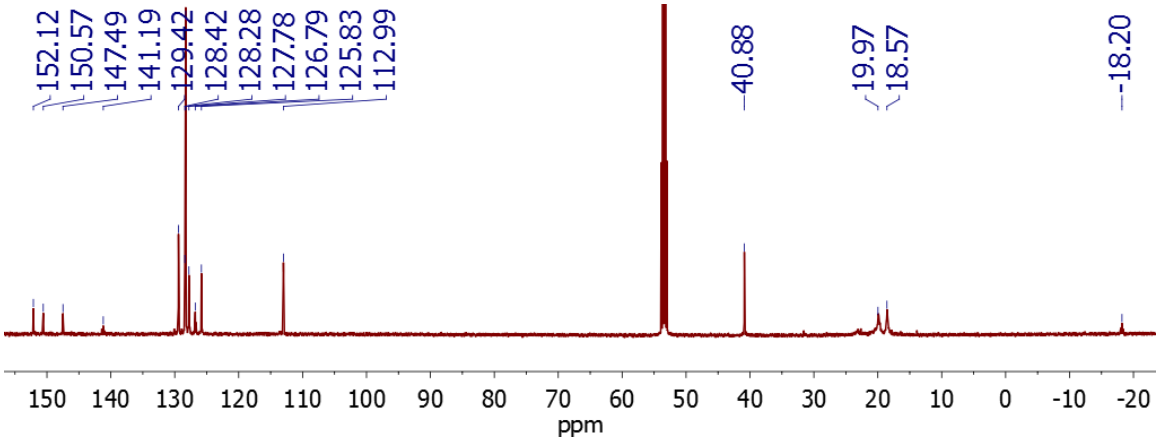

Figure A.122: ^{13}C{^{1}H} NMR Spectrum (C_6D_6, 25°C, 125.70 MHz) of 14

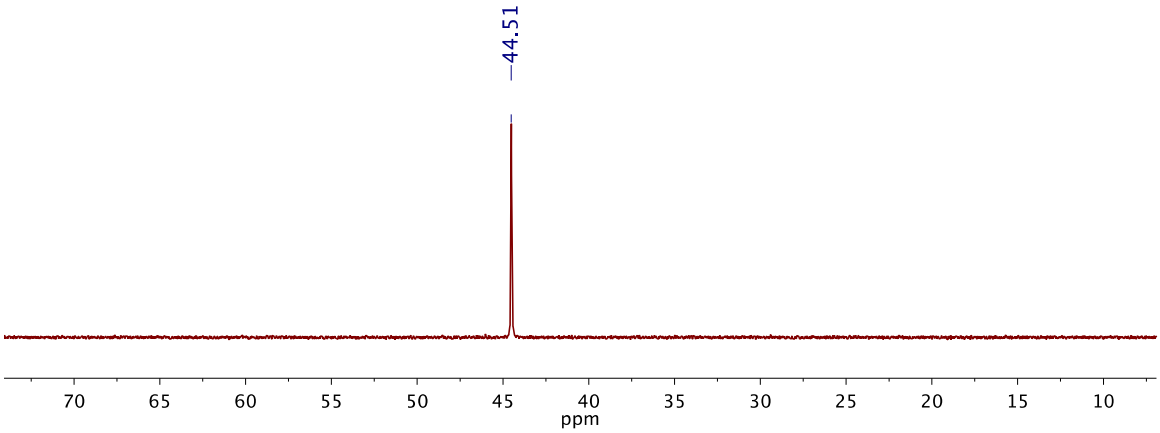

Figure A.123: ^{31}P{^{1}H} NMR Spectrum (C_6D_6, 25°C, 121.48 MHz) of 14

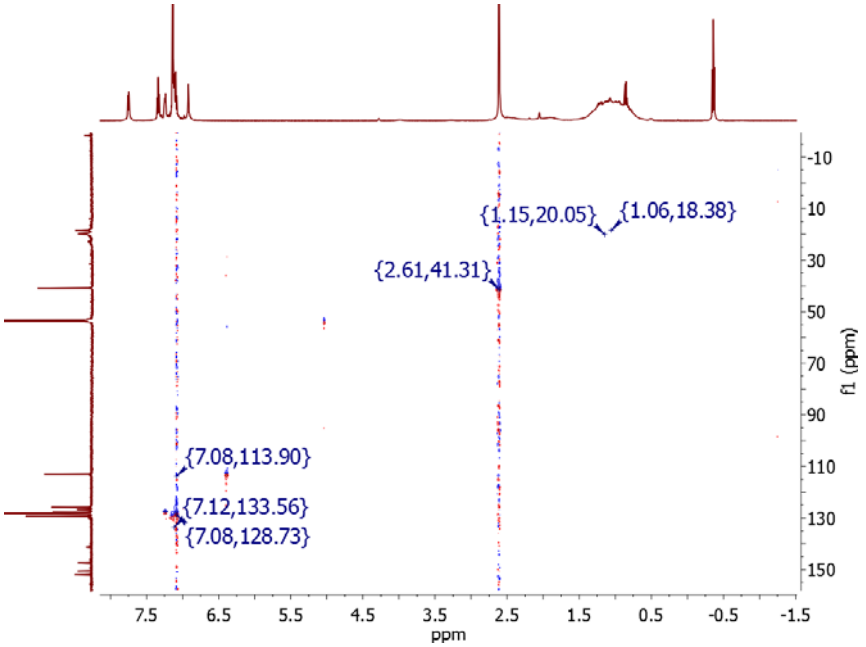

Figure A.124: ^{1}H-^{13}C HSQC NMR Spectrum (C_6D_6, 499.85, 125.70 MHz) of 14

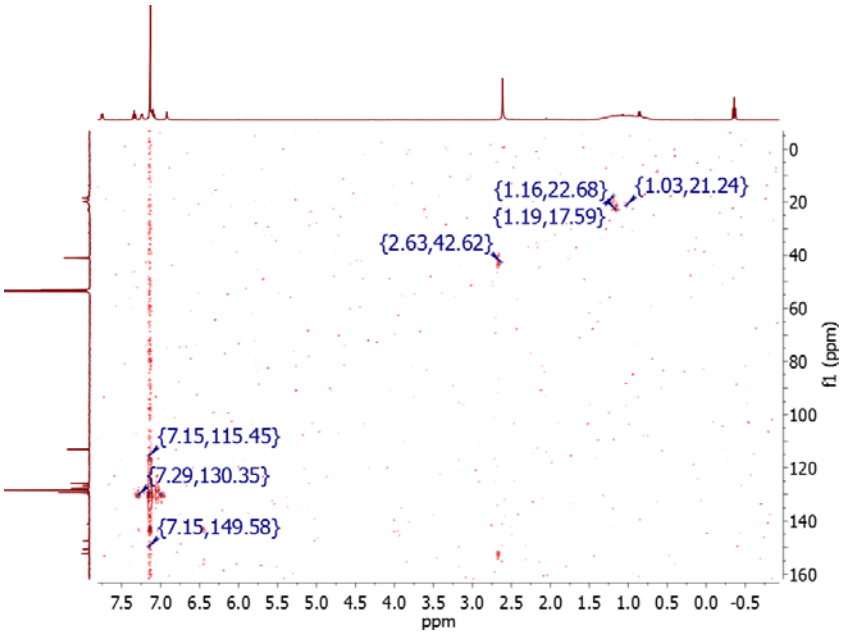

Figure A.125: ^{1}H-^{13}C HMBC NMR Spectrum (C_6D_6, 499.85, 125.70 MHz) of 14

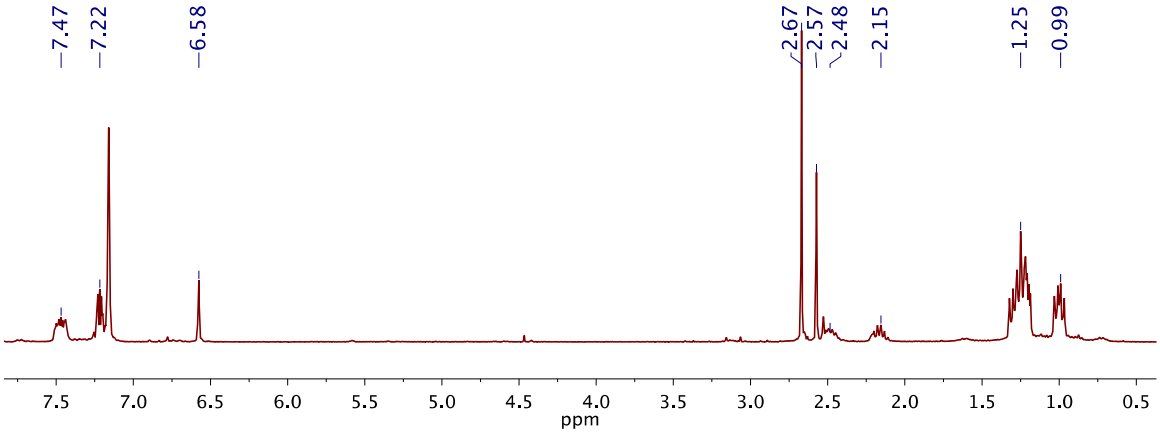

Figure A.126: ^{1}H NMR Spectrum (C_6D_6, 25°C, 499.85 MHz) of 16

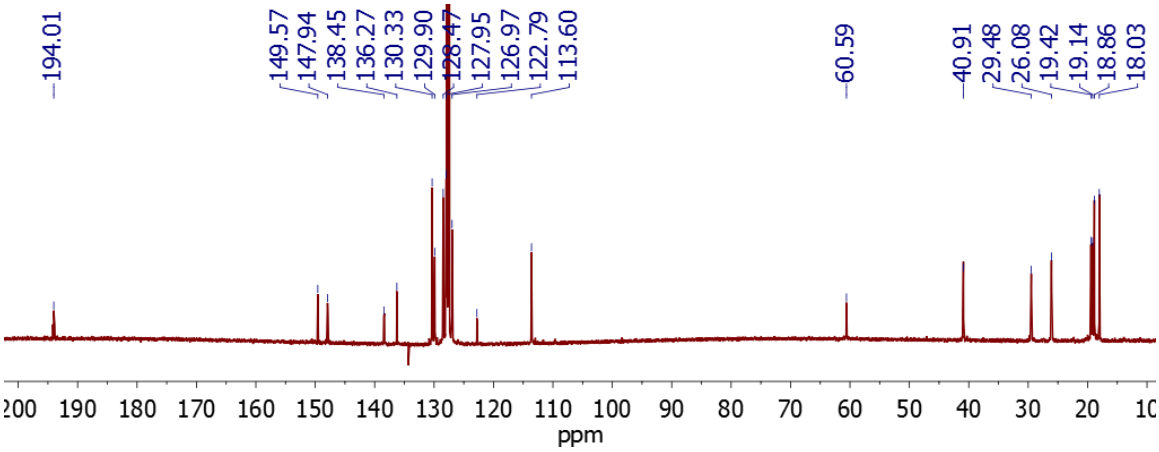

Figure A.127: ^{13}C{^{1}H} NMR Spectrum (C_6D_6, 25°C, 125.70 MHz) of 16

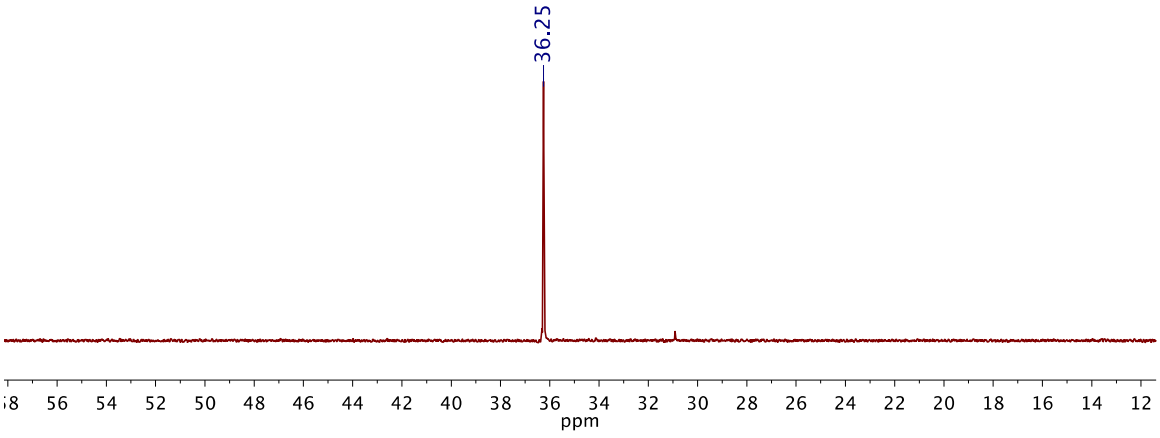

Figure A.128: ^{31}P{^{1}H} NMR Spectrum (C_6D_6, 25°C, 121.48 MHz) of 16

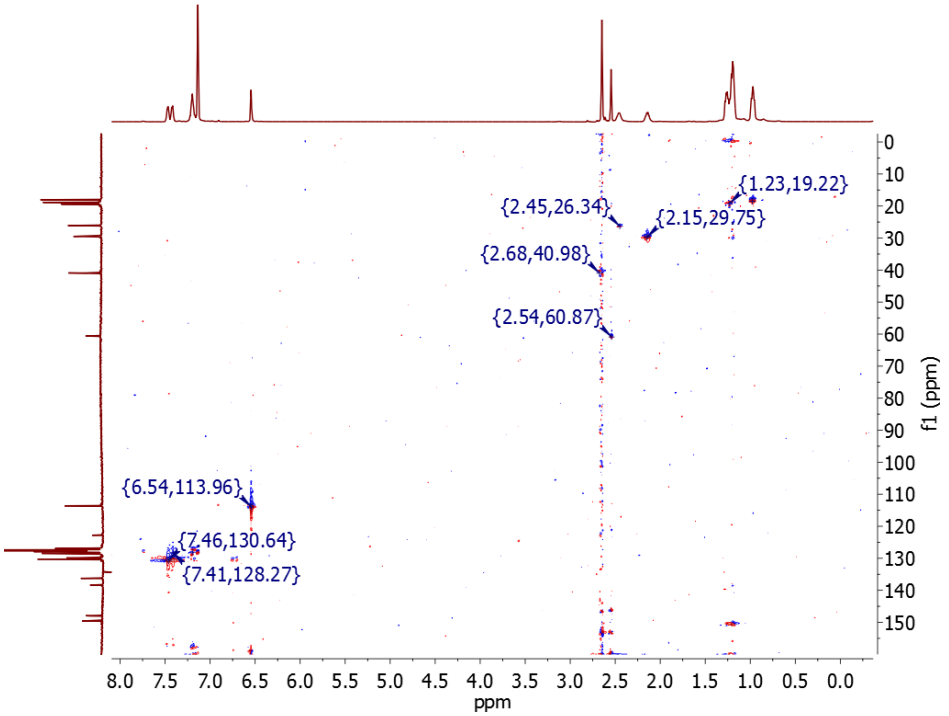

Figure A.129: ^{1}H-^{18}C HSQC NMR Spectrum (C_6D_6, 499.85, 125.70 MHz) of 16

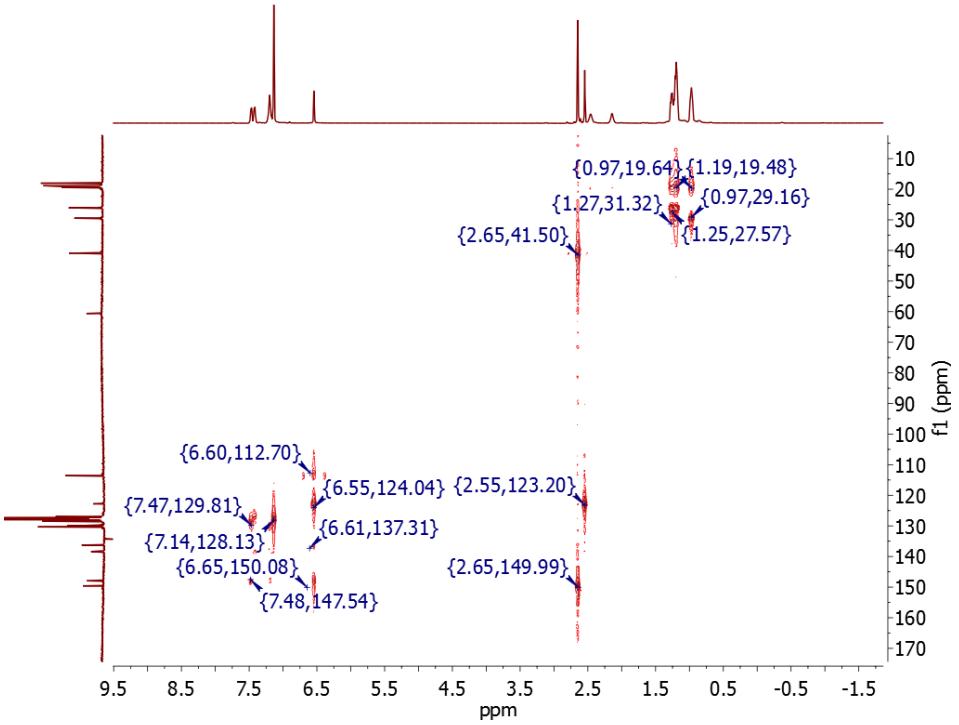

Figure A.130: ^{1}H-^{18}C HMBC NMR Spectrum (C_6D_6, 499.85, 125.70 MHz) of 16

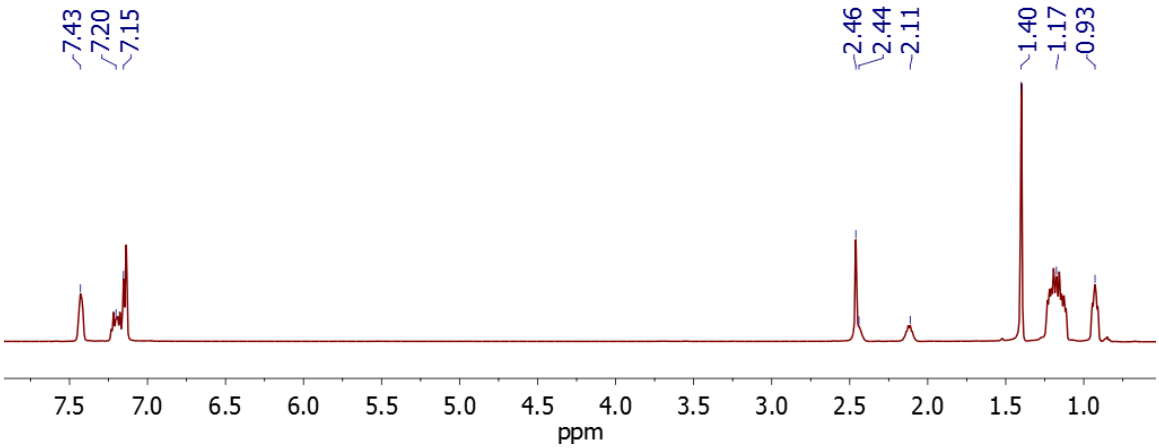

Figure A.131: ^{1}H NMR Spectrum (C_6D_6, 25°C, 499.85 MHz) of 16_{tBu}

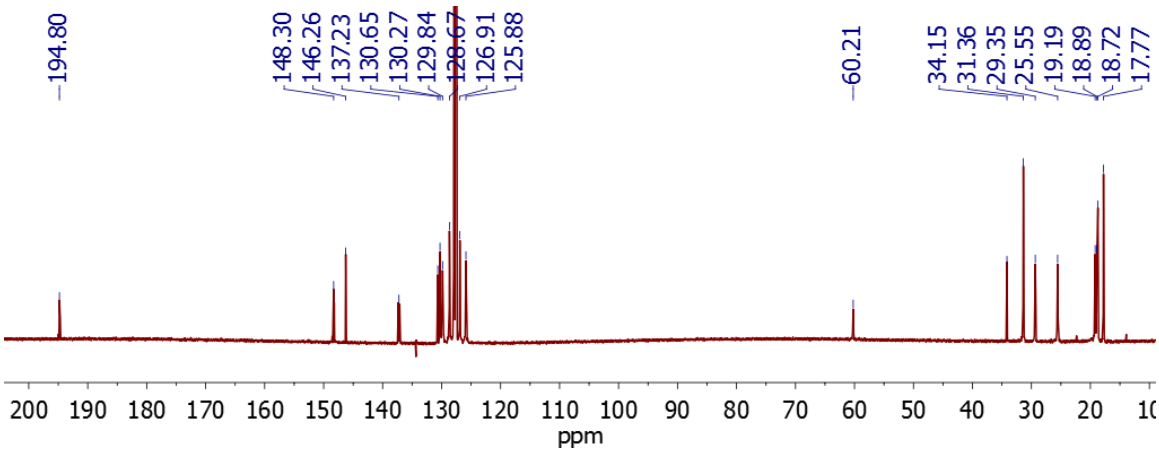

Figure A.132: $^{13}C\{^{1}H\}$ NMR Spectrum (C_6D_6, 25°C, 125.70 MHz) of 16_{tBu}

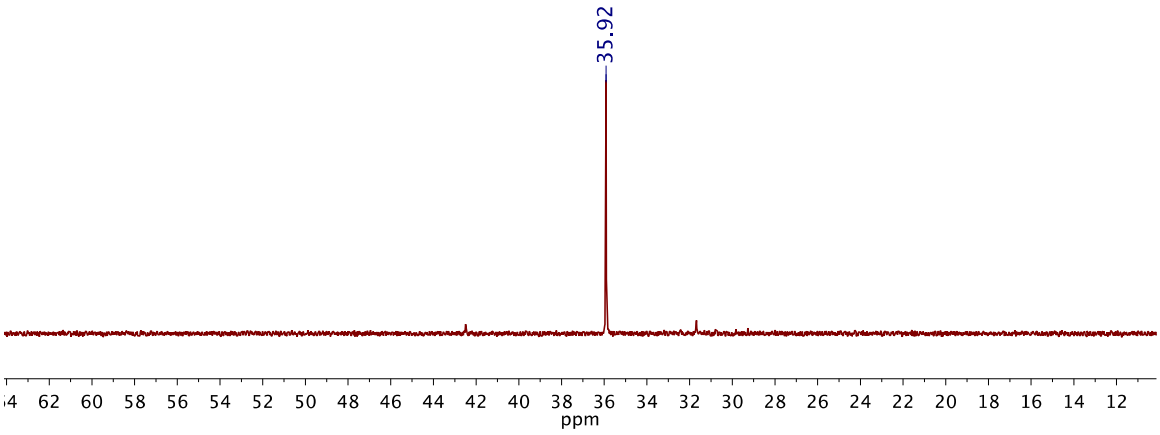

Figure A.133: $^{31}P\{^{1}H\}$ NMR Spectrum (C_6D_6, 25°C, 121.48 MHz) of 16_{tBu}

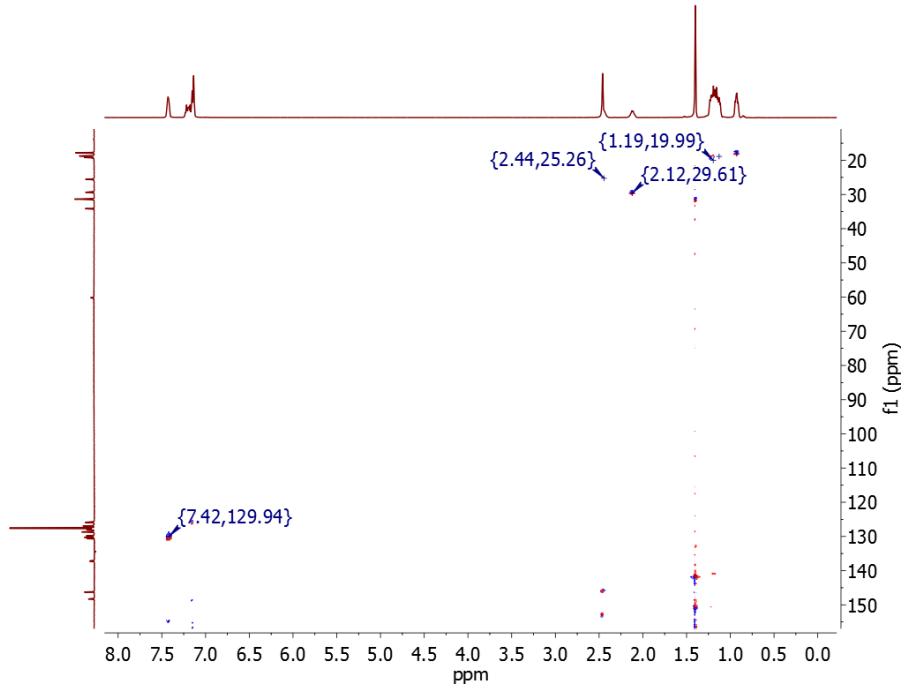

Figure A.134: ^{1}H-^{13}C HSQC NMR Spectrum (C_6D_6, 499.85, 125.70 MHz) of 16_{tBu}

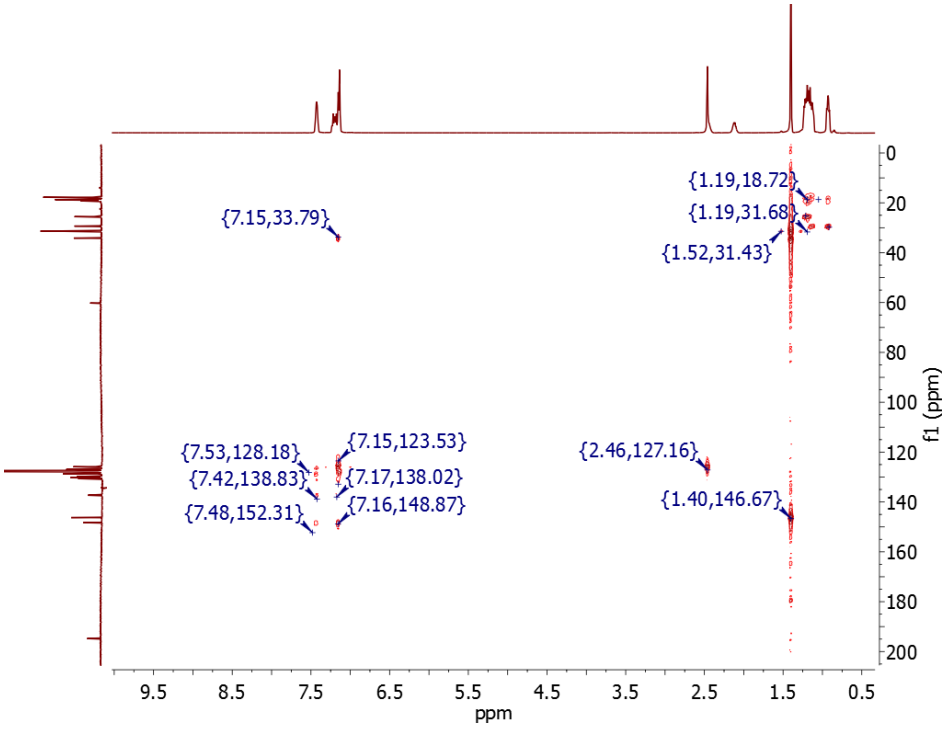

Figure A.135: ^{1}H-^{13}C HMBC NMR Spectrum (C_6D_6, 499.85, 125.70 MHz) of 16_{tBu}

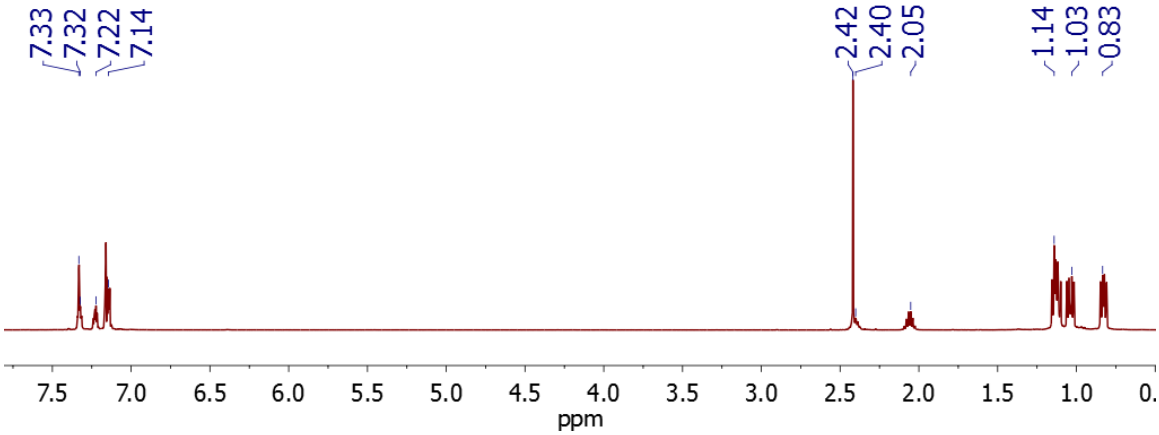

Figure A.136: ^{1}H NMR Spectrum (C_6D_6, 25°C, 499.85 MHz) of 16_{CF3}

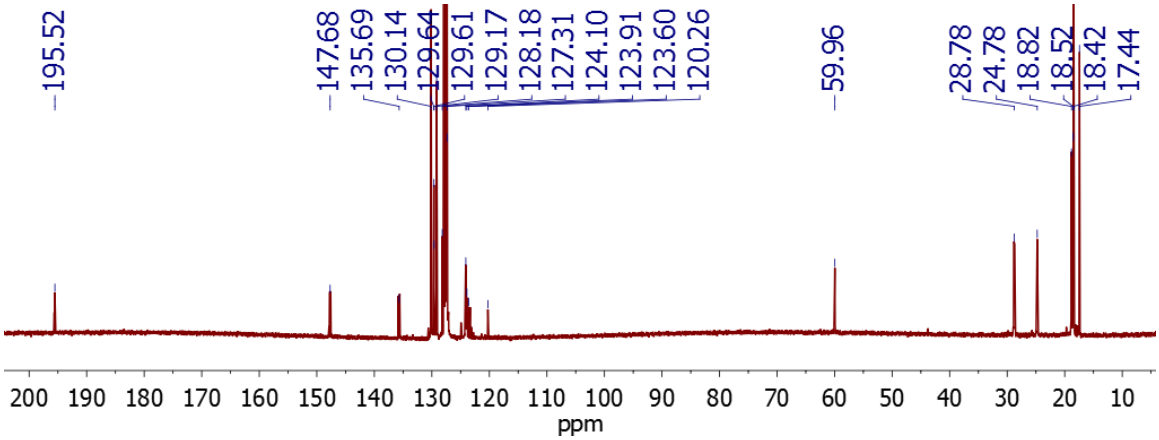

Figure A.137: ^{13}C NMR Spectrum (C_6D_6, 25°C, 125.70 MHz) of 16_{CF3}

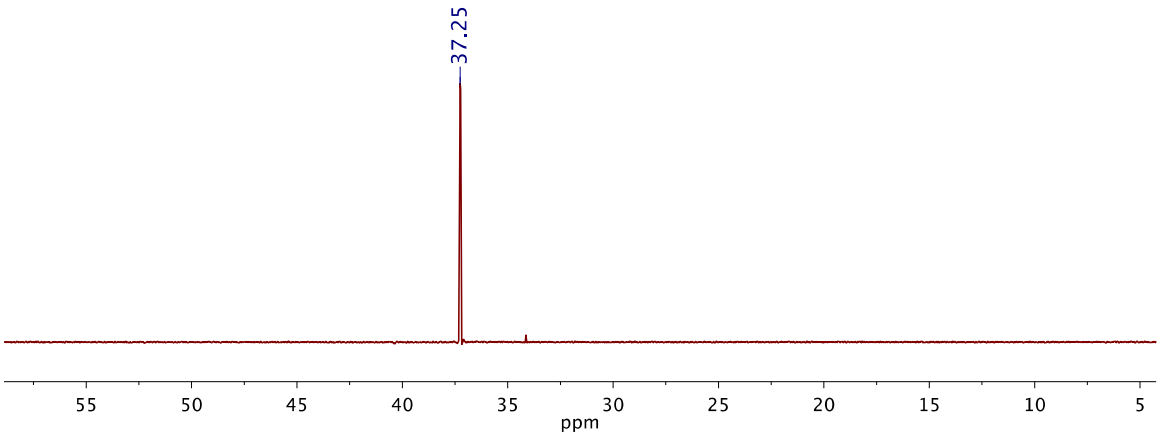

Figure A.138: ^{31}P{^{1}H} NMR Spectrum (C_6D_6, 25°C, 121.48 MHz) of 16_{CF3}

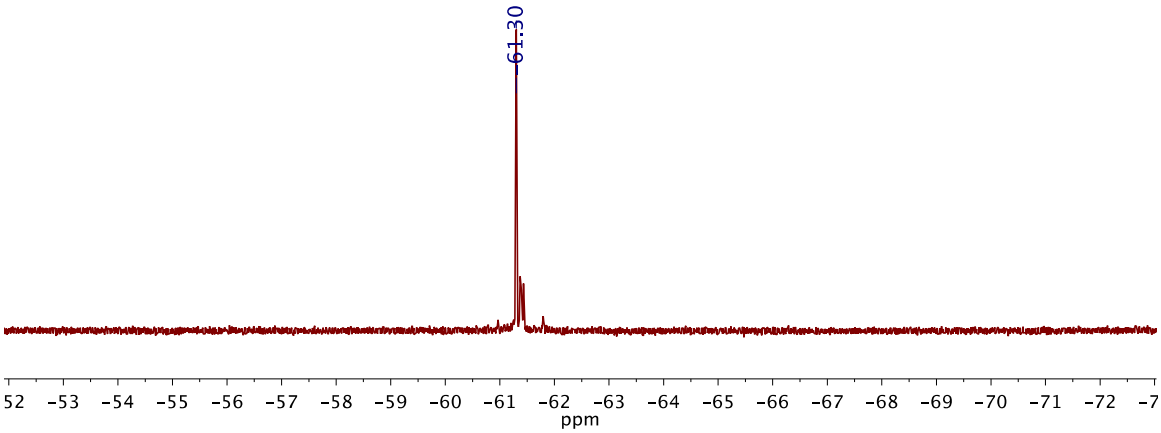

Figure A.139: $^{19}F\{^{1}H\}$ NMR Spectrum (C_6D_6, 282.33 MHz) of 16_{CF3}

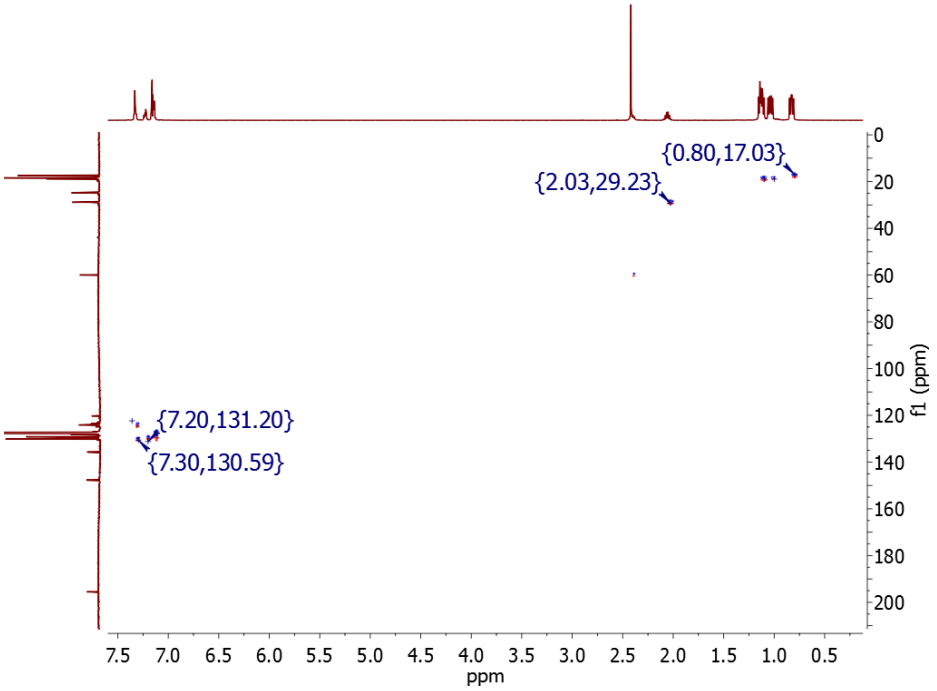

Figure A.140: ^{1}H-^{13}C HSQC NMR Spectrum (C_6D_6, 499.85, 125.70 MHz) of 16_{CF_3}

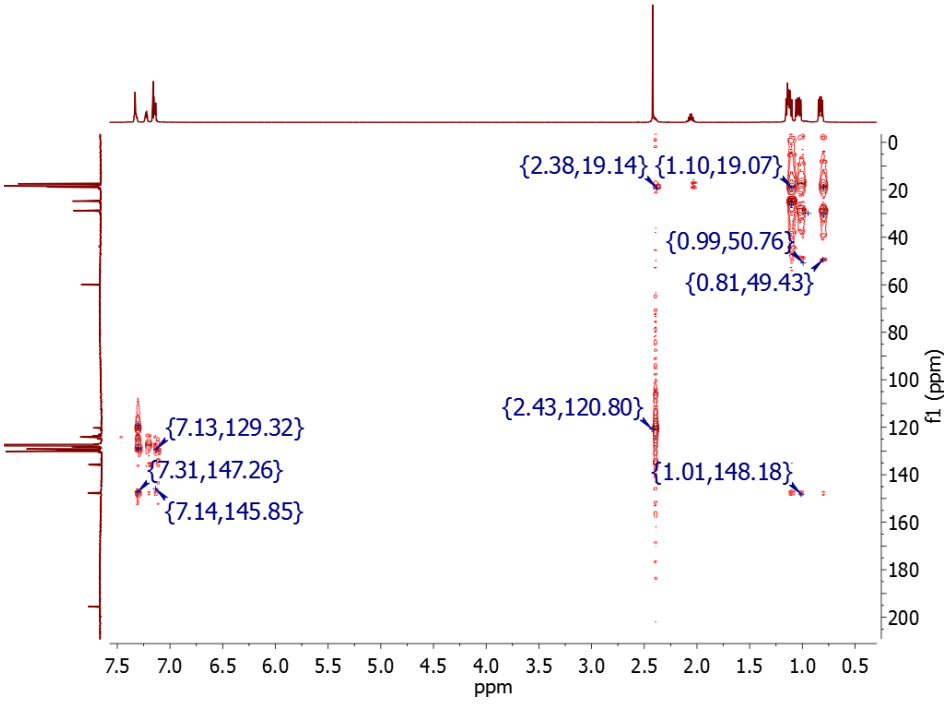

Figure A.141: ^{1}H-^{13}C HMBC NMR Spectrum (C_6D_6, 499.85, 125.70 MHz) of 16_{CF_3}

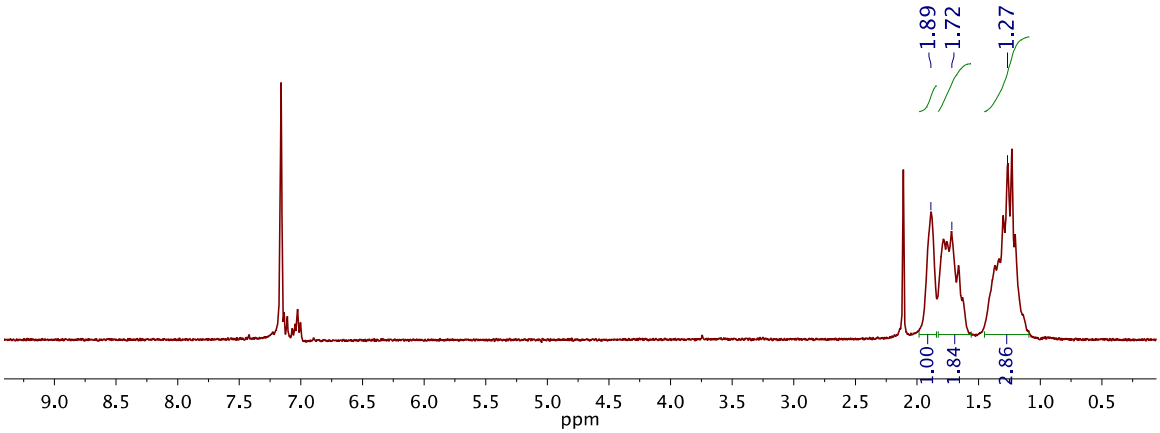

Figure A.142: ^{1}H NMR Spectrum (C_6D_6, 25°C, 300 MHz) of 18

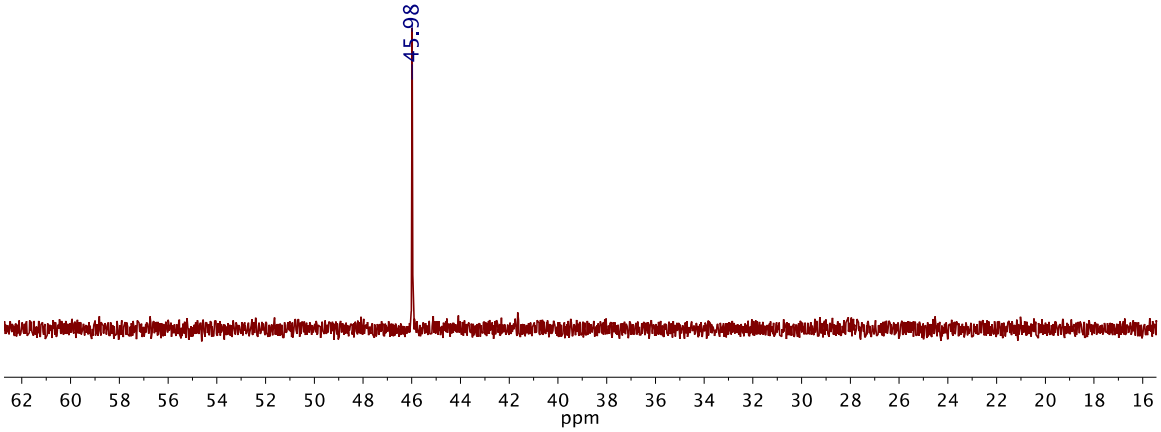

Figure A.143: $^{31}P\{^{1}H\}$ NMR Spectrum (C_6D_6, 25°C, 121.48 MHz) of 18

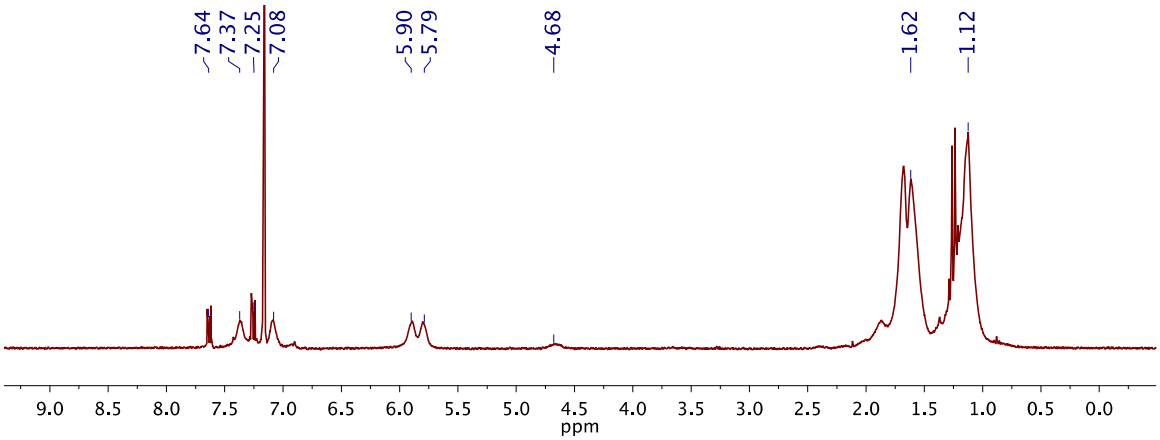

Figure A.144: ^{1}H NMR Spectrum (C_6D_6, 25°C, 300 MHz) of 19

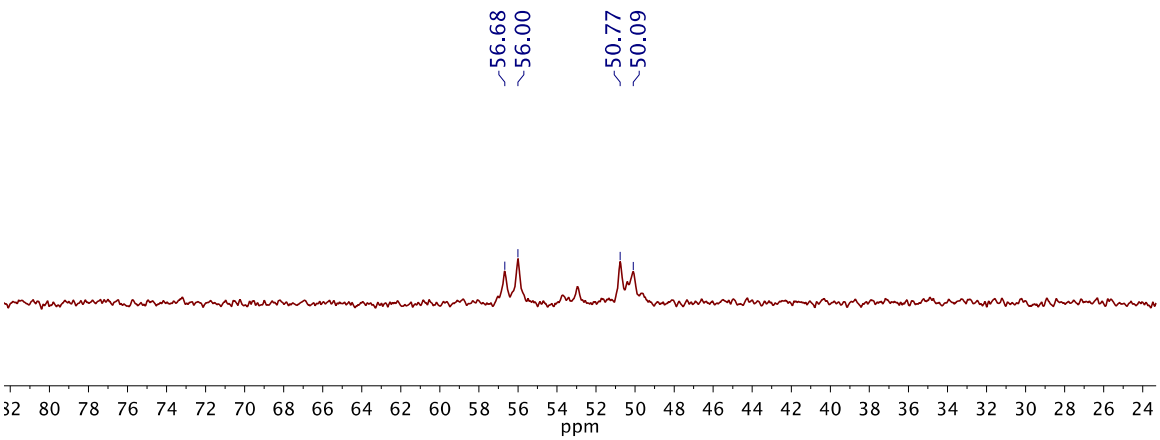

Figure A.145: $^{31}P\{^{1}H\}$ NMR Spectrum (C_6D_6, 25°C, 121.48 MHz) of 19

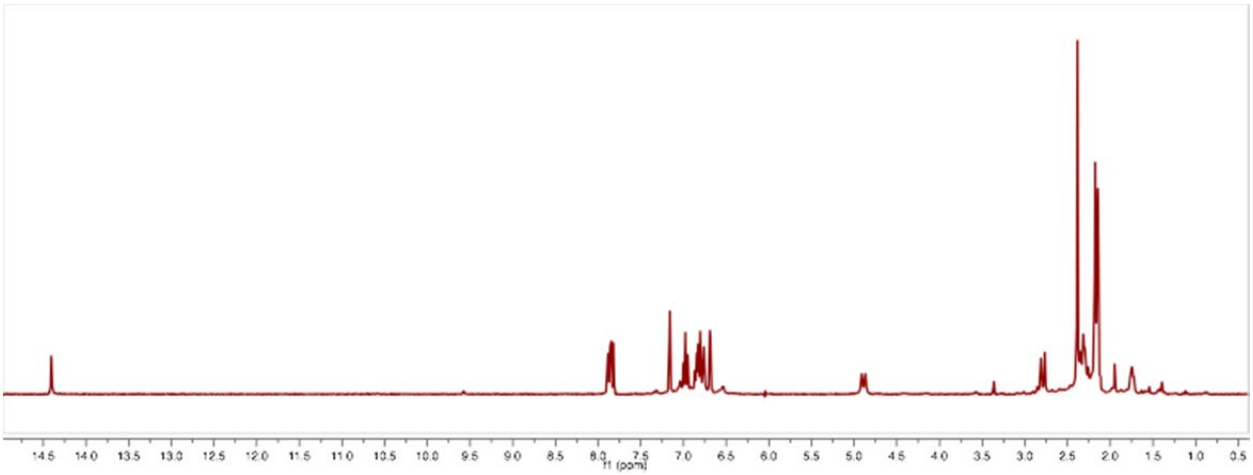

Figure A.146. ^{1}H NMR spectrum of 23 in C_6D_6.

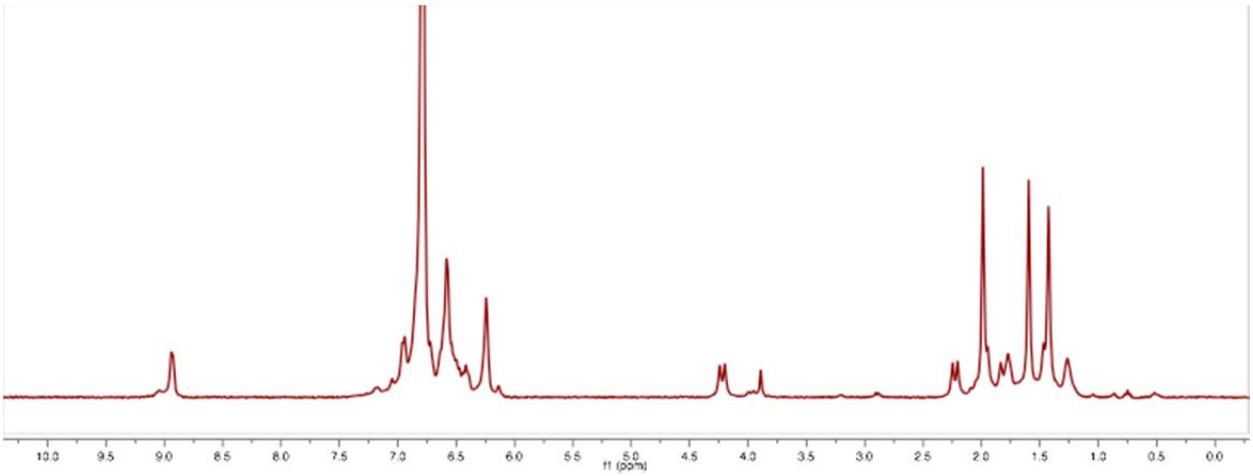

Figure A.147. ^{1}H NMR spectrum of 25 in C_6D_6.

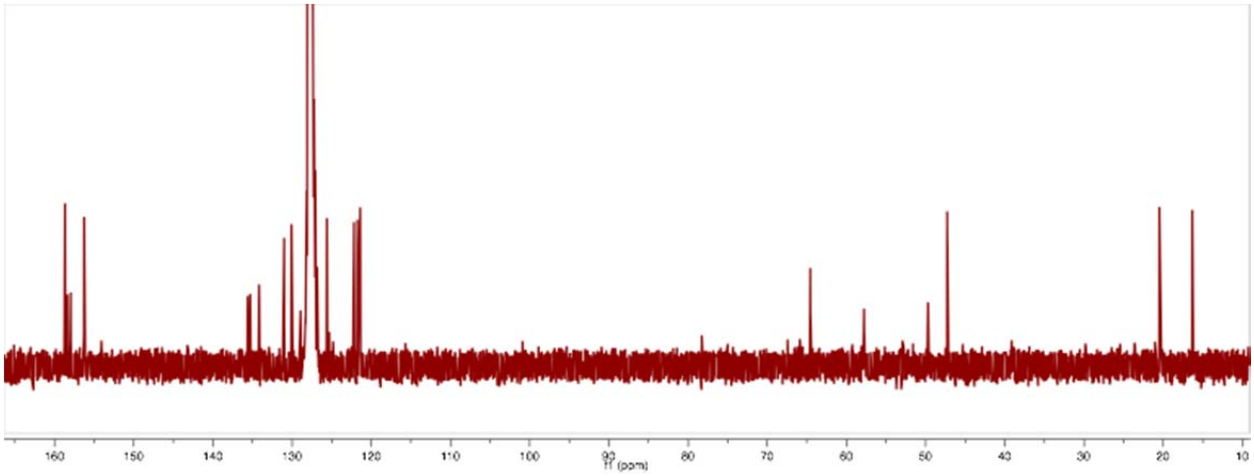

Figure A.148. ^{13}C NMR spectrum of 25 in C_6D_6.

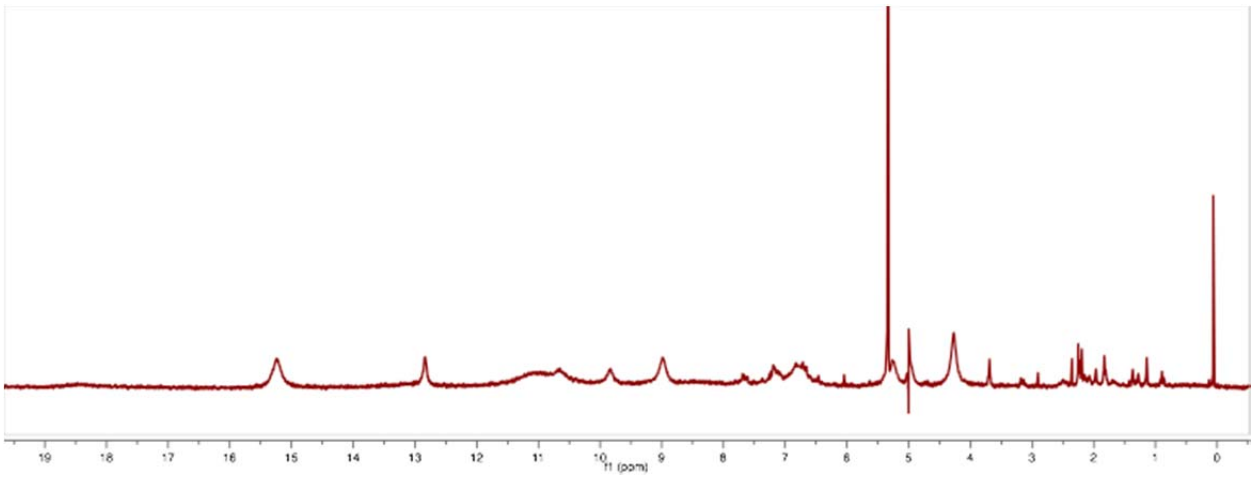

Figure A.149. ^{1}H NMR spectrum of 26 in CD_2Cl_2.

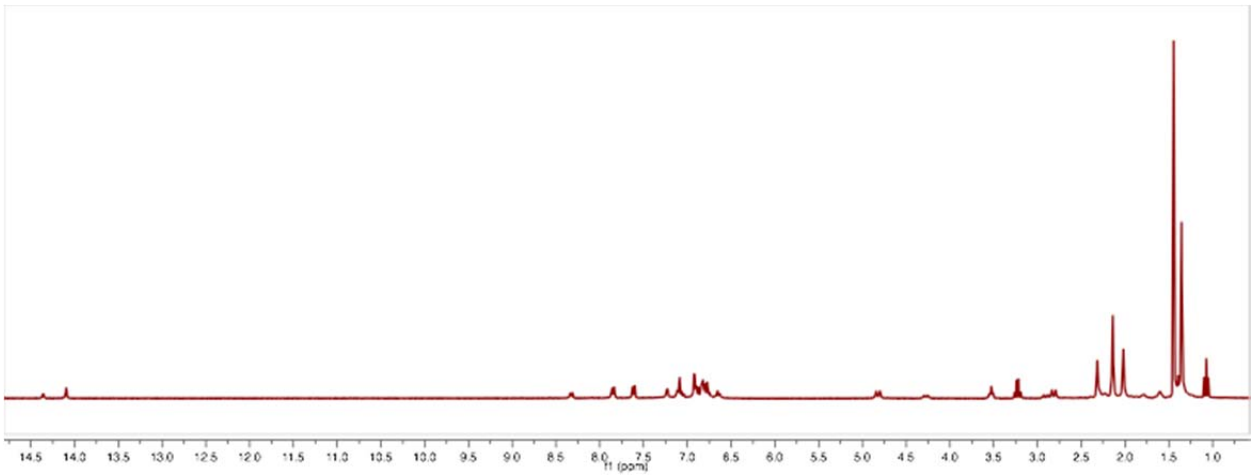

Figure A.150. ^{1}H NMR spectrum of 23^{tBu} in C_6D_6.

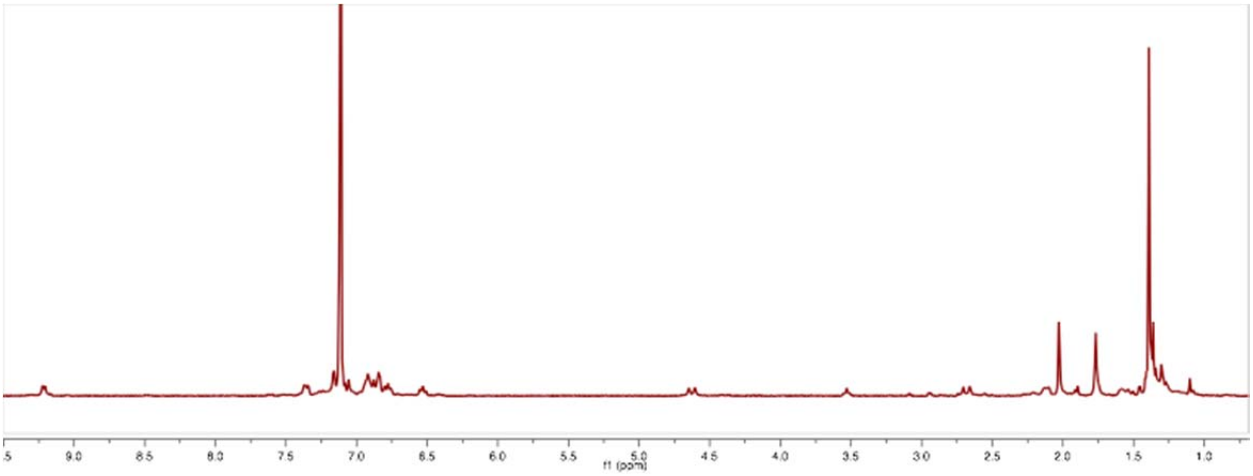

Figure A.151. ^{1}H NMR spectrum of 25^{tBu} in C_6D_6.

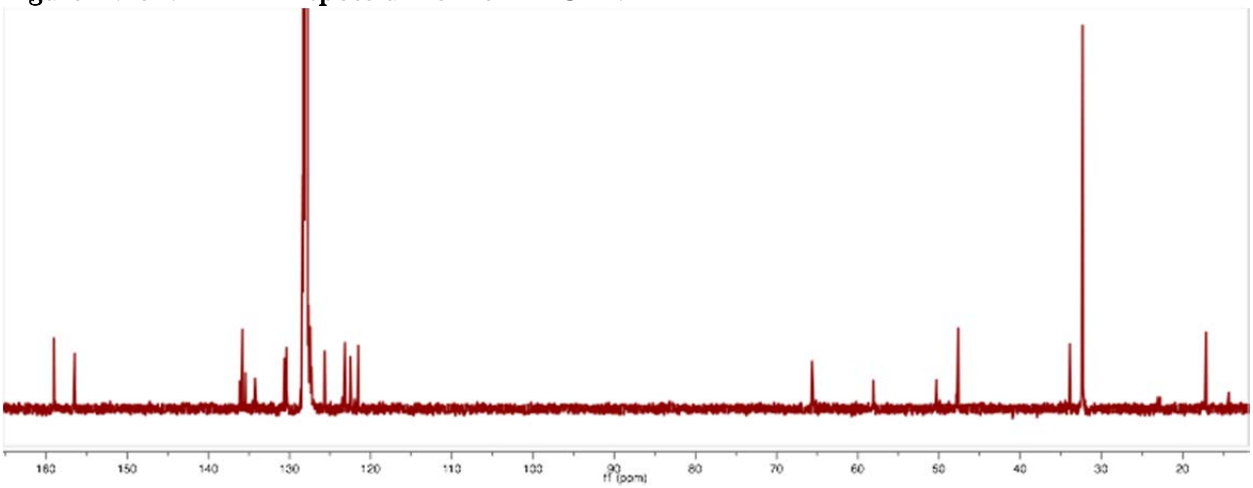

Figure A.152. ^{13}C{^{1}H} NMR spectrum of 25^{tBu} in C_6D_6.

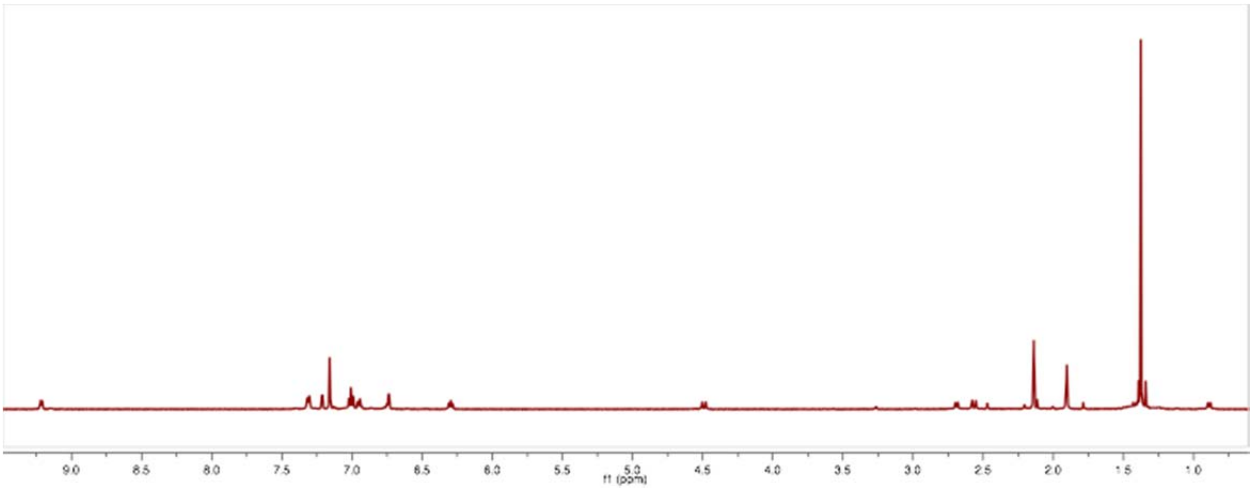

Figure A.153. ^{1}H NMR spectrum of 29^{tBu} in C_6D_6.

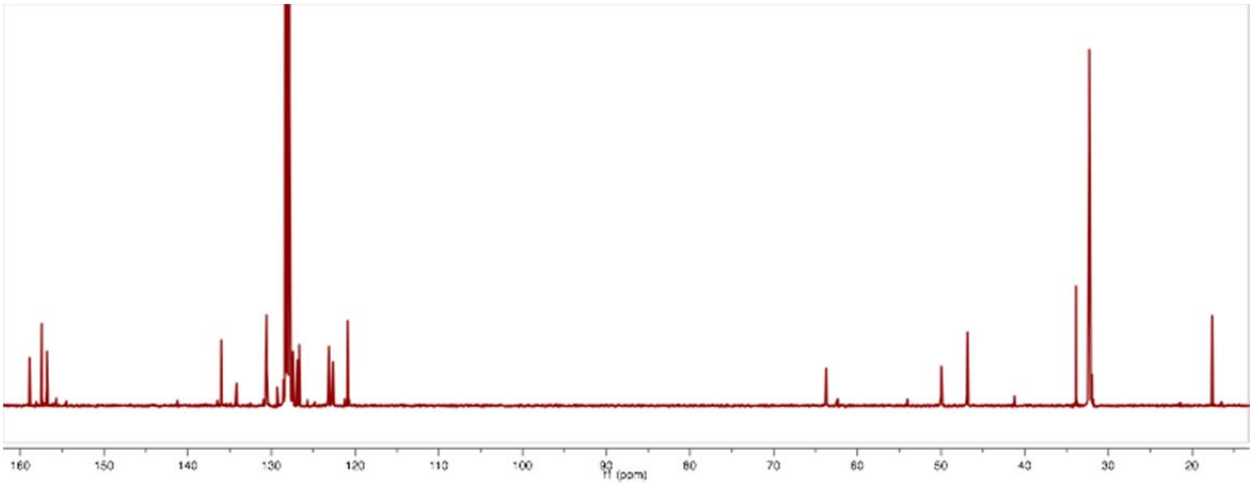

Figure A.154. $^{13}C\{^{1}H\}$ NMR spectrum of 29^{tBu} in C_6D_6.

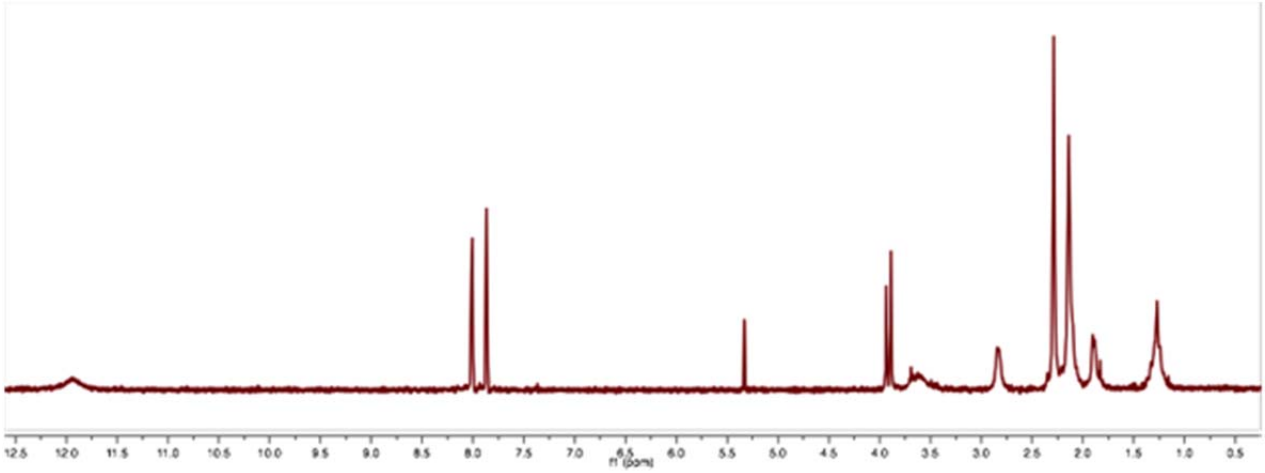

Figure A.155. ^{1}H NMR spectrum of 30^{NO2} in CD_2Cl_2

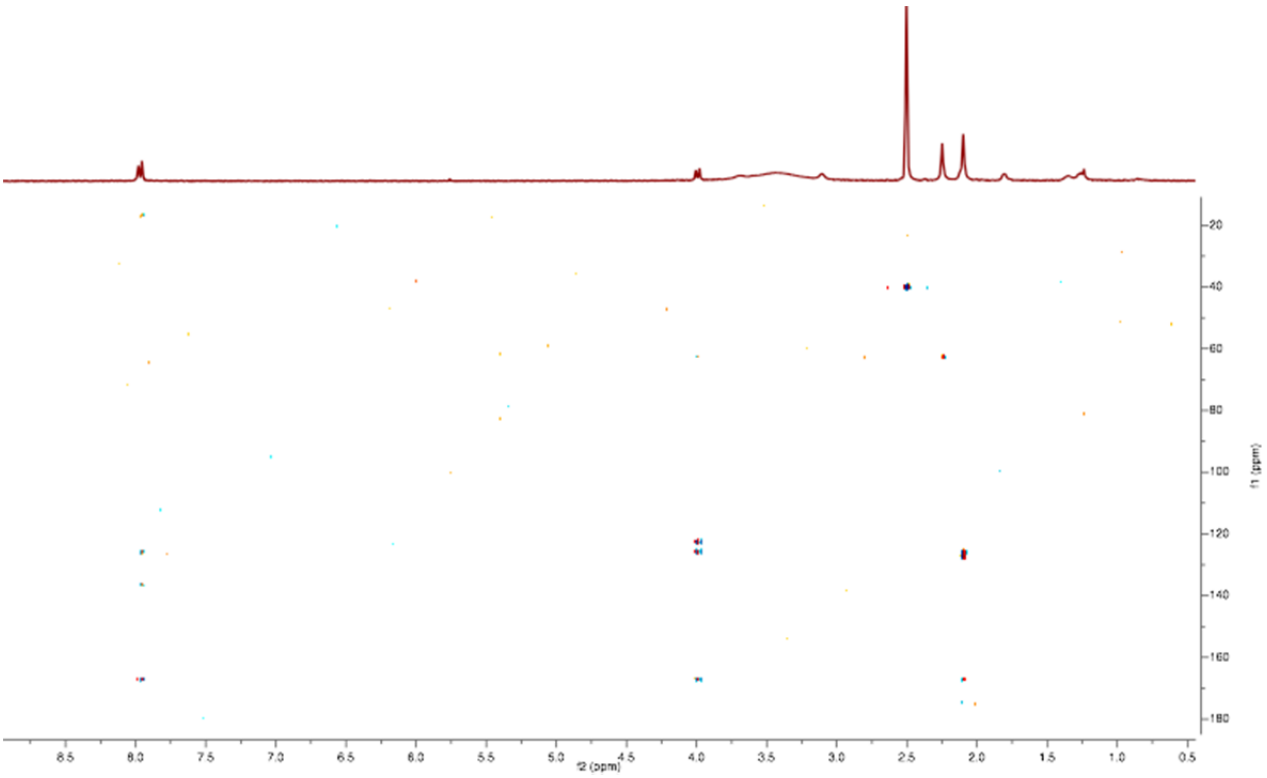

Figure A.156. ^{1}H-^{13}C gHMBCAD NMR spectrum of 30^{NO_2} in $(CD_3)_2SO$.

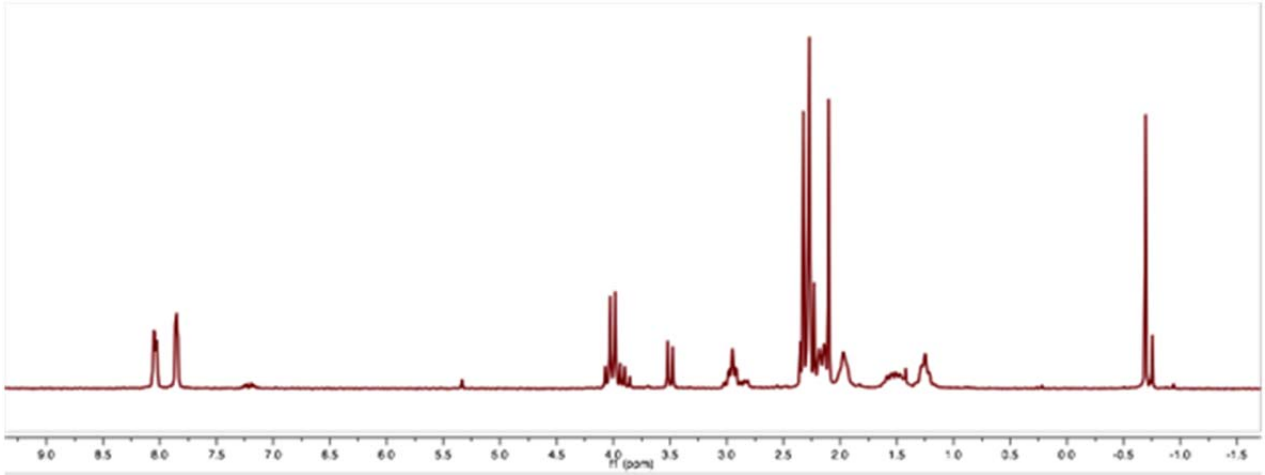

Figure A.157. ^{1}H NMR spectrum of 31^{NO_2} in CD_2Cl_2

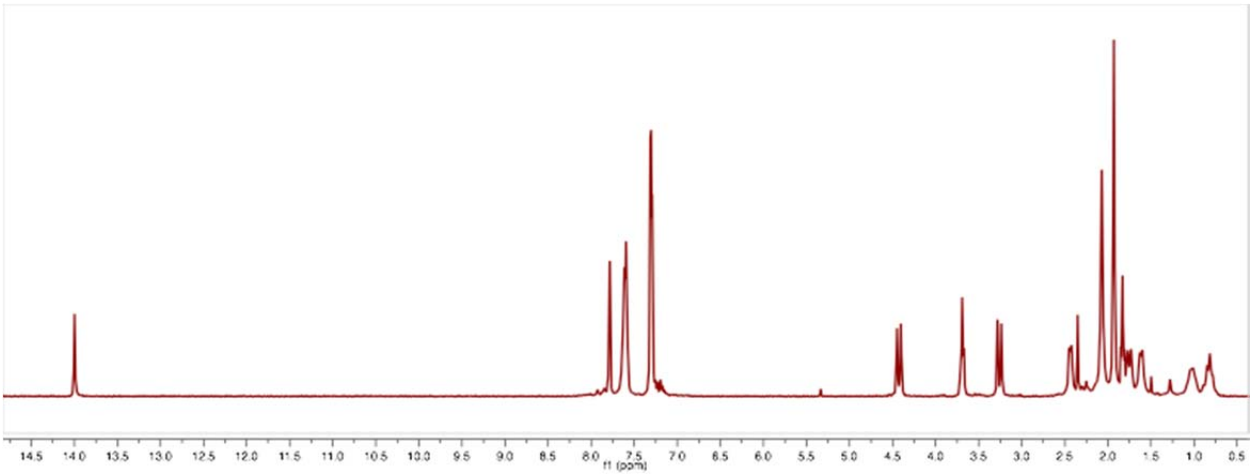

Figure A.158. ^{1}H NMR spectrum of 32^{NO_2} in CD_2Cl_2.

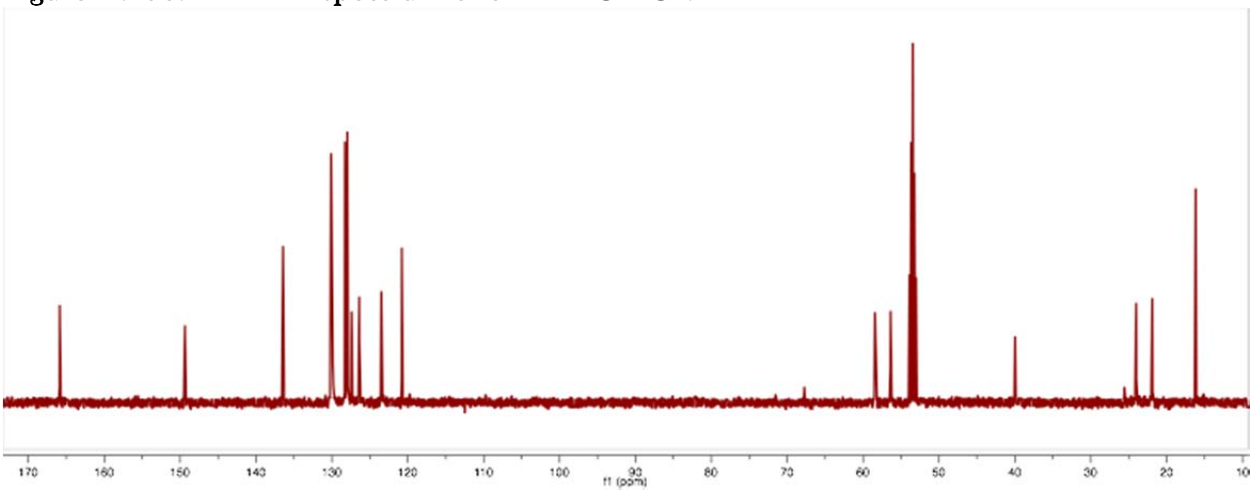

Figure A.159. $^{13}C\{^{1}H\}$ NMR spectrum of 32^{NO_2} in CD_2Cl_2.

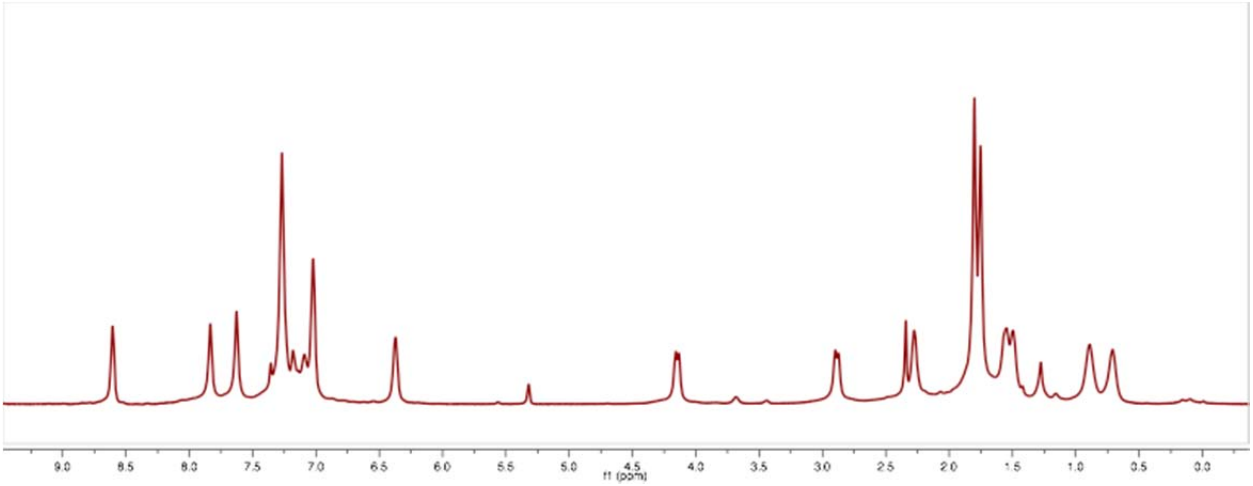

Figure A.160. ^{1}H NMR spectrum of 33^{NO_2} in CD_2Cl_2.

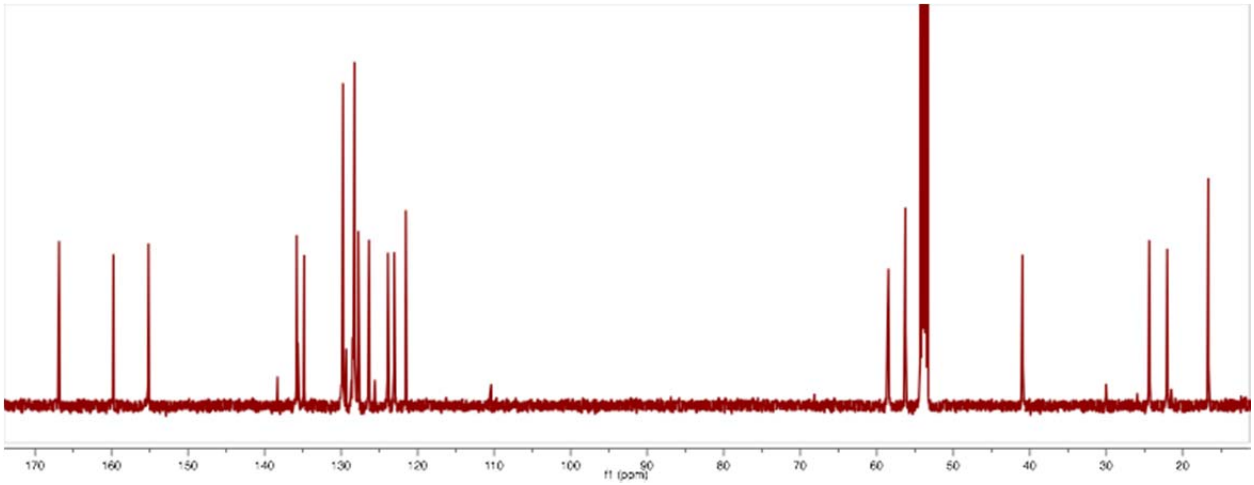

Figure A.161. $^{13}C\{^{1}H\}$ NMR spectrum of 33^{NO_2} in CD_2Cl_2.

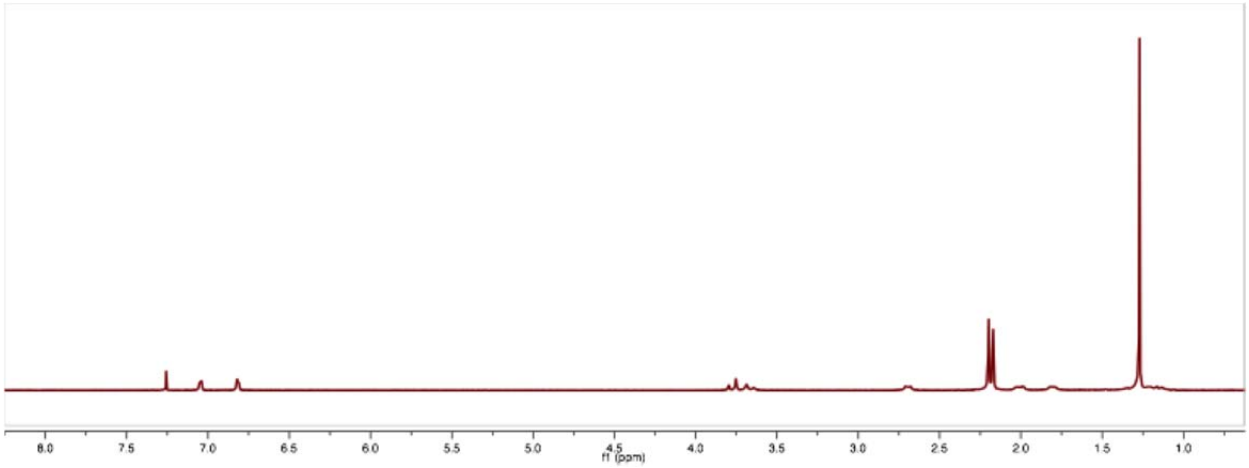

Figure A.162. ^{1}H NMR spectrum of 30^{tBu} in $CDCl_3$

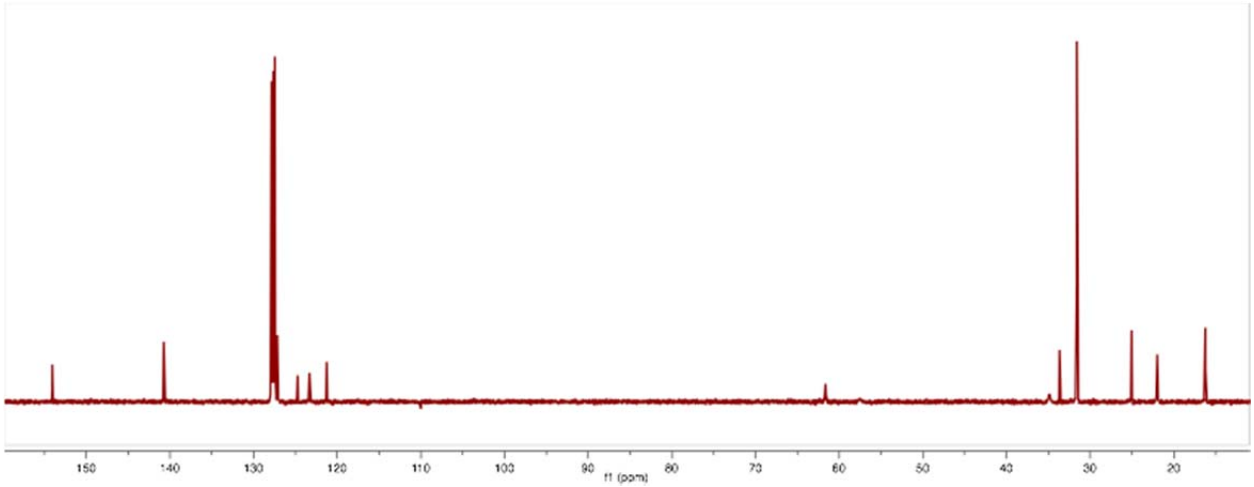

Figure A.163. $^{13}C\{^{1}H\}$ NMR spectrum of 30^{tBu} in C_6D_6

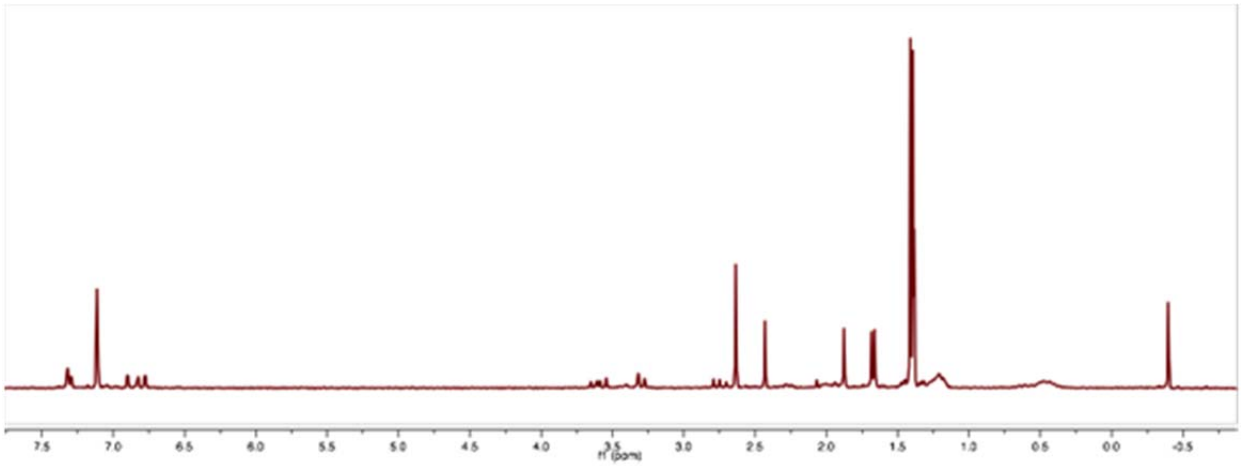

Figure A.164. ^{1}H NMR spectrum of 31^{tBu} in C_6D_6

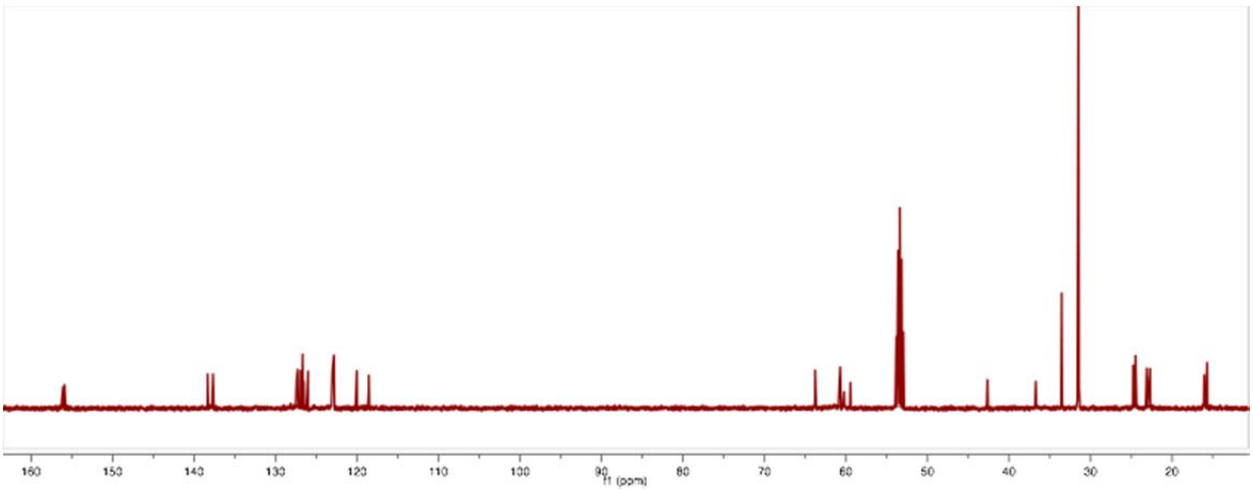

Figure A.165. $^{13}C\{^{1}H\}$ NMR spectrum of 31^{tBu} in CD_2Cl_2

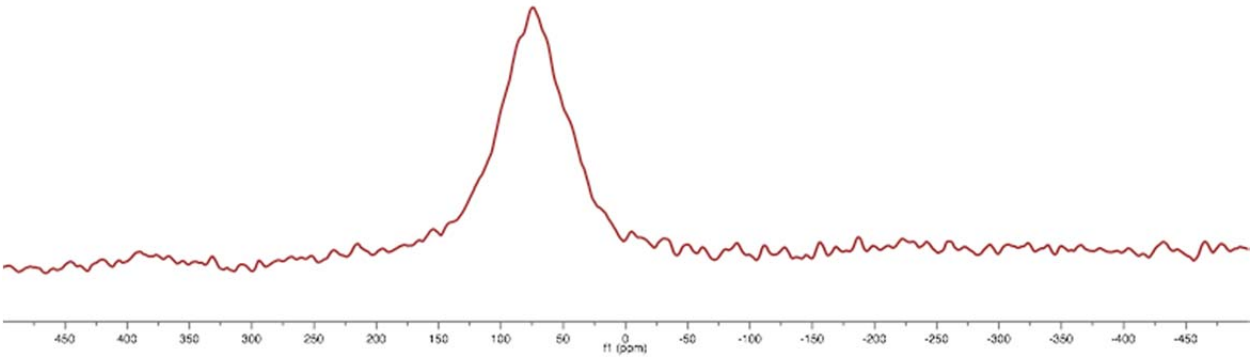

Figure A.166. ^{27}Al NMR spectrum of 31^{tBu} in CD_2Cl_2

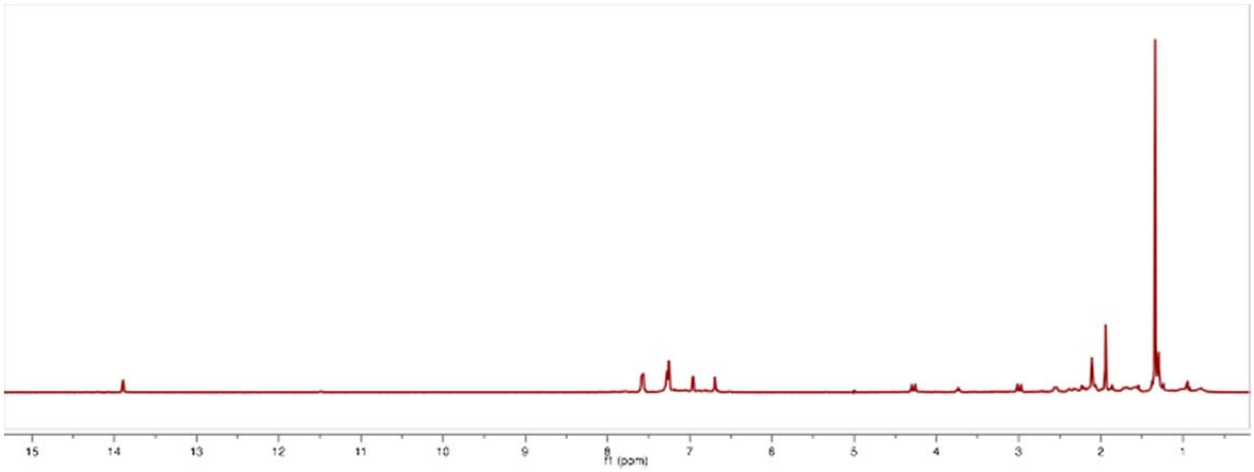

Figure A.167. ^{1}H NMR spectrum of 32^{tBu} in CD_2Cl_2.

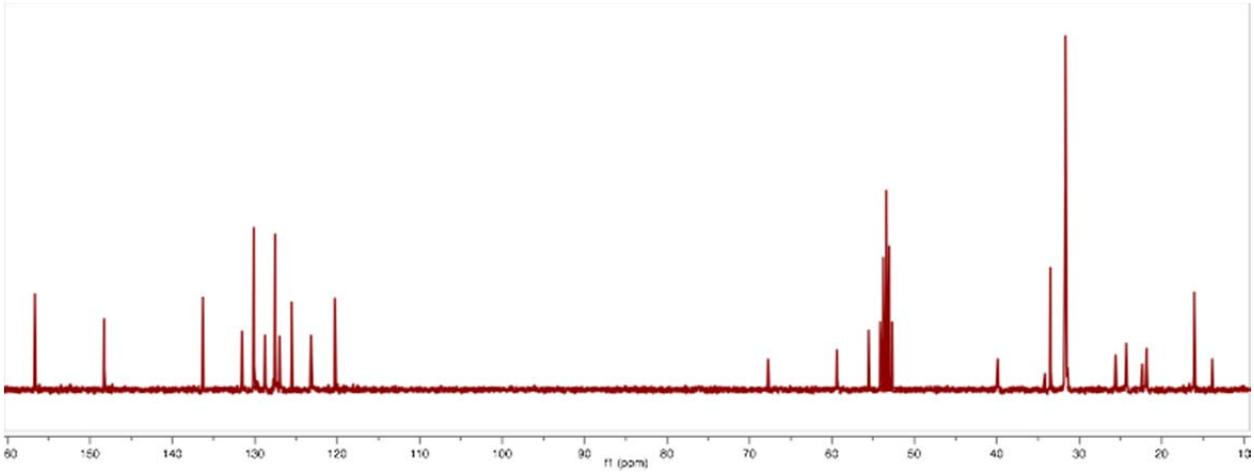

Figure A.168. $^{13}C\{^{1}H\}$ NMR spectrum of 32^{tBu} in CD_2Cl_2.

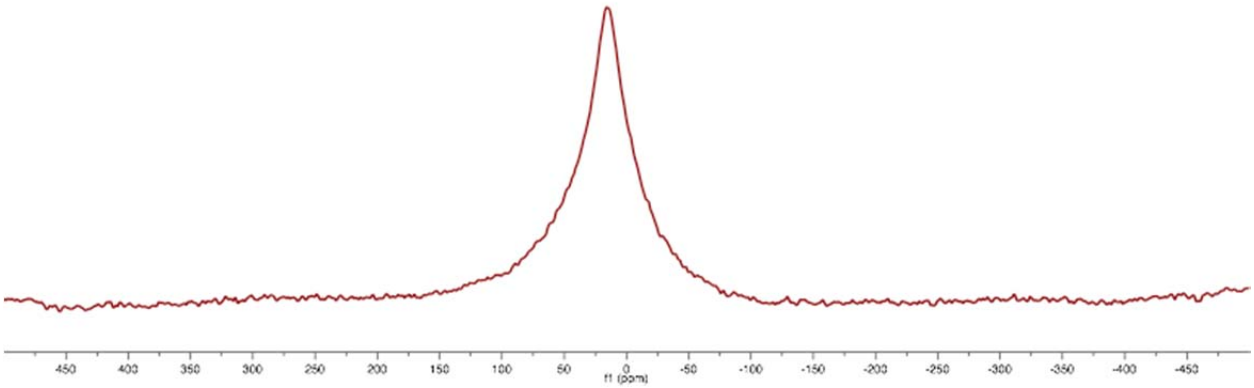

Figure A.169. ^{27}Al NMR spectrum of 32^{tBu} in CD_2Cl_2.

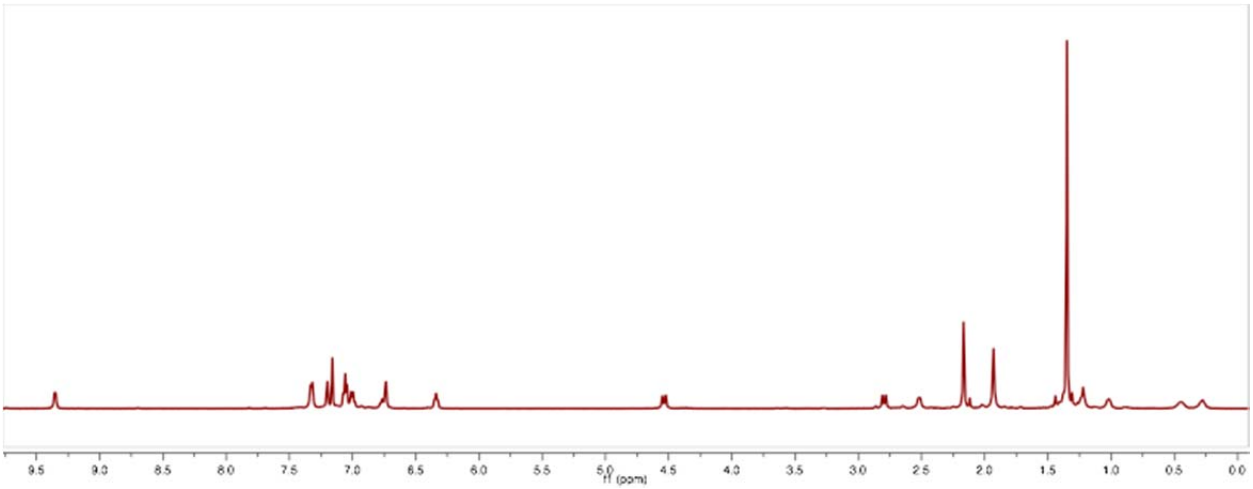

Figure A.170. ^{1}H NMR spectrum of 33^{tBu} in C_6D_6.

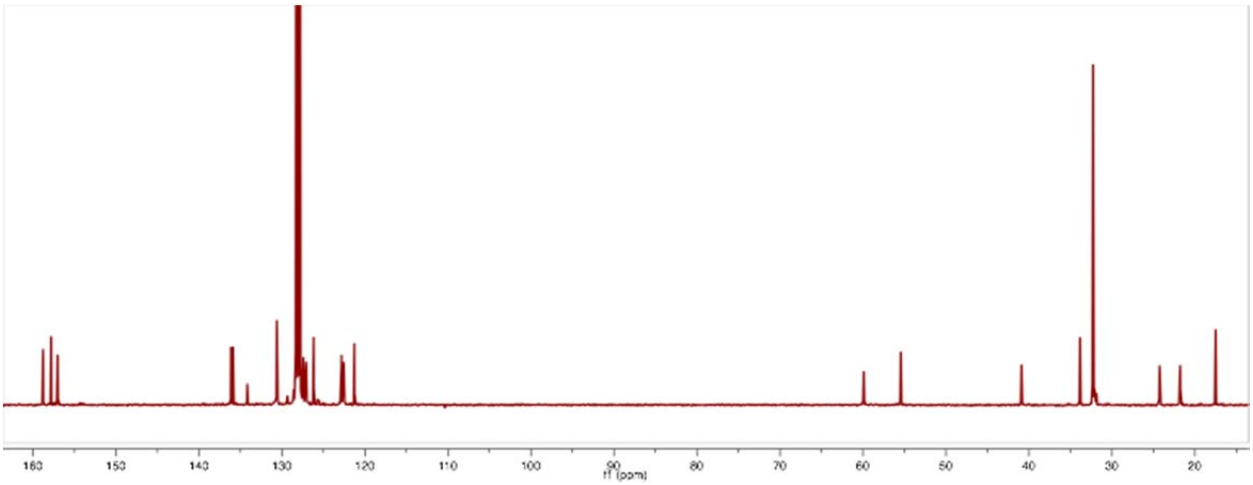

Figure A.171. ^{13}C{^{1}H} NMR spectrum of 33^{tBu} in C_6D_6.

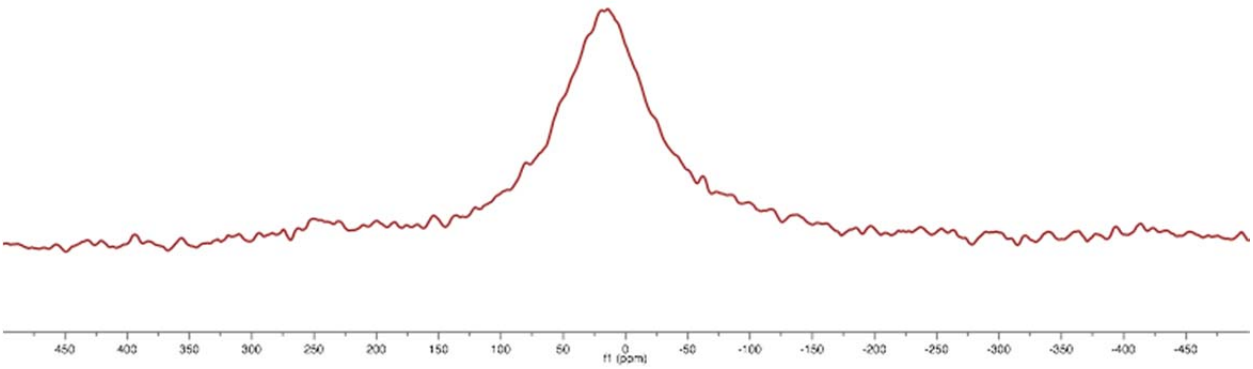

Figure A.172. ^{27}Al NMR spectrum of 33^{tBu} diphenylglyoxime macrocycle in C_6D_6.

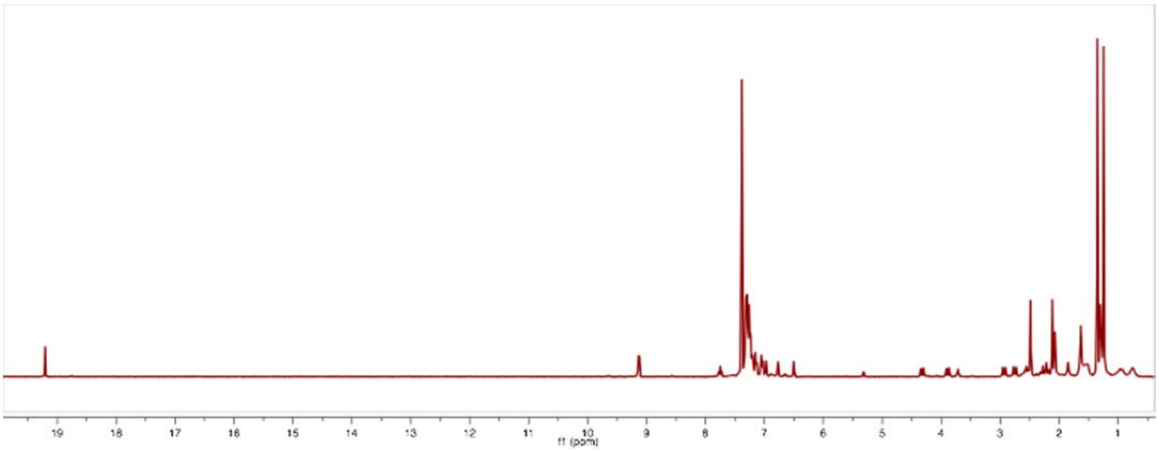

Figure A.173. ^{1}H NMR spectrum of 35 in in CD_2Cl_2.

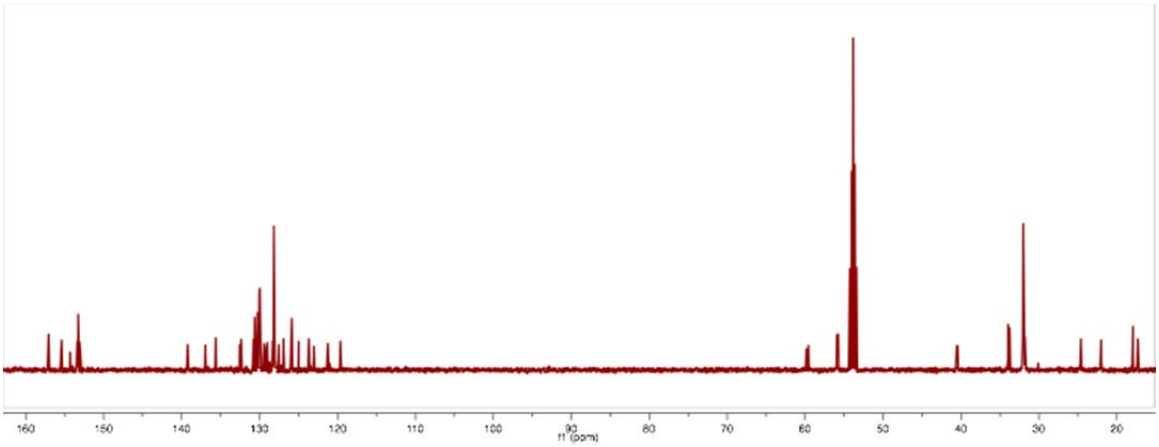

Figure A.174. $^{13}C\{^{1}H\}$ NMR spectrum of 35 in CD_2Cl_2.

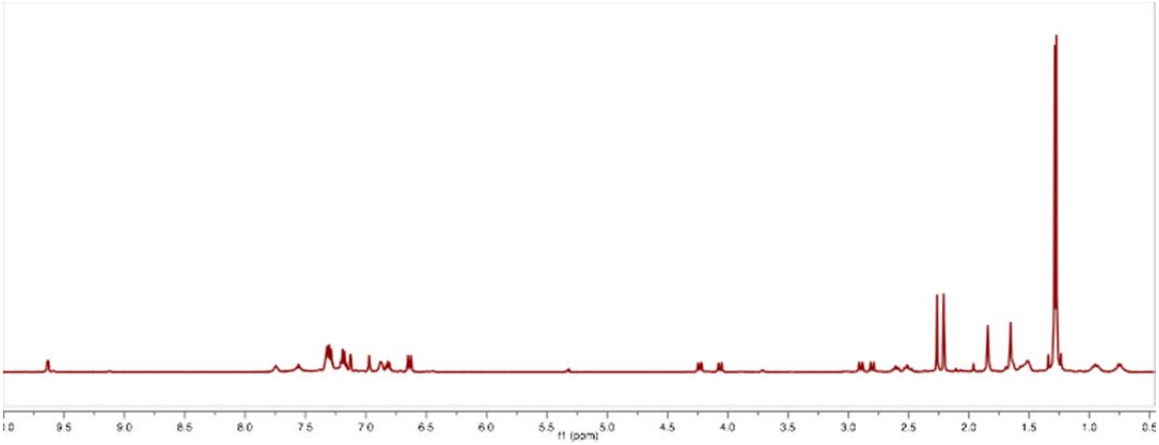

Figure A.175. ^{1}H NMR spectrum of 36^{tBu} in CD_2Cl_2.

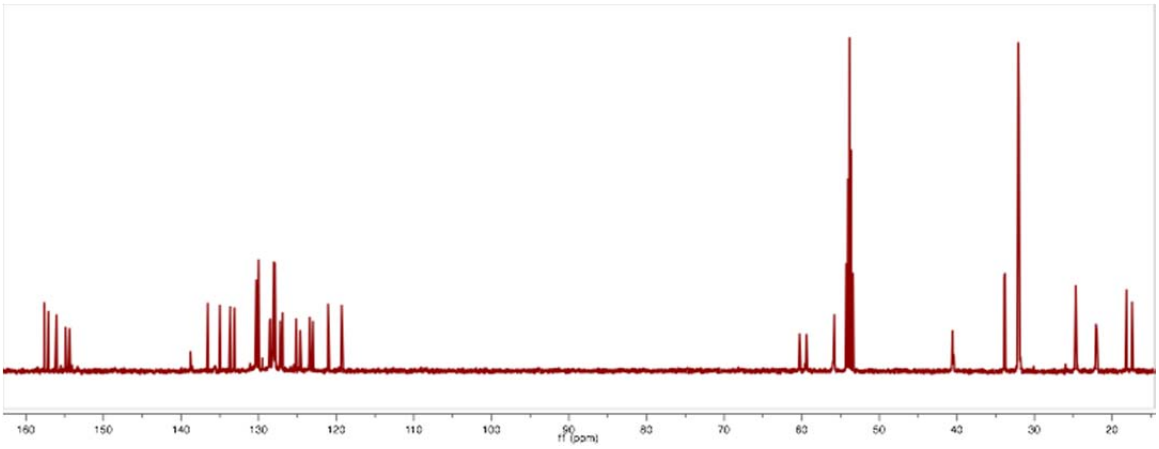

Figure A.176. $^{13}C\{^{1}H\}$ NMR spectrum of 36^{tBu} in CD_2Cl_2.

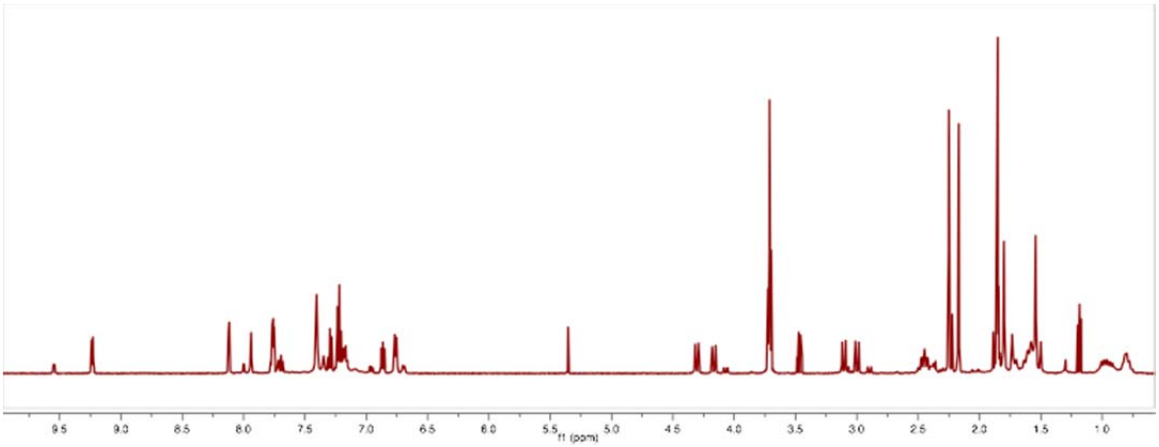

Figure A.177. ^{1}H NMR spectrum of crystals of 36^{NO2} in CD_2Cl_2 (contains THF and Et_2O).

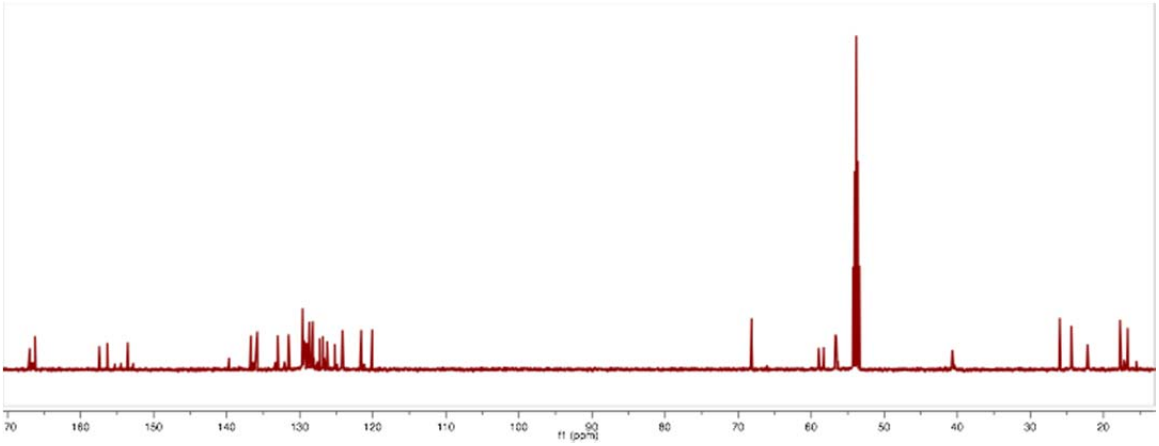

Figure A.178. $^{13}C\{^{1}H\}$ NMR spectrum of crystals of 36^{NO2} in CD_2Cl_2 (contains THF and Et_2O).

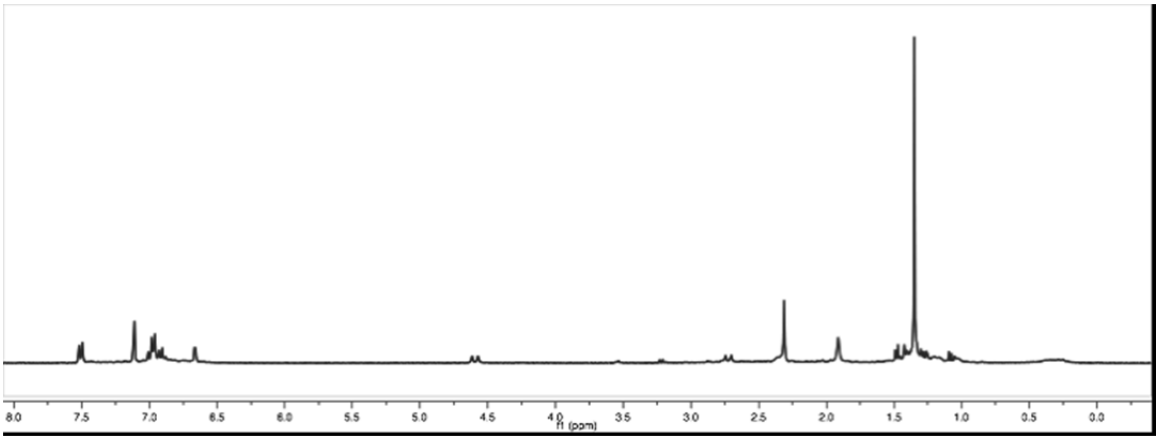

Figure A.179. ^{1}H NMR spectrum of 37 in C_6D_6.

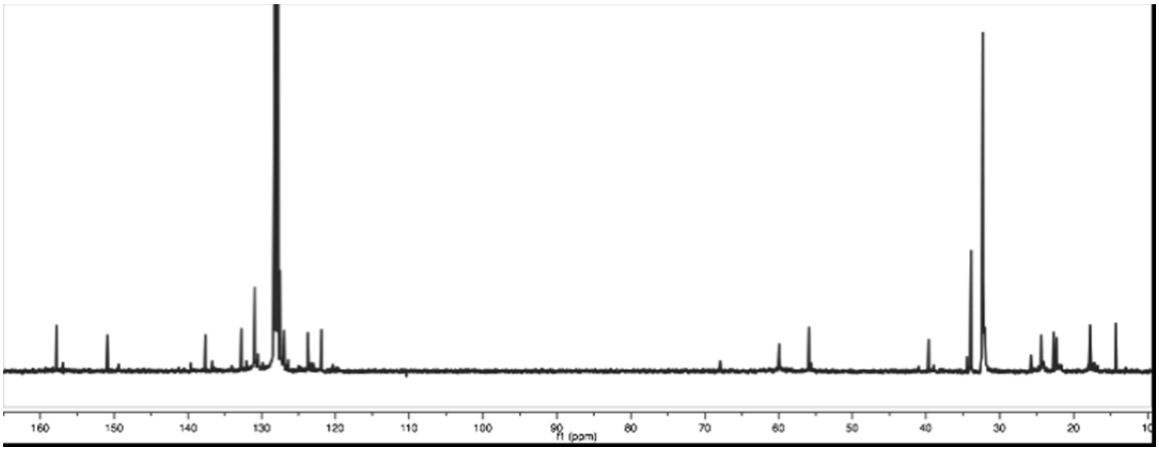

Figure A.180. $^{13}C\{^{1}H\}$ NMR spectrum of 37 in C_6D_6 (contains pentane and THF).